Novel phosphate-based cements

for clinical applications

Gemma Mestres

Supervisor: Prof. Maria-Pau Ginebra

PhD Thesis

Departament de Ciència dels Materials i Enginyeria Metal·lúrgica

E.T.S. d'Enginyeria Industrial de Barcelona

Universitat Politècnica de Catalunya

July 2012

Als meus avis, Josep i Eulàlia

Als meus pares, Jaume i Núria, i a la meva germana, Rosa

"It always seems impossible until it's done"

Nelson Mandela

I. Abstract (English)

This Thesis aims at the development of two novel families of inorganic phosphate cements with suitable characteristics for clinical applications in hard tissue regeneration or replacement. It is organized in two distinct parts.

The first part focuses at the development of silicon-doped α-tricalcium phosphate and the subsequent preparation of a silicon-doped calcium phosphate cement for bone regeneration applications. For this purpose, silicon-doped α-tricalcium phosphate was synthesized by sintering a calcium-deficient hydroxyapatite at 1250°C with different amounts of silicon oxide. The high temperature polymorph α-tricalcium phosphate was stabilized by the presence of silicon, which inhibited reversion of the β–α transformation, whereas in the Si-free α-tricalcium phosphate completely reverted to the β-polymorph. It was observed that the presence of Si did not alter the β–α transformation temperature. Both the Si-doped α-tricalcium phosphate and its Si-free counterpart were used as reactants in the formulation of calcium phosphate cements. While Si-doped α-tricalcium phosphate showed faster hydrolysis to calcium deficient hydroxyapatite, the composition, morphology and mechanical properties of both cements were similar upon completion of the reaction. When the samples were immersed in simulated body fluid, the Si-doped cement exhibited a faster deposition of an apatite layer on its surface than its Si-free counterpart, suggesting an enhanced bioactivity of the doped-cement. An *in vitro* cell culture study, in which osteoblast-like cells were exposed to a medium modified by the materials, showed a delay in cell proliferation and a stimulation of cell differentiation, the differentiation being more marked for the Si-containing cement. These results were attributed to the Ca depletion from the medium by both cements and to the continuous Si release detected for the Si-containing cement.

The second part of this Thesis is focused on the development of a new family of inorganic phosphate-based cements for biomedical applications, namely magnesium phosphate cements. The magnesium phosphate cements have been extensively used in civil engineering due to their fast setting, early strength acquisition and adhesive properties, properties that can be also of use for biomedical applications. However, there are some aspects that should be improved before they can be used in the human body, namely their high exothermic setting reaction and the release of

potentially harmful ammonium ions. Therefore, a new family of magnesium phosphate cements was explored as candidate biomaterials for hard tissue applications. These cements were prepared by mixing magnesium oxide with either sodium dihydrogen phosphate, ammonium dihydrogen phosphate or an equimolar mixture of both. The exothermia and the setting kinetics of the new cement formulations were tailored. The ammonium-containing magnesium phosphate cements resulted in struvite as the major reaction product, whereas the magnesium phosphate cement prepared with sodium dihydrogen phosphate resulted in an amorphous product. The magnesium phosphate cements studied showed an early compressive strength substantially higher than that of conventional apatitic calcium phosphate cements. Moreover, they showed antimicrobial properties against bacteria present in dental infections, which were attributed to the synergistic effect of a high osmolarity and high pH of the cement extracts. These properties make magnesium phosphate cements good candidates for endodontic applications. It is with this latter point in mind that some of the most relevant physico-chemical properties were further optimized and characterized. Particularly, their radiopacity was enhanced by the addition of bismuth oxide. The sealing efficiency of the magnesium phosphate cements and their adhesion to dentin were shown to be comparable or even higher than those presented by other inorganic cements used for endodontic treatments.

Resum (Catalan)

Aquesta Tesi té com a objectiu el desenvolupament de dues noves famílies de ciments inorgànics de base fosfat amb propietats adequades per a aplicacions clíniques en regeneració o substitució de teixits durs. La Tesi està organitzada en dues parts.

La primera part està centrada en el desenvolupament de fosfat tricàlcic α dopat amb silici i la subseqüent preparació de ciments de fosfat de calci dopats amb silici. Per a aquest objectiu, es va obtenir fosfat tricàlcic α dopat amb silici mitjançant la sinterització d'una hidroxiapatita deficient en calci amb diferents quantitats d'òxid de silici a 1250°C. La presència de silici va estabilitzar el polimorf d'alta temperatura (fosfat tricàlcic α), inhibint-se la reversió de la transformació $\beta-\alpha$, mentre que el fosfat tricàlcic α sense silici va revertir completament a polimorf β. La presència de silici no va alterar la temperatura de la transformació $\beta-\alpha$. Tant el fosfat tricàlcic α dopat amb silici com el seu homòleg sense silici van ser utilitzats com a reactius en la formulació de ciments de fosfat de calci. Si bé el fosfat tricàlcic α dopat amb silici va mostrar en les fases inicials una hidròlisi més ràpida a hidroxiapatita deficient en calci, un cop completada la reacció, la composició, morfologia i propietats mecàniques d'ambdós ciments van ser similars. L'estudi de bioactivitat mitjançant la immersió de les mostres en fluid corporal simulat va donar com a resultat la formació d'una capa d'apatita a la superfície del ciment dopat amb silici, més ràpida que al seu homòleg sense silici, fet que va suggerir una bioactivitat millorada del ciment dopat. L'estudi *in vitro*, en el qual cèl·lules osteoblàstiques es van exposar a un medi de cultiu que havia estat prèviament en contacte amb els ciments estudiats, va mostrar un retràs en la proliferació cel·lular i un estímul de la diferenciació cel·lular, aquest últim més marcat pel ciment que contenia silici. Aquests resultats es van atribuir a la reducció de calci en els medis en els quals estaven introduïts els ciments i a l'alliberament continu d'ions silici per part del ciment que en contenia.

La segona part d'aquesta Tesi està centrada en el desenvolupament d'una nova família de ciments inorgànics per a aplicacions mèdiques, els anomenats ciments de fosfat de magnesi. Aquests ciments s'han utilitzat extensament en enginyeria civil degut a la seva presa ràpida, elevades propietats mecàniques a temps curts i adhesivitat, propietats que poden ser de gran utilitat en aplicacions biomèdiques. No obstant, hi ha alguns aspectes que s'haurien de millorar

abans de poder utilitzar aquests ciments en el cos humà, com l'exotèrmia de reacció de presa o la possible alliberació d'ions amoni. Amb aquesta finalitat es planteja el desenvolupament d'una nova família de ciments de fosfat de magnesi amb possibles aplicacions clíniques. Aquests ciments es van preparar mitjançant la combinació d'òxid de magnesi amb dihidrogen fosfat de sodi, dihidrogen fosfat d'amoni o una barreja equimolar d'ambdós. L'exotèrmia i la cinètica de presa de les noves formulacions de ciment es van ajustar per tal de complir els requeriments clínics. Els ciments que contenien amoni van donar com a producte majoritari de reacció estruvita, mentre que els preparats amb dihidrogen fosfat de sodi van donar lloc a un producte amorf. Els ciments desenvolupats van presentar una resistència a la compressió superior als ciments apatítics de fosfat de calci, especialment a temps curts, i van mostrar propietats antimicrobianes contra bactèries presents en infeccions dentals. Aquestes propietats converteixen aquests ciments en bons candidats per aplicacions endodòntiques. Tenint en compte aquest últim punt, es va millorar la radiopacitat dels ciments i es va avaluar la capacitat de segellat dels ciments de fosfat de magnesi i la seva adhesió a la dentina, propietats que van resultar comparables o fins i tot superiors a les que presenten altres ciments inorgànics utilitzats en tractaments endodòntics.

Resumen (Spanish)

Esta Tesis tiene como objetivo el desarrollo de dos nuevas familias de cementos inorgánicos de base fosfato con propiedades adecuadas para aplicaciones clínicas en regeneración o sustitución de tejidos duros. La Tesis está organizada en dos partes.

La primera parte está centrada en el desarrollo de fosfato tricálcico α dopado con silicio y la subsecuente preparación de cementos de fosfato de calcio dopados con silicio. Para este objetivo, se preparó fosfato tricálcico α dopado con silicio mediante la sinterización de una hidroxiapatita deficiente en calcio con distintas cantidades de óxido de silicio a 1250°C. La presencia de silicio resultó en la estabilización del polimorfo de alta temperatura (fosfato tricálcico α), inhibiéndose la reversión de la transformación β–α, mientras que el fosfato tricálcico α sin silicio revertió completamente al polimorfo β. La presencia de silicio no alteró la temperatura de transformación β–α. Tanto el fosfato tricálcico α dopado con silicio como su homólogo sin silicio se utilizaron como reactivos en la formulación de cementos de fosfato de calcio. Si bien el fosfato tricálcico α dopado con silicio mostró una hidrólisis más rápida a hidroxiapatita deficiente en calcio, una vez completada la reacción, la composición, morfología y propiedades mecánicas de los dos cementos fueron similares. El estudio de bioactividad mediante inmersión en fluido corporal simulado mostró la formación de una capa de apatita en la superficie del cemento dopado con silicio, más rápida que en su homólogo sin silicio, lo que sugirió una mejora de la bioactividad del cemento dopado. El estudio *in vitro*, en el cual células osteoblásticas se expusieron a un medio de cultivo que había estado previamente en contacto con los cementos estudiados, mostró un retraso en la proliferación celular y un estímulo de la diferenciación celular, éste último más marcado en el cemento que contenía silicio. Estos resultados se atribuyeron a la reducción de calcio del medio de cultivo que había estado en contacto con los cementos y a la continua liberación de iones silicio por parte del cemento que contenía este elemento.

La segunda parte de esta Tesis está centrada en el desarrollo de una nueva familia de cementos inorgánicos para aplicaciones médicas, los cementos de fosfato de magnesio. Estos cementos se han utilizado extensamente en ingeniería civil, debido a su rápido fraguado, sus elevadas propiedades mecánicas a tiempos cortos y su adhesividad, propiedades que pueden ser

de gran utilizad en aplicaciones biomédicas. No obstante, hay algunos aspectos que requieren una mejora antes de utilizar estos cementos en el cuerpo humano, tales como su alta exotermia de reacción o la posible liberación de iones amonio. Con esta finalidad se plantea el desarrollo de una nueva familia de cementos de fosfato de magnesio para aplicaciones clínicas. Estos cementos se prepararon mediante la combinación de óxido de magnesio con dihidrógeno fosfato de sodio, dihidrógeno fosfato de amonio o una mezcla equimolar de ambos. La exotermia y la cinética de reacción de las nuevas formulaciones de cemento se ajustaron para cumplir con los requerimientos clínicos. Los cementos de fosfato de magnesio que contenían amonio resultaron en estruvita como producto mayoritario de la reacción, mientras que los preparados con dihidrógeno fosfato de sodio dieron lugar a un producto amorfo. Los cementos estudiados presentaron una resistencia a la compresión superior a los cementos apatíticos de fosfato de calcio, especialmente a tiempos cortos, y mostraron propiedades antimicrobianas contra bacterias presentes en infecciones dentales. Estas propiedades convierten a los cementos de fosfato de magnesio en buenos candidatos para aplicaciones endodónticas. Teniendo en cuenta este último punto, se optimizó la radiopacidad de los cementos, y se evaluó la capacidad de sellado de los cementos de fosfato de magnesio y su adhesión a la dentina, propiedades que resultaron ser comparables o incluso superiores a las que presentan otros cementos inorgánicos utilizados en tratamientos endodónticos.

II. Acknowledgements, agraïments, agradecimientos

Semblava que mai arribaria aquest dia. Però es veu que és cert que si tens paciència i vas treballant dia a dia tot acaba per arribar. Em disposo a escriure els agraïments de la Tesi, la qual ha representat una (llarga i) important etapa de la meva vida, i desenes de persones estan en els meus pensements.

Primer de tot vull fer el més sincer agraïment a la Maria Pau Ginebra, la directora d'aquesta Tesi, la qual no es pot ni arribar a imaginar la de coses que m'ha anat ensenyant, de forma pedagògica i exhaustiva, durant aquests últims quatre anys. Des de dissenyar el més eficientment possible un experiment, fins a discutir els resultats obtinguts per finalment donar-li forma de Tesi o article, passant per aprendre a redactar projectes. Pau, gràcies per haver-me donat la gran oportunitat que representa poder treballar al teu costat quan encara no em coneixies, adoptant-me al teu petit (ara és molt més gran!) grup de ciments.

En segon lloc voldria agrair al Xavier Gil, director del grup de Biomaterials, Biomecànica i Enginyeria de Teixits (BIBITE) per tirar endavant al grup, amb gran esforç i dedicació dia a dia. Xavier, et vull donar les gràcies per haver-me donat el teu vot de confiança durant tot aquest temps.

Voldria agrair sincerament a en Josep Anton Planell, el director de l'Institut de Bioenginyeria de Catalunya (IBEC), i a l'Òscar Castaño, un dels post-docs que ha tirat endavant la línia de biomaterials de l'IBEC, la oportunitat de em van donar per començar aquest gran projecte. Moltes gràcies per tot el que em vau ensenyar durant el meu primer any en contacte amb els biomaterials!

Tothom sap que, quan escrius alguna cosa, tens l'esperança de que algú s'ho llegirà. I al escriure la Tesi, tenir algú que s'ho llegeixi, t'ho comenti i, a més a més, et correigeixi l'anglès (abans de que passi per les estrictes correcciones de la Maria Pau) és el màxim que es pot demanar. Poques persones haurien tingut la generositat i paciència que has tingut tu, Jaume Navarro, llegint-te els capítols una i altra vegada. No saps com t'agraeixo la teva dedicació i minuciositat corregint-me la Tesi. De fet, saber que tu estaves "esperant" un capítol em donava

energia per seguir escrivint, i els teu *feedback* m'han permès anar millorant-los a poc a poc. Gràcies de tot cor!

A la vida, el record que et queda després de realitzar qualsevol projecte són les persones amb qui l'has viscut. De fet, crec que podria omplir pàgines i pàgines de noms i paraules d'agraïments, però intentaré ser breu. Per una banda, sento que amb cada un dels doctorands/tècnics/estudiants amb qui he compartit el despatx i els laboratoris, realment hem compartit molt més que un espai. Sou genials!

Edgar, no tengo palabras para describir lo que has significado para mi durante estos años: compañero, maestro, amigo... Eres una de las personas que más conocimiento me ha infundido y "tus broncas" siempre me han ayudado a hacer las cosas mejor. Hacemos muy buen equipo y espero de todo corazón que algún día podamos volver a trabajar juntos. ¡No sabes cuánto te echaré de menos!

Sara, tu siempre tan dulce y atenta en todo momento, eres una gran amiga. Hemos vivido muchos momentos importantes durante los últimos dos años, ¡que suerte que nos tocó compartir la oficina! ¡Gracias por los abrazos y las risas!

Montse, mil gràcies per la teva ajuda durant aquests anys! He après molt al teu costat, tant a ser més bona persona com a analitzar més acuradament els resultats. La teva passió per la ciència, la teva paciència i afany pel treball són increïbles! Gràcies per escoltar-me durant els meus últims mesos d'indecisió sobre el futur que m'espera!

Al departament de Ciència dels Materials de la UPC (CMEM) i, especialment, al grup de recerca BIBITE som una bona colla. Voldria dedicar unes paraules d'agraïment a tots ells. Per una banda, als que formen o han format part del grup de ciments: Montse Español, Cristina Canal, Edgar Montufar, Maite Valderas, Sara Gallinetti, David Pastorino, Yassine Maazouz, Román Pérez, Carolina Mochales (gràcies per ajudar-me a continuar el projecte del silici!) i Sergio del Valle (gracias por enseñarme a tener una gran disciplina en la sala de cultivos). Per altra banda, agraïr especialment l'ajuda rebuda al laboratori, utilitzant equips o en temes administratius, per part de Meritxell Molmeneu, Kim Albó, Pablo Sevilla, Lluis Delgado, Isaac López-Insa, Noelia Aparicio i Olga López. És difícil igualar el bon rotllo que transmet aquest grup. Gràcies a tots pels bons moments

que hem passat junts dia a dia: Marta Pegueroles, Tania Traykova, Daniel Rodríguez, José María Manero, Cristina Canal, Carles Mas, Emiliano Salvagni, Ana Guadalupe, Aleix Mestre, Marc Fernández, Jordi Guillem, Marta González, Virginia Paredes, Nathalia Marín, Carolina Herranz, Maria Godoy, Kiara Riccardi, María Isabel Castellanos, Andrea Colin, Mariana Motisuke, a més a més de tots els que he mencionat previament. També hem compartit molts i molt bon moments amb els investigadors i doctorants de l'IBEC: Elisabeth Engel, Damian Lacroix, Teresa Sanchis, Miguel Angel Mateos, Melba Navarro, Óscar Castaño, Clara Sandino, Andrea Malandrino, Andy Olivares, Aitor Aguirre, Johan Gustavsson, Tiziano Serra...

Recuerdo con una gran sonrisa a Giselle Ramirez, Carlos Botero y Zamir de Armas, con quien compartimos muchísimos momentos durante nuestros primeros años en la oficina. ¡Grandes compañeros! Tampoco voy a olvidar a Milena, Andy, Edgar, Sergio, Sara, Elena, Jordi Mir, Luis, Ravi, Yassine, Marc y Erik.

Me gustaría hacer también una mención especial a aquellos estudiantes que compartieron el día a día conmigo al realizar su proyecto final de carrera: Clémence Le Van, Yassine Maazouz, David Pastorino y Ruben Tayupo.

Un doctorat és una etapa durant la qual fas noves amistats, algunes de les quals sorgeixen de compartir projectes o senzillament els laboratoris. Voldria fer un agraïment especial al Conrado Aparicio, tan per ajudar-me a trobar un bon grup per fer l'estada com per compartir molt bons moments a l'altra banda de l'oceà, juntament amb la Jane i el Pablo. Sempre en mantindré un molt bon record! My stay in the School of Dentistry of the University of Minnesota gave me the oportunity to learn a lot from Dr. Sven-Ulrik Gorr, a great scientist and a wonderful person. Thank you so much to welcome me as an old-colleague in your lab from the first day and for stimulating me to do plenty of different experiments and experiences a part from those that we had already planned. I was also so lucky for sharing the lab with Mahsa Abdolhosseini, the greatest colleage and friend ever. I have learnt so much from you, Mahsa! Thank you so much for all your support, smiles, patience and hard work. I wish you all the best! ☺

Mi estancia en Granada también me permitió realizar un importante estudio para esta Tesis. Quiero agradecer la oportunidad que me dieron Manuel Toledano y Raquel Osorio para colaborar con su grupo de investigación. Allí, tuve la gran suerte de contar con la ayuda de Fátima

Sánchez desde el primer día. ¡Fátima, tu exactitud y perseverancia son envidiables! Te agradezco muchísimo tu ayuda, ánimo y cariño durante todos los días en que tuvimos el ensayo en marcha, ¡el cual que no fue corto! ¡Te deseo mucha suerte con todos tus retos!

I have always thought that a person is in a way constituted by all the experiences shared with other people during life. I really think that I would not have started my PhD if I would not have been part of the Catalytic Processes and Materials group of the University of Enschede in 2006-2007 as an Erasmus student. Specially my supervisor, Prof. Seshan, and also some of the PhD students, Berta, Davide and Cristiano, increased my devotion to science till the point that I learnt what I wanted to do in a future: research. Thank you all so much for be part of such a nice experience!

I a nivell personal, indubtablement, sóc qui sóc gràcies a la meva família i als meus amics. La bondat i força de voluntat dels meus avis, Josep i Eulàlia, dels meus pares, Jaume i Núria, i de la meva germana, Rosa, m'han fet créixer amb il·lusió per fer un món millor, sempre cuidant al màxim als meus. La veritat és que sempre he pensat que sóc molt afortunada amb la família que m'ha tocat, de debó. Gràcies a tots per formar-ne part! I un agraïment especial per la Vinyet i la Marina, de les quals sempre he rebut paraules de suport en moments delicats.

I un altre nucli que m'ha donat fortalesa és el grup d'amigues. Amigues de tota la vida, com la Mire, han sobrepassat qualsevol frontera després de 26 anys d'amistat incondicional. Hem passat de nenes a adolescents, a noies, a les persones que som ara. Res seria igual si tu no haguessis estat aquí. Gràcies per tots i cada un dels moments que hem compartit, i que estic segura que seguirem compartint! El grup d'amigues ja té una dècada i és una part molt especial de la meva vida. Moltes gràcies noies per ser com sou: Maria, Vicky, Pachi, Bet, Marta, Joana i Marina. I la colla d'amigues de la UAB, que cada dia és més fort, i ja esperant una nova incorporació!: Neus, Cristina, Marisa i Anna. Nenes, cada una de les nostres sortides dóna més sentit a la vida. És difícil mencionar totes les persones que són importants per la teva vida, però no puc deixar de mencionar l'Adrià, l'Aleix, el David, l'Anna i l'Alexandra.

A tots vosaltres, i tots aquells que sempre hi sereu presents, moltes gràcies per haver-me ajudat a tirar endavant aquest projecte i sobretot per endolcir cada dia la meva vida.

III. Index of contents

IV. Motivation, objectives and structure of this Thesis

Motivation

The motivation of this Thesis is originated by two different health problems. The **first issue of focus** is the prevalence of diseases or disorders and the large number of fractures occurring in an ageing population, which has increased the need for bone substitutes able to replace areas of bone that are too large to heal by themselves. The use of synthetic bioactive materials can overcome the limitations of the conventional treatments (*i.e.* autografts and allografts) [1].

Calcium phosphate cements (CPCs) are well-known for their excellent bioactivity and osteoconductivity owed to their similarity to the mineral phase of the bone [2]. The cements can be introduced into a bone defect by minimal invasive techniques and they can be used as drug delivery systems. However, the CPCs also have some drawbacks, such as slow resorption, poor mechanical properties [3] and lack of macroporosity [4]. Considerable efforts have been devoted to combine the intrinsic bone regeneration potential of CPCs with their ability to incorporate drugs, active molecules or specific ions for different therapeutic needs [3]. Silicon, specifically, is very important during the growth of bone and cartilage at early stages and also during bone remodelation [5].

The aim of the first part of this Thesis is to develop α-tricalcium phosphate doped with silicon, which will be used as the reactant of silicon-doped calcium phosphate cements for bone regeneration, with the expectation that these cements will have enhanced osteogenic properties than their silicon-free counterparts due to the presence of silicon.

The **second issue of focus** is the common damage of the hard tissues protecting the dental pulp (*i.e.* enamel and dentin) due to trauma or dental caries. This situation gives advantage to the oral microorganisms to infect the dental pulp, threatening the health of the whole tooth and even causing serious health problems to the individual if the infection is not eradicated. Depending on the grade of injury, the endodontic treatments aim either at the closure of the damaged hard tissue or at the removal of the diseased part of the pulp or at the removal of the entire pulp. If the

entire pulp is removed, the root canal has to be filled with a tightly sealing and antimicrobial material that prevents reinfection. However, there is still not a single material that fulfills all the requirements demanded by this application and therefore the root canal is usually obturated with the combination of two or more materials.

Magnesium phosphate cements (MPCs), which have been used in civil engineering for their fast setting and adhesive properties [6–8], were envisaged as a novel family of inorganic cements that could overcome the low mechanical properties of the calcium phosphate cements. Moreover, the chemical composition of this system allowed predicting their antimicrobial potential. Despite the unique benefits provided by these systems, only recently they have been proposed for clinical applications, specifically for bone regeneration [9–11]. At the best of our knowledge, the MPCs have not yet been suggested for endodontic applications.

The second part of the Thesis aims at the development of a novel system of antimicrobial MPCs tailored for clinical applications. This family of cements has been pointed out as promising candidates for endodontic applications, in which an infection of the root canal has to be battled.

Objectives

The main objectives of this Thesis are the following:

1. To develop a Si-doped calcium phosphate cement, using as a main reactant a Si-stabilized α-TCP, and to study the role of Si on the stabilization and hydrolysis reaction of this compound, as well as in the cell response to the Si-doped calcium phosphate cement.

2. To develop and characterize a new family of magnesium phosphate cements for clinical uses and to optimize their properties for endodontic applications.

Structure

This Thesis has been organized in two differentiated parts. The **first part** aims at the development of silicon-doped calcium phosphate cements for bone regeneration applications, and arises from the desire to improve the intrinsic bone regeneration potential of CPCs. The **second part** of this Thesis aims at the development of magnesium phosphate cements with high early compressive strength and tailored properties for clinical applications, which are envisaged to eradicate or prevent a localized infection.

Even though both Si-doped calcium phosphate cements and magnesium phosphate cements have several points in common, such as being inorganic phosphate cements intended to be used in clinical applications, their specific applications are different. Therefore, in order to facilitate the reading, this Thesis has been organized in two parts, each of them containing its own theoretical framework Chapter. This Thesis will conclude with a final Chapter in which the most relevant results will be recapitulated. Figure 1 shows the structure of this Thesis.
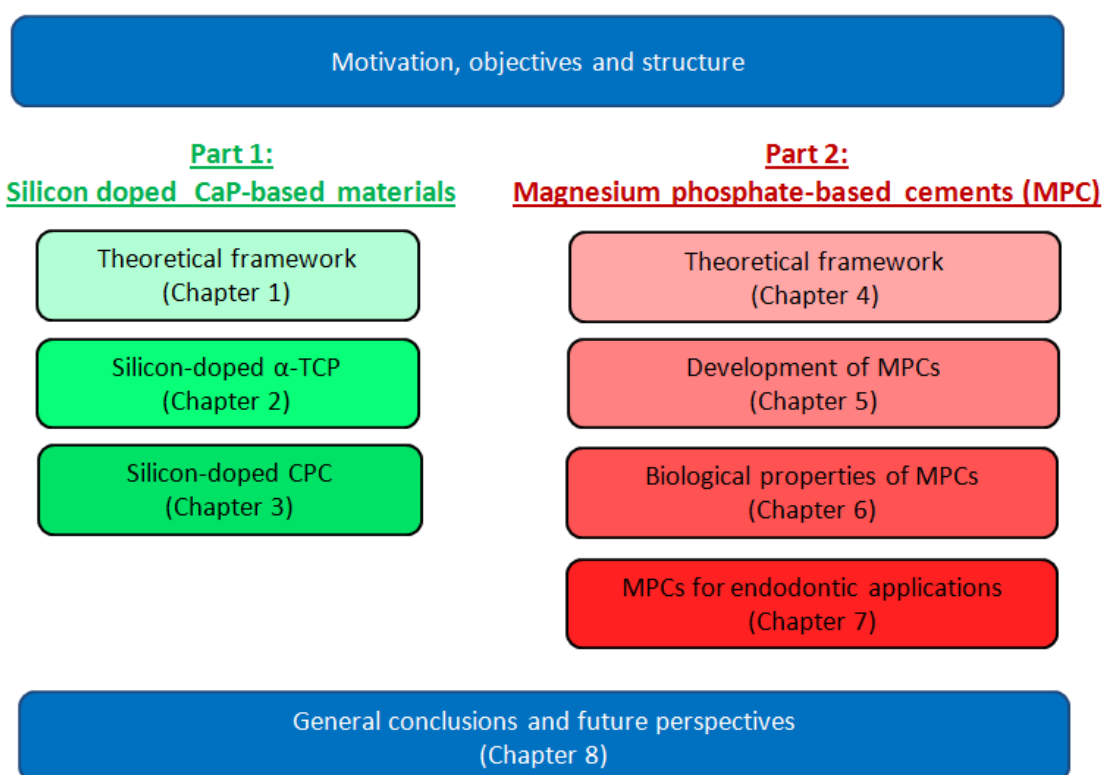

Figure 1. Structure of this Thesis.

References

[1] Juhash JA, Best SM. Bioactive ceramics: processing, structures and properties. J Mater Sci (2012) 47:610-624.

[2] Bose S, Tarafder S. Calcium phosphate ceramic systems in growth factor and drug delivery for bone tissue engineering: A review. Acta Biomaterialia 2011 (in press).

[3] Ginebra MP, Canal C, Espanol M, Pastorino D, Montufar EB. Calcium phosphate cements as drug delivery materials. Advanced Drug Delivery Reviews (in press).

[4] M.P. Ginebra. Cements as bone repair materials, In J.A. Planell (Ed.), Bone repair biomaterials. Woodhead Publishing Limited, Cambridge, England (2009), 271-308.

[5] Pietak et al. Silicon substitution in the calcium phosphate bioceramics. Biomaterials 28 (2007) 4023-4032.

[6] El-Jazairi B. Rapid repair of concrete pavings. Concrete 1982; 16: 12–15.

[7] Popovics S, Rajendran N, Penko M. Rapid hardening cements for repair of concrete. ACI Materials Journal 1987; 84: 64–73.

[8] Wilson AD, Nicholson JW. Acid–base cements: their biomedical and industrial applications. Cambridge, United Kingdom: Cambridge University Press, 1993.

[9] Klammert U, Vorndran E, Reuther T, Müller FA, Zorn K, Gbureck U. Low temperature fabrication of magnesium phosphate cement scaffolds by 3D powder printing. Journal of Materials Science: Materials in Medicine 2010; 21: 2947–2953.

[10] Großardt C, Ewald A, Grover LM, Barralet JE, Gbureck U. Passive and active *in vitro* resorption of calcium and magnesium phosphate cements by osteoclastic cells 2010; 16: 3687–3695.

[10] Vorndran E, Wunder K, Moseke C, Biermann I, Muller FA, Zorn K, Gbureck U. Hydraulic setting $Mg_3(PO_4)_2$ powders for 3D printing technology. Advances in Applied Ceramics 2011; 110: 476–481.

[11] Großardt C, Ewald A, Grover LM, Barralet JE, Gbureck U. Passive and active *in vitro* resorption of calcium and magnesium phosphate cements by osteoclastic cells 2010; 16: 3687–3695.

PART 1.

Silicon-doped calcium phosphate cements

for bone regeneration

"Not everything that counts can be counted, and not everything that
can be counted counts"

Albert Einstein

Part 1:

Silicon-doped calcium phosphate-based materials

Chapter 1. Theoretical framework
- Bones as living tissues that are able to self-remodelate small fractures
- Need of natural or synthetic bone grafts to heal large bone defects
- Intrinsic relevant properties of calcium phosphate-based materials and, especifically, of calcium phosphate cements (CPCs), for bone regeneration
- Twofold advantages brought by Si: i) stabilization of the α-TCP, and ii) potential enhancement of the biological properties of CPCs

Chapter 2. Silicon-doped α-TCP
- Development of Si-α-TCP. Optimization of the amount of Si
- Characterization of the Si-α-TCP

Chapter 3. Silicon-doped CPC
- Development of Si-CPC using Si-α-TCP as reactant
- Physico-chemical characterization of the Si-CPC
- Bioactivity studies of the Si-CPC
- Ion release studies
- Cell proliferation and differentiation

Chapter 1.

Theoretical framework

Table of Contents

1.1 Social context encouraging the development of novel biomaterials

Spanish population is aging since life expectancy in this country has increased almost linearly since the World War II [1]. As consequence of the increase of life expectancy, the bone fracture risks have increased as well. For instance, in Spain, a total of 318 new cases of hip fracture were recorded in 1988, and 490 in 2002. This represents an increase of 54% in the absolute number of hip fractures for the 14-year period (3.9% per year). [2]. The incidence of hip fractures have been reported to be more frequent in women compared to men [2], since a 26.1% of women who are 50 years old or older suffer from osteoporosis [3]. Figure 1.1 shows that the incidence of hip fracture starts increasing exponentially with age for people older than 65 years. In 2006 it was estimated that the 25,000 bone fractures that occur in Spain each year result in direct costs of more than €126 million and indirect costs of about €420 million [4].
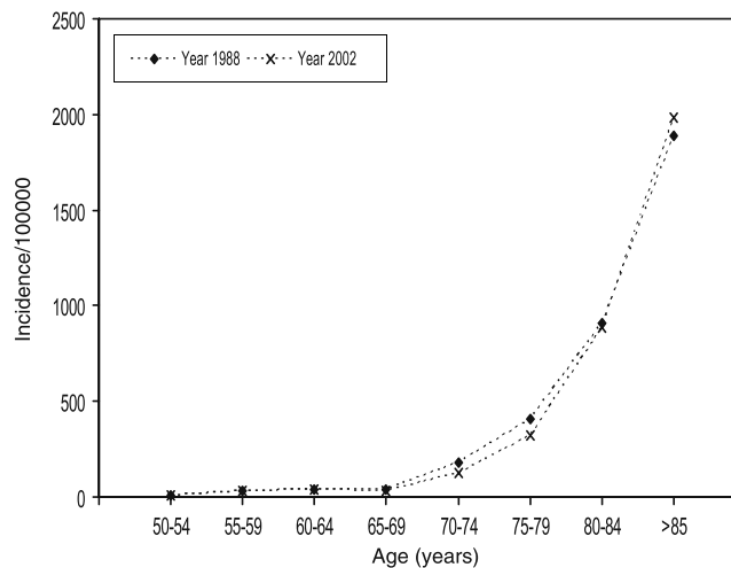
Figure 1.1. Overall age-specific incidence of hip fracture in Cantabria, Spain (from [2]).

Current medical treatments for severe bone injuries are problematic and may yield poor results [5]. Therefore, it is crucial to have a deep understanding of the bone from the biological point of view, in order to be able to perform a successful research focused on looking for new strategies to heal bone fractures.

1.2 Bone

1.2.1 Bone as a hierarchically organized tissue

Bone is a composite tissue with great stiffness and strength that constitute the skeleton. Bones have several functions: they are designed to protect vital organs of the body (*e.g.* skull or thorax), provide the frame for locomotion of the musculoskeletal system and withstand physiological load without breaking. Additionally, bone is a reservoir for many essential minerals, such as calcium and phosphate, and plays an important role in the regulation of ion concentration in extracellular matrix. Bone marrow contains mesenchymal stem cells (MSCs) and hematopoietic cells. MSC are multipotent stem cells that can differentiate into a variety of cell types, including: osteoblasts (bone cells), chondrocytes (cartilage cells), myocyte (muscle cell) and adipocytes (fat cells) [6] [5] [7].

Bone is a highly organized tissue that is hierarchically arranged at the macro- (tissue level), at the micro- (cellular), and at the nano-scale (molecular) [8].

1.2.1.1 Classification of bones (macroscopical organization)

The bones can be organized according to their shape, which is genetically programmed in order to attain a certain function. Four kinds of bones can be mentioned regarding their shape: long, short, flat and irregular bones. **Long bones** are those in which length exceeds width, having a cylindrical shape with thicker end portions, *e.g.* femur or humerus; **short bones** have the three dimensions similar, being cubelike, *e.g.* carpals of wrist; **flat bones** are thin and flattened, with light curvature, *e.g.* parietal bone of skull or ribs; **irregular bones** are those with complicated shapes, *e.g.* pelvis or vertebrae [7] (Figure 1.2).
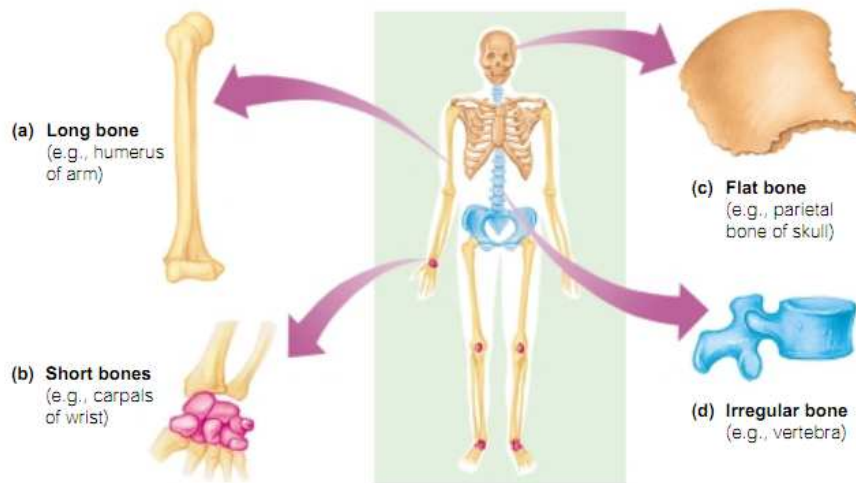
Figure 1.2. Classification of bones on the basis of their shape (from [7]).

The gross structure of a long bone is shown in Figure 1.3 a. The **diaphysis** makes up most of the bone's length and is composed of compact bone. The diaphysis is covered and protected by a fibrous connective tissue membrane, the **periosteum**. Hundreds of connective tissue fibers, called **Sharpey's fibers**, secure the periosteum to the underlying bone (Figure 1.3 c). The **epiphyses** are the ends of the long bone. Each epiphysis consists of a thin layer of compact bone enclosing an area filled with spongy bone. Articular cartilage, instead of a periosteum, covers its external surface.

Bone tissue has two major forms: the cortical or compact bone, and the cancellous, trabecular or spongy one. The bone tissue called **cortical** or **compact** is dense and forms most of the outer shell of a whole bone, which has variable thickness [9]. The **cancellous bone** forms a complex three-dimensional scaffold composed of short struts of bone material called trabeculae, being thus a porous material. [8]. The cortical bone embraces the trabecular one like a hull to protect the delicate trabecular scaffold from impact [8]. While cortical bone has four times the density of trabecular bone, its metabolic turnover is eight times lower [8]. The location of these bone types in a long bone is illustrated in Figure 1.3 b.
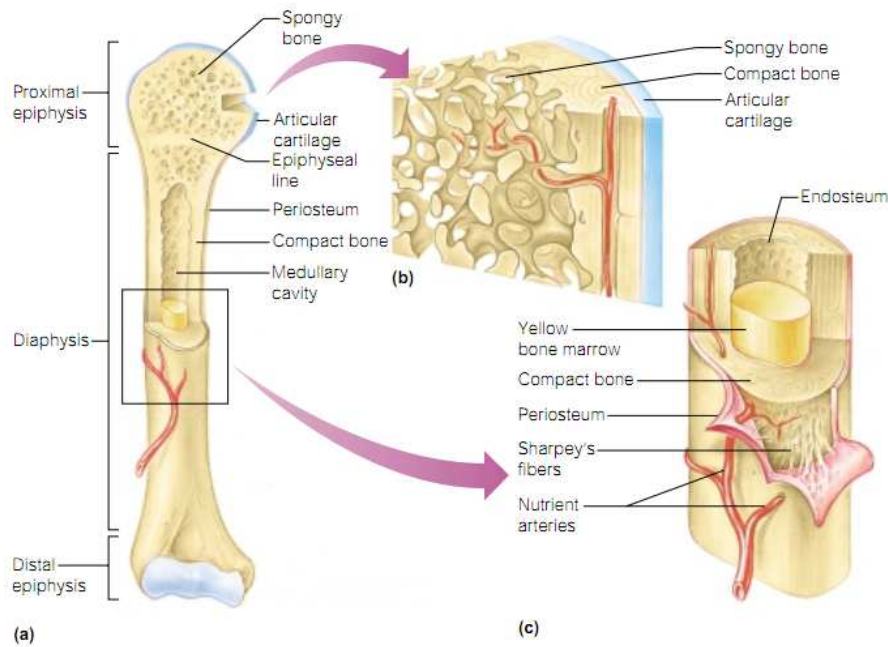
Figure 1.3. The structure of a long bone, a) anterior view with longitudinal section cuts away at the proximal end; b) pie-shaped, three-dimensional view of spongy bone and compact bone of the epiphysis; c) cross section of the shaft (diaphysis) (from [7]).

1.2.1.2 Bone structural organization (microscopical organization)

At the microscopic or cellular level, the organic and mineral phases are arranged into two forms of bone tissue: woven or primary bone, and lamellar bone.

The **woven bone** is typically found in both cortical and cancellous bone of young growing animals and also in adults after a bone injury. During normal maturation woven bone is gradually replaced by lamellar bone, so that in man, for example, there is normally no woven bone present after the age of 14–16 years [9]. Woven bone is an isotropic tissue with coarse collagen fibers which are randomly oriented [8]. The ratio of mineral to collagen in woven bone varies enormously, and hyper-mineralization is often observed. The woven bone can be understood as a temporary scaffold that bears a complete structure, and that precedes the lamellar bone [9].

The **lamellar bone** is formed from woven bone during the remodelling process. It is highly anisotropic and stress oriented, i.e. the tissue organization adapts and depends on the applied forces [8], and the mineral to collagen ratio is fixed. As shown in Figure 1.4, the lamellar bone consists of a number of concentrically arranged laminae, called **osteons** or **Haversian system**.

Osteons have a central lumen containing a blood vessel and also accommodate small vessels, arterioles and capillaries for microcirculation. While the blood vessels in the osteonal canal transport blood generally along the long axis of a long bone, it is the **Volkmann canals** that contain the blood vessels that transport blood generally perpendicular to the long axis of a long bone, connecting different osteonal systems, and also connecting to the outside of the bone [7] [9]. The mature bone cells, **osteocytes**, are found in tiny cavities within the matrix called **lacunae**, which are arranged in the lamellae around the Haversian canals. Tiny canals, **canaliculi**, radiate outward from the central canals to all lacunae, connecting all the bone cells to the nutrient supply.
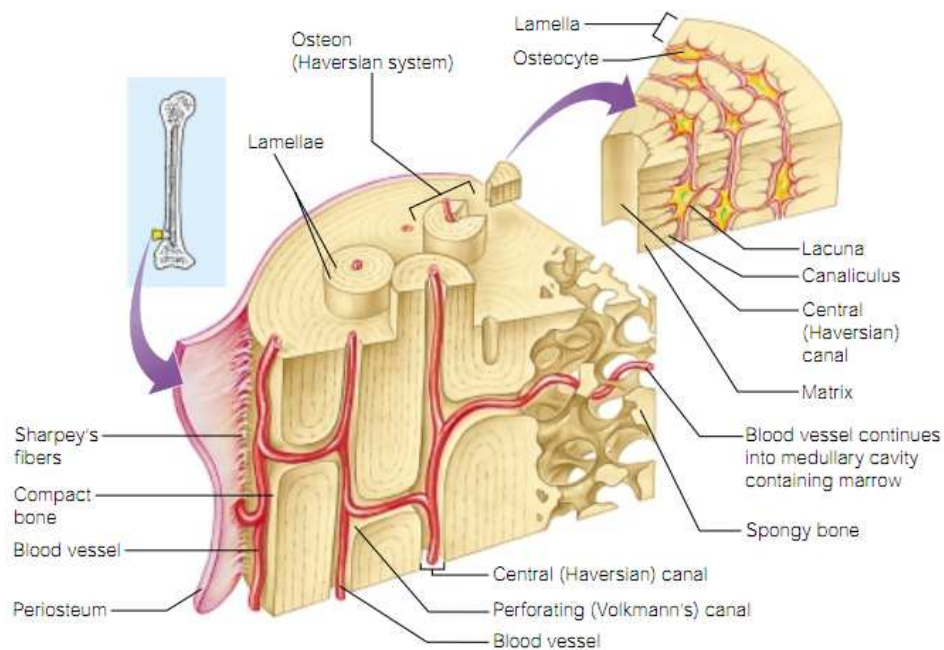
Figure 1.4. Microscopic structure of the compact bone. Diagram of a pie-shaped segment of compact bone (from [7]).

1.2.1.3 Bone composition (nanoscopical organization)

In general terms, bone tissue is a composite material made by ~ 50-60 wt% of an inorganic phase, ~ 30-40 wt% of an organic one, and up to 10 wt% of water [5] [10]. The inorganic phase is comprised by calcium orthophosphate crystals, precisely non-stoichiometric hydroxyapatites ($Ca_{10-x}(HPO_4)_x(PO_4)_{6-x}(OH)_{2-x}$, $0 < x < 1$), in the form of small plates of 2–3 nm thick and tens of nanometers in length and width [5]. The nanometric size and poor crystallinity of the natural apatites, combined with their non-stoichiometric composition and inner crystalline disorder [11],

provide the material with a higher solubility than mineral apatites. The organic phase consists mostly of collagenous proteins [5] [10] that align into triple helices that bundle into fibrils (1.5–3.5 nm diameter), which then bundle into collagen fibers (50–70 nm diameter).

Collagen builds up the bone matrix that is mechanically reinforced with apatitic nano-crystals [8] through a mechanism known as **biomineralization**. During this process, osteoblasts use the inorganic ions in body fluids (supersaturated in calcium phosphates, although their spontaneous precipitation is prevented by a buffering effect of the body) in order to produce hydroxyapatite that is afterwards incorporated at specific sites onto the collagen fibers, forming a complex-large-scale inorganic-organic composites [12]. Figure 1.5 shows that bone is formed by a systematic combination of hydroxyapatite crystals and collagen.
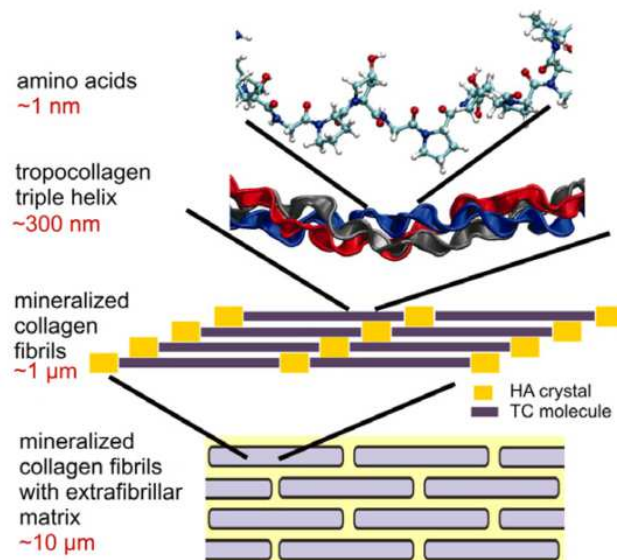
Figure 1.5. Geometry of the nanostructure of bone, showing several hierarchical features from atomic scale to microscale (from [13]).

1.2.2 Bone cells

The bones of vertebrates can be considered as ''living biominerals'' since there are cells inside them under permanent activity [11]. Bone cells are responsible for bone formation, resorption and repair, as well as for mineral homeostasis. The different sources of bone cells are mesenchymal stem cells (MSC) and hematopoietic progenitors cells [8].

There are five kinds of bone cells: osteoprogenitor, osteoblasts, osteoclasts, osteocytes and bone-lining cells. The cells are located upon the cellular interface, which includes the vasculature, the osteonal canals and the Volkmann canals, as well as the endosteum and the inner layer of the periosteum [9]. The function of each cell type is briefly explained below [9], and the morphology and location in the bone of each bone cell type are schematically shown in Figure 1.6.

• **Osteoprogenitor cells**: The pre-osteoblasts give rise to the bone-building osteoblasts, and the pre-osteoclasts give rise to bone-resorbing osteoclasts;

• **Osteoblasts**: Bone-forming cells, whose function is to synthesize and to secrete unmineralized collagenous bone matrix, the osteoid. They also participate in the calcification of bone, as they regulate the flux of calcium and phosphate in and out of the bone.

• **Osteoclasts**: Responsible for bone resorption. The osteoclasts are giant cells whose diameter ranges from 20 to over 100 µm and may contain from 2 to 50 nuclei;

• **Osteocytes**: Derive from osteoblasts that stayed behind as the mineralization front advances and, consequently, they become encased in the mineral matrix. The osteoblasts and osteocytes are extensively interconnected by the cell processes of the osteocytes, forming a connected cellular network important in signal transduction of mechanical stimuli;

▪ **Bone-lining cells**: They are believed to be derived from osteoblasts and/or osteoblasts precursors that have ceased their activity or differentiation and flattened out on bone surfaces.
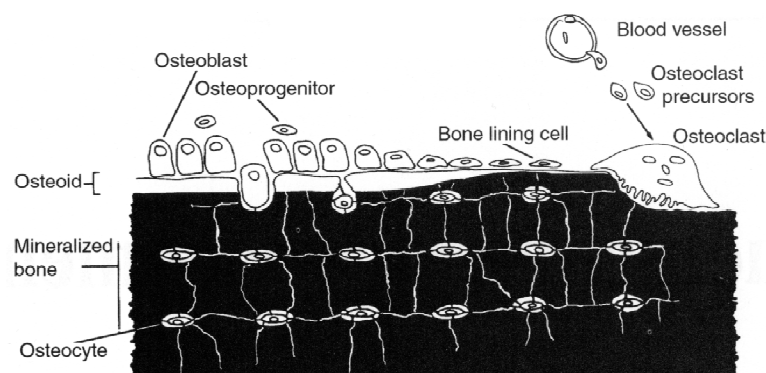
Figure 1.6. Schema of osteoblasts, osteocyte and osteoclasts (from [14]).

1.2.3 Mechanical properties of bone

Although bones are relatively light in weight [7], they have outstanding mechanical properties and are able to withstand repeated high impacts and compressive forces throughout the life-span of the organism. In fact, bone has a tensile strength similar to that of cast iron, but it is thrice lighter and ten times more flexible. The hierarchical features responsible for outstanding fracture resistance range from the nano- to the macro-scale are complex, and thus it is a challenge to replicate them in synthetic materials [8].

The mineral compound imparts hardness and stiffness, while the organic one increases the bone's toughness and resilience [8]. Collagen fibers are capable to dissipate energy, imparting tensile properties to bone [5] since the stresses are transferred in a zigzag manner [15].

The strength of cortical and trabecular bone to compressive and tensile forces, as well as its elastic modulus, is shown in Table 1.1.

Table 1.1. Compressive and tensile strength, and elastic modulus of both cortical and trabecular bone (data extracted from [16]).

	Cortical bone	Trabecular bone
Compressive strength (MPa)	100 – 230	2 – 12
Bending strength (MPa)	50 – 150	-
Young's Modulus (GPa)	7 – 30	0.05 – 0.5

1.2.4 Bones evolve lifelong. Tips to maintain them healthy

Most people reach their "peak bone mass" (maximal density and strength) in their 20s. After the peak bone mass is reached, bone density remains stable during adulthood, and then begins to decline. The bone density reached by each person depends essentially on the diet and on the physical exercise performed. Diet includes sufficient calcium intake and exposure to sunlight, which is necessary for production of vitamin D in the skin, this vitamin allows the absorption of calcium from food. Physical exercise maintains bones healthy since bones deteriorate if they are not used, just as muscles do. Bones need a variety of brief, frequent loads every day (*e.g.* walking and climbing stairs) to maintain their strength, and bones need to be loaded a bit more than usual (exercise) to improve their strength. Bones respond when they are "stressed," in other words,

when they are forced to bear more weight than they are used to. This can be achieved by "weight bearing" or impact exercises such as walking, running, lifting weights, jumping, or dancing [17].

1.2.5 Bone remodeling

Bone has a high complexity that can be reflected for its continuous removal and replacement throughout life. The skeleton of an individual is replaced several times during all his life by means of bone remodeling; this is, by resorbing the old bones and building them up again. This is a stochastic process that serves to continually rejuvenate the bone mineral, to remove bone matrix that is micro- or macroscopically damaged or has been functionally suboptimal, and to optimize bone architecture in response to functional loading. At a fundamental level, the removal and replacement of the extracellular matrix is necessary to establish and maintain bone mass and architecture [6].

The bone remodeling unit (BRU) describes the sequential activities of osteoclasts and osteoblasts that are spatially and temporally coupled to ensure that the removal of mineralized matrix is replaced by an equivalent quantity of new bone. Thus, over innumerable remodeling cycles, the collective activities of individual BRUs ensure that an organism's bone mass remains in constant balance and its skeletal architecture remains relatively unchanged [6]. However, dysfunction of either process may lead to excessive bone formation (osteopetrosis, osteosclerosis) or bone degradation (osteoporosis) [8].

The BRUs is a coordinated activity, commonly separated into four distinct phases: activation, resorption, reversal, and formation. The BRUs cycle starts with the activation of a resting bone surface in response to a stimulus. Groups of osteoclasts are recruited to the resorption site, and dissolve and resorb the mineralized bone matrix until a small piece of bone matrix is removed. As the osteoclastic activity subsides, a resorption cavity is formed, called **Howship's lacuna**. The resorptive tunnel excavated by the osteoclasts is eventually filled in by osteoblastic bone formation, producing a mature lamellar structure [6]. Figure 1.7 shows the stages conforming bone remodeling.
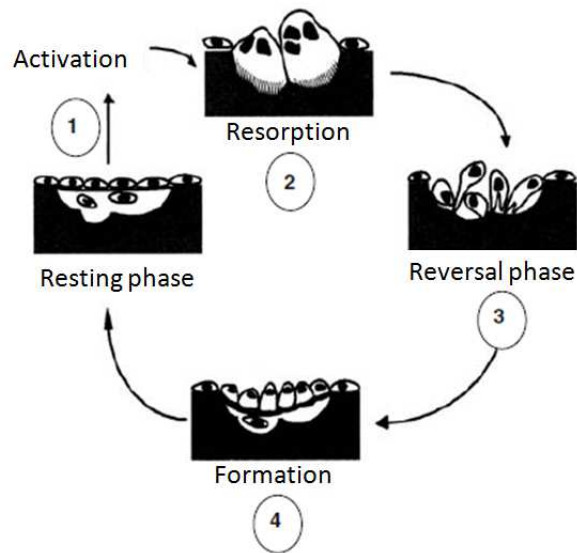
Figure 1.7. Representation of the life cycle stages of the bone remodeling process on a cortical bone surface. (from [6]).

1.2.6 Bone fractures

Despite their remarkable strength, bones are susceptible to fractures all their life. During youth, most fractures result from exceptional trauma that twists or smashes the bones. These fractures usually occur while practicing sports or in automobile accidents. In old age, bones have a lower mineral density and fractures occur more often due to their weakness [7]. Figure 1.8 shows a schema in which the different clinical procedures, which are described below, to heal a bone fracture depending on its size are indicated.
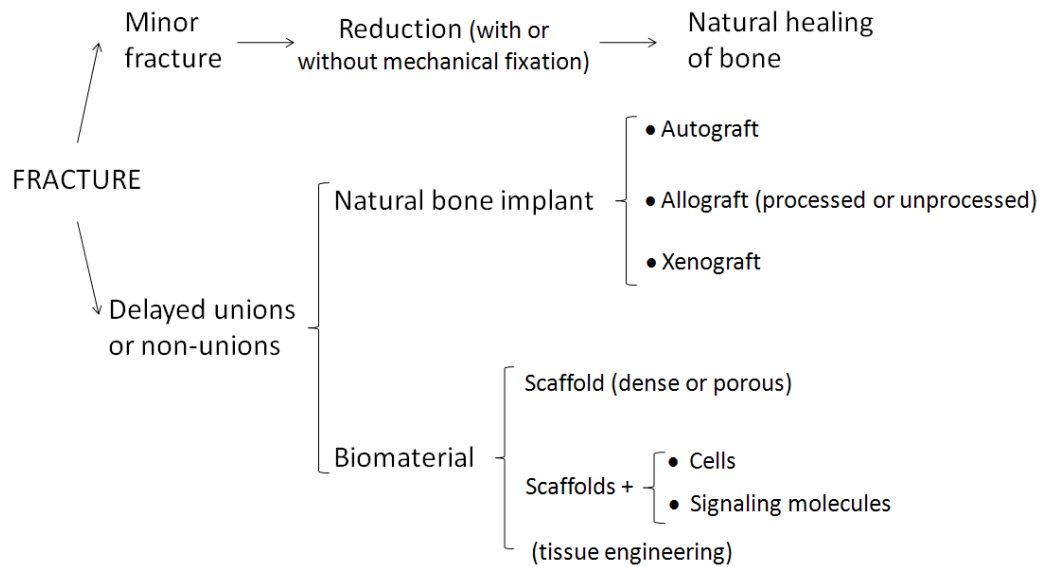
Figure 1.8. Schema of the strategies for bone healing after a minor fracture or a fracture causing delayed union or non-union is produced in the bone.

1.2.6.1 Spontaneous healing of bone fractures

When a minor fracture of a bone is produced, the fracture is treated by reduction, which is the realignment of the broken bone ends. In a closed reduction, the bone ends are coaxed back into their normal position by the physician's hands. In an open reduction (broken bone ends penetrate through the skin), surgery is performed and the bone ends are secured together with pins or wires (made of Fe, Co or Ti alloys). After the broken bone is reduced, it is immobilized by a cast or traction to allow the healing process to begin.

The healing time for a simple fracture is 6 to 8 weeks, but it is much longer for large bones and for the bones of elderly people because of their poorer circulation [7]. Injury initiates a cascade of healing events that recapitulate some of the steps of embryonic bone formation, which are described in biological stages involving inflammation, repair and remodeling (Figure 1.9) [5] [7]:

1. Blood vessels are ruptured when the bone breaks, resulting in the formation of a blood-filled swelling called **hematoma**. Bone cells deprived of nutrition die.

2. New capillaries grow into the clotted blood at the site of the damage, and phagocytes dispose of dead tissue. As this goes on, connective tissue cells form a mass of repair tissue, the **fibrocartilage callus**, which acts to "splint" the broken bone, closing the gap.

3. As more osteoblasts and osteoclasts migrate into the area and multiply, fibrocartilage is gradually replaced by a callus made of spongy bone, the **bony callus**.

4. Over the next few months, the bony callus is remodeled in response to the mechanical stresses placed on it, so that it forms a strong permanent "patch" at the fracture site.
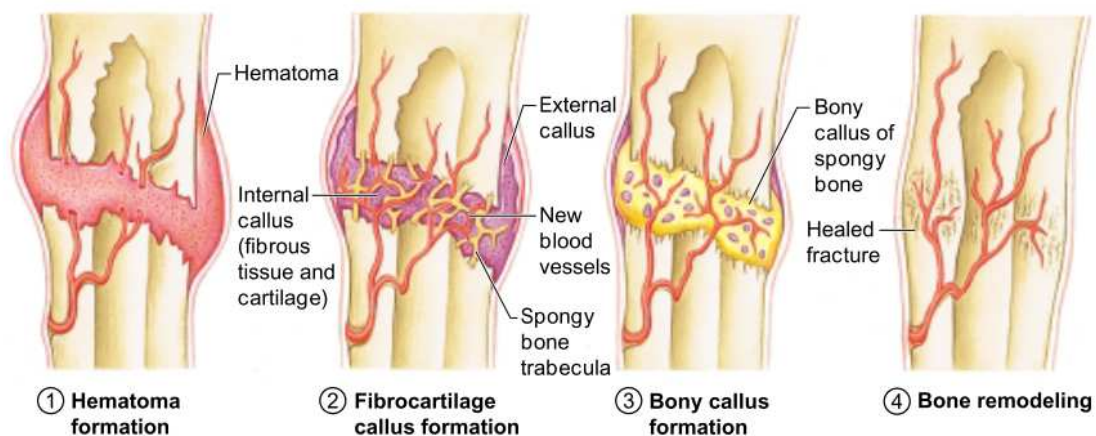
Figure 1.9. Stages in the healing of a bone fracture (from [7]).

1.2.6.2 Non-spontaneous healing of bone fractures

Although bone has its own ability to repair, the ability decreases with age and it can be also reduced by diseases or other factors. Moreover, spontaneous healing is limited to small bone defects [18]. The situation when bony bridging is delayed or does not occur is called **delayed union** or **non-unions**, respectively. The risk for non-unions can be greatly reduced if the defect (produced by the excision of bone tumor, other bone diseases or in cases of bone loss in accidents) is filled with a graft to which new bone can bond. The bone void fillers reduce the distance in the defect to be bridged [8] [18].

Bone grafting consists on filling the missing bone with a material that allows rapid bone regeneration and reconstruction of bone loss. Therefore, bone grafts have to comply with the following properties [19]:

i) to provide structural support/strength (immediate and static);

ii) to be **osteoconductive** (provide scaffolding for ingrowth of new bone);

iii) to be **osteoinductive** (stimulate new bone production in bone-forming cells);

iv) to favor **osteogenesis** (process of direct bone formation).

The bone graft sources can be natural (**bone grafts**), synthetic (**biomaterials**) or a mixture of a synthetic material supplemented with biological factors (treatment known as **tissue engineering**).

1.2.6.2.1 Natural bone grafts

Several natural bone grafts can be the choice in clinics for bone repair: autograft, allograft and xenograft, as schematically represented in Figure 1.10 [18] [19] [8] [20] [5].
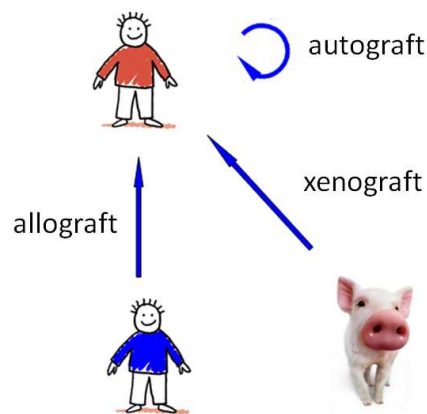
Figure 1.10. Schema of the three main sources of natural bone grafts.

• **Autograft:** the bone used is procured from the patient himself. It has no problems of biocompatibility or immunoresponse, and contains osteogenic cells and osteoinductive growth factors from the patient (such as bone morphogenetic proteins, BMPs). It is still regarded as the "golden standard", in other words, it is the most-used bone graft. The common problems related with this technique are the increase of operative time (double operation), blood loss,

postoperative pain, length of hospital stay, and cost. Moreover, the technique can only be used for the repair of small bone defects, since there are limited sites where bone can be harvested without loss of function. Other drawbacks presented by natural bone grafts are their lower effectiveness in irregularly shaped defects and their too fast resorption.

• **Allograft (unprocessed):** the bone used is provided by dead donors. The allografts have osteogenic cells and osteoinductive growth factors. Possible decrease of the osteogenic capacity due to an immunologic rejection, the limited supply of allografts and the risk of diseases transmission can be mentioned as main drawbacks.

• **Allograft (demineralized bone matrix, DBM):** the bone used is provided by dead donors but the risk of disease transmission is decreased by demineralizing the bone matrix. However, this treatment reduces the osteogenic capacity since not all growth factors and osteoinductive proteins survive the processing of the material.

• **Xenograft:** the bone is extracted from other species. The main drawback is the risk of immunologic rejection and transmission of diseases.

To date, the only graft having real osteogenic properties is the autograft. Achieving optimal bone regeneration with another graft would require the incorporation of growth factors that would produce an adequate local environment for cells to regenerate bone [19] [18]. The shortcomings of bone grafts together with the surgeon's desire for new bone grafting tools and their potential marketability has provided the stimulus to scientists for developing innovative and effective synthetic products over the last decade [19] [18] [20].

1.2.6.2.2 Synthetic bone grafts (biomaterials) and tissue engineering

a) Biomaterials

The first documented use of synthetic bone grafts, commonly known as **biomaterials** for bone regeneration, was reported in 1892 by van Meekeran, who treated large-bone defects with calcium sulfate.

The general requirements for ideal bone grafts are as follows:

i. Macroporosity (interconnected pores > 100 μm). Porous calcium phosphates provide mechanical fixation in addition to providing sites on the surface that allow chemical bonding between biomaterials and bone [21] and, moreover, permit the cell colonization [22]. Macroporosity in solid biomaterials is intentionally introduced by: (i) addition of various porogens (crystals or particles of either volatile or soluble substances) [23]; (ii) sintering spherical particles to generate porous three-dimensional bioceramics [24]; (iii) foaming methods [25].

ii. To fill effectively bone defects. In order to permit growth of new bone into bone defects, a suitable material should fill the defects. Otherwise, ingrowth of fibrous tissue might prevent bone formation within the defects.

iii. Biodegradation rate comparable to the formation of bone tissue. A biomaterial should be progressively resorbed by both **active** (resorption by osteoclasts) and **passive** (dissolution) **mechanisms**. In parallel, new bone should replace the space left by the newly resorbed biomaterial. The total substitution of the biomaterial by new bone formation should take between few months and about two years.

iv. Sufficient mechanical stability. The mechanical stability of a material is one of the characteristics that will determine its application. A biomaterial for bone regeneration should offer a superior compressive resistance than that of a cancellous bone graft, while remaining resorbable for the ingrowth of bone and vasculature to enable their remodelation into new bone over time [20].

b) Tissue engineering

Recently, since the knowledge regarding biomaterials has broadened, the interdisciplinarity between materials science and biology has been determined to be crucial [26]. Lately, grafts and implants that do not only mimic the body, but actually encourage the organism to "colonize" the foreign material itself have been proposed [27].

In the past decade, tissue engineering has emerged as a promising approach to orthopaedic repair. Utilizing a combination of cells, growth factors and/or biomaterials, the

principles of tissue engineering have been readily applied to the formation of a variety of connective tissues such as bone, cartilage, ligament or tendon, both *in vitro* and *in vivo* [28].

For the success of a tissue engineering treatment, the interaction between osteoconductive, osteoinductive and osteogenic elements is required. The **osteoconductive** scaffold is in charge of supporting bone growth at the same time that provides mechanical support, sites for cell attachment, vascular ingrowth, and a delivery vehicle for implanted growth factors and cells; **osteogenic** components include cells capable of bone production such as osteoprogenitor cells or differentiated osteoblasts; and **osteoinductive** factors include bioactive chemicals that induce recruitment, differentiation and proliferation of the proper cell types at an injury [5].

A key factor for the healing success of non-unions is the use of MSCs in cell-based strategies. The MSCs are promising tools for regenerative therapy due to their proliferation capabilities and their ability to build new tissue in a defect. However, due to the limited quantity of MSCs in the bone marrow (less than 0.001%), progenitor cells have to be extracted from the bone marrow of a patient, expanded *in vitro* and, finally, seeded onto a carrier for implantation into a defect (Figure 1.11) [5].
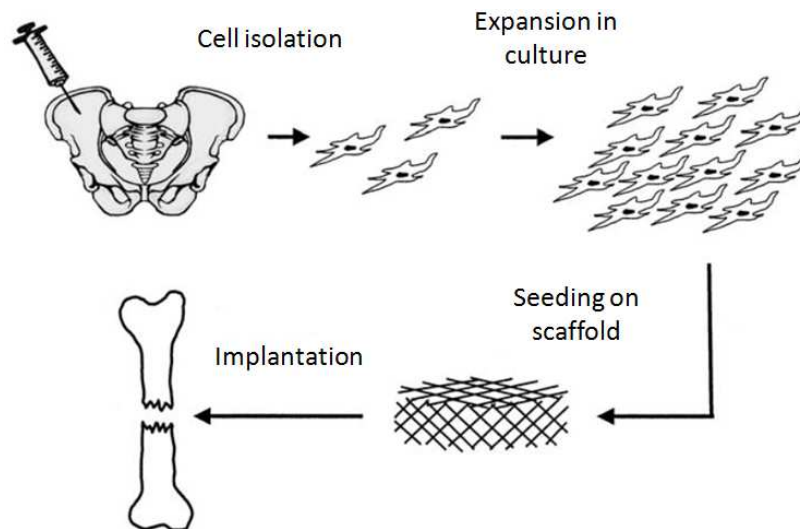
Figure 1.11. Cell transplantation: osteogenic cells may be isolated from the iliac crest, expanded in cell culture, seeded onto a scaffold and implanted into a defect (from [5]).

1.2.6.2.3 Pros and cons of natural grafts, biomaterials and tissue engineering

The advantages and drawbacks of the natural bone grafting techniques (autograft, allograft and xenograft) and those that use synthetic materials (biomaterials and tissue engineering) are summarized in Table 1.2. Tissue engineering is envisaged as the treatment that will produce better results and which might be worthy even though its high complexity.

Table 1.2. Advantages and drawbacks brought by natural bone grafting techniques such as autograft, allograft and xenograft and by synthetic bone grafts as biomaterials and tissue engineering strategy (from [18] [19] [8] [20] [5]).

Natural/synthetic bone graft	Bone graft source	Advantages	Drawbacks
Natural bone	**Autografts** (bone from the own patient) "golden standard"	✓ Provides support/strength ✓ Biocompatibility ✓ No immune response ✓ Contains osteogenic cells and osteoinductive growth factors ✓ Stimulates bone regeneration	✗ Increase of time endowed in surgery (double surgery) ✗ Blood loss ✗ Postoperative pain ✗ Length of hospital stay ✗ Cost
	Allografts (from a dead human donor)	✓ Provide support/strength ✓ Osteogenic cells and osteoinductive growth factors	✗ Osteogenic capacity may decrease due to an immunologic rejection ✗ Limited supply of allograft ✗ Risk of disease transmission
	Allografts (from a dead human donor) with demineralized bone matrix (DBM)	✓ Provide support/strength ✓ Risk of disease transmission decreases by a processing of the material	✗ Osteogenic capacity is reduced due to the material processing
	Xenografts (from other species)	✓ Provide support/strength ✓ Osteogenic cells and osteoinductive growth factors	✗ Risk of immunologic rejection ✗ Risk of diseases transmission

Natural/synthetic bone graft	Bone graft source	Advantages	Drawbacks
Synthetic material	**Biomaterials**	✓ Provide support/strength ✓ No risk of rejection ✓ No risk of diseases transmission ✓ Biocompatibility	✕ Does not contain osteogenic cells or osteoinductive growth factors ✕ Osteogenesis, osteoconduction and osteoinduction depend on material characteristics ✕ Resorption depends on the chemical and physical properties of material
	Tissue engineering	✓ Provide support/strength ✓ No risk of rejection ✓ No risk of diseases transmission ✓ Biocompatibility ✓ Osteogenic cells and osteoinductive growth factors	✕ Complex, long and expensive preparation: it requires to expand cells of patient and to grow them in the scaffold

The tissue engineering has been envisaged as a promising method to enhance bone regeneration, even though the strategy to carry out the process is very complex and the overall route is slow. The first step to guarantee a successful tissue engineering process is linked with the development of a biocompatible material with an ideal architecture and good chemical, physical, osteoconductive and osteoinductive properties. Therefore, from now on attention will be focused in the biomaterials.

1.3 Biomaterials for bone regeneration

Biomaterials emerged as an alternative strategy for the treatment of severe bone loss or fracture. Since antiquity, humans have used natural materials such as metals, polymers, glass or ceramics, to replace a part of their body that has been damaged [29]. The "biomaterial" term was defined for the first time in 1987, and since then its description has been considerably modified. In 1999, a "biomaterial" was defined as "*a material intended to interface with biological systems to evaluate, treat, augment or replace any tissue, organ or function of the body*" [30]. A recent definition makes the concept more precise "*substance that has been engineered to take a form which, alone or as part of a complex system, is used to direct, by control of interactions with components of living systems, the course of any therapeutic or diagnostic procedure, in human or veterinary medicine*" [31].

Biomaterials are classically classified in function of their chemical nature (subdivisions indicated in parenthesis) [31]:

i) **Metallic**: based on metallic bonds (pure metals and alloys);

ii) **Ceramic**: based on ionic bonds (glasses, glass-ceramics, ceramics and carbons);

iii) **Polymeric**: based on covalent bonds (thermosets, thermoplastics, elastomers and textiles);

iv) **Hybrids** or **composites** (combinations of ceramics and polymers).

Table 1.3 shows materials used nowadays as biomaterials and their respective applications.

Table 1.3. Classification of the materials in function of their chemical nature and their applications (modified from [32]).

MATERIALS				
Ceramic	Metallic	Polymeric	Composites	Natural
Alumina (Al_2O_3) Zirconia (ZrO_2) Calcium phosphates Calcium sulfates Bio-glass Bio-ceramics Carbon	Ti and Ti alloys Cr-Co alloys Stainless steels Au Pt Ag	Nylon Silicone Polyesters Polytetrafluoroethylene (PTFE) Polystyrene (PS) Polymethacrylate methyl (PMMA)	Carbon-carbon Resin Epoxy-graphite	Collagen Chitosan
APLICATIONS				
• Components of joint prosthesis • Coatings of metallic implants • Bone grafts	• Joint prosthesis • Osteosynthesis devices • Dental implants • Orthodontic material	• Sutures • Vascular prosthesis • Components of joint prosthesis • Drug release devices	• Heart valves • Root canal fillers • Dental restoration materials	• Artificial skin • Heart valves • Vascular prosthesis

The materials have been further classified as bioinert or bioactive according to their interaction with the host tissue [33]. The materials that have a minimal biological response from the physiological environment are known as **bioinert** and their function is simply to substitute a lost part of the body (**1st generation**). **Bioactive** materials, unlike bioinerts, are those that produce a positive interaction with the host tissue. The bioactive materials can be also classified as non-resorbable (**2nd generation**) or resorbable. Those bioactive materials that are as well resorbed with time (**3rd generation**) allow the regeneration of the tissue.

1.4 Calcium orthophosphates for bone substitution and regeneration

By definition, all calcium orthophosphates consist of three major chemical elements: calcium (oxidation state +2), phosphorus (oxidation state +5) and oxygen (reduction state -2), as a part of orthophosphate anions [34]. Calcium orthophosphates have been studied as bone repair

materials for the last 80 years [35]. One of the most used calcium phosphate is hydroxyapatite, $Ca_{10}(PO_4)_6(OH)_2$, since it is the most similar material to the mineral component of bones [11], in terms of chemical composition and crystalline structure. The hydroxyapatite is well accepted for the host bone and enhances bone regeneration, thus exhibiting the required properties for a biomaterial such as biocompatibility, bioactivity and osteoconductivity [11].

The calcium orthophosphates are usually classified by their Ca/P ratio since it is known that the lower the Ca/P ratio, the larger the acidity and solubility of the compound [11]. Table 1.4 shows a list of known calcium phosphates, including their standard abbreviations and their major properties.

Table 1.4. Properties of the biologically relevant calcium orthophosphates (modified from [36]).

Ca/P ionic ratio	Compound	Chemical formula	Solubility at 25°C (-log K_s)	pH stability range in aqueous solution at 25°C
0.5	Monocalcium phosphate monohydrate (MCPM)	$Ca(H_2PO_4)_2 \cdot H_2O$	1.14	0.0-2.0
0.5	Monocalcium phosphate anhydrous (MCPA)	$Ca(H_2PO_4)_2$	1.14	[b]
1.0	Dicalcium phosphate dihydrate (DCPD), brushite	$CaHPO_4 \cdot 2H_2O$	6.59	2.20-6.0
1.0	Dicalcium phosphate anhydrous (DCPA), monetite	$CaHPO_4$	6.90	[b]
1.33	Octacalcium phosphate (OCP)	$Ca_8(HPO_4)_2(PO_4)_4 \cdot 5H_2O$	96.6	5.5-7.0
1.5	α-Tricalcium phosphate (α-TCP)	$\alpha\text{-}Ca_3(PO_4)_2$	25.5	[a]
1.5	β-Tricalcium phosphate (β-TCP)	$\beta\text{-}Ca_3(PO_4)_2$	28.9 [b]	[a]
1.2-2.2	Amorphous calcium phosphate (ACP)	$Ca_xH_y(PO_4)_z \cdot nH_2O$; n = 3-4.5; 15-20% H_2O	25.7 ± 0.1 (pH = 7.40); 29.9 ± 0.1 (pH = 6.00); 32.7 ± 0.1 (pH = 5.28)	~ 5-12 [c]
1.5-1.67	Calcium deficient hydroxyapatite (CDHA)[d]	$Ca_{10-x}(HPO_4)_x(PO_4)_{6-x}(OH)_{2-x}$ $(0 < x < 1)$ [e]	~ 85.1	6.5-9.5
1.67	Hydroxyapatite (HA)	$Ca_{10}(PO_4)_6(OH)_2$	116.8	9.5-12
1.67	Fluroapatite (FA)	$Ca_{10}(PO_4)_6F_2$	120.0	7-12
2.0	Tetracalcium phosphate (TTCP), hilgentockite	$Ca_4(PO_4)_2$	38-44	[a]

[a] These compounds cannot be precipitated in aqueous solutions

[b] Stable at temperatures above 100°C

[c] Always metastable

[d] CDHA can be named as precipitated HA

[e] In the case x = 1 (Ca/P = 1.5), the chemical formula of CDHA is $Ca_9(HPO_4)(PO_4)_5(OH)$

Each calcium phosphate has a different solubility in an aqueous system, and the solubility of each calcium phosphate depends on the pH of the solution, as shown in Figure 1.12. In the solubility diagram a negative slope is observed at the acidic pH range, indicating that the solubility increases as the pH decreases, and a positive slope at the basic pH range, showing that the solubility increases as the pH increases. The diagram shows that for a given pH value, any salt whose isotherm lies below another will be relatively less soluble and thus more stable. Down to a pH of 4.2, HA is the least soluble calcium phosphate salt [36].
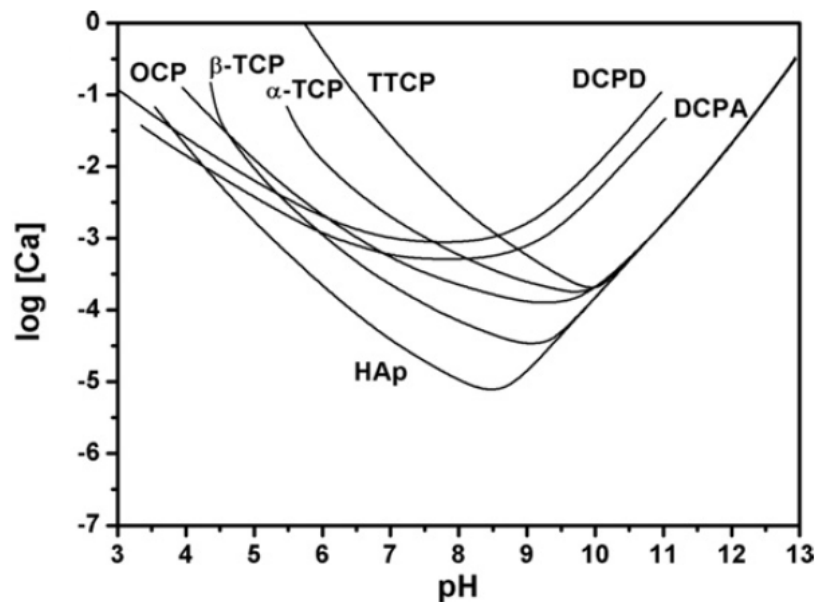
Figure 1.12. Solubility isotherms of different calcium phosphate salts in equilibrium with their solutions at 37°C in a representation of log [Ca] versus pH (from [36], redrawn by [37]).

Some calcium orthophosphates can be obtained by precipitation from an aqueous solution at low temperature (*e.g.* CDHA and brushite), while others can only be obtained at high temperature (*e.g.* α-TCP, HA, TTCP) [38], through a sintering process.

Sintering is of great importance to produce a variety of bioceramics with the required properties [34]. Several processes occur during sintering of calcium orthophosphates. Firstly, moisture, carbonates and all volatile chemicals remaining from the synthesis stage are removed as gaseous products. The removal of these gases facilitates the production of dense materials during sintering. Afterwards, there is an increase in crystal size and a decrease in the specific surface area. Finally, there is the chemical decomposition of all acidic orthophosphates, which transform into

other phosphates (*e.g.* 2 $HPO_4^{2-} \rightarrow P_2O_7^{4-} + H_2O$). Besides, sintering causes toughening of the ceramics [39]. The sintering process, together with the intrinsic solubility of the material, will also determine the stability under physiological conditions.

One of the most commonly used orthocalcium phosphate is hydroxyapatite. Although this compound can be prepared by several techniques, which can be divided into solid-state reactions and wet methods, pure hydroxyapatite (HA, $Ca_5(PO_4)_3(OH)$) can be only obtained by a sintering process. This is the reason why it can never be found in biological systems. Nevertheless, due to the chemical similarities to bone and teeth mineral, HA has been widely used as a coating on orthopedics (*e.g.* hip joint prosthesis) and dental implants. HA has been also implanted as a solid block or as HA particles in a bone defect [34].

1.4.3 Characteristics of calcium orthophosphates

Calcium orthophosphates fall into the categories of **bioactive** and/or **bioresorbable** materials [16]. Both the chemical and physical properties (crystallinity, porosity, *etc.*) of calcium phosphates will determine their level of bioactivity and bioresorbability.

Bioactive calcium phosphates are able to form a layer of biological apatite before interfacing directly with the hard tissue, resulting in the formation of a direct chemical bond with bone and providing good mechanical stabilization. Bioceramics made of dense HA are good examples of bioactive materials. Depending on the chemical and physical properties of the calcium phosphate, it can be **bioresorbable**, allowing a newly formed tissue to grow into any surface irregularities [40]. Porous scaffolds made of BCP (*i.e.* α or β-TCP + HA) [41] or bone grafts made of CDHA, TCP and/or ACP appear to be examples of bioresorbable materials [34].

The excellent biocompatibility and bioactivity that exhibit some calcium orthophosphates when used as biomaterials for hard tissues substitution has been associated to their similarity with the inorganic phases of biomineralized tissues. Indeed, calcium phosphate biomaterials should mimic the natural apatites, thus consisting on apatite crystals of nanometric dimensions, low crystallinity and non-stoichiometric composition [42].

1.4.4 Forms of calcium orthophosphates

Bioceramics of calcium orthophosphates are available in several physical forms: particles, blocks (dense or porous), injectable compositions, self-setting cements, coatings on metal implants, composites with polymers, *etc.* [43]. Figure 1.13 shows several calcium orthophosphates prepared in different forms.

Figure 1.13. Examples of calcium phosphate-based bone substitution materials (from [10]**).**

The mechanical properties of a ceramic are dependent on its form, shape and size. As expected, a macroporous calcium phosphate has a much lower mechanical properties than a dense material. However, in general, even dense calcium orthophosphate bioceramics possess poor mechanical properties. For this reason, the medical applications of calcium orthophosphates are currently focused on the production of non-load-bearing implants, such as pieces for middle ear surgery, bone defect filling material for oral or orthopedic surgery, or as coatings of dental implants and metallic prosthesis [11] [44].

The need of biomaterials for minimally invasive surgery has induced a larger development of self-setting bone cements, commonly known as calcium phosphate cements (CPCs) [36] [45] [46] [47] [48] [49].

1.5 Calcium phosphate cements (CPCs)

CPCs were discovered by LeGeros [50], and Brown and Chow [51] in the early 1980s. They demonstrated the formation of hydroxyapatite in a monolithic form at room or body temperature by means of a cementitious reaction. The CPCs are prepared by mixing one or more calcium phosphate powders with an aqueous solution. The mixture consists on a cement paste that can be injected into the bone defect, where it adapts perfectly to the cavity. The cement sets *in situ* through a dissolution-precipitation reaction. During this continuous process, the calcium phosphates are partially dissolved within the aqueous medium and they subsequently precipitate into the most insoluble calcium phosphate phase, with the hardening of the paste due to the entanglement of the formed crystals. Within minutes the cement paste has transformed into a solid body with mechanical properties (Figure 1.14).
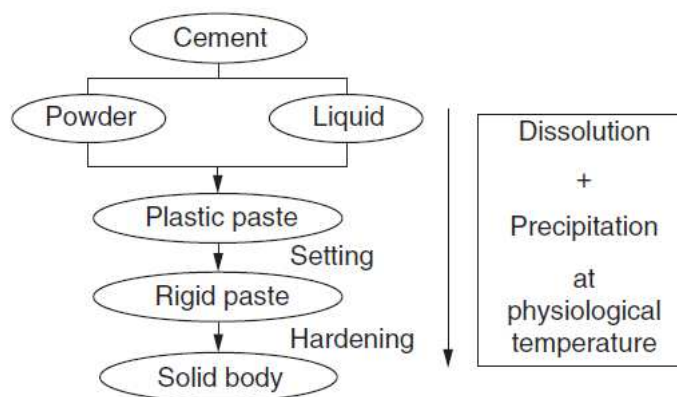
Figure 1.14. Rationale of calcium phosphate cements (from [38]).

1.5.1 Chemistry of CPCs

The CPCs are usually divided into two groups: the apatite CPC and the brushite CPC. The formation of a cement type or another depends upon the Ca/P ratio of the reactants and also upon the pH value of the cement paste. The cementious reaction results into precipitated hydroxyapatite (PHA or CDHA) when the pH > 4.2, and into brushite (DCPD) when the pH < 4.2 [38].

1.5.1.1 Apatite CPCs

The CPCs that lead to the formation of calcium deficient hydroxyapatite (CDHA) can be divided in three groups, taking into account the number and type of calcium phosphate used in the powder mixture [52].

(i) A single calcium phosphate. α-TCP is hydrolyzed in an aqueous solution, giving place to CDHA (Reaction 1.1) [53] [54] [55] [56] [57] [58] [59].

Reaction 1.1. $\qquad$ $3 \ \alpha\text{-}Ca_3(PO_4)_2 + H_2O \rightarrow Ca_9(HPO_4)(PO_4)_5(OH)$

(ii) One acidic and other alkaline calcium phosphate, which set following an acid-base reaction. TTCP usually acts as an alkaline compound, and can be combined with one or more calcium phosphates with lower Ca/P ratio to obtain CDHA (Reaction 1.2 and 1.3), without the formation of acids or bases as by-products [51].

Reaction 1.2. $\qquad$ $Ca_4(PO_4)_2O + CaHPO_4 \rightarrow Ca_5(PO_4)_3(OH)$

Reaction 1.3. $\qquad$ $Ca_4(PO_4)_2O + CaHPO_4 \cdot 2 \ H_2O \rightarrow Ca_5(PO_4)_3(OH) + 2 \ H_2O$
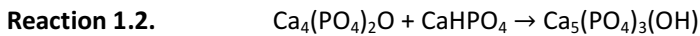
(iii) Calcium phosphates and other salts. A mixture of calcium phosphates with a Ca/P ratio lower than that of CDHA are used (α-TCP and MCPM), together with $CaCO_3$ as an additional source of calcium ions [60].

1.5.1.2 Brushite CPC

Brushite CPCs are acidic and metastable under physiological solutions [61]. Thus, they resorb much faster than apatite CPCs. Brushite CPCs are obtained as a result of an acid-base reaction (Reaction 1.4) [62].

Reaction 1.4. $\qquad$ $\beta\text{-}Ca_3(PO_4)_2 + Ca(H_2PO_4)_2 \cdot H_2O + 7 \ H_2O \rightarrow 4 \ CaHPO_4 \cdot 2H_2O$
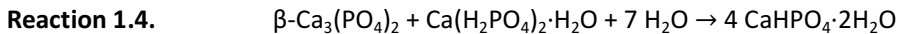
1.5.2 Processing parameters

The properties of a cement system such as its setting time, cohesion, viscosity, injectability, bioactivity, porosity and resorption, among others, depend on several processing parameters, which can be tailored to adjust them to a specific clinical application. On one hand, the powder

characteristics depend on its chemistry, the incorporation of additives such as seeds or accelerants, and the particle size distribution of the powder. On the other hand, the addition of additives to the liquid phase and its pH also has a significant influence on the cement properties. Also, while mixing the powder with the liquid, the porosity can be modified by the liquid to powder ratio or the mixing protocol. Finally, environmental factors such as temperature, humidity or pH can also have an effect on the resulting solid body. Figure 1.15 shows the processing parameters influencing the properties of CPCs for each factor involved in their preparation.
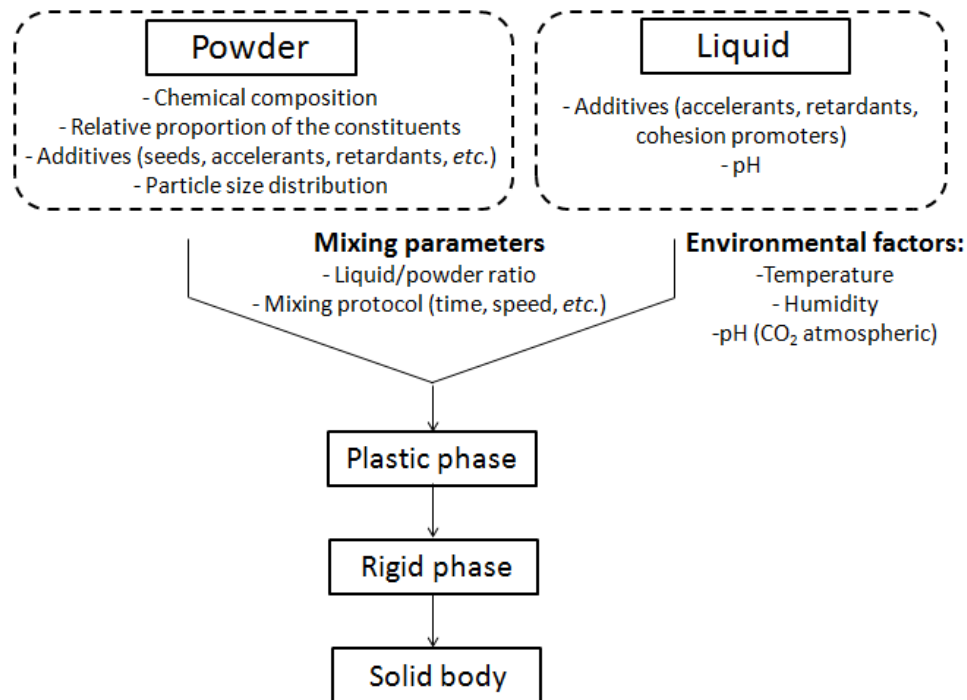
Figure 1.15. Processing parameters that affect the properties of a calcium phosphate cement (modified from [38]).

1.5.3 Setting and hardening of CPCs

CPCs must set slowly enough to provide sufficient time to the surgeon to perform implantation, but fast enough to prevent delaying the operation. Ideally, good mechanical properties should be reached within minutes after initial setting. The setting time of cements is commonly measured with Gillmore or Vicat needle methods. The purpose of both methods is to examine visually the surface of cement samples to decide whether the cement has already set, *i.e.* if no mark can be seen on the surface after indentation [63].

Gillmore needles have been used with success to measure the **initial setting time (t_I)** and **final setting time (t_F)** of calcium orthophosphate cements. A light and thick needle is used to measure the t_I, while a heavy and thin needle for the t_F. In clinics, the cement paste should be implanted before t_I and the wound could be closed after time t_F. The cement should not be deformed between t_I and t_F because in that stage of the setting process any deformation could induce cracks [49]. The **cohesion time (t_C)**, which is the time that a cement requires to no longer disintegrate when immersed in an aqueous solution [64], must be at least 1 min before t_I, so that a clinician has at least 1 min to mold and apply the material. The paste has to be introduced into the bone cavity after t_C and before t_I [64]. Figure 1.16 schematically shows the mentioned parameters.
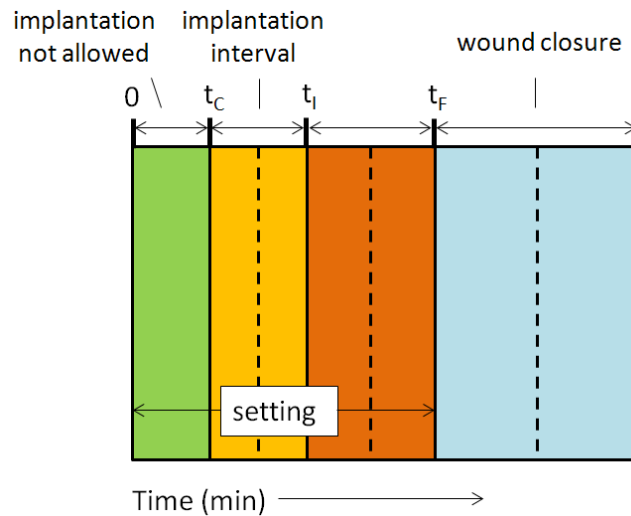
Figure 1.16. A diagram of the setting parameters relevant for a calcium orthophosphate cement. t_C stands for cohesion time, t_I stands for initial setting time, and t_F stands for final setting time (modified from [49]).

For dental applications, t_I must be close to 3 min, whereas for orthopedic applications it must be close to 8 min. However, if time t_F becomes greater than 15 min, in no case it will be tolerable for the clinicians [49] [64].

1.5.4 Advantages of CPCs

The CPCs have several advantages in comparison with the use of calcium phosphate ceramics [38] [35].

On one hand, physico-chemical properties such as i) ability to self-setting *in vivo*, ii) ease of preparation and handling; iii) moldeability, allowing a perfect adaptation to the implant site; iv) injectability, allowing the implantation by a minimally invasive surgical technique; and v) good osteoconductivity and occasional osteoinductivity can be mentioned as technical advantages.

On the other hand, several biological properties of CPCs can be pointed as advantageous, such as i) excellent biocompatibility and bioactivity; ii) resorption and replacement by newly formed bone after a period of time (osteotransductivity); and iii) chemical and physical similarity of the end-product to bone in the case of apatite cements, resulting in high bioactivity.

Other advantages shown by CPCs are: i) possibility to use them as carriers of antibiotics, anti-inflammatory drugs or growth factors, since the setting reaction takes place at low temperature; ii) no toxicity; and iii) low cost.

1.5.5 Drawbacks of CPCs

However, CPCs also present some problems. The main concerns of clinicians in respect to CPCs are the following [65]:

i) *In vivo* biodegradation of many formulations is slower than the growth rate of a newly forming bone;

ii) Mechanical weakness: limited use due to potential collapse of material. Metal supports are required for load-bearing areas;

iii) They can be washed out from surgical defect if excess of blood;

iv) Lack of macroporosity, especially interconnected pores, which prevents bone ingrowth. Moreover, the cements only degrade from the outside to the inside.

The mentioned drawbacks have stimulated the scientific community to continue studying the CPCs in order to improve some of their limitations.

1.6 Tricalcium phosphate (TCP)

In this section, emphasis is done to α-tricalcium phosphate since it is the reactant of apatite CPCs that will be used in the Thesis.

The chemistry of calcium phosphates is generally complex, and the phases with stoichiometry $Ca_3(PO_4)_2$ provide no exception [66]. The tricalcium phosphate (TCP, $Ca_3(PO_4)_2$ is constituted by 3 CaO (coded as C in the diagram phase) and 1 P_2O_5 (coded as P in the diagram phase), being therefore found as C_3P at 75% CaO − 25% P_2O_5 in the diagram phase (Figure 1.17). The TCP is a high temperature phase that exists under three crystallographic forms, α, α' and β. The β-TCP can only be prepared at temperatures above 800°C by thermal decomposition of CDHA or by solid-state interaction of acidic calcium orthophosphates [34]. The transition temperature from β-TCP to α-TCP is found at around 1125°C [67]. The α-TCP is thermodynamically stable between 1120 and 1470°C [68] in the absence of impurities, but it is metastable at room temperature. The α'-TCP, stable above 1430°C, is unable to survive quenching to room temperature [67]. Figure 1.17 shows the occurrence of these phases in the high temperature CaO-P_2O_5 phase diagram.
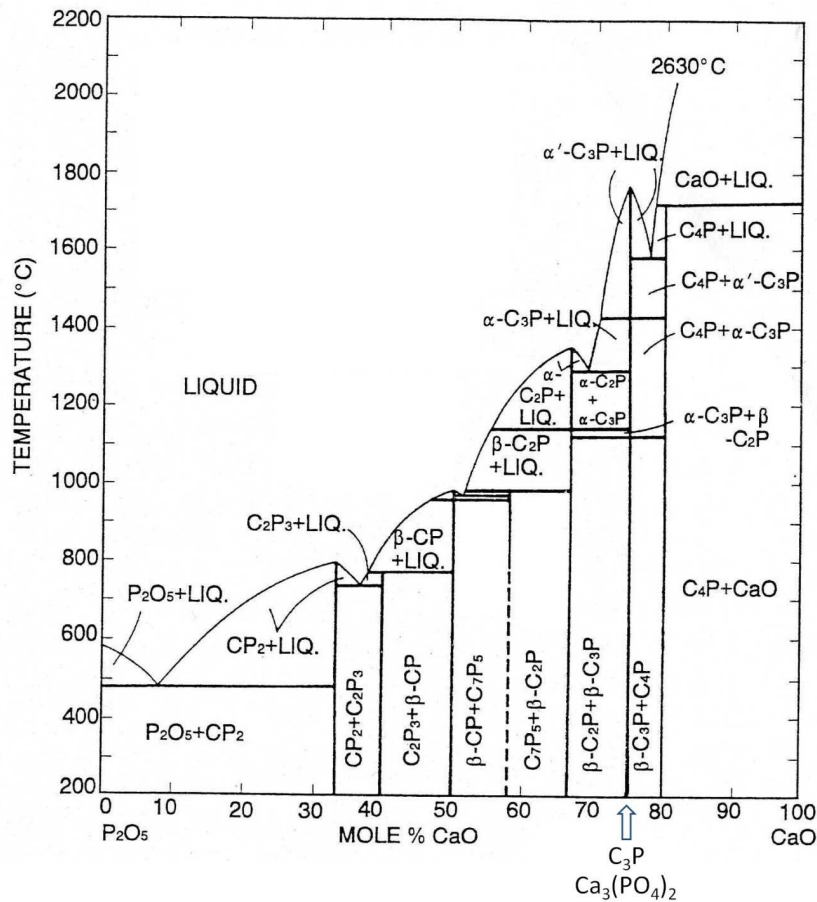
Figure 1.17. Equilibrium diagram for the system CaO-P$_2$O$_5$ with melting points and inversion temperatures, C = CaO, P = P$_2$O$_5$ (from [67]).

There is a general knowledge that α-TCP is an allotropic form unstable at low temperatures, since the β-α transformation reverts when cooling down to its transition temperature [10]. Therefore, α-TCP is usually prepared by heating a calcium phosphate mixture with a Ca/P ratio of 1.5 above ~ 1125 °C [67], retaining the α-phase by quenching above its transformation temperature, in order to prevent the reverse transformation. The quenching process entails certain drawbacks that are mainly the thermal shock that suffer both the material and the furnace.

1.6.1 The crystal structure of α-TCP

α-TCP crystallizes in a monoclinic space group P21/a, with cell parameters a = 12.887 ± 2, b = 27.280 ± 4, c = 15.219 ± 2 Å and β = 126.20 ± 1° at 25°C. The calculated density for Z = 24 was of

2.863 g/cm^3 [69]. A prominent subcell exists with b'' = b/3 [69]. Moreover, a pseudoorthorhombic cell with a' = 15.22, b' = 20.71, c' = 9.11 Å has been reported on ASTM card 9-348 and can be derived from the monoclinic cell by taking a' ~ c, b' ~ 2a cos (β-90°) and c' ~ b/3. Precession photographs and the intensity data show that the Laue symmetry of the subcell is 2/m [66].

The structure of α-TCP consists of calcium and phosphate ions arranged in columns along [001]. Both the pseudocell translation and the 2_1 axis are along b, giving a pseudounique slice of b/6 for α-Ca$_3$(PO$_4$)$_2$. Each cation column is surrounded by six cation-anion columns and each cation-anion column by alternate cation-cation and cation-anion columns [66]. Figure 1.18 shows two representations of the crystalline structure of the α-TCP.
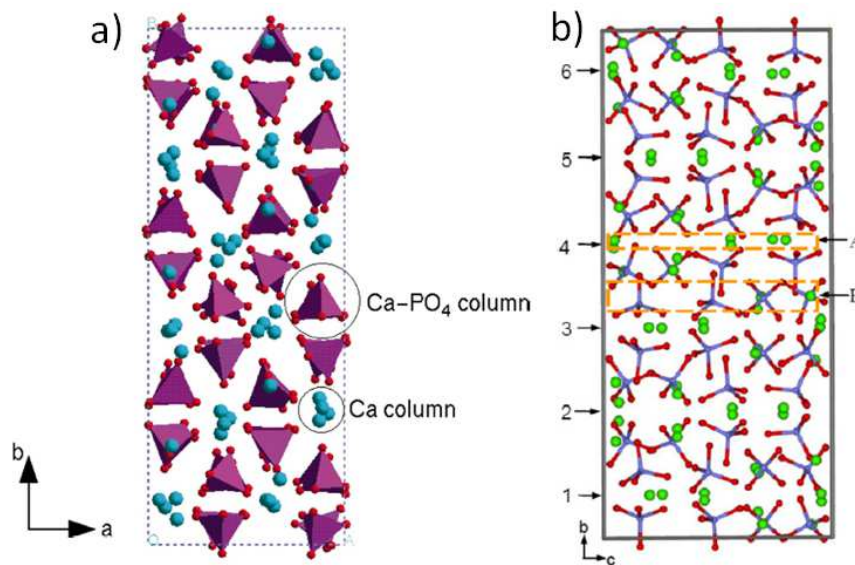
Figure 1.18. a) α-TCP unit cell projected on the (a, b) plane. (from [70]); and b) crystal structure of α-TCP projected along the a-axis; A, Ca column; B, Ca-PO$_4$ column; numerals 1-6 along the left side denote the six possible cutting positions for making surface models [71]. Tetrahedra represent PO$_4$ groups, and balls (blue (a) or green (b)) denote Ca atoms.

The fabrication process of the α-TCP allows the incorporation of different ions in its lattice depending on the composition of the starting materials [38]. Interestingly, the relative stability of the α and β-polymorphs is highly affected by the presence of some impurities [72]. Thus, whereas Mg is known as an element that stabilizes the β-phase [66] [72] [73] [74], Si is known to stabilize the α-form [66] [68] [75] [76] [77].

1.6.2 Si-stabilized α-TCP (Si-α-TCP)

The Ca_2SiO_4-$Ca_3(PO_4)_2$ binary system was first studied at the end of XIX century when silicocarnotite was described as a component of slag (by-product of smelting ore) [78].

Nurse *et al.* [75], and afterwards Fix *et al.* [68] and Barnes *et al.* [76] studied the phase equilibrium diagram for the binary system Ca_2SiO_4-$Ca_3(PO_4)_2$ and indicated that a new α-form containing silicon was stabilized down to low temperatures. The Ca_2SiO_4-$Ca_3(PO_4)_2$ binary system was first studied by means of X-ray diffraction using a high-temperature stage by Nurse *et al.* [75]. In order to be as close as possible to the equilibrium, the X-ray analysis was pursued through successively higher temperatures, heating the reactants at 1550°C for 20 h and then annealing the end-product at 500°C for 70 h. Nurse *et al.* determined from heating curves that in the system Ca_2SiO_4-$Ca_3(PO_4)_2$ a 2.8 wt% of Ca_2SiO_4 stabilized the α-form after the standard thermal process. Otherwise, if no Si was present in the phase, the β-TCP was the stable phase in these conditions.

The system was also studied by Fix *et al.* by holding the phases at every high-temperature for 21 days during synthesis and afterwards keeping the temperature for several hours for X-ray analysis [68]. The diagram of Fix *et al.* is shown in Figure 1.19.
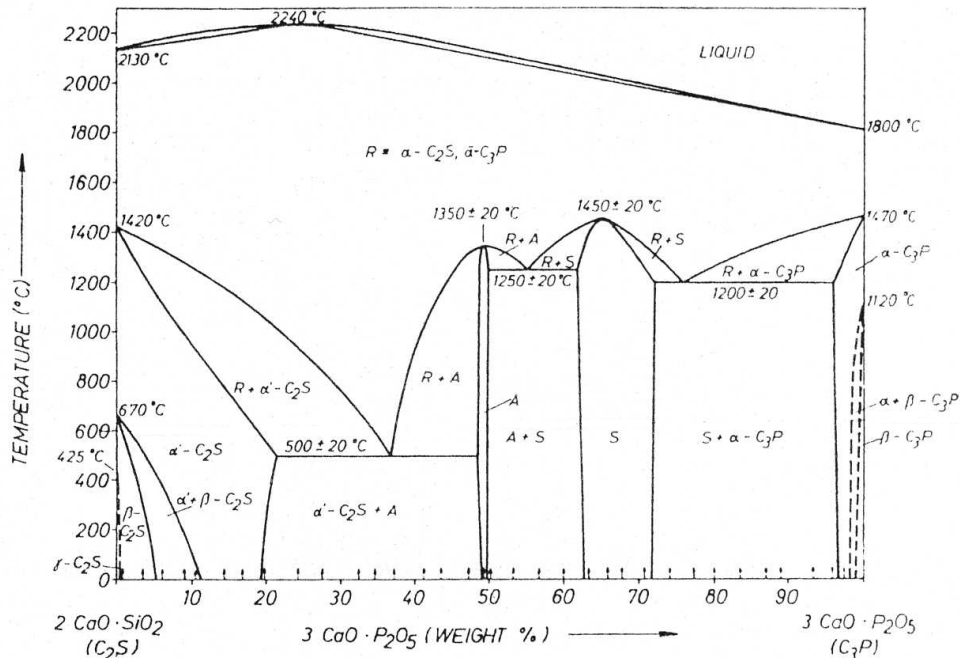

Figure 1.19. The system Ca_2SiO_4-$Ca_3(PO_4)_2$. α: nagelschmidtite, α-Ca_2SiO_4; α': α'-Ca_2SiO_4; A: A-phase, 2 Ca_2SiO_4·$Ca_3(PO_4)_2$; S: silicocarnotite, Ca_2SiO_4·$Ca_3(PO_4)_2$; α: α- $Ca_3(PO_4)_2$ (from [68]).

Si is believed to be introduced into the TCP structure exchanging PO_4^{3-} for SiO_4^{4-} groups. This substitution is non-isoelectronic, it means that the extra negative charge introduced by SiO_4^{4-} must be compensated by means of some mechanism [79]. The α-TCP lattice has to compensate the charge produced when Si^{4+} replaces P^{5+} either by the formation of O^{2-} vacancies or by the presence of Ca^{2+} in excess [80]. However, it is important to mention that the oxygen-deficient and the calcium-rich Si-α-TCP mechanisms are extreme cases. In fact, Si-α-TCP may contain both oxygen vacancies and Ca in excess to compensate the Si dopants [80].

1.6.3 α-TCP as a reactant of apatitic cements

α-TCP has a lower density and a higher free energy of formation compared to the low temperature β-polymorph [66], and is therefore more reactive and soluble, which makes it a much more efficient reactant for CPC. Upon contact with water, α-TCP hydrolyses to calcium deficient hydroxyapatite (CDHA), as shown in Reaction 1.5 [58]. CDHA is the compound precipitated as α-TCP dissolution progresses because, at physiological pH (7.2–7.4), it is the most stable of all calcium orthophosphates [37].

Reaction 1.5. $\quad 3\ \alpha\text{-}Ca_3(PO_4)_2 + H_2O \rightarrow Ca_9(HPO_4)(PO_4)_5(OH)$

In general, calcium-deficient hydroxyapatite (CDHA) exist in a wide range of compositions ($Ca_{10-x}(HPO_4)_x(PO_4)_{6-x}(OH)_{2-x}$ ($0 < x < 1$)) and is poorly crystalline [34]. Unsubstituted CDHAs (*i.e.* containing ions of Ca^{2+}, PO_4^{3-}, HPO_4^{2-} and OH^- only) do not exist in biological systems [34]. Several substitutions exist in bone mineral, in particular, carbonate ions are found at a concentration up to 8 wt%, and elements such as Na, Mg, K, Sr, Zn, Ba, Cu, Al, Fe, F, Cl and Si occur at trace (< 1 wt%) levels [67]. The main inorganic part of human normal and pathological calcifications are constituted by ion substituted CDHA, where the following substitutions occur: Na^+, K^+, Mg^{2+}, Sr^{2+} for Ca^{2+}; CO_3^{2-} for PO_4^{3-} or HPO_4^{2-}; F^-, Cl^-, CO_3^{2-} for OH^-, plus some water forms biological apatite. Therefore, ion substituted CDHA is a very promising compound for industrial manufacturing of artificial bone substitutes [34].

Scientists have focused many efforts in tailoring the ionic substitutions of synthetic apatites with the aim to improve their biological properties [42] [77] [81] [82] [83]. P*er se*, the ionic substitutions in apatites produce many modifications of bulk composition, crystal size,

morphology, surface composition, physico-chemical properties (zeta potential, surface energy, solubility) and materials properties (microstructure, texture, porosity). Therefore, it is difficult to determine which factors are involved in the biological behavior of the modified material [77].

1.7 Therapeutic ions for bone repair

It is well known that the presence of certain elements can facilitate the bone regeneration when released during the resorption of the material [11]. Until 20 years ago, gold was one of the most commonly used disease-modifying anti-rheumatic drugs and today it is still the subject of active research [84]. Other substances under several stages of acceptance and research include strontium as an anti-osteoporotic agent, vanadate as an anti-diabetic and bismuth as an anti-ulcer therapy. Also, most people apply daily fluoride or fluoro-phosphates to their teeth in order to combat caries. However, it is always important to keep the words of Paracelsus in mind: *"Everything is poisonous and nothing is non-toxic, only the dose makes something not poisonous"* [85]. The toxicity of inorganics depends on the species, dose and duration.

Single inorganic ions such as calcium (Ca) [86] [87], phosphorous (P) [88], silicon (Si) [89] [90] [91] [92], magnesium (Mg) [93] [94] [95], strontium (Sr) [96], zinc (Zn) [97] [98] [99], copper (Cu) [100] [101] [102] [103], manganese (Mn) [104], boron (B) [105] [106], vanadium (V) [107] and cobalt (Co) [108] are known to be involved in the bone metabolism, playing a physiological role in angiogenesis, growth and mineralization of bone tissues [109]. These effects make metal ions attractive for use as therapeutic agents in the fields of hard tissue engineering [84]. In fact, recent literature shows that these ions have attracted remarkable interest related with their possible use in the preparation of calcium phosphate-based biomaterials [42] [85] [109]. Table 1.5 revises the ions present in the hard tissues, which can be incorporated into calcium phosphate-based biomaterials in order to take advantage of their therapeutic effect.

Table 1.5. Effect to bone formation or bone remodeling of selected metallic ions when they are present in human bone metabolism in their normal concentration range, in a deficient concentration or in a concentration higher than the normal one. Compendium of published studies.

Element	Biological response *in vitro/in vivo*		
	Normal concentration	**Deficient concentration**	**Excessive concentration**
Calcium	• Favors osteoblast proliferation, differentiation and extracellular matrix (ECM) mineralization [86] • Activates Ca-sensing receptors in osteoblast cells, and increases expression of growth factors, *e.g.* IGF-I or IGF-II [87]	• Stimulates osteoclast activity [87]	• Stimulates osteoblast activity [87]
Phosphorus	• Stimulates expression of matrix gla protein (MGP) a key regulator in bone formation [88]	• Stimulates osteoclastic resorption and osteoblastic differentiation [110]	• Induces apoptosis of osteoblasts *in vitro* [111]
Silicon	• Essential for metabolic processes, formation and calcification of bone tissue [89] [90] • Dietary intake of Si increases bone mineral density [92] • Aqueous Si induces precipitation of HA [112] • Si(OH)$_4$ stimulates collagen I formation and osteoblastic differentiation [91]	• Causes problems in bone quality if present in a deficient concentration during early-bone formation stage [113]	• Improves bioactivity [42]
Magnesium	• Stimulates the beginning of the calcification process [114] [115] • Increases bone cell adhesion and stability (probably due to interactions with integrins) [95]	• Affects bone healing [116]	• Good tissue tolerance during degradation of Mg-biomaterial [85]

Element	Biological response *in vitro/in vivo*		
	Normal concentration	**Deficient concentration**	**Excessive concentration**
Strontium	• Improves the vertebral bone density and stimulates bone formation in rats (doses 0.19–0.34%) [117] [118]. Used for osteoporosis treatment [119]		• Defects in bone mineralization (doses > 0.4%) [117] [118]
Zinc	• Shows anti-inflammatory effect and stimulates bone formation *in vitro* by activation of protein synthesis in osteoblasts [98] • Increases ATPase activity, regulates transcription of osteoblastic differentiation genes, *e.g.* collagen I, ALP, osteopontin and osteocalcin [99]	• Decreases bone density [98]	• Inhibits osteoclast differentiation and promotes osteoblast activity [120]
Copper	• Favors angiogenesis of human endothelial cells [100] • Promotes synergetic stimulating effects on angiogenesis when associated with angiogenic growth factor FGF-2 [101] • Stimulates proliferation of human endothelial cells [102] • Induces differentiation of mesenchymal cells towards the osteogenic lineage [103]	• Is life threatening, causing cardiovascular deformities culminating in rupture [85]	
Manganese	• Influences regulation of bone remodeling [104]	• Reduces organic matrix synthesis and retards endochondral osteogenesis, increases possibility of bone abnormalities and decreases bone thickness or length [104]	• Inhibitor of loss of bone mass after ovariectomy [121]
Boron	• Stimulates RNA synthesis in fibroblast cells [106] • Dietary boron stimulates bone formation [105]		

1.8 Development of Si-containing calcium phosphates

1.8.1 Si as a therapeutic ion

The presence of Si in mammalian systems is quite variable. Si is present at a level of ~ 1 ppm in the serum, 2-10 ppm in the liver, kidney, lungs and muscles, 100 ppm in the bones and ligaments and 200-600 ppm in cartilages and other connective tissues [122]. Si is found in levels of 200-550 ppm in extracellular matrix compounds [122], implying a role for Si in these compounds. It has been hypothesized that Si acts as a biological cross-linking agent that contributes to the architecture and resilience of connective tissues [122].

The importance of Si for the health of the body, especially the growth of bone and cartilage at early stages, is nowadays a fact [77]. The role of Si as an essential element for birds, mammalians and probably other organisms was discovered in the 1970s through the studies of Carliste [89] [113] [123], Schwarz [124] and Seaborne [125]. In Carliste's studies, chicks were fed with Si-deficiency food and it was proved that the development of a healthy skeleton was linked to Si. The Si deficient animals showed lower levels of collagen, with no significant difference in the level of non-collagenous proteins [123]. The Si deficiency was also linked to deformities in the skull and teeth of rats [124]. In contrast, the Si supplemented to the diet of rats caused an increase of 33.8% of the growth rate compared to the Si deficient animals [124].

The effects of the dietary Si have also been recently evaluated with humans, analyzing the bone mineral density in hips of men and premenopausal women. Bone mineral density was reported to increase up to a 10% when the Si intake levels were high (> 40 mg Si/day), in comparison to lower ones (< 14 mg Si/day) [92].

1.8.2 Effect of Si on the chemistry and microstructure of α-TCP and CDHA

The Si that is introduced into α-TCP (Si-α-TCP) or into HA (Si-HA) is expected to modify the behavior of the material with its surrounding environment. However, there are still controversies regarding whether Si ions are the veritable reason of a positive biological response (**active mechanism**), or the presence of Si in the structure of the material causes chemical or

topographical changes at the surface that eventually lead to a change of the biological response (**passive mechanism**) [79] [126].

Concerning the passive mechanism, it is well known that Si modifies the chemistry and the microstructure of both Si-α-TCP and Si-HA. The incorporation of Si into HA has been more studied than the incorporation in α-TCP. Some changes that Si can induce to HA are indicated below.

i) decrease of the grain size [127] [81] [128] [129], increasing the triple point junctions per area and thus increasing the dissolution at the surface [130];

ii) modification of the surface topography [126], which can affect the cellular behavior [131];

iii) increase of the amorphous phase [127];

iv) increase of the electronegative surface (for Si-α-TCP and Si-HA) [77];

v) change of the protein conformation at the material surface [132].

1.8.3 Preparation of Si-doped α-TCP and Si-doped HA

The studies based on Si-doped calcium phosphate-based materials can be mainly divided in two groups, regarding the material that was evaluated: the Si-substituted HA (Si-HA) and the Si-substituted α-tricalcium phosphate (Si-α-TCP). Both materials have been the focus of many research efforts [77] [126].

The synthesis of both Si-α-TCP and Si-HA usually consists in a two-steps process. Firstly, a precursor is precipitated by wet chemical methods and, secondly, Si is incorporated into the crystalline structure of a calcium phosphate end-product through a thermal treatment [77] [42]. This process have been generally performed using Si as an organic compounds such as tetra ethyl or propyl ortho-silicate (TEOS or TPOS), silicon (IV) acetate ($Si(COOCH_3)_4$) [133] [134] [135] [128] [136] [127] or some form of nano-particulate silica; and the calcium phosphate used has been obtained by precipitation to have a nanocrystalline HA [80] [137] [138] [139] [129].

Even though the preparation of Si-α-TCP has been the aim of several studies, several works have shown that the α-phase is contaminated with other subproducts, namely HA, β-TCP or an amorphous phase [80] [137] [138] [140] [141].

1.8.4 Preparation of Si-doped CPC

Although there are several articles regarding the stabilization of the α-phase of TCP by Si doping and, undoubtedly, there are hundreds of papers and patents in the calcium phosphate cements (CPC) field, there are few works in which Si-doped CPCs (Si-CPC) are developed.

In 2006, Camiré *et al.* prepared Si-doped CPC from Si-α-TCP. *In vitro* tests with SBF resulted in the formation of a thicker apatite layer on the surface of a CPC containing 1 wt% Si in comparison with its Si-free counterpart. It should be highlighted, however, that the effect of Si on the stabilization of the α-phase could not be verified, since the α-TCP was stabilized by quenching the calcium phosphate in air from 1325°C [142].

In 2009, Motisuke *et al.* reported the preparation of a Si-CPC using Si-α-TCP [143]. However, since the reactivity of Si-α-TCP was low, the paper discussed different strategies to improve it. In 2011, Su *et al.* prepared Si-apatite cements with powder mixtures of tetracalcium phosphate, dicalcium phosphate anhydrous and 5 wt% sodium silicate [144]. Comparing with the analogous material free of Si, the results indicated a shorter setting time, higher compressive strength and higher degradability in Tris-HCl in the case of Si-CPC. The same material was modified by Cao *et al.* for the incorporation of macroporosity [145]. Similarly, Zhao *et al.* also showed improved results when calcium silicate (CS) was included to a CPC (CS/CPC) [146].

1.8.5 Assessment of the effect of Si on the performance of calcium phosphates

1.8.5.1 Predicting *in vivo* bioactivity in simulated body fluid (SBF)

The concept of **bioactivity** was employed for the first time in 1969 to designate a property of some bioceramics used for implant applications. A bioactive material was described as *"one that elicits a specific biological response at the interface of the material, which results in the formation of a bond between the tissue and the material"* [147]. In other words, a bioactive material creates an environment compatible with **osteogenesis** (bone growth), the mineralizing interface developing as a natural bonding junction between the living material (bone) and the non-living one (biomaterial) [148].

Not all materials can bond to living bone and each bioactive material has a different mechanism, time dependence, strength and thickness of the bonding zone. The rate of development of the interfacial bond can be referred as the **level of bioactivity** [148]. The bioactivity of a material is an important factor for the success of a bone implant, and many researchers have been interested in correlating the level of bioactivity *in vitro* with the real bioactivity capacity that would have the material when implanted into the body. The possibility to test the bioactivity of a material *in vitro* allows reducing remarkably the duration of the *in vivo* experiments and the number of animals used [149] and, in second place, saving a lot of time and money.

In 1991, Kokubo *et al.* proposed that an essential requirement for a biomaterial to bond to a living bone was the previous formation of bone-like apatite on the biomaterial's surface when implanted in the body [150]. In their study, it was proved that the formation of this apatite layer *in vivo* could be reproduced in a **simulated body fluid (SBF)**, a synthetic medium that contains ion concentrations nearly equal to those of human plasma [150]. Other studies have also correlated the ability to form apatite on the surface of different materials in SBF with the *in vivo* bone bioactivity of a material, being observed the same trend (HA < A-W < Bioglass) in both situations [151].

SBF has experienced some improvements in its formulation since 1990, when the original SBF was proposed by Kokubo *et al.* [152]. The original SBF lacked SO_4^{2-} ions that are contained in human blood plasma. Thus, the SBF was corrected by Kokubo *et al.* one year later [150] and, since then many researchers have been using the corrected-SBF (c-SBF), usually known simply as "SBF". A detailed recipe to prepare SBF was reported in 1995 by Cho *et al.* [153]. In 2003, Oyane *et al.* prepared a revised SBF (r-SBF): the Cl^- ion concentration was decreased and the HCO_3^- ion concentration was increased with the aim to get closer to the human blood plasma [154]. However, the calcium carbonate of the r-SBF had a strong tendency to precipitate. In 2004, Takadama *et al.* proposed a newly improved SBF (n-SBF) in which the Cl^- ion concentration was decreased to the level of human blood plasma [155]. A study compared the n-SBF with the c-SBF and it was shown that they did not differ in stability and reproducibility [155]. Hitherto, the c-SBF

(or simply SBF) has been the most commonly used medium to evaluate the bioactivity *in vitro* in the scientific community.

Studies evaluating the Z-potential of the surface of a hydroxyapatite immersed in SBF have increased the knowledge of the formation of the apatite layer. Kim *et al.* proposed several steps that lead to the formation of the apatite layer [156], as explained below.

The iso-electric point of HA in water is between 5 and 7 [157] [67], lower than the pH of the SBF, 7.4. Therefore, HA immersed in SBF presents negative surface charge by exposing hydroxyl and phosphate units in its crystal structure (Figure 1.20 a) [157]. The HA surface uses this negative charge to interact specifically with the positive calcium ions in the fluid, which subsequently attract phosphate groups, forming a Ca-rich ACP. The Ca ions are accumulated, which makes the Ca-rich ACP to acquire and to increase its positive charge. The Ca-rich ACP on the HA therefore interacts specifically with the negative phosphate ions in the fluid to form a Ca-poor ACP (rich in phosphate groups). This type of Ca-poor ACP has been observed as a precursor, which eventually crystallizes into bonelike apatite on various bioactive ceramics [158] [159] [160] [161]. The solubility of apatites in water is lower than that of any other calcium phosphate [36], and therefore the Ca-poor ACP in SBF could be thermodynamically stabilized by transforming into a crystal phase of apatite. Once formed in SBF, which is a medium supersaturated with respect to the apatite [162], the apatite grows spontaneously consuming the calcium and phosphate ions, and incorporating minor ions such as sodium, magnesium and carbonate. Thereby, a mineral bone-like regarding both its compositional and structural features is developed. The mechanism by which apatite is deposited on the HA is schematically shown in Figure 1.20 b.
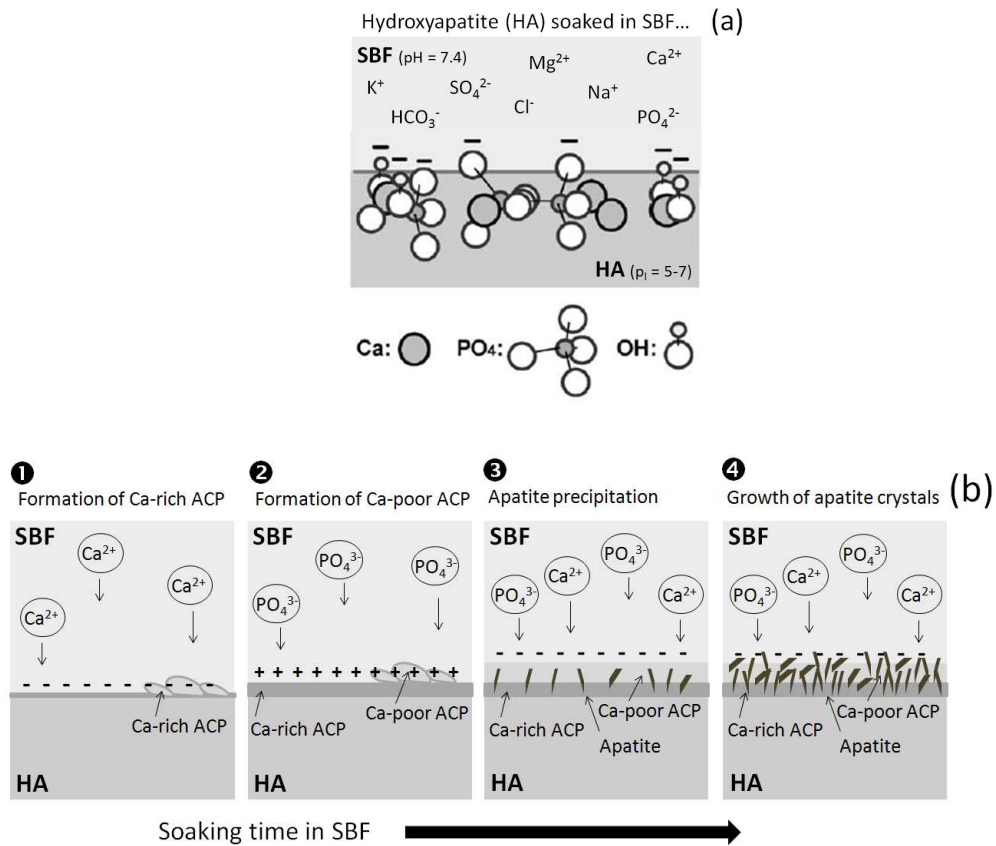
Figure 1.20. a) Schematic presentations of the origin of negative charge on the HA surface; b) process of bone-like apatite formation thereon in SBF (modified from [156]).

1.8.5.2 Influence of Si on *in vitro* cell behavior

In vitro cell studies are usually performed to predict the response that a material will have when implanted into the body. There are different strategies aimed at assessing the cell response to biomaterials: direct or indirect methods, as schematically shown in Figure 1.21. A **direct method** implies seeding the cells on the surface of the material, which can be a dense sample (Figure 1.21 a) or a porous scaffold (Figure 1.21 b). **Indirect methods** consist on evaluating the cell response in presence but not in direct contact with the material, either in the form of suspended particles (Figure 1.21 c) or bulk material (Figure 1.21 d). The cells medium can also be modified *in situ* by soaking into it a membrane (commercially named as insert or transwell) that contains the material (Figure 1.21 e). Another option is to put the cells in contact with an extract, a medium previously modified by the material (Figure 1.21 f).
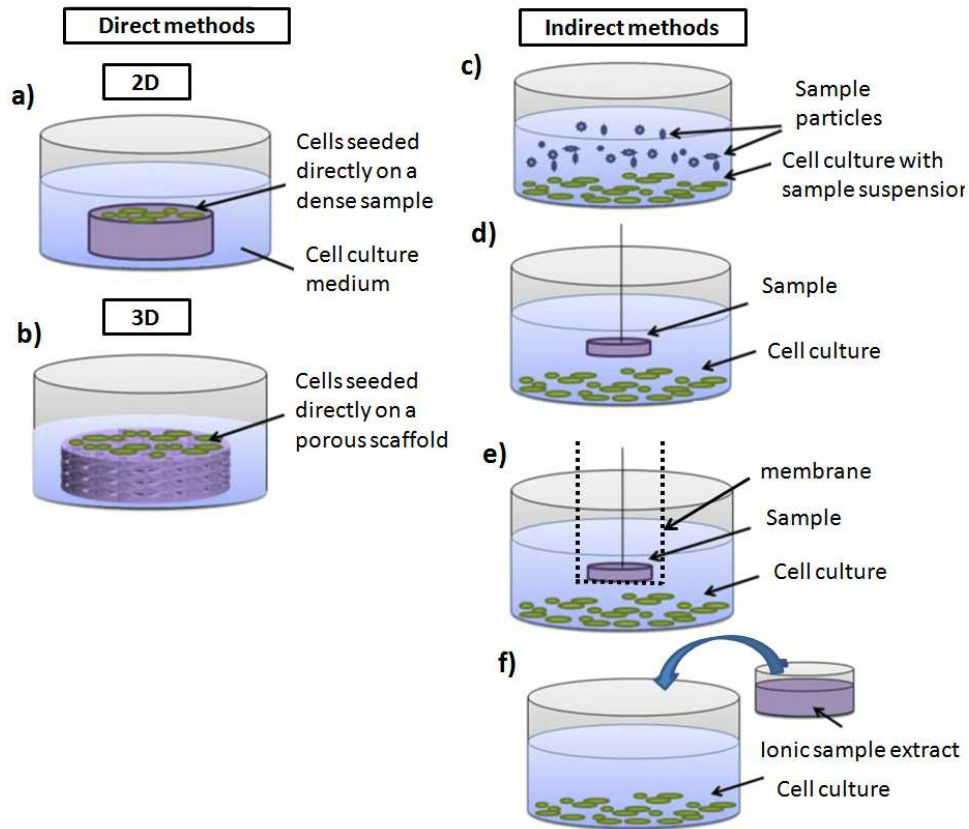
Figure 1.21. Different methods for analyzing the cellular response to degradable biomaterials (modified from [109]).

Every cell culture method evaluates differently the cell response, since the stimulatory factors are not the same. In the **direct methods**, the cells are affected by the surface properties of the material (density, porosity, crystallinity, chemistry, surface area, roughness, surface charge, chemistry, topography and hardness/stiffness) and also by the ionic modification of the medium. The **indirect methods** only evaluate the effect that the ion release/uptake from the material has on the cell behavior. Figure 1.22 shows a schematic overview of a few biological responses caused by the ions released by a material.
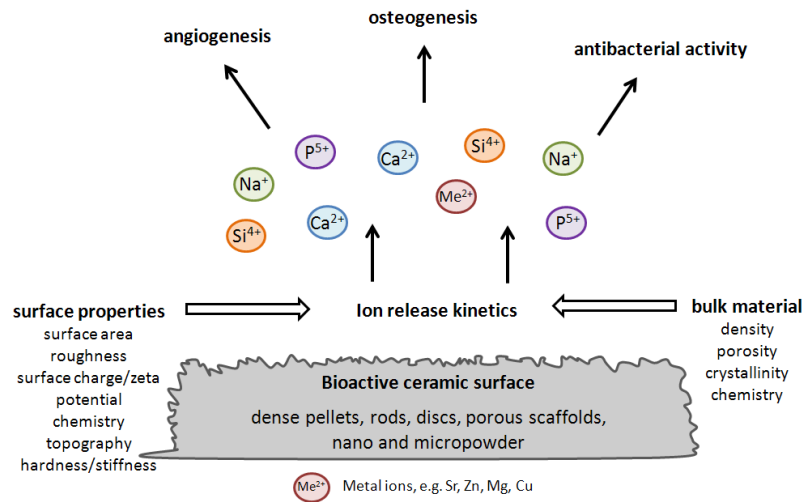
Figure 1.22. Overview of biological responses to ionic dissolution products of bioactive glasses (modified from [109]).

There are many studies evaluating the effect of Si on the material bioactivity and cell behavior, although the results are somehow controversial. However, there is a good number of works showing that Si released into the medium enhances osteoblast proliferation, differentiation and collagen production. Table 1.6 briefly summarizes some of the studies performed, including the Si concentration ([Si]) and the outcomes of each work.

Table 1.6. Effect of Si on *in vitro* cell behavior. Compendium of literature studies.

Materials used in the study, cells, incubation time	[Si] in medium	Cells behavior	References
• Study: Cells supplemented with orthosilicic acid • Cells: Human osteoblasts-like cells	0 to 50 μM (0-1.4 ppm Si)	Physiological concentrations of soluble Si increase osteogenesis by: • Stimulating collagen type I synthesis • Promoting osteoblasts differentiation	[91]
• Study: Human osteoblast supplemented with aqueous Si • Cells: Human osteoblasts • Incubation time: 48 h	0.1-100 ppm	Dose-dependent increase in osteoblast proliferation and cell differentiation through up-regulation of transforming growth factor beta (TGF-β)	[163]
• Study: Cells treated with dissolution products of Bioglass 45S5 (45 wt% SiO_2) • Cells: Human osteoblasts (isolated from the trabecular bone of femoral heads) • Incubation time: 48 h	16.5 ± 3.5 ppm	Osteogenesis and collagen synthesis is stimulated	[164]
• Study: Cells treated with ionic products of Bioglass (BG60S) • Cells: Osteoblasts derived from rat calvaria • Incubation time: 72 h	~ 40 ppm	Cell proliferation, differentiation, collagen segregation and cell viability is increased. It is speculated that Si might be the main cause	[165]
• Study: Cultures dosed with aqueous Si derived from Si-TCP • Cells: Rat osteoblast	0-100 ppm	Dose-dependent effect of Si	[166]
• Study: Cells cultured on dense Si-HA (1.97 wt% Si) • Cell type: MG-63 osteoblast-like cells • Incubation times: 0, 3, 6, 24 h	0.02 wt%	Cell proliferation is enhanced in Si-HA in comparison with HA	[136]

Materials used in the study, cells, incubation time	[Si] in medium	Cells behavior	References
• Study: Cells cultured in Si-HA • Cells: Human osteosarcoma cells (HOC)	-	• Si-HA is biocompatible and non-cytotoxic • Metabolic activity of cells cultured in direct contact is higher for Si-HA than for HA	[167]
• Study: Cells cultured over Si-HA (1-2 mol TEOS/1 mol HA) • Cells: Human osteosarcoma cells (HOC) • Incubation time: 1, 2, 3 and 7 days	Not measured	Stimulation of cell proliferation	[79]
• Study: Cells seeded on surfaces of Si-HA coatings • Cells: Primary human osteoblast-like cells (HOB) • Incubation time: 2, 4, 7 days	Not measured	• Good attachment of cells to HA and Si-HA, ECM formation • Level of mineral deposits is higher on Si-HA coatings than on HA • Higher cell growth, well-organised cytoskeletal architecture and enhanced biomineralisation were achieved on Si-HA	[168]
• Study: Cells were seeded on disks of Si-HA (0.8 wt % Si) • Cell type: Human osteoblast cells • Incubation time: From 1 to 27 days	Not measured	Higher cell number and ALP production when compared with HA	[169]
• Study: Cells in contact with Si-HA (1.5 wt% Si) • Cell type: Peripheral blood mononuclear cells (PBMC) and monocytes expressing the CD14 antigen	Not measured	• Si-HA allows differentiation of PBMC into mature osteoclasts • A higher osteoclastic resorption activity was observed for Si-HA	[170]
• Study: Cells in contact with Si-CPC (5 wt% sodium silicate) • Cell type: MG-63	Not measured	• Si-CPC promoted cell proliferation and differentiation	[144]
• Study: Calcium silicate (15wt%) was included to a CPC • Cell type: MC3T3-E1 and HUVEC cells • Incubation time: 1, 3 and 7 days	20-70 ppm	• Excellent biocompatibility and improved cell attachment, proliferation and differentiation of cells	[146]

1.8.5.3 Influence of Si on the *in vivo* biological response

Several studies claim that calcium phosphate based-materials doped with Si enhanced biological properties *in vivo* in comparison with their stoichiometric counterparts [79]. For instance, Patel *et al.* implanted granules of pure HA and Si-substituted HA in a rabbit model and observed an increase of bone ingrowth and bone-implant coverage [171]. This enhanced biological response was associated to an unknown mechanism that produced up-regulation in osteoblast cell metabolism, as reported by several works (Table 1.6). Similarly, Hing *et al.* showed that bone ingrowth was increased when 0.8 wt% Si was incorporated into the HA lattice of porous scaffolds [172].

Very few studies have been performed with *in vivo* studies using Si-CPC. Camiré *et al.* implanted Si-CPC in tibiae of rabbit model and observed that this material enhanced mesenchymal cell differentiation and increased osteoblast activity compared to CPC [142]. Cao *et al.* developed a macroporous Si-CPC and the scaffolds exhibited good biocompatibility, degradation and osteogenesis *in vivo* [145].

1.9 References

[1] Sandell R. El envejecimiento de la población, parte I: alcance y perspectivas en España consecuencias socioeconómicas. Real Instituto Elcano de Estudios Internacionales y Estratégicos, 2003; pp. 1–9.

[2] Hernández JL, Olmos JM, Alonso MA, González-Fernández CR, Martínez J, Pajarón M, Llorca J, González-Macías J. Trend in hip fracture epidemiology over a 14-year period in a Spanish population. Osteoporosis International 2006; 17: 464–470.

[3] Díaz Curiel M, García JJ, Carrasco JL, Honorato J, Pérez Cano R, Rapado A, Álvarez Sanz C. Prevalencia de osteoporosis determinada por densitometría en la población femenina española. Medicina Clínica (Barcelona) 2001; 116: 86–88.

[4] Gimeno A, Guanabens N, Monegal A, Peris P. Consulta de osteoporosis. Barcelona, Spain: Prous Science, 2005.

[5] Mistry AS, Mikos AG. Tissue engineering strategies for bone regeneration. Bone 2005; 94: 1–22.

[6] Bain SD, Gross TS. Structural aspects of bone resorption. In: Bone Resorption. Bronner F, Farach-Carson MC, Rubin J (editors). Hong Kong: Springer, 2005; pp. 58–66.

[7] Marieb EN. The skeletal system. In: Essentials of human anatomy and physiology, 2008; pp. 115–159.

[8] Döbelin N, Luginbühl R, Bohner M. Synthetic calcium phosphate ceramics for treatment of bone fractures. CHIMIA International Journal for Chemistry 2010; 64: 723–729.

[9] Cowin SC, Doty SB. Bone tissue. In: Tissue Mechanics. New York: Springer, 2007; pp. 341–384.

[10] Dorozhkin SV. Calcium orthophosphates. Journal of Materials Science 2007; 42: 1061–1095.

[11] Vallet-Regí M. Calcium phosphates as substitution of bone tissues. Progress in Solid State Chemistry 2004; 32: 1–31.

[12] Sato K. Mechanism of hydroxyapatite mineralization in biological systems. Journal of the Ceramic Society of Japan 2007; 115: 124–130.

[13] Buehler MJ. Molecular nanomechanics of nascent bone: fibrillar toughening by mineralization. Nanotechnology 2007; 18: 295102.

[14] Bilezikian JP, Raisz LG, Rodan GA (editors). Principles of Bone Biology. San Diego: Academic Press, 2001.

[15] Gupta HS, Seto J, Wagermaier W, Zaslansky P, Boesecke P, Fratzl P. Cooperative deformation of mineral and collagen in bone at the nanoscale. Proceedings of the National Academy of Sciences of the United States of America 2006; 103: 17741–17746.

[16] Kokubo T. Novel bioactive materials with different mechanical properties. Biomaterials 2003; 24: 2161–2175.

[17] International Osteoporosis Foundation (IOF) Committee. Move it or lose it. In: Invest in your bones report, 2005.

[18] Reis R, Weiner S (editors). Learning from nature how to design implantable biomaterials: from biomineralization fundamentals to biomimetic materials and processing routes. Proceedings of the NATO Advanced Study Institute, 171. New York: Kluwer Academic Publishers, 2004.

[19] Ilan DI, Ladd AL. Bone graft substitutes. Techniques 2003; 9: 151–160.

[20] Carson JS, Bostrom MPG. Synthetic bone scaffolds and fracture repair. Injury 2007; 38: S33–S37.

[21] Jones A, Arns C, Sheppard A, Hutmacher D, Milthorpe B, Knackstedt M. Assessment of bone ingrowth into porous biomaterials using micro-CT. Biomaterials 2007; 28: 2491–2504.

[22] Mastrogiacomo M, Scaglione S, Martinetti R, Dolcini L, Beltrame F, Cancedda R, Quarto R. Role of scaffold internal structure on in vivo bone formation in macroporous calcium phosphate bioceramics. Biomaterials 2006; 27: 3230–3237.

[23] Takagi S, Chow L. Formation of macropores in calcium phosphate cement implants. Journal of Biomedical Materials Research 2001; 12: 135–139.

[24] Ota Y, Kasuga T, Abe Y. Preparation and compressive strength behaviour of porous ceramics with β-Ca$_3$(PO$_3$)$_2$ fiber skeletons. Journal of the American Ceramic Society 1997; 80: 225–231.

[25] Montufar EB, Traykova T, Gil C, Harr I, Almirall A, Aguirre A, Engel E, Planell JA, Ginebra MP. Foamed surfactant solution as a template for self-setting injectable hydroxyapatite scaffolds for bone regeneration. Acta Biomaterialia 2010; 6: 876–885.

[26] Daw R, Tonzani S. Biomaterials. Nature 2009; 462: 425.

[27] Editorial. Boom time for biomaterials. Nature materials 2009; 8: 439.

[28] Lu HH, Subramony SD, Boushell MK, Zhang X. Tissue engineering strategies for the regeneration of orthopedic interfaces. Annals of Biomedical Engineering 2010; 38: 2142–2154.

[29] Huebsch N, Mooney DJ. Inspiration and application in the evolution of biomaterials. Nature 2009; 462: 426–432.

[30] Williams DF. The Williams dictionary of biomaterials. Liverpool, United Kingdom: Liverpool University Press, 1999.

[31] Williams DF. On the nature of biomaterials. Biomaterials 2009; 30: 5897–5909.

[32] Vallet-Regí M. Biocerámicas: regeneradoras de hueso y portadoras de sustancias biológicamente activas. Transatlántica de educación 2007; 3: 60–72.

[33] Best SM, Porter AE, Thian ES, Huang J. Bioceramics: past, present and for the future. Journal of the European Ceramic Society 2008; 28: 1319–1327.

[34] Dorozhkin SV. Calcium orthophosphates in nature, biology and medicine. Materials 2009; 2: 399–498.

[35] Dorozhkin SV. Calcium orthophosphate cements for biomedical application. Journal of Materials Science 2008; 43: 3028–3057.

[36] Chow LC. Development of self-setting calcium phosphate cements. Journal of the Ceramic Society of Japan 1992; 99: 927–936.

[37] Carrodeguas RG, De Aza S. α-tricalcium phosphate: synthesis, properties and biomedical applications. Acta Biomaterialia 2011; 7: 3536–3546.

[38] Ginebra MP. Calcium phosphate bone cements. In: Orthopaedic Bone Cements. Deb S (editor). Cambridge: Woodhead Publishing Limited, 2008; pp. 206–230.

[39] Khalil K, Kim S, Dharmaraj N, Kim K, Kim H. Novel mechanism to improve toughness of the hydroxyapatite bioceramics using high-frequency induction heat sintering. Journal of Materials Processing Technology 2007; 187–188: 417–420.

[40] Kim HM. Bioactive ceramics: challenges and perspectives. Journal of Ceramic Society of Japan 2001; 109: S49–S57.

[41] Daculsi G. Biphasic calcium phosphate concept applied to artificial bone, implant coating and injectable bone substitute. Biomaterials 1998; 19: 1473–1478.

[42] Boanini E, Gazzano M, Bigi A. Ionic substitutions in calcium phosphates synthesized at low temperature. Acta Biomaterialia 2010; 6: 1882–1894.

[43] LeGeros RZ, LeGeros J. Calcium phosphate bioceramics: past, present, future. Key Engineering Materials 2003; 240-242: 3–10.

[44] Burger E, Patel V. Calcium phosphates as bone graft extenders. Orthopaedics 2007; 30: 939–942.

[45] Bermúdez O, Boltong MG, Driessens F, Planell JA. Optimization of a calcium orthophosphate cement formulation occurring in the combination of monocalcium phosphate monohydrate with calcium oxide. Journal of Materials Science: Materials in Medicine 1994; 5: 67–71.

[46] Bermúdez O, Boltong MG, Driessens FCM, Planell JA. Development of some calcium phosphate cements from combinations of α-TCP, MCPM and CaO. Journal of Materials Science: Materials in Medicine 1994; 5: 160–163.

[47] Driessens FCM, Boltong MG, Bermúdez O, Planell JA, Ginebra MP, Fernández E. Effective formulations for the preparation of calcium phosphate bone cements. Journal of Materials Science: Materials in Medicine 1994; 5: 164–170.

[48] Huan Z, Chang J. Novel bioactive composite bone cements based on the beta-tricalcium phosphate-monocalcium phosphate monohydrate composite cement system. Acta Biomaterialia 2009; 5: 1253–1264.

[49] Driessens FCM, Planell JA, Boltong MG, Khairoun I, Ginebra MP. Osteotransductive bone cements. Proceedings of the Institution of Mechanical Engineers H: Journal of Engineering in Medicine 1998; 212: 427–435.

[50] LeGeros RZ, Chohayeb A, Shulman A. Apatitic calcium phosphates: possible dental restorative materials. Journal of Dental Research 1982; 61: 343–347.

[51] Brown W, Chow L. A new calcium phosphate setting cement. Journal of Dental Research 1983; 62: 672.

[52] Fernández E, Gil FJ, Ginebra MP, Driessens FCM, Planell JA, Best SM. Calcium phosphate bone cements for clinical applications, part II: precipitate formation during setting reactions. Journal of Materials Science: Materials in Medicine 1999; 10: 177–183.

[53] Monma H, Kanazawa T. The hydratation of α-tricalcium phosphate. Journal of Ceramic Society of Japan 1976; 84: 209–213.

[54] Monma H, Goto M, Komura T. Effect of additives on hydratation and hardening of tricalcium phosphate. Gypsum Lime 1984; 188: 11–16.

[55] Ginebra MP, Fernández E, Boltong M, Planell JA, Bermúdez O, Driessens FCM. Compliance of an apatitic calcium phosphate cements with some short-term clinical requirements in surgery, orthopaedics and dentistry. Clinical Materials 1994; 17: 99–104.

[56] Ginebra MP, Boltong M, Fernández E, Planell JA, Driessens F. Effects of various additives and temperature on some properties of an apatitic calcium phosphate cement. Journal of Materials Science: Materials in Medicine 1995; 6: 612–616.

[57] Ginebra MP, Fernández E, De Maeyer EAP, Verbeeck RMH, Boltong MG, Ginebra J, Driessens FCM, Planell JA. Setting reaction and hardening of an apatitic calcium phosphate cement. Journal of Dental Research 1997; 76: 905–912.

[58] Ginebra MP, Fernández E, Driessens F, Planell JA. Modeling of the hydrolysis of α-tricalcium phosphate. Journal of the American Ceramic Society 1999; 82: 2808–2812.

[59] Ginebra MP, Driessens FCM, Planell JA. Effect of the particle size on the micro and nanostructural features of a calcium phosphate cement: a kinetic analysis. Biomaterials 2004; 25: 3453–3462.

[60] Constantz BR, Ison IC, Fulmer MT, Poser RD, Smith ST, vanWagoner M, Ross J, Goldstein SA, Jupiter JB, Rosenthal DI. Skeletal repair by *in situ* formation of the mineral phase of bone. Science 1995; 267: 1796–1799.

[61] Brown P, Fulmer M. Kinetics of hydroxyapatite formation at low temperature. Journal of the American Ceramic Society 1991; 74: 934–940.

[62] Bohner M, Lemaitre J, Ring T. Hydraulic properties of tricalcium phosphate-phosphoric acid-water mixtures. In: Conference Proceedings of Third Euro-Ceramics: Engineering Ceramics, 1993.

[63] Dorozhkin SV. Calcium orthophosphate cements and concretes. Materials 2009; 2: 221–291.

[64] Khairoun I, Boltong MG, Driessens FCM, Planell JA. Limited compliance of some apatitic calcium phosphate bone cements with clinical requirements. Journal of Materials Science: Materials in Medicine 1998; 9: 667–671.

[65] Ginebra MP. Cements as bone repair materials. In: Bone repair biomaterials. Planell JA (editor). Cambridge: Woodhead Publishing Limited, 2009; pp. 271–308.

[66] Mathew M, Schroeder W, Dickens B, Brown W. The crystal structure of α-$Ca_3(PO_4)_2$. Acta Crystallographica B: Structural Science 1977; 33: 1325–1333.

[67] Elliott JC. Structure and chemistry of the apatites and other calcium orthophosphates. Amsterdam: Elsevier, 1994.

[68] Fix W, Heymann H, Heinke R. Subsolidus relations in the system $2CaO \cdot SiO_2 \cdot 3CaO \cdot P_2O_5$. Journal of the American Ceramic Society 1969; 52: 346–347.

[69] Mackay A. A preliminary examination of the structure of $Ca_3(PO_4)_2$. Acta Crystallographica 1953; 6: 743–744.

[70] Yin X, Stott MJ. Theoretical insights into bone grafting silicon-stabilized alpha-tricalcium phosphate. The Journal of Chemical Physics 2005; 122: 024709-1–9.

[71] Liang L, Rulis P, Ching WY. Mechanical properties, electronic structure and bonding of alpha- and beta-tricalcium phosphates with surface characterization. Acta Biomaterialia 2010; 6: 3763–3771.

[72] Ando J. Tricalcium phosphate and its variation. Bulletin of the Chemical Society of Japan 1958; 31: 196–201.

[73] Enderle R, Götz-Neunhoeffer F, Göbbels M, Müller FA, Greil P. Influence of magnesium doping on the phase transformation temperature of beta-TCP ceramics examined by Rietveld refinement. Biomaterials 2005; 26: 3379–3384.

[74] Carrodeguas RG, De Aza AH, Turrillas X, Pena P, De Aza S. New Approach to the β→α polymorphic transformation in magnesium-substituted tricalcium phosphate and its practical implications. Journal of the American Ceramic Society 2008; 91: 1281–1286.

[75] Nurse RW, Welch J, Gutt W. High-temperature phase equilibria in the system dicalcium silicate-tricalcium phosphate. Journal of the Chemical Society 1959; 220: 1077–1083.

[76] Barnes MW, Klimkiewicz M, Brown PW. Hydratation in the system Ca_2SiO_4-$Ca_3(PO_4)_2$ at 90^oC. Journal of the American Ceramic Society 1992; 75: 1423–1429.

[77] Pietak AM, Reid JW, Stott MJ, Sayer M. Silicon substitution in the calcium phosphate bioceramics. Biomaterials 2007; 28: 4023–4032.

[78] Stead J, Ridsdale C. Crystals in basic converter slag. Journal of the Chemical Society 1887; 51: 601–610.

[79] Vallet-Regí M, Arcos D. Silicon substituted hydroxyapatites: a method to upgrade calcium phosphate based implants. Journal of Materials Chemistry 2005; 15: 1509–1516.

[80] Sayer M, Stratilatov AD, Reid J, Calderin L, Stott MJ, Yin X, MacKenzie M, Smith TJN, Hendry JA, Langstaff SD. Structure and composition of silicon-stabilized tricalcium phosphate. Biomaterials 2003; 24: 369–382.

[81] Porter AE, Patel N, Skepper JN, Best SM, Bonfield W. Effect of sintered silicate-substituted hydroxyapatite on remodelling processes at the bone-implant interface. Biomaterials 2004; 25: 3303–3314.

[82] Li YW, Leong JC, Lu WW, Luk KD, Cheung KM, Chiu KY, Chow SP. A novel injectable bioactive bone cement for spinal surgery: a developmental and preclinical study. Journal of Biomedical Materials Research 2000; 52: 164–170.

[83] Denissen H, Klein C, Visch L, Van den Hooff A. Behavior of calcium phosphate coatings with different chemistries in bone. The International Journal of Prosthodontics 1996; 9: 142–148.

[84] De Wall SL, Painter C, Stone JD, Bandaranayake R, Wiley DC, Mitchison TJ, Stern LJ, DeDecker BS. Noble metals strip peptides from class II MHC proteins. Nature Chemical Biology 2006; 2: 197–201.

[85] Habibovic P, Barralet JE. Bioinorganics and biomaterials: bone repair. Acta Biomaterialia 2011; 7: 3013–3026.

[86] Maeno S, Niki Y, Matsumoto H, Morioka H, Yatabe T, Funayama A, Toyama Y, Taguchi T, Tanaka J. The effect of calcium ion concentration on osteoblast viability, proliferation and differentiation in monolayer and 3D culture. Biomaterials 2005; 26: 4847–4855.

[87] Marie P. The calcium-sensing receptor in bone cells: a potential therapeutic target in osteoporosis. Bone 2010; 46: 571–576.

[88] Julien M, Khoshniat S, Lacreusette A, Gatius M, Bozec A, Wagner EF, Wittrant Y, Masson M, Weiss P, Beck L, Magne D, Guicheux J. Phosphate-dependent regulation of MGP in osteoblasts: role of ERK1/2 and Fra-1. Journal of Bone and Mineral Research 2009; 24: 1856–1868.

[89] Carlisle EM. Silicon: a possible factor in bone calcification. Science 1970; 167: 279–280.

[90] Carlisle EM. Silicon: a requirement in bone formation independent of vitamin D1. Calcified Tissue International 1981; 33: 27–34.

[91] Reffitt DM, Ogston N, Jugdaohsingh R, Cheung HF, Evans BA, Thompson RP, Powell JJ, Hampson GN. Orthosilicic acid stimulates collagen type 1 synthesis and osteoblastic differentiation in human osteoblast-like cells *in vitro*. Bone 2003; 32: 127–135.

[92] Jugdaohsingh R, Tucker KL, Qiao N, Cupples LA, Kiel DP, Powell JJ. Dietary silicon intake is positively associated with bone mineral density in men and premenopausal women of the framingham offspring cohort. Journal of Bone and Mineral Research 2004; 19: 297–307.

[93] Staiger MP, Pietak AM, Huadmai J, Dias G. Magnesium and its alloys as orthopedic biomaterials: a review. Biomaterials 2006; 27: 1728–1734.

[94] Tsuboi S, Nakagaki H, Ishiguro K, Kondo K, Mukai M, Robinson C, Weatherell JA. Magnesium distribution in human bone. Calcified Tissue International 1994; 54: 34–37.

[95] Zreiqat H, Howlett CR, Zannettino A, Evans P, Schulze-Tanzil G, Knabe C, Shakibaei M. Mechanisms of magnesium-stimulated adhesion of osteoblastic cells to commonly used orthopaedic implants. Journal of Biomedical Materials Research 2002; 62: 175–184.

[96] Marie P, Ammann P, Boivin G, Rey C. Mechanisms of action and therapeutic potential of strontium in bone. Calcified Tissue International 2001; 69: 121–129.

[97] Brandão-Neto J, Stefan V, Mendonça B, Bloise W, Castro A. The essential role of zinc in growth. Nutrition Research 1995; 15: 335–358.

[98] Yamaguchi M. Role of zinc in bone formation and bone resorption. Journal of Trace Elements in Experimental Medicine 1998; 11: 119–135.

[99] Kwun IS, Cho YE, Lomeda RAR, Shin HI, Choi JY, Kang YH, Beattie JH. Zinc deficiency suppresses matrix mineralization and retards osteogenesis transiently with catch-up possibly through Runx 2 modulation. Bone 2010; 46: 732–741.

[100] Finney L, Vogt S, Fukai T, Glesne D. Copper and angiogenesis: unravelling a relationship key to cancer progression. Clinical and Experimental Pharmacology and Physiology 2009; 36: 88–94.

[101] Gérard C, Bordeleau LJ, Barralet JE, Doillon C. The stimulation of angiogenesis and collagen deposition by copper. Biomaterials 2010; 31: 824–831.

[102] Hu GF. Copper stimulates proliferation of human endothelial cells under culture. Journal of Cellular Biochemistry 1998; 69: 326–335.

[103] Rodríguez J, Ríos S, González M, Modulation of the proliferation and differentiation of human mesenchymal stem cells by copper. Journal of Cellular Biochemistry 2002; 85: 92–100.

[104] Medvecky L, Stulajterova R, Parilak L, Trpcevská J, Durisin J, Barinov S. Influence of manganese on stability and particle growth of hydroxyapatite in simulated body fluid. Colloids and Surfaces A: Physicochemical and Engineering Aspects 2006; 281: 221–229.

[105] Uysal T, Ustdal A, Sonmez M, Ozturk F. Stimulation of bone formation by dietary boron in an orthopedically expanded suture in rabbits. The Angle Orthodontist 2009; 79: 984–990.

[106] Nielsen F. Is boron nutritionally relevant? Nutrition Reviews 2008; 66: 183.

[107] Barrio D, Etcheverry S. Vanadium and bone development: putative signaling pathways. Canadian Journal of Physiology and Pharmacology 2006; 84: 677–686.

[108] Patntirapong S, Habibovic P, Hauschka P. Effects of soluble cobalt and cobalt incorporated into calcium phosphate layers on osteoclast differentiation and activation. Biomaterials 2009; 30: 548–555.

[109] Hoppe A, Güldal NS, Boccaccini AR. A review of the biological response to ionic dissolution products from bioactive glasses and glass-ceramics. Biomaterials 2011; 32: 2757–2774.

[110] Zhang R, Lu Y, Ye L, Yuan B, Yu S, Qin C, Xie Y, Gao T, Drezner MC, Bonewald LF, Feng JQ. Unique roles of phosphorus in endochondral bone formation and osteocyte maturation. Journal of Bone and Mineral Research 2011; 26: 1047–1056.

[111] Meleti Z, Shapiro I, Adams C. Inorganic phosphate induces apoptosis of osteoblast-like cells in culture. Bone 2000; 27: 359–366.

[112] Damen J, Ten Cate J. Silica-induced precipitation of calcium phosphate in the presence of inhibitors of hydroxyapatite formation. Journal of Dental Research 1992; 71: 453–457.

[113] Carlisle EM. Si: an essential element for the chick. Science 1972; 178: 619–621.

[114] Burnell J, Teubner E, Miller A. Normal maturational changes in bone matrix, mineral, and crystal size in the rat. Calcified Tissue International 1980; 31: 13–19.

[115] Bigi A, Foresti E, Gregorini R, Ripamonti A, Roveri N, Shah J. The role of magnesium on the structure of biological apatites. Calcified Tissue International 1992; 50: 439–444.

[116] Del Barrio R, Giro G, Belluci M, Pereira R, Orrico S. Effect of severe dietary magnesium deficiency on systemic bone density and removal torque of osseointegrated implants. International Journal of Oral and Maxillofacial Implants 2010; 25: 1125–1130.

[117] Grynpas M, Marie P. Effects of low doses of strontium on bone quality and quantity in rats. Bone 1990; 11: 313–319.

[118] Marie P, Garba M, Hott M, Miravet L. Effect of low doses of stable strontium on bone metabolism in rats. Mineral and Electrolyte Metabolism 1985; 11: 5–13.

[119] Shorr E, Carter A. The usefulness of strontium as an adjuvant to calcium in the remineralization of the skeleton in man. Bulletin of the Hospital for Joint Diseases Orthopaedic Institute 1952; 13: 59–66.

[120] Moonga B, Dempster D. Zinc is a potent inhibitor of osteoclastic bone resorption *in vitro*. Journal of Bone and Mineral Research 1995; 10: 453–457.

[121] Rico H, Gómez-Raso N, Revilla M, Hernández ER, Seco C, Páez E, Crespo E. Effects on bone loss of manganese alone or with copper supplement in ovariectomized rats: a morphometric and densitometric study. European Journal of Obstetrics & Gynecology and Reproductive Biology 2000; 90: 97–101.

[122] Schwarz K. A bound form of Si in glycosaminoglycans and polyuronides. In: Proceedings of the National Academy of Sciences 1973; 70: 1608–1612.

[123] Carlisle EM. Biochemical and morphological changes associated with long bone abnormalities in Si deficiency. Journal of Nutrition 1979; 110: 1046–1055.

[124] Schwarz K, Milne D. Growth promoting effects of Si in rats. Nature 1972; 239: 333–334.

[125] Seaborn C, Nielson F. Si depravation decreases collagen formation in wounds, bone and ornithine transaminase enzyme activity in liver. Biological Trace Element Research 2002; 89: 251–261.

[126] Bohner M. Silicon-substituted calcium phosphates – a critical view. Biomaterials 2009; 30: 6403-6406.

[127] Arcos D, Rodríguez-Carvajal J, Vallet-Regí M, Silicon incorporation in hydroxylapatite obtained by controlled crystallization. Chemistry of Materials 2004; 16: 2300–2308.

[128] Gibson I, Best SM, Bonfield W. Effect of silicon substitution on the sintering and microstructure of hydroxyapatite. Journal of the American Ceramic Society 2002; 85: 2771–2777.

[129] Li XW, Yasuda HY, Umakoshi Y. Bioactive ceramic composites sintered from hydroxyapatite and silica at 1,200°C: preparation, microstructures and in vitro bone-like layer growth. Journal of Materials Science: Materials in Medicine 2006; 17: 573–581.

[130] Porter AE, Best SM, Bonfield W. Ultrastructural comparison of hydroxyapatite and silicon-substituted hydroxyapatite for biomedical applications. Journal of Biomedical Materials Research A 2004; 68: 133–141.

[131] Curtis A, Wilkinson C. Tophographical control of cells. Biomaterials 1997; 18: 1573–1583.

[132] Botelho CM, Brooks RA, Kawai T, Ogata S, Ohtsuki C, Best SM, Lopes MA, Santos JD, Rushton N, Bonfield W. *In vitro* analysis of protein adhesion to phase pure hydroxyapatite and silicon substituted hydroxyapatite. Key Engineering Materials 2005; 284–286: 461–464.

[133] Ruys AJ. Silicon-doped hydroxyapatite. Journal of the Australian Ceramic Society 1993; 29: 71–80.

[134] Gibson IR, Jha L, Santos J, Best SM, Bonfield W. Effect of Si content on the chemical and phase composition of novel Si substituted hydroxyapatites. In: Bioceramics 1998; pp. 105-108.

[135] Gibson IR, Best SM, Bonfield W. Chemical characterization of silicon-substituted hydroxyapatite. Journal of Biomedical Materials Research 1999; 44: 422-428.

[136] Kim SR, Lee JH, Kim YT, Riu DH, Jung SJ, Lee YJ, Chung SC, Kim YK. Synthesis of Si, Mg substituted hydroxyapatites and their sintering behaviors. Biomaterials 2003; 24: 1389–1398.

[137] Langstaff SD, Sayer M, Smith TJN, Pugh SM, Hesp SA, Thompson WT. Resorbable bioceramics based on stabilized calcium phosphates, part I: rational design, sample preparation and material characterization. Biomaterials 1999; 20: 1727–1741.

[138] Pietak AM, Reid JW, Sayer M, Dunfield D, Smith TJN. Phase formation and evolution in the silicon substituted tricalcium phosphate/apatite system. Biomaterials 2005; 26: 2887–2897.

[139] Reid JW, Tuck L, Sayer M, Fargo K, Hendry JA. Synthesis and characterization of single-phase silicon-substituted alpha-tricalcium phosphate. Biomaterials 2006; 27: 2916–2925.

[140] Tuck L, Astala R, Reid JW, Sayer M, Stott MJ. Dissolution and re-crystallization processes in multiphase silicon stabilized tricalcium phosphate. Journal of Materials Science: Materials in Medicine 2008; 19: 917–927.

[141] Pietak AM, Reid JW, Sayer M. Electron spin resonance in silicon substituted apatite and tricalcium phosphate. Biomaterials 2005; 26: 3819–3830.

[142] Camiré CL, Saint-Jean SJ, Mochales C, Nevsten P, Wang JS, Lidgren L, McCarthy I, Ginebra MP. Material characterization and in vivo behavior of silicon substituted alpha-tricalcium phosphate cement. Journal of Biomedical Materials Research B 2006; 76: 424–431.

[143] Motisuke M, Carrodeguas RG, Zavaglia C. A comparative study between alpha-TCP and Si-alpha-TCP calcium phosphate cement. Key Engineering Materials 2009; 396–398: 201–204.

[144] Su J, Cao L, Yu B, Wang Z, Chen X, Li M. Study on preparation and properties of self-setting silicon hydroxyapatite bone cement. Journal of Inorganic Materials 2011; 26: 55–60.

[145] Cao L, Yu B, Wu G, Su J. Study on adulterate sodium silica apatite cement porous scaffolds for bone defect repair. Journal of Inorganic Materials 2011; 26: 591–596.

[146] Zhao Q, Qian J, Zhou H, Yuan Y, Mao Y, Liu C. *In vitro* osteoblast-like and endothelial cells' response to calcium silicate/calcium phosphate cement. Biomedical Materials 2010; 5: 35004.

[147] Hench LL, Splinter R, Allen W, Greenlee T. Bonding mechanisms at the interface of ceramic prosthetic materials. Journal of Biomedical Materials Research 1971; 5: 117–141.

[148] Cao W, Hench LL. Bioactive materials. Ceramics International 1996; 8842: 493–507.

[149] Kokubo T, Takadama H. How useful is SBF in predicting in vivo bone bioactivity? History 2006; 27: 2907–2915.

[150] Kokubo T. Bioactive glass ceramics: properties and applications. Biomaterials 1991; 12: 155–163.

[151] Oonishi H, Hench LL, Wilson J, Sugihara F, Tsuji E, Matsuura M, Kin S, Yamamoto T, Mizokawa S. A-W glass-ceramic and hydroxyapatite. Journal of Biomedical Materials Research 2000; 51: 37–46.

[152] Kokubo T, Kushitani H, Sakka S, Kitsugi T, Yamamuro T. Solutions able to reproduce *in vivo* surface-structure change in bioactive glass-ceramic. Journal of Biomedical Materials Research 1990; 24: 721–734.

[153] Cho SB, Nakanishi K, Kokubo T, Soga N, Ohtsuki C, Nakamura T, Kitsugi T, Yamamuro T. Dependence of apatite formation on silica gel on its structure: effect of heat treatment. Journal of the American Ceramic Society 1995; 78: 1769–1774.

[154] Oyane A, Kim HM, Furuya T, Kokubo T, Miyazaki T, Nakamura T. Preparation and assessment of revised simulated body fluids. Journal of Biomedical Materials Research A 2003; 65: 188–195.

[155] Takadama H, Hashimoto M, Mizuno M, Kokubo T. Round-robin test of SBF for *in vitro* measurement of apatite-forming ability of synthetic materials. Phosphorus Research Bulletin 2004; 17: 119–125.

[156] Kim HM, Himeno T, Kokubo T, Nakamura T. Process and kinetics of bonelike apatite formation on sintered hydroxyapatite in a simulated body fluid. Biomaterials 2005; 26: 4366–4373.

[157] Bell L, Posner A, Quirk J. Surface charge characteristics of hydroxylapatite and fluorapatite. Nature 1972; 239: 515–517.

[158] Hench LL. Bioceramics: from concept to clinic. Journal of the American Ceramic Society 1991; 74: 1487–1510.

[159] Neo M, Nakamura T, Ohtsuki C, Kokubo T, Yamamuro T. Apatite formation on three kinds of bioactive materials at an early stage *in vivo*: a comparative study by transmission electron microscopy. Journal of Biomedical Materials Research 1993; 27: 999–1006.

[160] Ohtsuki C, Kokubo T, Yamamuro T. Mechanism of apatite formation on $CaO–SiO_2–P_2O_5$ glasses in a simulated body fluid. Journal of Non-Crystalline Solids 1992; 143: 84–92.

[161] Filguerias M, Torre G, Hench LL. Solution effects on the surface reaction of a bioactive glass. Journal of Biomedical Materials Research 1992; 27: 445–453.

[162] Neuman WF, Neuman MW. The chemical dynamics of bone mineral. Chicago: The University of Chicago Press, 1958; p. 34.

[163] Keeting PE, Oursler MJ, Wiegand KE, Bonde SK, Spelsberg TC, Riggs BL. Zeolite A increases proliferation, differentiation, and transforming growth factor β production in normal adult human osteoblast-like cells in vitro. Journal of Bone and Mineral Research 1992; 7: 1281–1289.

[164] Xynos ID, Edgar AJ, Buttery LDK, Hench LL, Polak JM. Gene-expression profiling of human osteoblasts following treatment with the ionic products of Bioglass® 45S5 dissolution. Journal of Biomedical Materials Research 2001; 55: 151–157.

[165] Valerio P, Pereira MM, Goes AM, Leite MF. The effect of ionic products from bioactive glass dissolution on osteoblast proliferation and collagen production. Biomaterials 2004; 25: 2941–2948.

[166] Pietak AM. The role of silicon in Si-TCP bioceramics: a material and biological characterization. PhD Dissertation. Kingston, Ontario, Canada: Queen's University, 2004.

[167] Gibson I, Huang J, Best SM, Bonfield W. Enhanced *in vitro* cell activity and surface apatite layer formation on novel silicon- substituted hydroxyapatites. Bioceramics 1999; 12: 191–194.

[168] Thian ES, Huang J, Best SM, Barber ZH, Bonfield W. Silicon-substituted hydroxyapatite: the next generation of bioactive coatings. Materials Science and Engineering C 2007; 27: 251–256.

[169] Botelho CM, Brooks RA, Best SM, Lopes MA, Santos JD, Rushton N. Human osteoblast response to silicon-substituted hydroxyapatite. Journal of Biomedical Materials Research A 2006; 79: 723–730.

[170] Botelho CM, Brooks RA, Spence G. Differentiation of mononuclear precursors into osteoclasts on the surface of Si-substituted hydroxyapatite. Journal of Biomedical Materials Research A 2006; 78: 709–720.

[171] Patel N, Best SM, Bonfield W, Gibson IR, Hing KA, Damien E, Revell PA. A comparative study on the *in vivo* behavior of hydroxyapatite and silicon substituted hydroxyapatite granules. Journal of Materials Science: Materials in Medicine 2002; 13: 1199–1206.

[172] Hing KA, Revell PA, Smith N, Buckland T. Effect of silicon level on rate, quality and progression of bone healing within silicate-substituted porous hydroxyapatite scaffolds. Biomaterials 2006; 27: 5014–5026.

Chapter 2.

Development and characterization of

Si-doped α-tricalcium phosphate

Table of contents

2.1 Introduction

The interest of doping α-TCP with silicon (Si) is twofold. On one hand, Si can stabilize the α-phase at low temperatures, facilitating the fabrication process. Otherwise high-temperature thermal treatments are required and, in many cases, quenching has to be performed to avoid the reversion of the reconstructive β→α transformation. On the other hand, Si has a specific metabolic role connected to the bone growth, and it has attracted the interest of many scientists who considered that the incorporation of Si into calcium phosphate-based biomaterials was a promising way of improving the bioactivity [1], as well as the osteogenic potential of these materials.

2.2 Objectives

The main aim of this Chapter is to obtain a Si-stabilized α-TCP. In order to fulfill this purpose, the specific objectives of this Chapter are the following:

1. To develop a new method to stabilize α-TCP by Si doping.

2. To assess the effect of Si on the stabilization of the α-TCP phase and on the reversion of β→α transformation.

3. To evaluate the effect of impurities and specific surface area of the starting powders on the Si-stabilization of the α-phase.

4. To determine the effect of different amounts of Si on the stabilization of the α-phase.

5. To physico-chemically characterize the Si-α-TCP in terms of crystalline and amorphous phases, FTIR, lattice parameters and β→α transition temperature, comparing the results with an undoped α-TCP (control).

Figure 2.1 shows a schema of the procedure proposed to obtain Si-stabilized α-TCP (Si-α-TCP) and its Si-free counterpart (α-TCP), as well as the characterizations performed in this Chapter.
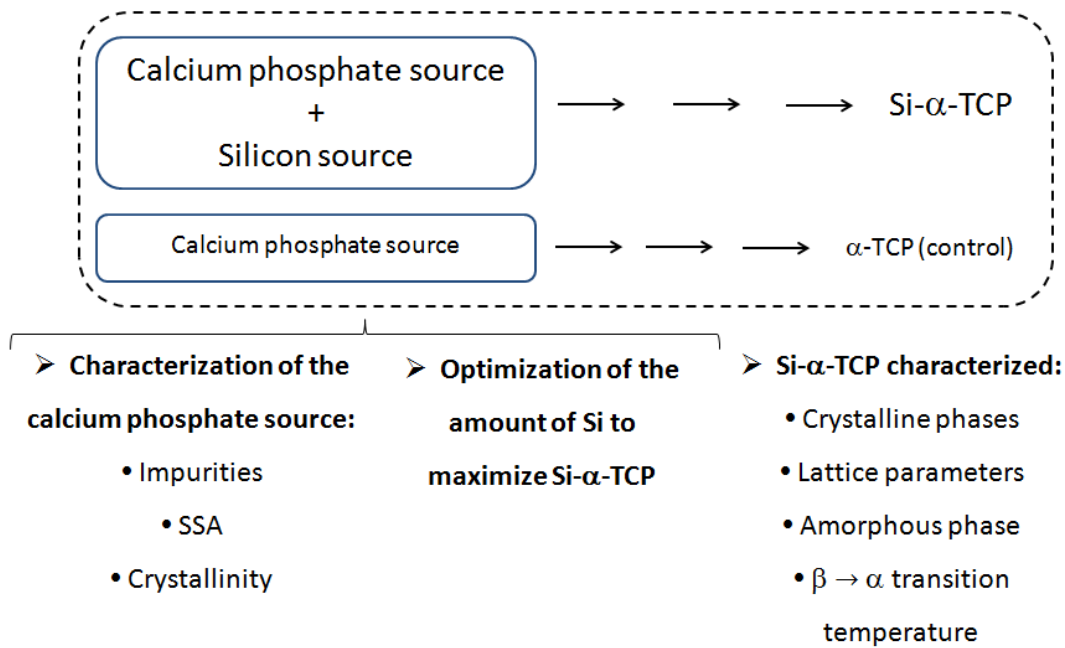
Figure 2.1. Schema of the studies performed in Chapter 2.

2.3 Materials and methods

2.3.1 Reactants

The effect of the addition of Si on the stability of the α-TCP was investigated. Two commercial hydroxyapatites (HA) were evaluated as potential starting reactants: **HA1** (Merck, ref. n. 1.02196.1000; calcined at 1000°C for 4 h) and **HA2** (CalbioChem, ref n. 391948). A colloidal silica in an aqueous dispersion (**SiO₂**, Cab-O-Sperse® 1030K) was used as Si source.

The ratio in which the HA and the SiO_2 were mixed was calculated using two complementary rationales: i) the Si-α-TCP required a Ca/(P+Si) ratio of 1.50, and ii) the HA was assumed to be stoichiometric, $Ca_5(PO_4)_3(OH)$. To fulfill the two established criteria, the reactants were mixed in a SiO_2/HA molar ratio of 0.32. In addition to this SiO_2/HA molar ratio, half and twice this ratio were also used to evaluate the effect of different amounts of Si. In order to evaluate the influence of Si, samples were also prepared with 0 wt% Si. Table 2.1 shows the SiO_2/(SiO_2+HA) wt% and the Si wt% for each SiO_2/HA molar ratio, and the amount added of each reactant.

Table 2.1. SiO$_2$/HA ratios used in this study, shown as SiO$_2$/(SiO$_2$+HA) wt% and Si wt%, and amount of reactants needed in each case.

SiO$_2$/HA (molar ratio)	SiO$_2$/(SiO$_2$+HA) (wt%)	Si (wt%)	Weight HA (g)	Weight SiO$_2$ dispersion (g)	Weight SiO$_2$ (g)
0	0	0		0	0
0.16	1.88	0.88		6.4	1.92
0.32	3.69	1.72	20	12.8	3.84
0.48	5.43	2.54		19.1	5.73

2.3.2 Preparation of Si-doped α-TCP (Si-α-TCP)

HA and SiO$_2$ were mixed at different SiO$_2$/(HA+SiO$_2$) weight ratios, namely 0, 1.88, 3.69 and 5.43, which correspond to 0, 0.88, 1.72 and 2.54 wt% Si, respectively, as detailed in Table 2.1. The procedure was as follows. Twenty g of HA were mixed with the needed amount of SiO$_2$ (Table 2.1). The colloidal SiO$_2$ was previously sonicated with 30 ml of distilled water for 5 min. An extra amount of water of 20 ml was added to the reactants mixture in order to improve its homogeneity. The slurry was milled in a planetary ball mill (Fritsch Pulverisette 6) using 3 agate balls (ϕ = 30 mm), at 350 rpm for 30 min. Finally, the mixture was dried for 24 h in a furnace at 110°C. The resultant powder was sintered at 1250°C for 2 h, with a heating and cooling rate of 5°C/min. No quenching was performed. The sample that resulted in higher amount of Si-stabilized α-TCP was selected for further characterization and was coded as **Si-α-TCP**. Figure 2.2 summarizes the steps followed for the obtaining of Si-α-TCP.
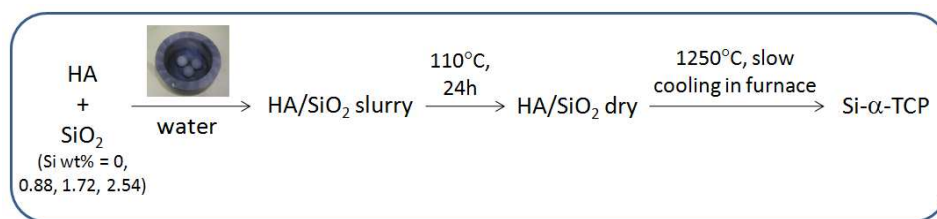
Figure 2.2. Flow chart of the preparation of Si-α-TCP.

Undoped α-TCP was prepared as control. The α-phase was stabilized through a thermal treatment (since no Si was added) followed by a quench. In order to determine the thermal treatment resulting in a higher amount of α-phase, the HA2 (which resulted to be Ca-deficient) was

sintered at different temperatures (1250, 1400 and 1450°C) for 2 h, with a heating rate of 5°C/min, and the sample was quenched in air to retain the α-phase at room temperature. Moreover, a thermal treatment at 1250°C slowly cooling down the temperature was performed in order to determine the influence of the fast cooling in the stabilization of the α-phase.

2.3.3 Physico-chemical characterization of the reactants

The chemical composition of the two HAs was measured in triplicate by inductively coupled plasma (ICP). Ca, P, Na, K, Si and Fe were analyzed by ICP-optical emission spectrometry (ICP-OES, Perkin Elmer Optima 3200 RL), and Mg, Al, Sr, Mn and Zn by ICP-mass spectrometry (ICP-MS, Perkin Elmer Elan 6000). Each HA was dissolved in an acidic aqueous solution (2% HCl) in a concentration of 750 ppm.

The specific surface area (SSA) of the reactants was analyzed in duplicate by N_2 adsorption (Micromeritics ASAP 2020) following the Brunauer–Emmett–Teller method (BET) theory. In the case of SiO_2, the dispersion was previously dehydrated and manually crushed.

The morphology of the commercial HAs was observed with a Scanning Electron Microscope (SEM, JEOL JSM 6400). The samples were mounted on a carbon fiber stuck on a copper foil and their conductance was increased creating a link with silver colloidal suspension between the sample and the carbon layer. The morphology of the colloidal SiO_2 was observed in a Transmission Electron Microscope (TEM, JEOL 1200 EX-II). The samples were prepared by diluting the colloidal dispersion with water, sonicating it for 5 min and, finally, disposing a drop on a cupper grate.

The phase composition of the reactants was assessed by high resolution X-ray powder diffraction (XRD, PANalytical, X'Pert PRO Alpha-1). The XRD measurements were done by scanning in Bragg Brentano geometry using a copper Kα radiation. The experimental conditions were: 2θ scan step 0.020° between 4-100°, counting time 150 s per point, voltage 45 kV and intensity 40 mA. The diffraction patterns were compared to the Joint Committee on Powder Diffraction Standards for HA (JCPDS #9-432), tridymite (JCPDS #42-1401) and β-cristobalite (JCPDS #82-0512) [2].

2.3.4 Physico-chemical characterization of Si-α-TCP

2.3.4.1 Phase quantification by X-ray diffraction

The phase composition of the sintered doped and undoped α-TCP was assessed by high resolution X-ray powder diffraction (XRD, PANalytical, X'Pert PRO Alpha-1). The same experimental conditions that were described in section 2.3.3 were used, including the structural model for α-TCP (JCPDS #9-348) [2]. Rietveld refinements were carried out with three different samples of each formulation in order to quantify the phases present. For this purpose the Inorganic Crystal Structure Database (ICSD) was used, including structural models for α-TCP (ICSD #923), β-TCP (ICSD #6191), HA (ICSD #151414) and β-cristobalite (ICSD #75483) [3]. Quality fits for phase quantification were obtained by refining the instrument displacement, scale factors and lattice parameters using a Thompson-Cox-Hastinge pseudo Voight*Axial divergence, FWHM/shape parameters, preferred orientation and background. The Rietveld refinements were performed using the software package FullProf Suite [4]. XRD spectra analyzed with Rietveld refinement were also used to calculate the lattice parameters of the main phase of each sample.

The presence of an amorphous phase was evaluated by the external standard method, adding a known amount of a zinc oxide standard (ZnO, Panreac ref n. 141786-1210) to the Si-α-TCP (prepared with 2.54 wt% Si) and to the α-TCP. Rietveld refinement was performed, including the structural model for ZnO (ICSD #26170) [3].

2.3.4.2 Phase transition temperatures (differential thermal analysis)

Differential thermal analysis (DTA, Netzsch STA-409) was performed at a heating rate of 5°C/min step from room temperature to 1300°C and an air flow of 80 ml/min. The samples (approximately 60 mg) were placed in Al_2O_3 crucibles and Al_2O_3 powders were used as standard. Four series were analyzed, namely the HA used as main reactant, the SiO_2/HA mixture with 2.54 wt% Si, and the sintered doped (2.54 wt% Si) and undoped α-TCP powders.

2.3.4.3 FTIR analysis

Fourier Transform Infrared spectra (FTIR) from 400 to 4000 cm^{-1} were obtained using an ABB FTLA 2000 spectrometer. A few milligrams of powder was mixed with KBr in a 3.33 wt% ratio,

in order to obtain semi-quantitative results. The mixture was pressed in a 6 mm diameter die at 5 t for 1 min to produce uniform and translucent discs for analysis.

2.3.5. Statistical analysis of the results

A Student's t-test was used to determine the statistically significant differences between the mean values of the different experimental groups. A difference between groups was considered to be significant at $p < 0.05$.

2.4 Results

2.4.1 Physico-chemical characterization of the reactants

2.4.1.1 Hydroxyapatite

The elemental composition data for the HA1 and HA2, measured by ICP, is shown in Table 2.2, and the Ca/P and the (Ca+Na)/P atomic ratio for HA1 and HA2 are shown in Table 2.3. On one hand, the HA1 had a high content of Mg (more than 2,500 ppm) and also had impurities such as Na, Sr, Al, Fe, Si and Mn in the order of hundreds of ppm. The Ca/P ratio of HA1 was close to 1.67, indicating that it was a nearly stoichiometric HA. On the other hand, HA2 had a concentration of Mg ions lower than 10 ppm and a remarkably high Na content (more than 16,000 ppm), which was consistent with its low Ca/P atomic ratio (1.43 ± 0.72), since Na ions could substitute Ca ones in the apatite crystal structure [5]. Thus, the HA2 was non-stoichiometric.

Table 2.2. Elemental compositional data of HA1 and HA2. Ca, P, Na, K, Si and Fe were measured by ICP-OES, and Mg, Al, Sr, Mn and Zn by ICP-MS.

	Ca (wt %)	P (wt %)	Na (ppm)	Mg (ppm)	Sr (ppm)	Al (ppm)
HA1	55.0±8.2	25.9±3.8	300.6±103.3	2534.0±67.6	166.9±6.5	221.0±10.2
HA2	51.7 ± 13.2	27.9 ± 6.8	$1.67 \cdot 10^{4} \pm 1.01 \cdot 10^{3}$	9.8±0.9	49.1±0.7	5.7±2.6

	Fe (ppm)	K (ppm)	Si (ppm)	Mn (ppm)	Zn (ppm)
HA1	212.6±9.6	0.0±0.0	372.2±16.5	90.2±1.6	8.0±3.0
HA2	23.3±7.8	127±41.5	3.1±0.3	0.4±0.1	180.2±88.0

Table 2.3. Atomic ratio of Ca/P and (Ca+Na)/P, and SSA of both HA1 and HA2.

	Ca/P atomic ratio	(Ca+Na)/P atomic ratio	SSA (m^2/g)
HA1	1.64 ± 0.48	1.65 ± 0.98	4.3 ± 0.2
HA2	1.43 ± 0.72	1.51 ± 0.85	71.1 ± 0.6

HA1 and HA2 were characterized in terms of XRD. All peaks corresponded to hydroxyapatite (Figure 2.3), indicating that the reactants did not have any impurity of other crystalline phases. The wide peaks of HA2 indicated that this reactant was poorly crystalline, in contrast to the high crystallinity ascribed to the sharp peaks of HA1.
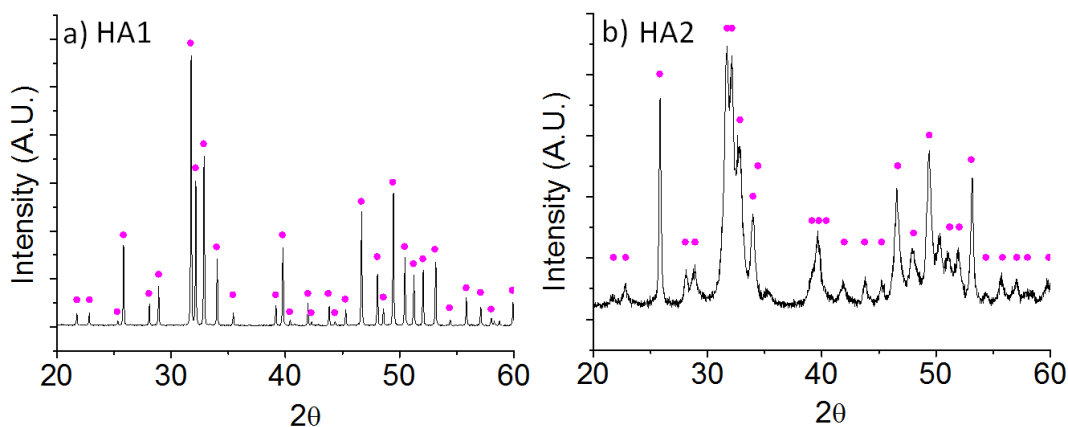
Figure 2.3. X-ray spectra of HA1 and HA2. The theoretical positions of the hydroxyapatite peaks are indicated. A.U. stands for arbitrary units.

HA2 was also characterized by FTIR. The spectrum showed the expected bands for this compound (Figure 2.4) [6]. The experimental values for HA2 were compared with the theoretical ones, as displayed in Table 2.4.
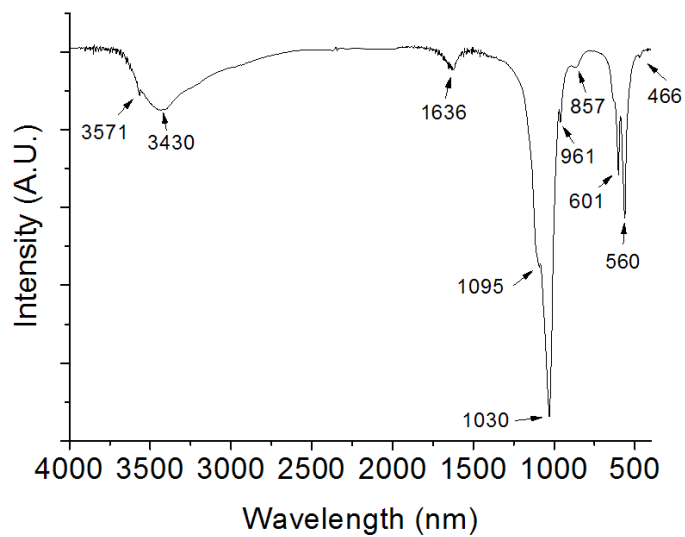

Figure 2.4. FTIR of HA2. A.U. stands for arbitrary units.

Table 2.4. Band assignments for HA2. Some abbreviations were used: sh: shoulder; s: strong band; w: weak; wd: wide.

Band assignment	Experimental values (cm^{-1}) HA2	Frequency (cm^{-1}) according to literature	References
OH stretching	3571 (w)	3572 (w)	[6]
OH water-adsorbed deformation	3430 (wd)	3400	[6]
OH water-adsorbed bending CO_3^{2-}	1636 (m)	1625 / 1648	[6] / [7]
PO_4^{3-}, ν_3	1095 (sh) / 1030 (s)	1085 (sh) / ~ 1035 (vs)	[6] / [6]
PO_4^{3-}, ν_1	961 (w)	965 (w)	[6]
P-O(H), deformation of HPO_4^{2-}, ν_5 CO_3^{2-}	857 (w)	870 (w) / 875	[6] / [7], [8]
OH, libration	-	632 (sh, vw)	[6]
PO_4^{3-}, ν_4	601 (m) / 560 (m)	605 (m) / 565 (m)	[6] / [6]
PO_4^{3-}, ν_2	466 (w)	~ 462 (sh)	[9]

The high SSA of HA2 (Table 2.3) was associated to the presence of nanometric crystals covering the surface of its rhomboedrical particles of 1-75 μm in size (Figure 2.5).
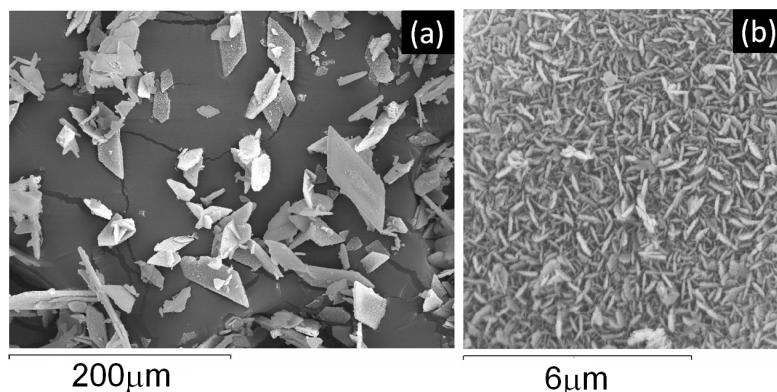
Figure 2.5. Morphology of HA2 observed by SEM: a) particles of powder; b) surface of the particles.

2.4.1.2 SiO$_2$

The dispersion of SiO$_2$ was composed of spherical nanoparticles with a size between 20 and 200 nm (Figure 2.6) and a surface area of 74.5 ± 6.4 m^2/g.
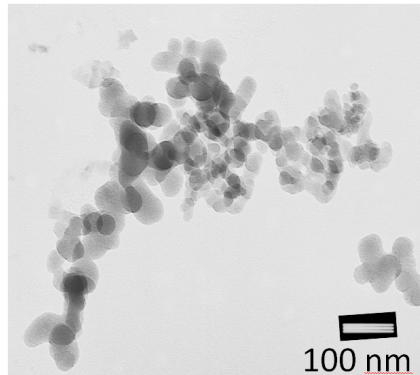
Figure 2.6. Morphology of the colloidal SiO$_2$ observed by TEM.

The X-ray diffraction spectrum of the colloidal SiO$_2$ showed wide bands centered at 22° and around 70° (Figure 2.7 a). The spectrum indicated that the compound had a poor crystallinity, which was associated to its small particle size. However, after a thermal treatment at 1250°C for 2 h, the SiO$_2$ transformed into crystalline compounds, mainly tridymite and a low amount of β-cristobalite (Figure 2.7 b).

Figure 2.7. X-ray spectra of colloidal SiO$_2$: a) raw material, and b) after a thermal treatment at 1250°C for 2 h. A.U. stands for arbitrary units.

The FTIR spectra of the SiO_2 of both the raw material and after sintering it at 1250°C for 2 h, is shown in Figure 2.8. As it can be observed, the thermal treatment slightly modified the bands shape and caused a small shift to them.
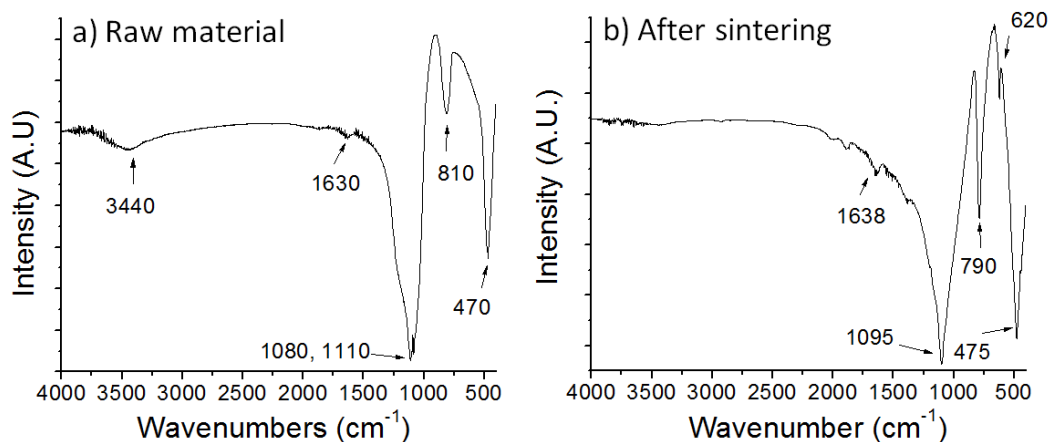
Figure 2.8. FTIR spectra of SiO_2: a) raw material; b) after thermal treatment at 1250°C for 2 h. A.U. stands for arbitrary units.
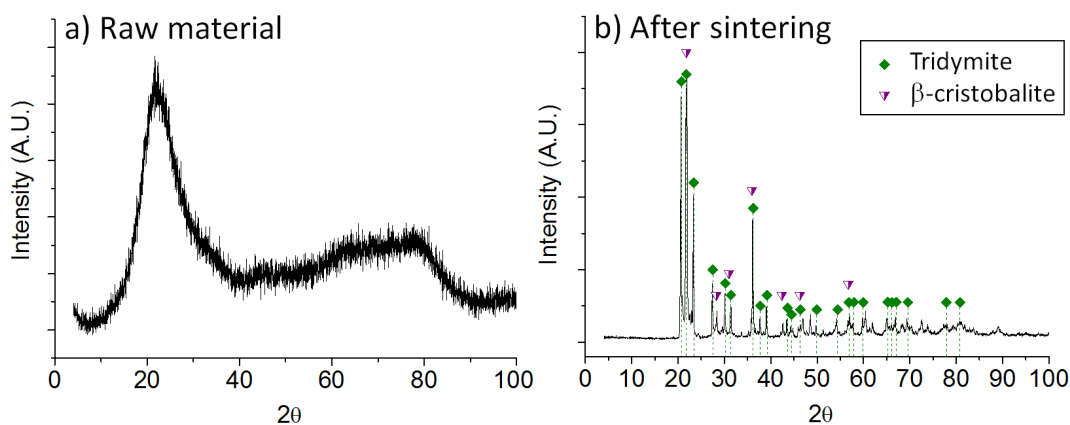
Table 2.5 indicates the bands assignation by comparing the experimental values with those reported in literature.

Table 2.5. Band assignments for SiO_2. Some abbreviations are used: sh: shoulder; s: strong band; w: weak; wd: wide.

Band assignment	Experimental values (cm^{-1})	Frequency (cm^{-1}) according to literature	References
OH water-adsorbed deformation	3440 (wd)	3400	[6]
O = C = O, carbonates	1630 (w)	1643	[7]
O-Si-O, cristobalite	1080, 1110 (s)	1080	[10]
O-Si-O, bending, cristobalite	810 (m)	800	[10]
O-Si-O, bending, cristobalite	470 (s)	481	[10]

2.4.2 Preparation of Si-stabilized α-TCP

2.4.2.1 Effect of the hydroxyapatite used as a starting reactant

Figure 2.9 shows the amount of crystalline phases (quantified by XRD) formed when hydroxyapatite (HA1 or HA2) was mixed with 1.72 wt% SiO_2, followed by sintering at 1250°C and cooling down slowly inside the furnace. The crystalline phases formed when no Si (0 wt%) was added are also indicated. Interestingly, the phases formed when no Si was added depended on the HA used. While HA1 remained untransformed, HA2 decomposed mainly into β-TCP, remaining only about 10 wt% of the initial compound. However, both HA1 and HA2 were partly stabilized into α-TCP when 1.72 wt% Si was added. On one hand, HA1 transformed in a mixture of α-TCP, β-TCP and HA, with a small quantity of β-cristobalite as subproduct. On the other hand, HA2 resulted in α-TCP as a majority phase, with β-TCP and β-cristobalite as subproducts.
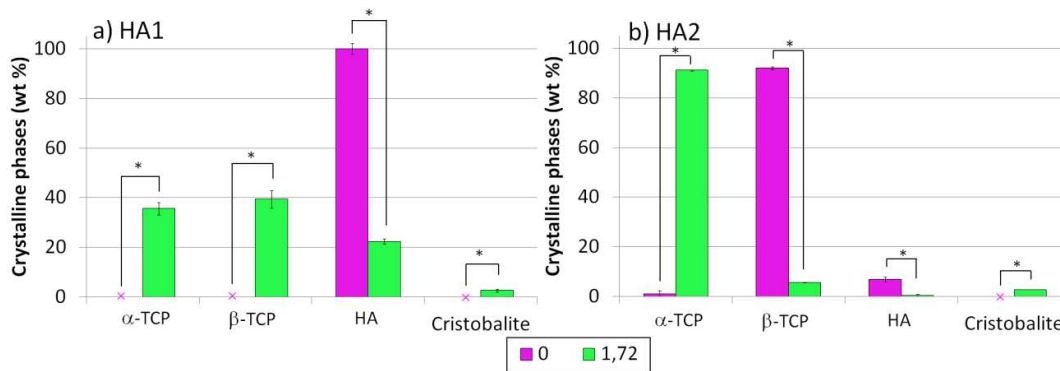
Figure 2.9. Distribution of the crystalline phases formed mixing HA with 0 or 1.72 wt% Si, subsequently sintering at 1250°C and cooling down slowly inside the furnace. Two HAs were used: a) HA1 and b) HA2. Error bars indicate standard deviation, n = 3. * indicates statistically significant differences.

➢ When 1.72 wt% Si was added, a higher amount of Si-α-TCP was obtained when using HA2 as initial reactant. This result was in accordance with the fact that the HA2 had a lower amount of Mg impurities, element known to be a β-stabilizer [11] [12]. Therefore, the **HA2 was selected** and, from now on, it will be coded as **HA**.

2.4.2.2 Effect of the amount of Si added

Figure 2.10 shows the effect of different amounts of Si (0, 0.88, 1.72 and 2.54 wt% Si) on the stabilization of the α-TCP phase after sintering the SiO_2/HA mixture at 1250°C for 2 h, and

subsequent slow cooling inside the furnace. The quantification of the crystalline phases was done including α-TCP, β-TCP, HA and β-cristobalite. The sample that did not contain Si (0 wt% Si) resulted in 1.0 ± 0.1 wt% α-TCP, 89.8 ± 0.3 wt% β-TCP and 9.2 ± 0.3 wt% HA. In contrast, the samples prepared with Si contained α-TCP as the main phase, with decreasing amounts of β-TCP when the amounts of added SiO_2 increased. The sample with 2.54 wt% Si resulted in a nearly single-phase α-TCP, namely 94.4 ± 1.8 wt% α-TCP, 2.2 ± 0.8 wt% β-TCP, 0.2 ± 0.1 wt% HA and 3.2 ± 1.0 wt% β-cristobalite, according to the Rietveld refinement. Thereby, this was the sample selected for further characterization, and was coded as **Si-α-TCP**.
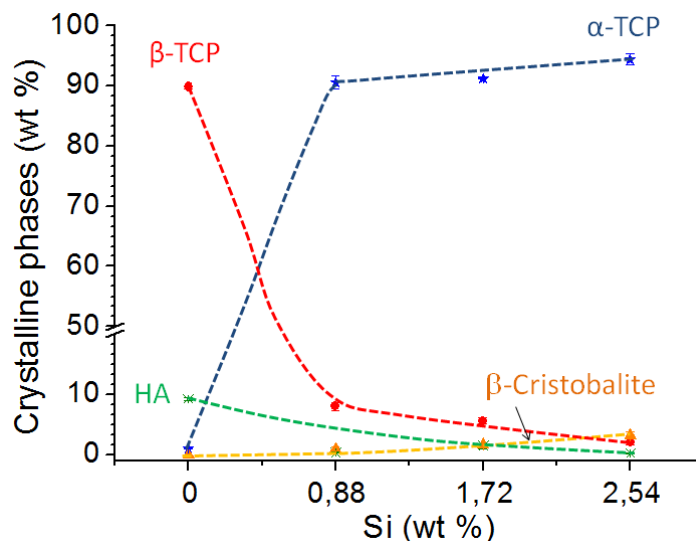
Figure 2.10. Crystalline phase composition as function of the Si wt%. The samples were sintered at 1250°C for 2h and cooled down in the furnace. Error bars indicate standard deviation, n = 3. The amount of α-TCP, β-TCP and HA showed statistically significant differences between 0 Si wt% and the other amounts of Si; the amount of β-TCP also showed statistically significant differences between both 0.88 and 1.72 wt% and 2.54 wt%; the amount of β-cristobalite showed statistically significant differences between 0 Si wt% and both 1.72 and 2.54 wt%.

Figure 2.11 shows a representative Rietveld profile analysis assuming the presence of α-TCP, β-TCP, HA and β-cristobalite for the Si-α-TCP.
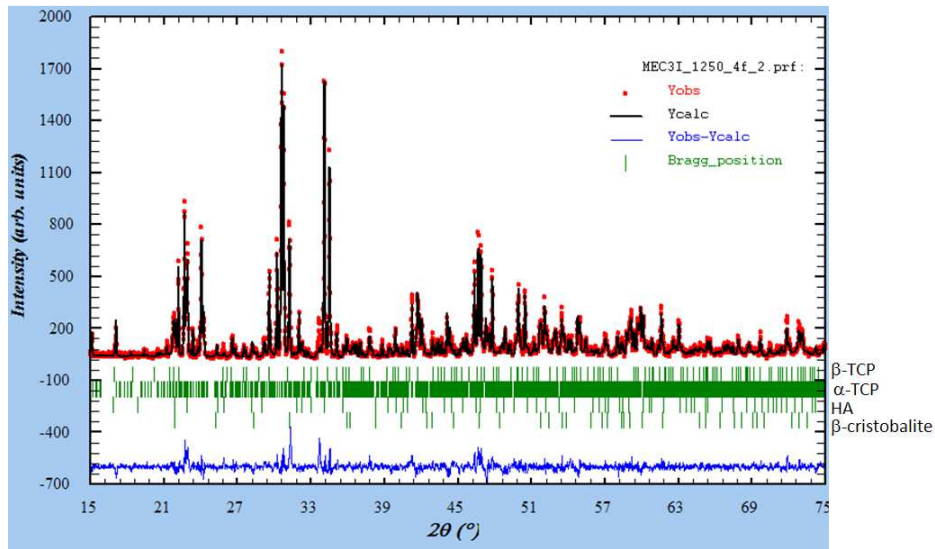
Figure 2.11. XRD pattern of HA mixed with 2.54 wt% Si sintered at 1250°C for 2 h and cooled down in the furnace, refined using the Rietveld method. The vertical lines mark the positions of the calculated Bragg peaks of the phases included in the refinement, which from top to bottom were β-TCP, α-TCP, HA and β-cristobalite.

➢ The amount of Si selected for the continuation of the study was **2.54 wt%**.

2.4.3 Preparation of undoped α-TCP

As previously observed, when HA2 (without any addition of Si) was sintered, cooling down the sample slowly inside the furnace, the phase stabilized was β-TCP (Figure 2.9 b). This indicated that the initial HA, which in fact was a CDHA (Ca/P = 1.43 ± 0.72), was transformed into TCP during the thermal treatment. However, the α-phase was only stabilized if Si was added (Figure 2.10). This result showed that the HA did not retain the α-TCP polymorph upon slow cooling down.

An alternative procedure to stabilize the α-phase without the addition of any external compound is quenching the sample in air right after the thermal treatment. Therefore, HA was submitted to several thermal treatments that included the quenching of the sample in order to find out which of them resulted in a higher amount of α-phase. Figure 2.12 confirms that the α-phase was only stabilized if the sample was quenched after the heating process, otherwise being formed β-TCP. As higher was the maximum heating temperature, the amount of HA decomposed and transformed into TCP was increased. Thus, a Si-free α-TCP (coded as **α-TCP**) was prepared by heating the HA at 1450°C for 2 h, followed by quenching the sample in air.
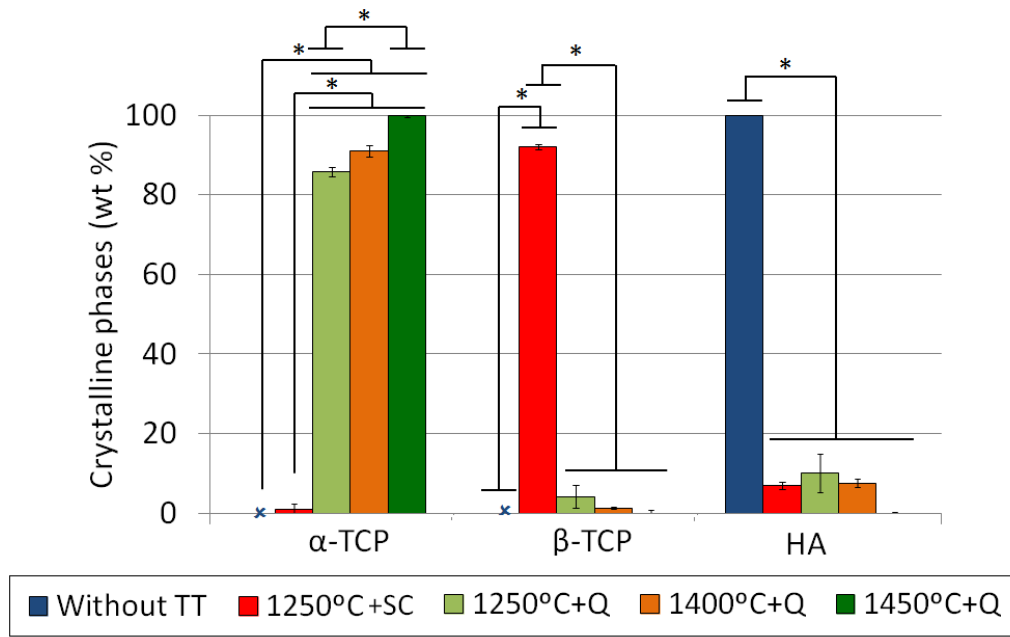
Figure 2.12. Crystalline phases resulting of performing the indicated thermal treatment to HA. "Without TT" stands for "without thermal treatment", "+SC" stands for slow cooling down, and quenching is indicated as "+Q". Every thermal treatment lasted for 2 h. Error bars indicate standard deviation, n = 2. * indicates statistically significant differences.

The conditions selected in order to prepare both Si-α-TCP and α-TCP are summarized in Figure 2.13.

➤ **Preparation Si-α-TCP:**
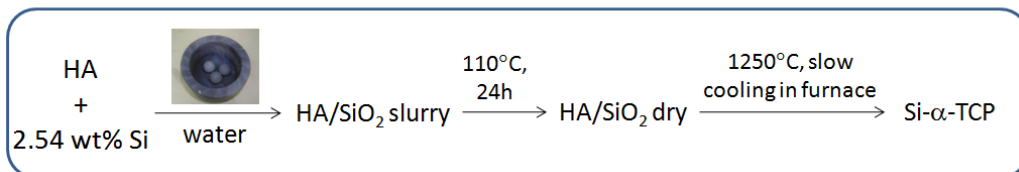
➤ **Preparation α-TCP (control):**
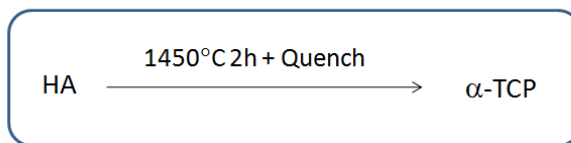
Figure 2.13. Flow charts in which the methodology followed to prepare Si-α-TCP and the thermal treatment applied to prepared α-TCP are indicated. HA stands for HA2, which was the calcium phosphate source selected.

2.4.4 Characterization of Si-α-TCP and α-TCP

2.4.4.1 Phase transition temperatures

The effect of SiO_2 addition in the phase transition temperatures was analyzed by differential thermal analysis (DTA). The curves obtained for the HA powder, the SiO_2/HA mixture prepared with 2.54 wt% Si, the Si-α-TCP and the α-TCP are shown in Figure 2.14. The heating curves for the SiO_2/HA mixture and the HA were similar (Figure 2.14 a and b). Two endothermic peaks, attributed to the loss of surface-bound water and to the loss of lattice water were respectively observed around 90°C and 510°C [13]. An exothermic peak indicated the HA transformation into β-TCP at 713°C, which in turn transformed into the α-form through an endothermic reaction upon subsequent heating, at 1148°C. When the HA sample was cooled down, an exothermic peak corresponding to the reverse transformation of α to β-TCP was observed at 996°C (Figure 2.14 b). Interestingly, this peak did not appear in the SiO_2/HA mixture (Figure 2.14 a), indicating that the α-phase was stabilized down to room temperature. When the α-TCP was heated up (Figure 2.14 d), an exothermic peak at 684°C was attributed to the transformation into β-TCP, whereas in the Si-α-TCP (Figure 2.14 c) only a diffuse band appeared around 750°C. The β to α endothermic transformation was produced upon subsequent heating, around 1150°C in both samples. During the cooling process, the α-TCP showed the expected exothermic peak corresponding to the α to β transformation at 978°C, whereas this transformation was not detected in the Si-α-TCP.
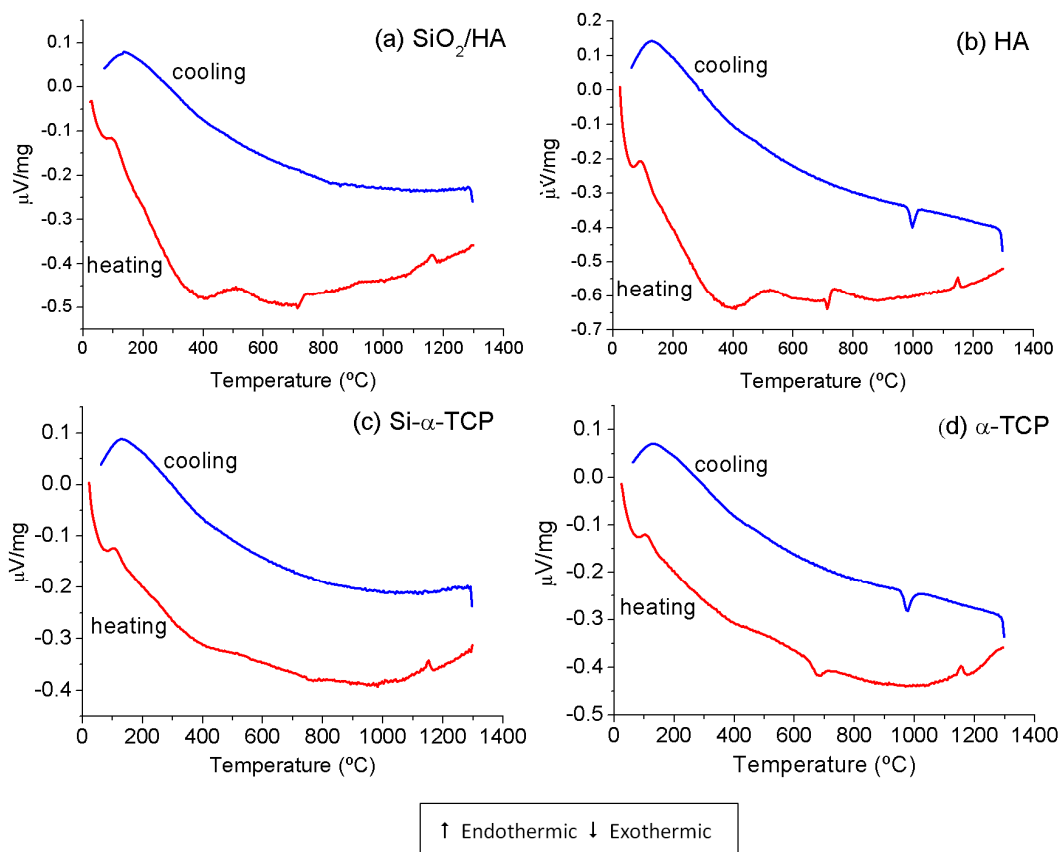
Figure 2.14. DTA analysis of reactants and products: a) SiO$_2$/HA powder mixture with 2.54 wt% Si, with no thermal treatment, b) HA, c) Si-α-TCP, and d) α-TCP.

2.4.4.2 Lattice parameters

The evaluation of the lattice parameters of both Si-α-TCP and α-TCP, calculated from the XRD spectra by the Rietveld method, showed no statistically significant differences between them (p > 0.05), as indicated in Table 2.6. However, the b and β parameters were larger for the experimental α-phases than for the α-TCP reported in literature [14], and the c parameter was slightly shorter.

Table 2.6. Lattice parameters obtained by Rietveld refinement method of Si-α-TCP and undoped α-TCP. The data indicate mean ± standard deviation, n= 3.

	a (Å)	b (Å)	c (Å)	β (°)
Si-α-TCP	12.9002 ± 0.001	27.3796 ± 0.002	15.1977 ± 0.001	126.4328 ± (0.004
α-TCP	12.8999 ± 0.0089	27.3789 ± 0.0143	15.2009 ± 0.0183	126.4368 ± 0.0384
α-TCP, reported in literature [14]	12.887 ± 0.002	27.280 ± 0.004	15.219 ± 0.002	126.20 ± 0.001

2.4.4.3 Amorphous phase

An external standard was added to the sample and the amorphous phase was quantified from the XRD spectra by the Rietveld method. The amount of amorphous phase was 13.8 ± 0.3 wt% for Si-α-TCP and 11.2 ± 0.2 wt% for α-TCP.

2.4.4.4 FTIR analysis

The FTIR spectra of α-TCP and of Si-stabilized α-TCP prepared with different Si wt%, are shown in Figure 2.15.
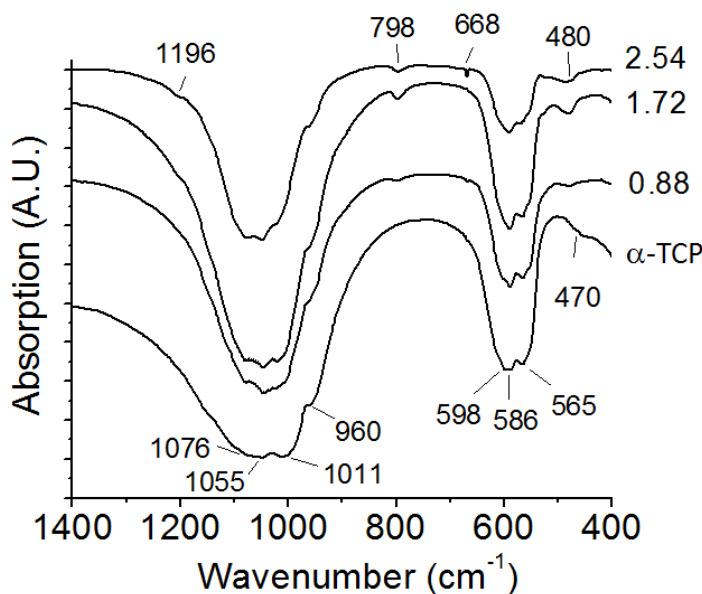
Figure 2.15. FTIR spectra of Si-α-TCP prepared with SiO_2/HA mixtures with 0.88, 1.72 and 2.54 wt% of Si, subsequently sintered at 1250°C for 2 h and cooled down slowly. The α-TCP spectra is also showed. A.U. stands for arbitrary units.

The wavenumbers of the α-TCP bands were in accordance with those reported in the literature [8], as displayed in Table 2.7. When the amount of added SiO_2 increased, the wide bands corresponding to ν_3 stretching (969-1155 cm^{-1}) and ν_4 bending (540-640 cm^{-1}) decreased their intensity and got narrower. This trend was associated to the increasing content of α-TCP. The bands located at 480, 798 and 1196 cm^{-1}, that slightly increased their intensity with the amount of SiO_2 added, were assigned to the O-Si-O vibration of β-cristobalite [10] [15]. In the sample with 2.54 wt% Si, a small sharp band was detected at 668 cm^{-1}. This band was also detected in a previous study on attenuated total reflection infrared spectroscopy of Si-stabilized tricalcium phosphate [16] and it can be attributed to the formation of $Si_2O_7^{6-}$ groups within the α-TCP structure [16] [17].

Table 2.7. Band assignments for α-TCP and Si-α-TCP. Some abbreviations were used: sh: shoulder; s: strong band; w: weak; wd: wide.

Band assignment	Experimental values (cm^{-1})		Frequency (cm^{-1}) according to literature	References
	α-TCP	Si-α-TCP		
	969-1155 (wd, s)	974-1144 (wd, s)	950-1100 (wd)	[8]
	-	-	1136 (sh)	[8]
	-	-	1100 (sh)	[8]
PO_4^{3-}, ν_3 stretching	1076 (sh)	1079 (sh)	1078 (sh)	[8]
	1055 (sh)	1048 (sh)	1045 (s)	[8]
	1011 (sh)	1018 (sh)	1010 (sh)	[8]
	-	-	990 (sh)	[8]
PO_4^{3-}, ν_1 stretching	960 (sh)	960 (sh)	960 (s)	[8]
	540-640 (wd)	543-632 (wd)	~ 550-600 (wd)	[8]
	-	-	609	[8]
(PO_4^{3-}) ν_4 bending	598 (sh)	-	595	[8]
	586 (sh)	586 (sh)	583	[8]
	565 (sh)	565 (sh)	562	[8]
PO_4^{3-}, ν_2	470 (w)	472 (w)	462 (w)	[8]
O-Si-O, bending, cristobalite	-	480 (w)	481	[10]
$Si_2O_7^{6-}$, bridging	-	668 (w)	668	[16]
O-Si-O, bending, cristobalite	-	798 (w)	800	[10]
O-Si-O, cristobalite	-	1196 (w)	1192	[15]

2.5 Discussion

α-TCP, which is a widely used compound for the preparation of apatitic cements, was stabilized by a simple process that consisted in mixing hydroxyapatite (HA) with silicon oxide (SiO_2), subsequently sintering the mixture and cooling it down slowly inside the furnace. A straight advantage of this process is that the α-phase is obtained without performing any quench after the thermal treatment, which simplifies substantially the production of the α-TCP.

Sayer *et al.* [18] [19] [20] [21] prepared Si-α-TCP following several steps. They precipitated hydroxyapatite via a basic precipitation reaction in an ammoniated aqueous mixture and,

afterwards, added the Si source either as an organic compound or as SiO_2. Subsequently, the sols were sprayed using a spray dryer and, finally, thermal treatments were performed, which aimed both at the removal of water and NO_2 associated with the precursor reactants and at the incorporation of Si to the crystalline structure of the calcium phosphate. The main differences between the strategy followed by Sayer *et al.* and the methodology explained in this Chapter are: i) the reactants used, in our case being inorganic commercial compounds, and ii) the procedure to mix these reactants, in this work, was done by ball milling, including some water to improve their homogenization. The methodology followed in this work resulted in a nearly single phase Si-α-TCP with a high reproducibility, which was ascribed to the simplicity and the low number of steps of the overall process.

Another work aiming at the Si-stabilization of α-TCP that followed a similar methodology was published by Li *et al.* [22]. In fact, Li *et al*. also mixed a commercial HA with SiO_2 using a ball mill. However, their mixture contained 10 wt% of SiO_2 (almost 5 wt% Si) and it was milled for 24 h; subsequently, the mixture was sintered at 1200°C to stabilize the α-phase. Li *et al*. reported that more than 24 wt% HA remained and that an amorphous phase was formed, which increased by adding higher quantities of SiO_2.

2.5.1 Factors influencing on the Si-stabilization of α-TCP

The effectiveness to stabilize α-TCP with Si was evaluated with two HAs and adding different amounts of Si.

2.5.1.1 Calcium phosphate source (HA)

It is well known that the relative stability of the different TCP polymorphs is strongly influenced by the presence of some impurities. For instance, Mg has been shown to increase the β→α transformation temperature, acting in practice as a beta-stabilizer [23] [11] [12]. On the other hand, it has been proved that Si stabilizes the alpha phase down to low temperatures [24] [25] [26] [27].

Two commercial HAs were used in this work, which differed in their impurities content (Table 2.2), their Ca/P ratio (Table 2.3), their SSA (Table 2.3) and their crystallinity (Figure 2.3). The

HA1, which was nearly stoichiometric, had impurities of betagen elements such as Na, Mg, Sr, Al and Fe. Mg, which is an ion known to stabilize the β-phase even in low concentrations [23] [11] [28] [12] [29], was the betagen element found in a higher amount (thousands of ppm). The elemental composition of the HA2 was very different, with less than 10 ppm of Mg, and less than 50 ppm of other betagen impurities such as Sr, Fe and Al. In contrast, HA2 had a low Ca/P ratio, indication that the HA was deficient in Ca, which was associated to the high concentration of Na ions occupying Ca sites [5]. The (Ca+Na)/P ratio of HA2 was 1.51 (calculated from the elemental composition resulting from the ICP-OES analysis).

The two HAs had very different SSA (Table 2.3). The low SSA of HA1 was due to the calcination performed to this compound, which increased its crystallinity as indicated by the sharp peaks of the XRD spectrum (Figure 2.3). In contrast, the HA2 had a very high SSA, due to the nanometric crystals covering its particles (Figure 2.5), which were the reason for the poor crystallinity of the compound, as observed by the wide peaks of the XRD spectrum.

When the HAs (without Si) were submitted at 1250°C, cooling down the samples inside the furnace, different results were observed. While HA1 remained stable, HA2 was decomposed mainly into β-TCP (Figure 2.9). The different thermostability of the HAs was associated to their distinct Ca/P ratio. Therefore, the nearly stoichiometric HA1 had a high thermostability, while the non-stoichiometric HA2 was not thermostable.

The initial studies were performed adding Si to the two HAs in order to evaluate the stabilization of the α-TCP after sintering the mixture and cooling it down slowly. It is interesting to note that, in these conditions, HA1 was decomposed into α-TCP, β-TCP and HA when 1.72 wt% Si was added (Figure 2.9). In contrast, HA2 resulted in about 90 wt% α-TCP by adding Si. The higher stability of α-TCP when using HA2 was associated to two different factors: i) the lower amount of betagenic impurities, such as Mg (less than 10 ppm), Sr, Fe and Al [23] of HA2, and ii) the higher SSA of HA2, which enhanced an intimate contact between the HA and the SiO_2. However, it was not possible to ascribe the stability of the α-phase to only one of these properties. Thus, **the calcium deficient hydroxyapatite (HA2) was selected** to synthesize Si-doped α-TCP.

2.5.1.2 Amount of Si

According to DTA (Figure 2.14) and to XRD (Figure 2.9 and 2.10), when no Si was added to HA2, the α-TCP phase that was formed over 1148°C was not retained upon slow cooling and it completely reverted to β-TCP, in spite of the low Mg concentration. Unlike what was reported in other studies [11] [12], it was necessary to quench the samples to obtain α-TCP. This behavior could be attributed to the high amount of Na impurities in the HA, which have also been reported to increase the stability of the β polymorph [30].

The minimum amount of Si necessary to effectively stabilize the α-phase is still not clear, since it depends on many factors, namely the Ca/(P+Si) ratio of the system, the method of introducing Si and the sintering conditions [27]. In the current work, it was observed that although 0.88 wt% Si was enough to produce 89.7 ± 1.1 wt% Si-α-TCP, an excess of Si (up to 2.54 wt% Si) increased the amount of stabilized α-TCP, together with residual β-cristobalite (Figure 2.10).

It is interesting to note that β-cristobalite is not the stable allotropic form of silicon oxide at 1250°C. In fact, the stable phase at this temperature was tridymite, which is the one that was obtained when sintering the colloidal SiO_2 dispersion at 1250°C in absence of hydroxyapatite (Figure 2.7 b). However, the presence of both Ca and Na are known to decrease the tridymite→β-cristobalite phase transformation temperature from 1470°C to lower values [31].

2.5.2 Characterization of Si-α-TCP and α-TCP

After the initial studies, the HA2, a calcium deficient hydroxyapatite that did not retain the α-phase at room temperature (Figure 2.10 and 2.14), and had low amounts of betagen elements (Table 2.2), was used as initial reactant. The sample containing 2.54 wt% Si, which was the one producing the highest amount of α-phase, was coded as **Si-α-TCP**.

The addition of SiO_2 to HA stabilized and retained the α-phase upon slow cooling, as assessed by XRD and DTA (Figures 2.10 and 2.14). The α→β retransformation did not take place when cooling down the Si-doped samples (Figure 2.14 a and c), in contrast to what happened in the Si-free samples, that showed this phase reversion (Figure 2.14 b and d). However, although some studies reported a reduction of the β→α transformation temperature with Si addition [24]

[25] [26] [27], in our case, very similar β→α transformation temperatures (1148-1150°C) were observed for both, the Si-free and the Si-containing samples. It is interesting to note that without the addition of Si, nearly pure α-TCP was produced only if the HA was heated up to 1450°C and quenched afterwards in order to stabilize the α-phase (Figure 2.12).

In addition to the crystalline phases, 13.8 ± 0.3 wt% and 11.2 ± 0.2 wt% of an amorphous phase was detected in Si-α-TCP and α-TCP, respectively. The existence of an amorphous phase in coexistence with Si-stabilized α-TCP has been previously associated with the formation of a non-crystalline Ca-Si-P-O phase and was directly related with the presence of Si in excess [19] [22]. However, the fact that an amorphous phase was also detected in the non-doped TCP would rather suggest the formation of a glassy phase in the system $CaO-Na_2O-P_2O_5$ [32]. The amorphous phase was expected to remain preferentially in the grain boundaries of the crystalline phase, as determined by Li *et al.* in SEM micrographs [22].

The α-TCP obtained had larger b and β parameters than the theoretical one, reported by Mathew [14], as shown in Table 2.6. The enlargement of the α-TCP lattice was associated to the lattice distortions produced by the presence of other ionic substitutions like Na. However, no statistically significant changes were detected in the lattice parameters of the Si-stabilized α-TCP (Table 2.6), unlike previous works that indicate the enlargement of the unit cell volume with Si incorporation [19] [21]. In fact, in the current study, the preexisting lattice distortions caused by Na ions may mask the effect of Si substitution in the modification of lattice parameters.

Finally, the comparison of the FTIR spectra of Si-containing and Si-free samples confirmed the presence of β-cristobalite in the Si-containing samples (Figure 2.15). Moreover, in addition to the β-cristobalite-related bands at 480, 668 and 798 cm^{-1}, a band at 668 cm^{-1} was also found in the sample with highest Si content, which was previously detected in Si-stabilized TCP and adscribed to $Si_2O_7^{6-}$ groups [16]. *Ab initio* calculations performed by Yin *et al.* suggested that $Si_2O_7^{6-}$ species could be formed within the Si-α-TCP structure after the incorporation and fusion of SiO_4^{4-} groups into the crystal lattice, through an oxygen-vacancy formation mechanism [17]. The incorporation of Si into the crystal lattice did not affect the position of the bands associated with phosphate group vibrations. This was in accordance with the close vibration energies of both Si-O and P-O bonds, since Si and P have a similar dipolar movement and atomic weight [18].

2.6 Conclusions

The conclusions that can be extracted from this Chapter are the following:

1. A new method to stabilize α-tricalcium phosphate with silicon was developed and optimized. The high temperature polymorph α-tricalcium phosphate was stabilized by the presence of silicon, which inhibited the reversion of the β→α transformation. This was achieved by the addition of 2.54 wt% colloidal silicon oxide to a calcium deficient hydroxyapatite and subsequent sintering at 1250°C for 2 h, followed by slow cooling. In the Si-free sample α-tricalcium phosphate completely reverted to the β-polymorph.

2. The addition of Si did not modify the β→α transformation temperature, which took place between 1148 and 1150°C regardless the presence of Si.

3. The Si-stabilization of the α-phase was enhanced using a calcium deficient hydroxyapatite that contained a low amount of Mg impurities and had a high SSA.

4. Fourier Transform Infrared analysis suggested the formation of $Si_2O_7^{6-}$ groups within the α-TCP structure, following an oxygen-vacancy formation mechanism.

5. No significant modifications in the lattice parameters were detected in the Si-α-TCP, probably because the crystal lattice was already distorted by a high quantity of Na ions present in the starting reactants.

6. Both Si-α-TCP and α-TCP contained about 10 wt% amorphous phase, which was attributed to the formation of a non-crystalline Ca-Na-P-O phase due to the high amount of Na impurities in the HA.

7. The Si in excess was transformed into β-cristobalite during the thermal treatment, instead of tridymite, probably due to the presence of both Ca and Na in the HA, decreasing the tridymite→β-cristobalite phase transformation temperature to lower values.

2.7 Acknowledgements

2.8 References

[1] Boanini E, Gazzano M, Bigi A. Ionic substitutions in calcium phosphates synthesized at low temperature. Acta Biomaterialia 2010; 6: 1882–1894.

[2] Joint Committee for Powder Diffraction Studies (JCPDS). International Center for Diffraction Data and American Society for Testing Materials. Powder diffraction file (Inorganic and Organic). Swarthmore (USA), 1991.

[3] Inorganic Crystal Structure Database (ICSD). Institut Laue-Langevin (ILL), Grenoble, France.

[4] Rodríguez-Carvajal J. Fullprof.2k Software. CEA-CNRS; 2007.

[5] Lin FH, Liao CJ, Chen KS, Sun JS. Preparation of high-temperature stabilized beta-tricalcium phosphate by heating deficient hydroxyapatite with $Na_4P_2O_7$ x $10H_2O$ addition. Biomaterials 1998; 19: 1101-1107.

[6] Ginebra MP, Fernández E, De Maeyer EAP, Verbeeck RMH, Boltong MG, Ginebra J, Driessens FCM, Planell JA. Setting reaction and hardening of an apatitic calcium phosphate cement. Journal of Dental Research 1997; 76: 905–912.

[7] Gibson IR, Best SM, Bonfield W. Chemical characterization of silicon-substituted hydroxyapatite. Journal of Biomedical Materials Research 1999; 44: 422-428.

[8] Radin S, Ducheyne P, The effect of calcium phosphate ceramic composition and structure on *in vitro* behavior, II: precipitation. Journal of Biomedical Materials Research 1993; 27: 25–34.

[9] Berry EE. The structure and composition of some calcium deficient apatites. Journal of Inorganic and Nuclear Chemistry 1967; 29: 317-327.

[10] Mollah M, Promreuk S, Schennach R, Cocke D, Guler R. Cristobalite formation from thermal treatment of Texas lignite fly ash. Fuel 1999; 78: 1277–1282.

[11] Enderle R, Götz-Neunhoeffer F, Göbbels M, Müller FA, Greil P. Influence of magnesium doping on the phase transformation temperature of beta-TCP ceramics examined by Rietveld refinement. Biomaterials 2005; 26: 3379–3384.

[12] Carrodeguas RG, De Aza AH, Turrillas X, Pena P, De Aza S. New Approach to the β→α polymorphic transformation in magnesium-substituted tricalcium phosphate and its practical implications. Journal of the American Ceramic Society 2008; 91: 1281–1286.

[13] Elliott JC. Structure and chemistry of the apatites and other calcium orthophosphates. Amsterdam: Elsevier, 1994.

[14] Mathew M, Schroeder W, Dickens B, Brown W. The crystal structure of α-$Ca_3(PO_4)_2$. Acta Crystallographica B: Structural Science 1977; 33: 1325–1333.

[15] Simon I, McMahon H. Study of the structure of quartz, cristobalite, and vitreous silica by reflection in Infrared. The Journal of Chemical Physics 1956; 21: 23–30.

[16] Dunfield D, Sayer M, Shurvell HF. Total attenuated reflection infrared analysis of silicon-stabilized tri-calcium phosphate. The Journal of Physical Chemistry B 2005; 109: 19579-19583.

[17] Yin X, Stott MJ. Theoretical insights into bone grafting silicon-stabilized alpha-tricalcium phosphate. The Journal of Chemical Physics 2005; 122: 024709-1–9.

[18] Langstaff SD, Sayer M, Smith TJN, Pugh SM, Hesp SA, Thompson WT. Resorbable bioceramics based on stabilized calcium phosphates, part I: rational design, sample preparation and material characterization. Biomaterials 1999; 20: 1727–1741.

[19] Sayer M, Stratilatov AD, Reid J, Calderin L, Stott MJ, Yin X, MacKenzie M, Smith TJN, Hendry JA, Langstaff SD. Structure and composition of silicon-stabilized tricalcium phosphate. Biomaterials 2003; 24: 369–382.

[20] Pietak AM, Reid JW, Sayer M, Dunfield D, Smith TJN. Phase formation and evolution in the silicon substituted tricalcium phosphate/apatite system. Biomaterials 2005; 26: 2887–2897.

[21] Reid JW, Tuck L, Sayer M, Fargo K, Hendry JA. Synthesis and characterization of single-phase silicon-substituted alpha-tricalcium phosphate. Biomaterials 2006; 27: 2916–2925.

[22] Li XW, Yasuda HY, Umakoshi Y. Bioactive ceramic composites sintered from hydroxyapatite and silica at 1,200°C: preparation, microstructures and *in vitro* bone-like layer growth. Journal of Materials Science: Materials in Medicine 2006; 17: 573–581.

[23] Ando J. Tricalcium phosphate and its variation. Bulletin of the Chemical Society of Japan 1958; 31: 196–201.

[24] Fix W, Heymann H, Heinke R. Subsolidus relations in the system $2CaO \cdot SiO_2 \cdot 3CaO \cdot P_2O_5$. Journal of the American Ceramic Society 1969; 52: 346–347.

[25] Nurse RW, Welch J, Gutt W. High-temperature phase equilibria in the system dicalcium silicate-tricalcium phosphate. Journal of the Chemical Society 1959; 220: 1077–1083.

[26] Barnes MW, Klimkiewicz M, Brown PW. Hydratation in the system Ca_2SiO_4-$Ca_3(PO_4)_2$ at 90^oC. Journal of the American Ceramic Society 1992; 75: 1423–1429.

[27] Pietak AM, Reid JW, Stott MJ, Sayer M. Silicon substitution in the calcium phosphate bioceramics. Biomaterials 2007; 28: 4023–4032.

[28] Reid JW, Fargo K, Hendry JA, Sayer M. The influence of trace magnesium content on the phase composition of silicon-stabilized calcium phosphate powders. Materials Letters 2007; 61: 3851–3854.

[29] Motisuke M, García Carrodeguas R, Zavaglia CAC. Mg-free precursors for the synthesis of pure phase Si-doped α-$Ca_3(PO_4)_2$. Key Engineering Materials 2008; 361–363: 199–202.

[30] Matsumoto N, Yoshida K, Hashimoto K, Toda Y. Thermal stability of β-tricalcium phosphate doped with monovalent metal ions. Materials Research Bulletin 2009; 44: 1889–1894.

[31] Ning CQ, Greish Y, El-Ghannam A. Crystallization behavior of silica-calcium phosphate biocomposites: XRD and FTIR studies. Journal of Materials Science: Materials in Medicine 2004; 15: 1227-1235.

[32] Navarro ME, Ginebra MP, Clement J, Martinez S, Avila G, Planell JA. Physicochemical degradation of titania-stabilized soluble phosphate glasses for medical applications. Journal of the American Ceramic Society 2003; 86: 1345–1352.

Chapter 3.

Development of silicon-doped calcium phosphate cement: study of its bioactivity and cell response

Table of contents

3.1 Introduction

This Chapter proposes the preparation of a Si-doped calcium phosphate cement (Si-CPC), using as main reactant the Si-α-TCP developed in Chapter 2. The aim to dope CPCs with Si is to improve some biological properties of the cement, such as its bioactivity and the cell response to the material [1], which are of high interest for medical applications. However, whether the biological improvements are associated to the Si itself or to the modifications that this ion causes to the physical properties of the material is still unclear [2]. Therefore, special attention will be paid to discern, when possible, between both factors.

3.2 Objectives

The main aim of this Chapter is to develop and to characterize a Si-doped calcium phosphate cement (Si-CPC). The specific objectives of this Chapter are the following:

1. To develop a Si-doped calcium phosphate cement (Si-CPC) with suitable characteristics for clinical applications, using alpha-tricalcium phosphate doped with silicon (Si-α-TCP) as reactant.

2. To characterize the Si-CPC in terms of chemical, physical and mechanical properties.

3. To evaluate the bioactivity of Si-CPC using Kokubo's method.

4. To evaluate the ion exchange of Si-CPC with two different immersion media.

5. To assess the cell response to the Si-CPC in terms of cell proliferation and differentiation.

In order to assess the role of Si in the mentioned studies, a Si-free CPC was included as a control in all tests. Figure 3.1 summarizes schematically the studies evaluated in this Chapter.
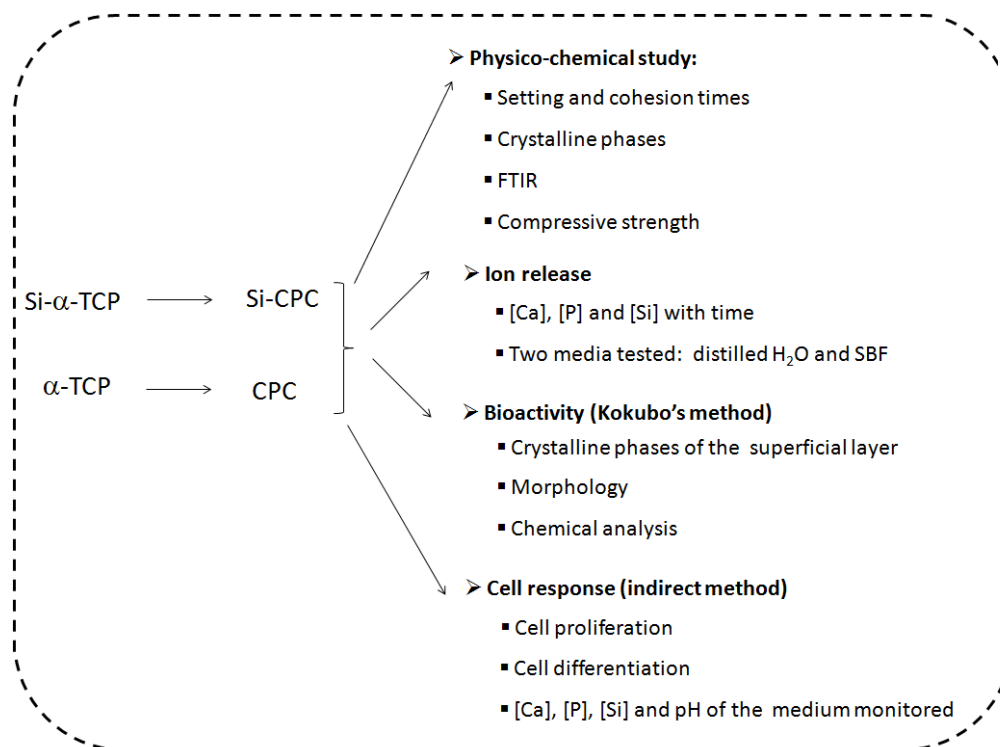
Figure 3.1. Schema of the studies evaluated in Chapter 3. [Ca], [P] and [Si] stands for the concentration of Ca, P and Si, respectively.

3.3 Materials and methods

3.3.1 Preparation of Si-CPC and CPC

The reactant used to prepare the Si-doped calcium phosphate cement (Si-CPC) was the Si-α-TCP developed in Chapter 2. Analogously, α-TCP was the reactant used to prepare the Si-free counterpart, namely CPC, which was used as a control. Briefly, Si-α-TCP was prepared from a SiO_2/HA mixture containing 2.54 wt% Si, sintered at 1250°C and cooled down slowly inside the furnace. α-TCP was prepared by heating the HA at 1450°C for 2 h, followed by quenching in air to stabilize the α-phase.

Fifty g of bulk material of α-TCP or Si-α-TCP were milled in a planetary ball mill (Fritsch Pulverisette 6) with 6 agate balls (ϕ = 30 mm), at 350 rpm for 30 min. Figure 3.2 shows the particle size distribution of both powders. The SSA of the milled powders, analyzed in duplicate, were 2.64 $\pm$ 0.12 m^2/g for Si-α-TCP and 2.55 $\pm$ 0.23 m^2/g for α-TCP.
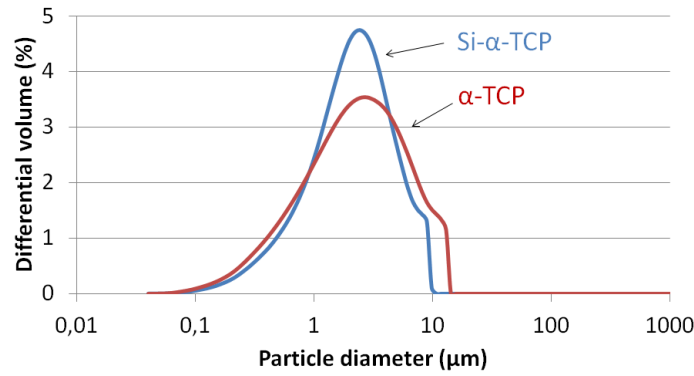
Figure 3.2. Particle size distribution of milled Si-α-TCP and α-TCP.

The cements were prepared by mixing the powder phase with distilled water in a liquid to powder ratio of 0.32 ml/g. Therein, the cement obtained with the Si-α-TCP powder was coded as **Si-CPC** and the cement obtained from α-TCP was coded as **CPC** (Figure 3.3).
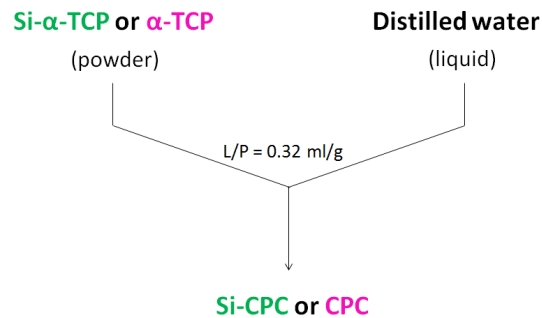
Figure 3.3. Schema of the preparation of Si-CPC and CPC. The codes used for the TCP reactants and the cements are indicated.

3.3.2 Physico-chemical characterization of Si-CPC and CPC

3.3.2.1 Setting time

The setting times of Si-CPC and CPC were measured in triplicate using the Gillmore needles, following the regulation ASTM-C266-89 [3]. The Gillmore needles is a device made of two solid elongated cylinders with a weight on the top of each of them. The "needle" that indicates the initial setting time (t_I) has a larger diameter and a lower weight, thus exerts a lower pressure than the "needle" used to evaluate the final setting time (t_F), which has a smaller diameter and a higher

weight. The standard values of diameter, weight and pressure for both needles are shown in Table 3.1.

Table 3.1. Standard values of the Gillmore needles [3].

	Weight (g)	Diameter (mm)	Pressure (MPa)
Needle for initial setting time	113.4 ± 0.5	2.12 ± 0.05	0.3
Needle for final setting time	453.6 ± 0.5	1.06 ± 0.05	5

3.3.2.2 Cohesion time

The cohesion of CPC pastes was evaluated by virtual inspection after introducing the paste in water at 37°C, as explained by Fernández *et al.* (method 1) [4]. The procedure consists of introducing the fresh cement in a plastic surface and then soaking it in distilled water. The cohesion time is the period of time from the moment when the liquid and powder are mixed (time zero) until the cement suffers no disintegration when soaked.

3.3.2.3 Compressive strength

Cement cylinders (6 mm diameter, 12 mm height) were prepared by filling Teflon cylindrical moulds and immersing them in Ringer's solution at 37°C for 8 h, 1 day and 7 days.

The compressive strength evolution with time was measured in wet conditions in a Universal testing machine (Adamel Lhomargy DY 32/34) equipped with a load cell of 10 kN at a crosshead speed of 1 mm/min. Eight specimens of 6 mm diameter and 12 mm height were tested at each time point. After performing this test, the setting reaction of the specimens was stopped by introducing them in acetone for 1 h and, subsequently, they were dried at 110°C overnight.

3.3.2.4 Crystalline phases

The phase composition at different reaction times was assessed by high resolution X-ray powder diffraction (XRD, PANalytical, X'Pert PRO Alpha-1). Measurements of XRD were done by scanning in Bragg Brentano geometry using a copper Kα radiation. The experimental conditions were: 2θ scan step 0.020° between 4-100°, counting time 150 s per point, voltage 45 kV and

intensity 40 mA. The diffraction patterns were compared with those of the Joint Committee on Powder Diffraction Standards for α-TCP (JCPDS #9-348), β-TCP (JCPDS #9-169), HA (JCPDS #9-432), and β-cristobalite (JCPDS #89-3607) [5]. Rietveld refinements were carried out in triplicate in order to quantify the phases present. For this purpose the Inorganic Crystal Structure Database (ICSD) was used, including structural models for α-TCP (ICSD #923), β-TCP (ICSD #6191), HA (ICSD #151414) and β-cristobalite (ICSD #75483) [6]. Quality fits for phase quantification were obtained by refining the instrument displacement, scale factors and lattice parameters using a Thompson-Cox-Hastinge pseudo Voight*Axial divergence, FWHM/shape parameters, preferred orientation and background. The Rietveld refinements were performed using the software package FullProf Suite [7].

3.3.2.5 FTIR

Fourier Transform Infrared spectra (FTIR) from 400 to 4000 cm^{-1} were obtained using an ABB FTLA 2000 spectrometer. A few milligrams of crunched cement were mixed with KBr in a 3.33 wt% ratio, in order to obtain semi-quantitative results. The mixture was pressed in a 6 mm diameter die at 5 t for 1 min to produce uniform and translucent disks for analysis.

3.3.2.6 Morphology

The microstructure of the cements was observed in fractured surfaces by scanning electron microscopy (SEM, JEOL JSM 6400). For this purpose, the specimens were previously coated with gold to improve their electrical conductivity.

3.3.2.7 Specific surface area

The specific surface area (SSA) of the set cements was analyzed by N_2 adsorption (Micromeritics ASAP 2020) following the Brunauer–Emmett–Teller method (BET theory).

3.3.3 Ion exchange of the samples in different media

3.3.3.1 Experimental design

Si-CPC and CPC disks of 15 mm diameter and 2.5 mm height were prepared using Teflon molds. The cement disks were set in distilled water at 37°C for 48 h, in order to guarantee an

almost complete transformation to CDHA. The setting reaction was stopped by immersing the cement disks in acetone for 1 h and, finally, the disks were dried at 110°C overnight. The hardened disks were sterilized by gamma radiation at 25 kGy.

Another set of samples was prepared in order to determine whether the Si ions released came from the colloidal SiO_2 in excess or from the Si ions incorporated into the crystalline structure of Si-CPC. These samples consisted of a mixture of SiO_2/HA with 2.54 wt% Si, and distilled water was added in 40 w/v % to improve homogeneity. No thermal treatment was performed. The slurry was dried at 110°C for 3 h and, afterwards, the powder was pressed in a 9 mm diameter die at 5 t for 1 min to produce disks of 4 mm height for analysis. The samples were coded as **SiO_2/HA**.

The ion exchange of Si-CPC and CPC was evaluated in two different media: distilled water (H_2O) and simulated body fluid (SBF). The ion exchange of SiO_2/HA was evaluated only in distilled H_2O. The study was performed by soaking the disks with media in a 24-well plate, having a surface/volume ratio equal to 3 cm^2/ml. The mentioned ratio was selected because it is commonly used for the preparation of extracts to evaluate the cytotoxicity of ceramics through an indirect method [8]. The amount of medium added was 1.0 ml to the Si-CPC and CPC disks, and 0.5 ml to the SiO_2/HA ones.

After different time periods, 6 h, 3, 7, 14 and 21 days for the CPCs, and 6 h, 3 days and 7 days for the SiO_2/HA, the media were collected for further analysis and pristine medium was added to all the samples. The assay was performed with 8 replicates for each sample. The media of each group of samples were collected together in order to have enough volume to quantify the ionic concentration.

3.3.3.2 Media of study

As mentioned previously, the study was performed with two different media, free of proteins and cells. The media were selected for the reasons indicated below.

▪ **Distilled water (H_2O)** was used as plain medium, which should allow the maximum solubilization of the material.

▪ **Simulated body fluid (SBF)** was used since it has a similar ionic concentration to the human physiological plasma. Moreover, this assay provided complementary data to the bioactivity study, which was performed with this medium.

With the aim to decrease the chances of bacterial contamination in the solutions, 1 v/v% of penicillin/streptomycin solution (Gibco, ref. n. 15140-122) was added to each medium. The possibility of adding sodium azide (NaN_3) as antibacterial agent was discarded due to the high toxicity of this compound [9].

3.3.3.3 Quantification of the ion release

The Ca, P and Si concentration in the media, from now on [Ca], [P] and [Si], were analyzed by inductively coupled plasma-optical emission spectrometry (ICP-OES, Perkin Elmer Optima 3200 RL). Previous to the quantification of these elements, each medium was filtered with a syringe-filter of polycarbonate membrane and pore size of 0.01 μm (Sterlitech, ref. n. PCT00113100) (Figure 3.4) in order to exclude any colloidal SiO_2 present (particles size of SiO_2 was higher than 0.01 μm, as shown in Chapter 2). The aim of this process was to ensure that ICP-OES would only detect the dissolved species. Finally, 1% HNO_3 was added to each solution in order to avoid the precipitation of any metallic ion.

Figure 3.4. Syringe, filter holder and filters (pore size of 0.01 μm) used to remove any present colloidal SiO_2 after soaking the samples.

3.3.4 *In vitro* bioactivity study of Si-CPC and CPC

3.3.4.1 Experimental design

The bioactivity of the CPCs was evaluated following Kokubo's method, by immersing the samples into a simulated body fluid (SBF) [10]. This assay allows evaluating the bioactivity of the

material *in vitro*. A new apatite layer should be deposited on the surface of the material in case of a positive response.

Cement disks (15 mm diameter and 2.5 mm height) were prepared and were set for 48 h in Ringer's solution, in order to guarantee an almost complete transformation to CDHA. Since it is known that SBF gets easily contaminated, the CPCs disks were sterilized by gamma radiation at 25 kGy.

The cement disks were soaked in 50 ml of SBF solution (surface/volume ratio of 10 mm^2/ml), as indicated in the guidelines of the bioactivity study *in vitro* established by Kokubo *et al.* [10]. The disks soaked in SBF were stored in a plastic container at 37°C (Figure 3.5) and the SBF solution was refreshed twice a week. The changes of media were performed in a fume hood previously sterilized with ethanol and UV light for 15 min. The same face of the disk was kept facing up during the study, in order to afterwards observe the microstructure of this surface. At different time periods, 7, 14, 28 and 56 days, the specimens were taken out from SBF and gently washed with distilled H$_2$O. Finally, the specimens were dried at 120°C over 3 h. One disk of Si-CPC and one of CPC were evaluated at every time point.
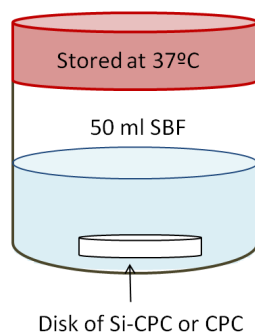
Figure 3.5. Experimental set-up for the *in vitro* bioactivity study.

3.3.4.2 Preparation of SBF

The preparation of SBF requires having all the recipients and instruments totally clean to avoid bacterial contamination and also to remove any residual particles that could induce the precipitation of the salts present in the SBF. Thus, the first step was to wash carefully all recipients and instruments to use in the following order: 1) solution of HCl 1M, 2) neutral soap and 3) distilled water.

The reactants (Table 3.2) were dissolved in a plastic jar with 800 ml of distilled water at 37°C. In order to avoid precipitation, each reactant was added after complete dissolution of the previous one, following the order indicated in Table 3.2. The pH of the solution, still at 37°C, was set to 7.40 with HCl 1 M. Finally, the solution was diluted to 1 L in a volumetric flask.

The SBF was stored at 4°C. Before its use, the SBF was filtered with a 0.22 μm pore size membrane (Millipore, GP Express™ Plus, ref. n. SCGPU01RE) and 1 v/v% of a commercial penicillin/streptomycin solution (Gibco ref. n. 15140-122) was added, even though the SBF protocol [10] does not contemplate the addition of any compound to avoid the contamination.

Table 3.2. Reactants used for the preparation of SBF. TRIS stands for tris-hydroxymethyl aminomethane ($(HOCH_2)_3CNH_2$).

Order	Compound	Amount (g or ml)	Purity	Commercial brand name, ref. n.
1	NaCl	8.036	≥ 99.5	Sigma, S9625
2	$NaHCO_3$	0.352	≥ 99.5	Sigma, S6297
3	KCl	0.225	≥ 99.5	Fluka, 60130
4	$K_2HPO_4 \cdot 3H_2O$	0.230	≥ 99.0	Sigma, P5504
5	$MgCl_2 \cdot 6H_2O$	0.311	≥ 99.0	Sigma-Aldrich, M0250
6	HCl 1.0 M	40	37 %	Panreac, 131020
7	$CaCl_2$	0.293	≥ 96.0	Sigma-Aldrich, C4901
8	Na_2SO_4	0.072	≥ 99.0	Sigma, S6547
9	TRIS	6.063	≥ 99.9	Panreac, 131940
	HCl 1.0 M	Amount needed to adjust the pH	37 %	Panreac, 131020

3.3.4.3 Characterization of the bioactivity

3.3.4.3.1 Crystalline phases (X-ray diffraction)

Si-CPC and CPC, unsoaked and soaked in SBF for 56 days, were ground and evaluated by X-ray powder diffraction (XRD, Panalytical, X'Pert PRO Alpha-1), using the same experimental conditions that were described in Section 3.3.2.

3.3.4.3.2 Crystallinity of the surface layer (glancing angle-X-ray diffraction)

With the aim to evaluate the composition of the apatite layer deposited on the surface of the cement, the disks immersed in SBF for 28 days were analyzed by glancing angle-X-ray diffraction (glancing angle-XRD, Bruker D8 Advance). Glancing angle-XRD allows reducing the penetration of X-rays into the specimen, therefore recording the diffraction pattern of thin layers with minimum contribution from substrate, which could overshadow the signal of the layer [11]. This is achieved by reducing the angle of incidence in comparison with the Bragg-Brentano geometry, also known as θ-2θ geometry (Figure 3.6 a). Hence, Grazing Incidence Angle Asymmetric Bragg (GIAB) geometry was used to perform the glancing angle-XRD (Figure 3.6 b).
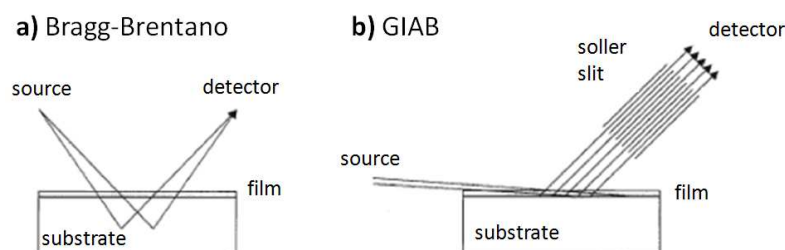
Figure 3.6. Schematic diagrams of three diffraction geometries: a) Bragg-Brentano or θ-2θ geometry; b) Grazing Incidence Angle Asymmetric Bragg (GIAB) geometry (modified from [11]).

The experimental conditions were: 2θ scan step 0.020° between 30° and 34°, counting time 8 s per point, voltage 40 kV and intensity 40 mA. The goniometer radius was 217.5°.

3.3.4.3.3 Morphology (Scanning electron microscopy, SEM)

The CPC disks that were immersed in SBF for 0, 7, 14, 28 and 56 days were observed with scanning electron microscope (SEM, JEOL JSM 6400). The presence of an apatitic layer was observed from two different visual perspectives: a) the surface and b) the transversal fracture. The transversal fracture allowed observing the morphological differences between the original CDHA and the apatite deposited on its surface. To carry out the morphological observations, a transversally fractured disk was mounted on a carbon fiber stuck on a copper foil (Figure 3.7).
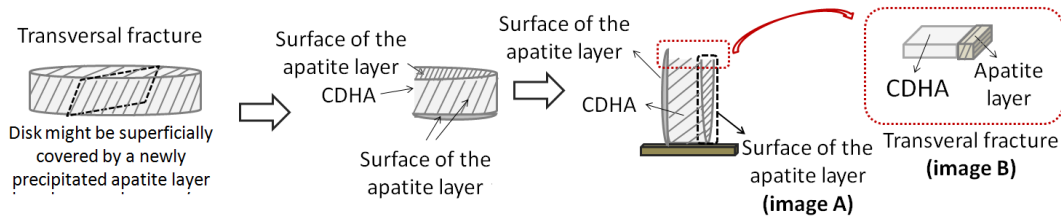
Figure 3.7. Preparation of the disk for the observation of the apatite layer (deposited on the surface of the CDHA). Both images taken with SEM are so marked: image A corresponds to the surface of the apatite layer and image B shows the transversal fracture, with the apatite layer growing on the surface of the set cement (CDHA).

3.3.4.3.4 Elemental analysis (energy dispersive spectroscopy, EDS)

The elemental composition of the Si-CPC, unsoaked or after being immersed in SBF for 28 days, was semi-quantitatively analyzed by energy dispersive spectroscopy (EDS). The fundaments of the EDS technique rely on the fact that each element has a unique atomic structure, which releases a characteristic X-ray when hit by a high-energy beam of charged particles such as electrons. The transversally fractured sample (image B of Figure 3.7) was embedded inside a polyacrilic resin and it was slightly polished to obtain a smooth surface that would cause a minimal dispersion of the radiation.

In the case of disks soaked in SBF, the elemental analysis was performed on two different areas: on the surface and on the core of the disk (0.5 mm far from the surface). The Ca/P, (Ca+Na)/P and (Ca+Na)/(P+Si) atomic ratios were determined, since the calcium phosphate source used for the preparation of α-TCP (CPC reactant) had a high Na concentration (Table 2.2). Three different spots were analyzed in each area.

3.3.5 Cell culture study

Human osteoblast-like Saos-2 (ATCC-HTB85) cells were used as cell model. The cells were maintained in cell culture flasks in an incubator with humidified atmosphere of 5% CO_2 in air at 37°C. McCoys medium (Sigma, ref. n. M8403) supplemented with 0.75% of L-glutamine (Gibco, ref. n. 25030), 1% penicillin/streptomycin (Gibco, ref. n. 15140), 2% of sodium pyruvate (Gibco, ref. n. 11360) and 15% of fetal bovine serum (Gibco, ref. n. 10270-106) was used. The culture medium was exchanged every second day. Upon confluence, cells were detached with a minimum amount

of trypsin-EDTA (Gibco, ref. n. 12605-028) that was inactivated with complete McCoys medium after 10 min. The cells were then re-cultured or used for the experiments.

The cell culture study was performed with an indirect method in order to assess the effect of the ionic exchange between the cements and the culture medium. This method allows discriminating the ion-exchange effects from the effect of the cements' surface properties (roughness, Z-potential, topography, *etc.*). Cement disks (15 mm diameter and 2.5 mm height) were prepared with Si-α-TCP or α-TCP. After 7 days of immersion in Ringer's solution at 37°C, the hardened disks were sterilized by gamma irradiation at 25 KGy to ensure complete reaction. The sterile disks were introduced into a 24-well plate and cell culture polycarbonate inserts (Thermo Scientific, Nunc, ref. n. 137052) with 0.4 μm pores were placed over them to allow the ionic exchange. Both disks and inserts were preconditioned for 24 h by introducing 1.5 ml of medium per well. After preconditioning them, the medium was removed and 25,000 cells were seeded in the insert with 1 ml of medium. Cells were also cultured in inserts placed in wells containing no material, as control series. Figure 3.8 schematically shows the set-up of the assay. The culture medium was exchanged every second day. Each cell culture experiment was performed twice, with 3 replicates in each experiment.
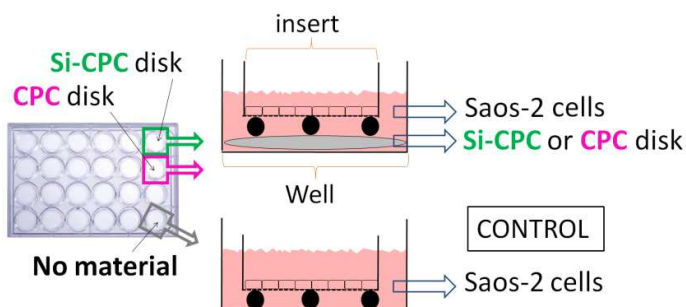
Figure 3.8. Schema of the experimental set-up of the *in vitro* study.

At each medium exchange and at the end of the culturing period, samples were collected from the medium to determine [P] and [Si] by using inductively coupled plasma-optical emission spectrometry (ICP-OES). [Ca] and pH were measured by means of a selective electrode (Ilyte: Ca^{2+}, K^+, Na^+, pH, Instrumentation Laboratory).

Cell proliferation and cell differentiation were evaluated at 6 h and at 3, 7, 14 and 21 days. At each time point, the inserts were rinsed twice with PBS to remove non-attached cells. The attached cells were lysed three times via freezing at -80°C and thawing at room temperature. The lysates were centrifuged at 1500 rpm for 10 min.

Cell proliferation was analyzed using a LDH Kit (Roche, ref n. 1644793), an indirect method to measure the number of alive cells before lysing. The LDH assay allows measuring the lactate dehydrogenase (LDH), a stable cytoplasmic enzyme that is released after plasma membrane rupture. LDH reduces yellow tetrazolium salt into a red formazan component, indicator of the enzymatic activity (Reaction 3.1). The reaction was incubated protected from light for 10 min and afterwards it was stopped with HCl 1 M. Finally, the LDH activity was determined spectrophotometrically in a plate reader (Power WaveX, Bio-Tek Instruments, USA; 490 nm). A calibration curve with decreasing concentrations of cells was created to express results as cell number.
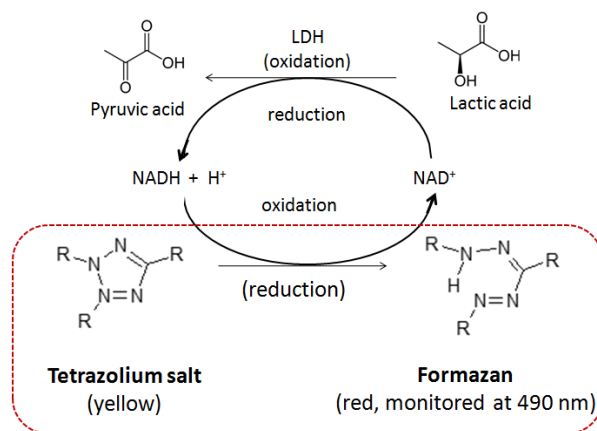
Reaction 3.1. Reaction to measure alive cells through the indirect reaction of lactate dehydrogenase (LDH), a cytoplasmatic enzyme, with a calorimetric reactant.

Alkaline phosphatase activity, an early marker of osteoblast differentiation that is expressed just before matrix mineralization begins [12], was measured using a colorimetric method based on the conversion of p-nitrophenyl phosphate to p-nitrophenol in the presence of alkaline phosphatase (ALP). ALP is a hydrolase enzyme responsible for removing phosphate groups from many types of molecules, process known as dephosphorylation (Reaction 3.2). The lysates

obtained in the previous section, which contained an unknown amount of ALP, were mixed with a phosphatase substrate solution (p-nitrophenyl phosphate, Sigma, ref n. P5994) and 2-amino-2-methyl-1-propanol buffer (AMP, Sigma Diagnostics Inc., ref n. A9226). The AMP is an alkaline buffer that was added because the ALP enzyme is more effective in an alkaline medium. The mixture was incubated protected from light for 25 min. The reaction was stopped with NaOH 1 M and the production of p-nitrophenol was determined spectrophotometrically in a plate reader (Power WaveX, Bio-Tek Instruments, USA; 490 nm) by measuring the absorbance at 405 nm. The values were calibrated to a standard curve prepared from known concentrations of p-nitrophenol (Sigma, ref n. N7660). The ALP activity was shown as the p-nitrophenol concentration normalized to both the number of cells and the reaction time.
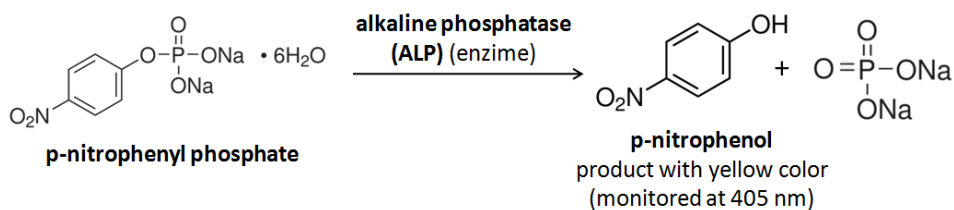
Reaction 3.2. Colorimetric reaction for the measurement of the ALP activity.

3.3.6 Statistical analysis of the results

A Student's t-test was used to determine the statistically significant differences between the mean values of the different experimental groups. A difference between groups was considered to be significant at $p < 0.05$.

3.4 Results

3.4.1 Physico-chemical characterization of Si-CPC and CPC

The initial setting time of Si-CPC was 8-9 min and its cohesion time was 6-8 min. The initial setting and cohesion times of undoped CPC were slightly longer, around 10-11 min and 8-10 min,

respectively. The setting and cohesion times were within the ranges established for clinical applications [13].

Figure 3.9 shows the evolution of the crystalline phases determined by X-ray diffraction and quantified by the Rietveld method. Both Si-α-TCP and α-TCP were hydrolyzed into CDHA, although Si-α-TCP reacted statistically significantly faster ($p < 0.05$), since after 8 h a 61 wt% of CDHA was already detected, compared to a 39 wt% for the α-TCP.
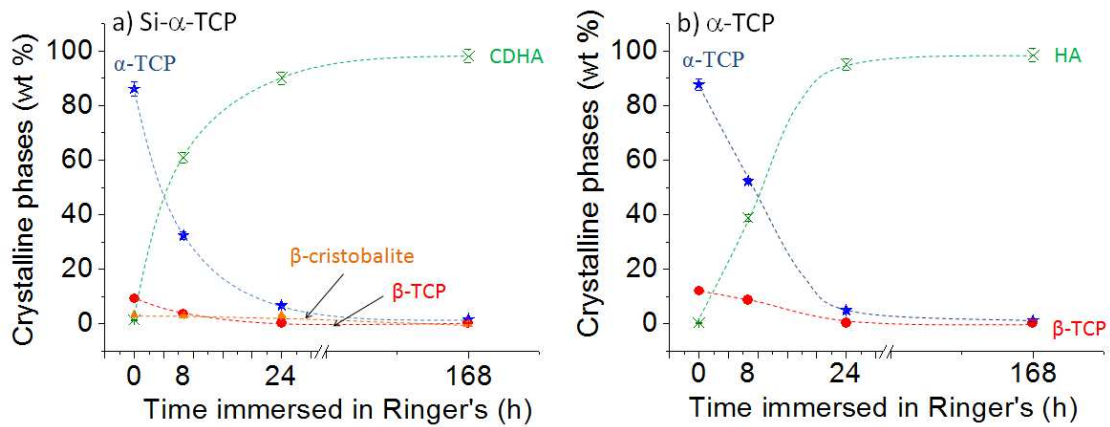
Figure 3.9. Phase composition of: a) Si-CPC and b) CPC, immersed in Ringer's solution for 0, 8, 24 and 168 h (7 days). Quantified by the Rietveld method, including models for α-TCP (★), β-TCP (●), CDHA (✳) and β-Cristobalite (▲). Error bars indicate standard deviation, n = 3.

The evolution of the compressive strength of both cements followed the progress of the setting reaction, as reported in Figure 3.10. Statistically significant differences ($p < 0.05$) were only found at 8 h of reaction, being the compressive strength of the Si-CPC higher than that of the undoped CPC.
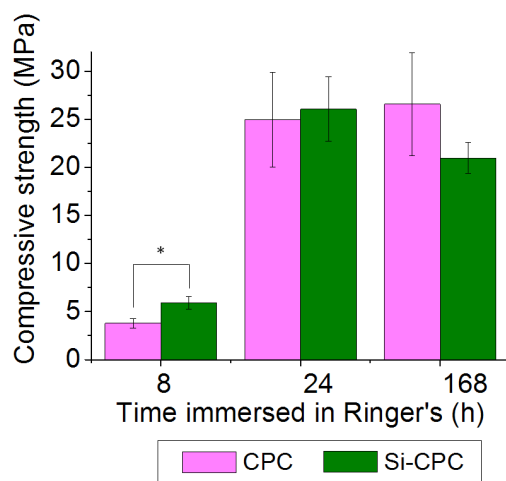
Figure 3.10. Compressive strength of the set cements after 8, 24 and 168 h (7 days) of immersion in Ringer's solution. Error bars indicate standard deviation, n = 8. * indicates statistically significant differences.

The setting reaction was also followed by FTIR (Figure 3.11 a). The evolution of the bands was consistent with the hydrolysis of the α-TCP to a precipitated HA, as previously reported [14] [15], and it is summarized in Table 3.3. The absorption bands at 962 cm^{-1} (v_1 of PO_4), 1035 and 1091 cm^{-1} (v_3 of PO_4), and 563 and 603 cm^{-1} (v_4 of PO_4), typical for apatite, become more pronounced with increasing reaction time. The bands located at 480, 798 and 1196 cm^{-1} were assigned to the O-Si-O vibration of β-cristobalite [16] [17]. Moreover, a small sharp band detected at 668 cm^{-1} was also observed in a previous study on attenuated total reflection infrared spectroscopy of Si-stabilized TCP [18], and it was attributed to the formation of $Si_2O_7^{6-}$ groups within the crystalline structure [18] [19].

When comparing the set cements (Si-CPC and CPC) after complete reaction (Figure 3.11 b), it was assessed that the additional bands detected in the Si-CPC coincided to those previously observed in the Si-α-TCP (Figure 3.11 a, at 0 h). However, interestingly, whereas the bands at 480, 798 and 1196 cm^{-1}, which were assigned to β-cristobalite, had the same intensity in the Si-CPC reacted for 7 days than in the Si-α-TCP (0 h), the band at 668 cm^{-1} was much smaller in the set Si-CPC.
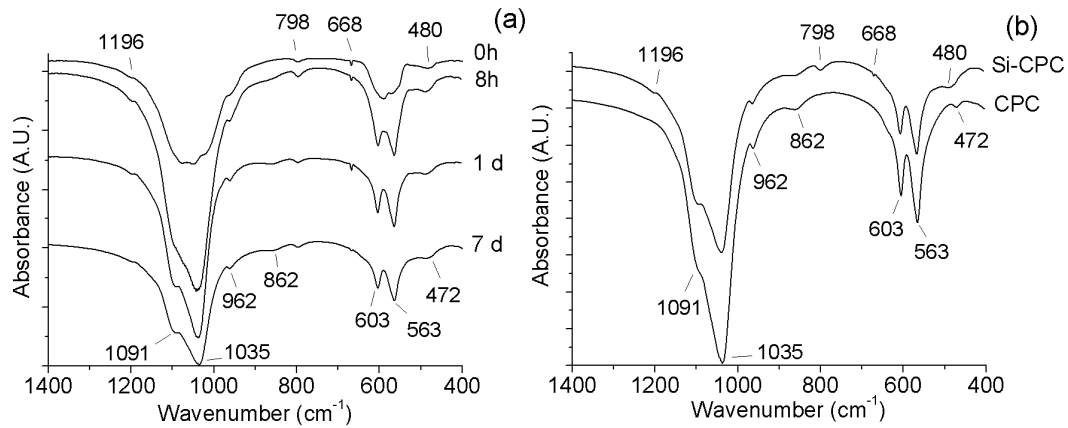
Figure 3.11. a) IR spectra of Si-α-TCP cement powder (0h) and the corresponding Si-CPC immersed in Ringer's solution for 8 h, 1 day and 7 days; b) Comparison of Si-CPC and CPC, immersed in Ringer's solution for 7 days. The bands indicated below the spectra are assigned to phosphate vibrations and the bands showed above are associated to O-Si-O vibrations. A.U. stands for arbitrary units.

Table 3.3. Band assignments for the CPC and the Si-CPC reacted for 7 days. Some abbreviations were used: sh: shoulder; s: strong band; vs: very strong band; m: medium band; w: weak band.

Band assignment	Experimental values (cm^{-1})		Frequency (cm^{-1}) according to literature for CDHA	References
	CPC 7 days	Si-CPC 7 days		
PO$_4^{3-}$, ν_3	1096 (sh)	1091 (sh)	1085 (sh)	[15]
	1039 (s)	1035 (s)	~ 1035 (vs)	[15]
PO$_4^{3-}$, ν_1	965 (w)	962 (w)	965 (w)	[15]
P-O(H), deformation of HPO$_4^{2-}$, ν_5	858 (w)	862 (w)	870 (w)	[15]
OH, libration	-	-	632 (sh, vw)	[15]
PO$_4^{3-}$, ν_4	603 (m)	603 (m)	605 (m)	[15]
	565 (m)	563 (m)	565 (m)	[15]
PO$_4^{3-}$, ν_2	472 (w)	472 (w)	~ 462 (sh)	[14]
O-Si-O, bending, cristobalite	-	480 (w)	481	[16]
Si$_2$O$_7$, bridging	-	668 (w)	668	[18]
O-Si-O, bending, cristobalite	-	798 (w)	800	[16]
O-Si-O, cristobalite	-	1196 (w)	1192	[17]

Figure 3.12 shows the microstructure of the Si-doped and undoped cements after 24 h of reaction. Both of them were formed by a network of needle-like entangled crystals. The SSA of the samples was 21.4 ± 1.1 and 21.6 ± 0.9 m^2/g for the Si-doped and the undoped CPC, respectively.
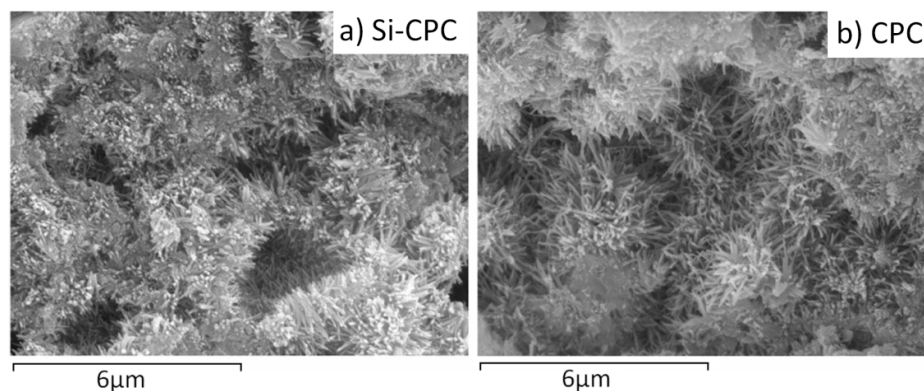
Figure 3.12. Microstructure of fracture surfaces of the cements, which were immersed in Ringer's solution for 24 h: a) Si-CPC; b) CPC.

3.4.2 Ion exchange of the Si-CPC and CPC

First of all, it should be emphasized that the medium was refreshed at every time point. This means that any change observed on the ionic concentration of the medium from one time point to the next one was consequence of the ionic release or uptake by the material to/from the medium.

3.4.2.1 Ion concentration of pristine media

The theoretical and the experimental [Ca], [P] and [Si] of each pristine media, quantified by ICP-OES, are shown in Table 3.4.

Table 3.4. Theoretical and experimental [Ca], [P] and [Si] of the media used for the ion exchange study, distilled H$_2$O and SBF. The experimental values (indicated as "Exp.") were quantified by ICP-OES. The concentrations under the detection limit are shown as "< DL".

	[Ca] (mM)		[P] (mM)		[Si] (mM)	
	Theoretical	Exp.	Theoretical	Exp.	Theoretical	Exp.
Distilled H$_2$O	0	< DL	0	< DL	0	< DL
SBF	2.5	2.31	1	0.98	0	< DL

3.4.2.2 Ion exchange in H_2O

Figure 3.13 shows the [Ca], [P] and [Si] of the distilled H_2O containing Si-CPC, CPC and SiO_2/HA disks. The three samples released small amounts of Ca ions along the study, increasing the [Ca] of the medium from 0 to about 0.06 mM. P ions were also released, producing a concentration between 5 and 11 mM in both Si-CPC and CPC, and 2-4 times higher in the case of SiO_2/HA. Finally, both SiO_2/HA and Si-CPC released similar amounts of Si ions, producing concentration between 1.5 and 2.5 mM.
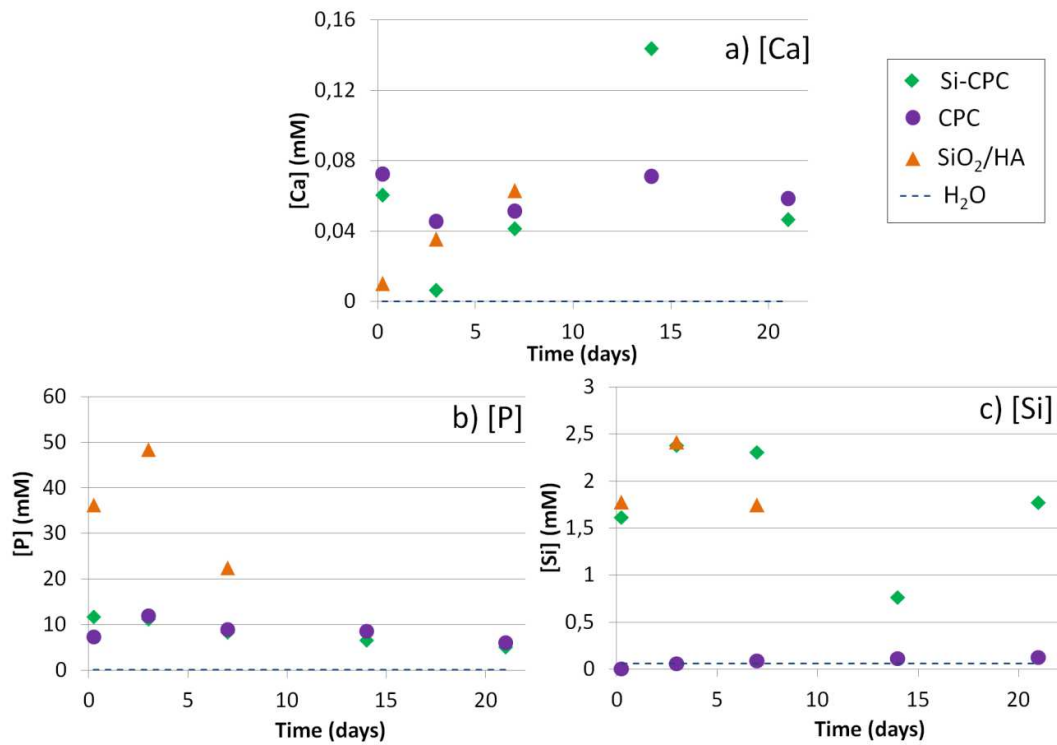
Figure 3.13. Evolution of the ionic concentration of distilled H_2O containing Si-CPC, CPC and SiO_2/HA (SiO_2/HA was only measured for 7 days): a) [Ca], b) [P], c) [Si]. A dashed line shows the ionic concentration of pristine distilled H_2O.

3.4.2.3 Ion exchange in SBF

In the case of soaking the disks in SBF, the scenario changed significantly, as shown in Figure 3.14. The [Ca] in SBF dropped from 2.31 to 0.25 mM after 3 days, probably uptaken by the CPC disks. After this time, the [Ca] decreased less at every time, showing that although the CPC disks kept uptaking Ca ions while refreshing the medium, they did so in a lower amount. Regarding the [P], the cements released this ion during the whole period of study. After only 6 h, the [P] of

SBF medium was 3-4 times higher than that of pristine SBF. However, this concentration decreased linearly with time, indicating that the samples released a lower amount of P with time. The Si-CPC released Si to the SBF medium during the whole study, producing a [Si] close to 2 mM.
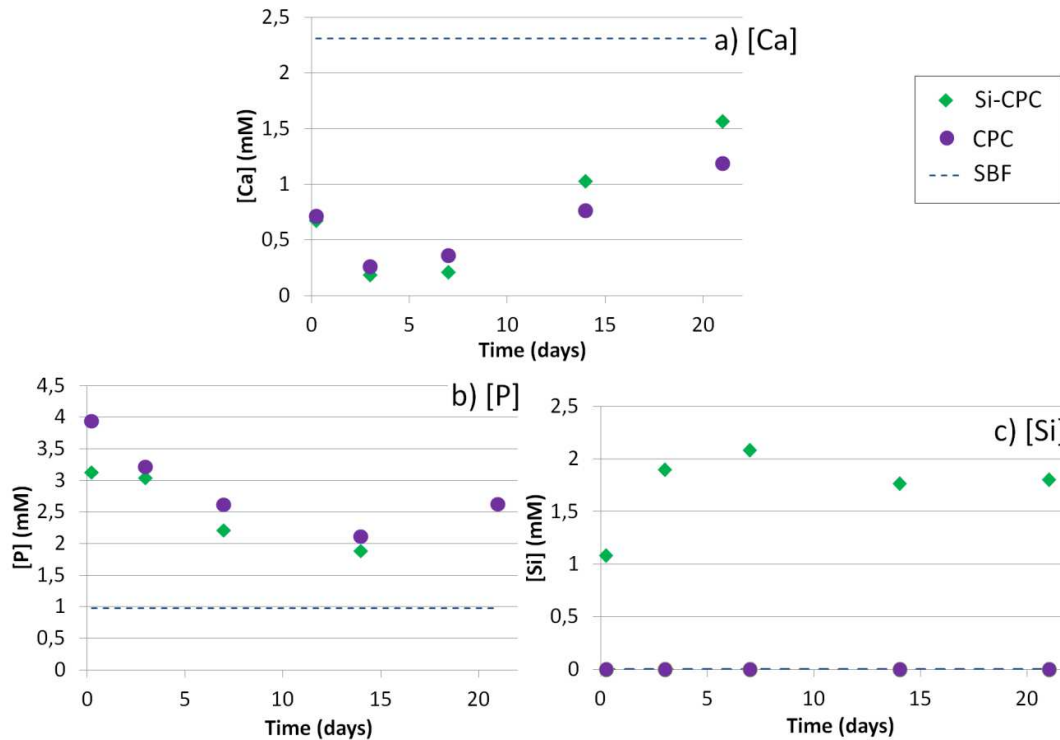
Figure 3.14. Evolution of the ionic concentration of SBF medium containing Si-CPC and CPC: a) [Ca], b) [P], c) [Si]. A dashed line shows the ionic concentration of pristine SBF.

3.4.3 Bioactivity study of the CPCs

3.4.3.1 Phase composition (X-ray diffraction)

Figure 3.15 shows XRD spectra of Si-CPC and CPC disks (both set in Ringer's for 48 h), prior and after immersion in SBF (0 h and 56 days, respectively). Prior to immersion in SBF, the cements were mainly composed by CDHA. No significant differences were detected between CPC and Si-CPC, and neither due to their immersion in SBF.
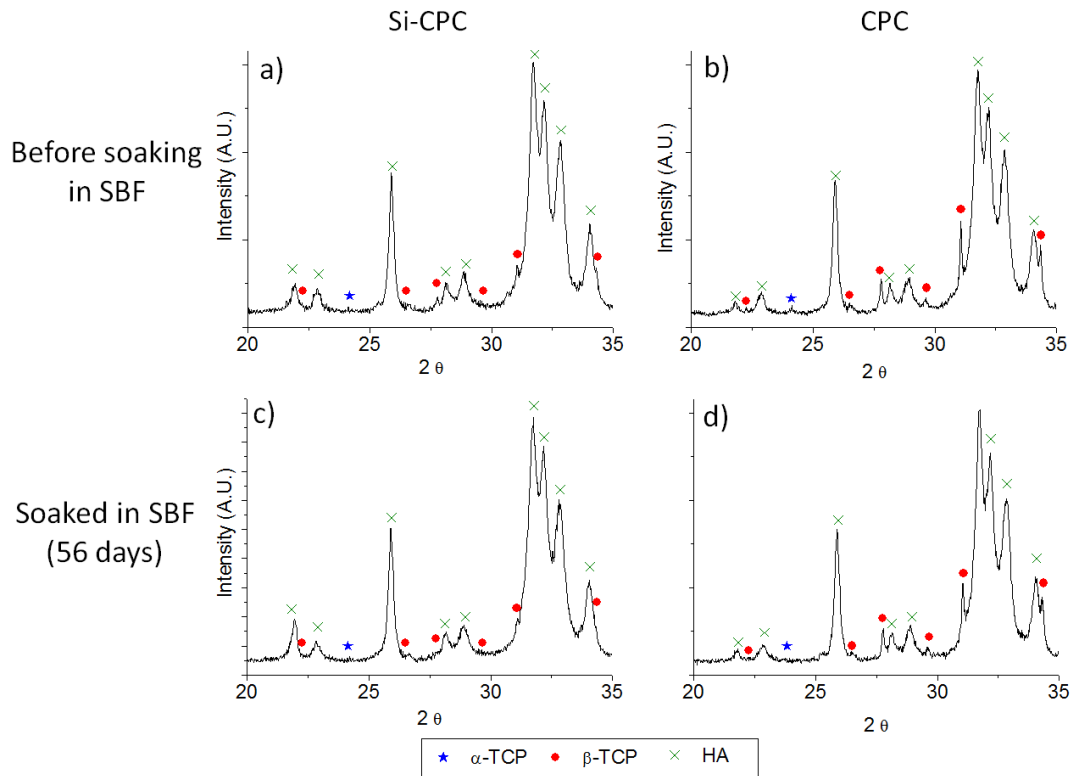
Figure 3.15. X-ray spectra of cement disks (set in Ringer's solution for 48 h), before soaking in SBF: a) Si-CPC and b) CPC, or soaked in SBF for 56 days: c) Si-CPC and d) CPC.

3.4.3.2 Crystallinity of the apatite layer (glancing angle-X ray diffraction)

In order to assess if an apatitic layer was deposited on the surface of the cement disks immersed in SBF, glancing angle-XRD was performed. The spectra of Si-CPC and CPC disks soaked in SBF solution for 28 days are compared with that of the corresponding unsoaked samples, as shown in Figure 3.16. The spectra of both Si-CPC and CPC unsoaked in SBF showed broad peaks at 31.8, 32.3 and 32.9°, which corresponded to the highest intensity peaks of HA with Miller index 211, 112 and 300, respectively. In contrast, the spectra of Si-CPC soaked in SBF showed much less intense peaks at the same positions, the peaks being barely differentiated due to their wideness (Figure 3.16 a). The CPC showed similar spectra prior and after immersion in SBF, with bands of similar width although they were slightly less intense after being soaked in SBF (Figure 3.16 b).
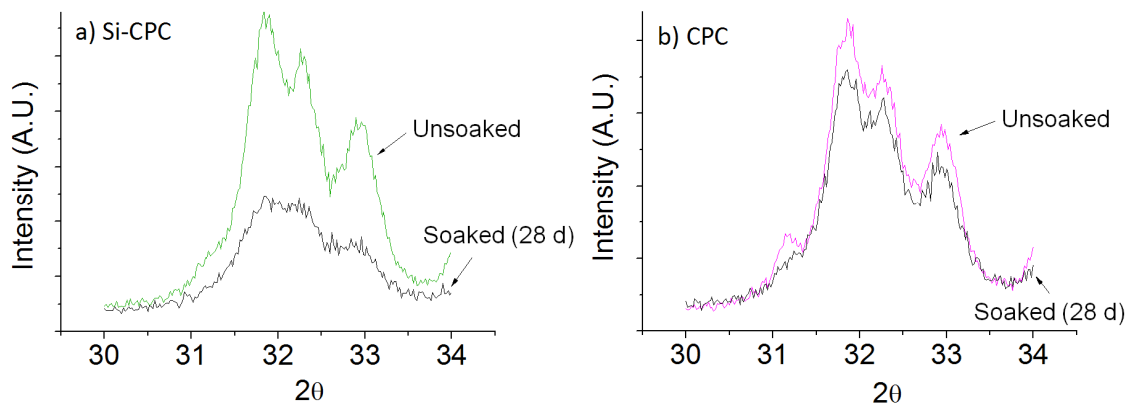
Figure 3.16. Glancing angle-XRD spectra of the set cements, which were unsoaked or soaked in SBF for 28 days: a) Si-CPC and b) CPC.

3.4.3.3 Morphology

The morphologies of the cement disks soaked in SBF for different time periods are shown in Figure 3.17 for Si-CPC and in Figure 3.18 for CPC, respectively. The morphology of both Si-CPC and CPC unsoaked in SBF was homogeneous, consisting of rosette-like networks made by nanometric crystals (Figure 3.17 b and 3.18 b).

Regarding Si-CPC soaked in SBF (Figure 3.17), the deposition of a new apatite layer was clearly observed after 14 days. The apatite layer was deposited over the rosette-like agglomerates. The transversal fracture showed that the layer was dense and about 3-5 μm thick (Figure 3.17 e). After 28 days, the apatite layer was thicker, about ~ 20 μm (Figure 3.17 g), and had a smooth texture that covered the entire surface (Figure 3.17 h). Similar morphologies were observed after 56 days (Figure 3.17 I and j).

Regarding CPC soaked in SBF (Figure 3.18), the deposition of an apatite layer on the surface of CPC was not observed as clearly as in the Si-CPC. After 14 days, some particles were observed on the surface of CPC (Figure 3.18 e), although their aspect was not the one expected for the formation of an apatite layer. Moreover, no evident sign of an apatite layer could be distinguished on the surface of CPC soaked in SBF for 28 days (Figure 3.18 g and h) and 56 days (Figure 3.18 l and j).

Although preventions were taken to avoid contamination, most of the SBF containing the cement disks were contaminated after 28 days, turning into a brown media with a strong smelling. The lacunas left by bacteria were also observed in some SEM images, as elongated dark embedded flecks (Figure 3.17 h and j).
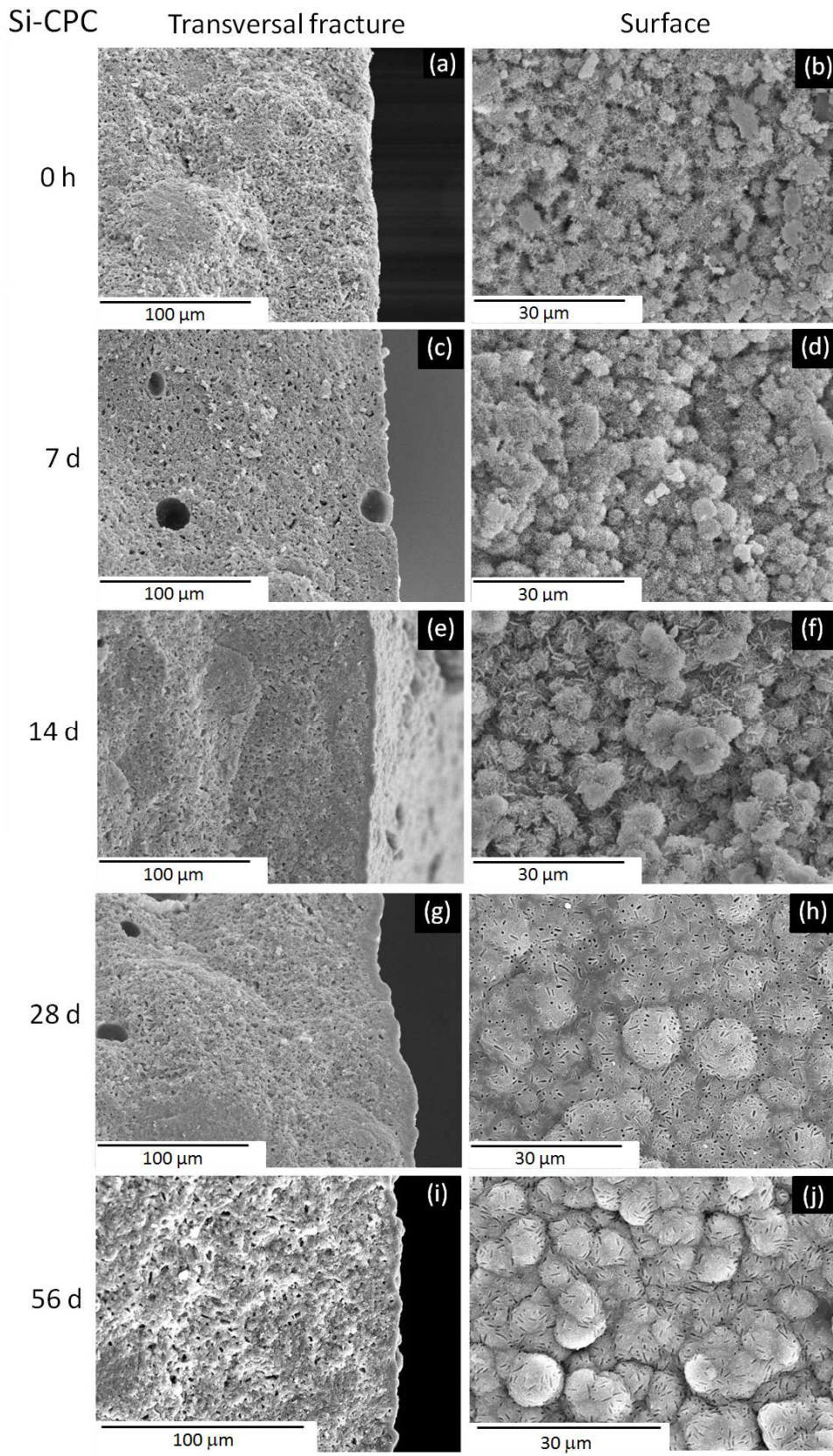
Figure 3.17. Morphology of Si-CPC soaked in SBF for: a, b) 0 h; c, d) 7 days; e, f) 14 days; g, h) 28 days; i, j) 56 days. The transversal fracture face is shown on the left image and the surface of the disk is shown on the right one.
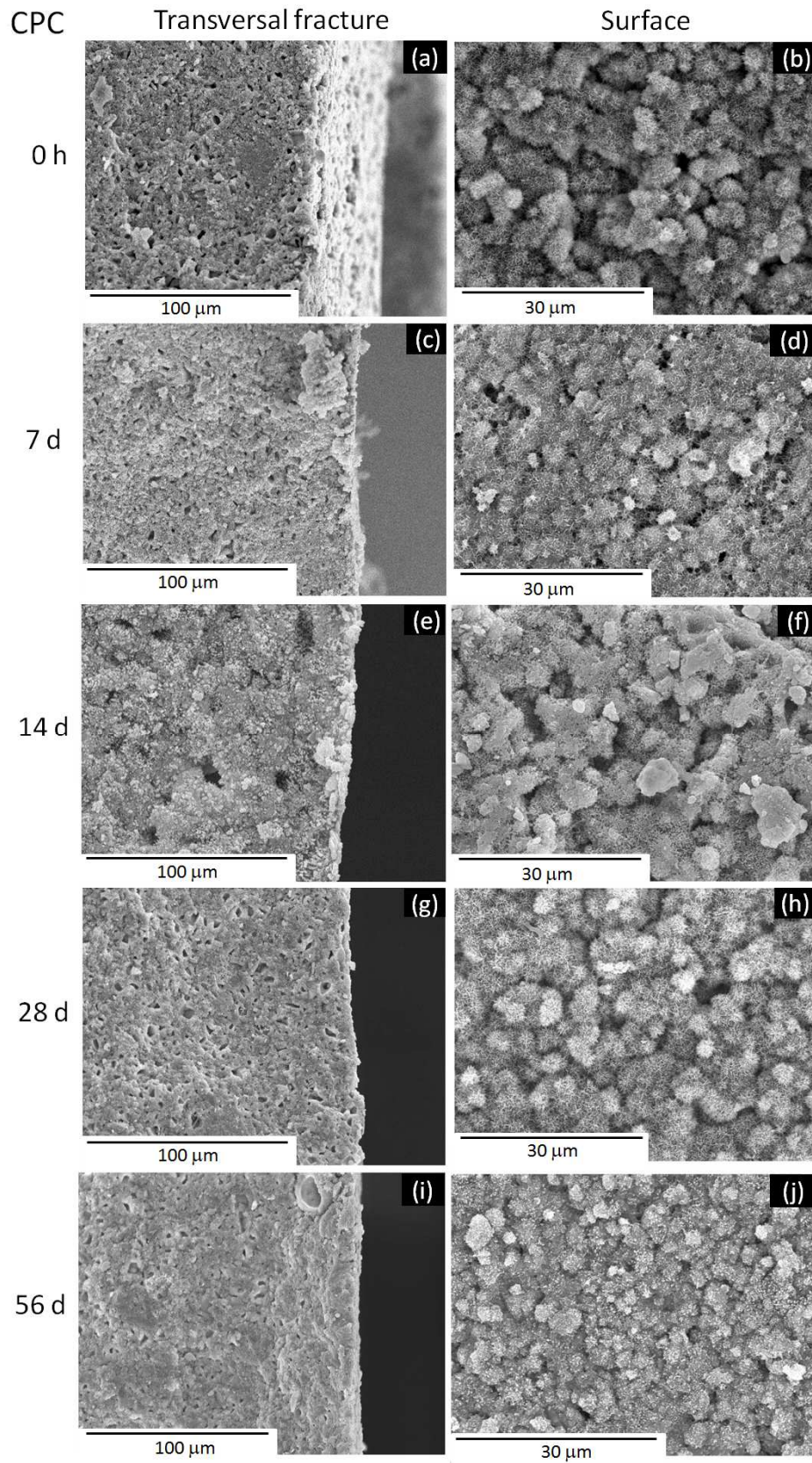
Figure 3.18. Morphology of CPC soaked in SBF for: a, b) 0 h; c, d) 7 days; e, f) 14 days; g, h) 28 days; i, j) 56 days. The transversal fracture face is shown on the left image and the surface of the disk is shown on the right one.

3.4.3.4 Elemental analysis (energy dispersive spectroscopy, EDS)

The elemental analysis was only performed with Si-CPC, since this was the formulation in which a new apatite layer was clearly observed on its surface. Table 3.5 shows the elemental composition of Si-CPC, unsoaked and soaked in SBF for 28 days, including the Ca/P, (Ca+Na)/P and (Ca+Na)/(P+Si) ratio. Two different areas of the soaked Si-CPC samples were analyzed: the surface and the cement core (0.5 mm far from the apatite layer).

Table 3.5. Elemental analysis by EDS (semi-quantitative results) of set Si-CPC, before soaking in SBF and soaked in SBF for 28 days. The soaked Si-CPC was analyzed on the surface and on the cement core (0.5 mm apart from the deposited apatite). The atomic % and the calculated atomic ratios are shown. The standard deviations are indicated in parenthesis.

Treatment	Analyzed area	Atomic (%)				Atomic ratios (calculated)		
		Ca	Na	P	Si	Ca/P	(Ca+Na)/P	(Ca+Na)/(P+Si)
Before soaking in SBF	Core	53,43 (0,55)	2,18 (0,43)	38,82 (0,33)	5,57 (0,35)	1.38 (0.06)	1.43 (0.24)	1.25 (0.31)
Soaked in SBF for 28 days	Core	53,31 (0,10)	2,33 (0,04)	38,89 (0,40)	5,47 (0,54)	1.37 (0.03)	1.43 (0.06)	1.25 (0.58)
	Surface	50,29 (0,91)	1,40 (0,18)	34,02 (1,23)	14,29 (2,32)	1.46 (0.05)	1.50 (0.21)	1.11 (0.76)

It is worth noting that the core area of Si-CPCs, soaked or unsoaked in SBF, resulted in similar elemental compositions, as determined by the atomic ratios. In contrast, the surface of the Si-CPC soaked in SBF had a higher Ca/P ratio and lower (Ca+Na)/(P+Si) ratio than the unsoaked Si-CPC.

3.4.4 Cell culture study

Figure 3.19 a represents the proliferation rate of Saos-2 cells grown in the inserts in presence of Si-CPC, CPC or control medium. The cells in contact with the medium containing either Si-CPC or CPC had a marked delay on cell proliferation. No statistically significant differences were observed between the Si-doped and the undoped CPC.

The ALP activity of the cells reached a maximum value at day 14 in all series and it was statistically significantly increased ($p < 0.05$) in the cells cultured in presence of Si-CPC or CPC, as

displayed in Figure 3.19 b. The values detected were similar for the cells in presence of both cements, except at day 14, when the ALP activity was statistically significantly higher (p < 0.05) for the cells in presence of Si-CPC as compared to CPC.
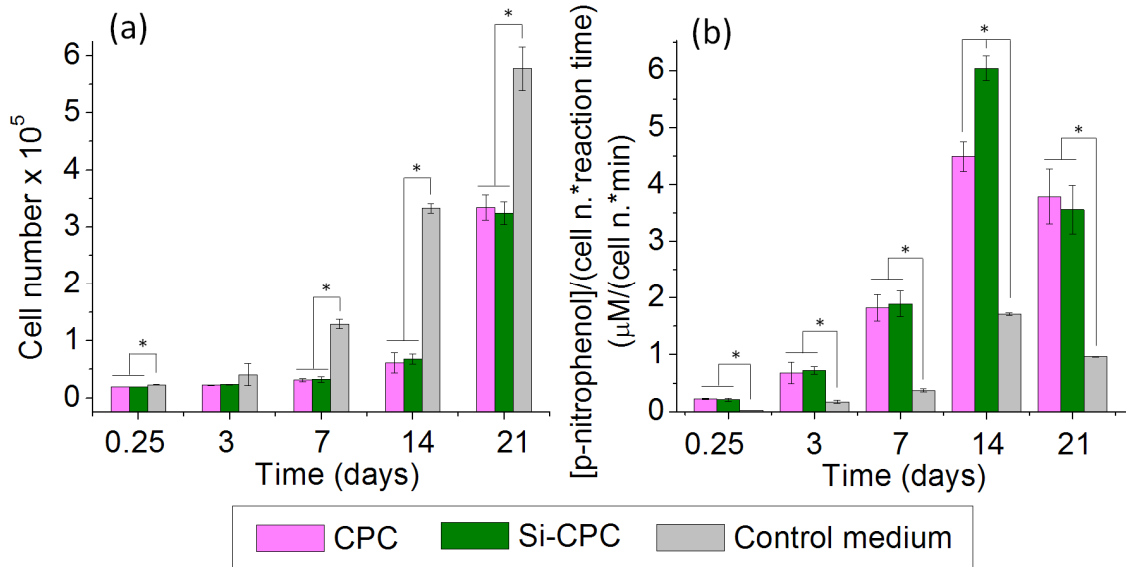
Figure 3.19. a) Cell proliferation measured by quantifying the LDH of lysed cells, for cells in contact with a medium containing Si-CPC or CPC, or in contact with control medium; b) Cell differentiation measured as [p-nitrophenol]/(cell number*reaction time), for cells in contact with a medium containing Si-CPC or CPC, or in contact with control medium. Errors bars indicate standard deviation, n = 3. * indicates statistically significant differences.

In parallel, the [Ca], [P] and [Si] and the pH in the media were quantified. The initial [Ca] in the control medium was 0.8 mM and decreased continuously with time, reaching a minimum value of 0.5 mM after 14 days (Figure 3.20 a). In presence of Si-CPC or CPC, [Ca] decreased sharply after only 6 h and remained low throughout all the study, between 0.05 and 0.1 mM, even though the medium was refreshed every second day. The [P] in the control medium decreased slightly during the culture period (Figure 3.20 b). In presence of Si-CPC or CPC, [P] showed an increase in the initial stages followed by a decrease, although the concentration was higher than in the control medium at all time-points. As expected, Si was detected only in presence of Si-CPC, with a concentration close to 1.5 mM during the whole culturing period (Figure 3.20 c). Finally, the pH of the control medium ranged between 7.7 and 7.4 (Figure 3.20 d). The pH was acidified at the initial stages in presence of Si-CPC, and subsequently evolved to more alkaline values. The same trend was observed for the CPC, although a higher dispersion of the measurements was found.
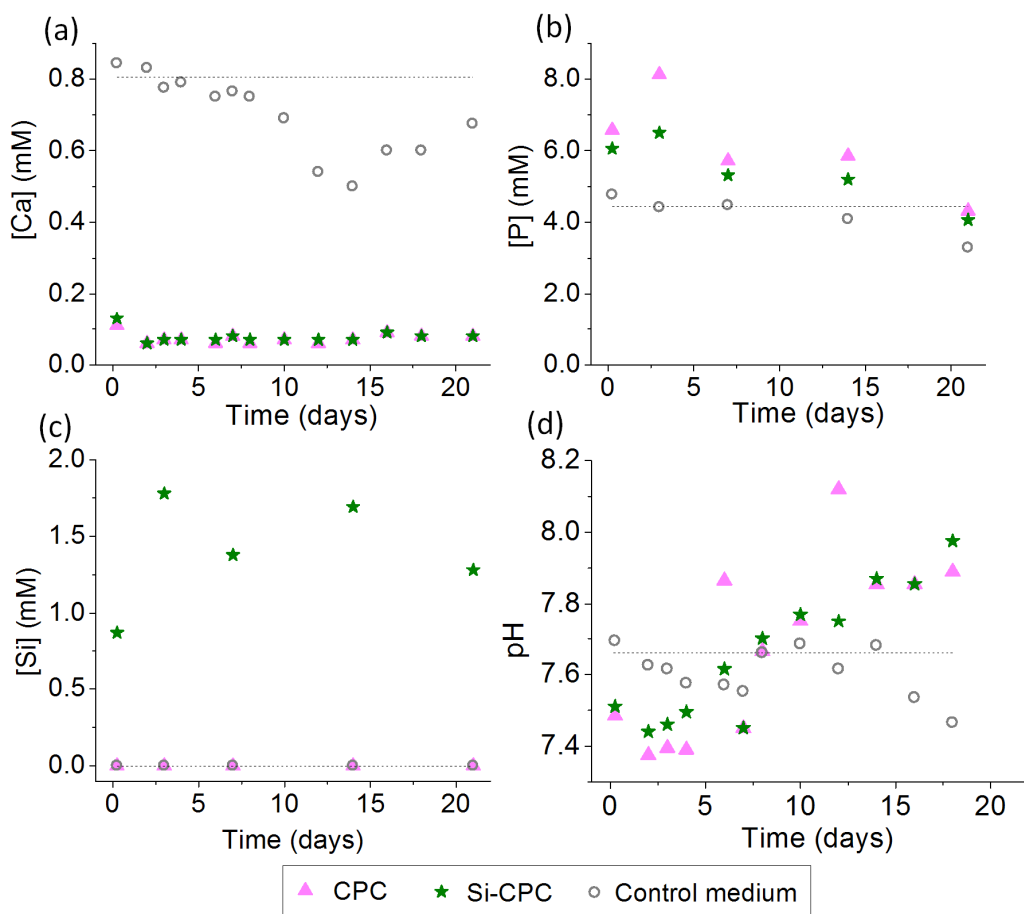
Figure 3.20. [Ca], [P], [Si] and pH in the medium in contact with Si-CPC or CPC and in the control medium at different times during the cell culture study. [P] and [Si] were measured by means of ICP-OES, and [Ca] and pH by means of a selective electrode: a) [Ca]; b) [P]; c) [Si]; d) pH. The dotted lines correspond to the initial values in the culture medium.

3.5 Discussion

3.5.1 Physico-chemical characterization of CPC and Si-CPC

Si-CPC had an appropriate handling time for clinical use. This means that, when used in clinics, the cement would set slowly enough to provide the surgeon with sufficient time to perform implantation, but at the same time would be fast enough to avoid delaying the operation [13].

The setting of both Si-CPC and CPC pastes was produced by a dissolution-precipitation mechanism that led the α-TCP hydrolysis to CDHA crystals (Figure 3.9 and 3.12). The setting kinetics of Si-CPC was shown to be faster than that of CPC, as revealed by a slightly shorter setting

and cohesion times, and a faster transformation to CDHA (Figure 3.9), specifically after 8 h. In fact, Si-CPC also led to slightly higher early strength development than CPC (Figure 3.10). The higher reactivity of the Si-doped CPC, also reported by Camiré *et al.* [20], could be a consequence of the higher solubility of the Si-α-TCP, caused by the lower stability of the doped crystalline structure [21]. The hydrolysis of both CPCs was almost complete after 24 h, as observed by XRD (Figure 3.9) and FTIR (Figure 3.11), and their morphology (Figure 3.12), SSA and mechanical properties (Figure 3.10) were similar.

No evidence was found that Si was incorporated into the precipitated HA produced by the setting reaction, which is in agreement with other reported works [22]. None of the bands associated to silicate incorporation into HA, *e.g.* at 888 or 890 [23] [24], 756 [24] and 504 [23] cm^{-1}, were detected in the FTIR spectra of Si-CPC (Figure 3.11). In fact, some authors claim that Si ions can only be introduced into the hydroxyapatite crystal lattice under high temperature conditions, which favor diffusion processes [25].

In Si-CPC, three bands detected by FTIR (1196, 798 and 480 cm^{-1}), which were stable with the reaction time (Figure 3.11 a), were attributed to β-cristobalite. However, the band attributed to $Si_2O_7^{6-}$ groups (668 cm^{-1}) decreased with time (Figure 3.11 a), being much smaller in the Si-CPC set for 7 days than in the Si-α-TCP (0 h). This would agree with the assignment of this band to $Si_2O_7^{6-}$ groups incorporated in the α-TCP structure (Figure 2.15), which would disappear upon TCP dissolution.

3.5.2 Ion exchange in different media

The ionic exchange produced between a solid compound (solute) and a medium (solvent) are regulated by a dynamic equilibrium known as solubility equilibrium. The relationship established between the solute and the solvent consists in the migration of individual ions or molecules between them. When equilibrium is reached, the rates of dissolution and precipitation are equal to one another and the solvent is said to be saturated. The concentration of the solute dissolved in a saturated solution indicates its solubility. In this study, the solutes were Si-CPC, CPC and SiO_2/HA disks, and the solvents were distilled H_2O and SBF. For Si-CPC and CPC, the study was carried out with the two solvents for 21 days, and the behavior of SiO_2/HA was evaluated only with

distilled H_2O for 1 week. The evolution of [Ca], [P] and [Si] was followed at different time points, the solvent being also refreshed at each interval. Another experimental factor that should be taken into account is that the media (modified by the materials) were filtered prior to their analysis in order to ensure that the atomic concentration observed only came from dissolved species.

When soaking Si-CPC or CPC disks in distilled H_2O, the disks were slightly dissolved and Ca and P ions were released to the medium. However, interestingly, the two samples produced a significantly higher [P] (around 5-10 mM) than [Ca] (around 0-0.15 mM) during the 21 days of the study (Figure 3.13), indication that the P ions were released in a greater amount than the Ca ones. This result indicated that the dissolution of the materials was incongruent, in other words, they modified the solvent (distilled H_2O) so that its molecular composition did not match that of the solute (Si-CPC or CPC). Therefore, although it would be expected that in distilled H_2O (solvent free of ions) the CDHA would maintain the same Ca/P ratio than the precursor of the cement (Si-α-TCP or α-TCP), *i.e.* Ca/P = 1.5, the ions released to the solvent indicated that the surface of the CPC disks might slowly increase their Ca/P ratio. The incongruent dissolution of the CPCs could be associated with the atomic reorganization of the superficial CDHA, which trended to form a more stoichiometric hydroxyapatite, thermodynamically more stable. In other words, the CDHA, which is a solid solution, would evolve from $Ca_{10-x}(HPO_4)_x(PO_4)_{6-x}(OH)_{2-x}$ with a x value of 1 ($Ca_9(HPO_4)(PO_4)_5(OH)$) to a x value closer to 0 (Reaction 3.3).

Reaction 3.3.

$$3\ \alpha\text{-}Ca_3(PO_4)_2 + H_2O\ \rightarrow\ Ca_9(HPO_4)(PO_4)_5(OH)\ \xrightarrow{\ Ca^{2+}\ }\ Ca_{10-x}(HPO_4)_x(PO_4)_{6-x}(OH)_{2-x}\ (0 < x < 1)$$

Ca/P = 1.5 $\quad\quad\quad\quad\quad$ Ca/P = 1.5 $\quad\quad\quad\quad\quad\quad\quad\quad\quad$ Ca/P > 1.5
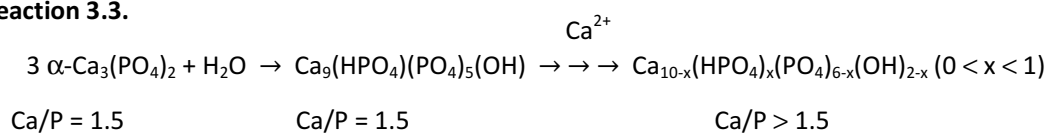
Regarding the dissolution of SiO_2/HA when immersed in distilled H_2O, it produced a [Ca] of the same order than that produced by the CPCs. However, SiO_2/HA released a significantly higher amount of P ions than the CPCs, the SiO_2/HA producing a [P] of 22-48 mM and the CPCs of 5-10 mM. This fact could be related to the higher SSA of the HA (about 71 m^2/g), increasing its dissolution in comparison with the CPCs, which SSA was close to 21 m^2/g.

Moreover, regarding to the release of Si ions, both SiO_2/HA and Si-CPC immersed in distilled H_2O released a similar amount of this ion, increasing the [Si] from 0 to around 2 mM. The

Si ions detected when SiO_2/HA was soaked in distilled H_2O could only come from a partial dissolution of SiO_2. However, the Si ions released by Si-CPC could either come from a partial dissolution of β-cristobalite (SiO_2 in excess that transformed during the thermal treatment applied to prepare Si-α-TCP) or from the release of Si ions incorporated into the crystal lattice of CDHA. It was indeed not possible to ascribe the release of Si to a unique source since the SiO_2/HA control contained SiO_2 whereas the Si-CPC contained the Si in excess as β-cristobalite.

A different scenario was observed when the CPC disks were soaked in SBF in comparison with that in distilled H_2O. In SBF, the initial [Ca] (2.31 mM) was significantly decreased at each time due to the uptake of Ca ions by the CPC disks, even though the medium was refreshed twice per week. However, after 3.5 days, the trend of [Ca] followed a positive slope, indicating that the CPC disks uptake a lower amount of Ca each time. Regarding the [P], the cements released P ions during the 21 days of the study. For the first 14 days, a negative slope indicated that the CPCs released a lower amount of P ions each time, and at 21 days the concentration remained approximately constant. The trends observed for [Ca] and [P] indicated that, after 21 days, the cements were closer to reach equilibrium with SBF. Finally, a [Si] around 1-2 mM was found at each time of study, indication that the β-cristobalite was slowly dissolved, as previously discussed.

When comparing the dissolution of Si-CPC with that of CPC, no significant differences were observed in the [Ca] and [P] in both distilled H_2O and SBF. Therefore, it was assumed that both CPC formulations had a similar solubility in the mentioned media. The fact that both CPC formulations had a similar solubility was an additional indication that, in Si-CPC, Si was not incorporated in the crystalline structure of CDHA, since it has been reported that the incorporation of SiO_4^{4-} increases the number of defects [1], decreasing the stability of its crystalline system [20] [21] [26]. Thus, in Si-CPC, Si would initially be in the form of β-cristobalite and, after immersion in SBF, it would be also included in the newly formed apatite layer, which contained the Si, Ca and P ions of the media, as determined by a chemical analysis (Table 3.5). The chemical analysis also showed that, after 28 days of immersion in SBF, the apatite layer had a higher Ca/P ratio and a higher amount of Si than the core area of Si-CPC. This result indicated again that the superficial CDHA was reorganized to form a CDHA more close to a stoichiometric HA.

A complete understanding of the underlying mechanisms of this ionic exchange would require monitoring all the ionic species in the immersion media, which is beyond the scope of this work. The ionic exchange can involve different situations in the material: substitution in the crystal lattice, on the crystal surface or in the hydration shell, or precipitation of different compounds. In any case, electroneutrality of the material must be preserved. In a previous study on ion reactivity of CDHA in standard culture media [27] it was shown that ionic substitution occurred between phosphate and carbonate, the latter one being incorporated in the apatite lattice and the former being released. However, with respect to the calcium uptake there is no clear explanation on the underlying mechanism. In another work on a similar CPC, it was hypothesized that the calcium uptake responded to a reorganization of the CDHA to a more stoichiometric HA, reducing its calcium deficiency [28], although no experimental evidence was provided.

3.5.3 Bioactivity study of the CPCs

The bioactivity study was evaluated by soaking Si-CPC and CPC disks in SBF for different intervals of time. The core area of Si-CPC and CPC shown to be similar by XRD (Figure 3.15), regardless of the immersion in SBF, since the apatite layer only modified the surface of the material. The microstructure of the surface fracture of the Si-CPC and CPC disks exhibited rosette-like agglomerates made by nanometric crystals prior SBF immersion (Figure 3.17 b and 3.18 b), whereas a new dense and smooth apatite layer covered the surface after immersion in SBF (Figure 3.17 e, f, g and h). In contrast, the microstructure of CPC disks soaked in SBF did not clearly reveal a new apatite layer on their surface (Figure 3.18). Glancing angle-XRD verified these results. On one hand, the formation of a poorly crystalline apatite on the surface of Si-CPC was corroborated (Figure 3.16 a), since the soaked Si-CPC had a glancing angle-XRD spectrum with broader peaks (indication of poorer crystallinity) than the unsoaked sample. On the other hand, the presence of a new apatite layer on the surface of CPC disks could not be elucidated by glancing angle-XRD, which showed peaks with similar width for both unsoaked and soaked samples (Figure 3.16 b).

The chemical analysis was only performed for Si-CPC disks, which were the samples that clearly exhibited the formation of a new apatite layer. The chemical composition of the core area of Si-CPC was the same regardless of the immersion in SBF (Table 3.5), because the SBF only modified the material's surface. Interestingly, the chemical analysis on the surface of Si-CPC disks

showed that the amount of Si ions present in the newly deposited apatite layer was about three times higher than that in the core area (Table 3.5). This result suggested that the Si ions released by Si-CPC were precipitated together with the Ca and P present in the medium, producing a layer of apatite containing the Ca, P and Si that was thermodynamically more stable. In fact, after immersion in SBF, the Ca/P ratio on the surface of the Si-CPC was also higher than that of the core area (Table 3.5), indication that the new apatite layer was constituted by CDHA more close to the stoichiometric one than that of the core area.

It is known that when a bioactive material is immersed in a physiological medium such as SBF, a chain of reactions are triggered. The evolution of this process has been well defined by materials containing SiO_2 such as Bioglass (24.5% Na_2O − 45%SiO_2 − 24.5% CaO − 6% P_2O_5) [29]. Firstly, there is an interaction between the material and the medium (either distilled H_2O or SBF), including the following steps: 1) formation of SiOH bonds; 2) polycondensation of Si-O-Si; 3) adsorption of amorphous $Ca-PO_4-CO_3$ phases; and 4) crystallization of a hydroxy carbonate apatite. Secondly, the material interacts with the tissue, adsorbing biological moieties and, afterwards, interacting with osteoblasts that create and crystallize the extracellular matrix [29]. Since the chemical composition of Si-CPC is very different than that of Bioglass, the interaction between the material and the medium would be different, but the interaction between the material and the tissue would probably follow a similar pattern.

The Si present in HA can promote the biomimetic precipitation by a combination of several factors: i) increasing the solubility of the materials via creation of defects in the lattice [1] [20] [21] [26], ii) creating a more electronegative surface due to the substitution of SiO_4^{4-} for PO_4^{3-} [30], and iii) generating smaller grains size [31] [32] [33] [34] with more triple point junctions per unit area, which facilitates increased dissolution at the surface [35]. In the current work, since Si-CPC had a similar solubility in SBF than CPC, the fact that a newly apatite layer was more evidently observed on the surface of Si-CPC disks than that of CPC disks was associated to the presence of SiO_4^{4-} groups on the surface of Si-CPC, increasing the electronegative charge of the material [30] [36]. Thus, preferential sites for nucleation would be provided and a higher adsorption of positive Ca ions would occur, resulting in a positive layer that attracts the phosphate groups, leading to the formation of the apatite layer [23] [37]. These explanations are schematically shown in Figure 3.21.

CPC: Ca, P

Ca   P   Ca   P

⊖   ⊖   ⊖   ⊖

Ca, P

Ca, P

P^{5+}
Ca^{2+}

Si-CPC: Ca, P, Si
(distorted lattice)

Si   Ca   P   Ca
Ca   P   Si
P   Ca   P   Ca

⊖⊖⊖⊖⊖⊖⊖⊖

SiO_4^{4-} (increases (-) charge)

P^{5+}, Si^{4+}
Ca^{2+}
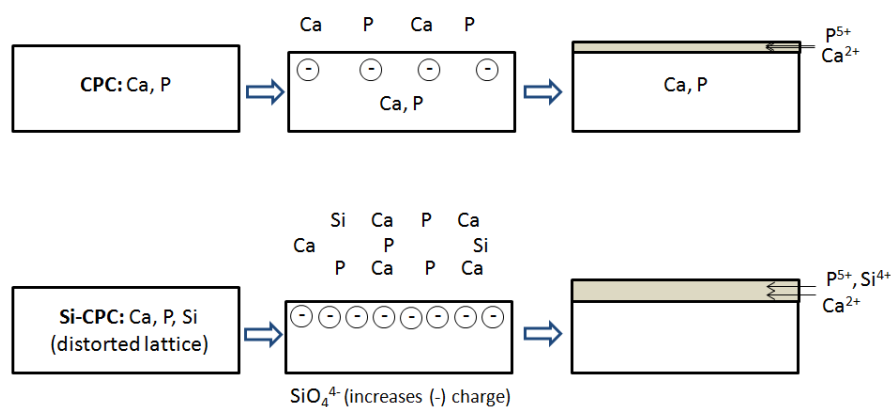
Figure 3.21. Comparative schema of the bioactivity kinetics for CPC and Si-CPC immersed in SBF solution.

As previously indicated, the deposition of the new apatite layer was not clearly observed on the surface of CPC samples. This fact was a surprising outcome of this study, since CDHA is well-known as a bioactive material [29]. However, under the conditions of the study, the apatite layer could have been deposited at longer time. Various bioactive materials can stimulate the formation of an apatite layer at different times, with diverse thickness and also by different mechanisms [29]. Regarding the different time at which the apatite layer can be observed, for instance, Kim *et al.* showed that the apatite forming ability of a $Na_2O-CaO-SiO_2$ glass varied largely with the composition of the material, from 0.5 to longer than 28 days [38]. Similarly, Balas *et al.* showed that after 6 weeks the Si-HA was more efficiently covered by an apatite layer than HA, which was associated with its higher efficiency trapping Ca ions from the solution [39]. Another *in vitro* study showed that HA maintained the same morphology after being immersed in SBF for 5 weeks, while Si-HA was clearly covered by an apatite layer that had a different morphology than the substrate [25]. Other works have also indicated that Si-substituted HA has a markedly enhanced *in vitro* apatite formation in SBF [23] [40].

Nevertheless, it is important to point out that the use of SBF to evaluate the bioactivity *in vitro* has recently been questioned [2]. Three main problems can be ascribed to this method. The first problem is that, although many improvements have been performed, none of the developed SBFs exactly simulates the composition of human blood serum, since the SBF i) has absence of proteins, which are known to play an essential role in controlling apatite nucleation [41] [42]; ii)

contains TRIS to buffer SBF solutions; and iii) the carbonate content is not controlled, although carbonates act as pH buffer in serum [43]. The second problem of SBF is that it is a highly supersaturated solution with respect to the apatite [44], which entails that i) special care has to be taken to prepare SBF with no precipitation [10], and ii) apatite can precipitate on any material surface with time (induction time), making it difficult to discern on the bioactive capacity of the material [2]. The third important limitation of testing the bioactivity of a material with SBF is that, in some cases, the method can lead not only to false positive but also to false negative results [52].

3.5.4 Cell culture study

Another objective of the study was to correlate the cell response with the ion exchange between the CPC formulations and the culture medium. For this reason the cells were cultured in inserts in presence of Si-CPC and CPC. The evolution of [Ca], [P], [Si] and pH in the culture medium surrounding the cells was monitored. The medium in presence of CPC and Si-CPC had very low [Ca] (Figure 3.20 a), suggesting a continuous Ca uptake by the cements, and a [P] higher than the control medium (Figure 3.20 b), in agreement with other works [45] [28] [46]. Si was detected only in the medium in contact with Si-CPC, at a concentration of approximately 1.5 mM (Figure 3.20 c). These results revealed that ion exchange between the CPC and the culture medium was taking place.

As shown in the present data, cell behavior was strongly affected by the shifts in ionic concentrations of the culture media. The proliferation pattern was very similar for the cells in presence of the two cements, being significantly delayed in comparison with the cells in the control medium (Figure 3.19 a). A similar delay in cell proliferation was reported in previous studies where osteoblastic-like cells were cultured in direct contact [45] [28] [46] [47] or in extracts of hydroxyapatite cements [46] [28]. Hempel *et al.* [28] verified that the low [Ca] and high [PO_4] in the culture media in presence of the CPC resulted in cell necrosis. Although it is clear that any modification of the pH as well as of the [Ca] and [PO_4] lead to a reduced proliferation, it is difficult to ascribe this effect to a specific ion. Several works have addressed the influence of [Ca] on the regulation of essential osteoblastic functions [48] [49]. However, only a few have evaluated the effect of lowering [Ca] in osteoblastic cells, which in fact appear to be opposite of those of elevating [Ca]. Thus, Dvorak *et al.* showed that lowering [Ca] to 0.5 mM decreased fetal rat

calvarial cell proliferation [48], and Shie *et al.* [50] reported a lack of osteoblastic MG63 cell proliferation in low [Ca] medium (0-0.35 mM). Farley *et al.* [51] showed that a decrease of [Ca] from 2 to 0.2 mM reduced Saos-2 cell proliferation. It is interesting to note that the Si found in the culture medium in presence of the Si-CPC did not produce any difference in cell proliferation compared with those cultured in presence of CPC, contrary to the results obtained in previous studies [52] [50] that reported an enhanced cell proliferation in presence of aqueous Si.

Moreover, the cells in presence of both CPC and Si-CPC showed a statistically significant increase of the ALP activity compared with the control medium ($p < 0.05$), although the kinetics was not affected (Figure 3.19 b). It is again difficult to ascribe this behavior to the concentration shift of a specific ion, especially if it is considered that the sensitivity to the ionic concentration depends on cell-type. In general it is accepted that elevations in [Ca] enhances osteoblastic differentiation [48] [49]. However, the role of [P] can be even more significant [53]. In fact, the results of our work are in good agreement with those reported by Farley *et al.* [51], who analyzed the effect of extracellular [Ca] and [P] on ALP activity and release in Saos-2 cells. They reported that the amount of ALP activity was directly dependent on [P] (medium containing 1.8 mM Ca and a [P] between 0.25-2.0 mM) and inversely dependent, although to a lower extent, on [Ca] (medium containing 1.0 mM P, and a [Ca] between 0.25-2.0 mM). These results are consistent with the increased ALP activity detected in our study in presence of the CPC, where [P] was increased and [Ca] was reduced. Enhanced cell differentiation was also reported in osteoblastic [46] and in human bone marrow osteoprogenitor cells [47] cultured on the surface of apatitic CPC, although in these studies, in addition to ionic concentrations, surface-related effects could also play a role.

Interestingly, the Si-containing CPC elicited a statistically significantly higher ($p < 0.05$) ALP activity at 14 days (Figure 3.19 b), when the maximum activity was reached. This result is in accordance with other studies that reported a favorable effect of Si-releasing compounds on the differentiation of osteoblastic-like cells [54]. Similarly, an enhanced ALP activity was found in rMSC cultured in contact or in presence of a bioactive glass, where [Si] levels in the culture medium were similar to those of the present study [55]. Lower [Si] were also shown to result in enhanced differentiation of the osteoblastic-like MG-63 cell line when soluble Si was added in the culture medium, in the form of orthosilicic acid [56]. In all these reported studies, as in the present work,

the enhanced cell differentiation cannot be attributed to a direct interaction of the cells with the materials, but to the Si released to the culture medium by the materials. However, the mechanism through which Si improves the bioactivity and the cellular response of a material is still unknown [52].

It is quite difficult to predict any *in vivo* response from these results, since it is not even possible to say that the same trend would have been observed if a direct method would have been used to perform the *in vitro* study. If cells would have been cultured on the surface of the material, the cell behavior would have been determined by both the ions released to the medium and the surface properties of the material. Moreover, the Si-CPC, which is expected to have a more electronegative charge than CPC, is foreseen to interact in a different way with proteins than CPC [57]. This could lead to differences in the interaction with integrins, consecutively triggering specific signals that may regulate many cellular functions such as cell attachment, proliferation and differentiation, or even mobility and shape [57].

3.6 Conclusions

This Chapter deals with the preparation of Si-doped CPC, using α-TCP doped with Si as a reactant. CPC prepared from undoped α-TCP was used as control. Si-CPC and CPC were characterized in terms of physico-chemical properties, ion exchange with two media, bioactive properties and cell behavior. The most outstanding conclusions extracted from this work are indicated below.

1. The Si-stabilized α-TCP was suitable for the fabrication of a cement (Si-CPC), with setting and cohesion times adequate for clinical applications. Si-stabilized α-tricalcium phosphate was completely hydrolyzed to a calcium deficient hydroxyapatite, showing a faster reaction kinetics than its Si-free counterpart, as proved by its shorter setting and cohesion times, as well as its higher earlier compressive strength. Upon complete reaction the crystalline phases, morphology and mechanical properties of both cements were similar.

2. The *in vitro* bioactivity of the CPC was enhanced by the addition of Si. The formation of an apatite layer when immersed in SBF was accelerated by in the Si-containing CPC as compared to the conventional CPC. This apatite layer formed had a higher Ca/P ratio and a higher Si content than the core material.

3. An *in vitro* study with osteoblast-like cells showed that the cell proliferation was decreased and the cell differentiation enhanced due to the modification of the ionic concentration of the medium by the cements. This was mainly ascribed to the strong decrease in [Ca], since both CPC and Si-CPC uptake Ca ions. Si-CPC further enhanced the ALP activity of the cells, which could be related to the release of Si ions.

3.7 Acknowledgements

3.8 References

[1] Boanini E, Gazzano M, Bigi A. Ionic substitutions in calcium phosphates synthesized at low temperature. Acta Biomaterialia 2010; 6: 1882–1894.

[2] Bohner M, Lemaitre J. Can bioactivity be tested in vitro with SBF solution? Biomaterials 2009; 30: 2175–2179.

[3] ASTM International C266-03. Standard test method for time of setting of hydraulic-cement paste by Gillmore needles.

[4] Fernández E, Boltong MG, Ginebra MP, Driessens FCM, Bermúdez O, Planell JA. Development of a method to measure the period of swelling of calcium phosphate cements. Journal of Materials Science Letters 1996; 15: 1004–1005.

[5] Joint Committee for Powder Diffraction Studies (JCPDS). International Center for Diffraction Data and American Society for Testing Materials. Powder diffraction file (Inorganic and Organic). Swarthmore (USA), 1991.

[6] Inorganic Crystal Structure Database (ICSD). Institut Laue-Langevin (ILL), Grenoble, France.

[7] Rodríguez-Carvajal J. Fullprof.2k Software. CEA-CNRS; 2007.

[8] Norma Española ISO No. 10993-12:1997. Biological evaluation of medical devices, part 12: simple preparation and reference materials, 1997; pp. 1–19.

[9] Russo I, Del Mese P, Viretto M, Doronzo G, Mattiello L, Trovati M, Anfossi G. Sodium azide, a bacteriostatic preservative contained in commercially available laboratory reagent, influences the responses of human platelets via the cGMP/PKG/VASP pathway. Clinical Biochemistry 2008; 41: 343–349.

[10] Kokubo T, Takadama H. How useful is SBF in predicting in vivo bone bioactivity? History 2006; 27: 2907–2915.

[11] Friedbacher G, Bubert H (editors). Surface and thin film analysis. Weinheim: Wiley-VCH, 2010.

[12] Aubin J, Liu F. The osteoblast lineage. In: Principles of bone biology. Bilezikian J, Raisz L, Rodan G (editors). San Diego: Academic Press, 1996; pp. 51–67.

[13] Dorozhkin SV. Calcium orthophosphate cements and concretes. Materials 2009; 2: 221–291.

[14] Berry EE. The structure and composition of some calcium deficient apatites. Journal of Inorganic and Nuclear Chemistry 1967; 29: 317–327.

[15] Ginebra MP, Fernández E, De Maeyer EAP, Verbeeck RMH, Boltong MG, Ginebra J, Driessens FCM, Planell JA. Setting reaction and hardening of an apatitic calcium phosphate cement. Journal of Dental Research 1997; 76: 905–912.

[16] Mollah M, Promreuk S, Schennach R, Cocke D, Guler R. Cristobalite formation from thermal treatment of Texas lignite fly ash. Fuel 1999; 78: 1277–1282.

[17] Simon I, McMahon H. Study of the structure of quartz, cristobalite, and vitreous silica by reflection in Infrared. The Journal of Chemical Physics 1956; 21: 23–30.

[18] Dunfield D, Sayer M, Shurvell HF. Total attenuated reflection infrared analysis of silicon-stabilized tricalcium phosphate. The Journal of Physical Chemistry B 2005; 109: 19579–19583.

[19] Yin X, Stott MJ. Theoretical insights into bone grafting silicon-stabilized alpha-tricalcium phosphate. The Journal of Chemical Physics 2005; 122: 024709-1–9.

[20] Camiré CL, Saint-Jean SJ, Mochales C, Nevsten P, Wang JS, Lidgren L, McCarthy I, Ginebra MP. Material characterization and *in vivo* behavior of silicon substituted alpha-tricalcium phosphate cement. Journal of Biomedical Materials Research B 2006; 76: 424–431.

[21] Sprio S, Tampieri A, Landi E, Sandri M, Martorana S, Celotti G, Logroscino G. Physico-chemical properties and solubility behaviour of multi-substituted hydroxyapatite powders containing silicon. Materials Science and Engineering C 2008; 28: 179–187.

[22] Tuck L, Astala R, Reid JW, Sayer M, Stott MJ. Dissolution and re-crystallization processes in multiphase silicon stabilized tricalcium phosphate. Journal of Material Science: Material Medicine 2008; 19: 917–927.

[23] Botelho CM, Lopes MA, Gibson IR, Best SM, Santos JD. Structural analysis of Si-substituted hydroxyapatite: zeta potential and X-ray photoelectron spectroscopy. Journal of Material Science: Material Medicine 2002; 13: 1123–1127.

[24] Leventouri T, Bunaciu CE, Perdikatsis V. Neutron powder diffraction studies of silicon-substituted hydroxyapatite. Biomaterials 2003; 24: 4205–4211.

[25] Vallet-Regí M, Arcos D. Silicon substituted hydroxyapatites: a method to upgrade calcium phosphate based implants. Journal of Materials Chemistry 2005; 15: 1509–1516.

[26] Porter AE, Patel N, Skepper J, Best SM, Bonfield W. Comparison of *in vivo* dissolution processes in hydroxyapatite and silicon-substituted hydroxyapatite bioceramics. Biomaterials 2003; 24: 4609–4620.

[27] Gustavsson J, Ginebra MP, Engel E, Planell JA. Ion reactivity of calcium-deficient hydroxyapatite in standard cell culture media. Acta Biomaterialia 2011; 7: 4242–4252.

[28] Hempel U, Reinstorf A, Poppe M, Fischer U, Gelinsky M, Pompe W, Wenzel KW. Proliferation and differentiation of osteoblasts on Biocement D modified with collagen type I and citric acid. Journal of Biomedical Materials Research B 2004; 71: 130–143.

[29] Cao W, Hench LL. Bioactive materials. Ceramics International 1996; 8842: 493–507.

[30] Pietak AM, Reid JW, Stott MJ, Sayer M. Silicon substitution in the calcium phosphate bioceramics. Biomaterials 2007; 28: 4023–4032.

[31] Arcos D, Rodríguez-Carvajal J, Vallet-Regí M, Silicon incorporation in hydroxylapatite obtained by controlled crystallization. Chemistry of Materials 2004; 16: 2300–2308.

[32] Porter AE, Patel N, Skepper JN, Best SM, Bonfield W. Effect of sintered silicate-substituted hydroxyapatite on remodelling processes at the bone-implant interface. Biomaterials 2004; 25: 3303–3314.

[33] Gibson I, Best SM, Bonfield W. Effect of silicon substitution on the sintering and microstructure of hydroxyapatite. Journal of the American Ceramic Society 2002; 85: 2771–2777.

[34] Li XW, Yasuda HY, Umakoshi Y. Bioactive ceramic composites sintered from hydroxyapatite and silica at 1,200°C: preparation, microstructures and in vitro bone-like layer growth. Journal of Materials Science: Materials in Medicine 2006; 17: 573–581.

[35] Porter AE, Best SM, Bonfield W. Ultrastructural comparison of hydroxyapatite and silicon-substituted hydroxyapatite for biomedical applications. Journal of Biomedical Materials Research A 2004; 68: 133–141.

[36] Thian ES, Huang J, Best SM, Barber ZH, Brooks RA, Rushton N, Bonfield W. The response of osteoblasts to nanocrystalline silicon-substituted hydroxyapatite thin films. Biomaterials 2006; 27: 2692–2698.

[37] Himeno T, Kim HM, Kaneko H, Kawashita M, Kokubo T, Nakamura T. Surface structural changes of sintered hydroxyapatite in terms of surface charge. In: Proceedings of the International Symposium on Ceramics in Medicine, Bioceramics 15. Besim Ben-Nissan D, Walsh W (editors). Uetikon- Zuerich: Trans Tech Inc, 2003; pp. 457–460.

[38] Kim HM, Miyaji F, Kokubo T, Ohtsuki C, Nakamura T. Bioactivity of Na_2O-CaO-SiO_2 glasses. Journal of the American Ceramic Society 1995; 78: 2405–2411.

[39] Balas F, Pérez-Pariente J, Vallet-Regí M. *In vitro* bioactivity of silicon-substituted hydroxyapatites. Journal of Biomedical Materials Research A 2003; 66: 364–375.

[40] Gibson I, Huang J, Best SM, Bonfield W. Enhanced *in vitro* cell activity and surface apatite layer formation on novel silicon- substituted hydroxyapatites. Bioceramics 1999; 12: 191–194.

[41] Juhasz J, Best SM, Auffret A, Bonfield W. Biological control of apatite growth in simulated body fluid and human blood serum. Journal of Materials Science: Materials in Medicine 2008; 19: 1823–1829.

[42] Garnett J, Dieppe P. The effects of serum and human albumin on calcium hydroxyapatite crystal growth. Biochemical Journal 1990; 266: 863–868.

[43] Teitelbaum S. Bone resorption by osteoclasts. Science 2000; 289: 1504–1508.

[44] Neuman WF, Neuman MW. The chemical dynamics of bone mineral. Chicago: The University of Chicago Press, 1958; p. 34.

[45] Knabe C, Driessens FCM, Planell JA, Gildenhaar R, Berger G, Reif D, Fitzner R, Radlanski RJ, Gross U. Evaluation of calcium phosphates and experimental calcium phosphate bone cements using osteogenic cultures. Journal of Biomedical Materials Research 2000; 52: 498–508.

[46] Engel E, del Valle S, Aparicio C, Altankov G, Asin L, Planell JA, Ginebra MP. Discerning the role of topography and ion exchange in cell response of bioactive tissue engineering scaffolds. Tissue Engineering A 2008; 14: 1341–1351.

[47] Oreffo ROC, Driessens FCM, Planell JA, Triffitt JT. Growth and differentiation of human bone marrow osteoprogenitors on novel calcium phosphate cements. Biomaterials 1998; 19: 1845–1854.

[48] Dvorak MM, Siddiqua A, Ward DT, Carter DH, Dallas SL, Nemeth EF, Riccardi R. Physiological changes in extracellular calcium concentration directly control osteoblast function in the absence of calciotropic hormones. Proceedings of the National Academy of Science 2004; 101: 5140–5145.

[49] Maeno S, Niki Y, Matsumoto H, Morioka H, Yatabe T, Funayama A, Toyama Y, Taguchi T, Tanaka J. The effect of calcium ion concentration on osteoblast viability, proliferation and differentiation in monolayer and 3D culture. Biomaterials 2005; 26: 4847–4855.

[50] Shie MY, Ding SJ, Changa HC. The role of silicon in osteoblast-like cell proliferation and apoptosis. Acta Biomaterialia 2011; 7: 2604–2614.

[51] Farley JR, Hall SL, Tanner MA, Wergedal JE. Specific activity of skeletal alkaline phosphatase in human osteoblast-line cells regulated by phosphate, phosphate esters, and phosphate analogs and release of alkaline phosphatase activity inversely regulated by calcium. Journal of Bone and Mineral Research 1994; 9: 497–508.

[52] Botelho CM, Brooks RA, Best SM, Lopes MA, Santos JD, Rushton N. Human osteoblast response to silicon-substituted hydroxyapatite. Journal of Biomedical Materials Research A 2006; 79: 723–730.

[53] Beck GR. Inorganic phosphate as a signaling molecule in osteoblast differentiation. Journal of Cellular Biochemistry 2003; 90: 234–243.

[54] Keeting PE, Oursler MJ, Wiegand KE, Bonde SK, Spelsberg TC, Riggs BL. Zeolite A increases proliferation, differentiation, and transforming growth factor β production in normal adult human osteoblast-like cells in vitro. Journal of Bone and Mineral Research 1992; 7: 1281–1289.

[55] Radin S, Reilly G, Bhargave G, Leboy PS, Ducheyne P. Osteogenic effects of bioactive glass on bone marrow stromal cells. Journal of Biomedical Materials Research A 2005; 73: 21–29.

[56] Reffitt DM, Ogston N, Jugdaohsingh R, Cheung HF, Evans BA, Thompson RP, Powell JJ, Hampson GN. Orthosilicic acid stimulates collagen type 1 synthesis and osteoblastic differentiation in human osteoblast-like cells *in vitro*. Bone 2003; 32: 127–135.

[57] Thian ES, Huang J, Best SM, Barber ZH, Bonfield W. Silicon-substituted hydroxyapatite: the next generation of bioactive coatings. Materials Science and Engineering C 2007; 27: 251–256.

PART 2.

Magnesium phosphate cements for

endodontic applications

"Man never made any material as resilient as the human spirit"

Bern Williams

Part 2:

Magnesium phosphate-based cements (MPC)

Chapter 4. Theoretical framework
- Magnesium phosphate-based cements (MPCs)
- MPCs for clinical applications
- Teeth, root canal therapy and root canal filling materials
- Properties required for root canal filling materials

⇩

Chapter 5. Development of MPCs
- Development of three formulations of MPCs
- Physico-chemical characterization

⇩

Chapter 6. Biological properties of MPCs
- Optimization of the MPCs for clinical applications
- Evaluation of the antimicrobial properties
- Evaluation of the cell viability

⇩

Chapter 7. Tailoring MPCs for endodontic applications
- Development of radiopaque MPCs
- Physico-chemical characterization
- Specific characterization for root canal filling materials

Chapter 4.

Theoretical framework

Table of contents

4.1 Magnesium phosphate-based cements

4.1.1 Brief history

Magnesium-phosphate-based ceramics were discovered during 1939-1940 by Prosen [1,2] and Earnshaw [3] as investment materials for casting alloys. Several patents have been issued in Europe and in the United States on similar materials [4], in which magnesium oxide reacted with phosphoric acid or a source of phosphorous pentoxide, forming magnesium dihydrogen phosphate hydrated [$Mg(H_2PO_4)_2 \cdot nH_2O$] as a reaction product. However, the high solubility of the end-product motivated a modification of the reaction, and ammonium, sodium or potassium phosphate salts were used instead of phosphoric acid.

Another modification that has suffered the initial MPC is the procedure to mix the reactants. Initially the MPC system was constituted by a phosphate compound in a liquid phase and magnesia in a powder phase, which had to be mixed prior to its application [5]. In 1974, they were developed as a two-components system, the powder product requiring only the addition of water prior to its application *in situ*, thus simplifying further the use of MPCs [6].

The number of publications (papers or patents) regarding magnesium phosphate cements from 1951 to 2011 was consulted on the Web of Knowledge[1] (www.accesowok.fecyt.es/). Two different searches were done to determine, on one hand, the number of publications in magnesium phosphate cements used in non-clinical applications (coded as MPC) and, on the other hand, the number of publications regarding magnesium phosphate cements used in medical applications (coded as MPC-biomaterial). The topic entrances executed are indicated below.

• MPC: "magnesium phosphate" cement NOT medicine, bone, clinics, biomaterials.

• MPC-biomaterial: "magnesium phosphate" cement AND medicine, bone, clinics, biomaterials

The search of MPC resulted in a total of 85 publications and it was reduced to 31 when the words related with clinics were included. The amount of publications regarding magnesium phosphate cements (MPCs) started to increase in the 1980s due to the use of this material for civil

---

[1] Study realized on 31st of March 2012

engineering. Between 1980 and 2000, about 40% of the total publications on this topic were published and 49 entries out of 85 were found from 2000 to 2011 (58% out of total). In contrast, regarding the MPC as a biocement, there were only 3 publications until 2000. However, in the 2000s decade, the interest about using MPC in clinical applications start increasing and 26 entries out of 28 (93% out of total) were found from 2000 to 2011. These data clearly indicated a very recent and increasing interest on this topic. Table 4.1 shows the number of publications per decade, including apart the publications of 2011. The accumulative percentage of the total publications for both MPC and MPC-biomaterial is plotted in Figure 4.1 in the period comprised between 1951 and 2011.

Table 4.1. Number of publications found, including papers or patents, using as entry either "magnesium phosphate" cement + NOT medicine, bone, clinics or biomaterials (coded as MPC) or "magnesium phosphate" cement AND medicine, bone, clinics or biomaterials (coded as MPC-biomaterial). Information extracted from the web of knowledge (www.accesowok.fecyt.es/) on 31st of March 2012.

Number of publications (papers or patents)		
Period of time	MPC	MPC-biomaterial
1951-1960	0	0
1961-1970	0	0
1971-1980	1	0
1981-1990	18	0
1991-2000	17	3
2001-2010	41	17
2011	8	9
Total	85	29
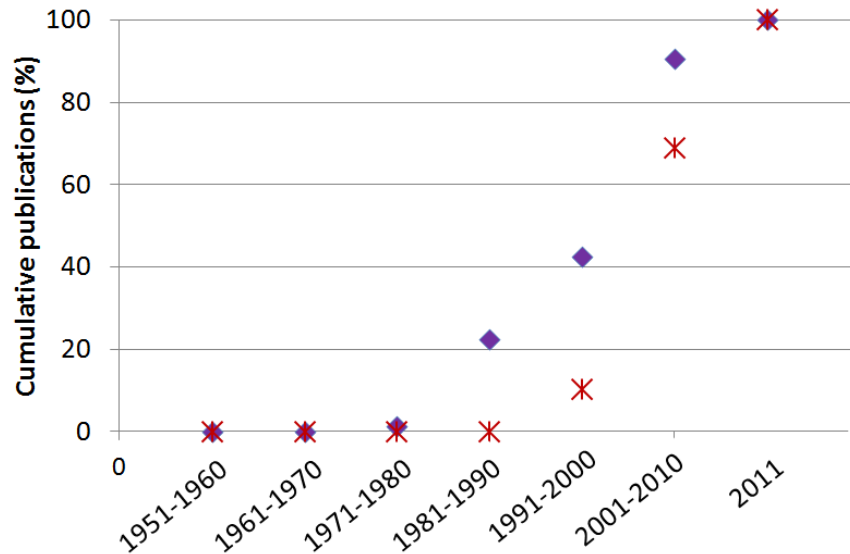
Figure 4.1. Accumulative percentage of publications (papers or patents) per decade, from 1951 to 2011, using as entry either "magnesium phosphate" cement + NOT medicine, bone, clinics or biomaterials (coded as MPC) or "magnesium phosphate" cement AND medicine, bone, clinics or biomaterials (coded as MPC-biomaterial). Information extracted from the web of knowledge (www.accesowok.fecyt.es/) on 31st of March 2012.

4.1.2 Use in civil engineering

Several magnesium phosphate-based cements were developed to be used as structural materials during the second half of the last century. Specifically, MPCs were used to repair concrete in the United States in early 1970s and in early 1980 in the United Kingdom [7].

The main advantages pointed out for the MPCs as concrete repair material are their quick setting and accelerated development of strength [8], their ease of application and their moderate cost. The fast early strength of MPC mortars made them suitable patching materials for concrete pavings, particularly where a minimum delay to traffic or any work disruption is of the utmost importance [7,9], as displayed in Figure 4.2. The MPC mortars have been used for patching and repair work of concrete in highways in cold regions, bridge decks, airport runways and industrial floors [7].
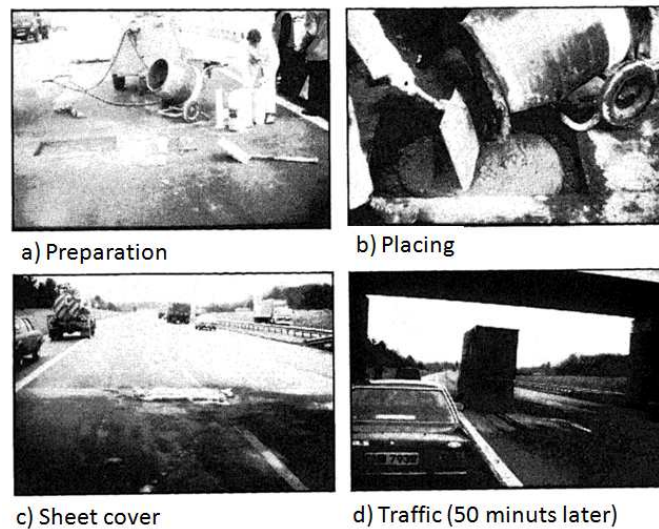
Figure 4.2. Thin bonded repair at joint of a motorway, in 1981. The traffic was opened 50 minutes after placing the cement (from [9]).

Ten years after the initial utilization of MPC mortar in the United States, there was evidence of its good and long performance as concrete patching materials [7]. Other studies evaluating the durability of the hardened MPC mortar and concrete when exposed to the action of freezing and thawing, showed excellent results. The cement dimensions showed to be stable after setting, with just 0.02% of expansion, which did not cause any excessive or detrimental stress to the repair area. The permeability of the material was also reported to be low, with an absorption below than 1% after 28 days. A good bonding to the substrate was also reported [7,9,10].

The reactants commonly used for the preparation of MPCs for patching were magnesia and ammonium hydrogen phosphate, blended with selected fine aggregates. When the powder was mixed with water, an exothermic reaction took place, producing mainly struvite ($MgNH_4PO_4 \cdot 6H_2O$) [7]. During the reaction, ammonia was released, which led to container corrosion and created an unpleasant environment odor, restricting its use to outdoor applications [11]. The material set in about 15 min at 20°C and after one hour its compressive strength was over 20 MPa. Its color and appearance were similar to that of ordinary Portland cement [7].

The fast setting and the exothermia of the magnesium phosphate cements has been tailored by adding retardants to the powder phase [12–14] and by calcining the MgO in order to decrease its reactivity [11,12,15].

4.1.3 Chemistry of magnesium phosphate cements

The phosphate bonded cements are formed by the reaction of metal cations, generally an oxide (*e.g.* MgO or ZnO), with phosphate anions (either phosphoric acid or an acid phosphate) [16]. The first magnesium phosphate cement developed was formed by a reaction between magnesium oxide (MgO) and phosphoric acid (H_3PO_4), forming magnesium dihydrogen phosphate hydrated [$Mg(H_2PO_4)_2 \cdot nH_2O$] as a reaction product (Reaction 4.1). The main drawbacks of this reaction are two: i) the resulting product sets very rapidly, thus allowing very little working time, and ii) the $Mg(H_2PO_4)_2 \cdot nH_2O$ formed is a water-soluble product.

Reaction 4.1. $MgO + H_3PO_4 \rightarrow Mg(H_2PO_4)_2 \cdot nH_2O$
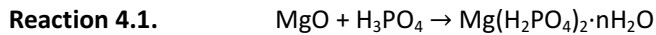
Ceramics with very low solubility can be formed by replacing one or two hydrogens of phosphoric acid by cations, which will also replace the hydrogens of the end product. Salts such as ammonium mono- or dihydrogen phosphate (($NH_4)_2HPO_4$ or $NH_4H_2PO_4$) [12,17], ammonium polyphosphate ($NH_4PO_3)_n$ [12], sodium polyphosphate (($NaPO_3)_n$) [18] or potassium dihydrogen phosphate (KH_2PO_4) [19] provide the necessary additional cation. Then, when MgO reacts with one of these phosphate salts, the major products can be represented by the formula $Mg(X_2PO_4)_2 \cdot nH_2O$ or $MgXPO_4 \cdot nH_2O$, where X is hydrogen (H), ammonium (NH_4), sodium (Na) or potassium (K). The general reactions are displayed in Reaction 4.2 and 4.3 and the reaction products are listed in Table 4.2.

Reaction 4.2. $MgO + XH_2PO_4 + H_2O \rightarrow Mg(X_2PO_4)_2 \cdot nH_2O$ X = H, NH_4, Na, K

Reaction 4.3. $MgO + X_2HPO_4 + H_2O \rightarrow MgXPO_4 \cdot nH_2O$ X = H, NH_4, Na, K
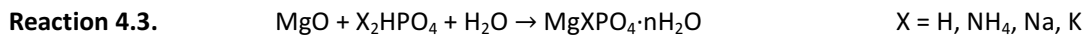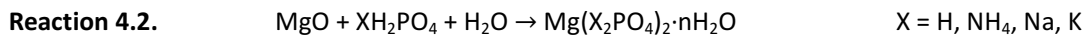
Table 4.2. Phases found in magnesium phosphate ceramics (from [16]).

Formula	Name	Reference
$Mg(H_2PO_4)_2 \cdot 2H_2O$	Magnesium dihydrogen phosphate	[18]
$Mg(H_2PO_4)_2 \cdot 4H_2O$	Magnesium dihydrogen phosphate	[18]
$MgHPO_4 \cdot 3H_2O$	Newberyite	[20]
$MgHPO_4 \cdot H_2O$; $MgHPO_4 \cdot 2H_2O$	Haysite	[21]
$Mg(NH_4 \cdot HPO_4)_2 \cdot 4H_2O$	Schertelite	[8,22–24]
$MgNH_4PO_4 \cdot 6 H_2O$	Struvite	[8,22–24]
$MgNH_4PO_4 \cdot H_2O$	Dittmarite	[8,22–24]
$MgK(PO_4)_2 \cdot 6H_2O$	Magnesium potassium phosphate	[7]
$Mg_3(PO_4)_2 \cdot 4H_2O$	Magnesium phosphate	[12]

Newberyite, struvite, magnesium potassium phosphate and magnesium phosphate are the most stable phases among the listed in Table 4.2 [16].

The phosphate bonded cements can be catalogued within the acid-base cements, because they are formed by a reaction between an acid and an alkaline compound [16]. The steps that form the acid-base cements have been summarized by Wilson *et al.* [25], Soudée *et al.* [26] and Wagh *et al.* [16,27]. The alkaline compounds that form acid-base cements (*e.g.* MgO) are sparsely soluble, in other words, they dissolve slowly and in a small fraction. On the other hand, acids (*e.g.* phosphate salt) are inherently soluble species. This implies that the acid solubilizes first, decreasing the pH and enhancing the dissolution of the bases, which occurs slowly. The dissolved species then react to form neutral complexes, which constitute a gel. When the gel crystallizes, a process that is inherently slow, it forms a solid in the form of a ceramic [16]. Coherent bonds can only be developed among precipitating particles that grow into crystalline structures and form a ceramic if the reaction rate is controlled properly.

This mechanism of reaction produces a protective coating of less soluble products on the surface of the MgO particles, inhibiting the reaction between the core of individual MgO particles and the solubilized acid compounds. In most cases, saturation of the gel is accomplished even before all the basic material, namely MgO, is totally dissolved. The process is illustrated in Figure

4.3. The unreacted particles of MgO form a second phase that is good for the overall strength and integrity of the ceramic since it resists crack propagation within the ceramic, providing rigidity to the matrix and improving the fracture toughness of the ceramic [16].
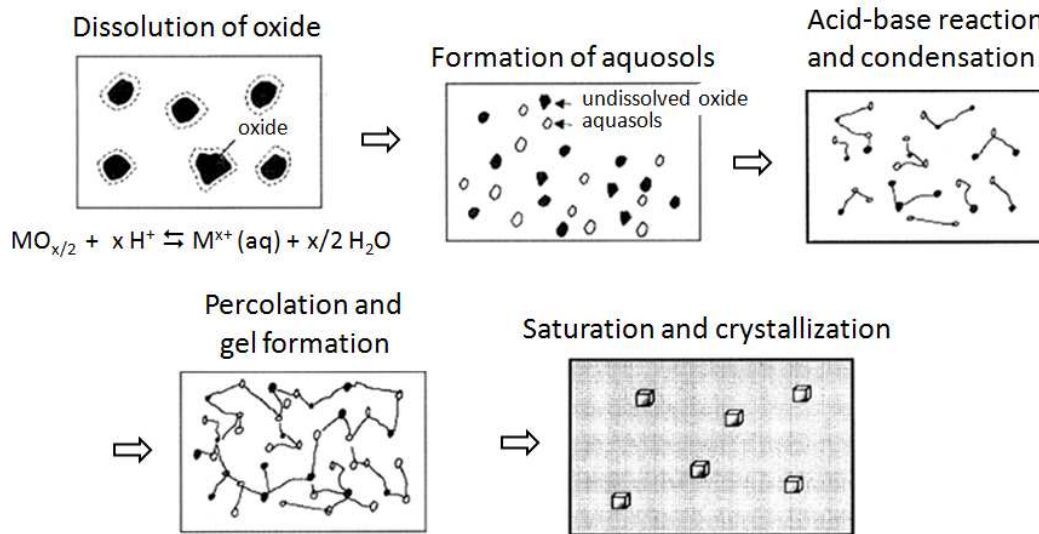
Figure 4.3. Pictorial representation of the formation of chemically bonded phosphate ceramic (from [16]).

4.2 Mg-based compounds as biomaterials

Mg is known to be an important trace element in bones and teeth. Indeed, despite its low concentration (generally between ~ 0.5 and 1.5 wt%), it plays a key role in bone metabolism, in particular during the early stages of osteogenesis [28]. Mg influences both matrix and mineral metabolism of bone by a combination of hormone effects and other factors that regulate skeletal and mineral metabolism. It has been proved that Mg stimulates osteoblast proliferation [29] and the level of Mg increases at the beginning of the calcification process, in comparison to the normal physiological values [30]. In contrast, Mg depletion affects all stages of skeletal metabolism adversely, causing cessation of bone growth, decreased osteoblastic and osteoclastic activity, osteopenia and bone fragility [31–33]. In fact, osteoporosis, a metabolic bone disorder characterized by decreased bone mass, which increases bone fragility, has been associated with low amounts of Ca, Mg and vitamin D intakes [34]. In conclusion, there is growing evidence that

Mg may be an important factor in the qualitative changes of the bone matrix that determine bone fragility [31,32,35].

Given the relevant role of Mg in bone metabolism [28], many research teams have worked, on one hand, in developing metallic implants based on Mg and its alloys and, on the other hand, in the preparation of both calcium-phosphate materials doped with Mg and magnesium phosphate-based materials.

The preparation of metallic implants based on Mg and its alloys has been recently considered. These materials are investigated as lightweight, degradable, load bearing orthopedic implants, which would remain present in the body and maintain mechanical integrity over a time scale of 12–18 weeks while the bone tissue heals, eventually being replaced by natural tissue [36]. The main problem of this metal is that it can corrode too quickly, producing hydrogen gas. However, several possibilities exist to tailor the corrosion rate of Mg [37]. A Mg alloy has also proved to have antimicrobial properties against *E. coli*, *P. aeruginosa* and *S. aureus* due to both the release of Mg ions and the increase of pH [38].

Many efforts have been focused on doping calcium phosphates with Mg. According to literature, the replacement of calcium by magnesium in hydroxyapatite (HA) is limited. This is related to the large size difference between Mg and Ca ions (~ 0.28 Å difference in radius according to the Pauling scale), which leads to strong distortions of the HA lattice and reduces its crystallinity [28]. These changes have a direct impact on the properties of Mg-HA, compared to its non-substituted analogous [39,40]: the solubility and biodegradability in physiological fluids is increased and the thermal conversion into β-tricalcium phosphate (β-TCP) is favored. The incorporation of Mg also plays an important role in the biological responses of bone cells. *In vivo*, Mg-doped HA has shown to enhance bioactivity and osteoconductivity with respect to free Mg-HA [29,39,41,42].

Magnesium phosphates may occur in physiological and pathological mineralized tissues [43,44]. Whitlockite (β-tricalcium magnesium phosphate) can be found in salivary gland stones, as well as in dental calculi [43], whilst struvite ($MgNH_4PO_4 \cdot 6H_2O$) and newberyite ($MgHPO_4 \cdot 3H_2O$) are found in kidney stones [44]. Interestingly, these phases can be synthesized into materials showing

promising properties for hard tissue regeneration, as it will be explained in Section 4.2.2. Magnesium phosphates such as cattiite ($Mg_3(PO_4)_2 \cdot 22H_2O$) and newberyite ($MgHPO_4 \cdot 3H_2O$) have showed low cytotoxicity and demonstrated biocompatibility toward osteoblastic cells. Therefore, magnesium phosphate materials are expected to possess a similar bone regenerative capacity to their calcium phosphate counterparts and offer an interesting alternative for a hard tissue engineering scaffold [45].

4.2.1 Calcium magnesium phosphate cements

The development of new materials is stimulated by the rising expectations of customers, who demand new products and higher standards of goods and services [46]. The phosphate bonded cements are characterized to be quick-setting, hard materials and stable in a wide range of pH. Moreover, another great advantage of phosphate bonded ceramics for biomaterials or dental applications is the fact that their structure is mainly made by phosphate groups [16] that, together with calcium, are the main elements constituting the inorganic phase of hard tissues.

In 1993, Driessens *et al.* evaluated over 100 formulations of calcium orthophosphates combining calcium phosphates containing sodium, potassium, magnesium, zinc, carbonate or chloride [47]. One year later, Ginebra *et al.* focused in the preparation of magnesium-containing calcium phosphate cements, which showed successful setting times and compressive strength at the composition $CaMg_2(PO_4)_2 \cdot xH_2O$ [48]. Moreover, this composition had an alkaline character during and after setting, indication that it could promote the precipitation of bone mineral from the body fluids [49].

In 1994, Driessens *et al.* reported three new formulations of calcium magnesium phosphate cements (CMPCs) that had appropriate setting time and compressive strength for clinical applications [50]. The end-product of the three formulations was $CaMg_2(PO_4)_2$ and it was the result of mixing: i) MCPM + MgO; ii) DCPA + MgO + $MgHPO_4 \cdot 3H_2O$; or iii) DCPD + MgO + $MgHPO_4 \cdot 3H_2O$. As a continuation of this work, the same authors performed an *in vivo* study one year later [51], in which the CMPC prepared with DCPA + MgO + $MgHPO_4 \cdot 3H_2O$ (formulation ii) was tested. Initially, $Mg(OH)_2$ was formed, although this phase was completely dissolved after 8 weeks,

being substituted by apatite. Even though that the use of CMPCs for bone regeneration was promising, no other papers were published until 10 years later.

In 2005, Driessens *et al.* prepared new formulations of CMPCs [52] using as reactants $Mg_3(PO_4)_2$, $MgHPO_4 \cdot 3H_2O$ and different calcium phosphate reactants, such as PHA, $CaHPO_4$, $CaHPO_4 \cdot H_2O$, β-TCP and α-TCP and a $(NH_4)_2HPO_4$ solution as liquid phase. The studied CMPCs formulations had a high early strength, which was envisaged as the main advantage of Mg incorporation. Similarly, a patent by Zimmermann indicated that CMPCs could be prepared with different mixtures of calcium phosphates, magnesium phosphates and ammonium phosphates, and claimed that these cements could be used for bone regeneration since they are biologically degradable [53].

In 2005, Lilley *et al.* incorporated Mg ions into brushite cements and found that the hydrolysis of brushite to hydroxyapatite was reduced with the presence of Mg [54]. A few years later, Klammert *et al.* indicated that the addition of Mg into brushite cements allowed to tailor their setting time and, moreover, enhanced cell proliferation and differentiation [55]. Klammert *et al.* [56] and Vomdran *et al.* [57] studied the effect of different Ca/P ratios when the CMPCs were prepared with reactants such as $MgHPO_4 \cdot 3H_2O$, $CaHPO_4$ and $CaCO_3$, with ammonium phosphate dissolved in the liquid phase. They reported a fast setting time of the cement and improved biological results due to the presence of Mg.

In 2006, Liu patented the formulations of CMPCs prepared with a combination of TTCP, DCPA and MgO, and ammonium phosphate was added either to the powder or liquid phase [58]. The-end products were HA and struvite. The main advantages claimed for the new formulation were its fast setting and high early compressive strength. Afterwards, these cement formulations were widely studied. In *in vitro* studies, good cell proliferation and differentiation was reported with set CMPCs prepared as dense [59,60] or as macroporous materials [61]. In *in vivo* studies, CMPCs exhibited not only good biocompatibility, biodegradability and osteoconductivity but also enhanced new bone formation [59].

In 2009, Gbureck patented a formulation that comprised magnesium calcium phosphate, ammonium salt and water. This formulation was claimed for bone replacement as bone filler or as

bone glue, which could also act as carrier of pharmaceutical agents. The advantages highlighted for this formulation were its simplicity, defined setting time, good mechanical properties and improved resorbability.

On one hand, one of the advantages that has been claimed for the CMPCs is their fast degradation, which has been proved in *in vitro* studies by soaking set cements in both SBF [62] [59] and Tris-HCl media [60,61,63], and also in *in vivo* studies [59]. On the other hand, a common drawback of the CMPC formulations containing ammonium phosphate is the release of ammonium species that can produce necrosis of the surrounding tissues, as reported by Lu *et al.* [63] and Jia *et al.* [60]. Lu *et al.* suggested using a calcium dihydrogen phosphate instead of ammonium phosphate species.

Table 4.3 summarizes the reactants used for the preparation of different CMPC formulations and the resulting end-products, as well as the main properties attributed to the Mg addition.

Table 4.3. Compendium of literature study showing the reactants used to prepare calcium magnesium phosphate cements (CMPC) for biomedical applications, the formed end-products and the most outstanding properties of the materials. Some abbreviations are used. MCPM: monocalcium phosphate monohydrate; DCPA: dicalcium phosphate anhydrous (monetite), DCPD: dicalcium phosphate dehydrate (brushite); TCP: tricalcium phosphate; OCP: octacalcium phosphate; TTCP: tetracalcium phosphate; FA: fluorapatite; HA: apatite.

Reactants				End-product	Most outstanding properties of the materials	Refs.
Ca (and P) source	Mg-source	P source	Additives (retardants or not)			
i) MCPM ii) DCPA iii) DCPD	i) MgO ii) MgO + MgHPO$_4$·3H$_2$O iii) MgO + MgHPO$_4$·3H$_2$O	(NH$_4$)$_2$HPO$_4$	-	CaMg$_2$(PO$_4$)$_2$ for the three formulations (after 1 day)	Short setting times	[50]
DCP	MgO + MgHPO$_4$·3H$_2$O	-	-	Magnesium phosphate crystals (instead of the expected CaMg$_2$(PO$_4$)$_2$) (after 1 day)	Injectable and good setting time Basic character that may promote bone mineral precipitation from the body fluids	[48]
DCPA	MgO + MgHPO$_4$·3H$_2$O	-	-	CDHA + Mg$_3$(PO$_4$)$_2$·8H$_2$O (after 8 weeks *in vivo*)	Partially degraded *in vivo*	[51]
HA, CaHPO$_4$, CaHPO$_4$·H$_2$O, β-TCP and α-TCP	Mg$_3$(PO$_4$)$_2$, MgHPO$_4$·3H$_2$O	(NH$_4$)$_2$HPO$_4$	-	Not evaluated	High compressive strength	[52]
α/β-TCP, Na$_2$HPO$_4$, KH$_2$PO$_4$	MgHPO$_4$·3H$_2$O, Mg$_3$(PO$_4$)$_2$	NH$_4^+$ in solution or salt		Not evaluated	High biodegradability. Claimed for bone regeneration applications	[53]
Mg-HA: [Mg(NO$_3$)$_2$·6H$_2$O + Ca(NO$_3$)$_2$] + H$_3$PO$_4$	-	-	CDHA, monetite, brushite (after 16 h)	The hydrolysis of brushite into hydroxyapatite was reduced due to the presence of Mg	[54]

Ca (and P) source	Mg-source	P source	Additives (retardants or not)	End-products	Most outstanding properties of the materials	Refs.
Mg-β-TCP: $Mg_xCa_{(x-3)}(PO_4)_2$, $0 < x < 3$ (prepared with $Mg(OH)_2$ + $MgHPO_4 \cdot 3H_2O$) + MCPM	-	Citric acid		$Ca_3Mg_3(PO_4)_4$ (after 24 h)	• Setting time was tailored • Promote the osteoblasts cells proliferation and differentiation	[55]
$Ca(H_2PO_4)_2 \cdot H_2O$	$Mg_{2.25}Ca_{0.75}(PO_4)_2$	$(NH_4)_2HPO_4$	-	Newberite and brushite (after 7 days)	• *In vivo*: higher resorption of CMPC than brushite, newberyite, struvite and hydroxyapatite	[56]
$CaHPO_4$, $CaCO_3$	$MgHPO_4 \cdot 3H_2O$, $Mg(OH)_2$ Different Mg/Ca ratios used: 1, 3, only-Mg	$(NH_4)_2HPO_4$	-	Mg/Ca ratio = 1: $Ca_{1.5}Mg_{1.5}(PO_4)_2$, or mixtures with $Mg_3(PO_4)_2$ for higher Mg/Ca ratios (after 24 h)	• Fast setting and high early compressive strength • *In vitro*: cell proliferation: 3 > only-Mg > 1 • *In vitro*: cell activity: only-Mg > 3 > 1	[57]
α or β-TCP, TTCP, OCP, $CaHPO_4 \cdot H_2O$, HA, FA	MgO	$NH_4H_2PO_4$	Borax (retardant)	Not evaluated	• End-products were HA and struvite • Fast setting and high early compressive strength	[58]
TTCP + DCPA	MgO	$NH_4H_2PO_4$	-	CDHA, TTCP, struvite and MgO (unreacted) (after 48 h)	• Fast setting and high early compressive strength • Fast degradation *in vitro* (SBF)	[62]
TTCP + DCPA	MgO	$NH_4H_2PO_4$	-	CDHA, TTCP, struvite and MgO (unreacted) (after 24 h)	• Fast setting and high early compressive strength • Fast degradation *in vitro* (SBF) • *In vitro*: good cell proliferation and differentiation • *In vivo*: good biocompatibility, biodegradability and osteoconductivity. Mg enhances new bone formation	[59]

Ca (and P) source	Mg-source	P source	Additives (retardants or not)	End-products	Most outstanding properties of the materials	Refs.
TTCP + DCPA	MgO	$NH_4H_2PO_4$	NaCl as porogen agent	CDHA and struvite (after 48 h)	• Fast degradation *in vitro* (Tris-HCl) • *In vitro*: good cell proliferation and differentiation • *In vivo*: good biocompatibility, biodegradation and osteogenesis	[61]
$Ca(H_2PO_4)_2·H_2O$	MgO	$NH_4H_2PO_4$ <u>not</u> added to avoid NH_3 release	-	$Ca_3(PO_4)_2$ and $Mg_3(PO_4)_2$ (after 7 days)	• Fast setting and high early compressive strength • Fast degradation *in vitro* (Tris-HCl) • *In vitro*: good cell proliferation and differentiation	[60]
$Ca(H_2PO_4)_2·H_2O$	MgO	$NH_4H_2PO_4$ <u>not</u> added to avoid NH_3 release	-	CDHA (after 48 h)	• Fast degradation *in vitro* (Tris-HCl) • Bioactivity in SBF: apatite layer formed at 7 days • *In vitro*: cell proliferation and enhanced differentiation (compared with Mg-free counterparts)	[63]

4.2.2 Magnesium phosphate cements

The MPCs for clinical applications have been mainly prepared with two different strategies. The first one uses farrangstonite ($Mg_3(PO_4)_2$) and ammonium phosphate as reactants and, in some cases, struvite was also added [64–68]. The second strategy consists on mixing MgO with a phosphate salt [69,70]. The main end-products resulting include phases such as struvite ($NH_4H_2PO_4 \cdot 6H_2O$) [65–68,70] and newberyite ($MgHPO_4 \cdot 3H_2O$) [64–68] and, in some occasions, one of the reactants ($Mg_3(PO_4)_2$ or MgO) remained unreacted. The reactants used for the preparation of different MPC formulations and the end-products formed, as well as the main properties attributed to the Mg addition, are summarized in Table 4.4.

The MPCs were designed with the idea to be used in the cement form, in order to take advantage of their intrinsic properties (*e.g.* ease of preparation, moldeability, injectability, self-setting *in vivo, etc.*). However, Klammert *et al.* and Vorndran *et al.* have recently proposed the use of MPCs for the preparation of scaffolds by a 3D powder printing method, preparing a layer of farringtonite powder ($Mg_3(PO_4)_2$ and a binder solution of phosphate salts such as ($NH_4)_2HPO_4$ and $NH_4H_2PO_4$ [64,67].

In vitro studies performed by Klammert *et al.* [64] and Gloβart *et al.* [65] showed that MPCs are cytocompatible for both osteoblast and osteoclasts-like cells. Moreover, the MPCs extracts produced neither mutagenicity nor potential carcinogenicity and MPC implanted *in vivo* was not toxic [69]. MPCs have been used in *in vivo* for bone repair [59,71], and also for other applications such as tendon-bone fixation [72,73] and augmentation of bone-screw interfaces [74], since magnesium phosphate-based cements have better adhesion to bone than their calcium phosphate counterparts [73,75].

Nevertheless, Jia *et al.* [60] and Lu *et al.* [63] suggested that ammonium phosphate reactants could compromise the biocompatibility of the material. Following this criterion, in this Thesis NaH_2PO_4 has been proposed as an alternative phosphate salt for the preparation of magnesium phosphate cements [70].

Table 4.4. Compendium of literature studies showing the reactants used to prepare MPC for biomedical applications, the end-products formed and the most outstanding properties of the materials.

Reactants			End-products		Refs.
Mg-source	P source (others)	Additives (retardants or not)		Most outstanding properties of the materials	
$Mg_3(PO_4)_2$	Powder: $(NH_4)_2HPO_4$ Binder solution: $NH_4H_2PO_4$ + $(NH_4)_2HPO_4$	-	$MgHPO_4 \cdot 3H_2O$ + unreacted $Mg_3(PO_4)_2$	• *In vitro*: cell viability was reduced, up to 60%, in comparison with the cell plastic tissue (control)	[64]
Powder: $Mg_3(PO_4)_2$	Binder solution: i) 2 M K_2HPO_4 + 0.5M $(NH_4)_2HPO_4$; or ii) 20% H_3PO_4	-	i) $MgKPO_4 \cdot 6H_2O$) (K-struvite); or ii) $MgNH_4PO_4 \cdot 6H_2O$) $MgHPO_4 \cdot 3H_2O$)	• K-Struvite long setting time, scaffolds do not maintain the structure • Both newberyite and struvite samples could be processed with good dimensional accuracy.	[67]
Powder: $Mg_3(PO_4)_2$	Powder: $NH_4H_2PO_4$ Liquid: pure $(NH_4)_2HPO_4$ or with $(NH_4)_2C_6H_6O_7$	-	Struvite + unreacted $Mg_3(PO_4)_2$	• Pastes can be injected only if $(NH_4)_2C_6H_6O_7$ is added and a powder liquid ratio of 2.5 g/ml is used	[68]
Struvite + $Mg_3(PO_4)_2$	$NH_4H_2PO_4$, $(NH_4)_2HPO_4$	-	Struvite + unreacted $Mg_3(PO_4)_2$	• Struvite samples have a higher solubility than brushite, monetite and CDHA	[65]
Struvite + $Mg_3(PO_4)_2$	$(NH_4)_2HPO_4$	-	Struvite + unreacted $Mg_3(PO_4)_2$	• *In vitro*: struvite had lower anchored molecule osteopontin and produced higher cellular growth and cell activity compared to brushite and CDHA	[66]

Mg-source	P source (others)	Additives (retardants or not)	End-products	Main results associated to Mg	Refs.
MgO	$NH_4H_2PO_4$	Retardant (not specified which one)	Not evaluated	• Extracts produced neither mutagenicity nor potential carcinogenicity • *In vivo*: no toxicity and good resorption	[69]
MgO	i) $NH_4H_2PO_4$ ii) NaH_2PO_4 iii) $NH_4H_2PO_4$ + NaH_2PO_4	Borax (retardant)	i and iii) Struvite + schertelite + unreacted MgO ii) Amorphous compound + unreacted MgO	• Fast setting and high early compressive strength • Antibacterial properties	[70]

4.2.3 MPCs for endodontic applications

In this Thesis, novel MPCs containing magnesium oxide in excess have been developed. It was envisaged that the developed MPCs could have antimicrobial properties since the magnesium oxide is an alkaline compound that could provide the cements with an analogous effect to that of calcium oxide or other alkaline compounds [76–78].

In this context, from now on, the theoretical framework reviews the main applications of cements with antimicrobial properties, which are usually applied in sites where an infection has to be prevented or battled. Even though antimicrobial cements are of great interest in orthopedics, this Thesis is focused to endodontic applications. Therefore, an introduction of the teeth, the root canal therapies and the root canal filling materials has been included.

4.3 Teeth

Teeth are dense structures found in the jaws of many vertebrates. The primary function of teeth is to tear and to chew food, while for carnivores they are also a weapon. Therefore, teeth have to withstand a range of physical and chemical processes, including compressive forces (up to ~ 700 N), abrasion and chemical attack due to acidic foods or products of bacterial metabolism. The roots of teeth are covered by the gums. The cutting edges of teeth are covered by an enamel layer of about 2 mm, which helps to prevent cavities on them [79].

A tooth is divided in the crown and the root. The cervix is the junction between both parts. Figure 4.4 shows a schema of the morphological structure of a tooth [80].

• The **crown** can be divided in the anatomical and the clinical crown. The anatomical crown is that portion of the tooth encased in enamel and the clinical crown is the part of the crown exposed (visible) in the mouth.

• The **root** is embedded in alveolar bone and is covered by cementum. The tooth may have between one and three roots, and the tip of each root is called apex. The apex of every root has a small opening (apical foramen) that allows the passage of blood vessels and nerves into the tooth.

• The **cervix** is a slight indentation that encircles the tooth and marks the junction of the crown with the root. The cementum joins the enamel at the cervix of the tooth and the point at which they join is called the cement-enamel junction.
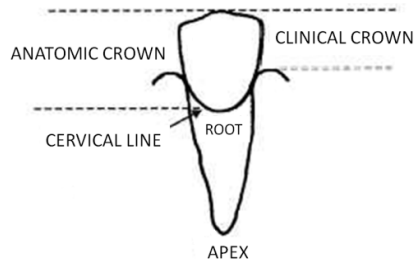
Figure 4.4. Anatomy of a tooth: crown, root and cervical line (from [80]).

4.3.1 Materials that constitute the tooth

Each tooth is built up with several materials: enamel, dentin, cementum and pulp, as displayed in Figure 4.5 [81]. The periodontium, the tissue that surrounds the teeth, is also included in this section.
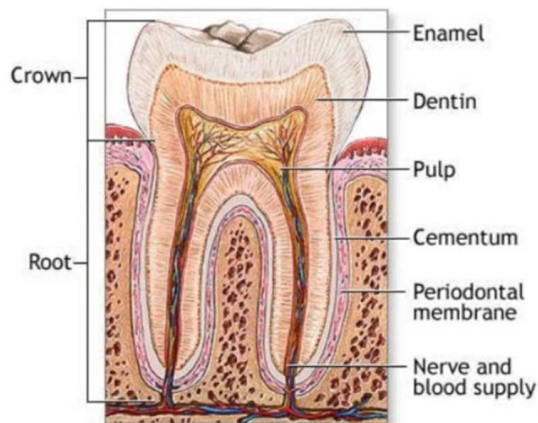
Figure 4.5. A schematic drawing of a tooth with its main parts indicated (from [82]).

The composition of each tooth compound as well as its main function is indicated below.

• The **enamel** is the hardest tissue in the human body and consists of approximately 96% inorganic minerals, 1% organic materials and 3% water. This highly mineralized substance covers the entire anatomic crown of the tooth and protects the dentin. The inorganic compound is mainly apatite.

• The **dentin** constitutes the largest portion of the tooth and it is more porous than enamel. Dentin, which consists of approximately 70% inorganic matter (calcium orthophosphate compounds) and 30% organic matter and water, is harder than bone but softer than enamel. Dentin is perforated by tubules that run between the cement-enamel junction and the pulp, through which pain stimuli are transmitted. The dentin can transform external stimuli into an appropriate message to cells and nerves in the pulp, which react to physiologic and pathologic stimuli due to the ability of the teeth of constant growth and repair [81,82].

• The **dental pulp** is a soft tissue of the tooth, with blood vessels and nerves that enter through the apical foramen. It is contained into the pulp chamber, which is located on the internal surface of the dentin walls [81].

• The **cementum** is a calcified tissue (55% organic and 45% inorganic material) that covers the roots of the teeth in a thin layer, being an essential part of both the tooth and the periodontium. The main function of cementum is to anchor the teeth to the bony walls of the tooth sockets in the periodontium [81].

• The **periodontium** are the tissues that surround and support the tooth. Their main functions are to support, to protect and to provide nourishment to the teeth. The periodontium consists of cementum, alveolar process of the maxillae and mandible, periodontal ligament and gingival [81].

4.3.2 Embryology of the tooth

The *in vivo* formation and development of a tooth is a very complex biological process, by which the teeth grow and erupt into the mouth after they are formed from embryonic cells. The materials forming the human teeth –enamel, dentin and cementum– must be all developed during the appropriate stages of fetal development [79]. Recent data confirmed the need to incorporate an extra amount of calcium in the diet of pregnant and nursing mothers to prevent early childhood dental caries.

In the odontogenesis phase, every tooth goes through three developmental processes which are categorized into growth, calcification and eruption periods. Figure 4.6 schematically shows the odontogenesis process [80] [83] [84]:

1) Growth: dental development usually begins in the fifth or sixth week of prenatal life. By the seventh week, skin cells of the mouth (**epithelium**) thicken along the ridge of the developing jaws creating the dental lamina. The tooth begins to take shape (morphodifferentiation process), and the enamel forming cells (**ameloblast**) and dentin forming cells (**odontoblast**) line up on a boundary line called dentino-enamel junction. At the end of morphodifferentiation, cells deposit the organic matrix along the boundary line (apposition process).

2) Calcification: process by which the organic tissue becomes hardened by the deposition of calcium phosphate components. Next, the tooth crown receives layers of enamel that start at the top of the crown and go downward over its sides to the cemento-enamel junction.

3) Eruption: after the crown of the tooth has been formed, the root begins to develop. Finally, the tooth erupts (movement of the tooth into its proper position in the mouth), process which takes about 3 years for permanent teeth. When primary teeth get ready to fall out and make way for the eruption of permanent teeth, they go through a process called exfoliation. The root of the primary tooth resorbs as the permanent tooth erupts from beneath. The primary teeth act as guides for the developing permanent teeth.
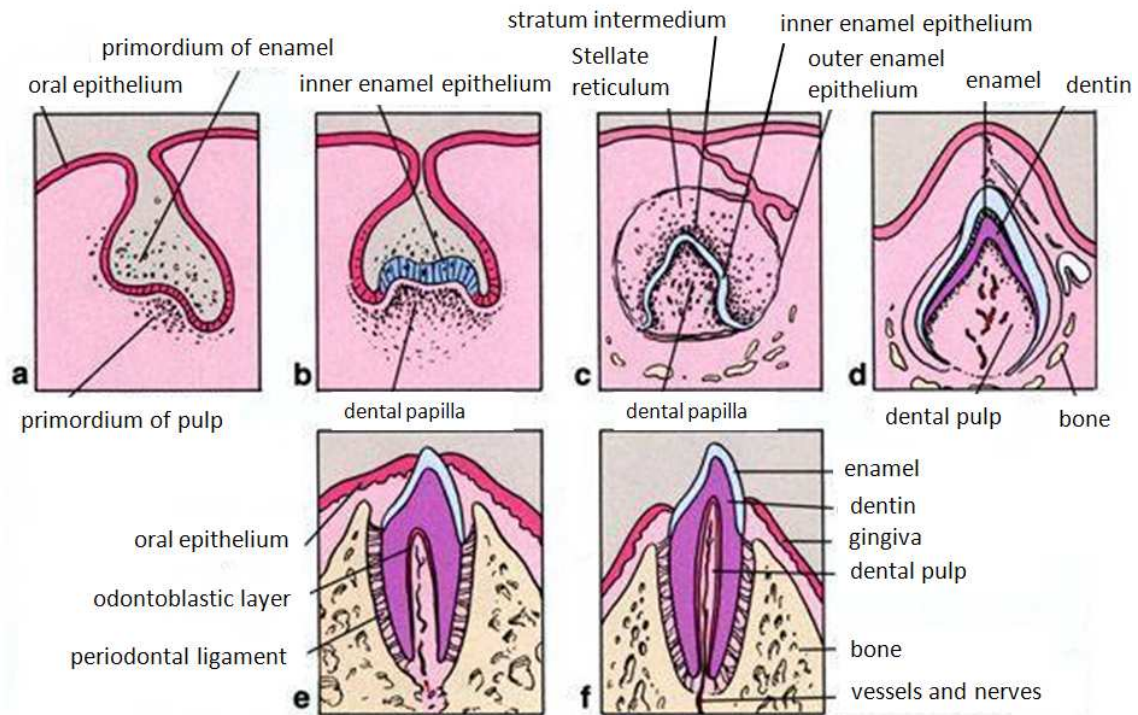
Figure 4.6. Stages in the development of a tooth [84]).

Enamel formation, or **amelogenesis**, is a highly regulated process involving precise genetic control as well as protein-protein interactions, protein-mineral interactions and interactions involving the cell membrane. At some point before the tooth erupts into the mouth, the ameloblasts (enamel forming cells) are broken down. Consequently, enamel has no way to regenerate itself because there is no biological process that repairs degraded or damaged enamel. Nevertheless, enamel is sufficiently porous to allow the diffusion of ions through this material and also chemical reactions can occur within its structure, producing a passive mineralization from saliva. However, the porosity of enamel also permits acidic dissolution to occur, due to caries or the injection of acidic food [79].

4.3.3 Dental pulp

Special emphasis to the dental pulp and its function will be given, since in case that the dental pulp is amputated or extracted after a bad infection, the root canal could potentially be filled with the materials developed in this part of the Thesis.

4.3.3.1 Anatomy of the pulp cavity

Pulp space is divided into the coronal and radicular regions. The pulp cavity consists of a pulp chamber (coronal), pulp horns (cornua), pulp canals (root canals, radicular pulp), lateral canals, apical foramen and accessory foramina, as displayed in Figure 4.7. In general, the shape and the size of the tooth determine the shape and the size of the pulp space [80]. Anatomy of the root canal can vary not only between tooth types but also within tooth types. Although at least one canal must be present in each root, some roots have multiple canals [81].
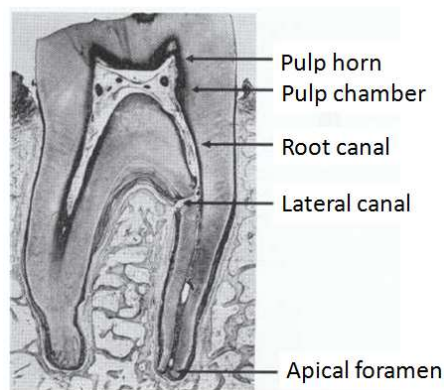
Figure 4.7. Anatomic regions of the root canal system highlighting the pulp horn, pulp chamber, root canal, lateral canal and apical foremen (from [81]).

4.3.3.2 Types of cells

The dental pulp contains different types of cells: odontoblasts, stem cells (preodontoblasts), fibroblasts and cells from the immune system [81]. Figure 4.8 shows a schema of the organization of the peripheral pulp that includes each cell type.

• The **odontoblasts** are the most distinctive cells of the dental pulp. They form a single layer at its periphery, synthesize the matrix and control the mineralization of dentin.

• The **stem cells** (**preodontoblasts)** are cells that have only been partly differentiated along the odontoblast line and can be totally differentiated into odontoblasts after an injury that results in a loss of the existing ones.

• The **fibroblasts** produce and maintain the collagen and ground substance of the pulp and alter the structure of the pulp in case of disease.

• The most prominent **cells of the immune system** in the dental pulp are **dendritic** cells. They recognize a wide range of foreign antigens and initiate the immune response. Other immune cells found in the dental pulp are **macrophages** and **neutrophils**.
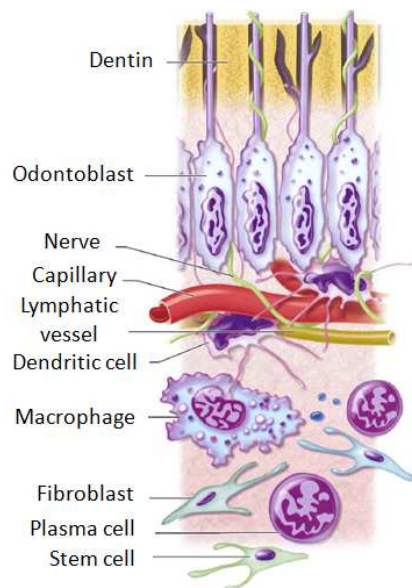
Figure 4.8. Diagram of the organization of the peripheral pulp (modified from [81]).

4.3.3.3 Extracellular components, blood vessels and innervations

The dental pulp is also made by extracellular components such as fibers, ground substance and calcifications, and also contains blood vessels and innervations [81].

The three main extracellular components in the dental pulp are: i) type I collagen, as the predominant **fiber**; ii) **pulp ground substance,** composed principally of glycosaminoglycans,

glycoproteins and water in the form of a sol-gel that supports the cells and acts as a medium for transport of nutrients and metabolites; and iii) **calcifications** [81].

The dental pulp has an extensive and unique vascular pattern and is also richly innervated by trigeminal afferent axons. Accordingly, they respond to stimuli that induce or threaten to induce injury to the pulp tissue and their activation may induce defensive, withdrawal-type reflexes in the masticatory muscles. The pain responses induced by external stimuli can be extremely intense.

4.3.3.4 Functions

The pulp performs five main functions, some formative and others supportive [81].

i) Induction: pulp participates in the initiation and development of dentin, which, when formed, leads to the formation of enamel. These events are interdependent: enamel epithelium induces the differentiation of odontoblasts, and odontoblasts and dentin induce the formation of enamel.

ii) Formation: odontoblasts participate in dentin formation in three ways: a) by synthesizing and secreting inorganic matrix; b) by initially transporting inorganic components to the newly formed matrix; and c) by creating an environment that permits mineralization of matrix. During early tooth development, dentinogenesis is generally a rapid process that forms **primary dentin**. After tooth maturation, dentin formation continues at a much slower rate, forming **secondary dentin**. Odontoblasts can also form a dentin in response to injury, *i.e.* the original dentin thickness is reduced due to caries, attrition, trauma or restorative procedures. This occurs through the induction, differentiation and migration of new odontoblasts or odontoblast-like cells to the exposure site. The so formed dentin (called **tertiary dentin**) is less organized than primary and secondary dentin and it is mostly localized in the site of the injury.

iii) Nutrition: pulp supplies nutrients that are essential for the initial formation of dentin and, afterwards, for dentin health, via dentinal tubules.

iv) Defense: odontoblasts form tertiary dentin in response to an injury. However, the structure of tertiary dentin may not afford the same degree of protection to the underlying pulp tissue than that of primary or secondary dentin. Dental pulp has also the ability to process and to identify

foreign substances and to elicit an immune response to their presence. This is a typical response of the pulp to dentinal caries.

v) Sensation: pulp transmits neural sensations mediated through enamel or dentin to the higher nerve centers. These stimuli are clinically expressed as pain, usually initiated by an inflammatory disease. The dense innervations of the pulp and dentin (Figure 4.9) give a morphological basis for the high sensitivity of these tissues [82].
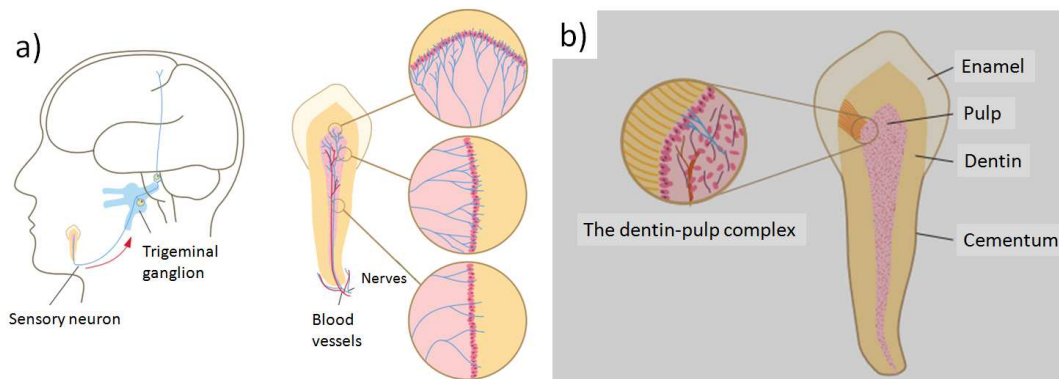
Figure 4.9. a) Schematic drawing that shows the innervations of the dental pulp and b) the interface zone between dentin and pulp (from[82]).

4.3.3.5 Preservation of the apex

A healthy pulp is protected by both the structure of the hard tissue and the intact periodontium [82]. However, these barriers may be damaged or reduced due to processes such as trauma, minor cracks in enamel and dentin, gaps in the cementum, root resorption, marginal gaps within restorations or root caries. [82]. Specifically, the 60-90% of school children worldwide have dental cavities [85]. The microorganisms take advantage of these imperfections, entering the tooth and going along the dentinal tubules (Figure 4.10).
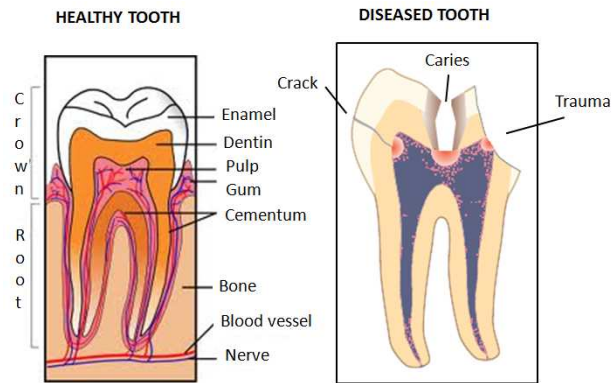
Figure 4.10. Schema of a healthy tooth versus a damaged one, which present imperfections such as cracks, caries or trauma (modified from [81]).

4.3.3.6 Microorganisms found in an infected pulp

Microorganisms colonizing a body site such as the root canal space may be either free-floating as single cells (planktonic form) or microbial biofilms. The term **microbial biofilm** is used when bacterial cells become densely packed and embedded in an extracellular matrix of polymers of host and microbial origin. Biofilms, most often composed of several morphotypes, grow in multilayers or as aggregates on the dentin walls of the root canal [82].

The many genera and species currently identified in root canal samples comprise obligate anaerobic and facultative anaerobic oral bacteria. Figure 4.11 shows a schema of the bacteria commonly found in endodontic infections.
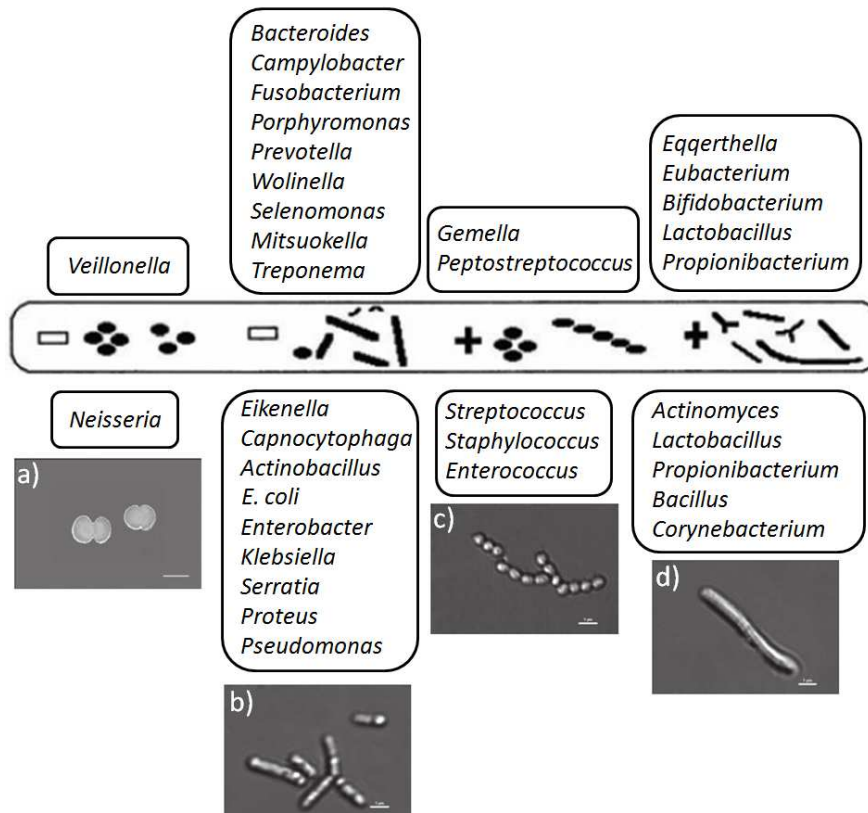
Figure 4.11. Overview of several important bacteria in endodontic infections and images of some of the them (scale bar indicates 1 µm): a) *Streptococcus enterococcus*, b) *Actinomyces lactobacillus*, c) *Neisseria veillonella*, d) *Capnocytophaga eikenella* (modified from [86] and [82]).

After microorganisms reach the dental pulp, an inflammatory reaction arises with the aim to neutralize and to eliminate any harmful agent, and also to repair the damaged tissue [82]. However, in certain occasion the natural mechanisms are not able to reduce the bacteria and pulp therapies have to be conducted to ensure the total disinfection and healing of the tooth.

4.4 Pulp therapies

Pulp therapy and subsequent restorative procedures should be designed not only to restore the mechanical integrity and appearance of the tooth but also to allow the pulp to recover and to protect it from further damage. Therefore, the dental pulp should seal tightly to prevent any access of bacterial organisms from the oral cavity through it. Thus, a material that provides antimicrobial properties, such as calcium oxide-based pastes, is desirable in many cases.

Nevertheless, it is generally accepted that the materials with antimicrobial properties also have certain cytotoxicity [87]. When applying this type of materials in a vital pulp, they produce an initial cauterization and a superficial necrosis of the tissue. However, as a side effect, the alkaline pH also stimulates the odontoblasts differentiation, which mineralizes hard tissue to form tertiary dentin and close the exposition of the pulp. In conventional clinical cases, the healing process takes about one week [82,88].

For extensive pulp lesions, the injured portion of the pulp should be removed and replaced by a temporary restoration at an early stage, allowing the recovery of the remaining pulp (the pulp is still inflamed after the infection) prior to the incorporation of a permanent restoration [81]. Sometimes the pulp is able to keep its functional state but, in other cases, in which severe lesions have persisted for a long time, the inflammatory response is so destructive that can induce the death of the tissue [82].

The endodontic treatments are distinguished in two groups, those in which the dental pulp is still vital and those in which necrosis of the pulp occurred [81,82]. When the dental pulp is vital but injured, the exposure of the pulp is closed with a restoration material, having previously partially extracted, if necessary, the injured tissue.

Depending on the grade of injury of the tissue, and thus on the extension of the treatment, the clinical procedures are named differently. The vital exposed pulp may be protected immediately by covering it and placing a restoration (**pulp capping**). If the exposure is large or seriously infected, it may be possible to remove the diseased part of the pulp, to cap the remaining pulp and, finally, to place a restoration (**pulpotomy**) [81]. In the case that the pulp is irreversibly injured or necrotic, a **pulpectomy** is performed, in which the totality of the dental pulp has to be extracted [82]. Several possibilities for pulpal protection are displayed in Table 4.5, together with a schema of the degree of injury of the tooth and a definition of the treatment.

Table 4.5. Definitions of the principal terms used in pulpal protection and vital pulp therapy, classified in function of the degree of injury of the tissue (images from [82]).

Term	Schema	Vital or necrotic pulp?	Definition
Direct pulp cap		Vital	A dental material placed directly on a mechanical or traumatic vital pulp exposure.
Pulp cap		Vital	The pulpal wound is sealed with a dental material (*i.e.* calcium hydroxide or MTA) to facilitate the formation of reparative dentin and maintenance of a vital pulp.
Step-wise caries excavation		Vital	A material is placed on a thin partition of remaining carious dentin that if removed might accidentally expose the pulp (for immature permanent teeth).
Partial pulpotomy		Vital	Surgical removal of a small diseased portion of vital pulp as a means of preserving the remaining coronal and radicular pulp tissues.
Pulpotomy (pulp amputation)		Vital	Surgical removal of the coronal portion of a vital pulp as a means of preserving vitality of the remaining radicular portion. It is usually performed as an emergency procedure for temporary relief of symptoms or therapeutic measure.
Pulpectomy (pulp extirpation)		Irreversible damaged or necrotic	Complete surgical removal of the vital pulp

The **pulpectomy**, which requires the extirpation of the pulp, is the most extreme case. This is an **endodontic treatment**, also known as non-surgical **root canal therapy**. The followed procedure to perform a root canal therapy is detailed below.

4.4.1 Root canal therapy

The **root canal therapy** or **pulpectomy** is a treatment performed to cure an infection of the dental pulp and to save the tooth (although not the pulp tissue) in a situation that the pulp is irreversibly damaged or necrotic.

A perennial problem in root canal therapy is the likelihood of recurrent infections, which are triggered by bacteria that reach the apex region of the tooth [87]. Therefore, in a root canal therapy, an essential step after removing the damaged pulp tissue is to disinfect the root canal and, subsequently, to obturate it with a sealing material to avoid another infection (**reinfection** or **secondary infection**). The disinfection process, carried out by means of mechanical instrumentation and irrigation of antimicrobial solutions, removes between 50 and 80% of the bacteria found in the root canal. Thus, if the root canal would be sealed like that and the bacteria would receive nutrients and have some room, they would quickly grow back and would cause again an infection [82]. In fact, secondary infection is the main cause of endodontic failure [89].

In order to avoid a secondary infection, two consecutive processes are usually performed to totally eliminate any remaining bacteria after the mechanical and chemical treatment: i) the root canal is obturated with a temporary disinfectant material (**inter-appointment dressing**) until the next follow-up appointment (after 7-10 days), and ii) the temporary filling is afterwards removed and any remaining bacteria are buried by a permanent filler of the root canal, expecting that the byproducts released by the material will kill the microorganisms and/or they will die for the lack of nutrients or space to grow up. Nevertheless, this only occurs in the case that the conducts to the periapical tissue are totally blocked and sealed by the root canal filler [82].

Therefore, the root canal therapy is usually done in more than one appointment [90]. In a first visit the root canal is chemically and mechanically cleaned and disinfected and an antibacterial inter-appointment dressing, such as calcium hydroxide, is incorporated into the root canal. In a follow-up appointment, a permanent root canal filler is introduced only if clinical signs of ongoing infection have disappeared [82]. Finally, if necessary, a coronal restoration is performed after the

root canal filler has set [91]. After an endodontic therapy, a tooth must be restored to functional and esthetic demands.

A general and simplified overview of the whole treatment is schematically indicated in Figure 4.12. However, it is important to keep in mind that every root canal therapy is slightly different depending on the clinical situation, mainly resulting in different timings of obturation.
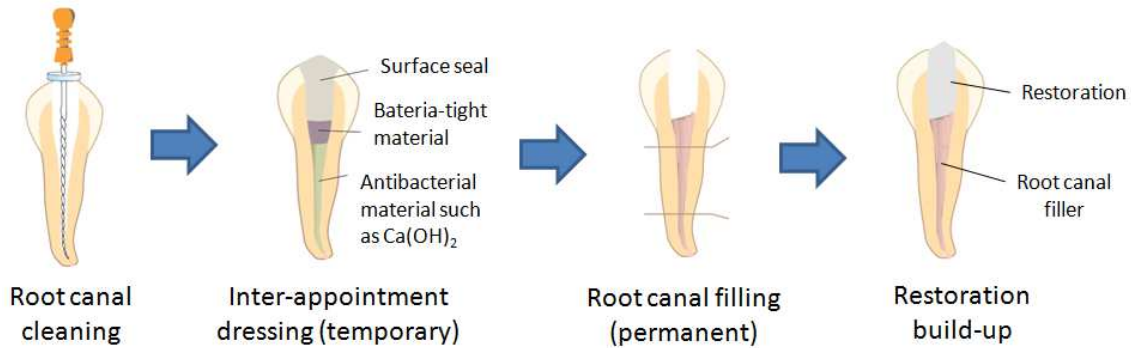
Figure 4.12. Schema of the main steps in an endodontic process (individual images modified from [82]).

4.4.2 Timing of root canal obturations

To determine how long it takes to complete a root canal treatment, the number of appointments necessary or the adequate timing, factors such as i) the patients' symptoms, ii) the pulp and periapical status and iii) the difficulty of the procedure should be considered. [81].

i) Patients' symptoms: obturation is contraindicated if the patient presents severe symptoms. Since these are emergency situations, it is preferable to manage the immediate problem and delay the definitive treatment [81].

ii) Pulp and periapical status:

• Vital pulp: the procedure may be completed in a single visit regardless of the inflammatory status of the pulp [81].

• Necrotic pulp without significant symptoms: canal preparation and obturation may be completed during the same appointment. However, multiple appointments are

advantageous in front of one-single appointment regarding to the healing of apical disease [81].

• Necrotic pulp with persistence of exudation in the canal during preparation: several visits are required. An inter-appointment dressing is introduced into the canal and the permanent sealing is not placed until the exudation stops [81].

iii) Difficulty of the procedure: those complex cases, which are time consuming, are better managed in multiple appointments [81].

4.4.3 General requirements for root canal filling materials

The aim of a root filling material is to provide a combination of an antibacterial agent that at the same time seals against the further ingress of bacteria, thus removing the pulpal antagonists and allowing the pulp to heal [87].

Briefly, the requirements for root canal materials are those that allow the dentist, first, to work comfortably with it (easy to apply and appropriate setting time), and second, to follow-up the treatment (radiopacity). Once implanted, the material should remain in the root canal permanently, sealing properly against bacteria (avoid reinfection) and, therefore, it should be stable with time (no degradation in physiological fluids), and should adhere and adapt to the dentin. The material may provide antimicrobial properties, further ensuring the bacterial death. As a side effect, the root canal filling should stimulate the periapical healing process. Finally, the material has to be biocompatible [82,89] and should not irritate local tissues or create general health problems such as allergies to patients and dental personnel [82]. Table 4.6 shows the general requirements that a root filling material has to fulfill regarding its technical, biological and handling properties.

Table 4.6. General requirements for a root canal filling material (modified from [82]).

Technical properties	Biological properties	Handling
• No shrinkage	• No general health problems or allergies for patients and dental personnel	• Setting in an adequate time, allowing sufficient time for obturation and radiographic control
• No solubilization in physiological fluids	• No irritation of local tissues	• Easy to apply
• Setting *in vivo*, no altered by the environmental humidity	• Sterile	• Easy to extract using solvent, heat or mechanical instrumentation
• Good adhesion and adaptation to dentin or combining materials (cones, sealers)	• Antimicrobial properties	
• Low porosity and water adsorption	• Stimulation of the periapical healing process	
• No tooth discoloration		
• Radiopacity		

There is still no commercial material that fulfills all the requirements indicated in Table 4.6, as reported in the literature [82,86]. This is the reason why a combination of endodontic materials to fill the root canal is usually employed [86].

The root canals are usually obturated using a combination of two or more materials in order to improve the performance of a single root canal filler. The primary obturating material, known as **core,** acts as a piston and a paste known as **sealer**, can be spread onto it, filling voids and attaching the core material to the dentin wall. The core comprises the bulk of material that fills the canal space and can be solid or semisolid (paste). The sealer is in paste form and, in fact, it is the material that comes into contact with the tissues of the root canal (*i.e.* dentin) [89].

4.5 Properties required for root canal filling materials and assessment of these properties

4.5.1 Radiopacity

Root canal sealers should have sufficient radiopacity to allow a clear distinction between the implanted material and the surrounding anatomic structures [82,92,93]. In fact, during an endodontic treatment, the evaluation of the quality of the root fillings can only be controlled by radiographic examination.

The X-ray is an electromagnetic radiation exhibiting wave-like behavior as it travels through the space. It has both electric and magnetic field components, which oscillate in phase perpendicular to each other and perpendicular to the direction of energy propagation. When an X-ray photon collides with an atom, the atom may absorb the energy of the photon and boost an electron to a higher orbital level or, if the photon is very energetic, it may knock an electron from the atom altogether, causing the atom to ionize. Generally, a larger atom (with higher atomic number) is more likely to absorb an X-ray photon, since larger atoms have greater energy differences among orbital electrons. Therefore, the materials made of larger atoms (*e.g.* lead) absorb the electromagnetic radiation, thus having a high stopping power in front of X-rays.

X-ray equipments are specifically designed to take advantage of the absorption difference between hard tissues (bones or teeth) and soft tissues, allowing physicians to examine different structures in the human body. Soft tissues are composed by atoms smaller than calcium and phosphorus, which are the most predominant atoms making up hard tissues; hence X-rays reveal the contrast differences among those chemically different structures.

Bismuth oxide (Bi_2O_3) has been widely used as radiopaque agent for intraoral dental materials, such as root canal fillers. For instance, Bi_2O_3 is the radiopacifying agent added to the mineral trioxide aggregate (MTA), a commercial root canal filler: the white MTA (WMTA) contains 16.13 wt% Bi_2O_3 and the grey MTA (GMTA) contains 15.90 wt % Bi_2O_3 [94]. Bi_2O_3 is insoluble in water [95] and exhibits low toxicity although it contains a heavy metal atom such as bismuth (atomic number 83).

Assessment of the radiopacity

In scientific literature, several methodologies to measure the radiopacity of a material for endodontic applications have been reported. However, most of the studies have been based in the protocol explained in the UNE-EN ISO 6876 standard (Dental root canal sealing materials) [92] and in the UNE-EN ISO 9917-1 standard (Dentistry. Water-based cements, part I) [96]. In these two standards for dental cements, the radiopacity of a sample is compared to that of an aluminum stepwedge. On one hand, the UNE-EN ISO 6876 standard establishes that a disk of 1 mm thickness has an adequate radiopacity if its optical density is higher than that of an aluminum piece of 3 mm thickness. On the other hand, the UNE-EN 9917-1 ISO standard establishes that a disk of 1 mm thickness has an adequate radiopacity if its optical density is higher than that of an aluminum piece of the same thickness. The optical density can be transformed in equivalent millimeters of aluminum thickness by means of a calibration curve of the aluminum stepwedge.

Different experimental conditions employed in the characterization of dental materials are summarized in Table 4.7.

Table 4.7. Compendium of different experimental conditions used to assess the radiopacity of dental materials. Some abbreviations are used: MTA: mineral trioxide aggregate; CPC: calcium phosphate cements; BSB: bismuth salicylite basic; AH Plus is the commercial name of a resin-type sealer. "eq. mm Al" stands for equivalent millimeters of aluminum thickness.

Material of study	Thickness of disks (mm)	Radiopacity (mean eq. mm Al)	Equipment	Distance between sample and the radiation source	Voltage (kV)	Intensity (mA)	Exposition time (s)	Reference
MTA	1	6.03	General Electric, Milwaukee	33.5 cm	50	10	18 pulses/s	[97]
MTA	2	4 mm (equivalent to addition 17.65 wt% Bi_2O_3)	Gendex 765 DC	40 cm	65	7	0.25	[98]
Pure CPC $SrCO_3$/CPC	3	2.5 5	Gendex Oralix AC generator	–	75	7.5	0.26	[99]
Bi-doped CPC: CPC + x wt% BSB CPC	5	Image contrast values: BSB = 5: 0.85 ± 0.003 BSB = 25: 0.89 ± 0.008 BSB = 0 (CPC): 0.55 ± 0.027	MXR-160A, Shenzhen	1 cm	60	10	0.7	[100]
Gutta-percha AH Plus	1	9.8 ± 0.3 11.2 ± 0.3	Spectro 70 X	30 cm	70	8	0.2	[101]
$CaCO_3$-calcium phosphate $CaCO_3$: 9.2 wt% or 8.2 wt% if milled	4	4	Philips MG 103/2.5	70 cm	65	10	–	[102]

4.5.2 Material stability

The stability of a material aimed to be used as root canal filler is an essential requirement to guarantee that the sealing provided by the filler will endure. Moreover, those materials with antibacterial properties should not compromise the stability of the material due to the release of antibacterial substances [82].

Assessment of the stability of a material

The stability of the materials has been studied in a wide range of conditions. Fridland *et al.* evaluated the degradation of MTA, a commercial root canal filling, following the UNE-EN ISO 6876 standard ("Materials for Dental Root Canal Sealing"). Interestingly, although the material fulfilled the requirement for root canal filling materials established in the UNE-EN ISO 6876 standard (the degradation was lower than 3 wt% after 24 h, following the protocol indicated [92,103]), it showed a great degradation in a longer period of 78 days [104]. Therefore, Fridland's studies showed the importance of performing assays for long periods of time.

There are also some studies that evaluated the degradation of materials such as calcium phosphate cements, magnesium phosphate cements or a mixture of both [59–62]. In general, the materials showing a high biodegradation rate were pointed out to be used for bone regeneration applications.

Table 4.8 schematically shows different protocols used to evaluate the degradation of different inorganic cements with time.

Table 4.8. Compendium of experimental conditions used to evaluate the stability of several materials with time. Some abbreviations are used: CPC: calcium phosphate cement; CMPC: calcium magnesium phosphate cement; MPC: magnesium calcium phosphate cement.

Material	Material/medium ratio. Medium. Static or dynamic conditions	Time points of study (medium refreshed)	Characterization of the degradation	Weight loss (%)	References
MTA	1 disk ($\varnothing$ = 20 mm, h = 2mm)/50ml. Distilled water. Static	24 h (medium not refreshed)	Weight of material dissolved in medium was evaluated after evaporation of medium (study follows ISO 6876 standard)	1.8–2.8 wt% (depending of L/P ratio)	[103]
MTA	1 disk ($\varnothing$ = 20 mm, h = 2mm)/50ml. Distilled water. Static	1, 2, 5, 9, 14, 21, 30, 50, and 78 days (medium was not refreshed)	Weight of material dissolved in medium was evaluated after evaporation of medium (study follows ISO 6876 standard)	16–24 wt% (depending of L/P ratio), after 78 days	[104]
CPC and CMPC	0,2 g/ml ($\varnothing$ = 10 mm, h = 3 mm). SBF. Dynamic (100 rpm)	90 days (medium refreshed every 2 days)	• Weight loss (specimens dried at 60°C) • SEM	CPC ~ 3 wt%; CMPC ~ 60 wt%	[59,62]
CMPC	0,2 g/ml (10x10x10mm). Tris HCl, pH = 7.4. Dynamic (100 rpm)	Every 7 days (and medium also refreshed), up to 90 days	• Weight loss (specimens dried at 60°C) • [Ca], [Mg], [P] by ICP	CPC ~ 30 wt%; MCPC ~ 85 wt%	[61]
CPC and MCPD	0,5 g/g. Tris HCl, pH = 7.4. Static.	Every 7 days (medium refreshed every 3 days), up to 90 days	• Weight loss (dried, temperature not specified) • [Ca], [Mg], [P] by ICP • pH	CPC ~ 10 wt%; MCPC ~ 85 wt%	[60]
Magnesium doped apatite	0,2 g/ml ($\varnothing$ = 10 mm h = 3 mm). Tris HCl, pH = 7.4. Dynamic (100 rpm)	Every 7 days for 28 days, and every 14 days until day 84 (medium refreshed at every time point)	• Weight loss (dried at 60°C)	8–50 wt%	[63]

4.5.3 Dentin-cement bonding strength

The root canal filling material should adapt and adhere to the dentin, thus decreasing the risk of interfacial bacterial leakage [82], and also increasing the changes of the material to remain in place under dislocation forces [105].

Adhesive cements have been tested as root canal filling materials in an attempt to improve the sealing quality of sealers. Materials such as cyanoacrylate, calcium phosphate, polycarboxylate and glass ionomer cements have been explored. Although appearing favorable in biocompatibility tests and in long-term clinical follow-up studies, the materials have never gained great popularity. Likely reasons are their short setting time and difficulty of removal for retreatment [82].

Assessment of the dentin-cement bonding strength

The bonding strength between a root canal filling material and dentin has commonly been evaluated by means of a **push-out test**. Although the experimental conditions among different works change slightly, the rationale of the assay consists on pressing the surface of a material placed in a sliced root canal and quantifying the strength necessary to displace the cement from its initial position. Reyes-Carmona *et al.* evaluated the bonding strength of different cements after storing the obturated roots for 72 h at 37°C [106].

4.5.4 Sealing ability

Many studies (about 25% of the current endodontic literature) are devoted to leakage or sealability [82]. The term bacterial leakage, also commonly referred as **microleakage**, is used to imply the bacterial elements penetrating the margins of dental restorations. Materials that do not seal tight may allow bacteria to enter along the margins of the restoration. Microleakage can seriously affect the health condition of the apical zone and, in fact, the main cause of failure of endodontic treatments is the lack of seal of the root canal filling [82].

Leakage mainly occurs between the root canal filling and the root canal wall, although there are some reports also showing leakage between the sealer and the core material or

throughout the sealer [82]. Leakage is influenced by the root canal filling material itself and by a number of other factors, such as [82]:

i) **Root canal anatomy and preparation.** Unsuitable cleaning and shaping impede the correct application of the root canal filling material.

ii) **Coronal leakage.** Bacteria may penetrate an obturated root canal within few days/weeks if the access cavity is not sufficiently sealed.

iii) **Smear layer.** Removal of the smear layer (layer of microcrystalline and organic particle debris that covers the root canal walls), using citric acid (10–50%) or ethylenediaminetetraacetic acid (EDTA, 17%), may influence leakage. Although controversial results have been reported, most authors indicate that the leakage is decreased if the smear layer is removed, since the sealer can penetrate better into the dentinal tubules.

iv) **Hemostasis/dryness of the root canal.** The wall of the root canal must be clean and dry for tight adaptation of the sealer to the wall.

v) **Root canal filling material:** the material has to be stable, adhere to dentin and should have lack of pores.

vi) **Sealer thickness and obturation technique.** Thick layers of root canal sealers showed more leakage than a thin one, which indicated that the sealer is more responsible for microleakage than the core material, probably due to the fact that most sealers contain pores and dissolve faster than the core material.

Assessment of the sealing ability

Nowadays, there is no commercial root canal filling material that can totally prevent leakage. Therefore, a bacteria-tight coronal restoration is of critical importance to ensure the success of root canal treatment [82].

Results reported in the literature regarding microleakage of root canal filling materials depend greatly upon the methods being used. Therefore, data should be regarded with caution.

The *in vitro* tests that have been more often performed include dye penetration, with additional pressure, centrifugation or vacuum. Bacterial penetration and fluid transport have also been used [82]. A widely used technique nowadays is the liquid pressure method, proposed by Derkson *et al.* for restorative materials [107], which allows quantifying root canal filling microleakage through a non-destructive testing. Table 4.9 shows a summary of leakage tests carried out with different root canal fillers, reported in literature.

Table 4.9. Compendium of different studies to evaluate the leakage of root canal filling materials. All tests were performed using single-root human teeth, otherwise it is indicated. Some abbreviations are used: GP: gutta-percha, MTA: mineral trioxide aggregate; WMTA: white MTA; GMTA: grey MTA; PCS: pulp canal sealer. Several endodontic materials were tested: GuttaFlow is a powdered gutta-percha with nanosilver particles, Epiphany is a resin cement, Resilon is a polymer-based material, AH Plus is a resin, Coltosol, pulp canal sealer (PCS) and Kerr Canal Sealer are zinc oxide cements, and TC are experimental accelerated Tetrasilicate Cement.

Material under study	Control material	Use of gutta-percha?	Times of study	Method to evaluate leakage	Leakage of the materials studied	References
MTA FMTA	AH Plus	Yes, warm	24 h, 48 h; 1 and 2 weeks; 1, 3 and 6 months	Fluid filtration SEM/EDX	24 h: 0.26 ± 0.20 µl/min 48 h: 0.21 ± 0.17 µl/min	[108]
GuttaFlow using different obturation methods	AH Plus	Control yes; experimental groups: half of the groups	1 week; 1.5 and 3 months	Fluid filtration	1 week: With GP: 0.07 ± 0.048 µl/min Only cement: 0.018 ± 0.009 µl/min	[109]
Epiphany/Resilon Coltosol	AH Plus/GP	Yes, Resilon and GP	Immediately and 6 months	Fluid filtration	Immediately: Epiphany/Resilon: 0.075 ± 0.075 µl/min AH Plus/GP: 0.05 ± 0.025 µl/min	[110]
MTA Pulp Canal Sealer (PCS)	GP and PCS, apex sealed off with bonding agent and varnish	Yes, warm	24 h and 28 days	Fluid filtration Leaching (ICP-AAS and SEM)	24 h: MTA:0.075 ± 0.075; 24 h: PCS: 0.05 ± 0.075 28 days: MTA: 0.09 ± 0.075; 28 days: PCS: 0.08 ± 0.075	[111]
GMTA WMTA Kerr Canal Sealer	GP and Kerr Canal sealer, coated with varnish	Only Kerr Canal Sealer	From 0 to 42 days	Turbidity test (bacteria, %)	42 days: GMTA 10% WMTA: 38%; Gutta+Kerr: 82%	[112]

Material under study	Control material	Use of gutta-percha?	Times of study	Method to evaluate leakage	Leakage of the materials studied	References
MTA (bovine incisors)	Lateral GP Warm GP	Yes, control	1 week	1% methylene blue	GP lateral: 0.59 ± 0.63 µl/min Warm GP: 0.76 ± 0.86 µl/min MTA: 8.65 ± 4.24 µl/min	[113]
As a retrogradate material TC-1 TC-2	WMTA	Yes	4, 24 and 48 h; 1 and 2 weeks; 3 months	Fluid filtration pH XRD	3h: 0.9 ± 0.2; 24h: 0.8 ± 0.5; 48h: 0.4 ± 0.3; 1 week: 0.1 ± 0.2; 2 weeks: 0.1 ± 0.6; 12 weeks: 0.0 ± 0.0 µl/min	[114]
Apical part: GP + AH Plus sealer or unfilled Root-end: gMTA (filled or 3mm)	Completely covered with 2 layers of nail varnish	Half of the groups	Up to 75 days (until bacteria penetrate)	Bacterial penetration	Roots obturated with GP and AH plus sealer showed a lower average time for bacterial leakage	[115]
GP and AH Plus sealer, different post space preparation	Cyanocrylate cement	Half of the groups	1 month	Fluid filtration	Intrinsic permeability of system: 0.029 ± 0.04 Immediate removal GP: 1.26 ± 0.45 Delayed removal GP: 1.11 ± 0.29 MTA apical filling: 0.61 ± 0.33 (units: $\mu l \cdot cmH_2O^{-1} \cdot min^{-1}$)	[116]

4.5.5 Biocompatibility

It has to be taken into account that root canal sealers and filling materials are exposed to the periradicular tissue at the apical and lateral foraminae, so superior tissue tolerance to sealer is required to minimize local and systemic side effects [117]. Therefore, *in vitro* and *in vivo* assays are recommended to evaluate the material biocompatibility.

Many works inaccurately obviate the importance of the biocompatibility of the materials aimed to endodontic applications, probably because they are not aimed at bone regeneration. For example, there are several studies regarding alkaline calcium phosphate cements intended for root canal filling or pulp capping that do not mention a word regarding the material biocompatibility [76–78,99]. However, the successful commercialization of MTA has recently encouraged the evaluation of its cytotoxicity and, nowadays, there are many works regarding this aspect of MTA. These results, which are controversial because they are highly dependent on the experimental conditions used, will be discussed in the Discussion section of Chapter 6.

4.6 Materials commonly used to fill the root canals

As previously explained, the root canals are usually obturated using a combination of the **core**, which acts as a piston, and the **sealer**, a paste that can be spread onto the core material, filling voids and attaching it to the dentin wall [89]. Figure 4.13 shows a schema of different types of root canal fillings, divided as core obturating materials or as sealers [81].
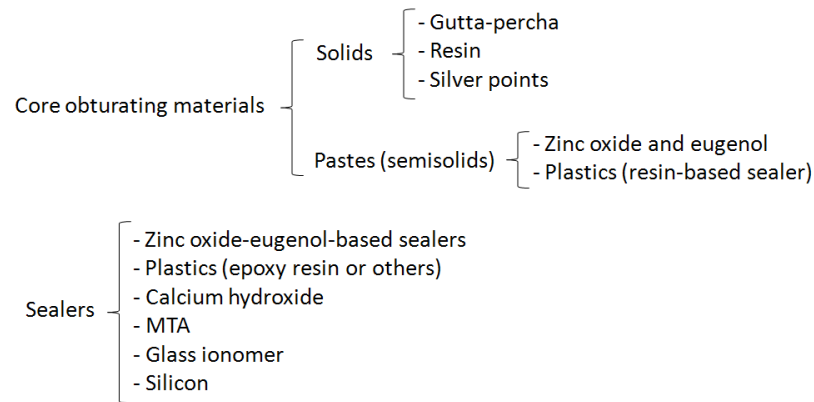
Figure 4.13. Schema of the types of root canal filling materials.

4.6.1 Core obturating materials

The core obturating materials can be divided into solid materials and pastes (semisolids) [81]. The solids are generally used accompanied with a sealer, whilst the pastes have to be considered as dough core materials that are used alone.

• **Solids:** The gutta-percha core has been a dominant material for endodontic obturations for more than a century [89]. Gutta-percha is the name given to narrow cones whose primary ingredient is zinc oxide (70-75%) and approximately 20% of gutta-percha, which gives the cone its unique properties such as plasticity. The gutta-percha is an inelastic natural latex (a polymer of isopropene) produced from the sap (fluid transported through the transport tissues) of some tropical trees [81,89]. Other obturating materials are resin-based polymers and silver points, although they have been used in a lower extent than gutta-percha [81].

• **Pastes (semisolids):** The idea of using a paste or a cement as a core obturating material is appealing, since the paste could be simply injected into the canal to length, filling it entirely. In addition, this method would permit using a material that would adhere to dentin and create an absolute seal. However, the concept presents significant practical difficulties, such as lack of length control, unpredictability, shrinkage and toxicity of ingredients [81]. The main paste cores in the market are zinc oxide and eugenol, which are mixed pure to intermediate thickness, or resin-based pastes made by epoxy (*e.g.* AH series) [81].

4.6.2 Sealers

The concept of using a sealer is that it fills the irregularities between the prepared canal and the core material, thus providing a fluid-tight sealing [81,89]. Generally, the major types of sealers are zinc-oxide-eugenol-based, resin-based (mainly made with epoxy), glass ionomer, calcium hydroxide-based, silicone paste and mineral trioxide aggregate (MTA) cement [81].

Nevertheless, none of the mentioned sealers have ideal properties. On one hand, the main drawback of both zinc-oxide-eugenol and resin-based sealers is their toxicity [81,89]. On the other hand, both glass-ionomer and calcium hydroxide-based sealers degrade with time, threatening the sealing of the obturation [81,89]. Therefore, the two later sealers are only recommended for temporary restoration. In fact, calcium hydroxide has commonly been used as inter-appointment dressing due to its antimicrobial properties [81]. Regarding silicone pastes, their main disadvantage is that they do not display any antibacterial activity. Finally, mineral trioxide aggregate (MTA) has proved to support hard-tissue repair at root-ends and root exposures, and it is therefore a good sealing candidate.

4.6.3 Gold standard for root canal filling

Nowadays, the gold standard for root canal filling is a combination of a few gutta-percha points with a sealer.

4.7 Dough core obturating materials with intrinsic antimicrobial properties

Cements with antimicrobial properties have been pointed out as good candidates for preventing or treating certain infections. In the endodontic context, they could be applied to treat infections occurring in the dental pulp or to remove remaining bacteria in the root canal in a root canal treatment.

In fact, endodontic fillers have been provided with a permanent antiseptic effect to ensure the total disinfection of the root canal and microcanals. With this aim, materials containing formaldehyde or iodoform have been used. Nevertheless, these materials are unacceptable for

their high toxicity, even causing chronic inflammation in some cases, in spite of their good physical properties [86]. Also, some additives such as silver oxide have been added to root canal filling materials to potentiate their antimicrobial properties [81].

Alkaline materials have also been used as root canal fillers due to their biological and pharmacological advantages, such as disinfecting the dentinal tubules and rendering a therapeutic environment surrounding the roots. Calcium oxide-based pastes have intrinsic antimicrobial properties due to their high pH [82]. Two of the main calcium oxide-based pastes that have been used as core obturating materials, calcium hydroxide and mineral trioxide aggregate (MTA), are described below.

4.7.1 Calcium hydroxide

Calcium hydroxide-based materials (pH ~ 12.5) have been used since 1930s as inter-appointment dressing in pulpectomy treatments, in some apexification techniques and as a component of several root canal sealers [117]. These materials are commonly used as temporal dressing due to their low mechanical properties [88] and their high solubility.

The two main reasons for using calcium hydroxide as a root-filling material are, on one hand, the stimulation of the periapical tissues, which maintains the health or promotes healing and, on the other hand, its antimicrobial potential. The very high pH of calcium hydroxide causes an initial degenerative response in the immediate vicinity to the material, this necrosis being rapidly followed by a mineralization and ossification response because calcium hydroxide encourages both reparation and active calcification, stimulating the periapical tissues to recover [117] [118].

Several studies have compared the cytotoxic effects of calcium hydroxide with that of other root canal sealers [117]. Cell culture tests using either human periodontal ligament cells or monolayer or multilayer mouse cells have shown calcium hydroxide-based materials to be less toxic compared with zinc oxide eugenol and resin-based sealers [119–122].

4.7.2 Mineral trioxide aggregate (MTA)

The mineral trioxide aggregate (MTA) is a commercial cement mainly composed by CaO ($\sim$ 60 − 67 wt%) and SiO_2 (19 − 25 wt%) that derives from the Portland cement. It was developed in the Loma Linda University (California, United States) in 1993 [123] and since then it has been proved to have a good performance in endodontic applications [124].

Nowadays, MTA is used as pulp capping, end-root canal filling or core obturating material and it has antimicrobial properties due to its high alkalinity (pH $\sim$ 12.5) [82]. Moreover, it has been reported that the MTA also shows high compressive strength, lower dissolution with time than calcium hydroxide [82], good sealing ability and adequate biocompatibility [104,125].

Even though the MTA is commercialized and widely used in clinics, it still shows significant drawbacks:

✗ **Low stability** with time due to its high content in calcium oxide [94,126,127], which transforms into calcium hydroxide after hydration. The high solubility of calcium hydroxide (0.160 g/100 g H_2O at 20°C, K_{sp} = 5.3 at 25°C [95]) allows predicting that MTA will dissolve with time [103]. In fact, a long-time stability study showed that 24% of MTA was dissolved after 78 days when using the liquid to powder ratio recommended by the manufacturer [104];

✗ **Long setting time**, between 3 and 4 hours [126,128], which forces to postpone the final restoration of the tooth in a later follow-up appointment (period during which a moist cotton pellet is temporarily placed in direct contact with the material [94]). Moreover, there is the risk that saliva removes MTA from the tooth cavity or that MTA irritates the surrounding tissues [129];

✗ **Bad handling properties** [124,128,130]: MTA paste may lose its consistency if an excessive amount of water is added, even when using the liquid to powder ratio recommended by the manufacturers [103];

✗ **High cost** [130].

Although this cement has been the aim of a large number of works, it still presents several problems. Therefore, several studies indicated strategies to reduce its setting time [131], to

improve its handling properties [132], to increase its antimicrobial properties [133] or to enhance its purity [134].

The lack of root canal filling materials with excellent properties opens a door to the development of new materials with enhanced performance as root canal fillers.

4.8 References

[1] Prosen EM. Refractory materials for use in making dental casting. US Patent No. 2,152,152; 1939.

[2] Prosen EM. Refractory material suitable for use in casting dental investments. US Patent No. 2,209,404; 1941.

[3] Earnshaw R. Investments for casting cobalt–chromium alloys, part II. British Dental Journal 1960; 108: 429–440.

[4] Sherif F, Michaels ES. Fast-setting cements from solid phosphorous pentoxide containing materials. US Patent 4,505,752; 1985.

[5] Elvery C. Improvements relating to mouldable compositions. UK Patent 593,172; 1945.

[6] Horvitz H, Gray A. Matrix forming composition. UK Patent 1,454,333; 1974.

[7] El-Jazairi B. Rapid repair of concrete pavings. Concrete 1982; 16: 12–15.

[8] Popovics S, Rajendran N, Penko M. Rapid hardening cements for repair of concrete. ACI Materials Journal 1987; 84: 64–73.

[9] El-Jazairi B. The properties of hardened MPC mortar and concrete relevant to the requirements of rapid repair of concrete pavements. Concrete 1987; 21: 25–31.

[10] Yang Q, Zhu B, Wu X. Characteristics and durability test of magnesium phosphate cement-based material for rapid repair of concrete. Materials and Structures 2000; 33: 229–234.

[11] Li Z, Chau CK, Qiao F. Setting and strength development of magnesium phosphate cement paste. Advances in Cement Research 2009; 21: 175–180.

[12] Sugama T, Kukacka LE. Characteristics of magnesium polyphosphate cements derived from ammonium polyphosphate solutions. Cement and Concrete Research 1983; 13: 407–416.

[13] Seehra S, Gupta S, Kumar S. Rapid setting magnesium phosphate cement for quick repair of concrete pavements – characterisation and durability aspects. Cement and Concrete Research 1993; 23: 254–266.

[14] Hall DA. The effect of retarders on the microstructure and mechanical properties of magnesia–phosphate cement mortar. Cement and Concrete Research 2001; 31: 455–465.

[15] Carvalho M, Segadães A. The hydration of magnesium phosphate cements: effect of powder characteristics on the reaction kinetics. Materials Science Forum 2008; 591: 833–838.

[16] Wagh AS. Chemically bonded phosphate ceramics: 21st century materials with diverse applications. Hurst E (editor). Oxford: Elsevier, 2004.

[17] Sherif F, Via F, Post L, Toy A. Improved fast-setting cements from ammonium phosphate fertilizer solution. European Patent No. EP0203485; 1986.

[18] Demotakis ED, Klemperer W, Young JF. Polyphosphate chain stability in magnesia–polyphosphate cements. Materials Research Symposium Proceedings 1992; 45: 205–210.

[19] Hurst E, Wagh AS, Singh D, Jeong SY. Chemically bonded phosphate ceramics. In: Oh C (editor). Handbook of mixed waste management technology. Boca Raton: CRC Press, 2001.

[20] Belopolsky AP, Shpunt SY, Shulgina MN. Physicochemical researches in the field of magnesium phosphates (the system $MgO–P_2O_5–H_2O$ at 80°C). Journal of Applied Sciences 1950; 23: 873–884.

[21] Abdelrazig B, Sharp J. Phase changes on heating ammonium magnesium phosphate hydrates. Thermochimica Acta 1988; 129: 197–215.

[22] Abdelrazig B, Sharp J, El-Jazairi B. The microstructure and mechanical properties of mortars made from magnesia-phosphate cement. Cement and Concrete Research 1989; 19: 247–258.

[23] Abdelrazig B, Sharp J, El-Jazairi B. The chemical composition of mortars made from magnesia-phosphate cement. Cement and Concrete Research 1988; 18: 415–425.

[24] Abdelrazig B, Sharp J, Siddy P, El-Jazairi B. Chemical reactions in magnesia-phosphate cement. Proceedings of the British Ceramic Society 1984; 35: 141–154.

[25] Wilson AD, Nicholson JW. Acid–base cements: their biomedical and industrial applications. Cambridge: Cambridge University Press, 1993.

[26] Soudée E, Péra J. Mechanism of setting reaction in magnesia-phosphate cements. Cement and Concrete Research 2000; 30: 315–321.

[27] Wagh AS, Jeong SY. Chemically bonded phosphate ceramics, I: a dissolution model of formation. Journal of the American Ceramic Society 2003; 86: 1838–1844.

[28] Laurencin D, Almora-Barrios N, de Leeuw NH, Gervais C, Bonhomme C, Mauri F, Chrzanawski W, Knowles JC, Newport RJ, Wong A, Gan Z, Smith ME. Magnesium incorporation into hydroxyapatite. Biomaterials 2001; 32: 1826–1837.

[29] Landi E, Tampieri A, Mattioli-Belmonte M, Celotti G, Sandri M, Gigante A, Fava P, Biagini G. Biomimetic Mg- and Mg,CO_3^- substituted hydroxyapatites: synthesis characterization and *in vitro* behavior. Journal of the European Ceramic Society 2006; 26: 2593–2601.

[30] Bigi A, Foresti E, Gregorini R, Ripamonti A, Roveri N, Shah J. The role of magnesium on the structure of biological apatites. Calcified Tissue International 1992; 50: 439–444.

[31] Sojka JE, Weaver CM. Magnesium supplementation and osteoporosis. Nutrition Reviews 1995; 53: 71–74.

[32] Wallach S. Effects of magnesium on skeletal metabolism. Magnesium and Trace Elements 1990; 9: 1–14.

[33] Rude R, Grubr H. Magnesium deficiency and osteoporosis: animal and human observations. The Journal of Nutritional Biochemistry 2004; 15: 710–716.

[34] Percival M. Bone health and osteoporosis. Applied Nutrition Science 1999; 5: 1–5.

[35] Danil'chenko SN, Kulik AN, Bugai AN, Pavlenko PA, Kalinichenko TG, Ul'yanchich NV, Sukhodub LF. Determination of the content and localization of magnesium in bioapatite of bone. Journal of Applied Spectroscopy 2005; 72: 899–905.

[36] Witte F, Kaese V, Haferkamp H, Switzer E, Wirth CJ, Windhagen H. *In vivo* corrosion of four magnesium alloys and the associated bone response. Biomaterials 2005; 26: 3557–3563.

[37] Staiger MP, Pietak AM, Huadmai J, Dias G. Magnesium and its alloys as orthopedic biomaterials: a review. Biomaterials 2006; 27: 1728–1734.

[38] Robinson DA, Griffith RW, Shechtman D, Evans RB, Conzemius MG. *In vitro* antibacterial properties of magnesium metal against *Escherichia coli*, *Pseudomonas aeruginosa* and *Staphylococcus aureus*. Acta Biomaterialia 2010; 6: 1869–1877.

[39] Landi E, Logroscino G, Proietti L, Tampieri A, Sandri M, Sprio S. Biomimetic Mg-substituted hydroxyapatite: from synthesis to *in vivo* behavior. Journal of Materials Science: Materials in Medicine 2008; 19: 239–247.

[40] Bigi A, Falini G, Foresti E, Gazzano M, Ripamonti A, Roveri N. Magnesium influence on hydroxyapatite crystallization. Journal of Inorganic Biochemistry 1993; 49: 69–78.

[41] Luoma H. The role of magnesium in the aetiology and prevention of caries: some new findings and implications. Magnesium Research 1988; 1: 223–230.

[42] Gomes S, Renaudin G, Jallot E, Nedelec J. Structural characterization and biological fluid interaction of sol-gel-derived Mg-substituted biphasic calcium phosphate ceramics. ACS Applied Materials Interfaces 2009; 1: 505–513.

[43] Burnstein L, Boskey A, Tannenbaum P, Posner A, Mandel I. The crystal chemistry of submandibular and parotid salivary gland stones. Journal of Oral Pathology & Medicine 1979; 8: 284–291.

[44] Miano R, Germani S, Vespasiani G. Stones and urinary tract infections. Urology International 2007; 79: 32–36.

[45] Tamimi F, Le Nihouannen D, Bassett DC, Ibasco S, Gbureck U, Knowles J, Wright A, Flynn A, Komarova SV, Barralet JE. Biocompatibility of magnesium phosphate minerals and their stability under physiological conditions. Acta Biomaterialia 2011; 7: 2678–2685.

[46] Prosser HJ, Wilson AD. Development of materials based on acid–base reaction cements. Materials & Design 1986; 7: 262–266.

[47] Driessens FCM, Boltong MG, Bermúdez O, Planell JA. Formulation and setting times of some calcium orthophosphate cements – a pilot-study. Journal of Materials Science: Materials in Medicine 1993; 4: 503–508.

[48] Ginebra MP, Boltong MG, Driessens FCM, Bermúdez O, Fernández E, Planell JA. Preparation and properties of some magnesium-containing calcium phosphate cements. Journal of Materials Science: Materials in Medicine 1994; 5: 103–107.

[49] Driessens FCM, Verbeeck R. Bio-minerals. Verlag der Zeitschrift für Naturforschung 1986; 41: 468–471.

[50] Driessens FCM, Boltong M, Bermúdez O, Planell JA, Ginebra MP, Fernández E. Effective formulations for the preparation of calcium phosphate bone cements. Journal of Materials Science: Materials in Medicine 1994; 5: 164–170.

[51] Driessens FCM, Boltong MG, Zapatero MI, Verbeeck MH, Bonfield W, Bermúdez O, Fernández E, Ginebra MP, Planell JA. *In vivo* behaviour of three calcium phosphate cements and a magnesium phosphate cement. Journal of Materials Science: Materials in Medicine 1995; 6: 272–278.

[52] Driessens FCM, Boltong M, Wenz R, Meyer J. Calcium phosphates as fillers in struvite cements. Key Engineering Materials 2005; 284-286: 161–164.

[53] Zimmermann M. Magnesium ammonium phosphate cement composition. US Patent 7,942,963 B2; 2011.

[54] Lilley KJ, Gbureck U, Knowles JC, Farrar DF, Barralet JE. Cement from magnesium substituted hydroxyapatite. Journal of Materials Science: Materials in Medicine 2005; 16: 455–460.

[55] Klammert U, Reuther T, Blank M, Reske I, Barralet JE, Grover LM, Kübler AC, Gbureck U. Phase composition, mechanical performance and *in vitro* biocompatibility of hydraulic setting calcium magnesium phosphate cement. Acta Biomaterialia 2010; 6: 1529–1535.

[56] Klammert U, Ignatius A, Wolfram U, Reuther T, Gbureck U. *In vivo* degradation of low temperature calcium and magnesium phosphate ceramics in a heterotopic model. Acta Biomaterialia 2011; 7: 3469–3475.

[57] Vorndran E, Ewald A, Müller FA, Zorn K, Kufner A, Gbureck U. Formation and properties of magnesium-ammonium-phosphate hexahydrate biocements in the Ca-Mg-PO$_4$ system. Journal of Materials Science: Materials in Medicine 2011; 22: 429–436.

[58] Liu C. Inorganic bone adhesion agent and its use in human hard tissue repair. US Patent No. 7,094,286 B2; 2006.

[59] Wu F, Wei J, Guo H, Chen F, Hong H, Liu C. Self-setting bioactive calcium-magnesium phosphate cement with high strength and degradability for bone regeneration. Acta Biomaterialia 2008; 4: 1873–1884.

[60] Jia J, Zhou H, Wei J, Jiang X, Hua H, Chen F, Wei S, Shin J, Liu C. Development of magnesium calcium phosphate biocement for bone regeneration. Journal of the Royal Society, Interface 2010; 7: 1171–1180.

[61] Wei J, Jia J, Wu F, Wei S, Zhou H, Zhang H, Shin JW, Liu C. Hierarchically microporous/macroporous scaffold of magnesium-calcium phosphate for bone tissue regeneration. Biomaterials 2010; 31: 1260–1269.

[62] Wu F, Su J, Wei J, Guo H, Liu C. Injectable bioactive calcium-magnesium phosphate cement for bone regeneration. Biomedical Materials 2008; 3: 1–7.

[63] Lu J, Wei J, Yan Y, Li H, Jia J, Wei S, Guo H, Xiao T, Liu C. Preparation and preliminary cytocompatibility of magnesium doped apatite cement with degradability for bone regeneration. Journal of Materials Science: Materials in Medicine 2011; 22: 607–615.

[64] Klammert U, Vorndran E, Reuther T, Müller FA, Zorn K, Gbureck U. Low temperature fabrication of magnesium phosphate cement scaffolds by 3D powder printing. Journal of Materials Science: Materials in Medicine 2010; 21: 2947–2953.

[65] Großardt C, Ewald A, Grover LM, Barralet JE, Gbureck U. Passive and active *in vitro* resorption of calcium and magnesium phosphate cements by osteoclastic cells. Tissue Engineering A 2010; 16: 3687–3695.

[66] Ewald A, Helmschrott K, Knebl G, Mehrban N, Grover LM, Gbureck U. Effect of cold-setting calcium- and magnesium phosphate matrices on protein expression in osteoblastic cells. Journal of Biomedical Materials Research B: Applied Biomaterials 2011; 96: 326–332.

[67] Vorndran E, Wunder K, Moseke C, Biermann I, Muller FA, Zorn K, Gbureck U. Hydraulic setting $Mg_3(PO_4)_2$ powders for 3D printing technology. Advances in Applied Ceramics 2011; 110: 476–481.

[68] Moseke C, Saratsis V, Gbureck U. Injectability and mechanical properties of magnesium phosphate cements. Journal of Materials Science: Materials in Medicine 2011; 22: 2591–2598.

[69] Yu Y, Wang J, Liu C, Zhang B, Chen H, Guo H, Zhong G, Qu W, Jiang S, Huang H. Evaluation of inherent toxicology and biocompatibility of magnesium phosphate bone cement. Colloids and surfaces B: Biointerfaces 2010; 76: 496–504.

[70] Mestres G, Ginebra MP. Novel magnesium phosphate cements with high early strength and antibacterial properties. Acta Biomaterialia 2011; 7: 1853–1861.

[71] Waselau M, Samii VF, Weisbrode S, Bertone AL. Effects of a magnesium adhesive cement on bone stability and healing following a metatarsal osteotomy in horses. American Journal of Veterinary Research 2007; 68: 370–378.

[72] Gulotta LV, Kovacevic D, Ying L, Ehteshami JR, Montgomery S, Rodeo SA. Augmentation of tendon-to-bone healing with a magnesium-based bone adhesive. The American Journal of Sports Medicine 2008; 36: 1290–1297.

[73] Thomopoulos S, Zampiakis E, Das R, Kim HM, Silva MJ, Havlioglu N, Gelberman RH. Use of a magnesium-based bone adhesive for flexor tendon-to-bone healing. Journal of Hand Surgery 2009; 34: 1066–1073.

[74] Hirvinen LJM, Litsky AS, Samii VF, Weisbrode S, Bertone AL. Influence of bone cements on bone-screw interfaces in the third metacarpal and third metatarsal bones of horses. American Journal of Veterinary Research 2009; 70: 964–972.

[75] Farrar DF. Bone adhesives for trauma surgery: a review of challenges and developments. International Journal of Adhesion and Adhesives 2012; 33: 89–97.

[76] Serraj S, Michaïlesco P, Margerit J, Bernard B, Boudeville P. Study of a hydraulic calcium phosphate cement for dental applications. Journal of Materials Science: Materials in Medicine 2002; 13: 125–131.

[77] Gbureck U, Knappe O, Grover LM, Barralet JE. Antimicrobial potency of alkali ion substituted calcium phosphate cements. Biomaterials 2005; 26: 6880–6886.

[78] Gbureck U, Knappe O, Hofmann N, Barralet JE. Antimicrobial properties of nanocrystalline tetracalcium phosphate cements. Journal of Biomedical Materials Research B 2007; 83: 132–137.

[79] Dorozhkin SV. Calcium orthophosphates in nature, biology and medicine. Materials 2009; 2: 399–498.

[80] Prabhu S (editor). Textbook of oral and maxillofacial anatomy, histology, and embryology. New Delhi: Oxford University Press, 2006.

[81] Torabinejad M, Walton RE, editors. Endodontics: principles and practice. St. Louis: Saunders Elsevier, 2009.

[82] Bergenholtz G, Hørsted-Bindslev P, Reit C, editors. Textbook of endodontology. Chichester: Wiley-Blackwell, 2009.

[83] Pispa J, Thesleff I. Mechanisms of ectodermal organogenesis. Developmental Biology 2003; 262: 195–205

[84] Power R. Oral anatomy. In: Dentist training manual for military dentists. Port Richey: Integrated Publishing, 2007.

[85] World Health Organization. Oral health. In: Fact Sheet n. 318; 2007.

[86] Tronstad L. Clinical endodontics: a textbook. New York: Thieme, 2003.

[87] van Noort R. Introduction to dental materials. London: Mosby, Elsevier, 2007.

[88] Macchi RL. Materiales dentales. Buenos Aires: Panamerica, 2007.

[89] Ørstavik D. Materials used for root canal obturation: technical, biological and clinical testing. Endodontic topics 2005; 12: 25–38.

[90] Torabinejad M, Khademi AA, Babagoli J, Cho Y, Johnson WB, Bozhilov K, Kim J, Shabahang S. A new solution for the removal of the smear layer. Journal of Endodontics 2003; 29: 170–175.

[91] Ingle JI, Newton CW, West JD, Gutmann JL, Glickman GN, Korzon BH, Martin H. Obturation of the radicular space. In: Ingle's Endodontics. Ingle JI, Bakland LK, Baumgartner JC (editors). Hamilton: BC Decker Inc, 2008.

[92] Norma Española UNE-EN ISO No.6876. Dental root canal sealing materials, 2003.

[93] Beyer-Olsen E, Ørstavik D. Radiopacity of root canal sealers. Oral Surgery Oral Medicine Oral Pathology 1981; 51: 320–328.

[94] Roberts HW, Toth JM, Berzins DW, Charlton DG, Mi M. Mineral trioxide aggregate material use in endodontic treatment: a review of the literature. Dental Materials 2007; 4: 149–164.

[95] Lide D. CRC Handbook of Chemistry and Physics (internet version). Boca Raton: CRC, 2010.

[96] Norma Española UNE-EN ISO No. 9917-1. Dentistry. Water-based cements, part I: powder/liquid acid-base cements, 2007.

[97] Guerreiro-Tanomaru JM, Duarte MAH, Gonçalves M, Tanomaru-Filho M. Radiopacity evaluation of root canal sealers containing calcium hydroxide and MTA. Brazilian Oral Research 2009; 23: 119–123.

[98] Bueno CEDS, Zeferino EG, Manhães LRC, Rocha DGP, Cunha RS, De Martin AS. Study of the bismuth oxide concentration required to provide Portland cement with adequate radiopacity for

endodontic use. Oral Surgery, Oral Medicine, Oral Pathology, Oral Radiology, and Endodontics 2009; 107: 6569.

[99] Romieu G, Garric X, Munier S, Vert M, Boudeville P. Calcium-strontium mixed phosphate as novel injectable and radio-opaque hydraulic cement. Acta Biomaterialia 2010; 6: 3208–3215.

[100] Chen F, Liu C, Mao Y. Bismuth-doped injectable calcium phosphate cement with improved radiopacity and potent antimicrobial activity for root canal filling. Acta Biomaterialia 2010; 6: 3199–3207.

[101] Carvalho-Junior JR, Correr-Sobrinho L, Correr AB, Sinhoreti MAC, Consani S, Sousa-Neto MD. Radiopacity of root filling materials using digital radiography. International Endodontic Journal 2007; 40: 514–520.

[102] Tadier S, Le Bolay N, Girod-Fullana S, Cazalbou S, Charvillat C, Labarrère M, Boitel D, Rey C, Combes C. Co-grinding significance for calcium carbonate-calcium phosphate mixed cement. Part II: effect on cement properties. Journal of Biomedical Materials Research B 2011; 99: 302–313.

[103] Fridland M, Rosado R. Mineral trioxide aggregate (MTA) solubility and porosity with different water-to-powder ratios. Journal of Endodontics 2003; 29: 814–817.

[104] Fridland M, Rosado R. MTA solubility: a long term study. Journal of Endodontics 2005; 31: 376–379.

[105] Saghiri MA, Shokouhinejad N, Lotfi M, Aminsobhani M. Push-out bond strength of mineral trioxide aggregate in the presence of alkaline pH. Journal of Endodontics 2010; 36: 1856–1859.

[106] Reyes-Carmona JF, Felippe MS, Felippe WT. The biomineralization ability of mineral trioxide aggregate and Portland cement on dentin enhances the push-out strength. Journal of Endodontics 2010; 36: 286–291.

[107] Pashley DH, Derkson ME. Microleakage measurement of selected restorative materials: a new *in vitro* method. Journal of Prosthetic Dentistry 1986; 56: 435–440.

[108] Gandolfi MG, Prati C. MTA and F-doped MTA cements used as sealers with warm gutta-percha. Long-term study of sealing ability. International Endodontic Journal 2010; 43: 889–901.

[109] Brackett MG, Martin R, Sword J, Oxford C. Comparison of seal after obturation techniques using a polydimethylsiloxane-based root canal sealer. Techniques 2006; 32: 1188–1190.

[110] Santos J, Tja L, Ferraz C, Zaia A, Alves M, Goes MD, Carrilho M. Long-term sealing ability of resin-based root canal fillings. International Endodontic Journal 2010; 43: 455–460.

[111] Camilleri J, Gandolfi MG, Siboni F, Prati C. Dynamic sealing ability of MTA root canal sealer. International Endodontic Journal 2011; 44: 9–20.

[112] Al-Hezaimi K, Naghshbandi J, Oglesby S. Human saliva penetration of root canals obturated with two types of mineral trioxide aggregate cements 2005; 31: 453–456.

[113] Vizgirda PJ, Liewehr FR, Patton, WR, Mcpherson, JC, Buxton TB. A comparison of laterally condensed gutta-percha, thermoplasticized gutta-percha and mineral trioxide aggregate as root canal filling materials. Journal of Endodontics 2004; 30: 103–106.

[114] Gandolfi MG, Sauro S, Mannocci F. New tetrasilicate cements as retrograde filling material: an *in vitro* study on fluid penetration. Journal of Endodontics 2007; 33: 742–745.

[115] Parirokh M, Askarifard S, Mansouri S, Haghdoost AA, Raoof M, Torabinejad M. Effect of phosphate buffer saline on coronal leakage of mineral trioxide aggregate. Oral Surgery Oral Medicine Oral Pathology Oral Radiology and Endodontics 2009; 51: 187–191.

[116] Yildirim T, Tas T. The evaluation of the influence of using MTA in teeth with post indication on the apical sealing ability. Oral Surgery Oral Medicine Oral Pathology 2009; 108: 471–474.

[117] Desai S, Chandler N. Calcium hydroxide-based root canal sealers: a review. Journal of Endodontics 2009; 35: 475–480.

[118] Manhart M. The calcium hydroxide method of endodontic sealing. Oral Surgery Oral Medicine Oral Pathology 1982; 54: 219–224, 1982.

[119] Beltes P, Koulaouzidou E, Kotoula V, Al E. *In vitro* evaluation of cytotoxicity of calcium hydroxide-based root canal sealers. Endodontics & Dental Traumatology 1995; 11: 245–249.

[120] Geurtsen W, Leyhausen G. Biological aspects of root canal filling materials – histocompatibility, cytotoxicity, and mutagenicity. Clinical Oral Investigations 1997; 1: 5–11.

[121] Huang FM, Tai KW, Chou MY, Chang YC. Cytotoxicity of resin-, zinc oxide-eugenol-, and calcium hydroxide-based root canal sealers on human periodontal ligament cells and permanent V79 cells. International Endodontic Journal 2002; 35: 153–158.

[122] Vajrabhaya L, Sithisarn P. Multilayer and monolayer cell cultures in a cytotoxicity assay of root canal sealers. International Endodontic Journal 1997; 30: 141–144.

[123] Torabinejad M, Watson T, Pitt Ford TR. Sealing ability of a mineral trioxide aggregate when used as a root end filling material. Journal of Endodontics 1993; 19: 591–595.

[124] Walker MP, Diliberto A, Lee C. Effect of setting conditions on mineral trioxide aggregate flexural strength. Journal of Endodontics 2006; 32: 334–336.

[125] Abdullah D, Pitt Ford TR, Papaioannou S, Nicholson J, McDonald F. An evaluation of accelerated Portland cement as a restorative material. Biomaterials 2002; 23: 4001–4010.

[126] Asgary S, Parirokh M, Eghbal M, Brink F. Chemical differences between white and gray mineral trioxide aggregate. Journal of Endodontics 2005; 31: 101–103.

[127] Silva HF, Andrade V, Méndez G, Medellin R, Al E. Análisis fisicoquimico del mineral trióxido agregado (MTA) por difracción de rayos X calorimetría y microscopía electrónica de barrido. Revista ADM 2000; 57: 125–131.

[128] Jafarnia B, Jiang J, He J, Wang YH, Safavi KE, Zhu Q. Evaluation of cytotoxicity of MTA employing various additives. Oral Surgery, Oral Medicine, Oral Pathology, Oral Radiology, and Endodontics; 2009: 107: 739–744.

[129] Bodanezi A, Carvalho N, Silva D, Bernardineli N, Bramante CM, Garcia RB, de Moraes IG. Immediate and delayed solubility of mineral trioxide aggregate and Portland cement. Journal of Applied Oral Science; 2008: 16: 127–131.

[130] Islam I, Chng H, Yap A. X-ray diffraction analysis of mineral trioxide aggregate and Portland cement. International Endodontic Journal 2006; 39: 220–225.

[131] Wang X, Sun H, Chang J. Characterization of $Ca_3SiO_5/CaCl_2$ composite cement for dental application. Dental Materials 2008; 24: 74–82.

[132] Lovato K, Sedgley C. Antibacterial activity of EndoSequence root repair material and ProRoot MTA against clinical isolates of *Enterococcus faecalis*. Journal of Endodontics 2011; 37: 1542–1546.

[133] Odabaş ME, Cinar C, Akça G, Araz I, Ulusu T, Yücel H. Short-term antimicrobial properties of mineral trioxide aggregate with incorporated silver-zeolite. Dental Traumatology; 2011; 27: 189–194.

[134] Camilleri J. Characterization and hydration kinetics of tricalcium silicate cement for use as a dental biomaterial. Dental Materials 2011; 27: 836–844.

Chapter 5.

Effect of processing parameters on the setting reaction of magnesium phosphate cements

Table of Contents

5.1 Introduction

Magnesium-phosphate-based cements (MPC) were first discovered during 1939–1940 by Prosen [1,2] as refractory materials for use in casting dental alloys. They consisted of a mixture of magnesium oxide and phosphoric acid, and formed water-soluble magnesium dihydrogen phosphate [$Mg(H_2PO_4)_2 \cdot nH_2O$] as a reaction product. Later, ceramics with very low solubility were formed by replacing the phosphoric acid for a salt such as ammonium dihydrogen phosphate. Several magnesium-phosphate-based cements (MPC) were developed for use as structural materials during the second half of the last century.

MPCs are essentially acid-base cements and can react at room temperature. Dead-burned magnesia is used as the alkaline component, whereas ammonium phosphates are the preferred acid components, either as diammonium hydrogen phosphates ($(NH_4)_2HPO_4$) [3] or ammonium dihydrogen phosphate ($NH_4H_2PO_4$) [4–7]. Their fast setting and early strength attainment and also their adhesive properties were some of the most relevant features of these cements, which are used in civil engineering for rapid repair of roads, industrial floors and airport runways [4,6,8]. The main problem with ammonium magnesium phosphate cements is that, during setting and even after, they tend to release ammonia [9–11].

Despite the unique benefits provided by these systems, they have not been exploited in clinical applications up to date. Only recently, the use of ammonium-magnesium phosphate cements (ammonium-MPCs) in combination with calcium phosphate cements (CPCs) has been proposed for bone regeneration applications [12–15]. The combined CPC-ammonium-MPCs were shown to be biocompatible and osteogenic *in vivo* [13,15]. Additionally, a recent study reported that both mutagenicity and potential carcinogenicity were negative for ammonium MPC extracts [16]. In a different context, the growing interest in biodegradable magnesium alloys for medical application has fostered numerous studies on the effect of the release of magnesium ions *in vivo*. It has been shown that local magnesium release in bone not only has not any adverse effect [17] but also enhances osteoclast and osteoblast activity [18,19], thus reinforcing the hypothesis that Mg^{2+} ions play a key role in bone metabolism [20,21].

Nevertheless, the use of the ammonium magnesium phosphate cements may present some problems in clinical applications. On one hand, the use of an ammonium salt may compromise the biocompatibility of the cement. In fact, ammonia released during processing and storage is one of the problems associated with these mortars [9–11], which leads to container corrosion and creates an unpleasant environmental odor, restricting their use to outdoor applications. On the other hand, the fast acid-base reaction leads to an exothermic process [4,9] that should be strictly controlled to avoid tissue necrosis.

In this context, this Chapter aims at the development of novel formulations of MPCs that do not compromise the cement biocompatibility due to the ammonium release or the exothermy.

5.2 Objectives

This Chapter aims at the development of a novel family of inorganic cements, the magnesium phosphate cements (MPCs), with enhanced properties for clinical applications. In order to fulfill this purpose, the specific objectives are the following:

1. To prepare MPCs with a low amount or without ammonium-compounds in order to reduce or avoid the release of ammonia or ammonium ions to the surrounding tissues.

2. To control the exothermy of the setting reaction by the adjustment of the granulometry, the reactivity of MgO and/or the addition of a retarding agent.

3. To characterize the paste of the MPC formulations by assessing the setting times and the injectability.

4. To evaluate the phase composition, microstructure, mechanical properties, specific surface area, skeletal density and pore size distribution of the MPC formulations.

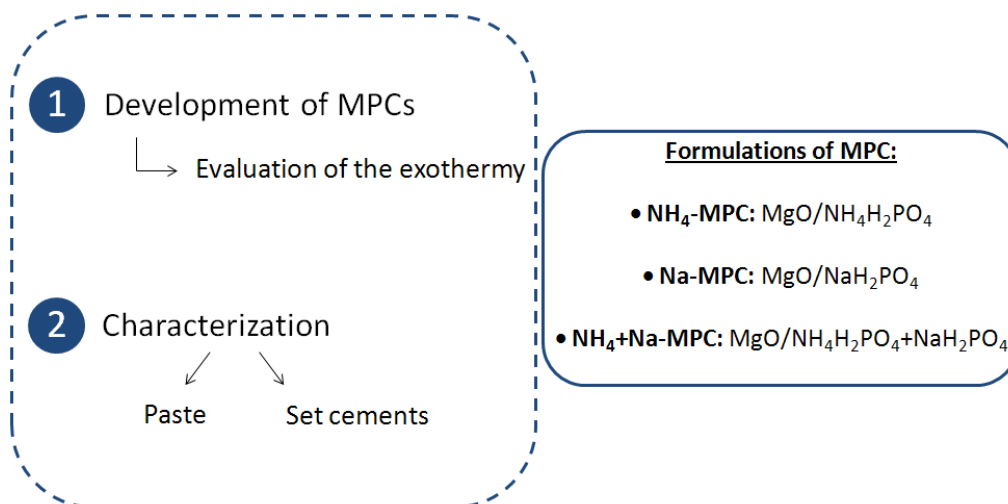Figure 5.1 schematically shows the structure of this Chapter.

Figure 5.1. Schema of the studies evaluated in Chapter 5.

5.3 Materials and methods

5.3.1 Powder phase

The powder phase of the cement consisted of a mixture of heavy magnesium oxide (MgO, Merck, ref n. 105867), as the basic component, and an acid component that was either ammonium dihydrogen phosphate ($NH_4H_2PO_4$, Panreac ref n. 131126.1210), sodium dihydrogen phosphate (NaH_2PO_4, Fluka ref n. 71496) or an equimolar mixture of both.

Since the reaction between MgO and the phosphate salt is an acid-base one, an exothermic process takes place [4,9]. In order to control the exothermy of this process and to protect the tissues that would surround the cement *in vivo*, three different strategies were employed: i) the MgO was calcined in order to decrease its reactivity, ii) a retardant was added to the powder phase, and iii) the particle size of all reactants was controlled by milling.

The MgO was calcined at 1475°C for 6 h to decrease its reactivity [22,23]. After the thermal treatment, 50 g of the MgO powder were milled in a planetary ball mill (Fritsch, Pulverisette 6), using an agate jar and 4 agate balls (ϕ = 30 mm) at 150 rpm for 15 min. The ammonium and sodium phosphate salts were also milled (50 g), following two different milling protocols in order to obtain coarse and fine powders for each salt. Sodium tetraborate decahydrate ($Na_2B_4O_7 \cdot 10H_2O$, Fluka, ref

n. 72000), known also as borax, was added to the powder phase as a retardant of the reaction [24–28]. Previously, 50 g of borax were milled at 150 rpm during 15 min.

The particle size distribution was characterized by laser diffraction (Beckman Coulter LS 13 320), after sonicating the powder in ethanol in order to avoid particle agglomeration. Table 5.1 shows the particle size of the reactants after applying the different milling protocols, and also after being calcined for different time periods in the case of MgO.

Table 5.1. Milling protocols and particle size distribution of the magnesium oxide, the two phosphate salts and the retardant used as reactants for the MPCs. D_i (D_{10}, D_{50} and D_{90}) stands for the average particle size where i% of the sample volume is smaller than Di.

	Powder size	Milling protocol	D_{10} (μm)	D_{50} (μm)	D_{90} (μm)
Magnesium source					
MgO (1475°C 6 h)	Coarse	150 rpm–15 min	0.55 ± 0.44	4.75 ± 0.68	27.49 ± 6.65
Phosphate source					
$NH_4H_2PO_4$	Coarse	150 rpm–15 min	16.99 ± 5.58	274.97 ± 13.70	550.4 ± 23.3
	Fine	350 rpm–60 min	1.97 ± 0.52	14.15 ± 6.32	35.89 ± 8.20
NaH_2PO_4	Coarse	150 rpm–15 min	11.89 ± 7.24	185.51 ± 97.99	446.7 ± 111.98
	Fine	350 rpm–30 min	1.59 ± 0.18	7.07 ± 0.83	29.21 ± 4.38
Retardant					
Borax	Coarse	150 rpm–15 min	13.48 ±4.77	66.77 ± 15.82	214.47 ± 55.76

5.3.2 Cement preparation

Three series of MPC were prepared by combining MgO with either ammonium dihydrogen phosphate, sodium dihydrogen phosphate or an equimolar mixture of both. A MgO/phosphate salt molar ratio of 3.8/1 was employed, since it is known that, in the case of ammonium magnesium phosphate cements, an excess of magnesia ensures reaction completion and enhances strength development [5,25,29]. The powder was mixed with distilled water at a liquid to powder ratio of 0.13 ml/g, forming a cement paste that resulted in a solid body after hardening, as schematically

shown in Figure 5.2. The formulations were named as NH_4-MPC, Na-MPC and NH_4+Na-MPC, respectively, accounting for the type of phosphate salt used.
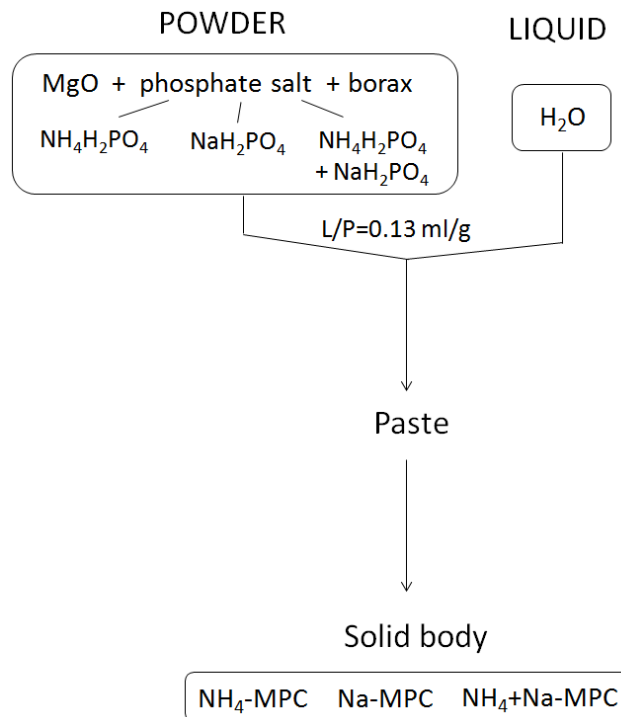

Figure 5.2. Schematic representation of the reactants included in the powder phase, which when mixed with water, give place to the cement paste that resulted in a solid body after hardening. The three MPC formulations are indicated, as well as the phosphate salts that originated them.

5.3.3 Optimization of the MPC formulation

The cement exothermy while setting was a crucial parameter to control in order to avoid high levels of heat causing irreversible damages to the surrounding tissues [30]. The exothermy of the cements was evaluated at room temperature. The temperature evolution of the cements during the setting reaction was followed by introducing a type K thermocouple (Thermometer RS 1313) into 1.5 g of cement paste placed in a plastic container. When monitoring the temperature evolution, time zero was the moment in which the liquid phase was added to the powder.

The exothermy of the cement was adjusted gradually. Firstly, the effect of the phosphate salts granulometry on the exothermy was evaluated, being selected the milling protocol that produced a lower exothermy. Secondly, the amount of borax required was assessed (Figure 5.3).
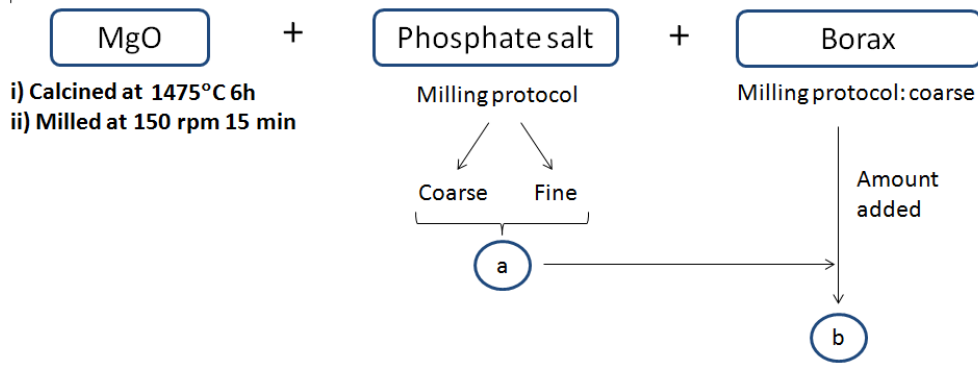
Figure 5.3. Processing of the reactants to establish an appropriate exothermy.

The MPC formulations with an adequate exothermy for clinical requirements were selected for subsequent characterization.

5.3.4 Physico-chemical characterization studies

Both the cement paste and the cement set at different time points of immersion were characterized. Except for the evaluation of the mechanical properties, the set cements were characterized after stopping the setting reaction by introducing the cements in acetone for 1 h and afterwards drying them at 37°C for 24 h. Figure 5.4 schematically indicates the techniques that were used to characterize both the cement paste and the set cement. The techniques used are briefly explained beyond.
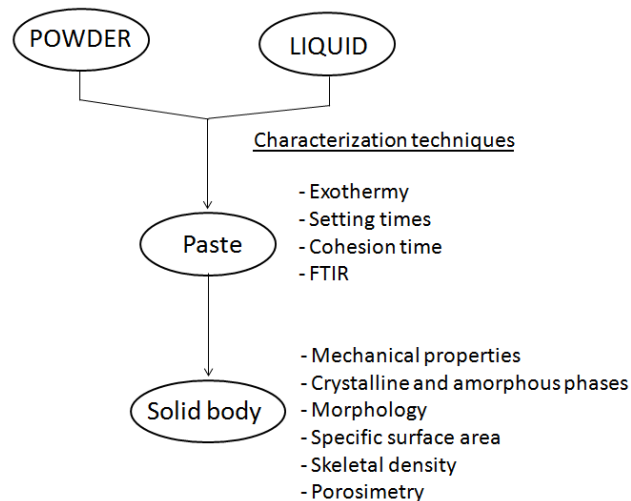

Figure 5.4. Schema of the cement preparation and of the characterization of both the cement paste and the solid body.

5.3.4.1 Setting and cohesion time

The setting times of the cement paste were determined with the Gillmore needles, as explained in Chapter 3 (Section 3.3.2.1). The cohesion time was measured by virtual inspection of the cement, as explained in Chapter 3 (Section 3.3.2.2).

5.3.4.2 *In situ* setting evolution by FTIR

The fresh cements (0.5 − 1 min after the liquid phase was added to the powder) were analyzed using a Fourier-transform infrared spectroscopy (FTIR, Spectrum GX, Perkin Elmer). The three MPC formulations were prepared without the addition of borax in order to simplify the system. In other words, to only evaluate the reactions between the main reactants and thus avoid any interference of borax, which is known to interact with MgO [24,31]. A small amount of paste was deposited on the surface of a cell that consisted of two Hastelloy plates containing a pair of diamond windows that enabled samples to be compressed to an ideal thickness for transmission measurements. This means that pre-preparation was minimal and the fresh cement was ready for direct analysis on an FTIR microscope stage. The analysis was performed *in situ* at regular intervals of time for a period of 60 min.

5.3.4.3 Mechanical properties

Cylindrical Teflon molds (6 mm in diameter and 12 mm in height) were filled with the cement paste and were immersed in Ringer's solution at 37°C to simulate physiological conditions. After different periods of time (1 h, 2 h, 1 day and 7 days) the specimens were removed from the molds and the compressive strength was measured in wet conditions using a Universal testing machine (Adamel Lhomargy DY 32/34) equipped with a load cell of 10 kN at a crosshead speed of 1 mm/min. Ten specimens were tested for each time point.

5.3.4.4 Crystalline phases

The phase composition of the MPCs at different time points (1 h, 2 h, 1 and 7 days) was assessed by X-ray powder diffraction (XRD, PANalytical, X'Pert PRO Alpha-1). The samples used to test the mechanical properties were introduced in acetone for 1 h to stop the reaction and

afterwards were dried at 37°C for 24 h. The cements were pulverized by crushing them in an agate mortar.

The XRD measurements were done using Bragg Brentano geometry using a Cu K_α radiation. The step-scanning was performed with an integration time of 50 s using a 2θ scan step of 0.017° between 4 and 50°. Indexing of the peaks was carried out by means of cards JCPDS #79-0612 for MgO; JCPDS #85-0881 for $NH_4H_2PO_4$; JCPDS #84-0112 for NaH_2PO_4; JCPDS #12-0258 for $Na_2B_4O_7 \cdot 10H_2O$; JCPDS #77-2303 for struvite, $MgNH_4PO_4 \cdot 6H_2O$; and JCPDS # 16-0353 for schertelite, $Mg(NH_4 \cdot HPO_4)_2 \cdot 4H_2O$ [32].

5.3.4.5 Morphology

The microstructure of both the reactants and fracture surfaces of the cements (set in Ringer's solution for 1 h and 7 days) was observed by Field Emission Scanning Electron Microscopy (FESEM, JEOL JSM-7001F). The samples were placed on a carbon fiber stuck on a copper layer. For the cements, colloidal silver was used to paint a line from the top of the cement to the holder.

5.3.4.6 Specific surface area

The specific surface area of MPCs set for 7 days in Ringer's solution was analyzed by N_2 adsorption (Micromeritics ASAP 2020) following the BET (Brunnauer – Emmet – Teller) theory. Two replicates were performed for each formulation.

5.3.4.7 Skeletal density

The skeletal density of MPCs set for 7 days in Ringer's solution was measured by helium pycnometry (Micromeritics AccuPyc 1330). Three replicates were performed for each formulation.

5.3.4.8 Porosimetry

The total porosity and the pore size distribution of MPCs set for 7 days in Ringer's solution were evaluated by mercury intrusion porosimetry (MIP, Micromeritics AutoPore IV 9500). Cylindrical specimens (6 mm diameter and 12 mm height) set in Ringer's solution for 7 days were evaluated. One assay was performed for each formulation.

5.3.5. Statistical analysis of the results

A Student's t-test was used to determine the statistically significant differences between the mean values of the different experimental groups. A difference between groups was considered to be significant at $p < 0.05$.

5.4. Results

5.4.1 Optimization of the MPC formulations

a) Effect of phosphate salt type and granulometry

The effect of both the type of phosphate salt and the powder granulometry on the exothermy of the three MPCs to which 3 wt% borax was added is shown in Figure 5.5. The cements prepared with sodium dihydrogen phosphate presented lower exothermy. Moreover, the maximum temperature appeared at shorter times, around 5 min, suggesting a faster reaction. In the cements prepared with ammonium dihydrogen phosphate, the maximum temperature was reached after 12 min, and the MPC prepared with an equimolar mixture of both phosphate salts, reached the maximum temperature at an intermediate time. Moreover, in all cases, a clear effect of the powder fineness was observed, the use of coarse powder reducing the exothermy of the reaction, as expected. Therefore, the coarse powder was selected for the continuation of the studies.
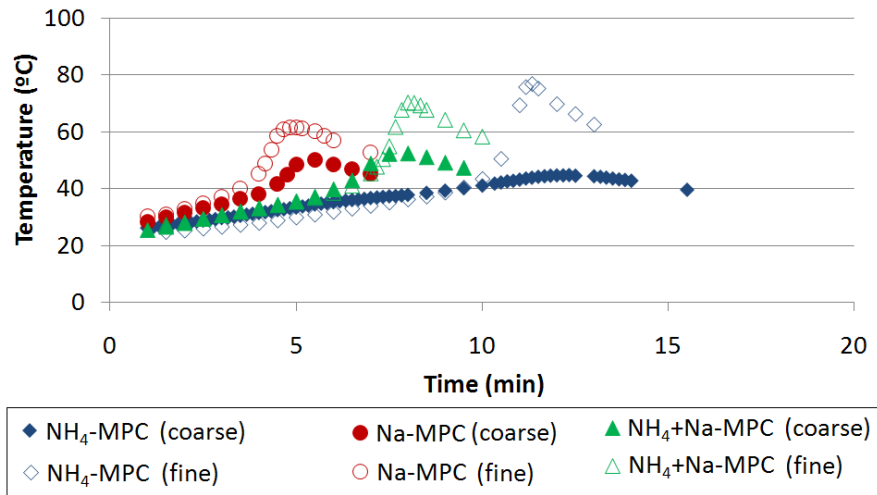
Figure 5.5. Temperature evolution for NH_4-MPC, Na-MPC and NH_4+Na-MPC using different powder granulometry for the phosphate salt.

The particle size distribution of the reactants used for the preparation of MPCs is shown in Figure 5.6.

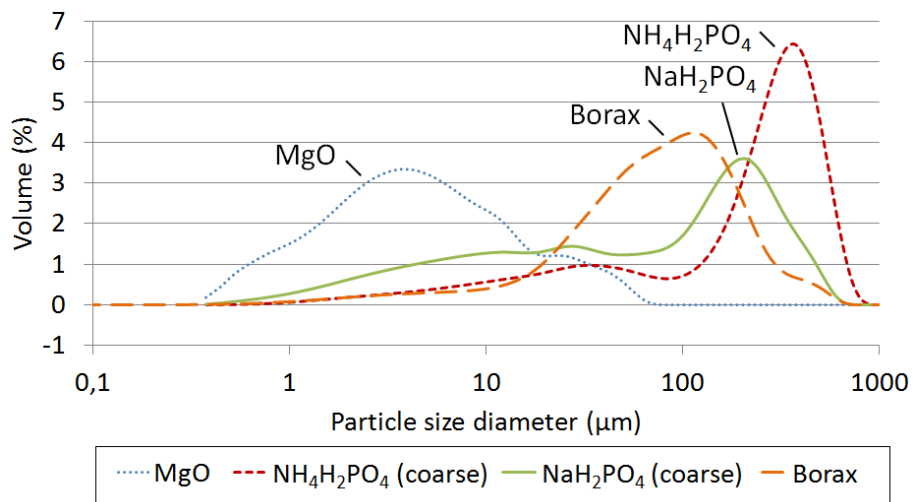**Figure 5.6.** Particle size distribution of the reactants of MPCs: MgO calcined at 1475°C for 6h and milled at 150 rpm for 15min, coarse $NH_4H_2PO_4$ and NaH_2PO_4, and borax.

b) Effect of borax

Figure 5.7 shows the effect of the amount of borax in the temperature evolution. In all cases, an increasing amount of borax resulted in a decrease of the maximum temperature reached

and, simultaneously, in a delay of the time at which this maximum temperature was reached, retarding the setting reaction. It is interesting to note that borax was more effective in reducing the exothermy of the reaction in the case of NH_4-MPC than in the other two formulations. In the NH_4-MPC the maximum temperature was reduced from 110 to 42°C when adding 3 wt% borax, whereas in the Na-MPC this temperature was reduced from 61 to 42°C and in the NH_4+Na-MPC from 67 to 44°C.
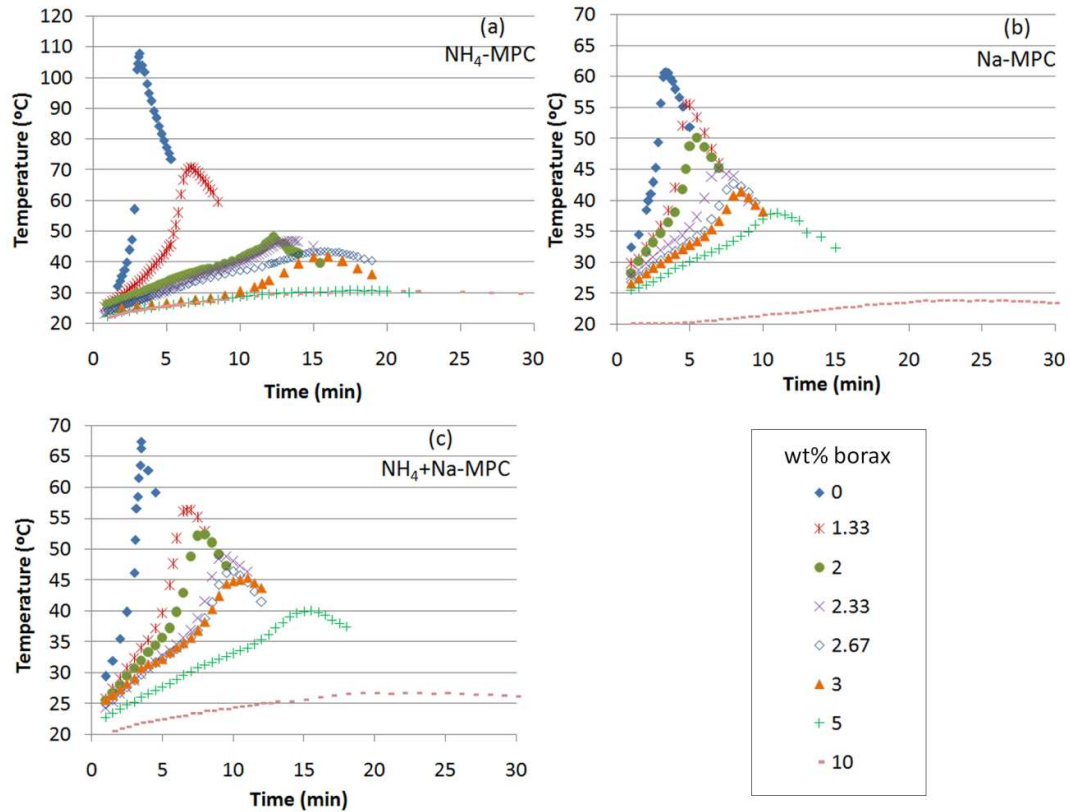

Figure 5.7. Temperature evolution of: a) NH_4-MPC, b) Na-MPC and c) NH_4+Na-MPC with different amounts of coarse borax (wt%).

For the succeeding studies, a concentration of 3 wt% borax was selected since it was considered that the exothermy was low enough to be compatible with clinical applications [33].

5.4.2 Physico-chemical characterization of MPCs

5.4.2.1 Setting and cohesion times

The initial (t_I) and the final (t_F) setting times, and the time at which the maximum temperature was reached (t_{Tmax}) for the three MPC formulations containing 3 wt% borax are displayed in Table 5.2. The initial and final setting times of a CPC are included, for comparison [34].

Table 5.2. Initial setting time (t_I), final setting time (t_F), time at which the highest temperature was reached (t_{Tmax}) and cohesion time (t_C) for the three MPC formulations The average $\pm$ standard deviation is shown, n = 3. The initial and final setting times of an apatitic CPC are given for comparison [34].

MPC formulation	t_I (min)	t_F (min)	t_{Tmax}(min)	t_C (min)
NH_4-MPC	15 $\pm$ 1	16 $\pm$ 1	15.0 $\pm$ 08	$\geq$ 20
Na-MPC	8 $\pm$ 2	9 $\pm$ 2	8.2 $\pm$ 0.4	$\geq$ 10
NH_4+Na-MPC	12 $\pm$ 2	13 $\pm$ 2	10.5 $\pm$ 0.4	$\geq$ 15
CPC	9	19	–	–

The Na-MPC was the formulation with shortest initial and final setting times, followed by NH_4+Na-MPC and, finally, NH_4-MPC. In contrast to what happens in CPCs, the initial and final setting times were very close, and t_{Tmax} was very similar to t_I in all MPCs. The cohesion time was slightly longer than the final setting time in the three formulations.

5.4.2.2 *In situ* setting evolution by FTIR

FTIR allowed evaluating *in situ* the setting evolution of the MPC formulations. This study was done without the addition of borax to the powder phase in order to simplify the system, since it is known that borax can react with MgO [24,31].

Figure 5.8 a shows the setting evolution for NH_4-MPC prepared without borax, at different setting times. It is interesting to note that there was a quick evolution of the bands during the first 10 min (mostly between 500 – 1500 cm^{-1}), indication of the fast reaction between MgO and $NH_4H_2PO_4$. However, after 10 min, the bands were not significantly modified, showing that most of the end-products were already formed.

Figure 5.8 b shows the spectrum of the NH$_4$-MPC after 60 min of setting reaction. The position of most of the bands was in accordance with that of struvite and MgO, and the position of the phosphate groups matched with those reported for CDHA. Table 5.3 displays the experimental values and the wavenumbers reported in the literature.
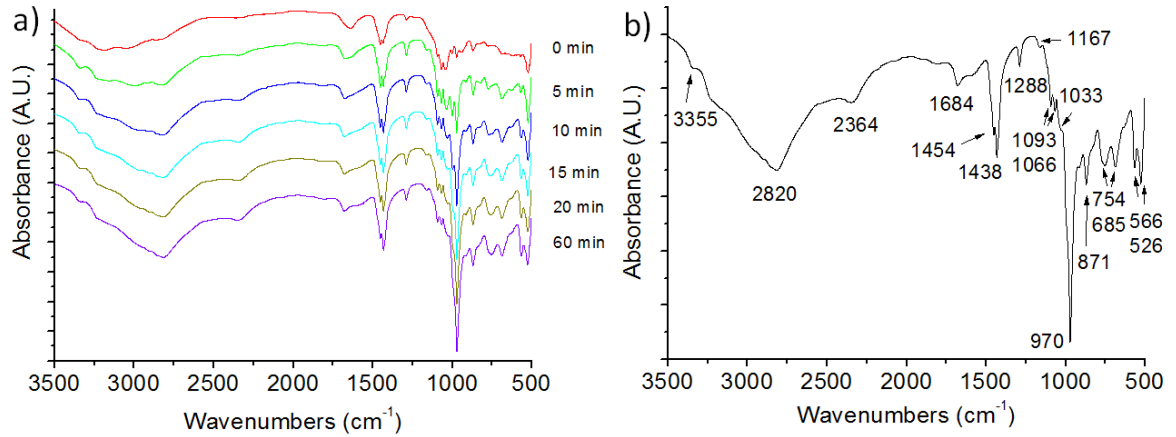

Figure 5.8. FTIR spectra of NH$_4$-MPC (without borax): a) at different setting times and b) after 60 min of reaction.

Table 5.3. Band assignments for NH_4-MPC (without borax) after 60 min of setting. The experimental values are compared with those reported in literature. Some abbreviations are used: sh: shoulder; s: strong band; vs: very strong; m: medium; w: weak; wd: wide.

Band assignment		Experimental values (cm^{-1})	Compound, frequency (cm^{-1}) according to literature	Refs.
Water of crystallization	OH, NH stretching	3355 (wd)	Struvite, 3276.9 (wd)	[35]
	OH, bending	2364 (wd)	Struvite, 2400 (wd)	[36]
	δ(HOH)	1684 (wd)	Struvite, 1680	[36]
	H_2O	1438 (s)	$Mg_3(PO_4)_2$+$Ca_3(PO_4)_2$, 1432.2	[37]
NH_4^+ units	ν_1, NH	2820 (wd)	Struvite, $2800 - 3000$	[35]
	ν_4, NH	1454 (sh)	Struvite, 1451	[36]
	NH	1288 (m)	Struvite, 1263	[36]
	NH, librational	754 (m)	Struvite, 754	[36]
	NH, librational	685 (m)	Struvite, 690.9	[35]
PO_4^{3-} units	PO_4^{3-}, ν_3	1167 (w)	CDHA, 1136 (sh)	[38]
	PO_4^{3-}, ν_3	1093 (w)	CDHA, 1085 (sh)	[39]
	PO_4^{3-}, ν_3	1066 (w)	Struvite, 1064.7	[35]
	PO_4^{3-}, ν_3	1033 (sh)	CDHA, 1045 (vs)	[38]
	PO_4^{3-}, ν_1	970 (s)	CDHA, 960 (m), 965 (w),	[38,39]
	PO_4^{3-}, ν_4	566 (m)	CDHA, 562 (w)	[38]
	HPO_4^{2-}, ν_5	871 (m)	CDHA, 870 (w)	[39]
Metal-oxygen bonds	MgO	526 (m)	Struvite, 510.4	[35]

The setting evolution of Na-MPC (prepared without borax) by FTIR showed a fast modification of the bands during the first 20 min (Figure 5.9 a), indication that a reaction between MgO and NaH_2PO_4 was taking place. After this time, when probably the major part of the end-product was already formed, the position and shape of the bands remained similar until the end of the study.

Figure 5.9 b indicates the bands present in the spectrum of Na-MPC after 60 min of setting. The position of the bands was associated to that of struvite and MgO, and the phosphate groups were linked to that of CDHA. Table 5.4 compiles the experimental values and compares them with those reported in literature.
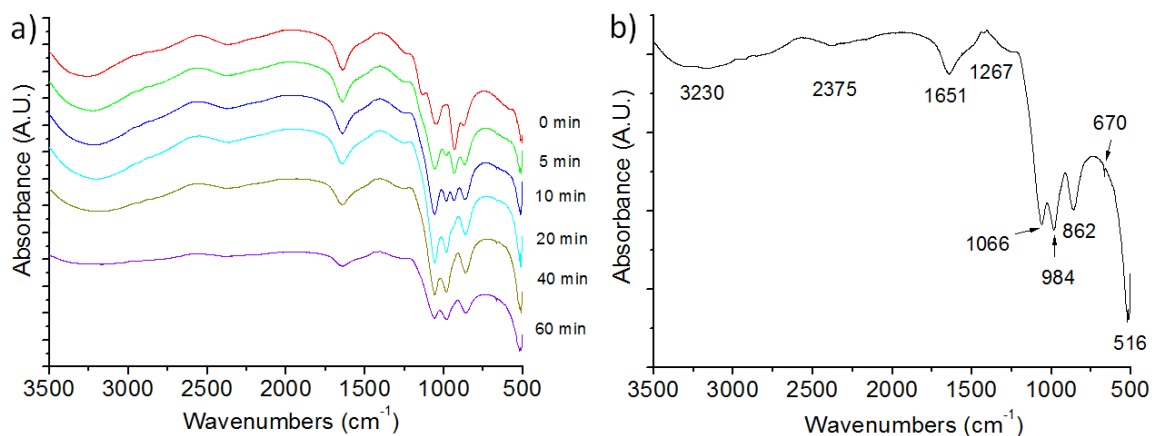

Figure 5.9. FTIR spectra of Na-MPC (without borax): a) at different setting times, and b) after 60 min of setting.

Table 5.4. Band assignments for Na-MPC (without borax) after 60 min of setting. The experimental values are compared with those reported in literature. Some abbreviations are used: sh: shoulder; s: strong band; vs: very strong; m: medium; w: weak; wd: wide.

Band assignment		Experimental values (cm^{-1})	Compound, frequency (cm^{-1}) according to literature	Refs.
Water of crystallization	OH stretching	3230 (wd)	Struvite, 3276.9 (w)	[35]
	OH	2375 (wd)	Struvite, 2400 (broad)	[36]
	OH water-adsorbed bending	1651 (wd,s)	CDHA, 1640 (w)	[39]
	OH libration	670 (w)	CDHA, 632 (sh, vw)	[39]
PO$_4^{3-}$ units	PO$_4^{3-}$, ν_3	1066 (m)	Struvite, 1064.7	[35]
	PO$_4^{3-}$, ν_1	984 (m)	CDHA, 960 (m), 965 (w)	[38,39]
	δ_{OH} of HPO$_4^{2-}$	1267 (sh)	CDHA, 1215 (sh, w)	[39]
	HPO$_4^{2-}$, ν_5	862 (m)	CDHA, 870 (w)	[39]
Metal-oxygen bonds	MgO	516 (s)	Struvite, 510.4	[35]

Figure 5.10 a shows the spectra of NH_4+Na-MPC (without borax) at different reaction times. A fast evolution of the bands was observed for the first 10 min (mainly between 500 and 1500 cm^{-1}), indication that the reactants were transforming into the end-products. Afterwards, the spectra evolved slightly. Figure 5.10 b shows the spectrum of NH_4+Na-MPC after 60 min of reaction. The position of the bands was associated with that of struvite and MgO, and the phosphate groups were linked to that of CDHA. Table 5.5 displays the experimental values and the wavenumbers reported in the literature.
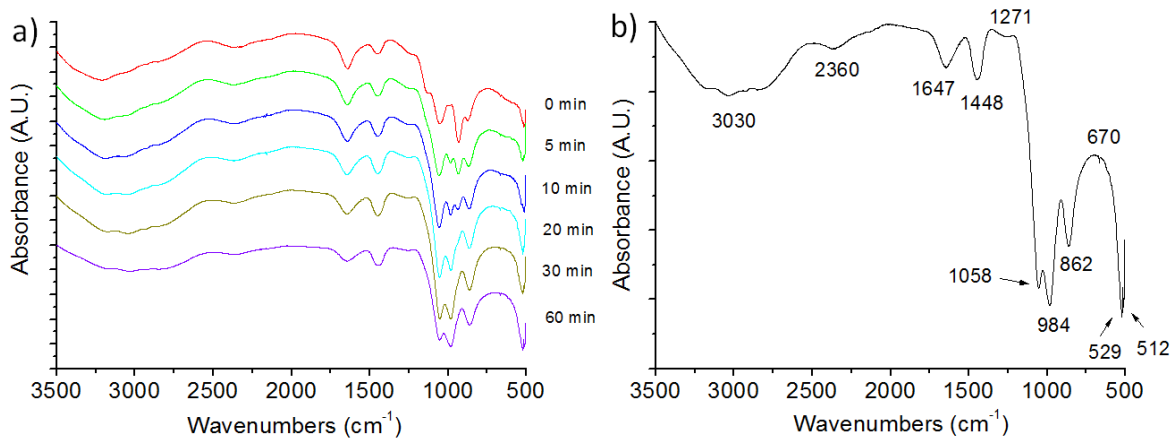

Figure 5.10. FTIR spectra of NH_4+Na-MPC (without borax): a) at different setting times and b) after 60 min of setting.

Table 5.5. Band assignments for the NH$_4$+Na-MPC (without borax) after 60 min of setting. Some abbreviations are used: sh: shoulder; s: strong band; vs: very strong; m: medium; w: weak; wd: wide

Band assignment		Experimental values (cm^{-1})	Compound, frequency (cm^{-1}) according to literature	Refs.
Water of crystallization	OH	3030 (wd)	Struvite, 3276.9	[35]
	OH	2360 (wd)	Struvite, 2400 (broad)	[36]
	OH water-adsorbed bending	1647 (m)	CDHA, 1640 (w)	[39]
	OH libration	670 (w)	CDHA, 632 (sh, vw)	[39]
NH$_4^+$ units	ν_4, NH	1448 (m)	Mg$_3$(PO$_4$)$_2$+Ca$_3$(PO$_4$)$_2$, 1432.2	[37]
	NH $^-$	1271 (m)	Struvite, 1263	[36]
PO$_4^{3-}$ units	PO$_4^{3-}$, ν_3	1058 (s)	Struvite, 1064.7	[35]
	PO$_4^{3-}$, ν_1	984 (s)	CDHA, 960 (m), 965 (w)	[38,39]
	HPO$_4^{2-}$, ν_5	862 (m)	CDHA, 870 (w)	[39]
Metal-oxygen bonds	MgO	512 (s)	Struvite, 510.4	[35]
	MgO	529 (s)	Struvite, 522.4	[35]

5.4.2.3 Mechanical properties

Figure 5.11 shows the compressive strength of MPC formulations at different reaction times. The strength evolution of an apatitic calcium phosphate cement (CPC) is included for comparison [39]. After 1 h, the three MPC formulations showed compressive strength values close to 30 MPa, in contrast to the apatitic CPC that achieved only 1 MPa. After 2 h, the compressive strength of all MPC formulations ranged between 30 and 50 MPa, whereas the CPC attained only 5 MPa. After 1 day, all MPCs reached a compressive strength close to 50 MPa, which was maintained after 7 days except for the NH$_4$+Na-MPC, in which case a decrease to less than 20 MPa was observed. The maximum compressive strength of the CPC was around 35 MPa.
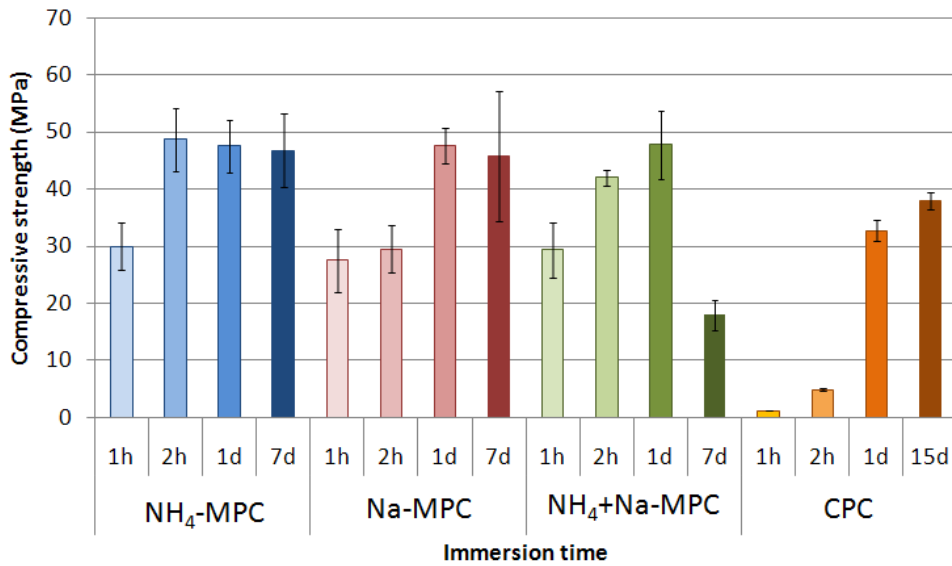
Figure 5.11. Compressive strength for the three MPC formulations after 1 h, 2 h, 1 day (1d) and 7 days (7d) immersion in Ringer's solution at 37°C. Error bars indicate the standard deviation, n = 10. The strength evolution of a CPC is included for comparison [39].

5.4.2.4 Crystalline phases

The XRD patterns obtained for the different formulations after 0 h (initial powder), 1 h, 1 and 7 days of immersion in Ringer's solution are shown in Figure 5.12. In all formulations the presence of MgO in excess was still detected after 7 days. In contrast, the phosphate salts used as reactants were not detected either in Na-MPC or in NH$_4$+Na-MPC, even at short times, suggesting rapid dissolution. Only small amounts of NH$_4$H$_2$PO$_4$ were observed in NH$_4$-MPC up to 1 day.

The compounds formed after cement hardening depended on the phosphate salt used as starting reactant. Thus, in the case of NH$_4$-MPC, schertelite (Mg(NH$_4$·HPO$_4$)$_2$·4H$_2$O) and a small amount of struvite (MgNH$_4$PO$_4$·6H$_2$O) appeared after 1 h setting. After 1 and 7 days the cement mainly consisted of struvite, although some schertelite was still present, coexisting with unreacted MgO. In NH$_4$+Na-MPC a similar phase evolution was observed, with schertelite and struvite being detected after 1 h and a progressive increase in the intensity of the peaks corresponding to struvite with reaction time. After 7 days the main product was struvite, coexisting with unreacted MgO and a small quantity of schertelite. Finally, in Na-MPC no crystalline phases apart from MgO were detected, and only a very small and wide shoulder around 2θ ~ 31° was observed in the baseline of the XRD pattern, indicating that the reaction product was an amorphous phase.
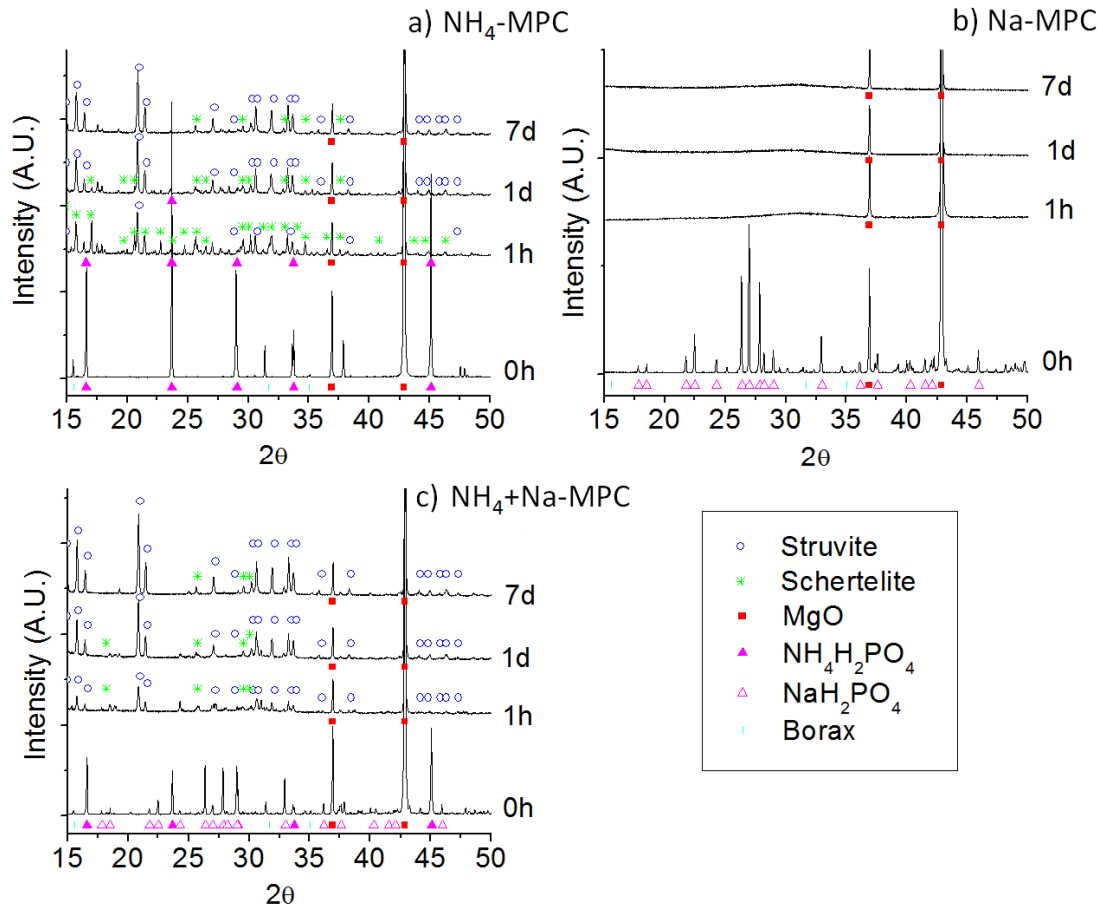
Figure 5.12. XRD of set MPC for 0 h, 1 h, 1 day and 7 days in Ringer's solution at 37°C: a) NH$_4$-MPC, b) Na-MPC, c) NH$_4$+Na-MPC. A.U. stands for arbitrary units.

5.4.2.5 Morphology of reactants and end-products

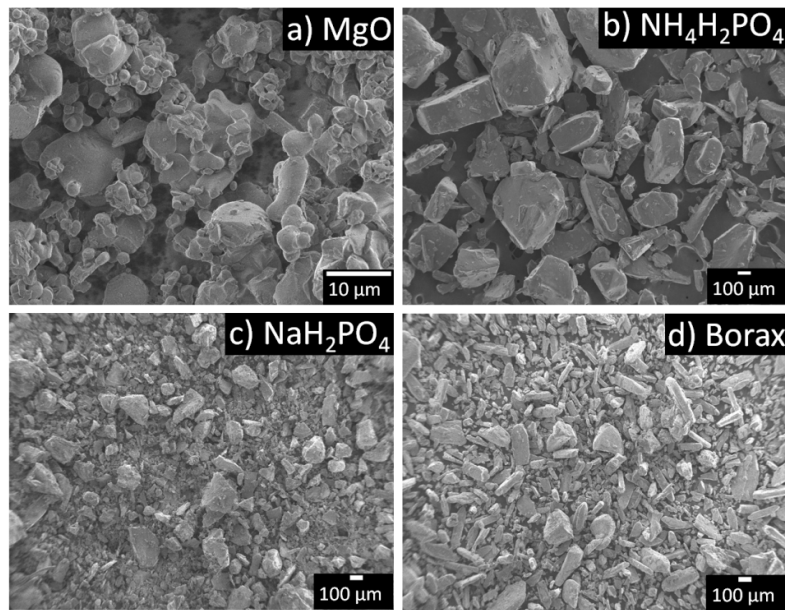The morphology of the initial reactants is shown in Figure 5.13.

Figure 5.13. Morphology of the main reactants, milled at 150 rpm for 15 min: a) MgO, b) $NH_4H_2PO_4$, c) NaH_2PO_4 and d) borax.

Figure 5.14 shows the microstructure corresponding to fractured surfaces of the three MPCs after 1 h and 7 days of reaction. After 1 h of reaction, the NH_4-MPC microstructure consisted of a vitreous-like matrix covering elongated particles (Figure 5.14 a). After 7 days of immersion in Ringer's solution (Figure 5.14 b), the morphology was more homogenous, with a rough appearance. The Na-MPC after 1 h of reaction (Figure 5.14 c) showed a vitreous gel-like morphology, with a few particles being distinguished underneath a smooth glassy phase. Numerous cracks were observed, which could presumably be created during the drying of the hydrated gel-like phase. After 7 days (Figure 5.14 d), some particles embedded in a continuous matrix were clearly distinguished, which could correspond to the unreacted MgO in the sodium magnesium phosphate matrix. The morphology of the NH_4+Na-MPC (Figure 5.14 e and f) was intermediate between the two previous ones, with some features typical of each of them, which is in agreement with its composition, that contains both sodium and ammonium dihydrogen phosphate.
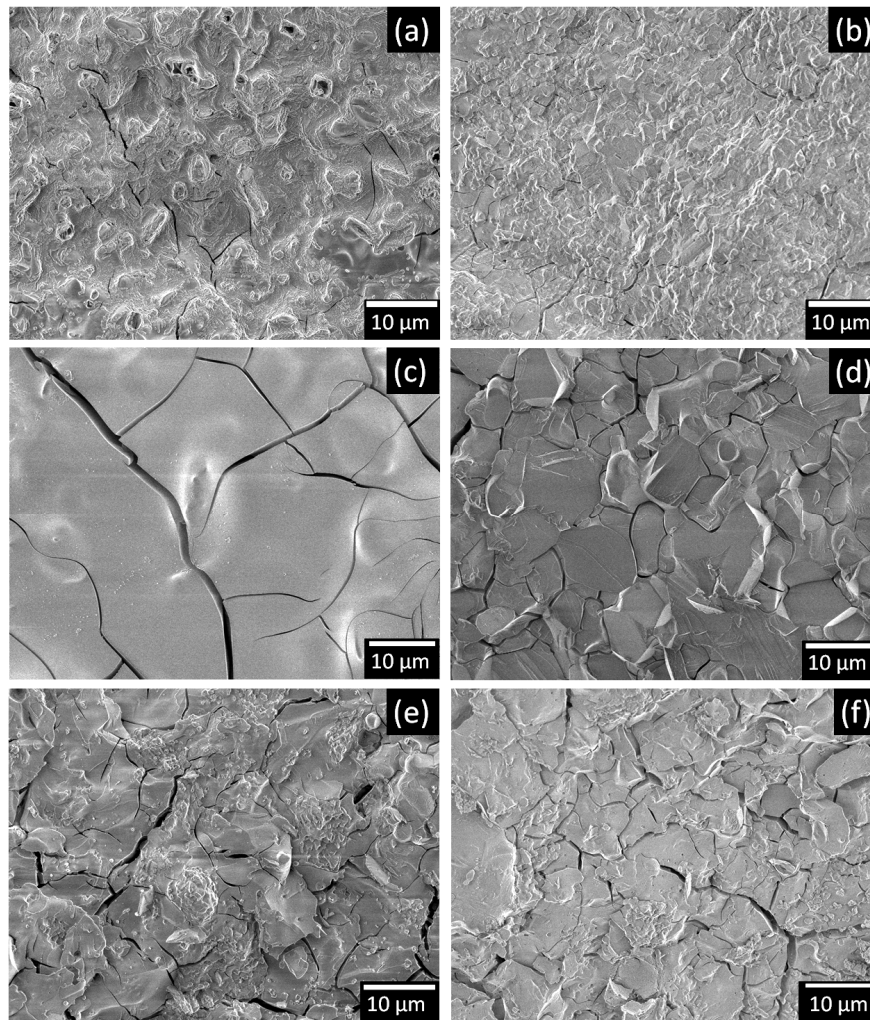
Figure 5.14. Microstructure of the fracture surface of MPC after 1 h: a) NH$_4$-MPC, c) Na-MPC and e) NH$_4$+Na-MPC, and 7 days: b) NH$_4$-MPC, d) Na-MPC and f) NH$_4$+Na-MPC. The cements were immersed in Ringer's solution at 37°C.

5.4.2.6 Specific surface area, skeletal density and porosimetry

Table 5.6 shows the specific surface area (SSA) and the skeletal density for the MPC formulations after immersion in Ringer's solution for 7 days. The lowest value of SSA was obtained for the Na-MPC series, whereas both NH$_4$-MPC and NH$_4$+Na-MPC had similar SSA values. The trend for the SSA was the following: Na-MPC < NH$_4$-MPC < NH$_4$+Na-MPC, and the values of skeletal density were very similar for the three formulations.

Table 5.6. Specific surface area (SSA, m^2/g) and skeletal density (g/cm^3) of the three MPC formulations after 7 days of immersion in Ringer's solution. The average ± standard deviation is shown, n = 2 for SSA and n = 3 for skeletal density.

	SSA (m^2/g)	Skeletal density (g/cm^3)
NH$_4$-MPC	7.63 ± 0.82	2.46 ± 0.06
Na-MPC	3.95 ± 0.31	2.53 ± 0.04
NH$_4$+Na-MPC	7.83 ± 0.93	2.49 ± 0.01

The entrance pore diameter distribution, measured by means of mercury intrusion porosimetry, is shown in Figure 5.15. In general, all the specimens presented a bimodal pore size distribution, with a band around 0.03 µm (30 nm) and another one close to 10 µm. However, the pores around 10 µm or higher did not match with the morphology of the cement (Figure 5.14) and could be attributed to some cracks formed during the drying process.
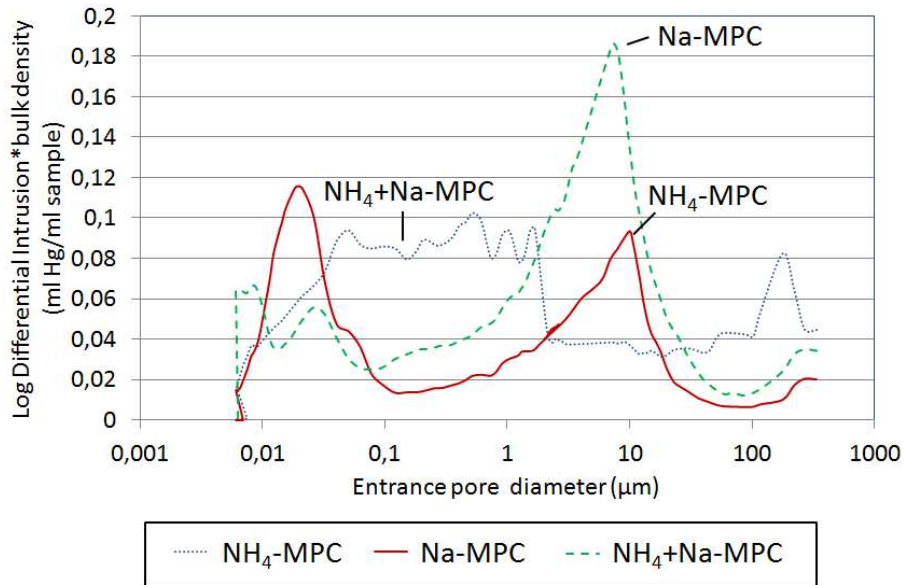

Figure 5.15. Distribution of the entrance pore diameter of MPC formulations after being immersed in Ringer's solution for 7 days.

Table 5.7 shows the results of total open porosity of the three MPC formulations set for 7 days. It should be mentioned that the total open porosity might be overestimated due to the

formation of some cracks during the drying process of the material, as previously explained. The trend of total open porosity was Na-MPC < NH$_4$+Na-MPC < NH$_4$-MPC.

Table 5.7. Total open porosity (%) of the three MPC formulations after being immersed in Ringer's solution for 7 days.

NH$_4$-MPC	Na-MPC	NH$_4$+Na-MPC
28.16	17.13	25.50

5.5 Discussion

The MPC formulations all consist on a mixture of MgO, which is sparsely soluble [9,40], with highly soluble acid phosphates. It is known that in this type of cements, the setting reaction involves three steps: i) first, the acid phosphate dissolves, releasing phosphate anions and forming an acid phosphate solution of low pH; ii) MgO dissolves gradually in the low pH solution and releases cations; iii) the phosphate anions react with the newly released cations in an acid-base reaction, and form a coordinated network that consolidates around the unreacted MgO (which is present in excess), resulting in a hardened ceramic body [9,29,31,41,42]. The mechanism of setting resembles the hydratation of Portland cement but it is faster in the case of MPC [25].

5.5.1 Exothermy

The results obtained in this study show that, as expected, the reaction kinetics and exothermy of the reaction (Figures 5.5 and 5.7) strongly depend on the solubility of the phosphate salt used. Interestingly, Na-MPC exhibited setting kinetics faster than those of NH$_4$-MPC, which was evident from both the temperature evolution and the setting times, which were in fact in close agreement, as shown in Table 5.2. According to these results the speed of reaction was: Na-MPC > NH$_4$+Na-MPC > NH$_4$-MPC. This correlates well with the higher solubility in water of sodium dihydrogen phosphate (94.5 wt%) compared with ammonium dihydrogen phosphate (40.5 wt%) [40]. Moreover, according to Figures 5.5 and 5.7 the maximum temperature reached during the cement reaction was lower when the MPC was prepared with sodium dihydrogen phosphate.

The fineness of the phosphate salt powder and the amount of borax were two processing parameters that were shown to be efficient for controlling the reaction kinetics and the heat

evolved during the setting reaction (Figures 5.5 and 5.7). As shown in Figure 5.7, the addition of borax effectively reduced the maximum temperature reached during the setting reaction, simultaneously increasing the time needed to reach the maximum temperature. In previous studies the mechanism of retardation by borax was associated with the adsorption of $B_4O_7^{2-}$ ions on the surface of MgO particles and to the subsequent formation of amorphous magnesium borate compounds covering the MgO grains, which would hinder their subsequent reaction [9,24,31]. Figure 5.16 schematically shows a possible mechanism of action of borax in an ammonium magnesium phosphate cement. In this respect it is interesting to note that, according to our results, the retarding effect of borax was more significant for NH_4-MPC, followed by NH_4+Na-MPC and, finally, Na-MPC. This can be related to the fact that the dissolution of borax, a sodium tetraborate decahydrate, could be hindered in the formulations containing sodium phosphate, by the presence of sodium ions in solution.
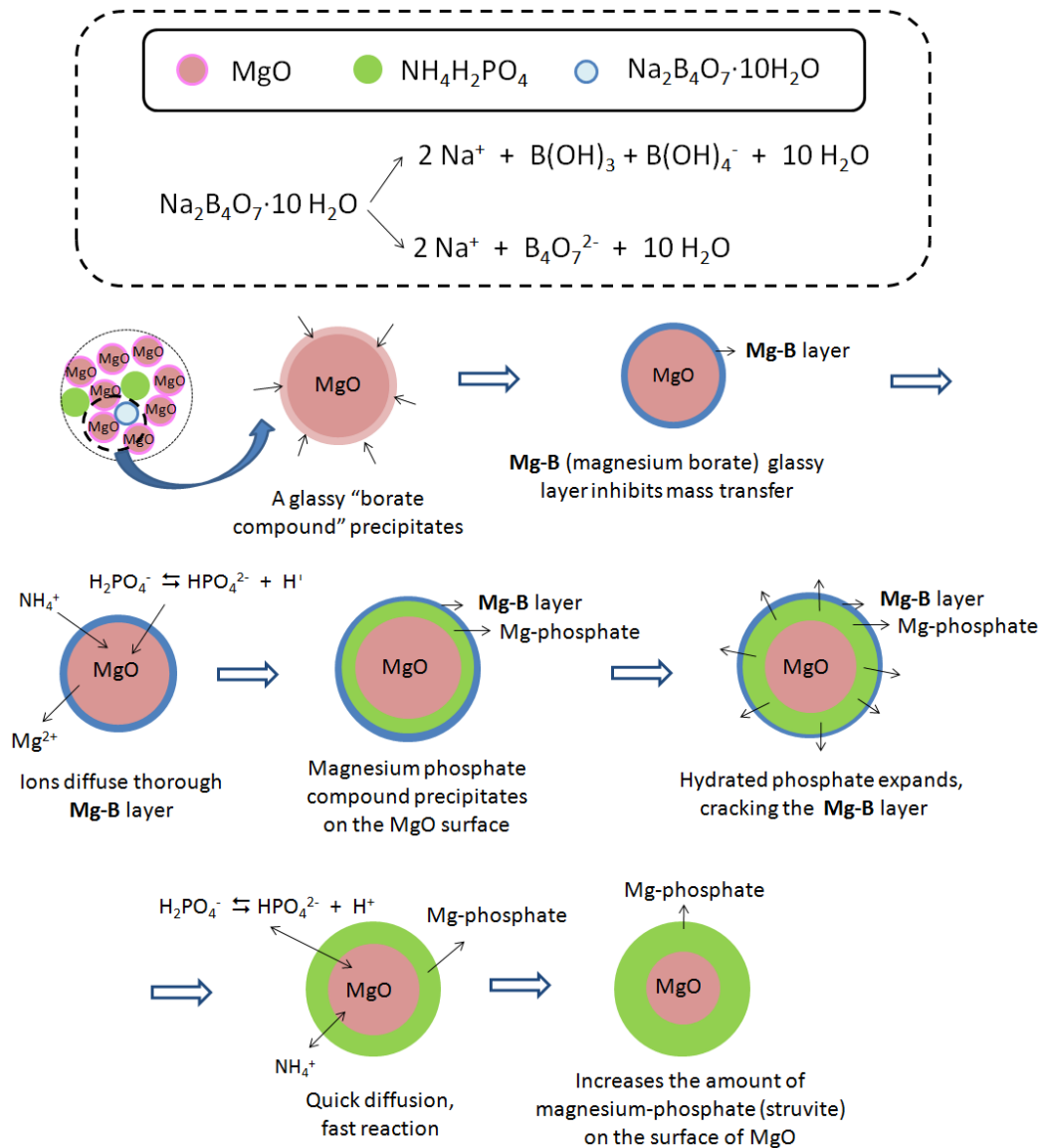
MgO NH$_4$H$_2$PO$_4$ Na$_2$B$_4$O$_7$·10H$_2$O

$$Na_2B_4O_7 \cdot 10\,H_2O \nearrow 2\,Na^+ + B(OH)_3 + B(OH)_4^- + 10\,H_2O$$
$$\searrow 2\,Na^+ + B_4O_7^{2-} + 10\,H_2O$$

MgO MgO MgO
MgO MgO
MgO MgO
MgO MgO

MgO

A glassy "borate compound" precipitates

Mg-B layer

MgO

Mg-B (magnesium borate) glassy layer inhibits mass transfer

$H_2PO_4^- \rightleftharpoons HPO_4^{2-} + H^+$

NH$_4^+$

MgO

Mg^{2+}

Ions diffuse thorough Mg-B layer

Mg-B layer
Mg-phosphate

MgO

Magnesium phosphate compound precipitates on the MgO surface

Mg-B layer
Mg-phosphate

MgO

Hydrated phosphate expands, cracking the Mg-B layer

$H_2PO_4^- \rightleftharpoons HPO_4^{2-} + H^+$ Mg-phosphate

MgO

NH$_4^+$

Quick diffusion, fast reaction

Mg-phosphate

MgO

Increases the amount of magnesium-phosphate (struvite) on the surface of MgO

Figure 5.16. Schematic representation of the effect of borax as retarding agent in the reaction between MgO and phosphate salts in an ammonium magnesium phosphate cement.

In this Chapter three cement formulations were selected with the aim of obtaining a fast setting MPC which could be used in clinical applications, with a moderately exothermic reaction in order to avoid protein denaturation and tissue necrosis [33]. The formulations with coarse phosphate salts and 3 wt% borax were selected as meeting these criteria. It has to be mentioned, however, that there are specific clinical situations where a cement with an exothermic setting reaction could be of interest. This would be the case, for instance, for the treatment of vertebral

bone tumors, where implantation of an exothermic cement would allow the application of local hyperthermia at the tumor site at the same time as biomechanical stabilization was achieved.
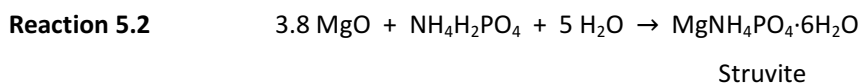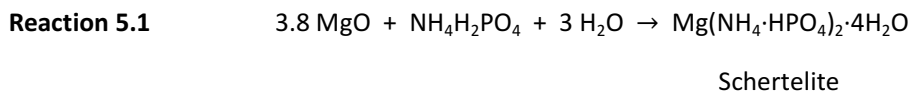
5.5.2 Setting and cohesion times

The consistency of the three selected MPC formulations and also their setting times were acceptable for clinical applications, with setting times between 8 and 15 min (Table 5.2) [43]. The *in situ* setting evolution by FTIR confirmed the fast evolution of the cement paste, the main reactions occurring during the initial 10 or 20 min (Figures 5.8, 5.9 and 5.10).

A characteristic feature of the three MPCs studied was that in all cases the final setting time was very close to the initial setting time (Table 5.2). The setting process was very fast, their transition from a plastic paste to a solid body taking place in about 1 min once the initial setting time had been reached.

5.5.3 Crystalline phases

With respect to the chemical reaction responsible for setting of the different MPCs, the XRD studies revealed that the reaction of MgO with either $NH_4H_2PO_4$ or NaH_2PO_4 resulted in different compounds. Both NH_4-MPC and NH_4+Na-MPC were developed by step-reactions: first it was formed an intermediate phase of low stability until the formation of a more stable phase [9]. After only 1 h, schertelite was formed, which was partially transformed into struvite after 1 day (Figure 5.12 a and c). The initial formation of schertelite, a tetrahydrate magnesium ammonium dihydrogen phosphate with Mg/P molar ratio of 0.5, could be associated to the low availability of magnesium ions at the beginning of the reaction. The appearance of schertelite as an intermediate product of the reaction was also previously reported [7,44–46]. After 7 days, when MgO was further dissolved, the initial compound was almost completely transformed into struvite (Figure 5.12 a), a magnesium ammonium phosphate hexahydrated with a Mg/P molar ratio of 1, which is in agreement with previous studies [5,12,29,42].

Apart from the higher Mg/P ratio required for the formation of struvite than for schertelite, struvite also requires a higher amount of molecules of water than schertelite (Reaction 5.1 and 5.2).

Reaction 5.1 $3.8 \, MgO + NH_4H_2PO_4 + 3 \, H_2O \rightarrow Mg(NH_4 \cdot HPO_4)_2 \cdot 4H_2O$

Schertelite

Reaction 5.2 $3.8 \, MgO + NH_4H_2PO_4 + 5 \, H_2O \rightarrow MgNH_4PO_4 \cdot 6H_2O$

Struvite

The liquid to powder ratio used for the preparation of NH_4-MPC (L/P = 0.13 ml/g) did not provide enough amount of water for the formation of struvite or schertelite (0.010 mols of H_2O were added for 0.006 mols of $NH_4H_2PO_4$, being required 0.018 mols of H_2O to form schertelite and 0.030 mols of H_2O to form struvite). In the case that no extra water would be available, dittmarite, a magnesium ammonium phosphate monohydrated ($MgNH_4PO_4 \cdot H_2O$), would be formed. However, if the cements absorb water from the environment, they gradually transform in a compound thermodynamically more stable, at the end being formed struvite. This indicates that factors such as the availability of Mg ions and of water governs the composition of the final product of MPCs [25,47]. Figure 5.17 schematically shows the step-reactions developed for NH_4-MPC.
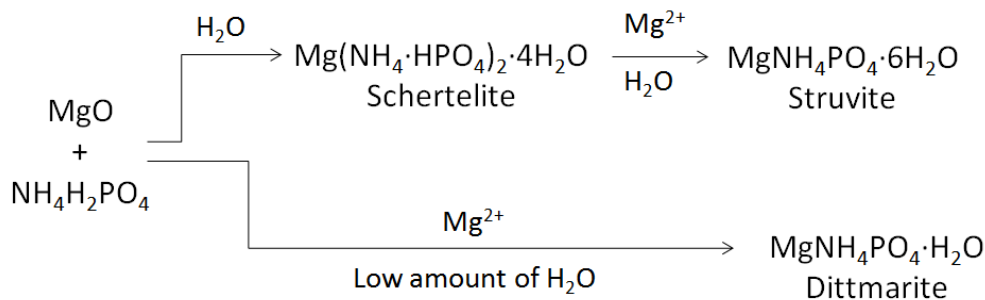

Figure 5.17. Step-reactions occurring between MgO and $NH_4H_2PO_4$ in a humid or dry environment.

Regarding the Na-MPC, XRD was not a useful technique to determine the phase composition of the end-product due to its amorphous nature. The presence of a broad hump around $2\theta \sim 31°$ (Figure 5.12 b) was compatible with the formation of an amorphous magnesium sodium phosphate. The fact that several magnesium sodium phosphate salts have their main diffraction peaks in the range of $31–33°$ makes difficult to hypothesize if a specific poorly crystalline sodium magnesium salt was formed. It could be speculated that both the fast dissolution of NaH_2PO_4 in water and the poor solubility of borax in the matrix (which was hindered

by the presence of Na ions) enhanced the fast setting reaction of the cement, leading to the formation of a precipitate with amorphous nature instead of the ceramic with organized structure formed in NH_4-MPC [9]. However, since the NH_4-MPC also reacted very fast, the most plausible hypothesis was that the magnesium sodium phosphate inherently formed a low organized crystalline or quasi-amorphous structure.

NH_4+Na-MPC, which was constituted by an equimolar amount of $NH_4H_2PO_4$ and NaH_2PO_4, might also form the amorphous sodium magnesium phosphate phase, although the hump around $2\theta \sim 31°$ was probably masked by the crystalline peaks of struvite.

In all cases, unreacted MgO was detected in the hardened paste (Figure 5.12), which was expected for two reasons. On one hand, because there was a 3.8 M excess of this compound over the phosphate salts; on the other hand, due to the low solubility of MgO in water [40]. As anticipated, the dissolution of the acid phosphates was much faster. In fact they were not detected in the sodium containing MPCs even after 1 h, whereas in the NH_4-MPC only a small amount of ammonium dihydrogen phosphate remained after 1 day (Figure 5.12). This can be correlated to the higher solubility of the sodium dihydrogen phosphate (94.5 wt%) as compared to the ammonium dihydrogen phosphate (40.5 wt%) [40].

5.5.4 *In situ* setting evolution by FTIR

The bands observed by FTIR for NH_4-MPC and NH_4+Na-MPC after 60 min of reaction (Figure 8 b and 10 b) were associated to vibration of groups such as PO_4^{3-}, NH_4^+ and MgO, and were in accordance with the formation of struvite ($MgNH_4PO_4 \cdot 6H_2O$) [35,47] and the presence of MgO in excess. Moreover, the presence of a band close to 870 cm^{-1}, associated to HPO_4^{2-} groups, could indicate the formation of schertelite ($Mg(NH_4 \cdot HPO_4)_2 \cdot 4H_2O$). Therefore, FTIR results showed a good accordance with the phases determined by means of XRD.

Fewer bands were observed in Na-MPC after 60 min of reaction (Figure 9 b). The detected bands indicated that the end-product contained covalent bonds such as MgO, PO_4^{3-} and HPO_4^{2-}, which also matched with the formation of an amorphous sodium magnesium phosphate compound.

5.5.5 Mechanical properties

It is worth noting that the early compressive strength of all MPC formulations was much higher than that of CPCs (Figure 5.11), which are the hydraulic cements most used as synthetic bone grafts in bone regeneration applications. In these cements, brushite or hydroxyapatite is formed through dissolution and reprecipitation of one or more calcium phosphates when in contact with water. The apatitic cements, which are more resistant than brushite ones, reach compressive strengths of typically 35–40 MPa after several days reaction [39], as reported in Figure 5.11. The three MPC formulations showed compressive strengths around 30 times higher than a CPC after 1 h, and 6–10 times higher after 2 h. At longer reaction times, although the differences were smaller, the MPCs continued to show higher compressive strengths, except for NH_4+Na-MPC at 7 days, which showed a strong drop in strength. Similar maximum strengths were reached irrespective of the crystalline or amorphous nature of the final products. Interestingly, the hardening mechanism also appeared to be different from that reported in apatitic CPCs, where complexation between plate- or needle-like apatite crystals is responsible for progressive stiffening of the paste [39]. In MPCs no needle- or plate-like crystals were found, but a continuous matrix with polyhedral phases was observed. The early strength acquisition by the MPC formulations is an advantage for several clinical applications, where the cement can be subjected to moderate loading situations, allowing for mobility of the patient early after cement implantation.

The hardening kinetics of MPC formulations followed the trend Na-MPC < NH_4+Na-MPC < NH_4-MPC (Figure 5.11). Surprisingly, this trend was opposed to the kinetics determined by the setting time and the exothermy. In other words, although the Na-MPC was the formulation that set faster, it was also the one needing longer immersion time in order to reach its maximum compressive strength. And vice versa for the NH_4-MPC. Regarding the chemical composition, the Na ions contained in the Na-MPC may hinder the dissolution of the retardant. This would permit a faster reaction between the MgO and the phosphate salt, thus accelerating the setting of the cement. However, the Na-MPC would require longer times to reach its maximum strength, since the whole process of hardening would be delayed.

The longer time required by Na-MPC to reach its maximum compressive strength (Figure 5.11) was in accordance with the slow formation of end-products, which provided the strength to

the material, since a hump around $2\theta \sim 31°$ was not clearly observed by XRD until 1 day (Figure 5.12). In contrast, the faster formation of struvite and schertelite in NH_4-MPC and NH_4+Na-MPC, enhanced the attainment of high early compressive strength for these formulations.

5.5.6 Morphology, SSA, skeletal density and porosity

The microsctructure of NH_4-MPC suggested the coexistence of an amorphous matrix among the elongated particles after 1 h of reaction (Figure 5.14 a), although no background directly attributable to an amorphous phase was observed in the XRD patterns. This glassy-like structure was assigned to the formation of an amorphous borate compound coating, as previously reported [9,24,31].

The skeletal density of NH_4-MPC (Table 5.6) was higher than the expected value for struvite, which skeletal density is 1.71 g/cm^3 [40]. This could be associated to a high amount of unreacted MgO (skeletal density of 3.6 g/cm^3 [40]), since 50.8 wt% MgO was added and only 25.9 wt% MgO would react (1 mol MgO should stoichiometrically react with 1 mol of $NH_4H_2PO_4$). For the NH_4-MPC, a skeletal density of 2.46 g/cm^3 indicated that 39.7 wt% MgO remained unreacted and 60.3 wt% struvite was formed.

The formation of an amorphous hydrated gel in the Na-MPC observed by XRD (Figure 5.12 b), was consistent with the SEM images obtained after 1 h of reaction (Figure 5.14 c), where a glassy morphology was observed. In fact, the amorphous phase observed could be a mixture of both the sodium magnesium phosphate formed and the borate compound. Finally, the cracks on the surface (Figure 5.14 c) were compatible with the cracking produced during the drying process of a highly hydrated gel.

The Na-MPC, which was the only formulation that gave place to an amorphous compound, had a lower SSA than the other two formulations (Table 5.6). The lower SSA of Na-MPC was related with its flat surface (Fig. 5.14 c and d), and matched with the higher skeletal density (Table 5.6) and the lower porosity of the composition (Table 5.7).

5.6 Conclusions

The conclusions of this Chapter can be summarized as follows:

1. A novel family of magnesium phosphate cements (MPC), including formulations with different compositions, was developed. The MPC reactants consisted of sintered MgO and a phosphate salt, either $NH_4H_2PO_4$, NaH_2PO_4 or a mixture of both. The three different formulations were prepared, namely NH_4-MPC, Na-MPC and NH_4+Na-MPC.

2. The exothermy of the reaction was adjusted lower than 45°C by sintering the MgO at 1475°C for 6 h, by using phosphate salts with a coarse particle size and by adding sodium tetraborate decahydrate (borax) as retardant.

3. The setting times were adequate for clinical applications, with very similar initial and final setting times due to the fast cement setting.

4. The main product of the ammonium-containing cements was struvite ($MgNH_4PO_4 \cdot 6H_2O$), and schertelite ($Mg(NH_4 \cdot HPO_4)_2 \cdot 4H_2O$) was an intermediate product of the reaction. The Na-MPC formed an amorphous sodium magnesium phosphate phase. Unreacted MgO was found in all formulations due to the addition in excess of this reactant.

5. The novel MPCs exhibited high early compressive strength ($30 - 50$ MPa after $1 - 2$ h), which was significantly superior to a CPC ($1 - 5$ MPa after the same time). After 1 day, the three MPC formulations had a compressive strength about 50 MPa.

6. The morphology of NH_4-MPC and NH_4+Na-MPC showed elongated particles covered by a glassy layer, which was associated to the precipitation of a borate compound on the surface of MgO particles, thus retarding the reaction between the MgO and the phosphate salts. The amorphous product of Na-MPC resulted in a glassy-like microstructure.

7. The skeletal density of NH_4-MPC set for 7 days in Ringer's solution was higher to that of struvite due to the presence of unreacted MgO. Na-MPC had a higher skeletal density, lower specific surface area and lower total porosity than the other formulations.

5.7 Acknowledgements

5.8 References

[1] Prosen EM. Refractory materials for use in making dental casting. US Patent No. 2,152,152; 1939.

[2] Prosen EM. Refractory material suitable for use in casting dental investments. US Patent No. 2,209,404; 1941.

[3] Sugama T, Kukacka LE. Characteristics of magnesium polyphosphate cements derived from ammonium polyphosphate solutions. Cement and Concrete Research 1983; 13: 407–416.

[4] El-Jazairi B. Rapid repair of concrete pavings. Concrete 1982; 16: 12–15.

[5] Abdelrazig B, Sharp J, Siddy P, El-Jazairi B. Chemical reactions in magnesia-phosphate cement. Proceedings of the British Ceramic Society 1984; 35: 141–154.

[6] Popovics S, Rajendran N, Penko M. Rapid hardening cements for repair of concrete. ACI Materials Journal 1987; 84: 64–73.

[7] Abdelrazig B, Sharp J, El-Jazairi B. The chemical composition of mortars made from magnesia-phosphate cement. Cement and Concrete Research 1988; 18: 415–425.

[8] Wilson AD, Nicholson JW. Acid–base cements: their biomedical and industrial applications. Cambridge: University Press, 1993.

[9] Wagh AS. Chemically bonded phosphate ceramics: 21st century materials with diverse applications. Hurst E, editor. Oxford: Elsevier, 2004.

[10] Michałowski T, Pietrzyk A. A thermodynamic study of struvite+water system. Talanta 2006; 68: 594–601.

[11] Bhuiyan MIH, Mavinic DS, Koch FA. Thermal decomposition of struvite and its phase transition. Chemosphere 2008; 70: 1347–1356.

[12] Liu C. Inorganic bone adhesion agent and its use in human hard tissue repair. US Patent No. 7,094,286 B2; 2006.

[13] Wu F, Wei J, Guo H, Chen F, Hong H, Liu C. Self-setting bioactive calcium-magnesium phosphate cement with high strength and degradability for bone regeneration. Acta Biomaterialia 2008; 4: 1873–1884.

[14] Wu F, Su J, Wei J, Guo H, Liu C. Injectable bioactive calcium-magnesium phosphate cement for bone regeneration. Biomedical Materials 2008; 3: 1–7.

[15] Wei J, Jia J, Wu F, Wei S, Zhou H, Zhang H, Shin JW, Liu C. Hierarchically microporous/macroporous scaffold of magnesium-calcium phosphate for bone tissue regeneration. Biomaterials 2010; 31: 1260–1269.

[16] Yu Y, Wang J, Liu C, Zhang B, Chen H, Guo H, Zhong G, Qu W, Jiang S, Huang H. Evaluation of inherent toxicology and biocompatibility of magnesium phosphate bone cement. Colloids and Surfaces B: Biointerfaces 2010; 76: 496–504.

[17] Witte F, Kaese V, Haferkamp H, Switzer E, Wirth CJ, Windhagen H. *In vivo* corrosion of four magnesium alloys and the associated bone response. Biomaterials 2005; 26: 3557–3563.

[18] Percival M. Bone health and osteoporosis. Applied Nutrition Science 1999; 5: 1–5.

[19] Boanini E, Gazzano M, Bigi A. Ionic substitutions in calcium phosphates synthesized at low temperature. Acta Biomaterialia 2010; 6: 1882–1894.

[20] Stendig-Lindberg G, Tepper R, Leichter I. Trabecular bone density in a two year controlled trial of peroral magnesium in osteoporosis. Magnesium Research 1993; 6: 155–163.

[21] Toba Y, Kajita Y, Masuyama R, Takada Y, Suzuki K, Aoe S. Dietary magnesium supplementation affects bone metabolism and dynamic strength of bone in ovariectomized rats. Journal of Nutrition 2000; 130: 216–220.

[22] Eubank WR. Calcination studies of magnesium oxides. Journal of the American Ceramic Society 1951; 34: 225–229.

[23] Soudée E, Péra J. Influence of magnesia surface on the setting time of magnesia–phosphate cement. Cement and Concrete Research 2002; 32: 153–157.

[24] Sugama T, Kukacka LE. Characteristics of magnesium polyphosphate cements derived from ammonium polyphosphate solutions. Cement and Concrete Research 1983; 13: 407–416.

[25] Sarkar AK. Phosphate Cement-Based Fast-Setting Binders. Ceramic Bulletin 1990; 69: 234–238.

[26] Seehra S, Gupta S, Kumar S. Rapid setting magnesium phosphate cement for quick repair of concrete pavements – characterisation and durability aspects. Cement and Concrete Research 1993; 23: 254–266.

[27] Yang Q. Factors influencing properties of phosphate cement-based binder for rapid repair of concrete. Cement and Concrete Research 1999; 29: 389–396.

[28] Wagh AS, Jeong SY. Chemically bonded phosphate ceramics, I: a dissolution model of formation. Journal of the American Ceramic Society 2003; 86: 1838–1844.

[29] Soudée E, Péra J. Mechanism of setting reaction in magnesia-phosphate cements. Cement and Concrete Research 2000; 30: 315–321.

[30] Dunne NJ, Orr J. Thermal characteristics of curing acrylic bone cement. ITBM-RBM 2001; 22: 88–97.

[31] Yang Q, Zhu B, Wu X. Characteristics and durability test of magnesium phosphate cement-based material for rapid repair of concrete. Materials and Structures 2000; 33: 229–234.

[32] Joint Committee for Powder Diffraction Studies (JCPDS). International Center for Diffraction Data and American Society for Testing Materials. Powder diffraction file (Inorganic and Organic). Swarthmore (USA), 1991.

[33] Samali A, Holmberg CI, Sistonen L, Orrenius S. Thermotolerance and cell death are distinct cellular responses to stress: dependence on heat shock proteins. FEBS letters 1999; 461: 306–310.

[34] Ginebra MP, Fernández E, Driessens FCM, Boltong MG, Muntasell J, Font J, Planell JA. The effects of temperature on the behaviour of an apatitic calcium phosphate cement. Journal of Materials Science: Materials in Medicine 1995; 6: 857–860.

[35] Chauhan CK, Joseph KC, Parekh BB, Joshi MJ. Growth and characterization of struvite crystals. Indian Journal of Pure & Applied Physics 2008; 46: 507–512.

[36] Cahil A, Najdoski M, Stefov V. Infrared and Raman spectra of magnesium ammonium phosphate hexahydrate (struvite) and its isomorphous analogues, IV: FTIR spectra of protiated and partially deuterated nickel ammonium phosphate hexahydrate and nickel potassium phosphate hexahydrate. Journal of Molecular Structure 2007; 834–836: 408–413.

[37] Jia J, Zhou H, Wei J, Jiang X, Hua H, Chen F, Wei S, Shin J, Liu C. Development of magnesium calcium phosphate biocement for bone regeneration. Journal of the Royal Society, Interface 2010; 7: 1171–1180.

[38] Radin S, Ducheyne P. The effect of calcium phosphate ceramic composition and structure on *in vitro* behavior, II: precipitation. Journal of Biomedical Materials Research 1993; 27: 25–34.

[39] Ginebra MP, Fernández E, De Maeyer EAP, Verbeeck RMH, Boltong MG, Ginebra J, Driessens FCM, Planell JA. Setting reaction and hardening of an apatitic calcium phosphate cement. Journal of Dental Research 1997; 76: 905–912.

[40] Lide D. CRC Handbook of Chemistry and Physics (internet version). Boca Raton: CRC, 2010.

[41] Neiman R, Sarma AC. Setting and thermal reactions of phosphate investments. Journal of Dental Research 1980; 59: 1478–1485.

[42] Hall DA, Stevens R, El-Jazairi B. Effect of water content on the structure and mechanical properties of magnesia – phosphate cement mortar 1998; 56: 1550–1556.

[43] Driessens FCM, Planell JA, Boltong MG, Khairoun I, Ginebra MP. Osteotransductive bone cements. Proceedings of the Institution of Mechanical Engineers, H: Journal of Engineering in Medicine 1998; 212: 427–435.

[44] Miyaji T, Utsumi K, Suzuki E, Shimizu Y. Deterioration of phosphate-bonded investment on exposure to 100% relative humidity atmosphere. The Bulletin of Tokyo Medical and Dental University 1982; 29: 53–62.

[45] Abdelrazig B, Sharp J. Phase changes on heating ammonium magnesium phosphate hydrates. Thermochimica Acta 1988; 129: 197–215.

[46] Abdelrazig B, Sharp J, El-Jazairi B. The microstructure and mechanical properties of mortars made from magnesia-phosphate cement. Cement and Concrete Research 1989; 19: 247–258.

[47] Sarkar AK. Hydration/dehydration characteristics of struvite and dittmarite pertaining to magnesium ammonium phosphate cement systems. Journal of Materials Science 1991; 26: 2514–2518.

Chapter 6.

Magnesium phosphate cements for clinical applications: optimization of the formulations and biological properties

Table of contents

6.1 Introduction

The use of materials in clinical applications is conditioned by their biocompatibility. In the case of acid-base cements such as magnesium phosphate cements (MPCs), a first step to guarantee an adequate biocompatibility is to control the exothermy of the cements in order that the surrounding tissues can tolerate the released heat. The knowledge gained in Chapter 5, regarding the role of the processing parameters in the exothermy of MPCs, is applied in this Chapter to further reduce the exothermy of MPCs when assessing this property in conditions closer to a real situation.

A second step to evaluate the biocompatibility of a material is to determine the viability of cells when they are in contact with it. Furthermore, microbiological studies can also inform about the interaction of the material with prokaryotic cells that can lead to an infection. The overall results should permit to speculate a potential application for the material.

6.2 Objectives

The objectives of this Chapter are the following:

1. To optimize the MPC formulations in order to ensure that mild or no damage of the surrounding tissues would occur when implanting the material.

2. To evaluate the antimicrobial properties of the formulations of MPC and to determine the influence of the cement aging.

3. To evaluate the cell cytotoxicity of the MPC formulations using preosteoblast-like cells, and to determine if the cytotoxicity depends on the cement aging.

Figure 6.1 schematically shows the studies performed in this Chapter.
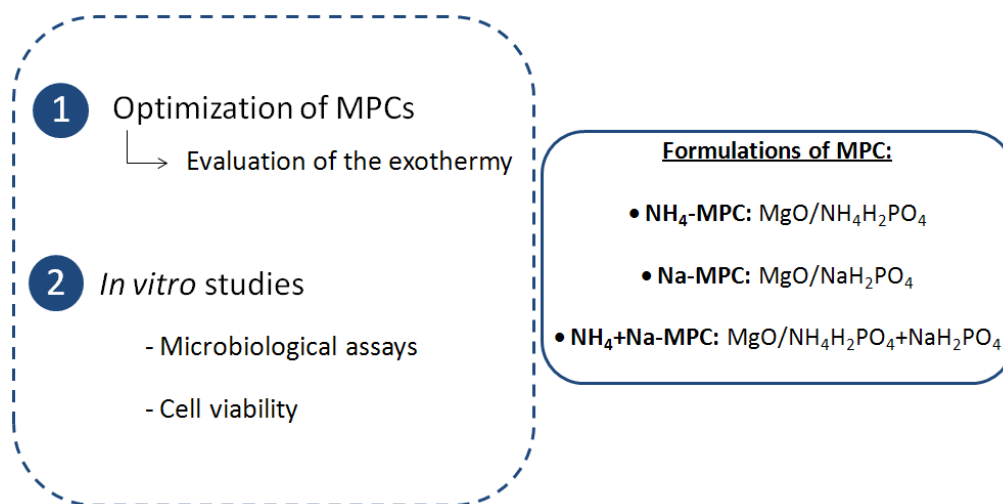
Figure 6.1. Schema of the studies explained in Chapter 6.

6.3 Materials and methods

6.3.1 Powder phase

The reactants constituting the powder phase were the same that have been reported in Chapter 5 (Section 5.3.1). However, they were differently processed in order to ensure that the exothermy would not injure the surrounding tissues.

Briefly, the powder phase of the cement consisted of a mixture of heavy magnesium oxide (MgO, Merck, ref n. 105867) and a phosphate salt that was either ammonium dihydrogen phosphate ($NH_4H_2PO_4$, Panreac ref n. 131126.1210), sodium dihydrogen phosphate (NaH_2PO_4, Fluka ref n. 71496), or an equimolar mixture of both. Sodium borate decahydrated ($Na_2B_4O_7 \cdot 10H_2O$, Fluka, ref n. 72000), known also as borax, was added to the powder phase as a retardant of the reaction [1–5].

The MgO was sintered at 1475°C for 6 or 12 h, in order to reduce its reactivity [6,7]. Afterwards, 50 g of the calcined MgO was milled in a planetary ball mill (Fritsch, Pulverisette 6), using an agate jar and 4 agate balls (ϕ = 30 mm) at 150 rpm during 15 min. The ammonium and sodium phosphate salts were milled at 150 rpm during 15 min, producing coarse powders, which resulted in a moderate exothermy when used as reactants of the cement, as shown in Chapter 5

(Section 5.4.1). Fifty g of borax were milled following two different protocols, in order to produce fine (350 rpm during 30 min) and coarse (150 rpm during 15 min) powders.

The particle size distribution was characterized by laser diffraction (Beckman Coulter LS 13 320), after sonicating the powder in ethanol in order to avoid particle agglomeration. Table 6.1 shows the particle size of the reactants after applying the mentioned processing parameters.

Table 6.1. Milling protocols and particle size distribution of the magnesium oxide, the two phosphate salts and the retardant, used as reactants for the MPCs. D_i (D_{10}, D_{50} and D_{90}) stands for the average particle size where i% of the sample volume is smaller than Di.

	Powder size	Milling protocol	D_{10} (µm)	D_{50} (µm)	D_{90} (µm)
Magnesium source					
MgO (1475°C 6 h)	Coarse	150 rpm-15 min	0.55 ± 0.44	4.75 ± 0.68	27.49 ± 6.65
MgO (1475°C 12 h)			0.34 ± 0.02	5.20 ± 0.31	27.2 ± 1.27
Phosphate source					
$NH_4H_2PO_4$	Coarse	150 rpm-15 min	16.99 ± 5.58	274.97 ± 13.70	550.4 ± 23.3
NaH_2PO_4			11.89 ± 7.24	185.51 ± 97.99	446.7 ± 111.98
Retardant					
Borax	Coarse	150 rpm-15 min	13.48 ± 4.77	66.77 ± 15.82	214.47 ± 55.76
	Fine	350 rpm - 30 min	2.36 ± 0.14	16.17 ± 1.00	35.98 ± 2.10

6.3.2 Cement preparation

The same formulations described in Chapter 5 (Section 5.3.2) were used. Briefly, each MPC formulation was constituted by MgO and a phosphate salt, $NH_4H_2PO_4$, NaH_2PO_4 or a mixture of both. The MgO/phosphate salt ratio was 3.8. Therefore, each formulation was named as NH_4-MPC, Na-MPC and NH_4+Na-MPC, respectively, accounting for the type of phosphate salt used. The cement was prepared with a liquid to powder ratio of 0.13 ml/g.

6.3.3 Assessment of the exothermy

The exothermy of the MPCs was controlled in order to avoid high levels of heat, which could cause irreversible damages to the surrounding tissues [8]. The exothermy of the cements was adjusted gradually. Firstly, the effect of the fineness of borax and, afterwards, of the calcination time of MgO was assessed, selecting at each step the process that reduced more the exothermy. Finally, the amount of borax needed was determined, as indicated in Figure 6.2.
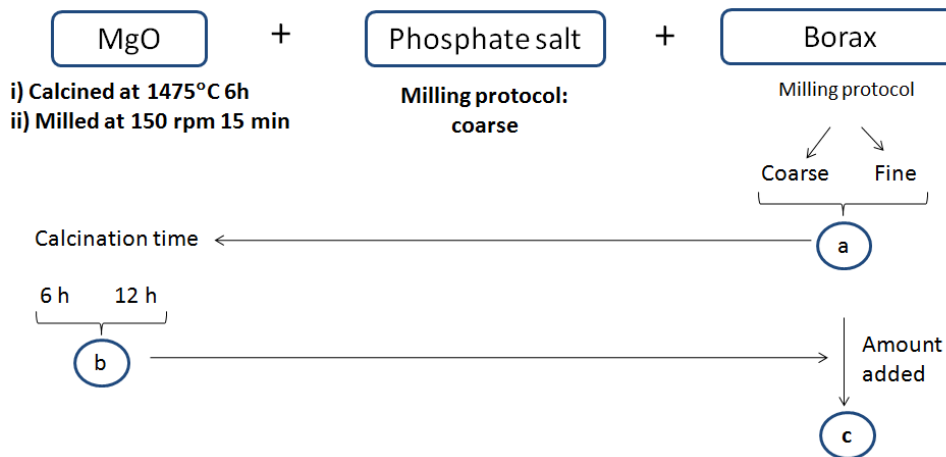
Figure 6.2. Processing of the reactants to reduce the exothermy of the cement down to safety levels.

The temperature evolution of the cements during the setting reaction was followed by introducing a type K thermocouple (Thermometer RS 1313) in 1.5 g of cement paste placed in a plastic container, immersed into an isostatic bath at 37°C. The thermocouple passed through a small hole made on the container's seal, which was placed to avoid heat dissipation. When monitoring the temperature evolution, the moment at which the liquid phase was added to the powder was considered as time zero.

Dunne *et al.* determined the maximum exothermy that the tissues surrounding a material can bear without suffering any harmful effect [8]. In the mentioned study, the exothermy during the curing process of the acrylic cements was evaluated, and the authors proposed to quantify the exothermy using a thermal coefficient that took into account the period of time at which each temperature remained constant. Therefore, the thermal coefficient evaluated the thermal history of the potential biomaterial and allowed predicting if the surrounding tissues would be severely

damaged or if, otherwise, the suffered injury would be mild or inexistent. The experimental curve of Figure 6.3 shows the period of time in which a temperature ranging from 40 to 75°C could be tolerated by the body (bottom left of Figure 6.3). On the contrary, when a temperature higher than 40°C was maintained for a longer period of time or when the reached temperature was higher than 70°C, the tissue might suffer an irreversible damage (top right of Figure 6.3). A temperature between 37 and 44°C caused a minimal damage to the tissue and thus the thermal coefficient was calculated considering that this range of temperature would cause an irreversible damage only if the exposition time was longer than 10.000 s.
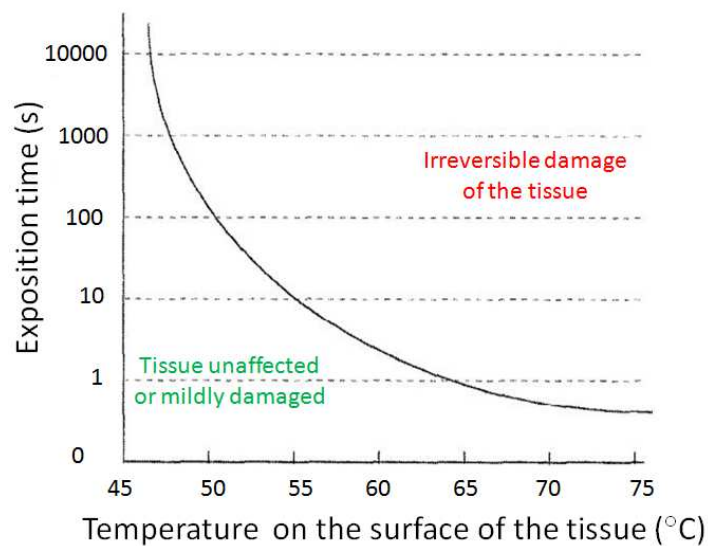
Figure 6.3. Experimental curve that indicates the periods of time during which a determined temperature would only cause a mild damage to the surrounding tissue (bottom left) or an irreversible one (top right) (modified from [8], which extracted the data from [9]).

The thermal coefficient was calculated by integrating a function f(T) between the initial temperature and the final temperature of the exothermy curve (Equation 6.1), in which f(T) function (Equation 6.2) was the fraction between the period of time in which a cement stayed at a determined temperature range divided by the maximum time that tissues could bear this temperature without suffering any irreversible damage (see Appendix A.2 for further details).

Equation 6.1 $\qquad$ Thermal coefficient $= \int_{T_i}^{T_f} f(T) dT$

Equation 6.2

$$f\,(T) = \frac{\text{time spent at temperature T}}{\text{maximum time at which no tissue damage occurs at temperature T}}$$

Dunne *et al.* considered that when the f(T) value was higher than 1, the exothermy could produce an irreversible damage to the surrounding tissues, whether a f(T) value lower than 1 would only produce mild or no damages [8], as summarized in Table 6.2.

Table 6.2. Expected effect that the exothermy will have to the tissues in function of the f(T) value.

f(T)	Effect of the exothermy to the tissue
> 1	May produce irreversible damages
< 1	Only produces mild or no damages

6.3.4 Assessment of the physico-chemical properties of the optimized MPCs

6.3.4.1 Characterization of the cement paste

The paste was evaluated in terms of setting and cohesion times using the Gillmore needles or by visual inspection, respectively, as explained in Chapter 3 (Section 3.3.2.1). In this Chapter, the setting times and cohesion times were evaluated while maintaining the cements at 37°C.

The injectability of a cement paste is defined as the percentage of cement that can be extruded through a syringe when a similar force to the one that could be done by hand is applied. In general, it is considered that a human hand can apply a force between 100 and 200 N [10]. The most restrictive force (100 N) was selected and thus the assay ended when the force applied to the cell load reached 100 N [11–13]. Figure 6.4 shows a schematic representation of the used experimental setup.

Prior to injection   During injection
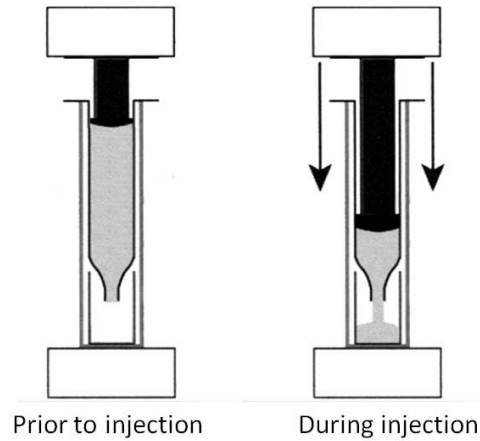
Figure 6.4. Schematic representation of the experimental setup used to quantify the injectability, before and during the injection process (modified from [14]).

The cement paste (prepared with 2.2 g of powder to have a volume around 2 ml) was transferred into a 5 ml syringe (BD Discardit™ II) with 2 mm-aperture. The paste was extruded using a mechanical testing machine (Bionix® MTS 370) with a load cell of 1 kN. Two min 30 s after the liquid contacted the cement powder, the syringe piston started being displaced at a cross-head speed of 15 mm/min (Figure 6.5).
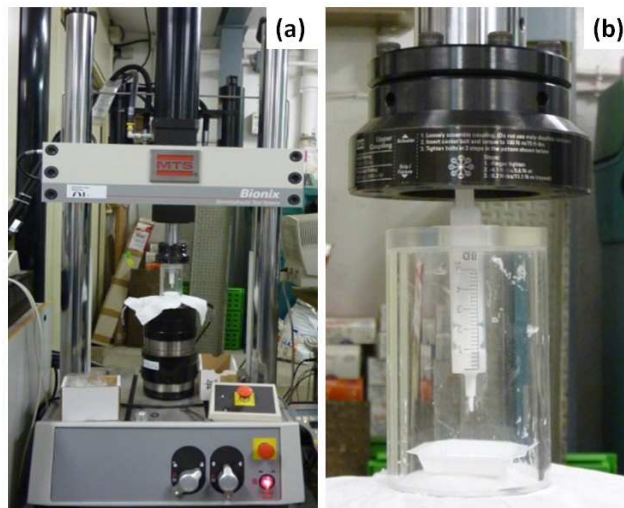
Figure 6.5. a) Universal testing machine performing an injectability test by displacing the syringe piston, and b) extrusion of the cement paste during the injectatility test.

The injectability of the paste was calculated by weighting the syringe before the assay, empty ($w_{syringe}$) and containing the cement paste ($w_{initial}$), and by weighting it again with the

remaining paste after the assay (w_{after}). The % of injectability was calculated as indicated in the Equation 6.3. Three replicates of each formulation were tested.

Equation 6.3.

$$\text{Injectability (\%)} = \left(1 - \left(\frac{w_{after} - w_{syringe}}{w_{initial} - w_{syringe}}\right)\right) * 100$$

A load/displacement curve was obtained for each paste. These curves inform about the load profile along paste injection and thus give information about the injectability of the paste.

6.3.4.2 Characterization of the set cements

The cement was introduced in Teflon molds ($\varnothing$ = 6 mm, h = 12 mm) and were set in Ringer's solution for different time points (1 h, 2 h, 1 day and 7 days). The compressive strength was measured with the set specimens following the protocol detailed in Section 5.3.4.3.

Afterwards, the set cements were characterized after stopping the setting reaction by introducing the cements in acetone for 1 h and drying them at 37°C for 24 h. The experimental procedures described in Chapter 5 were followed to evaluate the crystalline phases (Section 5.3.4.4), the morphology of the fracture surfaces (Section 5.3.4.5), the specific surface area (SSA, Section 5.3.4.6), the skeletal density (Section 5.3.4.7) and the porosimetry (Section 5.3.4.8).

The morphology of the fracture surfaces was evaluated with the optimized formulations and also with cements free of borax in order to determine the influence of the retardant in the microstructure of the cements.

6.3.5 Antimicrobial assays and anti-biofilm activity

Doses of 1.5 g of the cement powders were prepared in plastic containers, were individually sealed in plastic bags and were sterilized by gamma rays (25 kGy) (Aragogamma, Barcelona, Spain). The cements were prepared in a sterile environment right before their use.

6.3.5.1 Bacterial culture conditions

The antimicrobial properties of the MPCs were tested against *Escherichia coli*, strain DH5α (Invitrogen, Carlsbad, CA), *Pseudomonas aeruginosa,* strain PAO1, and *Aggregatibacter*

actinomycetemcomitans, strain JP2. The latter two strains were kind gifts from Dr. Donald Demuth, University of Louisville (Kentucky, USA). The bacterial strains were selected for their presence in caries or endodontic infections (*E. coli* and *P. aeruginosa*) [15–17] or in periodontitis infections (*A. actinomycetemcomitans*) [18].

E. coli and *P. aeruginosa* were grown in Luria Bertani broth (LB, Difco, ref. n. 244620) and *A. actinomycetemcomitans* in Brain Heart Infusion broth (BHI, Bacto, ref. n. 237500). The bacterial growth conditions either in liquid (broth media) or in solid (agar plates) are shown in Table 6.3. The density of bacterial cultures was quantitated by spectroscopy at 600 nm and converted to approximate colony forming units per volume (CFU/ml), as indicated in Table 6.3.

Table 6.3. Conditions of the bacterial growth in liquid and solid media for the three bacterial species.

	E. coli	*P. aeruginosa*	*A. actinomycetemcomitans*
Broth media	Luria Bertani (LB)	Luria Bertani (LB)	Brain Heart Infusion (BHI)
Liquid culture conditions	200 rpm, 37°C, overnight	200 rpm, 37°C, overnight	Static, 35°C, 2 days
Oxygen conditions	Aerobic	Aerobic	Semi-anaerobic (sealed plastic box with a candle inside*)*
OD_{600} ↔ CFU/ml	1 ↔ $1 \cdot 10^9$ CFU/ml	1 ↔ $1 \cdot 10^{10}$ CFU/ml	0.3 ↔ $1 \cdot 10^9$ CFU/ml
Agar plate culture conditions	35°C, 24 h	35°C, 24 h	35°C, 48 h

6.3.5.2 Preparation of cement extracts

To test the antimicrobial effect of the cements, MPCs was prepared as explained above with a liquid to powder ratio of 0.13 ml/g. The cement was either allowed to set for 1 h at room temperature (**fresh-cement**), or was set for 1 h at room temperature and then further incubated in Ringer's solution for 24 h (**aged-cement**). This allows for the complete transformation of the cements to their reaction products. The fresh- and aged-cements were then incubated in broth (LB or BHI) or in phosphate buffered saline solution (PBS, Gibco, ref. n. 18912-014) for 72 h, using a cement mass *versus* medium volume ratio of 0.85 g/ml. The resulting solutions (**cement extracts**) were centrifuged at 3000 rpm for 5 min to remove particulates prior to use. The extracts prepared

from fresh-cements were termed as **fresh-cement extracts** and the extracts prepared from aged-cements were termed as **aged-cement extracts**. The preparation of the fresh- and aged-cements, as well as the preparation of their extracts, is schematically shown in Figure 6.6.
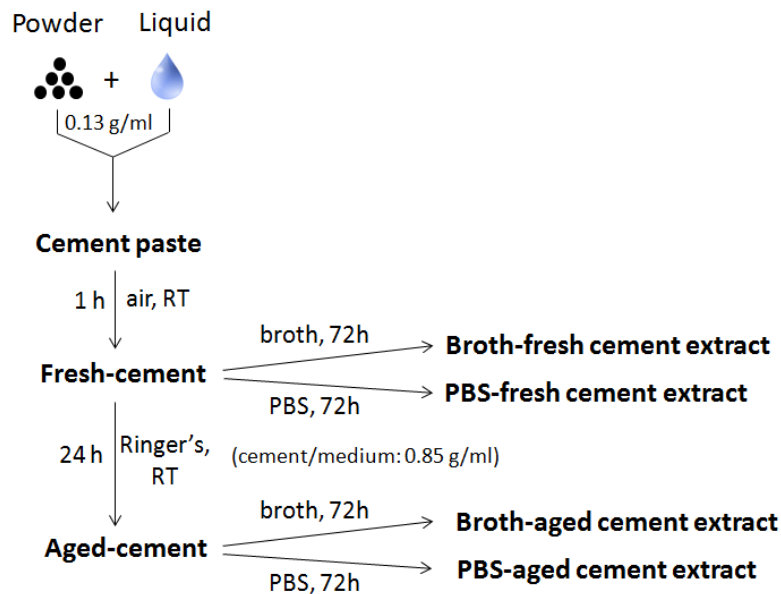

Figure 6.6. Schema of the followed steps to prepare fresh- and aged-cements, as well as fresh- and aged-cement extracts. RT stands for room temperature.

The osmolarity of the PBS-extracts was quantified by means of an Osmometer (Roebling 1313 DR), which quantifies the amount of ionic species in a solution by evaluating their freezing point. This technique is based on the reduction of the freezing point of a solution by the presence of electrolyte particles, which is called freezing point depression [19].

In order to have a more specific information regarding the ionic species dissolved in the extracts, the concentration of Mg, P and Na (from now on [Mg], [P] and [Na]) in the PBS-extracts was quantified by means of inductively coupled plasma-optical emission spectrometry (ICP-OES, Perkin Elmer Optima 3200 RL) after diluting each extract 50-fold with HNO_3 1%. However, it should be considered that the contribution of the NH_4^+ released by the ammonium-containing cements could not be obtained, since this technique does not permit to quantify nitrogen. Four replicates of each extract were analyzed by both the Osmometer and the ICP-OES. The pH of the extracts was measured in triplicate using a pH-meter (Beckman Coulter, A51705).

6.3.5.3 Antibacterial assays

6.3.5.3.1 Agar diffusion test

One approach to determine the antibacterial activity of cement formulations was the agar diffusion test (ADT). Bacteria (10^7 CFU) were cultured on agar plates. Three cavities (12 mm diameter) were punched in the agar and filled with the cements. The Na-MPC and NH_4+Na-MPC were injected with 5-ml syringes with a 2 mm-aperture, and the NH_4-MPC was applied with a spatula due to its low injectability. After 48 h of incubation at 35°C, inhibition of bacterial growth around the cement plugs was measured using a 1 mm-precision ruler. The inhibition zone was calculated from the diameter of the inhibition zone ($\varnothing_{iz}$) and the diameter of the cement-filled cavity ($\varnothing_c$), according to Equation 6.4 [20]. Images of the plates were taken with a Kodak Image Station 4000R. The study was performed in duplicate.

Equation 6.4. $\qquad$ Inhibition zone size (mm) $= \frac{\varnothing_{iz} - \varnothing_c}{2}$

6.3.5.3.2 Growth curves

Bacterial growth curves were obtained by inoculating 10^6 CFU/ml in broth (control) or in broth-cement extracts. The samples were kept on an orbital shaker (Stovall Belly Dance Shaker) for 24 h at 35°C in order to favor the bacterial growth. At different time points, the viable bacteria were quantified by plating 100 µl of diluted aliquots in duplicate on agar plates. CFUs were enumerated on the plates after incubation for 24 h (*E. coli* and *P. aeruginosa*) or 48 h (*A. actinomycetemcomitans*) at 35°C (Table 6.3). Growth curve assays were carried out in duplicate.

6.3.5.3.3 Bactericidal activity

Bactericidal activity of the extracts was evaluated by incubating 10^6 CFU/ml in PBS (control) or in PBS-cement extracts. PBS was the chosen medium because although it has a similar osmolarity than bacteria's cytoplasm, not causing osmotic pressure to bacteria, it inhibits the bacterial growth because it is free of nutrients, and thus the bacterial death was not masked by the bacterial growth. After 2 h at 35°C, 100 µl of diluted aliquots were plated in duplicate on agar plates. CFUs were determined after 24 h (*E. coli* and *P. aeruginosa*) or 48 h (*A.

actinomycetemcomitans) of incubation at 35°C. The % of surviving bacteria was calculated according to Equation 6.5, where CFU_{sample} is the number of colonies enumerated in the cement extract or PBS (control) and CFU_{PBS} is the number of colonies enumerated in the PBS (control).

Equation 6.5. $\qquad$ Viable bacteria (%) $= \dfrac{CFU_{sample}}{CFU_{PBS}} * 100$

To evaluate whether the antimicrobial effects of the extracts were related to their pH, bactericidal assays were performed using an alkaline buffer prepared with 0.2 M glycine (Sigma Aldrich, ref. n. 410225) and 0.2 M NaOH (Fischer Scientific, ref. n. BP359) brought to a final pH between 9-11. Bacteria (10^6 CFU/ml) were incubated in the alkaline buffer for 2 h at 35°C. Afterwards, 100 µl of diluted aliquots were plated in duplicate on agar plates to determine the % of viable bacteria, as described above. Bactericidal activity assays were carried out in duplicate.

6.3.5.3.4 Anti-biofilm activity

Bacterial biofilms were formed by incubating $2 \cdot 10^7$ CFU/ml of *P. aeruginosa* in 96-well plates for 24 h at 35°C. Following incubation, the plates were washed twice with PBS to remove unattached bacteria. 125 µl of broth (control) or of broth-fresh-cement extracts were added to each well in order to evaluate the bacterial growth in each extract. The samples were kept on the orbital shaker for 24 h at 35°C and then washed twice with PBS to remove detached bacteria. Surviving bacteria were quantified by a chemiluminiscent assay for ATP quantitation using the manufacturers' protocol (BacTiter Glo; Promega, ref n. G8231). Every sample was quantitated in triplicate by luminescence in a multi-mode plate reader (Biotek, Synergy HT) using a sensitivity of 125.

The % of surviving bacteria living in the biofilm was calculated according to Equation 6.6, where I_{sample} is the intensity of the luminescence signal of the extract or PBS (control) and I_{PBS} is the intensity of the luminescence signal of the PBS (control).

Equation 6.6. $\qquad$ Viable bacteria in biofilm (%) $= \dfrac{I_{sample}}{I_{PBS}} * 100$

The anti-biofilm activity study was run twice.

6.3.6 Studies with eukaryotic cells: cell viability

6.3.6.1 Cells and culture conditions

Rat preosteoblast-like MC3T3-M1 cells were used as a cell model to test the cytotoxicity of the cement extracts. The cells were maintained in complete medium (MEM Alpha medium, GIBCO, ref. n. 12571) supplemented with 10 v/v% fetal bovine serum (Hyclone ref. n. SH30071-03) and 1 v/v% of penicillin/streptomycin (GIBCO, ref. n. 15140) at 37°C in a humid atmosphere with 5% CO_2. The culture medium was renewed every third day. Upon confluence, cells were detached with 5 ml of trypsin-EDTA (GIBCO, ref. n. 25300) that was inactivated with complete medium after 10 min. The cells were then centrifuged at 1000 rpm for 10 min and the pellet was resuspended in complete medium. Finally, the cells were re-cultured or used for the experiment.

6.3.6.2 Preparation of cement extracts

Cement extracts were prepared to test the cytotoxicity of the cement. For this purpose, the cements were either allowed to set for 1 h at room temperature (**fresh-cement**), or allowed to set for 1 h at room temperature and then further incubated in Ringer's solution for 24 h (**aged-cement**). The fresh- and aged-cements were then incubated in complete medium either for 5 or 72 h (**5h-extract** or **72h-extract**, respectively), using a cement mass *versus* medium volume ratio of 0.85 g/ml. The resulting solutions (cement extracts) were centrifuged at 3000 rpm for 5 min to remove particulates prior to use. The extracts prepared from fresh-cements were termed as **fresh-cement extracts** and the extracts prepared from aged-cements were termed as **aged-cement extracts**. The preparation of the fresh- and aged-cements, as well as the preparation of their extracts, is schematically shown in Figure 6.7.
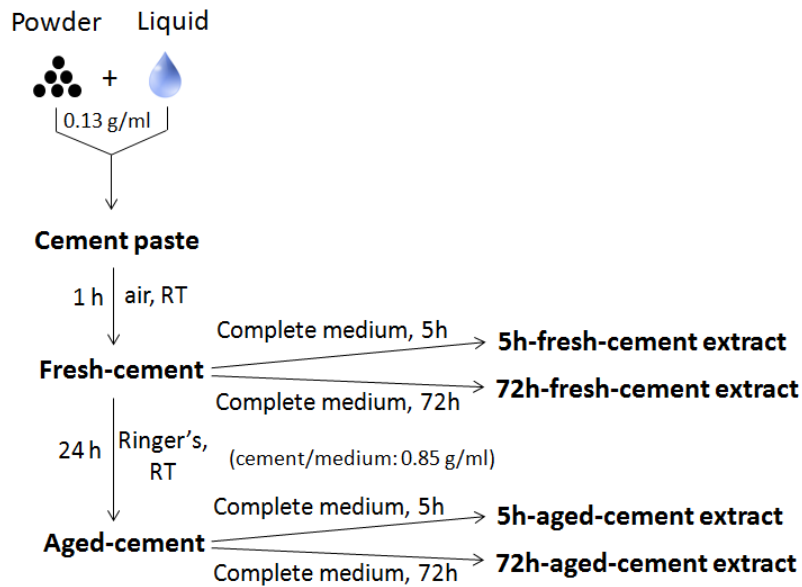
Figure 6.7. Schema of the followed steps to prepare the 5h and 72h-extracts, using the corresponding fresh- and aged-cements. RT stands for room temperature.

6.3.6.3 Experimental study

Cells (10^4 cells/well) were seeded in 96-well plates and incubated for 20 ± 3 h. After this period, cells were adhered on the plastic surface and unattached cells were removed by washing each well twice with PBS. Finally, cells were incubated with 100 µl of cement extract prepared with fresh- or aged-cement for a period of 5 h or 72 h (5h-fresh-cement extract, 72h-fresh-cement extract, 5h-aged-cement extract or 72h-aged-cement extract). Every extract was used undiluted (1-1), with a 2-fold (1-2) or a 10-fold (1-10) dilution. Control samples consisted on incubating cells with complete medium (negative control) or with complete medium supplemented with 1 v/v% triton X-100 (Sigma Aldrich, T9284) (positive control). Complete medium was added in wells free of cells as blank. Every sample was tested in triplicate and the whole experiment was repeated twice (n = 6).

After 24 h of incubation, each well was washed twice with PBS to remove the unattached cells and cell viability was determined using CellTiter-Glo reagent (Promega, ref. n. G7571), as described by the manufacturer. The reagent extracted the ATP from the cells and then supported a luminescent reaction. The luminescence signal was directly proportional to the ATP present, thus being directly related to the number of metabolically active cells. A calibration curve with

decreasing concentration of cells was created to convert the results to cell numbers. The luminescence was read in a plate reader (Biotek, Synergy HT) with a sensitivity of 125.

6.3.7 Statistical analysis of the results

A Student's t-test was used to determine the statistically significant differences between the mean values of the different experimental groups. A difference between groups was considered to be significant at $p < 0.05$.

6.4 Results

6.4.1 Exothermy

a) Effect of the environmental temperature

The exothermy of MPCs, which powder contained MgO sintered at 1475°C for 6 h, coarse phosphate salts and 5 wt% of coarse borax, was evaluated. Figure 6.8 compares the temperature evolution of MPCs when the plastic flask that contained the cement was maintained either at room temperature (RT) or at 37°C. The maximum temperature attained was substantially higher when the cements set at 37°C than at RT, the temperatures increasing from 31 to 57°C for NH_4-MPC and from 40 to 62°C for Na-MPC. Moreover, the maximum temperature was reached at a shorter time when the cement set at 37°C, the time being reduced from 18 to 6 min for NH_4-MPC and from 9 to 3 min for Na-MPC, respectively.
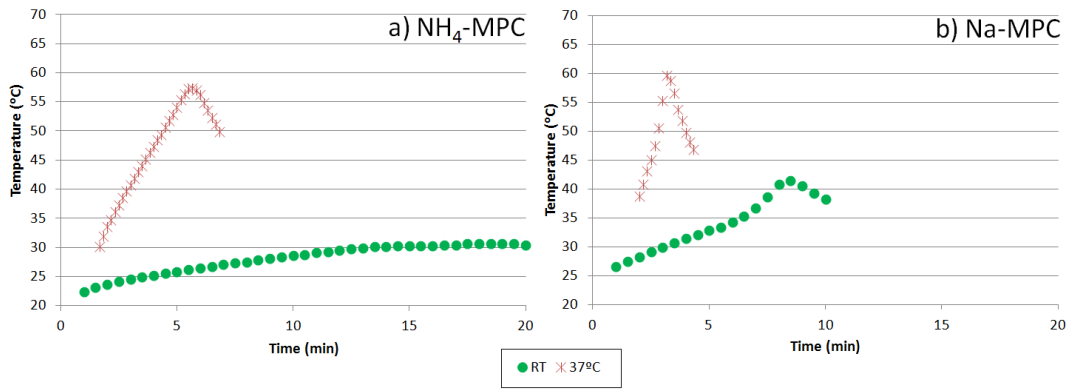
Figure 6.8. Temperature evolution of: a) NH$_4$-MPC and b) Na-MPC, while setting at room temperature (RT) and at 37°C. The cements were prepared with MgO calcined at 1475°C for 6 h (milled at 150 rpm for 15 min), with coarse phosphate salts and 5 wt% of coarse borax was added.

The significant increase of exothermy when the cements were in an environment at 37°C indicated that the reactants had to be further processed in order to optimize the exothermy at this temperature. The exothermy of the cements was adjusted gradually, following the directions proved to be efficient in Chapter 5. The effect of the exothermy was assessed for, firstly, the fineness of borax and, secondly, the calcination time of MgO.

b) Effect of the borax fineness

Figure 6.9 compares the exothermy of the MPCs containing 5 wt% of borax of two different particles size, coarse and fine. When the fine borax was used, the maximum reached temperature decreased about 10°C in NH$_4$-MPC and about 3°C in Na-MPC. The time to reach the maximum temperature was approximately the same in both cements. The fine borax was selected for the following studies due to its more efficient reduction of the exothermy than the coarse one.
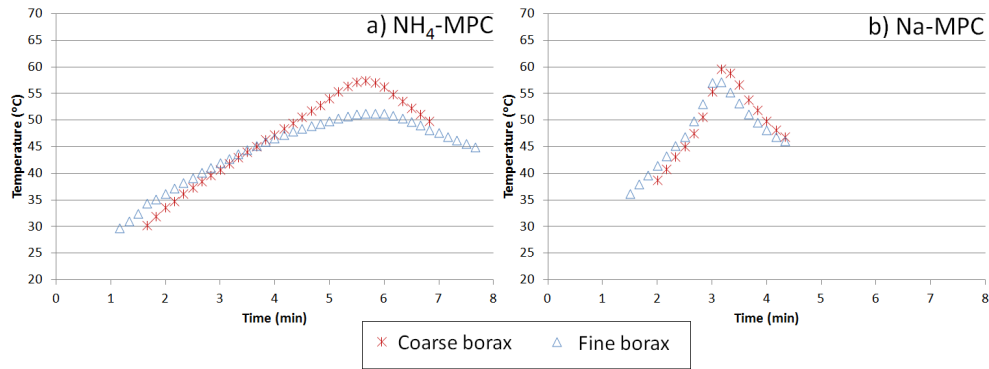
Figure 6.9. Temperature evolution of: a) NH$_4$-MPC and b) Na-MPC, with 5 wt% of either coarse or fine borax, while setting at 37°C. The cements were prepared with MgO calcined at 1475°C for 6 h (milled at 150 rpm for 15 min) and with coarse phosphate salts.

c) Effect of the calcination time of MgO

Figure 6.10 shows the temperature evolution of NH$_4$-MPC and Na-MPC containing 5 wt% of fine borax in function of the calcination time of MgO. The cements that were prepared with MgO calcined for 12 h where slightly less exothermic than those containing MgO calcined for 6 h, the maximum temperature decreasing about 5°C in both cements. The time to reach the maximum temperature was significantly increased for Na-MPC prepared with MgO calcined for 12 h, from 3 to 4.5 min, and was unmodified for NH$_4$-MPC. Therefore, from now on, the cements were prepared with MgO calcined for 12 h.
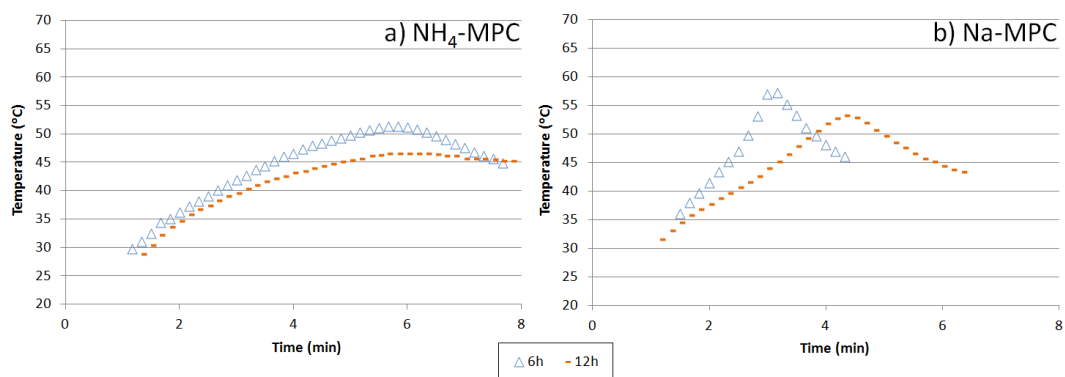

Figure 6.10. Temperature evolution of: a) NH$_4$-MPC and b) Na-MPC, prepared with MgO calcined at 1475°C for 6 and 12 h (milled 150 rpm 15min), while setting at 37°C. The cements were prepared with coarse phosphate salt and 5 wt% of fine borax was added.

The studies explained above indicated that the exothermy could be efficiently reduced using fine borax and calcining the MgO at 1475°C for 12 h. Figure 6.11 shows the particle size distribution of the processed reactants.
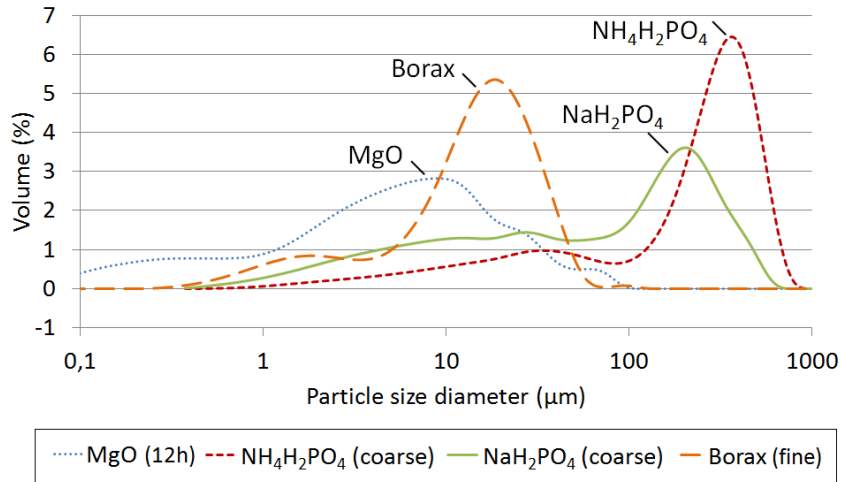
Figure 6.11. Particle size distribution of the MPC reactants: MgO calcined at 1475°C for 12 h (milled at 150 rpm for 15min), coarse $NH_4H_2PO_4$ and NaH_2PO_4, and fine borax.

d) Effect of the amount of borax

Finally, the amount of borax required to ensure the safety of the surrounding tissues was determined. Figure 6.12 shows the temperature evolution of the three formulations of MPC with different amounts of borax.
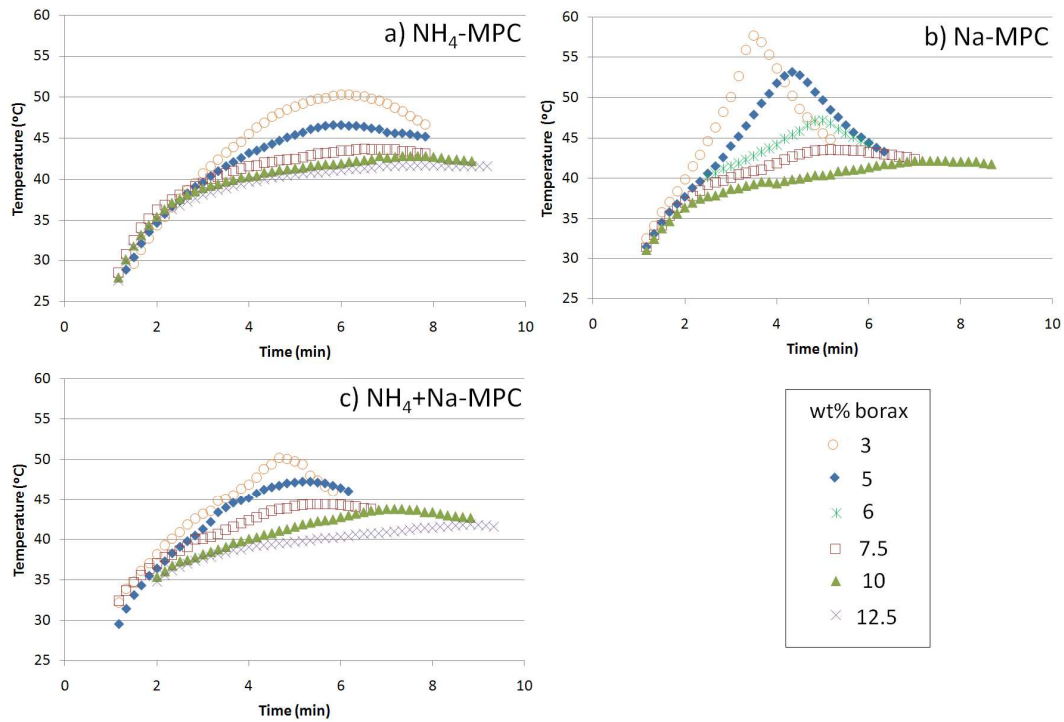
Figure 6.12. Temperature evolution of: a) NH$_4$-MPC, b) Na-MPC and c) NH$_4$+Na-MPC, with different amounts of fine borax, while setting at 37°C. All cements were prepared with MgO calcined at 1475°C for 12 h (milled at 150 rpm for 15min) and with coarse phosphate salts.

The amount of borax necessary to get cements with innocuous exothermy for the surrounding tissues was determined with the thermal coefficient of every temperature evolution (Figure 6.13). The amount of borax selected to prepare the MPCs was 6 wt%, since this was the lowest amount that resulted in a thermal coefficient lower than 1 for the three formulations, although the NH$_4$-MPC and NH$_4$+Na-MPC already had a thermal coefficient lower than 1 when 5 wt% of borax was added.
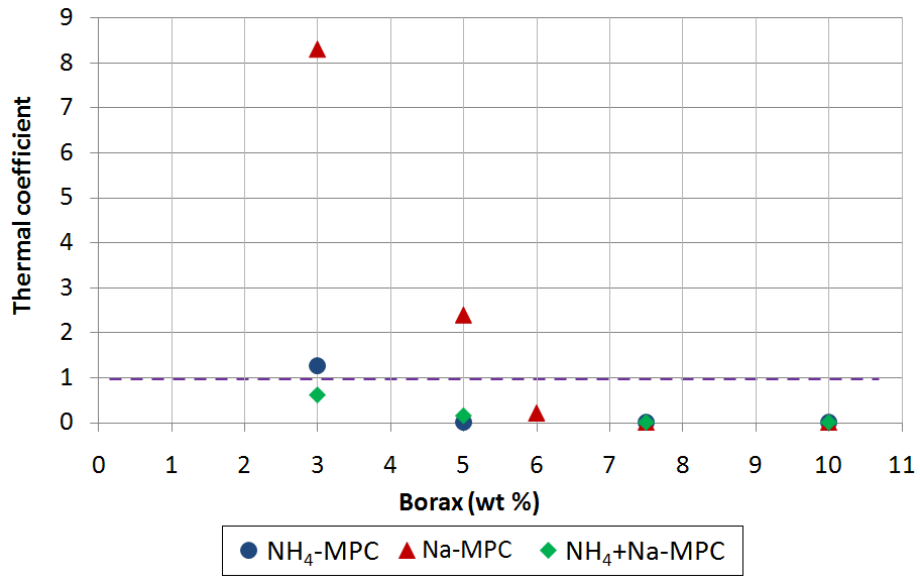
Figure 6.13. Thermal coefficient of the NH_4-MPC, Na-MPC and NH_4+Na-MPC prepared with different amounts of fine borax. All cements were prepared with MgO calcined at 1475°C for 12 h (milled at 150 rpm for 15min) and with coarse phosphate salts.

6.4.2 Physico-chemical characterization of MPCs

6.4.2.1 Setting and cohesion time

The final setting and the cohesion time of the three MPC formulations are shown in Table 6.4. The initial setting times are not shown since they were very similar to the final setting times, being just about one minute apart in every case. The cohesion time was slightly shorter than the final setting time in the case of Na-MPC and NH_4+Na-MPC, and it was halved in the case of NH_4-MPC.

Table 6.4. Final setting times (t_F) and cohesion times (t_C) of the MPCs. The average ± standard deviation is shown, n = 3.

MPC formulation	t_F (min)	t_C (min)
NH_4-MPC	14±2	≤ 6
Na-MPC	7±1	≤ 6
NH_4+Na-MPC	8.5±1	≤ 7

6.4.2.2 Injectability

The load/displacement curves displayed for the three MPC formulations showed the three typical stages of an injectable material (Figure 6.14). The first stage was an initial transient regime in which the applied load increased rapidly until it reached the yield load corresponding to the force needed for the paste starting to flow. In the second stage, pastes flowed in steady state conditions at a constant load that is referred to as injection load. In the final stage, the load increased again either because the syringe was empty or because the paste was not injectable anymore.

The yield load was between 14 and 16 N for the three formulations, with no significant differences among them ($p > 0.05$). However, the displacement of the piston was different for each MPC formulation, following the trend NH_4+Na-MPC > Na-MPC > NH_4-MPC, which was consistent with the amount of paste injected for each formulation (Table 6.5).
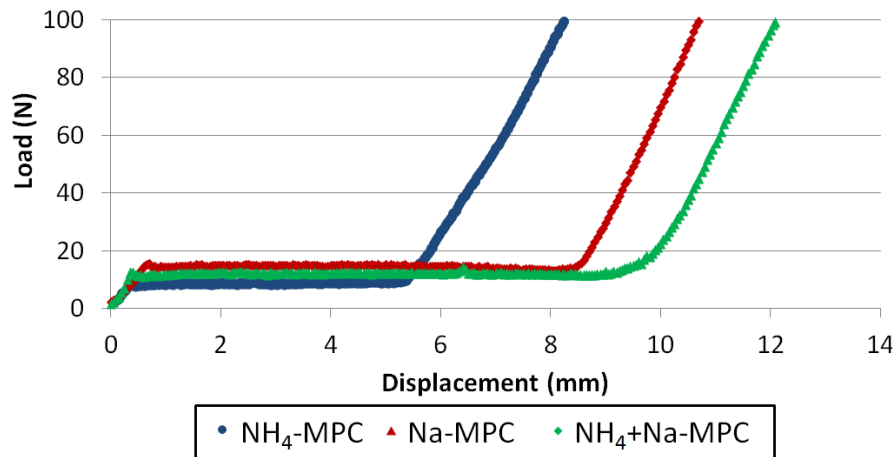

Figure 6.14. Load/displacement curves (displacement of the MTS piston and, therefore, of the syringe plunger) for the MPC formulations.

Table 6.5 shows the injectability for each formulation. NH_4+Na-MPC was the most injectable formulation, followed by Na-MPC, and both formulations had a significantly higher injectability than NH_4-MPC ($p < 0.05$).

Table 6.5. Injectability (%) of the MPC formulations. The average ± standard deviation is shown, n = 3.

NH$_4$-MPC	Na-MPC	NH$_4$+Na-MPC
41.4 ± 14.0	74.4 ± 13.0	86.4 ± 3.4

6.4.2.3 Mechanical properties

The compressive strength after 7 days of immersion in Ringer's solution is shown in Table 6.6. NH$_4$-MPC and NH$_4$+Na-MPC had similar compressive strengths, with values higher than 40 MPa. However, the compressive strength of Na-MPC was about 31 MPa, significantly lower ($p <$ 0.05) than that of the other two formulations. For NH$_4$-MPC, the compressive strength was also tested after 2 h, which showed a value of 16.0 ± 4.0 MPa (Table 6.6).

Table 6.6. Compressive strength of the MPC formulations immersed in Ringer's solution for 7 days at 37°C. The compressive strength of NH$_4$-MPC after 2 h of immersion in Ringer's solution is also shown. The average ± standard deviation is shown, n = 10.

Time points	NH$_4$-MPC	Na-MPC	NH$_4$+Na-MPC
2 h	43.4 ± 11.1	30.8 ± 3.0	46.1 ± 6.2
7 d	16.0 ± 4.0	–	–

6.4.2.4 Crystalline phases

Figure 6.15 shows the XRD of the cement powder (0 h) and of the cement immersed in Ringer's solution for 7 days. The phases formed for each MPC formulation were the same than those observed in Chapter 5 (Section 5.4.2.4). Briefly, NH$_4$-MPC and NH$_4$+Na-MPC transformed into struvite and schertelite, and Na-MPC gave place to an amorphous compound. Unreacted MgO was found in all formulations.
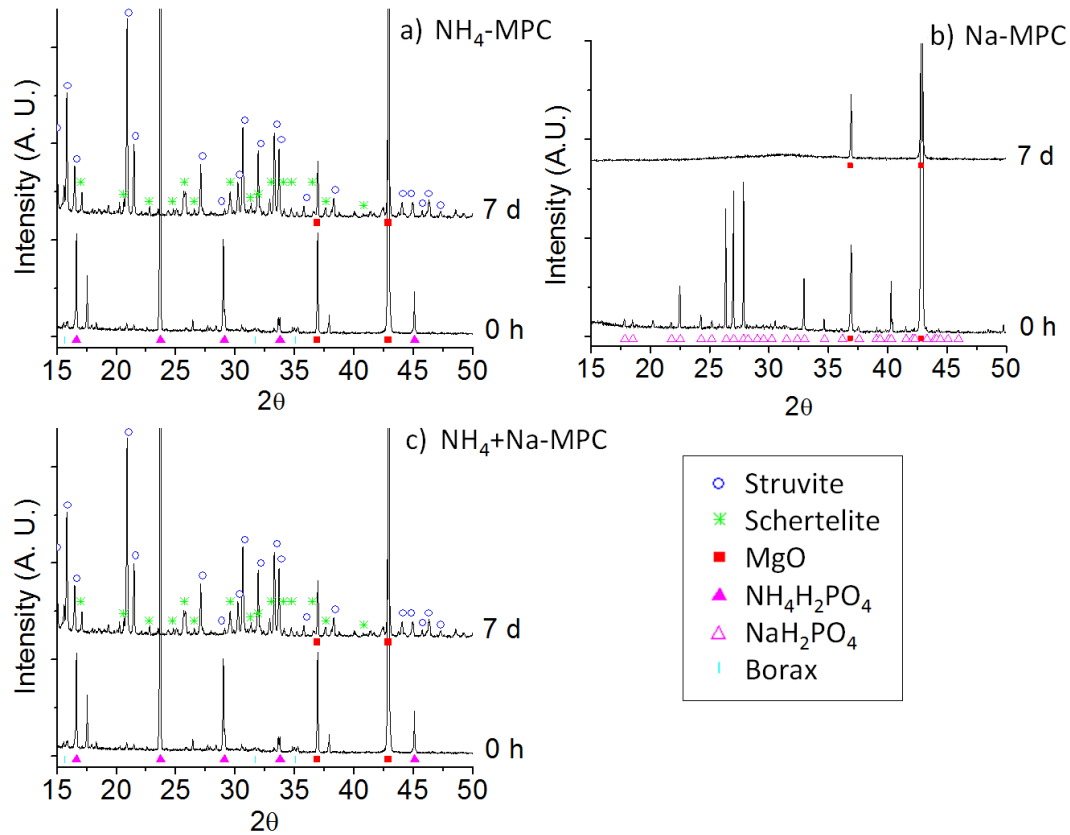
Figure 6.15. XRD of MPC formulations set for 0 h and 7 days in Ringer's solution at 37°C: a) NH$_4$-MPC, b) Na-MPC and c) NH$_4$+Na-MPC. A.U. stands for arbitrary units.

6.4.2.5 Morphology

The microstructures of surface fractures of MPCs set in Ringer's solution for 7 days are displayed in Figure 6.16. The microstructures of MPCs that did not contain borax in the powder phase are also included, in order to evaluate the influence of borax on the morphology of the cements.

Interesting differences were observed between those MPC containing borax and those without borax. For instance, NH$_4$-MPC without borax (Figure 6.16 b) was composed of elongated particles. In contrast, an amorphous layer was observed on the fracture surfaces of NH$_4$-MPC prepared with borax (Figure 6.16 a). Whilst Na-MPC prepared with borax was covered by a glassy layer (Figure 6.16 c), the morphology of the same formulation without borax showed some particles between 20 and 60 μm embedded into a vitreous matrix (Figure 6.16 d). Finally, the fracture surface of NH$_4$+Na-MPC containing borax (Figure 6.16 e) was also covered by a glassy

layer, whereas the NH$_4$+Na-MPC that did not contain borax had a more heterogeneous microstructure (Figure 6.16 f).
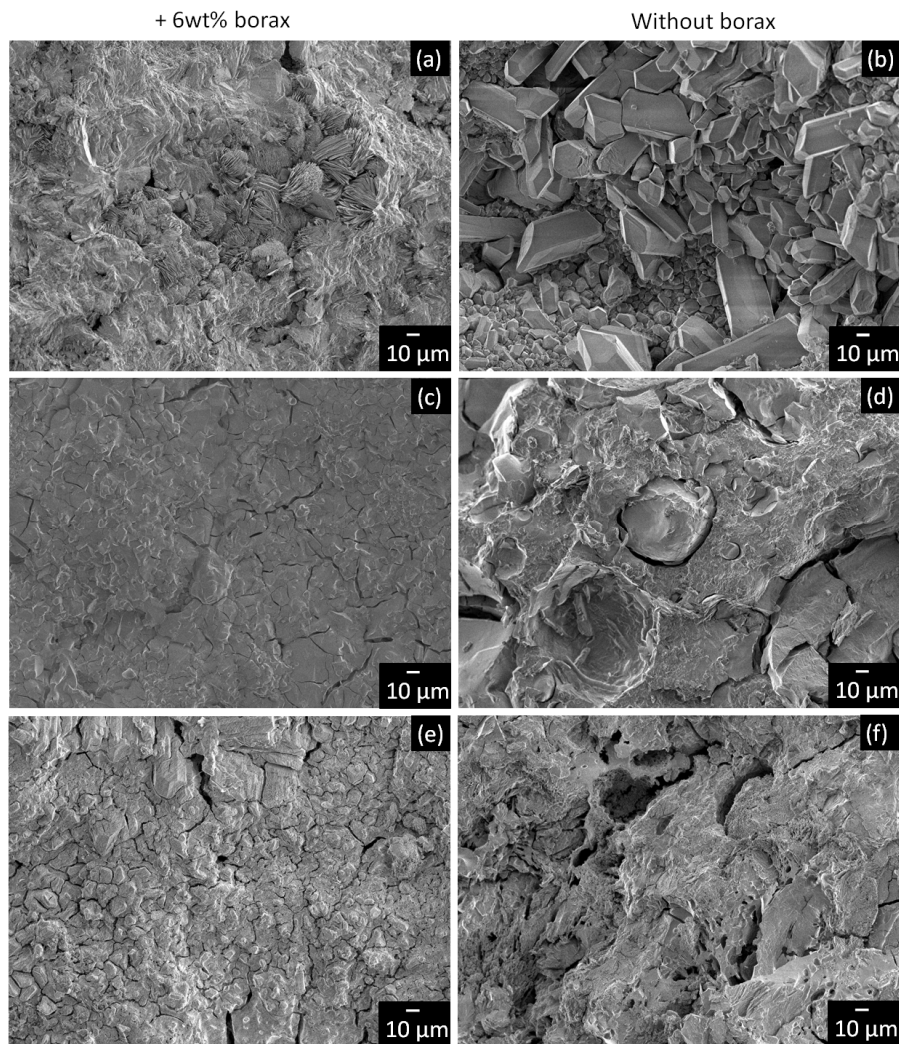
Figure 6.16. Microstructure of the MPC prepared with 6 wt% of borax: a) NH$_4$-MPC, c) Na-MPC and e) NH$_4$+Na-MPC, and without borax: b) NH$_4$-MPC, d) Na-MPC and f) NH$_4$+Na-MPC. The cements were immersed for 7 days in Ringer's solution at 37°C.

6.4.2.6 Specific surface area, skeletal density and porosimetry

Table 6.7 shows the specific surface area (SSA) and the skeletal density for MPC formulations after immersion in Ringer's solution for 7 days. The trend for the SSA was Na-MPC < NH$_4$-MPC < NH$_4$+Na-MPC and for the skeletal density it was NH$_4$-MPC < NH$_4$+Na-MPC < Na-MPC.

Table 6.7. Specific surface area (SSA, m^2/g) and skeletal density (g/cm^3) of the three formulations of MPC after 7 days of immersion in Ringer's solution at 37°C. The average ± standard deviation is shown, n = 2 for SSA and n = 3 for skeletal density.

	SSA (m^2/g)	Skeletal density (g/cm^3)
NH$_4$-MPC	1.85 ± 0.19	2.43 ± 0.02
Na-MPC	1.76 ± 0.26	2.64 ± 0.02
NH$_4$+Na-MPC	2.43 ± 0.40	2.59 ± 0.02

Figure 6.17 shows the entrance pore diameter distribution, measured by means of mercury intrusion porosimetry. In general, the three MPC formulations showed a peak around 0.01-0.02 µm, and NH$_4$-MPC and NH$_4$+Na-MPC also showed a wide peak around 1 µm. Finally, the three MPC formulations showed a peak of entrance pore diameter around 10 µm that could be associated to the presence of cracks on the surface of the cements (Figure 6.16), occurring during the drying process of the samples.
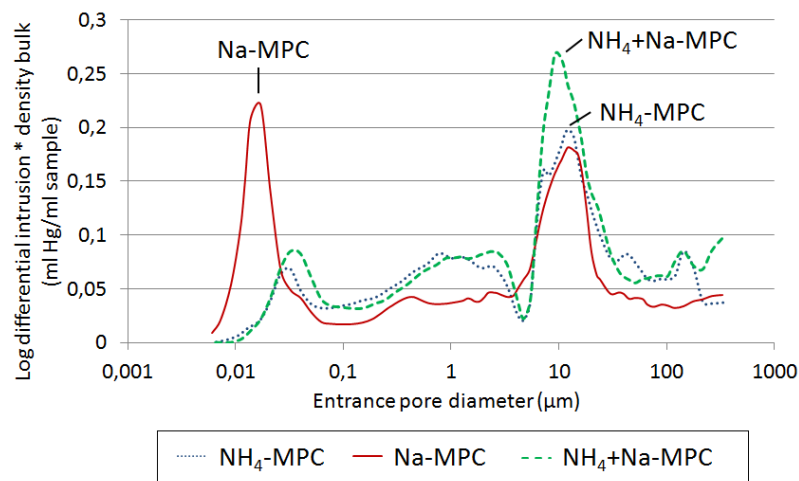

Figure 6.17. Distribution of the entrance pore diameter of MPC formulations after being immersed in Ringer's solution for 7 days.

Table 6.8 shows the results of total open porosity of the three MPC formulations set for 7 days. Na-MPC was the formulation exhibiting a lower total open porosity, followed by NH$_4$-MPC and NH$_4$+Na-MPC.

Table 6.8. Total open porosity (%) of the three MPC formulations after being immersed in Ringer's solution for 7 days.

NH$_4$-MPC	Na-MPC	NH$_4$+Na-MPC
30.84	28.80	35.08

6.4.3 Antimicrobial assays

6.4.3.1 Agar diffusion test

Every MPC formulation caused growth inhibition of the Gram negative bacteria *E. coli*, *P. aeruginosa* and *A. actinomycetemcomitans*, which was observed as a clear ring around the cement samples inserted into an agar plate seeded with bacteria (Figure 6.18).
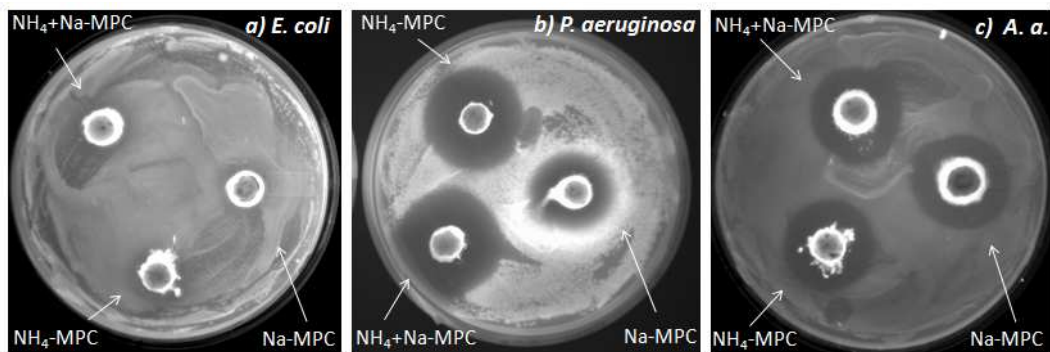
Figure 6.18. Agar diffusion test of the three fresh-cement formulations in: a) *E. coli*, b) *P. aeruginosa*; c) *A. actinomycetemcomitans (A.a.)*.

The inhibition zone for each bacterial strain and MPC formulation is shown in Table 6.9. Although no statistically significant differences were observed between MPC formulations (p > 0.05), NH$_4$+Na-MPC was the formulation that caused the largest inhibition zone. The inhibition zones were greater for *P. aeruginosa* than for *A. actinomycetemcomitans*, and both were significantly larger than that for *E. coli* (p < 0.05).

Table 6.9. Inhibition zone size that appeared around the fresh NH$_4$-MPC, Na-MPC and NH$_4$+Na-MPC formulations after the incubation time of the three bacterial strains studied: *E. coli*, *P. aeruginosa* and *A. actinomycetemcomitans*. The data indicate mean ± standard deviation, n = 2.

	Inhibition zone size (mm)		
	E. coli	*P. aeruginosa*	*A. actinomycetemcomitans*
NH$_4$-MPC	4.2 ± 1.6	10.5 ± 1.0	9.6 ± 3.0
Na-MPC	3.3 ± 1.2	7.1 ± 1.3	8.6 ± 0.1
NH$_4$+Na-MPC	4.5 ± 1.0	11.4 ± 0.8	9.8 ± 2.1

6.4.3.2 Growth curves

Bacterial growth curves were obtained for the fresh- and aged-cement extracts for the three bacterial species.

a) Fresh-cement extracts

The growth curves of the three bacterial species inoculated in broth (control) or in broth-fresh-cement extracts are shown in Figure 6.19. *E. coli* grew exponentially in broth, whereas no growth was evident when bacteria were incubated with the fresh-NH$_4$-MPC or NH$_4$+Na-MPC extracts (Figure 6.19 a). Fresh-Na-MPC extract caused a decline in CFU suggesting that this extract had bactericidal activity. Similar results were obtained with *P. aeruginosa*, with a sharper decrease in CFU for Na-MPC (Figure 6.19 b). Finally, all three fresh-MPC extracts caused the killing of *A. actinomycetemcomitans*, as evidenced by a decline of CFU over time (Figure 6.19 c).

Figure 6.19. Growth curve of a) *E. coli,* b) *P. aeruginosa* and c) *A. actinomycetemcomitans*, inoculated in broth (control) or in broth-fresh-cement extracts. The absence of bacteria on the plates (no surviving CFUs) is indicated with the corresponding symbol at 10^{-1} CFU/ml. Error bars indicate the standard deviation, n = 4. Since it is difficult to appreciate the error bars, which are smaller than the symbols, the mean and standard deviation values are displayed in Appendix A.3.

b) Aged-cement extracts

The retention of the antibacterial properties after cement setting was studied in the aged-cement extracts. The growth curves of the three bacterial species inoculated in broth (control) or in broth-aged-cement extracts are shown in Figure 6.20. Whereas all three species exhibited exponential growth in broth, bacterial counts (CFU/ml) were drastically reduced in 2-4 h in aged-Na-MPC extract. In contrast, *E. coli* (Figure 6.20 a) and *P. aeruginosa* (Figure 6.20 b) had similar behaviors when incubated in aged-NH$_4$-MPC or NH$_4$+Na-MPC extracts, with an exponential growth with time, the amount of bacteria after 24 h not being significantly different than that in control (p > 0.05). Differently, viable *A. actinomycetemcomitans* decreased with time (Figure 6.20 c), with none surviving bacteria neither in aged-NH$_4$-MPC nor in NH$_4$+Na-MPC extracts after 8 h.
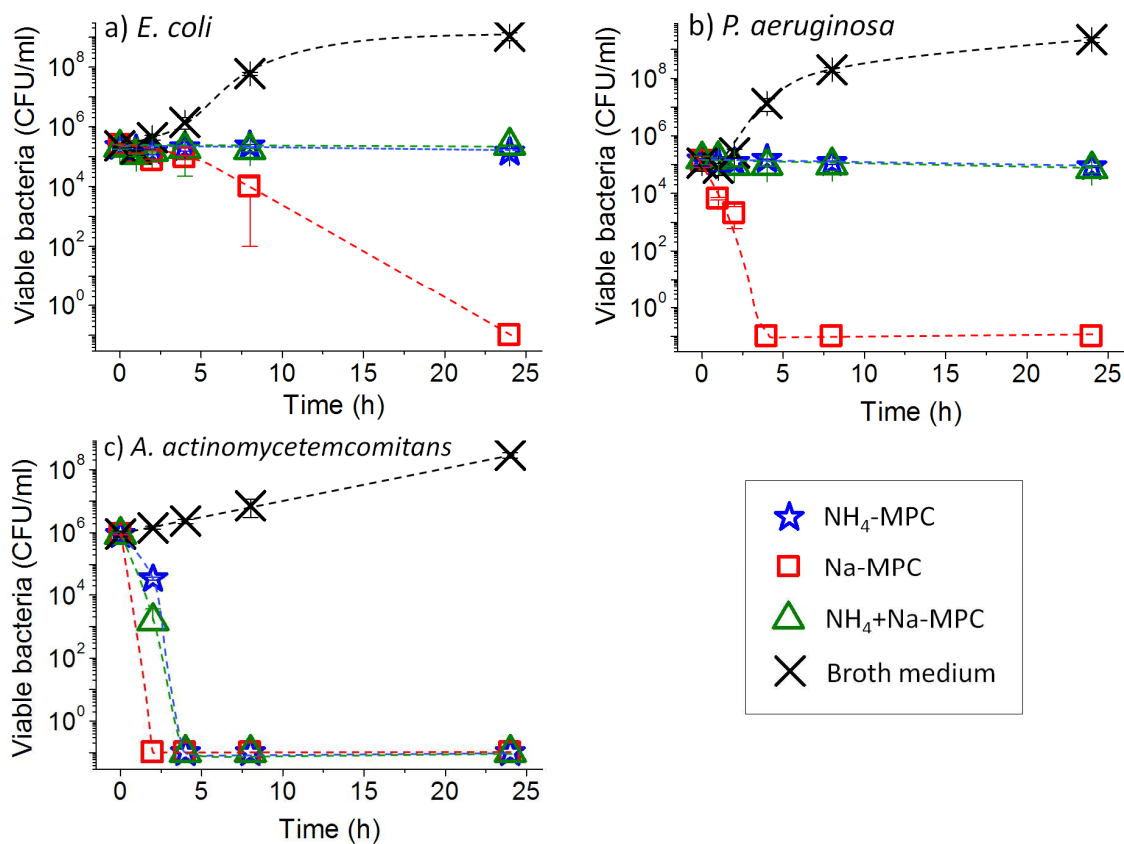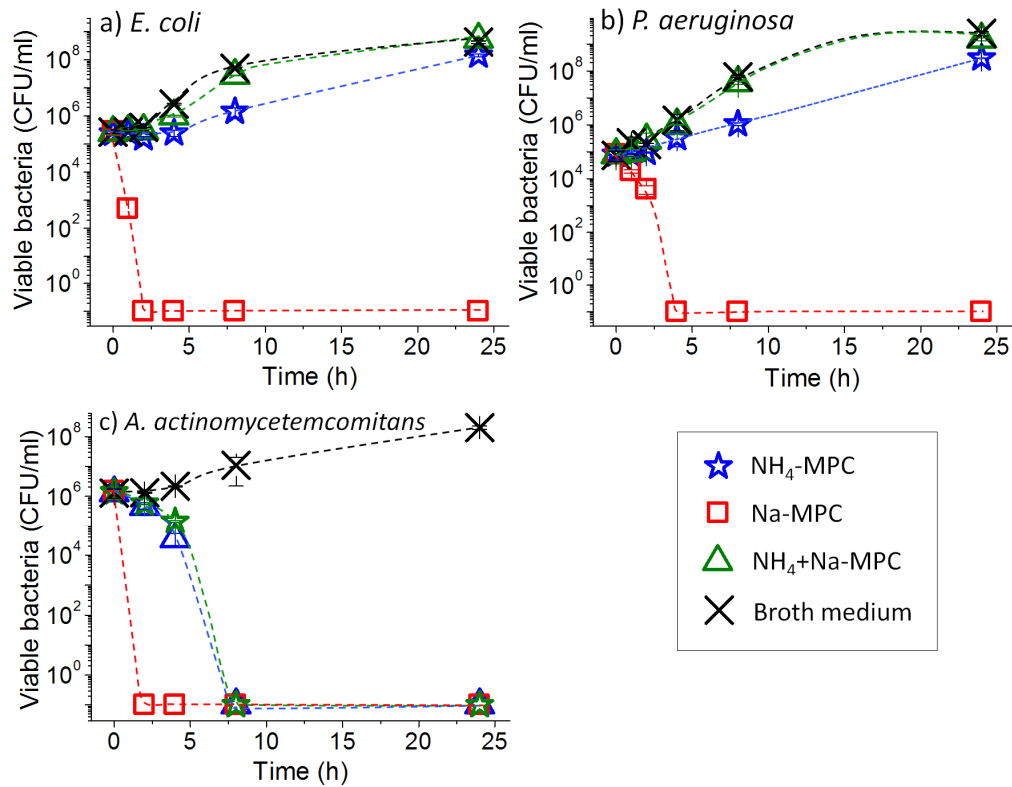
Figure 6.20. Growth curve of a) *E. coli,* b) *P. aeruginosa* and c) *A. actinomycetemcomitans,* inoculated in broth (control) or in broth-aged-cement extracts. The absence of bacteria on the plates (no surviving CFUs) is indicated with the corresponding symbol at 10^{-1} CFU/ml. Error bars indicate the standard deviation, n = 4. Since it is difficult to appreciate the error bars, which are smaller than the symbols, the mean and standard deviation values are displayed in Appendix A.3.

The pHs of the broth-fresh-cement and of the broth-aged-cement extracts are summarized in Table 6.10. The fresh-Na-MPC extract was alkaline (pH 10.1 ± 0.6), whereas the NH$_4$-MPC and NH$_4$+Na-MPC extracts were slightly acidic. All the aged-cement extracts were alkaline, the Na-MPC having the higher pH.

Table 6.10. pH of the broth-cement extracts, prepared by immersing fresh- or aged-cements in broth (LB or BHI) during 72 h. The ratio between the cement paste and the immersion media was 0.85 g/ml. The data indicate mean ± standard deviation, n = 3.

Cement formulation	Broth-fresh-cement extract	Broth-aged-cement extract
NH$_4$-MPC	5.8 ± 0.5	9.1 ± 0.4
Na-MPC	10.1 ± 0.6	11.9 ± 0.3
NH$_4$+Na-MPC	6.5 ± 0.3	10.4 ± 0.2
Control (pristine broth)	7.3 ± 0.2	

6.4.3.3 Bactericidal activity of the cement extracts

The results of the growth curves suggested that the three fresh-MPC formulations had a bacteriostatic or, in some cases, bactericidal activity. To verify this assertion, bacteria were incubated for 2 h in PBS (control), in PBS-fresh-cement or in PBS-aged-cement extracts. Subsequently, the CFUs were enumerated and the % of viable bacteria was calculated. The results are displayed in Figure 6.21.

The viability of the bacteria in contact with the PBS-fresh-cement extracts from all MPC formulations significantly decreased when compared with that of the control ($p < 0.05$) (Figure 6.21 a), especially for the Na-MPC extracts, where only 1.3 ± 1.1 % of *P. aeruginosa* survived, while no viable bacteria of either *E. coli* or *A. actinomycetemcomitans* were found.

Regarding the bactericidal activity of the PBS-aged-cement extracts, the Na-MPC was the most bactericidal extract, as displayed in Figure 6.21 b, exhibiting 100% bactericidal activity against *E. coli* and *A. actinomycetemcomitans*, whereas 9.2 ± 1.4 % of *P. aeruginosa* survived under these conditions. NH_4+Na-MPC extract also exhibited 100% bactericidal activity against *E. coli* and *A. actinomycetemcomitans*, and NH_4-MPC significantly reduced ($p < 0.05$) the amount of viable bacteria in comparison with that in the control. *P. aeruginosa* was the most resistant strain, the amount of viable bacteria being similar than that in control ($p > 0.05$) after incubation in NH_4-MPC or NH_4+Na-MPC extracts.
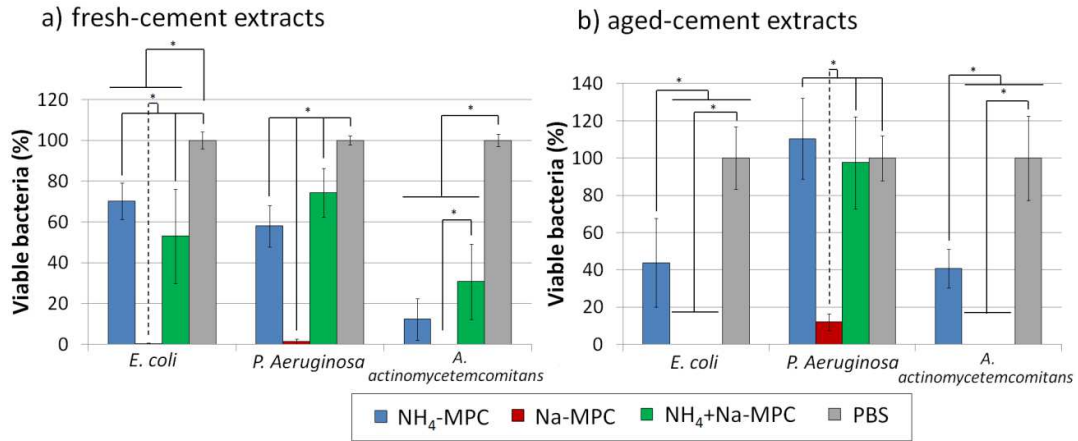
Figure 6.21. Bactericidal activity of the PBS-cement extracts, using PBS as control: a) fresh-cement extracts and b) aged-cement extracts. Bacteria were incubated in the PBS extracts for 2 h at 35°C, and plated on agar to determine surviving CFUs. Results presented as percentage of bacterial viability. Error bars indicate the standard deviation, n = 4. * indicates statistically significant differences (p < 0.05).

In order to determine if the bactericidal effect found in the extracts could be related to their pH, the three bacterial species were incubated for 2 h in an alkaline buffer with different pH values (Figure 6.22). The viability of *E. coli* was reduced at pHs higher than 10.0, remaining no surviving bacteria at pH 11.0. The viability of *P. aeruginosa* gradually decreased with increasing pH, with 11.3 ± 8.6% surviving bacteria detected at pH 11.0. *A. actinomycetemcomitans* also exhibited a decreasing viability with the increasing pH, with no surviving bacteria detected at pH 10.5 or higher.
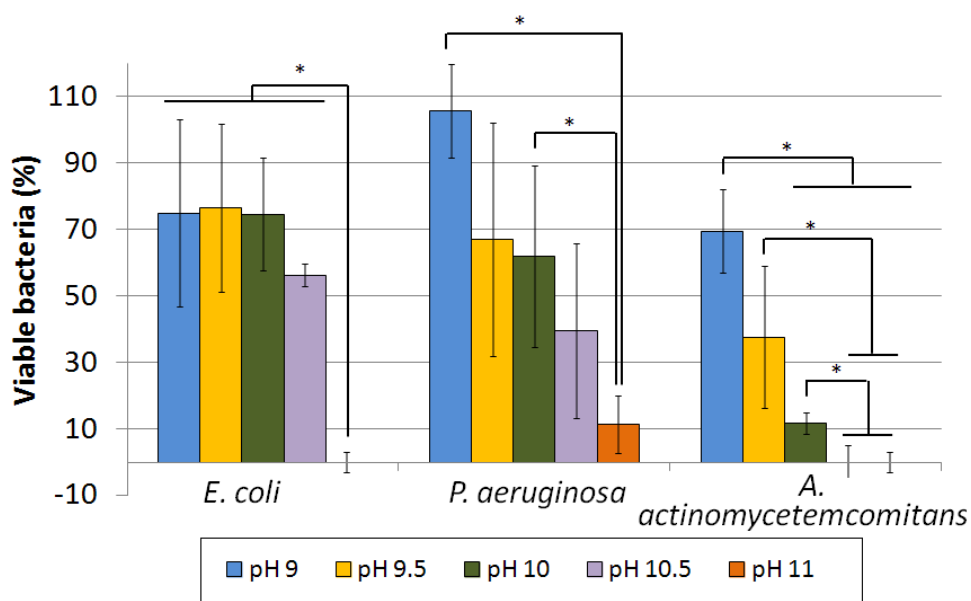
Figure 6.22. Bactericidal activity of buffer solutions set at pHs between 9 and 11. Bacteria were incubated in the buffer for 2 h at 35°C and plated on agar to determine surviving CFUs. Results are presented as percentage of bacterial viability. Error bars indicate the standard deviation, n = 4. * indicates statistically significant differences ($p < 0.05$).

The pHs of the PBS-fresh-cement and of the PBS-aged-cement extracts are summarized in

Table 6.11.

Table 6.11. pH of the PBS-cement extracts, prepared by immersing fresh- or aged-cements in PBS during 72 h. The ratio between the cement paste and the immersion media was 0.85 g/ml. The data indicate mean ± standard deviation, n = 3.

Cement formulation	PBS-fresh-cement extract	PBS-aged-cement extract
NH_4-MPC	6.3 ± 0.4	9.1 ± 0.6
Na-MPC	9.7 ± 0.1	11.4 ± 0.6
NH_4+Na-MPC	6.5 ± 0.2	9.9 ± 0.5
Control (pristine broth)	7.0 ± 0.2	

The osmolarity of the PBS-extracts as well as the [Mg], [P] and [Na] is shown in Figure 6.23, where the values of pristine PBS are indicated as a dashed line. The osmolarity of the extracts indicates the total amount of ionic species dissolved in the solution. The ICP analysis indicated the [Mg], [P] and [Na], thus informing about which was the ionic contribution in the osmolarity of the

extract. However, ICP did not permit to quantify the [N] resulting from the NH_4^+ released by the ammonium-containing cements, and thus the osmolarity was the technique providing the complete picture of the total amount of ionic species dissolved in the extract.

Both osmolarity and [Mg], [P] and [Na] of fresh- and aged-cement extracts of any formulation were significantly higher ($p < 0.05$) than that of PBS and, interestingly, the parameters were significantly higher ($p < 0.05$) for the fresh-cement extracts than that for the aged-ones, except for the osmolarity of Na-MPC, which difference was not statistically significant. The trend of osmolarity observed for the fresh-cements was NH_4-MPC > NH_4+Na-MPC > Na-MPC. Finally, NH_4+Na-MPC extracts had both osmolarity and ionic concentration ([Mg], [P] and [Na]) between that of NH_4-MPC and Na-MPC extracts.

Regarding the fresh-cement, it should be noted that the ionic concentration of Mg (between 1.5 and 6.5 mM) was much lower than that of the P (between 400 and 725 mM) or Na (between 750 and 1100 mM, excluding NH_4-MPC).
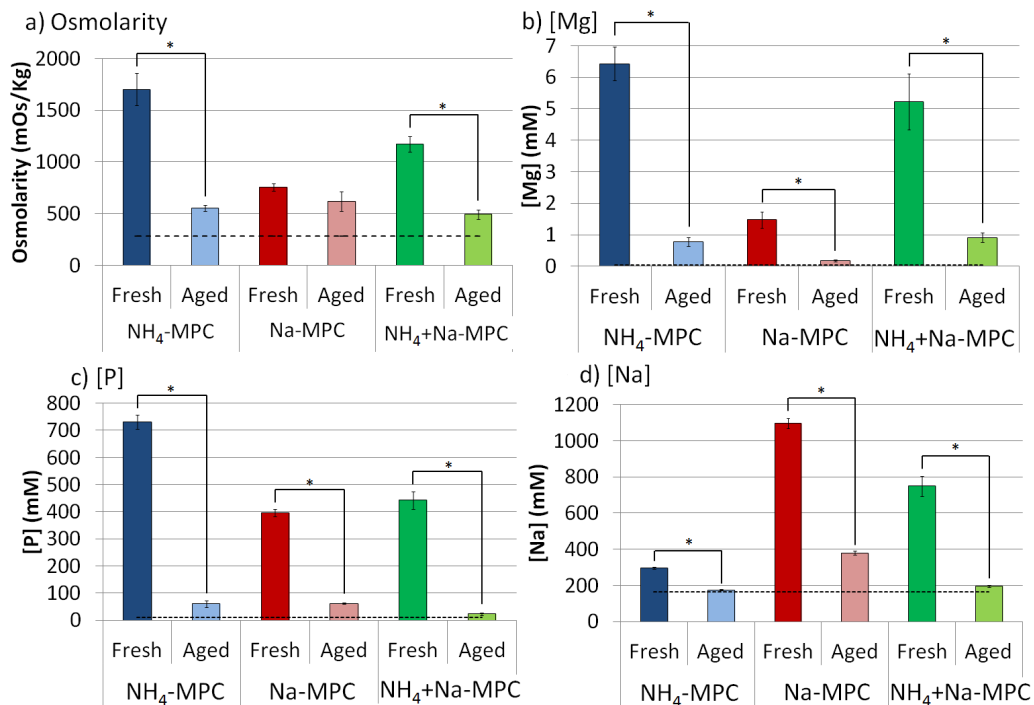
Figure 6.23. Osmolarity and ionic concentration of the three MPC formulations extracts, prepared by immersing fresh- or aged-cements in PBS for 72 h. The osmolarity and ionic concentration were quantified by means of an osmometer or ICP-OES, respectively: a) Osmolarity, b) [Mg], c) [P] and d) [Na]. The ratio between the cement paste and the immersion media was 0.85 g/ml. The dashed line indicates the ionic concentration of PBS. Error bars indicate the standard deviation, n = 4. * indicates statistically significant differences ($p < 0.05$).

6.4.3.4 Anti-biofilm activity

The incubation of *P. aeruginosa* biofilm for 24 h with broth-fresh-cement extracts (Figure 6.24) resulted in a reduction of the amount of metabolically active bacteria in the biofilms by $99.93 \pm 0.11\%$ for the Na-MPC aged-cement extracts. In contrast, NH_4-MPC and NH_4+Na-MPC reduced $92.65 \pm 1.60\%$ and $77.02 \pm 10.96\%$, respectively, the amount of metabolically active bacteria.
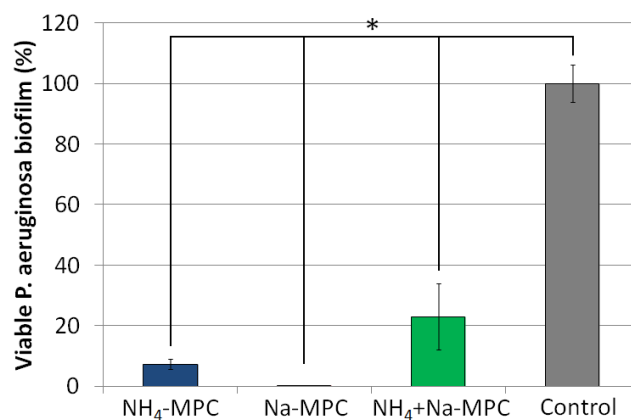
Figure 6.24. Bactericidal activity of broth-fresh-cement extracts against *P. aeruginosa* biofilm after 24 h of incubation at 35°C. Error bars indicate the standard deviation, n = 6. * indicates statistically significant differences ($p < 0.05$).

6.4.4 Cell viability

Figure 6.25 shows the cell viability after MC3T3-M1 cells were for 24 h with fresh- or aged-cement extracts, prepared immersing the cements for 5 or 72 h in complete medium. In general terms, it can be noted that, on one hand, the aged-cement extracts (both 5 and 72h-extracts) resulted in higher cell viability than their fresh-cement counterparts. On the other hand, the cell viability trends regarding the formulations were NH_4+Na-MPC > Na-MPC > NH_4-MPC for the fresh-cements and NH_4-MPC > NH_4+Na-MPC > Na-MPC for the aged-cements, regardless of the preparation time of the extract. Nevertheless, all 5h-extracts showed higher cell viability than 72h-extracts. As expected, the cell viability was increased by diluting more the cement extracts.

The 5h-fresh-cement extracts (Figure 25 a) prepared with Na-MPC and NH_4+Na-MPC had a cell viability higher than 90 % when were 10-fold diluted, whereas their NH_4-MPC counterparts extracts had a viability of 10 % with the same dilution. In contrast, the undiluted 5h-aged-cement extracts prepared with NH_4-MPC had a cell viability of about 90% and when prepared with NH_4+Na-

MPC of about 70%, and the Na-MPC counterparts had a viability of 60 % when the extract was 2-fold diluted.

The 72h-fresh-cement extracts (Figure 25 b) prepared with NH_4+Na-MPC resulted in a cell viability of 70% when 10-fold diluted, being necessary a higher dilution to obtain values of similar viability for the other two formulations. The 72h-aged-cement extracts prepared with NH_4-MPC and NH_4+Na-MPC reached a cell viability of about 70% when 2-fold diluted, and Na-MPC had to be 10-fold diluted to produce a cell viability of about 90 %.
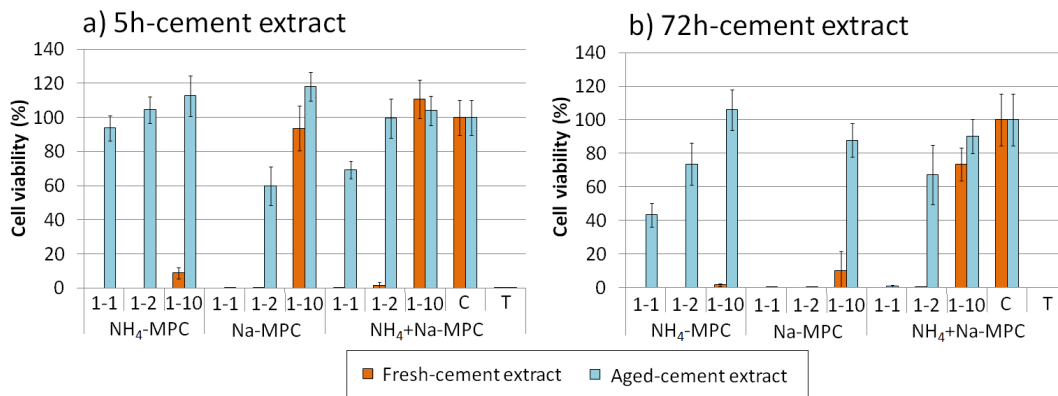
Figure 6.25. Cell viability after cells were in contact with NH_4-MPC, Na-MPC and NH_4+Na-MPC extracts for a period of 24 h. The extracts were prepared immersing the fresh- or aged-cement in complete medium for: a) 5h (5h-cement extract) or b) 72 h (72h-cement extract). 1-1, 1-2 and 1-10 stands for undiluted, 2-fold dilution and 10-fold dilution, respectively. C stands for negative control (complete medium) and T stands for positive control (1 wt% triton), which was prepared supplementing with Triton the complete medium. Error bars indicate standard deviation, n = 6.

Table 6.12 displays the pH of the fresh- and aged-cement extracts prepared with complete medium. While fresh NH_4-MPC and NH_4+Na-MPC led to slightly acidic extracts when prepared either for 5 h and 72h, fresh-Na-MPC led to alkaline extracts, being significantly more alkaline (p < 0.05) the extracts prepared for 72 h. The three formulations of aged-cements produced alkaline mediums, the pH trend being NH_4-MPC < NH_4+Na-MPC < Na-MPC. The aged-cement extracts prepared for 72 h had a significantly higher alkalinity (p < 0.05) than those prepared for 5 h.

Table 6.12. pH of the three MPC formulation extracts, prepared by immersing fresh- or aged-cements in complete medium either for 5 or 72 h. The ratio between the cement paste and the immersion media was 0.85 g/ml. The data indicate mean ± standard deviation, n = 2.

Cement formulation	5h-extract		72h-extract	
	Fresh-cement	Aged-cement	Fresh-cement	Aged-cement
NH_4-MPC	6.0 ± 0.2	7.7 ± 0.4	6.1 ± 0.1	9.0 ± 0.3
Na-MPC	7.8 ± 0.2	9.9 ± 0.3	10.4 ± 0.1	11.6 ± 0.2
NH_4+Na-MPC	6.5 ± 0.1	9.0 ± 0.4	6.9 ± 0.1	10.6 ± 0.3
Control (pristine medium)	7.3 ± 0.2			

6.5 Discussion

6.5.1 Exothermy

The effect of the environmental temperature was shown to be a determinant factor for the cement exothermy during the setting reaction. The exothermy was significantly higher when the cement was in an environment at 37°C than in one at RT (Figure 6.8), fact that can be explained in two different ways. On one hand, the initial temperature of the cement was already about 13°C higher when the cement was maintained at 37°C than at RT (around 24°C). On the other hand, the higher temperature favored the dissolution of the reactants and thus their reaction was faster. Moreover, the faster reaction in the cements maintained at 37°C also permitted a lower dissipation of the heat, the temperature increasing even more. Moreover, the cements prepared at 37°C reached the maximum temperature in a third of the time than the ones prepared at RT due to their faster reaction.

Three parameters were shown to be relevant to reduce the exothermy of the MPCs. On one hand, since Chapter 5 showed that the particle size of the reactants (*i.e.* phosphate salts) was an important parameter to control the exothermy of the cement, in this Chapter it was chosen to decrease the particle size of borax in order to further reduce the exothermy. Indeed, the finer were the particles of borax (Figure 6.9), the lower was the maximum temperature reached for the cement. This observation was associated with the higher specific surface area of the borax, being increased its contact with MgO and thus being potentiated its efficiency. On the other hand, the

longer the calcinations of the MgO, the lower the exothermy of the MPC formulations (Figure 6.10). This result was associated with the sintering of the MgO particles, decreasing its reactivity and thus slowing down the reaction between MgO and the phosphate salts. Finally, the addition of borax effectively reduced the maximum temperature reached during the setting reaction, increasing simultaneously the time needed to reach it, as shown in Figure 6.12.

The overall results indicated that an adequate exothermy at 37°C could be obtained by sintering the MgO at 1475°C for 12 h, using coarse phosphate salts and adding 6 wt% of fine borax.

6.5.2 Physico-chemical characterizations

6.5.2.1 Setting times

The setting times of the MPCs evaluated at 37°C (Table 6.4) were shorter than those of the MPCs evaluated at room temperature (Table 5.2). However, these results have to be evaluated carefully, discerning three simultaneous effects: i) for the MPCs evaluated at 37°C, the reactants were processed in order to further reduce the exothermy of the cements, intrinsically increasing the setting time; ii) a higher evaporation of the liquid phase occurs at 37°C than at room temperature, thus decreasing the setting times; and iii) the reactants dissolve faster at 37°C than at room temperature, thus allowing a faster reaction between them. Since the setting times of the MPCs were shorter when evaluated at 37°C than at room temperature, the environmental temperature was shown to be a more determinant factor for the setting time than any of the processing performed to the reactants.

6.5.2.2 Injectability

The load/displacement curves of Na-MPC and NH_4+Na-MPC indicated that the paste was injected at a constant load (Figure 6.14). However, a small part of the paste remained in the syringe, indication that filter pressing might have taken place. Filter pressing, which is a phenomenon occurring simultaneously to the paste flow, occurs when the pressure required to filter the liquid through the cement particles is lower than the pressure required to inject the paste, causing phase separation [10]. The filter pressing causes that the paste initially injected has

a higher L/P ratio and, consequently, the paste in the bottom of the syringe has a lower L/P ratio than the nominal one, its viscosity being higher and thus being more difficult to inject.

The load/displacement curve of NH_4-MPC showed an early increment of the load needed for the continuous flow of the paste (Figure 6.14). This could indicate that clogging of the syringe aperture occurs, reducing the injectability of the paste. The clogging of the syringe could be attributed to the large particle size of the $NH_4H_2PO_4$ (Figure 6.11).

The displacement reached by the syringe plugger when the force started to increase in third stage of the load/displacement curve (Figure 6.14) matched with the injectability of each material: NH_4+Na-MPC > Na-MPC >> NH_4-MPC (Table 6.5).

It should be mentioned that most surgeons complain that bone cements (*e.g.* calcium phosphate cements, CPCs), are poorly injectable [21]. In contrast, scientists consider CPCs as injectable materials. This discrepancy comes from the fact that the injectability of cements is not clearly defined. In principle, any cement paste can be claimed to be injectable. The question is how injectable it really is [10]. The results of injectability are linked to the experimental setup parameters. The variables that have a higher effect on injectability of the pastes are: the aperture of the syringe, the amount of paste used to start the extrusion and the force limit of the experiment. For instance, if a force limit of 200 N would have been used in this study, which other studies assure that is the normal force that a hand can apply to a syringe [10], the injectability of the MPC formulations would have been higher.

6.5.2.3 Crystalline phases

The end-products after 7 days of immersion in Ringer's solution (Figure 6.15) were the same than those observed in Section 5.4.2.4 and discussed in Section 5.5.3, as expected, since the same initial compounds were used. Briefly, NH_4-MPC and NH_4+Na-MPC formed struvite and a smaller amount of schertelite, and Na-MPC formed an amorphous phase. Unreacted MgO was detected in the three formulations. Borax was not detected by XRD and no phase related with this compound (*e.g.* luneburgite) was observed.

6.5.2.4 Compressive strength

The compressive strength of the MPC formulations (containing 6 wt% borax) after 7 days of immersion in Ringer's solution (Table 6.6) were similar to the values displayed in Figure 5.11, where MPCs were prepared with 3 wt% borax. Nevertheless, the scenario was quite different if comparing the compressive strength of NH_4-MPC after 2 h (Table 6.6). After 2 h, NH_4-MPC containing 6 wt% borax reached a third of the compressive strength (16.0 ± 4.0) that was reached for the NH_4-MPC prepared with 3 wt% borax (48.7 ± 5.6 MPa). The delay on hardening of the MPCs optimized to ensure adequate exothermy at 37°C was associated to the addition of a higher amount of borax, with a finer particle size, and to the longer sinterization time of MgO.

6.5.2.5 Morphology, SSA, skeletal density and porosity

The microstructure of the fracture surfaces of MPCs containing 6 wt% borax (Figure 6.16) were similar to those of the MPCs prepared with 3 wt% borax developed (Figure 5.14). This indicated that the extra addition of borax had no influence in the morphology of the cements.

In contrast, comparing the microstructures of those MPCs containing borax with those prepared without borax, interesting differences were revealed, especially for NH_4-MPC. In NH_4-MPC prepared without borax (Figure 6.16 b), elongated particles were displayed, instead of the glassy phase observed when the samples contained borax (Figure 6.16 a). The morphology of NH_4-MPC without borax was in accordance with that previously reported for schertelite, described as either cuboids or thick plates [22]. The morphology of Na-MPC prepared without borax (Figure 6.16 d) showed an amorphous matrix with some incrusted particles which were probably covered by a glassy layer when borax was included in the powder phase (Figure 6.16 c). Finally, the NH_4+Na-MPC containing borax had a more homogeneous microstructure (Figure 6.16 e) than those containing no borax (Figure 6.16 f).

The glassy layer observed when the MPCs contained borax was associated to the dissolved borax forming an amorphous magnesium borate compound on the surface of the MgO particles, as explained in Chapter 5 (Section 5.5.6).

The skeletal density of NH_4-MPC (Table 6.7) was higher than the expected value for struvite (skeletal density of 1.71 g/cm^3 [23]). This could be associated to a high amount of unreacted MgO (skeletal density of 3.6 g/cm^3 [23]), since 50.8 wt% MgO was added and only 25.9 wt% MgO should react (1 mol MgO should stoichiometrically react with 1 mol of $NH_4H_2PO_4$). A skeletal density of 2.43 g/cm^3 for NH_4-MPC indicated that, theoretically, it contained 61.9 wt% struvite and 38.1 wt% MgO.

The total open porosity of the three MPC formulations was about 30% or lower (Table 6.8), being mainly formed by nanometric pores intrinsically present in the microstructures of cements. However, the total open porosity could be overestimated due to the contribution of superficial cracks (Figure 6.16) —that appeared during the drying process of the samples—, producing pore entrance diameter peaks around 10 μm (Figure 6.17). In fact, no pores of this size were present in the microstructure of the cements.

6.5.3 Antimicrobial assays and anti-biofilm activity

The potential antimicrobial properties of the MPCs were envisaged due to the addition of MgO in excess, a basic compound that could provide the cements with an effect analogous to calcium oxide or alkaline compounds [24–26].

6.5.3.1 Agar diffusion test

The bacterial inhibition of the three formulations was evaluated by the agar diffusion test (Figure 6.18). NH_4+Na-MPC was the formulation that presented the largest inhibition area, followed by NH_4-MPC and, finally, Na-MPC. The size of the inhibition zone is indicative of the pathogen's susceptibility to grow close to the material and, in fact, it is dependent on the diffusion of the solubilized ionic species from the cement through the agar gel [27,28]. In this regard, it must be pointed out that NH_4+Na-MPC, which was the formulation with lower viscosity, was the one that favored more the diffusion of solubilized ions from the cement paste. It is important to note, therefore, that the outcome of this test can be considerably affected by the liquid to powder ratio of the cement paste [27].

6.5.3.2 Growth curves

The antibacterial properties of the fresh- and aged-MPCs were also evidenced by bacterial growth curves performed with broth-cement extracts. While the three bacterial strains incubated in broth grew exponentially with time, their growth remained inhibited or the number of viable bacterial colonies decreased when incubated with **fresh-cement** extracts (Figure 6.19).

For the **fresh-cement** extracts, it could be speculated that the antimicrobial properties of the extracts were directly correlated with their pH (Table 6.10), the slightly acidic pH of NH_4-MPC and NH_4+Na-MPC (pH 6.3 ± 0.4 and 6.5 ± 0.2, respectively) inhibiting the growth of *E. coli* and *P. aeruginosa*, while the alkaline Na-MPC extract (pH 10.1 ± 0.6) slowly killing these bacterial strains (Figure 6.19). However, since the pH of the NH_4-MPC and NH_4+Na-MPC was very close to neutrality, it was questioned whether there could be another factor involved in the antimicrobial properties of the cement extracts.

When bacteria were immersed in **aged-cement** extracts (Figure 6.20), only the Na-MPC formulation (pH 11.9 ± 0.3) reduced the viable bacteria, even though the NH_4-MPC and NH_4+Na-MPC also produced alkaline extracts (pH 9.1 ± 0.4 and 10.4 ± 0.2, respectively). This result suggests that there could be a pH threshold over which the medium turns to be a toxic solution for the three bacterial strains. However, the lack of antibacterial properties of the aged-NH_4+Na-MPC extract, whose pH (pH 10.4 ± 0.2) was even higher than that of the fresh-Na-MPC extract (pH 10.1 ± 0.6) that reduced to zero the viable bacteria, reinforced the hypothesis that in some cases (there was another factor influencing the bactericidal activity of the extracts in addition to the pH.

The fact that the number of viable *A. actinomycetemcomitans* was reduced with time when it was immersed in any of the cement extracts (cements of any formulation, used as either fresh or aged) was associated with a higher sensibility of this strain to slightly alkaline or acidic pHs in comparison with that of the other strains tested.

6.5.3.3 Bactericidal activity

The bactericidal activity test consisted on the quantification of the viable bacteria remaining after their immersion in media free of nutrients for a short period of time (*i.e.* 2 h). The

media used in this assay were free of nutrients (buffer medium ranging between 9 and 11, PBS-extracts and pristine PBS as control) in order to avoid bacterial growth and thus directly associate the reduction of viable bacteria with the bactericidal effect of the extract.

a) pH and osmolarity of the MPCs extracts

The pH values of the extracts (Table 6.11) can be explained by the chemical composition of MPCs. On one hand, MgO is alkaline, although sparsely soluble in water [23,29]. On the other hand, the phosphate salts are acidic and very soluble in water [23]. When the cements were immersed in an aqueous medium, the phosphate salts were dissolved first, thus decreasing the pH of the medium. This explains the lower pH of the fresh-cement extracts than that of the aged-ones. The higher pH of Na-MPC extracts in comparison with that of the ammonium-containing cements could be associated to a faster dissolution of the MgO or of the formed amorphous sodium magnesium phosphate compound, releasing alkaline groups that would increase the pH of the medium.

Both fresh- and aged-cement extracts had statistically significant higher values ($p < 0.05$) of both osmolarity and ionic concentration ([Mg], [P] and [Na]) than that of the pristine PBS (Figure 6.23), showing that the cement released ionic species probably until the saturation of the extract. Moreover, within the extracts, the fresh-cement extracts had a higher osmolarity and also a significantly higher [Mg], [P] and [Na] ($p < 0.05$) than the analogous aged-ones, suggesting that most ions were released during the first 24 h due to the higher solubility of the phosphate salts. This result was in accordance with the lower pH of the fresh-cement extracts than of the aged-ones (Table 6.11).

The high [P] and [Na] found in fresh-cement extracts was associated with the high dissolution of the phosphate salts and the low [Mg] could be attributed to the low solubility of MgO [23], which as long as it was dissolved reacted with the phosphate salts, producing the end-products. It should be noted that the fresh-NH_4-MPC extracts also had a statistically significantly higher ($p < 0.05$) [Na] than the pristine PBS due to the dissolution of the retardant, a sodium tetraborate decahydrate. Interestingly, the osmolarity of the fresh-cement extracts followed the trend NH_4-MPC > NH_4+Na-MPC > Na-MPC, which showed the amount of ionic species that were

released from the cements. In other words, this trend indicated that in the present conditions NH$_4$-MPC was the most soluble formulation, followed by NH$_4$+Na-MPC and, finally, Na-MPC.

b) Bactericidal activity of cement extracts

In order to interpret the bactericidal activity of the extracts, it should be considered that the cements modified both the pH and the osmolarity of the extract. In general, three different situations were found: a) highly alkaline extracts with moderate osmolarity (*e.g.* aged-Na-MPC), b) almost neutral pH extracts with very high osmolarity (*e.g.* fresh-NH$_4$-MPC and NH$_4$+Na-MPC), or c) alkaline extracts with moderate osmolarity (*e.g.* aged-NH$_4$+Na-MPC). The osmolarity was considered to be moderate when it was significantly higher than that of the pristine PBS (285 $\pm$ 1 mOs/Kg).

The bactericidal effects of different pH buffers were evaluated to understand the effect of pH on the bacterial strains under study. In general, the higher was the pH of the extract, the higher was the reduction of viable bacteria for the three bacterial species (Figure 6.22). However, the intensity of this effect differed for each bacterial strain. Specifically, 100 % of *E. coli* was killed at pH 11, 11.3 $\pm$ 8.6% of *P. aeruginosa* survived at the same pH and no *A. actinomycetemcomitans* survived at pH 10.5 or higher. It is interesting to note that *A. actinomycetemcomitans* was the most sensitive strain to pH changes, whilst *P. aeruginosa* was the most robust one [30]. These results were associated with the fact that every microorganism has a definite pH range and a pH optimum for growth, and that although they often grow over wider ranges of pH and far from their optimal one, they have tolerance limits since drastic variations in cytoplasmic pH can harm microorganism's enzymes and membrane transport proteins [27].

Nevertheless, the fact that a buffer solution with pH 10 only killed around 30% of *E. coli* (Figure 6.22), whilst a cement extract with similar pH (*i.e.* fresh-Na-MPC extract, pH = 9.7 $\pm$ 0.1) had 100% bactericidal activity against this bacterial strain (Figure 6.21 a), showed that at certain ranges of pH, the bactericidal effect was not only due to the alkalinity of the medium but that other factors, such as the osmolarity of the medium, could be involved. It is known that bacteria immersed in high osmolarity media may suffer hyperosmotic stress, which stimulates the synthesis of several proteins to maintain the internal osmotic conditions, whilst decreases the synthesis of

several others, as bacteria adjust to the new external environment [31]. Bacteria that cannot adapt to the osmotic changes usually die when their membranes are ruptured due to osmotic pressure. Moreover, it should be highlighted that although single parameters such as pH modification and moderate osmotic conditions might have relatively minor effects to bacteria, their combination can have a profound synergistic effect [32], as reported by Schwan *et al.* for the transcription of specific bacterial genes.

The bactericidal activity tests indicated that the **fresh-Na-MPC** extracts reduced the number of viable bacteria between 98.5 and 100 % of the three bacterial strains (Figure 6.21 a), and the **aged-Na-MPC** ones reduced 100% viable *E. coli* and *A. actinomycetemcomitans*, and 90.8 ± 1.4 % *P. aeruginosa* (Figure 6.21 b). On one hand, the high bactericidal effect of the **fresh-Na-MPC** extract against the three bacterial strains could be associated to the synergistic effect of both its alkaline pH (9.7 ± 0.1) and its moderate osmolarity (755 ± 36 mOs/Kg), which was 2.5-fold times higher than that of pristine PBS (286 ± 0.6 mOs/Kg). On the other hand, the high bactericidal effect of the **aged-Na-MPC** extract against *E. coli* and *A. actinomycetemcomitans* could be mainly related to its very high pH (11.4 ± 0.6), which probably was over the pH threshold that turned the solution into a toxic one for the bacteria under evaluation, by irreversibly damaging the enzymes and the membrane transport proteins of bacteria.

Surprisingly, the **fresh-Na-MPC** extract killed more efficiently the *P. aeruginosa* than the analogous aged-one. This could indicate that, particularly for this bacterial strain that is robust to pH changes of the medium (Figure 6.22) [30], the synergistic effect caused by the high osmolarity and the alkalinity of the extract could be specially potentiated from the side of osmolarity. Therefore, the fresh-cement extract (osmolarity 755 ± 36 mOs/Kg and pH 9.7 ± 0.1) would accentuate the osmotic stress conditions in front to the aged-cement extract (osmolarity 619 ± 96 mOs/Kg and pH 11.4 ± 0.6), reducing the viable bacteria more effectively.

Both **fresh-NH$_4$-MPC** and **fresh-NH$_4$+Na-MPC** extracts significantly reduced (p < 0.05) the population of viable bacteria of the three bacterial strains in comparison the control (Figure 6.21 a), which could be mainly attributed to the very high osmolarity of the extracts (1703 ± 155 and 1171 ± 73 mOs/Kg, respectively), which were 6-fold and 4-fold times that of the pristine PBS. Moreover, the slightly acidic pH (pH 6.3 ± 0.4 and 6.5 ± 0.2, respectively) could also contribute to

the bactericidal potential of the extracts by creating a synergistic effect. The bactericidal activity was even more pronounced for the **aged-NH$_4$-MPC** and **aged-NH$_4$+Na-MPC** for *E. coli* and *A. actinomycetemcomitans* (Figure 6.21 b). This antimicrobial activity was probably due to the synergistic effect of the alkaline pH (9.1 $\pm$ 0.4 and 9.9 $\pm$ 0.5, respectively) and the moderate osmolarity (553 $\pm$ 29 mOs/Kg and 495 $\pm$ 46 mOs/Kg, respectively). The higher efficiency for the aged-NH$_4$+Na-MPC could be associated to the higher alkalinity of this extract (9.9 $\pm$ 0.5), which in the present synergistic conditions could be over the pH threshold of both strains, causing irreversible damages to some of their enzymes and proteins. The number of viable *P. aeruginosa* after incubation with aged-NH$_4$-MPC and aged-NH$_4$+Na-MPC did not change significantly (p > 0.05), since this strain is robust to pH changes [30] and the osmolarity of the extracts was moderate.

6.5.3.4 Bacterial growth curve *versus* bactericidal activity

The growth curve assays (Figure 6.19 and 6.20) and the bactericidal activity tests (Figure 6.21) showed a good correlation regarding the effectiveness of each MPC formulation on the reduction of viable bacteria. It should be highlighted that the growth curve study was performed with broth-extracts and shows a balance between the growth and the death of bacteria, whilst the bactericidal activity test was conducted with PBS-extracts and only reveals the reduction of bacteria, since a medium free of nutrients inhibits bacterial growth.

In general, two different situations were found. In the first situation, the bactericidal efficiency of the cement extracts was about 100% and caused no bacterial growth. This was the case of fresh- and aged-Na-MPC in all bacterial strains and also of fresh- and aged-NH$_4$-MPC and NH$_4$+Na-MPC for *A. actinomycetemcomitans*. In the second situation, the cement extracts significantly reduced the viable bacteria and the bacterial growth was delayed or inhibited. This was the case of fresh- and aged-NH$_4$-MPC for *E. coli* and of fresh-NH$_4$-MPC for *P. aeruginosa*. However, *E. coli* immersed in aged-NH$_4$+Na-MPC extract showed an inconsistent result since its bactericidal effect was 100% but bacteria grew exponentially with time.

For both groups of tests it was observed that the bacterial viability in MPC extracts depended, on one hand, on the pH (Table 6.10 and 6.11) and, on the other hand, on the osmolarity (Figure 6.23) of each extract. The osmolarity and the pH was different for each cement formulation

(osmolarity: NH_4-MPC > NH_4+Na-MPC > Na-MPC; pH: Na-MPC > NH_4-MPC ~ NH_4+Na-MPC) and also depended on the aging time of the cement (osmolarity: fresh > aged; pH: aged > fresh). In most cases, the pH modification and the moderate osmolarity of the extract produced a synergistic effect which efficiently reduced the viable bacteria. In other cases, the pH of the extract was over a pH threshold, killing the totality of bacteria due to the harmful effect for certain enzymes and proteins of bacteria. It should be noted that the pH threshold seemed to be slightly higher for the extracts prepared in broth than for those prepared in PBS, since the bacteria would be able to adapt better in the broth extract.

Moreover, each bacterial strain was differently affected by the mentioned parameters. For instance, *P. aeruginosa* seemed to be more affected by a high ionic concentration than by a high pH, since a higher efficiency to inhibit bacterial growth in broth (growth curve assay) or to kill this strain in PBS (bactericidal activity assay) was observed for the fresh-cement extracts. This could be explained for the robusticity of *P. aeruginosa* to alkaline pHs [30]. In contrast, *A. actinomycetemcomitans* was more sensitive to the modifications of the media than the other two strains, being observed a reduction of viable bacteria with time and also 100% of bacterial death in the bactericidal activity test in any cement extract.

In conclusion, the growth curve and the bactericidal activity assays allowed predicting that, *in vivo*, the alkalinity of Na-MPC would provide the implantation site with bactericidal properties against *E. coli*, *P. aeruginosa* and *A. actinomycetemcomitans*, whilst the NH_4-MPC and NH_4+Na-MPC would provide it with a bacteriostatic effect against the same bacterial strains.

6.5.3.5 Anti-biofilm activity

The anti-biofilm activity showed that the fresh-Na-MPC-extracts reduced the viable biofilm-*P. aeruginosa* almost in their totality, whether fresh-NH_4-MPC and fresh-NH_4+Na-MPC extracts left 8 and 22 % of biofilm-bacteria alive, respectively (Figure 6.24). This data could be correlated with the results after 24 h of the growth curve performed with planktonic *P. aeruginosa* (Figure 6.19 b), where no viable bacteria were found in the Na-MPC extract, and the viable bacteria in fresh-NH_4-MPC and in NH_4+Na-MPC extracts represented about 0.003-0.004 % of the viable bacteria present in pristine broth. However, the population of viable biofilm-bacteria was higher

than that of the planktonic bacteria due to the higher resistance of bacterial communities to antimicrobial substances [33,34].

As previously explained (Section 6.5.3.3), the Na-MPC reduced the population of viable bacteria more effectively than NH_4-MPC and NH_4+Na-MPC. Briefly, the bactericidal activity of this extract was caused by the synergistic effect of both its alkalinity and moderate osmolarity.

6.5.4 Cell viability

The antimicrobial properties observed for the MPCs could consequently compromise the viability of eukaryotic cells. Therefore, cell viability tests were performed in order to evaluate the cytotoxicity of the material to preosteoblastic cells. The cell viability of the extracts (Figure 6.25) allowed evaluating the effect of several factors: the cement formulation (NH_4-MPC, Na-MPC or NH_4+Na-MPC), the cement aging (fresh or aged), the preparation time of the extract (5h or 72h-extract) and the dilution of the extract (1-1, 1-2 or 1-10).

Even though the osmolarity of the extracts prepared with complete medium was not evaluated, it was assumed to be similar to the values found with the PBS-extracts (Figure 6.23). Table 6.13 summarizes the results of cell viability in the undiluted 72 h-cement extracts, which are the most harmful extracts for cells, together with their pH values and their osmolarity.

Table 6.13. Cell viability, pH and osmolarity for the undiluted 72 h-cement extracts prepared in complete medium (except for the osmolarity, which values are from PBS-extracts).

	NH_4-MPC		Na-MPC		NH_4+Na-MPC		Pristine medium
	Fresh	Aged	Fresh	Aged	Fresh	Aged	
Cell viability (%)	0	43.5 ± 7.0	0	0	0	1 ± 0.7	100 %
pH	6.1 ± 0.1	9.0 ± 0.3	10.4 ± 0.1	11.6 ± 0.2	6.9 ± 0.1	10.6 ± 0.3	7.3 ± 0.2
Osmolarity (mOs/Kg)	~ 1700	~ 550	~ 750	~ 620	~ 1170	~ 500	~ 285

As observed in Table 6.13, except for aged-NH_4-MPC extracts, the cell viability was close to zero. This could be ascribed either to the high osmolarity of the extract (1170 – 1700 mOs/Kg) or to

its high alkalinity (pH 10.4 – 11.6), the former case occurring in fresh-cement extracts and the latter in the aged-ones. However, in both cases, the synergistic effect caused by the osmolarity and the pH modification of the extracts would be specifically harmful for the cells. In contrast, the aged-NH_4-MPC extract showed a cell viability over 40 % due to the moderate osmolarity of the extract (~ 550 mOs/Kg) and its slight alkalinity (pH 9.0 ± 0.3).

Looking to the whole cell viability study (Figure 6.25), aged-cement extracts had higher cell viability than the fresh-cement ones. These results suggested that the high osmolarity of the media was a more detrimental factor than their alkalinity, since aged-cement extracts had a higher pH and a lower osmolarity than fresh-ones. However, the cell viability results showed that around 40–70% of cells survived at pH around 9 (*e.g.* aged-5h-NH_4+Na-MPC-extract and aged-72h-NH_4-MPC-extract), but that they did not survive at a pH close to 10 (*e.g.* aged-5h-Na-MPC-extract). These results verified that cells, like bacteria, have a pH threshold over which an irreversible damage is caused to certain enzymes and proteins of cells.

The higher viability of cells in aged-cement extracts than in their fresh-counterparts allowed speculating that, *in vivo*, their cytotoxicity would be reduced with time. This result was also in agreement with a study performed by Ghoddusi *et al.* [35], which showed that the fresh-MTA (cement for endodontic applications) was more cytotoxic than the aged-one.

Cytotoxicity studies performed with MTA have been reported. However, the lack of normalization of these studies makes difficult to compare the results between different works. On one hand, Ko *et al.* [36] showed that the cell viability of MTA extracts (prepared in a surface/volume ratio of 6.3 cm^2/ml) was 25% for MTA set for 1 h or 30% for MTA set for 24 h, and that the cell viability of MTA increased by placing the cement disks in 100% humidity at 37°C for 48 h or more. On the other hand, Ribeiro *et al.* [37] reported only a slight cytotoxicity of MTA, probably due to the low cement/volume ratio of 1000 μg/ml (1 mg/ml) used. This concentration was 850 times lower than the one used in the current study (0.85 g/ml = 850 mg/ml). Ghoddusi *et al.* [35] evaluated the cytotoxicity of MTA with the L929 cell line by preparing extracts of 1 g cement/5 g medium ratio. These extracts, which were evaluated neat and diluted up to 1/100, showed a good biocompatibility of the cement. Nevertheless, it has to be pointed out that the neat extract was already 3.5 times more diluted than the one used in the current study. Finally, it is

important to remark that even though an alkaline root canal filler such as MTA may lead to cell toxicity *in vitro*, successful results in clinical studies have been repeatedly reported [38].

There are also several studies regarding the cytotoxicity studies performed with $Ca(OH)_2$, which has been conventionally used as an inter-appointment dressing material. Cell culture tests using either human periodontal ligament cells, monolayer or multilayer mouse cells have shown calcium hydroxide-based materials to be less toxic compared with zinc oxide eugenol and resin-based sealers [39–43].

6.5.5 Antimicrobial properties *versus* cell viability

It is generally accepted that materials showing antimicrobial properties induce some inflammatory response in the local tissues, while those that do not elicit an inflammatory response are, at best, bacteriostatic. In other words, it is difficult to reconcile both the biocompatibility and the antimicrobial properties of a material, since this would require a high degree of selectivity in the biological response [17]. However, it is essential to avoid a chronic inflammation, which could lead to the loss of the tooth, the opposite of the intended outcome [44]. Therefore, it is important to evaluate the cytotoxicity level of the MPCs and also to determine whether this cytotoxicity decreases with time.

For the purposes of this work, the antimicrobial properties and the cell viability of fresh- and aged-cement extracts were evaluated. The bacteriological assays showed that the extracts of the three fresh- and aged-cement formulations reduced the viable bacteria, Na-MPC doing so in its totality. In general, this antimicrobial effect was fostered by the synergistic effect of the alkalinity and the moderate osmolarity of the extract. As it could be expected, the eukaryotic cells were similarly affected by the cement extracts. However, interestingly, the cell viability was significantly increased for the aged-cement extracts, showing that the cells were more robust to slight alkaline pH (*i.e.* pH ~ 9) than to high osmolarity. The importance of this result relies on the lower cytotoxicity that the cements would have after aging.

Extrapolating these results to a hypothetic situation in which MPCs would be used to obturate an infected cavity, such as a root canal during an endodontic treatment, it could be expected that the cement would kill any remaining microorganism contaminating the wound site

(root canals and microtubules) from the very beginning. Consequently, as a side effect, the tissue in contact with the alkaline cement (apical part) would suffer superficial necrosis that could trigger an inflammatory response. However, after a few days, the material would reduce its cytotoxicity against eukaryotic cells, the inflammation response would decrease, new eukaryotic cells would be able to grow back and, finally, the surrounding tissue would recover. Indeed, commercialized alkaline root canal fillers such as MTA, which led to cell toxicity *in vitro* [36], have shown successful results in clinics [38].

Similarly, epoxy resin sealers guarantee the balance between both antimicrobial properties and biocompatibility due to their short period of antimicrobial activity. These materials are supposed to be toxic only for a short period of time during which the material is reacting, although long enough to kill residual bacteria. After setting, they should not be harmful anymore, leaving time for the surrounding tissues to heal [44].

6.6 Conclusions

The conclusions that can be extracted from this Chapter are the following:

1. MPCs were optimized to avoid tissue-damaging exothermy in physiological conditions by adding 6 wt% of borax and calcining the MgO for 12 h at 1475°C. These modifications performed to the cements did not significantly modify their physico-chemical properties regarding to their crystalline phases, microstructure, mechanical properties, specific surface area, skeletal density and porosimetry after 7 days of immersion in Ringer's solution.

2. The agar diffusion test showed that the three MPC formulations inhibited bacterial growth of *E. coli*, *P. aeruginosa* and *A. actinomycetemcomitans*. However, the obtained results had to be considered as qualitative and dependent on the cement diffusion through the agar.

3. Both fresh- and aged-Na-MPC extracts showed bactericidal properties against *E. coli*, *P. aeruginosa* (as free floating single bacteria or as biofilm) and *A. actinomycetemcomitans*. The antimicrobial potency of this formulation was fostered by the synergistic effect of the elevated pH and the moderate or high osmolarity of the extract.

4. Both fresh-NH$_4$-MPC and NH$_4$+Na-MPC extracts showed bacteriostatic properties against *E. coli*, *P. aeruginosa* and *A. actinomycetemcomitans*, which was associated to the synergistic effect of a high osmolarity and the slight pH modification.

5. Fresh-MPC extracts reduced osteoblastic-like cells viability. However, the cell viability increased by aging the cements, probably due to the lower osmolarity of the resulting extracts.

6.7 Acknowledgements

months later than I did. His experience in microbiology together with his sense of humor also made the daily life in the laboratory more interesting.

A smaller but not less important part of this work was done before my stage. Ana Guadalupe Rodríguez showed me the basics of working with bacteria and helped me performing the first studies. I really want to thank her patience and the knowledge she gave me. The preliminary studies shown in this Chapter were carried out with the very valuable help of Sonia Triviño (Optical Department of the Technical University of Terrassa, Barcelona, Spain). I would like to thank as well Dr. Marisol Marqués for the useful discussions about the possible methods to evaluate the antimicrobial properties of the cements.

6.8 References

[1] Sugama T, Kukacka LE. Characteristics of magnesium polyphosphate cements derived from ammonium polyphosphate solutions. Cement and Concrete Research 1983; 13: 407–416.

[2] Sarkar AK. Phosphate Cement-Based Fast-Setting Binders. Ceramic Bulletin 1990; 69: 234–238.

[3] Seehra S, Gupta S, Kumar S. Rapid setting magnesium phosphate cement for quick repair of concrete pavements – characterisation and durability aspects. Cement and Concrete Research 1993; 23: 254–266.

[4] Yang Q, Wu X. Factors influencing properties of phosphate cement based binder for rapid repair of concrete. Cement and Concrete Research 1999; 29: 389–396.

[5] Wagh AS, Jeong SY. Chemically bonded phosphate ceramics, I: a dissolution model of formation. Journal of the American Ceramic Society 2003; 86: 1838–1844.

[6] Eubank WR. Calcination studies of magnesium oxides. Journal of the American Ceramic Society 1951; 34: 225–229.

[7] Soudée E, Péra J. Influence of magnesia surface on the setting time of magnesia–phosphate cement. Cement and Concrete Research 2002; 32: 153–157.

[8] Dunne NJ, Orr J. Thermal characteristics of curing acrylic bone cement. ITBM-RBM 2001; 22: 88–97.

[9] Moritz AR, Henriques FC Jr. Studies of thermal injury, II: the relative importance of time and surface temperature in the causation of cutaneous burns. The American Journal of Pathology 1947; 23: 695–720.

[10] Bohner M, Baroud G. Injectability of calcium phosphate pastes. Biomaterials 2005; 26: 1553–1563.

[11] Khairoun I, Boltong MG, Driessens F, Planell JA. Some factors controlling the injectability of calcium phosphate bone cements. Journal of Materials Science: Materials in Medicine 1998; 9: 425–428.

[12] Khairoun I, Driessens F, Boltong MG, Planell JA, Wenz R. Addition of cohesion promotors to calcium phosphate cements. Biomaterials 1999; 20: 393–398.

[13] Romieu G, Garric X, Munier S, Vert M, Boudeville P. Calcium-strontium mixed phosphate as novel injectable and radio-opaque hydraulic cement. Acta Biomaterialia 2010; 6: 3208–3215.

[14] Ginebra MP, Rilliard A, Fernández E, Elvira C, San Román J, Planell JA. Mechanical and rheological improvement of a calcium phosphate cement by the addition of a polymeric drug. Journal of Biomedical Materials Research 2001; 57: 113–118.

[15] Cheung G, Ho M. Microbial flora of root canal-treated teeth associated with asymptomatic periapical radiolucent lesions. Oral Microbiology and Immunology 2001; 16: 332–337.

[16] Wade WG, Munson MA, de Lillo A, Weightman AJ. Specificity of the oral microflora in dentinal caries, endodontic infections and periodontitis. International Congress Series 2005; 1284: 150–157.

[17] van Noort R. Endodontic materials. Introduction to dental materials. London: Mosby, Elsevier; 2007.

[18] Slots J. Predominant cultivable organisms in juvenile periodontitis. Scandinavian Journal of Dental Research 1976; 84: 1–10.

[19] Ge X, Wang X. Estimation of freezing point depression, boiling point elevation, and vaporization enthalpies of electrolyte solutions. Industrial & Engineering Chemistry Research 2009; 48: 2229–2235.

[20] Guida A, Towler M, Wall J, Hill RG, Eramo S. Preliminary work on the antibacterial effect of strontium in glass ionomer cements. Journal of Materials Science Letters 2003; 22: 1401–1403.

[21] Ishikawa K. Effects of spherical tetracalcium phosphate on injectability and basic properties of apatitic cement. Key Engineering Materials 2003; 240–242: 369–372.

[22] Abdelrazig B, Sharp J, El-Jazairi B. The microstructure and mechanical properties of mortars made from magnesia-phosphate cement. Cement and Concrete Research 1989; 19: 247–258.

[23] Lide DR, editor. Handbook of chemistry and physics. Boca Raton: CRC Press; 2010. p. 4.43–4.101.

[24] Serraj S, Michaïlesco P, Margerit J, Bernard B, Boudeville P. Study of a hydraulic calcium phosphate cement for dental applications. Journal of Materials Science: Materials in Medicine 2002; 13: 125–131.

[25] Gbureck U, Knappe O, Grover LM, Barralet JE. Antimicrobial potency of alkali ion substituted calcium phosphate cements. Biomaterials 2005; 26: 6880–6886.

[26] Gbureck U, Knappe O, Hofmann N, Barralet JE. Antimicrobial properties of nanocrystalline tetracalcium phosphate cements. Journal of Biomedical Materials Research B 2007; 83: 132–137.

[27] Prescott LM, Harley JP, Klein DA. Microbiology. New York: McGraw-Hill; 2005.

[28] de Souza-Filho FJ, Soares ADJ, Vianna ME, Zaia AA, Ferraz CCR, Gomes BPFDA. Antimicrobial effect and pH of chlorhexidine gel and calcium hydroxide alone and associated with other materials. Brazilian Dentistry Journal 2008; 19: 28–33.

[29] Wagh AS. Magnesium phosphate ceramics. In: Hurst E, editor. Chemically bonded phosphate ceramics: 21st century materials with diverse applications. Amsterdam: Elsevier; 2004. p. 97–111.

[30] Xiong YQ, Caillon J, Drugeon H, Potel G, Baron D. Influence of pH on adaptive resistance of *Pseudomonas aeruginosa* to aminoglycosides and their postantibiotic effect. Antimicrobial Agents and Chemotherapy 1996; 40: 35–39.

[31] Brogden KA, Minion FC, Cornick N, Stanton TB, Zhang Q, Nolan LK, Wannemuehler MJ, editors. Virulence Mechanisms of Bacterial Pathogens. Washington: ASM Press, 2007.

[32] Schwan WR, Lee JL, Lenard FA, Matthews BT, Beck MT. Osmolarity and pH growth conditions regulate fim gene transcription and type 1 Pilus expression in uropathogenic *Escherichia coli*. Infection and Immunity 2002; 70: 1391–1402.

[33] Mah T, O'Toole G. Mechanisms of biofilm resistance to antimicrobial agents. Trends in Microbiology 2001; 9: 34–39.

[34] Drenkard E. Antimicrobial resistance of *Pseudomonas aeruginosa* biofilms. Microbes and Infection 2003; 5: 1213–1219.

[35] Ghoddusi J, Tavakkol Afshari J, Donyavi Z, Brook A, Disfani R, Esmaeelzadeh M. Cytotoxic effect of a new endodontic cement and mineral trioxide aggregate on L929 line culture. International Endodontic Journal 2008, 3: 17–23.

[36] Ko H, Yang W, Park K, Kim M. Cytotoxicity of mineral trioxide aggregate (MTA) and bone morphogenetic protein 2 (BMP-2) and response of rat pulp to MTA and BMP-2. Oral Surgery, Oral Medicine, Oral Pathology, Oral Radiology, and Endodontics 2010; 109: 103–108.

[37] Ribeiro DA, Sugui MM, Matsumoto MA, Duarte MAH, Marques MEA, Salvadori DMF. Genotoxicity and cytotoxicity of mineral trioxide aggregate and regular and white Portland cements on Chinese hamster ovary (CHO) cells in vitro. Oral Surgery, Oral Medicine, Oral Pathology, Oral Radiology, and Endodontics 2006; 101: 258–261.

[38] Roberts HW, Toth JM, Berzins DW, Charlton DG, Mi M. Mineral trioxide aggregate material use in endodontic treatment: a review of the literature. Dental Materials 2007; 4: 149–164.

[39] Beltes P, Koulaouzidou E, Kotoula V, Al E. In vitro evaluation of cytotoxicity of calcium hydroxide-based root canal sealers. Endodontics & Dental Traumatology 1995; 11: 245–249.

[40] Geurtsen W, Leyhausen G. Biological aspects of root canal filling materials – histocompatibility, cytotoxicity, and mutagenicity. Clinical Oral Investigations 1997; 1: 5–11.

[41] Huang FM, Tai KW, Chou MY, Chang YC. Cytotoxicity of resin-, zinc oxide-eugenol-, and calcium hydroxide-based root canal sealers on human periodontal ligament cells and permanent V79 cells. International Endodontic Journal 2002; 35: 153–158.

[42] Vajrabhaya L, Sithisarn P. Multilayer and monolayer cell cultures in a cytotoxicity assay of root canal sealers. International Endodontic Journal 1997; 30: 141–144.

[43] Desai S, Chandler N. Calcium hydroxide-based root canal sealers: a review. Journal of Endodontics 2009; 35: 475–480.

[44] Bergenholtz G, Hørsted-Bindslev P, Reit C. Textbook of endodontology. Singapore: Wiley Blackwell; 2009.

Chapter 7.

Tailoring magnesium phosphate cements for endodontic applications

Table of contents

7.1 Introduction

Any material intended to be used as root canal filling material, apart from being biocompatible, should fulfill other requirements. One of the most essential requirements is to **seal tightly against bacteria**, in other words, to avoid the penetration of bacteria through the material or through the interface between the filling material and the dentin [1]. In order to ensure the sealing, the material has to remain **stable with time** [1–3]. Moreover, the material should have a high **bonding strength**, reducing the risk of bacterial leakage in the interface between the filling material and the root canal. A good bonding strength also ensures the mechanical stability of the root canal filler material during basic functions such as mastication [4].

In summary, the aim of a root filling material is to act as an effective and permanent antibacterial barrier [5]. However, there is still no commercial material that fulfills all the requirements for root canal filling and, for this reason, a combination of two endodontic materials is usually employed [1,6]. Therefore, the concept of using a paste as a unique filling material makes it more appealing since it would be a simple method to fill and seal the root canal.

The magnesium phosphate cements (MPCs), which have been used in civil engineering, are proposed in this Thesis as novel materials for clinical applications. With this aim, the physico-chemical properties of the MPCs have been tailored and their biological properties have been evaluated (Chapter 6). The antimicrobial properties of the MPCs (Chapter 6) allowed pointing them out as potential candidates for endodontic treatments and, specifically, for root canal filling. However, the MPCs should be provided with radiopacity in order to be used in the mentioned applications.

7.2 Objectives

The objectives of this Chapter are the following:

1. To modify the MPC formulations (optimized in Chapter 6) in order to provide them with radiopacity (cements coded as **RAD-MPC**).

2. To characterize the physico-chemical properties of the RAD-MPC.

3. To evaluate some specific properties relevant for endodontic applications:

    i) Stability;

    ii) Dentin-cement bonding strength;

    iii) Sealing ability.

The following schema shows the studies performed in this Chapter.
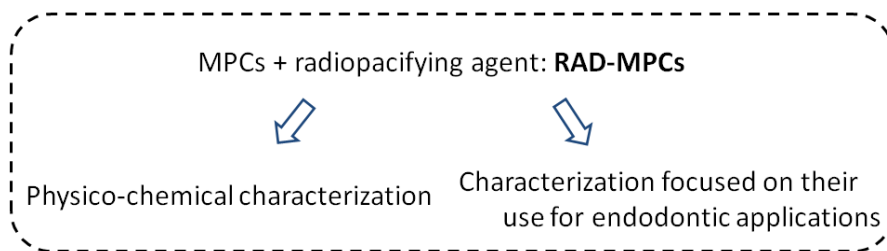
Figure 7.1. Schema of the parts composing Chapter 7.

7.3 Materials and methods

7.3.1 Powder phase

The three magnesium phosphate cement (MPC) formulations optimized in Chapter 6 were further modified to provide the cements with radiopacity. This novel family of cements is coded as RAD-MPC. Briefly, MPC formulations consisted of a combination of magnesium oxide (MgO, Merck, ref. n. 105867) and either ammonium dihydrogen phosphate ($NH_4H_2PO_4$, Panreac, ref. n. 131126.1210), sodium dihydrogen phosphate (NaH_2PO_4, Fluka ref. n. 71496) or an equimolar mixture of the two phosphate salts. A sodium borate decahydrated, $Na_2B_4O_7 \cdot 10H_2O$, known also as borax (Fluka, ref n. 72000), was added as a retardant of the reaction, and bismuth oxide (Bi_2O_3, Sigma Aldrich ref. n. 223891) was included as a radiopacifying agent.

The processing parameters performed to the reactants and their particle size distribution were described in Chapter 6 (Table 6.1). However, the $NH_4H_2PO_4$ was milled more energetically in this Chapter in order to improve its moldeability and its injectability. Fifty g of $NH_4H_2PO_4$ was milled

in a planetary ball mill (Fritsch, Pulverisette 6), using an agate jar and 4 agate balls (ϕ = 30 mm) at 350 rpm during 30 min. The particle size distribution was characterized by laser diffraction (Beckman Coulter LS 13 320) after sonicating the powder in ethanol in order to avoid particle agglomeration. The D_{10}, D_{50} and D_{90} (μm) of the milled powder was 1.97 $\pm$ 0.52, 14.15 $\pm$ 6.32 and 35.89 $\pm$ 8.20, respectively, D_i accounting for the average particle size where i% of the sample volume is smaller than Di. Figure 7.2 shows the particle size distribution of the main reactants of RAD-MPC.
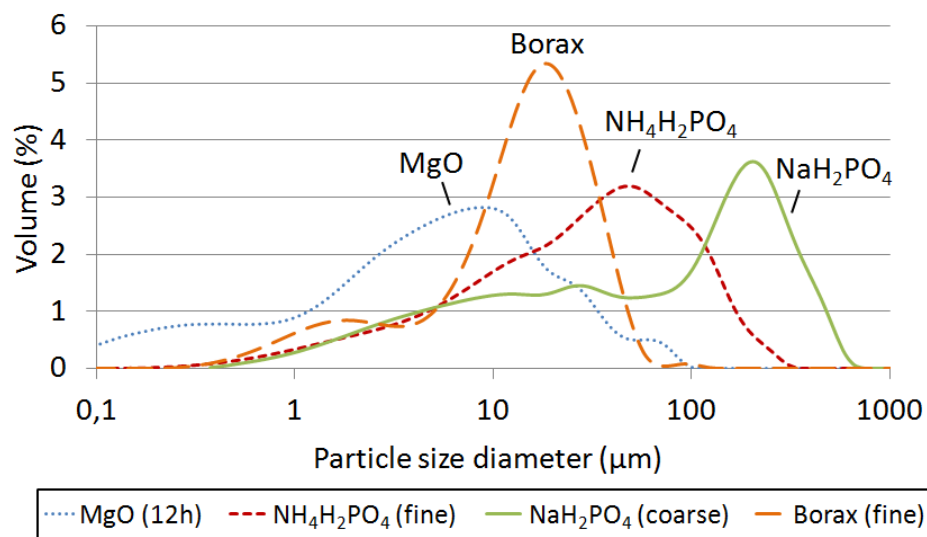
Figure 7.2. Particle size distribution of the processed reactants: MgO sintered at 1475°C for 12 h (milled at 150 rpm for 15 min), $NH_4H_2PO_4$ milled at 350 rpm for 30 min (fine), NaH_2PO_4 milled at 150 rpm for 15 min (coarse) and borax milled at 350 rpm for 30 min (fine).

The Bi_2O_3 was characterized in terms of crystalline phases by X-ray powder diffraction (XRD, PANalytical, X'Pert PRO Alpha-1), of morphology by Field Emission Scanning Electron Microscopy (FESEM, JEOL JSM-7001F) and of particle size distribution by laser diffraction (Figure 7.3). The specific surface area of this compound, which was analyzed by N_2 adsorption (Micromeritics ASAP 2020) following the BET (Brunnauer – Emmet – Teller) theory, was 0.37 $\pm$ 0.15 m^2/g.
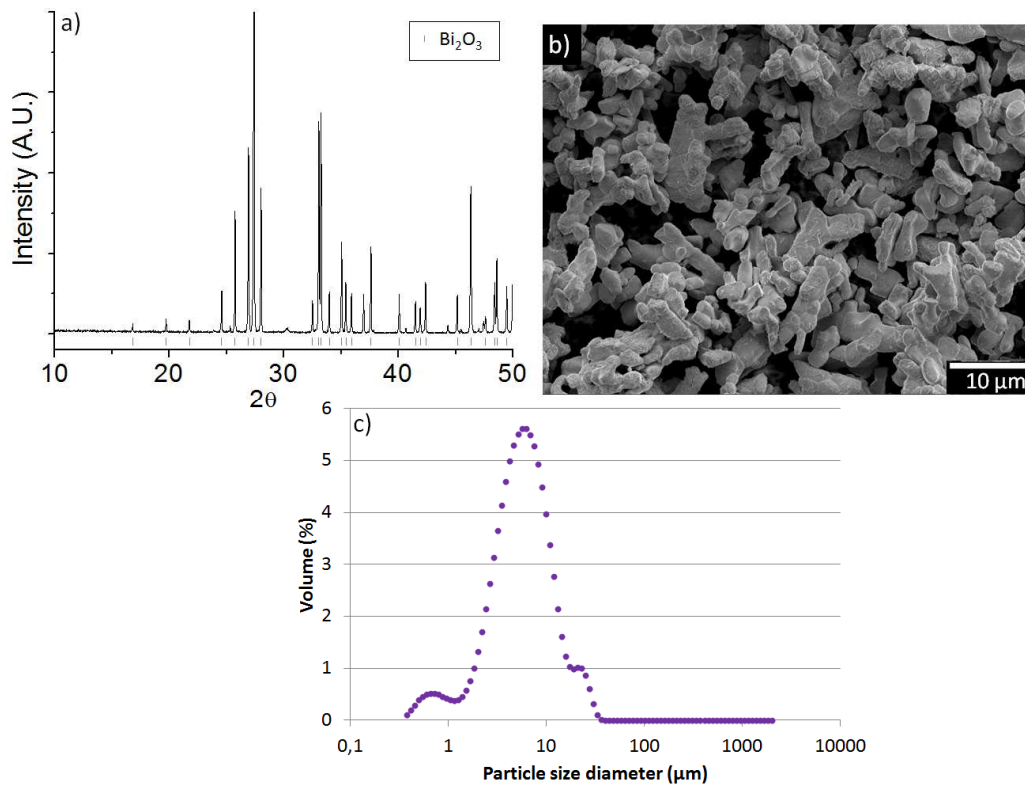
Figure 7.3. a) Characterization of Bi_2O_3: a) XRD, the theoretical position of Bi_2O_3 are indicated, b) morphology and c) particle size distribution.

7.3.2 Cement preparation

The cement was prepared as explained in section 5.3.2, with the difference that Bi_2O_3, which is yellow, was added to the cement powder that after being manually homogenized with a spatula became a matt yellow powder (Figure 7.4 a). Magnesium phosphate cements were prepared by mixing the powder phase with distilled water in a L/P ratio of 0.13 ml/g. The mixture of the powder and the liquid phase gave place to a paste that set within minutes into a solid body (Figure 7.4 b). The resulting cements were named NH_4-MPC, Na-MPC and NH_4+Na-MPC, respectively, accounting for the type of phosphate salt used.
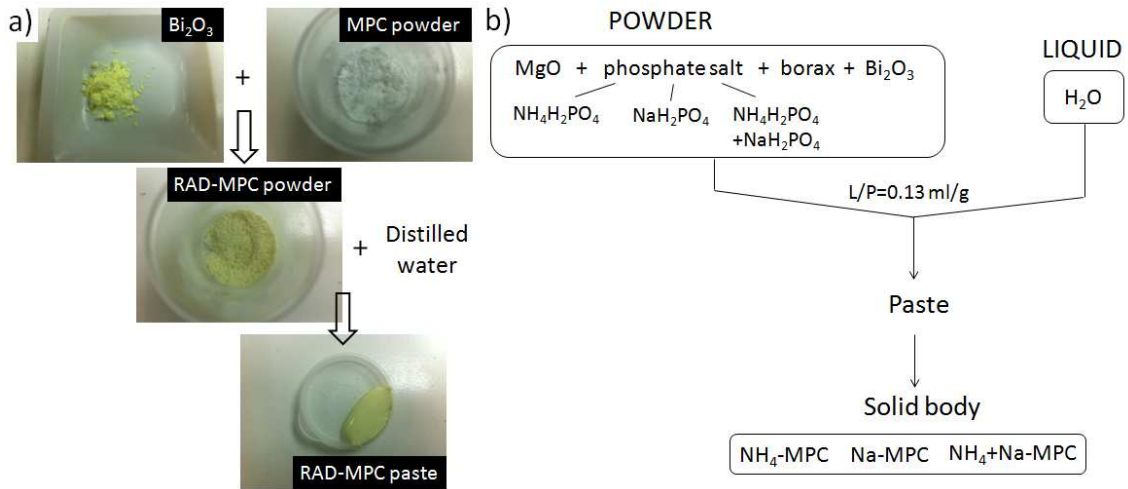
Figure 7.4. a) Appearance of: Bi_2O_3 powder, powder phase of Na-MPC, mixture of Bi_2O_3 with the powder phase, and Na-MPC paste; b) schema in which are shown the reactants that constitute the powder and the process until the hardening of the cement.

The experimental methodology to tune the RAD-MPC formulations consisted on further modifying the MPCs (optimized in Chapter 6) through a two-steps process, as schematically shown in Figure 7.5. Firstly, the amount of Bi_2O_3 needed to produce radiopaque cements was determined and, secondly, the amount of borax required in order to maintain the cements' exothermy within tolerable levels for the surrounding tissues was evaluated.
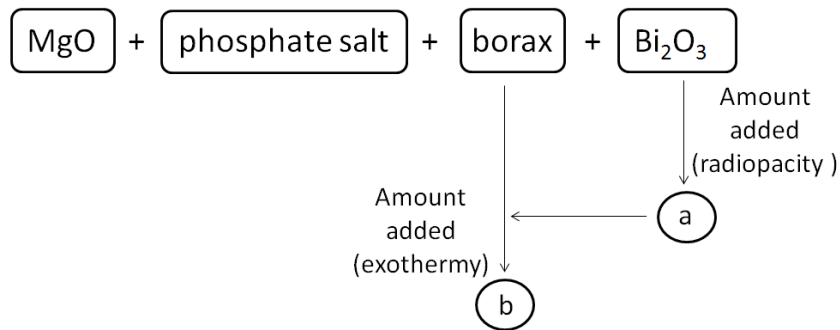
Figure 7.5. Experimental procedure to determine the amount of Bi_2O_3 and borax required to produce MPC cements with appropriate radiopacity and exothermy, respectively.

7.3.3 Radiopacity assessment

The amount of radiopacifying agent (Bi_2O_3) that had to be included in RAD-MPC was determined following the radiopacity criterion established in the UNE-EN ISO 6876 standard ("Dental root canal sealing materials") [7].

7.3.3.1 Sample preparation

Disks of RAD-MPC formulations containing different amounts of Bi_2O_3 were prepared. Since the commercial MTA contains about 16 wt% Bi_2O_3 [8], samples of RAD-MPC were prepared with lower and higher amounts of Bi_2O_3 than that in MTA. Therefore, RAD-MPC disks ($\varnothing$ = 15 mm, thickness = 2 mm) were prepared including 0, 10, 15, 20, 30, 40 wt% Bi_2O_3, and 0 wt% borax. Since the samples thickness is a determinant factor to evaluate the radiopacity, abrasive paper was used to reduce the thickness of each disk to exactly 2 mm.

7.3.3.2 Aluminum standard

The radiopacity of the cement disks was compared with that of an aluminum step-wedge that served as an internal standard for each radiographic exposure (Figure 7.6), as recommended by the UNE-EN ISO 6876 standard [7]. The use of a step-wedge allowed calculating the radiopacity of each sample in terms of equivalent millimeters of aluminum thickness [9].
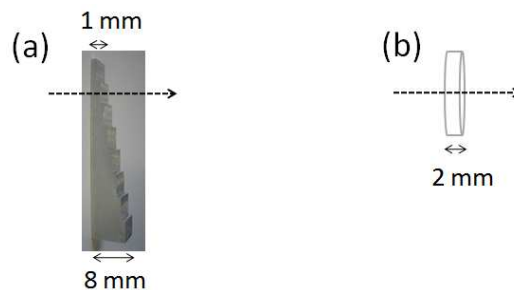
Figure 7.6. Schema in which is represented a X-ray going through a) an aluminum step-wedge and b) a 2 mm-thickness disk.

The aluminum step-wedge had the dimensions indicated in Figure 7.7.

Figure 7.7. Aluminum step-wedge used as a standard of the radiopacity tests. The step-wedge was made at the Mechanical Workshop of the Department of Material Science and Metallurgy of the Technical University of Catalonia.

An aluminum alloy #6082 was used to make up the step-wedge. The impurities contained in this alloy are indicated in Table 7.1.

Table 7.1. Impurities of the aluminum alloy #6082 (wt %).

Al	Cr	Cu	Fe	Mg	Mn	Si	Ti	Zn	Other (total)
95.2–98.3	< 0.25	< 0.10	< 0.50	0.60–1.20	0.40–1.0	0.70–1.30	< 0.10	< 0.20	< 0.15

7.3.3.3 Radiopacity quantification

According to UNE-EN ISO 6876 standard, which reports the required radiopacity for dental root canal sealing materials [7,9], a 1 mm-thickness material is 100 % radiopaque when its optical density on X-ray imaging is that of an aluminum piece of 3 mm-thickness.

The image processing software Adobe Photoshop (CS4 portable) was used to determine the grey scale values (optical density) of the sample regions, as reported by Carvalho-Junior *et al.* [10]. Five regions of the disk were randomly selected to measure their grey scale values. Each region was averaged over an area of 11 x 11 pixels. The radiopacity was quantified from the range of grey levels, which lower value (R = G = B = 0) represented the black color and their higher value (R = G = B = 255) matched with the white one. The level of grey was expressed as means ± standard deviation of R = G = B.

A calibration curve of the grey scale values (0 < R = G = B < 255) of the aluminum step-wedge (thickness from 1 to 8 mm) was created to convert the grey scale (optical density) of the samples to equivalent millimeters of aluminum thickness (Figure 7.8).
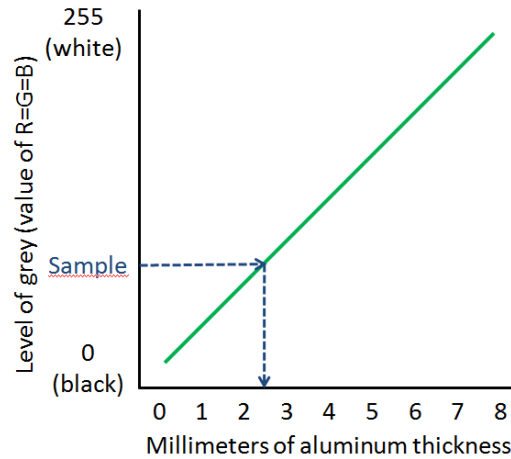
Figure 7.8. Calibration curve of the aluminum standard, and interpolation of the level of grey of a sample to determine the equivalent millimeters of aluminum thickness.

7.3.3.4 X-ray equipment

A portable X-ray unit was used (SATALEC X Mind). Since the size of the radiographies is small (4 x 2.2 cm), the images of the disks had to be taken one by one. The parameters used were: V = 70 kV, I = 8 mA, exposition time: 0.250 s and focal distance between the X-ray source and the samples of 37 cm. Figure 7.9 shows the X-ray cannon in the working position to analyze the radiopacity of a cement disk.
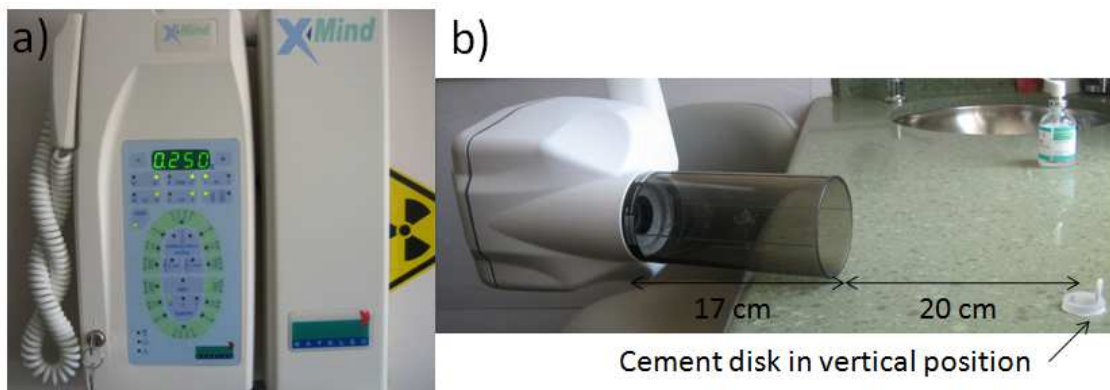
Figure 7.9. a) Portable X-ray unit and b) X-ray cannon 37 cm far from the disk, which was kept in a vertical position in order that the X-rays go through its thickness.

7.3.4 Physico-chemical characterizations of RAD-MPC

After selecting the optimal amount of Bi_2O_3 to have an adequate radiopacity, samples including 0, 1 and 3 wt% borax were prepared and their exothermy and setting times were evaluated, as described in Sections 6.3.3 and 3.3.2.1, respectively. The thermal coefficient was calculated (Section 6.3.3), indicating that only those formulations with a coefficient value lower than 1 were eligible for clinical applications. Both the exothermy and the setting times assays were used to determine the adequate amount of borax that should be added to comply with the clinical requirements. The resulting formulations were coded as **RAD-MPC**.

The three formulations of RAD-MPC were physico-chemically characterized with the techniques detailed in Chapter 5 and 6. The injectability of the pastes was characterized using a mechanical testing machine (Bionix® MTS 370) until the cell load reached 100 N (Section 6.3.4.1). The RAD-MPC formulations were also characterized after different times of immersion in Ringer's solution (0.9 wt% NaCl), in terms of mechanical properties (Section 5.3.4.3), crystalline phases (XRD) including also the card JCPDS # 710465 for Bi_2O_3 [11] (Section 5.3.4.4), morphology and chemical analysis by energy dispersive X-ray spectrometry (Section 5.3.4.5 and 3.3.4.3.4, respectively), specific surface area (Section 5.3.4.6), skeletal density (Section 5.3.4.7) and porosimetry (Section 5.3.4.8).

7.3.5 Specific characterizations for endodontic cements

7.3.5.1 Material stability

The stability of the RAD-MPCs was evaluated in static conditions. Cement disks (Ø = 15 mm, h = 2 mm), which were set in air for 20 min, were soaked in 50 ml of a phosphate buffer solution (PBS, Gibco, ref. n. 18912-014). After 2 h of soaking, the cement disks were weighted, these values accounting for the initial weight (w_0). The disks were maintained immersed in PBS at 37°C for a total period of 60 days, during which the solution was refreshed every 3.5 days. At every time point, the cement was weighted immersed into a fresh PBS solution using an analytical balance (Sartorius BP 211 D). The weight change (%) at every time point was calculated as indicated in Equation 7.1, where w_0 is the specimen's weight after 2 h and w_t is the specimen's

weight at time t. A positive weight change indicated a weight gain, while a negative weight change indicated a weight loss. The study was performed with five specimens for each formulation.

Equation 7.1. $$\text{Weight change } (\%) = \frac{w_t - w_0}{w_0}$$

It is important to highlight that this study was done under more drastic conditions than the actual ones in the root canal (the disk was soaked in a high amount of liquid that was frequently refreshed to avoid the ionic saturation of the medium), with the aim to accelerate the solubilization process of the material.

The pH of the degradation medium was monitored with a pH-meter (Crison MM 41). The pH was evaluated with 5 replicates. The magnesium, phosphorus and sodium concentration, from now on [Mg], [P] and [Na], were quantified using different analytical methods.

a) Quantification of the [Mg]

The [Mg] of the medium was quantified by a complexometric titration [12], specifically a back titration, which is a method commonly used to determine the total hardness of fresh water (combined concentration of Mg^{2+} and Ca^{2+}). Briefly, the Mg ions in the sample were complexed with ethylenediaminetetraacetic acid (EDTA, Panreac, ref. n. 131669). Then, Eriochrome Black T (EBT, Fluka, ref. n. 32751) was added as dye indicator and magnesium chloride hexahydrated ($MgCl_2 \cdot 6H_2O$, Panreac, ref. n. 131356) was used as titrating agent. To ensure an alkaline pH, NH_4Cl/NH_3 buffer was also added. The dye–metal ion complex is less stable than the EDTA–metal ion complex. Therefore, the Mg ions from $MgCl_2 \cdot 6H_2O$ complexed the EBT dye only when all EDTA molecules were already complexed, the dye changing color from blue to pink in the process. The [Mg] were evaluated with 5 replicates. The titration process is schematically shown in Figure 7.10 and the reactants concentration and volumes used are indicated in Table 7.2.
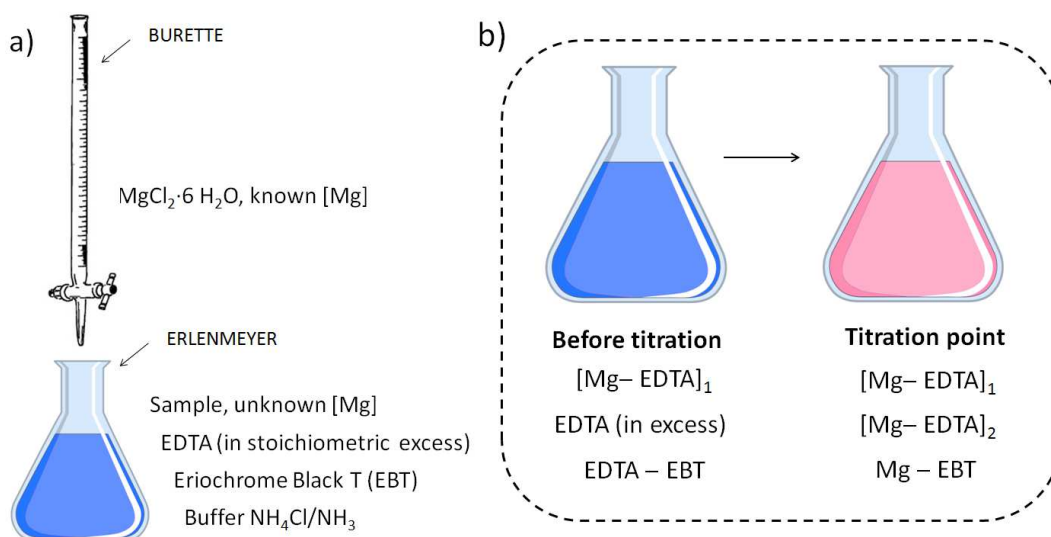
Figure 7.10. a) Schema of the titration process, where the reactants used are indicated, and b) color changes observed during the titration process, the formation of molecular complexes responsible of them are indicated. EBT stands for Eriochrome Black T.

Table 7.2. Concentration and volume of the reactants used for the titration.

Reactant	Concentration, [ ] (mM)	Volume, V (ml)
Sample	Unknown	25
$MgCl_2 \cdot 6\,H_2O$	0.3125 – 0.625	10 – 40
EDTA	5	3 – 9
EBT	28.9	2 – 3 drops
NH_4Cl/NH_3	1300/7330	10

The [Mg] of the sample was calculated knowing that both the Mg ions of the sample and the added Mg ions (as $MgCl_2 \cdot 6H_2O$) reacted with the totality of molecules of EDTA, at this moment the dye changing its color. The [Mg] of the sample was calculated as shown in Equation 7.2, where [EDTA] and [Mg] is the concentration of EDTA and Mg, respectively, and V is the volume of the compound displayed as a subscript.

Equation 7.2.
$$\text{mols Mg}_{\text{sample}} + \text{mols Mg}_{\text{added}} = \text{mols EDTA}$$

$$\text{mols Mg}_{\text{sample}} = \text{mols EDTA} - \text{mols Mg}_{\text{added}}$$

$$[\text{Mg}]_{\text{sample}} \cdot V_{\text{sample}} = [\text{EDTA}] \cdot V_{\text{EDTA}} - [\text{Mg}]_{\text{added}} \cdot V_{\text{Mg added}}$$

$$[\text{Mg}]_{\text{sample}} = \frac{[\text{EDTA}] \cdot V_{\text{EDTA}} - [\text{Mg}]_{\text{added}} \cdot V_{\text{Mg added}}}{V_{\text{sample}}}$$

b) Quantification of [P]

The [P] was quantified by a colorimetric method reported by Chen *et al.* [13]. The experimental procedure consisted on mixing 300 µl of sample with 300 µl of a reagent recently prepared in a 48 well plate. The reagent contained 1 volume of sulfuric acid 6 N, 1 volume of ammonium orthomolybdate 2.5 %, 1 volume ascorbic acid 10% and 2 volumes of distilled water. Briefly, the phosphate groups of the sample reacted with the ammonium orthomolybdate in the acidic solution, and the formed phosphomolybdic acid was reduced with ascorbic acid converting the solutions to blue color (Figure 7.11). The optical density of the colored solution was recorded using a plate spectrophotometer (Biotek, Synergy HT). This optical density was linearly proportional to the concentration of phosphates in the sample. A calibration curve with different concentrations of NaH_2PO_4, which [P] ranged between 10^{-4} and 10^{-6} M, was obtained. The [P] was calculated with 3 replicates of each cement formulation, each of them being quantified in triplicate (n = 9).

(PO$_4^{3-}$, sample)

+

12 (NH$_4$)$_2$MoO$_4$
Ammonium orthomolybdate

(Phosphomolybdic acid, H$_3$PMo$_{12}$O$_{40}$)

H$_3$PMo$_{12}$O$_{40}$
Phosphomolybdic acid

+

Ascorbic acid

PMo$_{12}$O$_{40}^{7-}$ (reduced) **BLUE**

Phosphomolybdate complex

+

(oxydized)

Dehydroascorbic acid
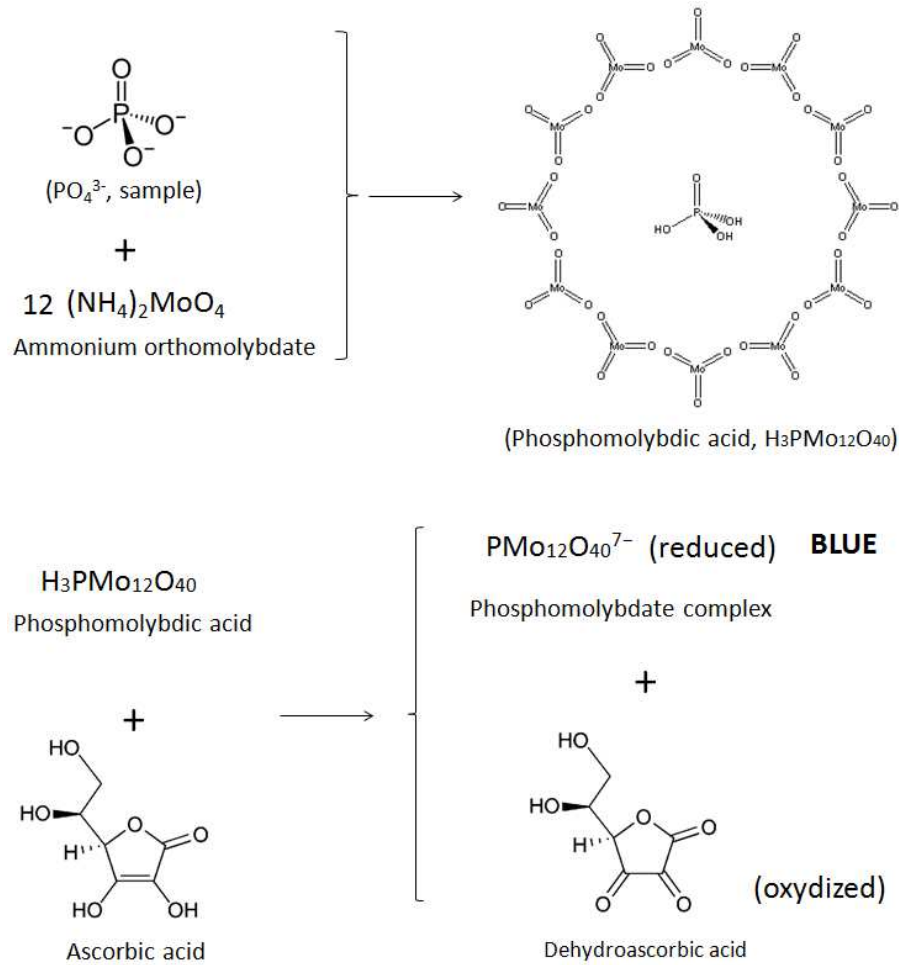
Figure 7.11. Step-reaction in which the ammonium orthomolybdate reacts with phosphate groups to result in a colored phosphomolybdate complex.

c) Quantification of [Na]

The [Na] was measured by means of a selective ion electrode (Ilyte: Ca^{2+}, K$^+$, Na$^+$, pH, Instrumentation Laboratory.

7.3.5.2 Dentin-cement bonding strength (push-out test)

The bonding strength between the cements and the dentin was evaluated by means of a push-out test. This study was performed obturating single-root human teeth with the cements under study. Briefly, the test consisted on pressing the surface of a cement placed in a sliced root canal and quantifying the needed stress to displace the cement from its original position.

It should be underlined that the dentin-cement bonding strength assays are displayed together with the specific characterization for endodontic cements, although this test was not performed with the RAD-MPC formulation, but with the MPCs optimized in Chapter 6. Grey MTA (Dentsply, Pro-root) was used as control.

Human extracted teeth were obtained as clinical waste specimens without identifying data. The project was exempt (exemption #4) from IRB review (University of Minnesota, Minnesota, USA). Before use, every tooth was placed in 5% sodium hypochlorite solution (NaClO) for 1 h for surface disinfection and periodontal ligament removal, followed by storage in 1% NaClO solution at 4°C for a period no longer than 1 month. Every tooth was individually measured with the aim to perform the tests using the coronal third of the root canal (Figure 7.12 a). Then, the teeth were fixed perpendicularly to a glass surface with wax (Figure 7.12 b) and were embedded in resin (Figure 7.12 c). The resin containing the teeth were cut with a low speed diamond saw (Buehler Isomet) through the apical and coronal areas marked previously (Figure 7.12 d).

The root canals were enlarged using Gates Glidden burs mounted using a slow-speed dental handpiece, progressively increasing their diameter until reaching 1.1 mm (Figure 7.12 e). The root canals were irrigated with 17% EDTA solution (a calcium chelating agent) for 2 min to remove the smear layer [14], followed by rinsing with sterile normal saline solution (0.9 wt% NaCl in water) and, finally, root canals were dried with paper points. Each cement was placed into the root canal using a lentulo spiral and was laterally compacted with endodontic pluggers (Figure 7.12 f). A single operator conducted all procedures.

After storing the obturated roots embedded in resin for 24 h in 100% relative humidity, they were sectioned horizontally into 2-mm slices, using a low-speed diamond saw (Figure 7.12 g).
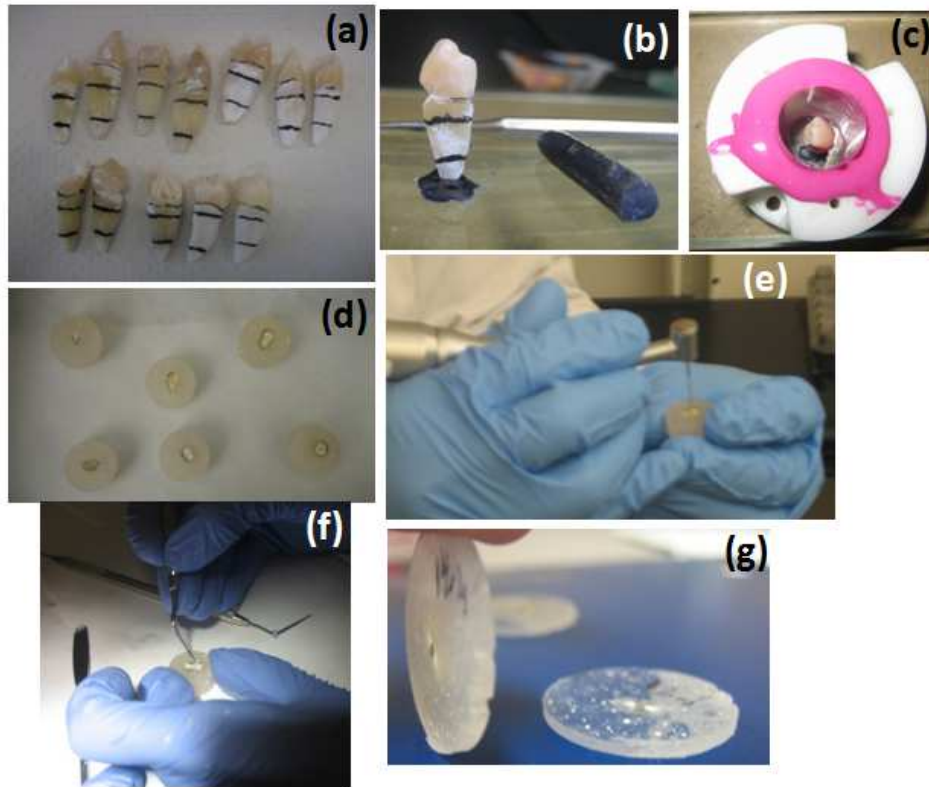
Figure 7.12. Process to prepare the teeth to finally obtain cemented root slices: a) single-root canal teeth with marks for cutting, b) tooth perpendicularly fixed in a glass surface with wax, c) tooth perpendicular to a glass surface and inside a circular mold, prepared for the addition of resin, d) teeth embedded inside resin with their coronal and apical parts cut, e) shaping the root canal to a diameter of 1.1 mm, f) cement obturation into the root canal and g) 2 mm-thickness slices containing the cemented root embedded in resin.

The push-out test was performed in a universal testing machine (Material Test System, TS 810) (Figure 7.13 a). The resin layer containing the cemented tooth was stuck on a steel holder (Figure 7.13 b), the apical part of the root facing up (to avoid blockage due to the root conical morphology) and matching the hole of the holder ($\varnothing$ = 2 mm) with the root canal ($\varnothing$ = 1.1 mm). The steel holder was fixed in the universal testing machine and, finally, a 1-mm diameter pin was used to push the cement perpendicularly at a speed rate of 0.5 mm/min, until the pin was displaced 1 mm (Figure 7.13 c). Figure 7.13 d schematically summarizes the parameters used for the push-out test.
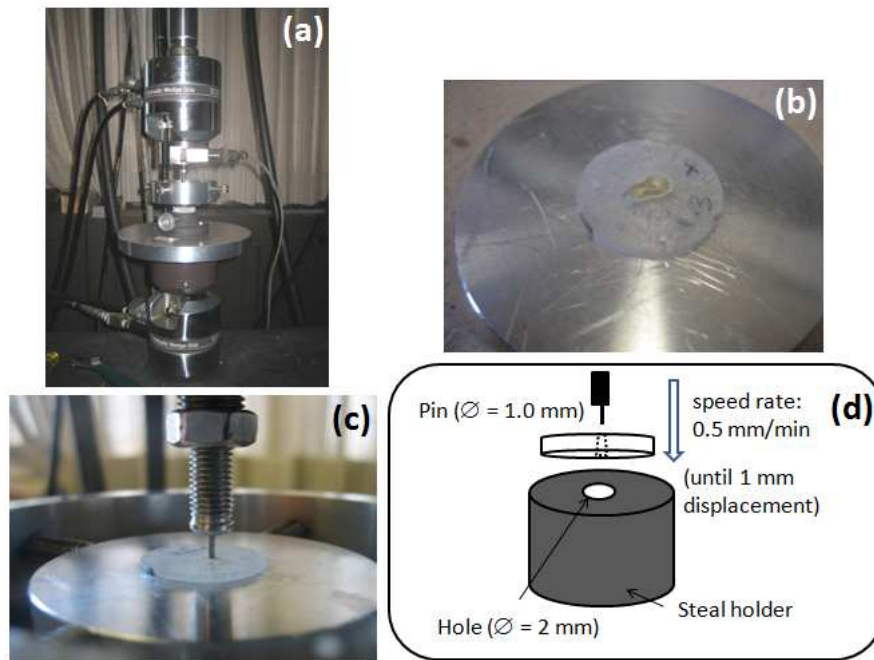
Figure 7.13. a) Universal testing machine to perform the push-out test, b) layer of cemented teeth sticked in the steel holder, c) pin perpendicular to the root slice, pressing into the surface of cement and d) schema of the push-out test where the conditions used are indicated.

The bonding strength (MPa) between the cement and the dentin was determined by a quotient between maximum load (N) and bonding surface (mm^2), as indicated in Equation 7.3. The bonding surface between cement and dentin (Figure 7.14) was calculated as displayed in Equation 7.4, where r is the radius of the cement (mm) and h is the height of the root slice (mm). Twelve specimens were assayed for each formulation.

Equation 7.3. $$\text{Bonding strength (MPa)} = \frac{\text{Maximum load (N)}}{\text{Bonding surface (mm}^2)}$$

Equation 7.4. $$\text{Bonding surface (mm}^2) = 2 \cdot \pi \cdot r \cdot h$$
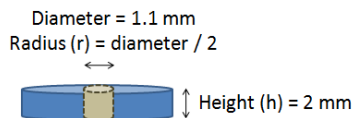
Figure 7.14. Schema that represents a tooth slice which root canal was obturated with cement. The height of the slice was 2 mm and the diameter of the root was 1.1 mm.

7.3.5.3 Sealing ability (microleakage test)

A microleakage test was carried out in order to evaluate the sealing ability of the RAD-MPC. The preparation of the samples and the technique employed in this study are described below.

7.3.5.3.1 Root canal filling

The study was performed with 86 single-rooted human premolar teeth extracted for surgical or periodontal reasons. The selected teeth had similar root length (13.5 ± 2.0 mm) and similar root canal diameter. Teeth with root fractures, root caries or multiple canals were excluded. The teeth were stored in 0.5 % chloramines T (Sigma-Aldrich) at 4°C for preventing bacterial growth, for no longer than one month. Human specimens were obtained with a protocol that was reviewed and approved by the Institutional Ethics Committee (University of Granada, Granada, Spain).

The teeth were decoronated using a low speed diamond saw (Struers, Minitorm) and the root length was standarized to approximately 12 mm. The cleaning and shaping of the root canal was performed as described below. Firstly, Gates Glidden drills (Dentsply International Inc.) size #2 and #3 were used to open the upper third of the root canal system. Secondly, canal patency was achieved with Flex-o-file (Dentsply International Inc.) size #15. Working length was measured and established 0.5 mm shorter than apical foramen. Finally, instrumentation was performed with a crown-down technique using endodontic rotatory nickel-titanium file instruments (Dentsply International Inc.) mounted on a low-speed hand-piece to a size #30. At each instrument change, the intracanals were irrigated with 5.25 % sodium hypochlorite (NaOCl, Panreac) by means of a 27-gauge needle supported in a syringe (Microlance ref. n. 300635). At the end of canal instrumentation, every root canal was irrigated with 17 % EDTA for 3 min (MD-Cleanser, Meta Biomed), a calcium chelating agent that removes the smear layer [14]. A final irrigation with 5.25 % NaOCl, followed with distilled water, was performed. Finally, every tooth was dried with paper points (Dentsply International Inc.). A single operator conducted all procedures.

Teeth were obturated with four different cements: experimental NH_4-MPC, Na-MPC and NH_4+Na-MPC, and grey MTA (ProRoot, Dentsply International Inc.) was used for comparison. MTA cement was prepared with a liquid to powder ratio of 0.33 ml/g, as indicated by the manufacturer [8]. The teeth were randomly divided in 8 groups of 10 teeth each, since the four cement types were applied either as root canal sealers together with gutta-percha, or as root canal fillers without gutta-percha. The cements were introduced into the root using a lentulo spiral [15] [16]. When the cements were applied as sealers, a few gutta-perchas point size #30 were slightly coated with the cement and placed into the canal to working length. Lateral compaction was achieved using endodontic pluggers [17]. When using cements as fillers, the cement was also placed into the canal using a lentulo spiral and was laterally compacted with endodontic pluggers. In both cases, excess of gutta-percha and/or cement was removed from the coronal portion of the root canal and a 3 mm coronally space was created to insert the fluid filtration device. The space was filled with Cavit (3M ESPE) as a provisional restoration [18].

Positive and negative controls were prepared using three teeth for each group. Positive controls were prepared introducing a cotton pellet into the root canals, and negative controls by obturating the teeth with resin AHPlus [19] and gutta-percha. The roots of the negative control were entirely covered with a double layer of varnish in order to ensure their perfect sealing.

X-ray images of each tooth were taken to assess the correct placement of the material along the root canal, as well as to detect the presence of any void in the filling material. Finally, teeth were stored in PBS solution at 37°C for 24h.

7.3.5.3.2 Fluid filtration system

After storing the obturated root canals in PBS for 24 h, the teeth were covered with 2 layers of varnish up to 2 mm of the apical site, in order to seal off any microcrack that they could have. The provisional restoration was removed and the coronal part was fixed on a Plexiglass support (2.1^2 x 0.6 cm) with cyanocrylate adhesive (Rocket, Corona). Previously, the Plexiglass support was pierced and penetrated by an 18-gauge needle (Figure 7.15 a), which was introduced

2 mm into the root coronal portion (Figure 7.15 b). To measure the microfiltration of the obturated roots, the other side of the 18-gauge needle was introduced into an 18-gauge polyethylene tubing (Tygon R-3603) of the fluid filtration system.
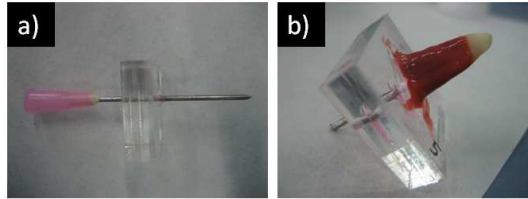
Figure 7.15. Preparation of the fluid filtration system: a) 18-gauge needle pierced in the Plexiglass support, b) coronal part of the tooth fixed on the Plexiglass support, 2 mm of the needle penetrating the root canal.

The fluid flow of the obturated root canal was measured using a liquid flow sensor (Sensirion, ASL 1600), which was connected between the source of hydraulic pressure and the root specimen. A constant hydraulic pressure of 6.86 kPa was generated by suspending a syringe filled with 60 ml of deionized water 70 cm above the sensor. Figure 7.16 a shows a schema of the fluid filtration system and Figure 7.16 b displays the pictures of the system that was actually used.
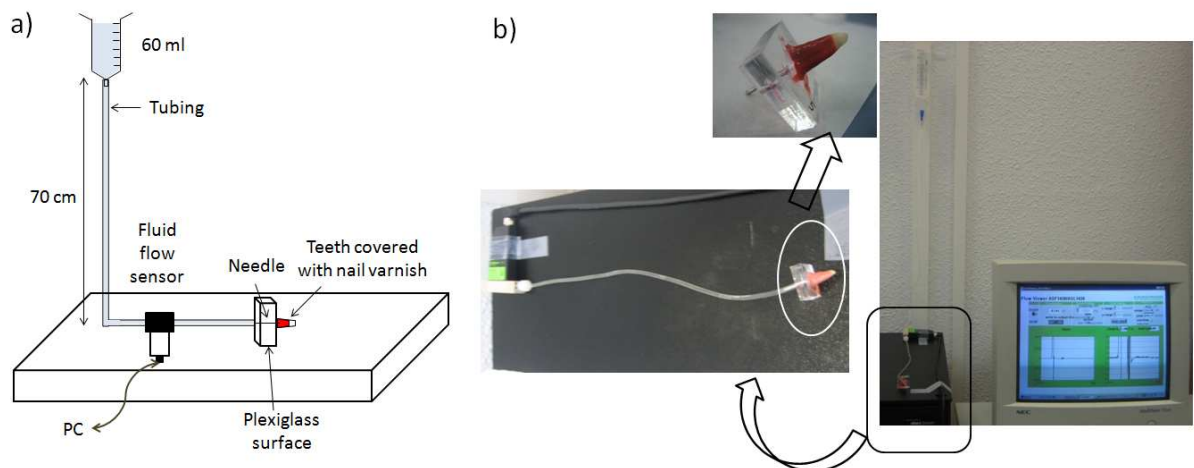
Figure 7.16. a) Schema of the fluid filtration system, b) pictures of the fluid filtration system that was actually used.

The fluid flow rate of every specimen (out of 10 for each formulation) was measured for 30s and repeated 10 times in succession, after 5 min of fluid stabilization. Therefore, n = 100. The fluid flow through the root canal of the specimens was measured at different time periods: 24 and 48 h, 1 and 2 weeks, and 1, 3 and 6 months. During the whole study, the specimens were stored at 37°C in PBS and the medium was refreshed every 2 weeks.

7.3.6 Statistical analysis of the results

A Student's t-test was used to determine the statistically significant differences between the mean values of the experimental groups. A difference between two groups was considered to be significant at $p < 0.05$.

7.4 Results

7.4.1 Radiographic assessment

Figure 7.17 a displays the radiographic image of the aluminum step-wedge, where it can be observed that the thicker was the step, the more radiopaque (whiter) was the X-ray image. The level of grey (optical density) of each step was used to draw the calibration curve of the step-wedge (Figure 17 b).

Aluminum thickness (mm)	R = G = B
1	3.4 ± 0.5
2	32.6 ± 0.5
3	60.8 ± 1.3
4	86.0 ± 1.0
5	110.2 ± 1.5
6	137.0 ± 2.1
7	159.2 ± 1.1
8	177.4 ± 1.1

$$y = 25,045x - 16,879$$
$$R^2 = 0,9966$$
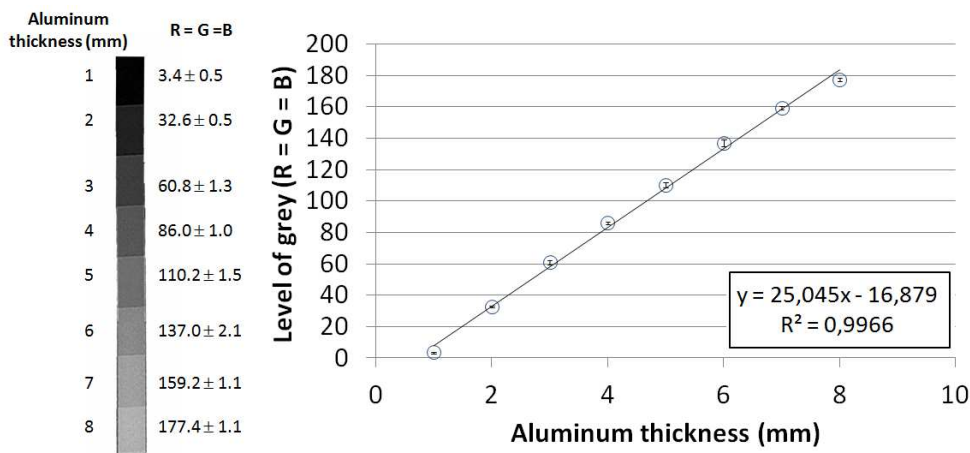
Figure 7.17. a) X-ray image of the aluminum step-wedge, where the level of grey for each step is indicated, b) calibration curve of the aluminum step-wedge. The data and error bars indicate mean ± standard deviation, n = 5.

A linear regression of the calibration curve resulted in Equation 7.5, which was used to determine the equivalent millimeters of aluminum thickness of each sample.

Equation 7.5.
$$\text{Level of grey} = (25.045 \cdot \text{Al thickness}) - 16.879$$

$$\text{Al thickness} = \frac{\text{Level of grey} + 16.879}{25.045}$$

Figure 7.18 shows the X-ray images of the cement disks of the three RAD-MPC formulations prepared with different amounts of Bi_2O_3. It should be noted that the X-ray images of the RAD-MPC disks prepared with $10 - 20$ wt% Bi_2O_3 showed several white dots, which were attributed to conglomerates of the radiopacifying agent.
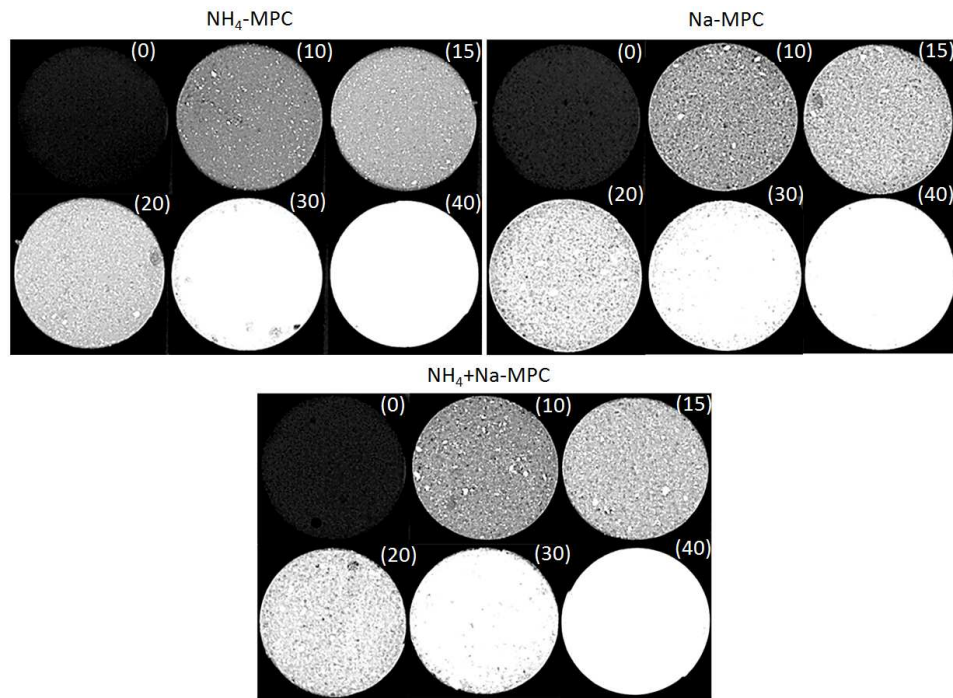
Figure 7.18. a) X-ray images of the specimens prepared with NH_4-MPC, Na-MPC and NH_4+Na-MPC to which different amounts of Bi_2O_3 were added. The amounts of Bi_2O_3 added are indicated on the top right corner of each image in wt%.

The level of grey of each sample was used in Equation 7.5 to determine its equivalent millimeters of aluminum thickness. Figure 7.19 shows the equivalent millimeters of aluminum thickness for each MPC formulation prepared with different amounts of Bi_2O_3. The cement itself, without the addition of Bi_2O_3, had between 1.3 and 1.7 equivalent millimeters of aluminum. The

radiopacity also depended on the formulation and the following trend was observed: Na-MPC > NH$_4$+Na-MPC > NH$_4$-MPC. The radiopacity rose to values between 5.7 and 6.5 equivalent millimeters of aluminum when 10 wt% of Bi$_2$O$_3$ was added and a maximum radiopacity of about 11 equivalent millimeters of aluminum was reached with 30 – 40 wt% Bi$_2$O$_3$.
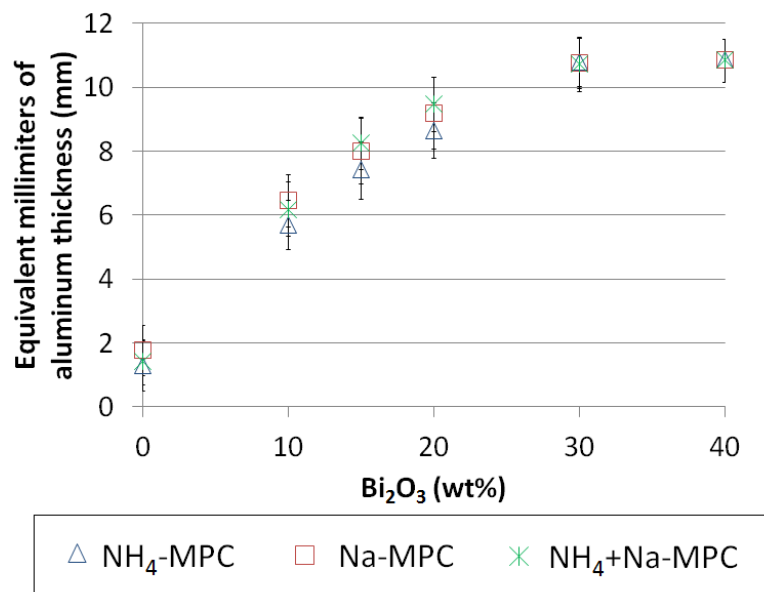
Figure 7.19. Equivalent millimeters of aluminum thickness *versus* amount of Bi$_2$O$_3$ (wt %) added to the cement powder. Error bars indicate the standard deviation, n = 5.

It is important to keep in mind that the equivalent millimeters of aluminum thickness were interpolated from the linear regression done with the aluminum step-wedge, which ranged from 1 to 8 mm. Thereafter, any value of radiopacity higher than 8 equivalent millimeters of aluminum thickness was out of the scale and should be considered as an approximation.

According to UNE-EN ISO 6876 standard [7], a root canal filling material of 1 mm thickness should have a radiopacity of 3 equivalent millimeters of aluminum thickness. Therefore, in the current situation, a disk of 2 mm thickness should have a radiopacity of 6 equivalent millimeters of aluminum. Equation 7.5 was used to calculate the minimal amount of Bi$_2$O$_3$ required for each formulation to comply with the ISO standard. The results indicated that a minimal amount of 11.2, 9.7 and 9.9 wt% should be added to NH$_4$-MPC, Na-MPC and NH$_4$+Na-MPC, respectively. Therefore, an amount of Bi$_2$O$_3$ of 10 wt% was selected since the radiopacity of the ammonium-free and the ammonium-reduced formulations complied with the ISO standard, ensuring that the cement would

be distinguished from hard tissues such as dentin. For comparison, a commercially used cement for root canal filling, MTA, contains around 16 wt % Bi_2O_3 [8].

➤ **10 wt% Bi_2O_3 was selected.**

7.4.2 Assessment of the exothermy and the setting times

The addition of the radiopacifying agent modified physical properties of the cement: the exothermy diminished and the setting times increased. This reduction of the exothermy allowed decreasing the amount of borax (retardant) that had to be added in the RAD-MPCs, in comparison with the MPCs without Bi_2O_3.

In order to determine the amount of borax that had to be added to the RAD-MPCs, the cements were prepared with different amounts of borax, and the exothermy and the setting times were evaluated. Figure 7.20 shows the temperature evolution of the three RAD-MPC formulations prepared with 0, 1 and 3 wt% of borax.
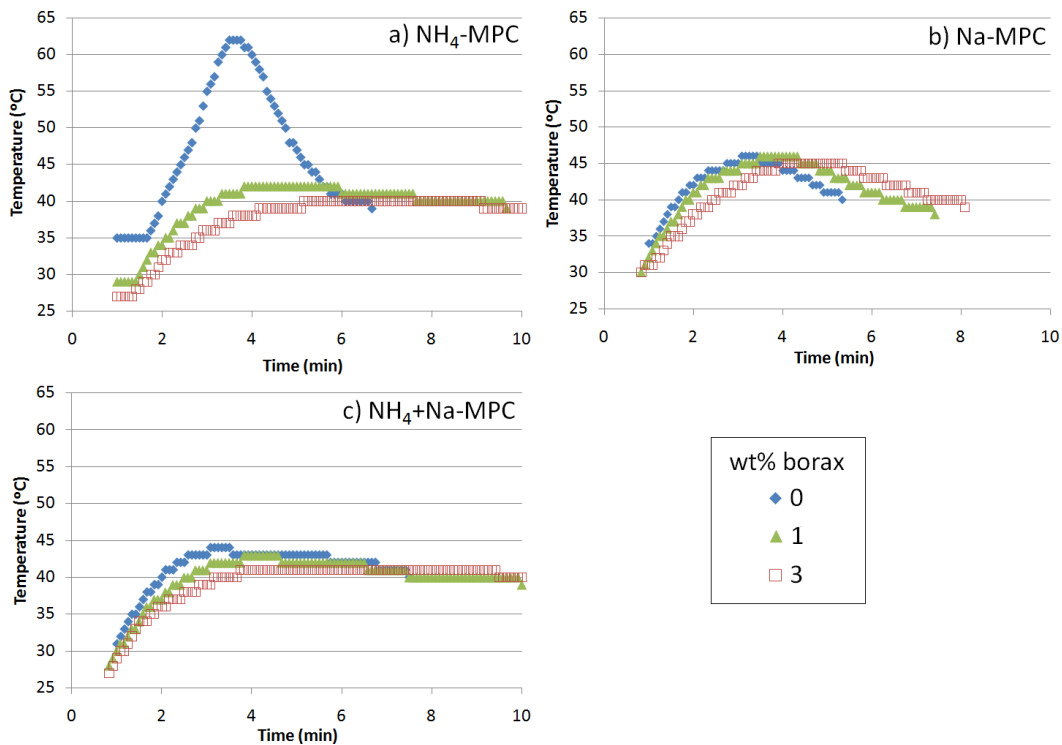
Figure 7.20. Temperature evolution of: a) NH_4-MPC, b) Na-MPC and c) NH_4+Na-MPC prepared with 10 wt% Bi_2O_3, and to which 0, 1 and 3 wt% borax was added.

Table 7.3 shows the thermal coefficients of the three cement formulations prepared with different amounts of borax. A thermal coefficient lower than 1 was required to ensure that the material would cause mild or no damages to the surrounding tissues [20]. Therefore, at least 1 wt% of borax had to be added to the cements, since NH_4-MPC prepared without borax had a thermal coefficient higher than 1.

Table 7.3. Calculated thermal coefficients of NH_4-MPC, Na-MPC and NH_4+Na-MPC containing 10 wt% Bi_2O_3 when 0, 1 and 3 wt% borax was added.

Added borax (wt%)	NH_4-MPC	Na-MPC	NH_4+Na-MPC
0	**> 1**	< 1	< 1
1	< 1	< 1	< 1
3	< 1	< 1	< 1

The initial and final setting times of the three cement formulations containing 10 wt% of Bi_2O_3 and 0, 1 and 3 wt% of borax are shown in Figure 7.21.
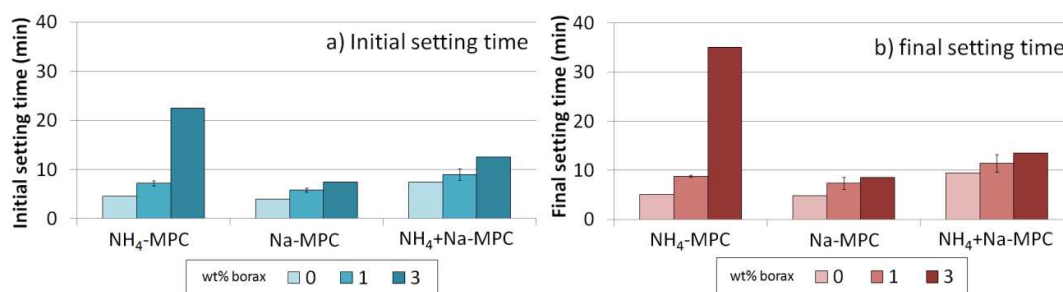
Figure 7.21. a) Initial setting times and b) final setting times of NH_4-MPC, Na-MPC and NH_4+Na-MPC containing 10 wt% Bi_2O_3 when 0, 1 and 3 wt% borax was added to the cement powder. For 1 wt% of borax, the error bars indicate the standard deviation, n = 3.

When no borax was added, both the initial and final setting times were very similar, and the times were short for the three cement formulations (initial setting times were between 4 and 8 min). The addition of 1 wt% of borax increased slightly the setting time of the three cement formulations (initial setting time values between 6 and 9 min). The trend was Na-MPC < NH_4-MPC < NH_4+Na-MPC when 1 wt% borax was added. A 3 wt% of borax increased substantially the setting time of NH_4-MPC, which then had an initial setting time of 22.5 min and a final setting time of 35

min. In contrast, the setting times of the other two formulations increased moderately, that of NH$_4$+Na-MPC more than that of Na-MPC.

An amount of borax of 1 wt% was selected for the continuation of the study because the exothermy of the three cement formulations would not cause any damage to the surrounding tissues and the setting times were adequate for dental applications [21].

➢ **1 wt% of borax was selected.**

From now on, 10 wt% of Bi$_2$O$_3$ and 1 wt% of borax were included to the powder phase of the MPC formulations, which were coded as **RAD-MPC**.

7.4.3 Physico-chemical characterizations of the RAD-MPC

7.4.3.1 Injectability

Figure 7.22 shows the load/displacement curves during extrusion of the RAD-MPC pastes through a 2 mm-aperture syringe. Na-MPC and NH$_4$+Na-MPC showed the typical load/displacement curves of the injectability tests, which contain three relevant stages, as explained in Section 6.4.2.2.

The yield force of Na-MPC was 18 N and that of NH$_4$+Na-MPC was 13 N. Afterwards, the paste was continuously injected when a constant load was applied to the syringe plugger. However, when a small portion of the paste was left inside the syringe, after the piston had been displaced about 7.5 mm for Na-MPC and about 8.0 mm for NH$_4$+Na-MPC, the load start increasing linearly until 100 N was reached, which was the limit load used for this assay. The injectability curve of NH$_4$-MPC had a different pattern than the curve of the other two formulations. After the piston was displaced about 1.0 mm, the load started increasing, until the maximum load was reached. The displacement of the piston when the load started to increase, which was similar for Na-MPC and NH$_4$+Na-MPC and much lower for NH$_4$-MPC, indicated the injectability of the pastes. The lower injectability of NH$_4$-MPC was associated to a major filter pressing occurring for this formulation.
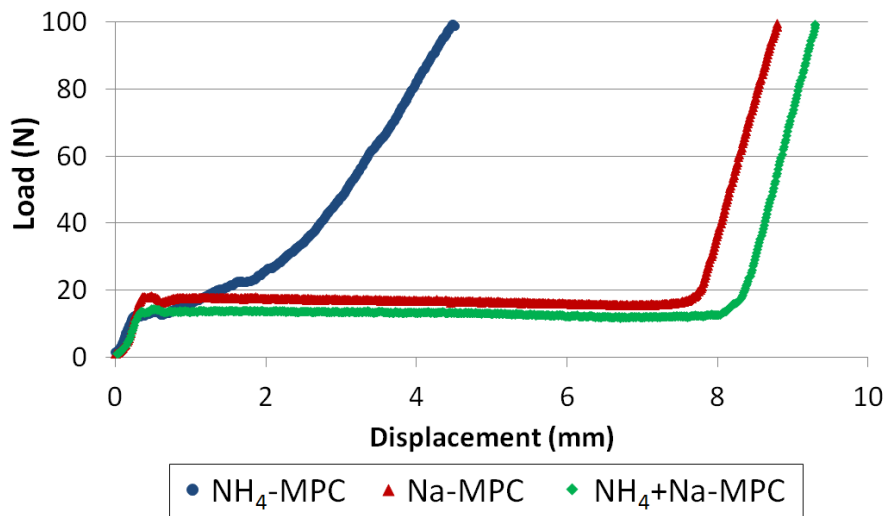
Figure 7.22. Load/displacement curves for the RAD-MPC formulations.

Table 7.4 shows the injectability of the three RAD-MPC formulations. The paste of Na-MPC and that of NH_4+Na-MPC were injected almost totally, with injectability values around 90 %. In contrast, only about 36 % of NH_4-MPC paste was injected.

Table 7.4. Injectability of the three RAD-MPC formulations. The data indicate mean ± standard deviation, n = 3.

NH_4-MPC	Na-MPC	NH_4+Na-MPC
35.8 ± 1.0	88.9 ± 0.6	90.3 ± 0.2

7.4.3.2 Compressive strength

Figure 7.23 shows the compressive strength of the cements after immersion in Ringer's solution for 1 h, 2 h, 1 day and 7 days. The strength evolution of an apatitic CPC is included for comparison [22]. After 1 h of immersion, the RAD-MPC exhibited compressive strength values between 12.3 and 17.2 MPa, in contrast with the 1.2 ± 0.1 MPa of the CPC. After 2 h, there was higher disparity in the compressive strength of the three formulations, with a higher value for NH_4-MPC (33.8 ± 3.0 MPa), followed by NH_4+Na-MPC (23.9 ± 2.4 MPa) and, finally, Na-MPC (17.3 ± 2.1 MPa). The compressive strength of CPC after 2 h was 4.9 ± 0.2 MPa. After 1 day the three RAD-MPC formulations reached their maximum strength. At this time, there were not significant differences (p > 0.05) in the compressive strength of the three formulations, which ranged

between 39.6 ± 3.6 MPa (Na-MPC) and 46.0 ± 6.5 MPa (NH$_4$+Na-MPC). The compressive strength of CPC after 1 day was 32.7 ± 1.8 MPa, slightly lower than that of MPCs. At 7 days the only formulation that showed a significant change on strength was NH$_4$+Na-MPC, which dropped to 31.5 ± 4.4 MPa.
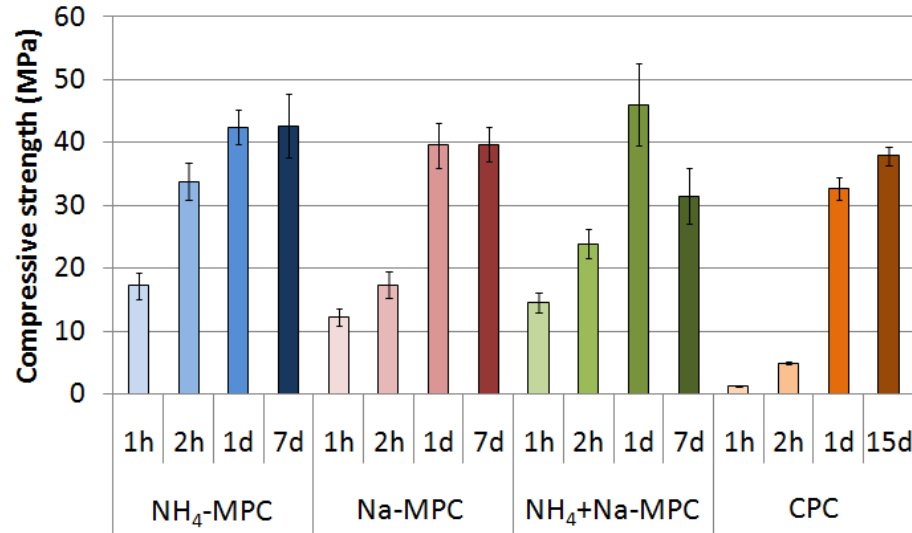
Figure 7.23. Compressive strength of the three RAD-MPC formulations after 1 h, 2 h, 1 and 7 days of immersion in Ringer's solution at 37°C. The strength evolution of a CPC has been included for comparison [22]. The error bars indicate the standard deviation, n = 10.

7.4.3.3 Phase composition

Figure 7.24 shows the evolution of the phase composition of the three RAD-MPC formulations, at time zero (initial powder) and after 1 h, 1 day and 7 days of immersion in Ringer's solution. The spectrum of the cement powder (0 h) showed all the reactants present in each formulation, except for borax, which was added in only 1 wt%. After 1 h of immersion in Ringer's solution, both NH$_4$-MPC and NH$_4$+Na-MPC formulations resulted in struvite and schertelite, which also coexisted after 1 day and 7 days, with a gradual increase of the amount of struvite with time. In contrast, Na-MPC spectra showed a hump centered at 2θ ~ 31° that was associated to an amorphous phase and slightly increased with time. The observation of an amorphous phase was not clear for the NH$_4$+Na-MPC, probably because crystalline peaks masked the presence of the hump. The radiopacifying agent (Bi$_2$O$_3$) was unaltered with time.
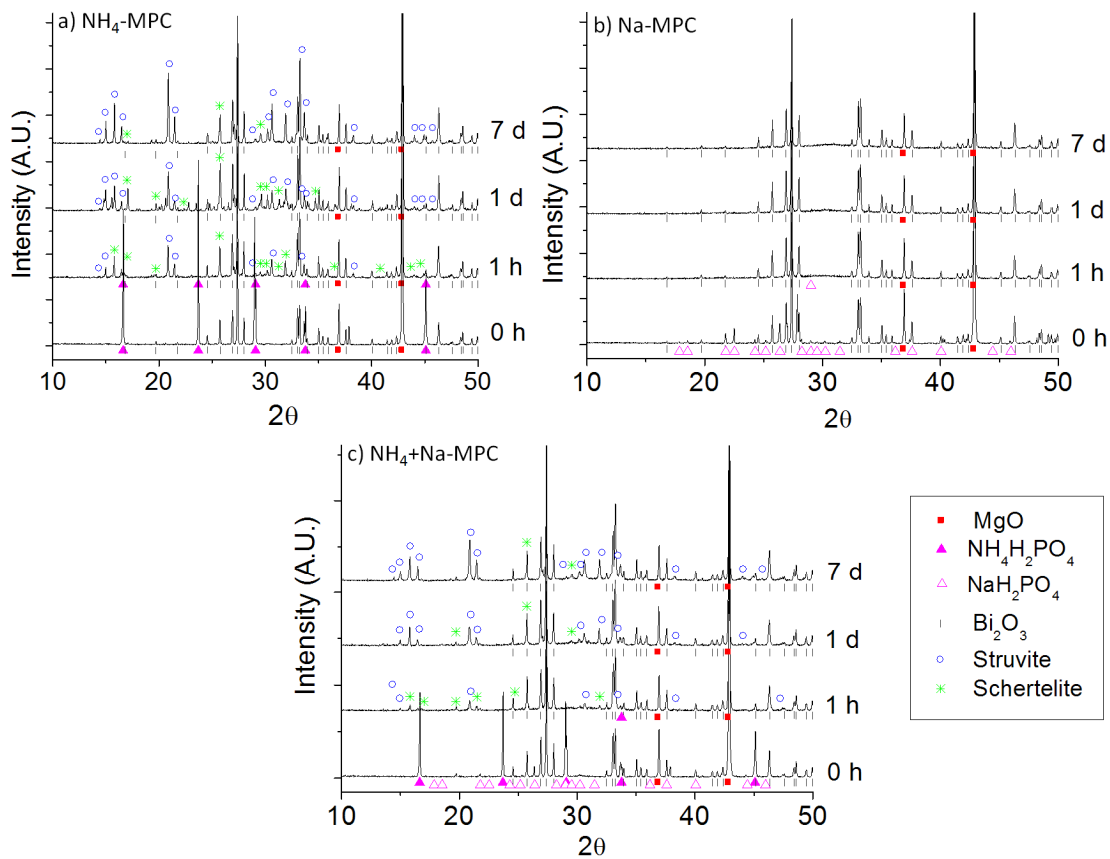
Figure 7.24. XRD of RAD-MPC formulations set for 0 h (initial powder), 1 h, 1 day and 7 days in Ringer's solution at 37°C: a) NH$_4$-MPC, b) Na-MPC, c) NH$_4$+Na-MPC. A.U. stands for arbitrary units.

7.4.3.4 Morphology

Figure 7.25 shows the morphologies at low magnification (40x) of fracture surface of the cements after 7 days of immersion and Figure 7.26 shows the same samples at high magnification (2000x). Some pores of 10–50 μm of entrance size were distributed heterogeneously on the fracture surface of NH$_4$-MPC (Figure 7.25 a). Figure 7.25 b displays some large cracked particles embedded in the matrix of Na-MPC. Finally, NH$_4$+Na-MPC showed a few pores without the presence of embedded particles (Figure 7.25 c).
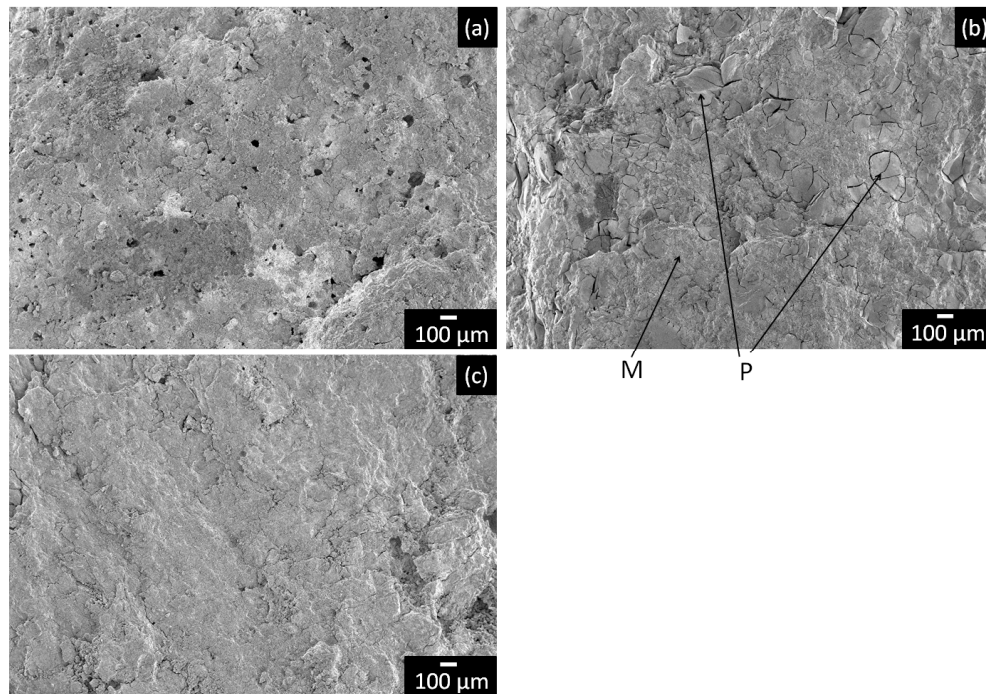
Figure 7.25. Microstructure at 40x of fracture surfaces of the RAD-MPC formulations after immersion in Ringer's solution for 7 days at 37°C: a) NH_4-MPC, b) Na-MPC and c) NH_4+Na-MPC. For Na-MPC, a few particles (P) and the matrix (M) are indicated.

Figure 7.26 shows the microstructure of RAD-MPC after immersion in Ringer's solution for 1 h and 7 days. The microstructures of the three formulations after 1 h were similar, showing a glass-like morphology with some cracks. After 7 days, NH_4-MPC and NH_4+Na-MPC showed elongated particles of different sizes embedded in a glassy-like matrix, being significantly smaller the particles observed in NH_4+Na-MPC. The morphology of Na-MPC was a flat and cracked surface. The presence of Bi_2O_3 (morphology of Bi_2O_3 is shown in Figure 7.3) was not clearly distinguished.
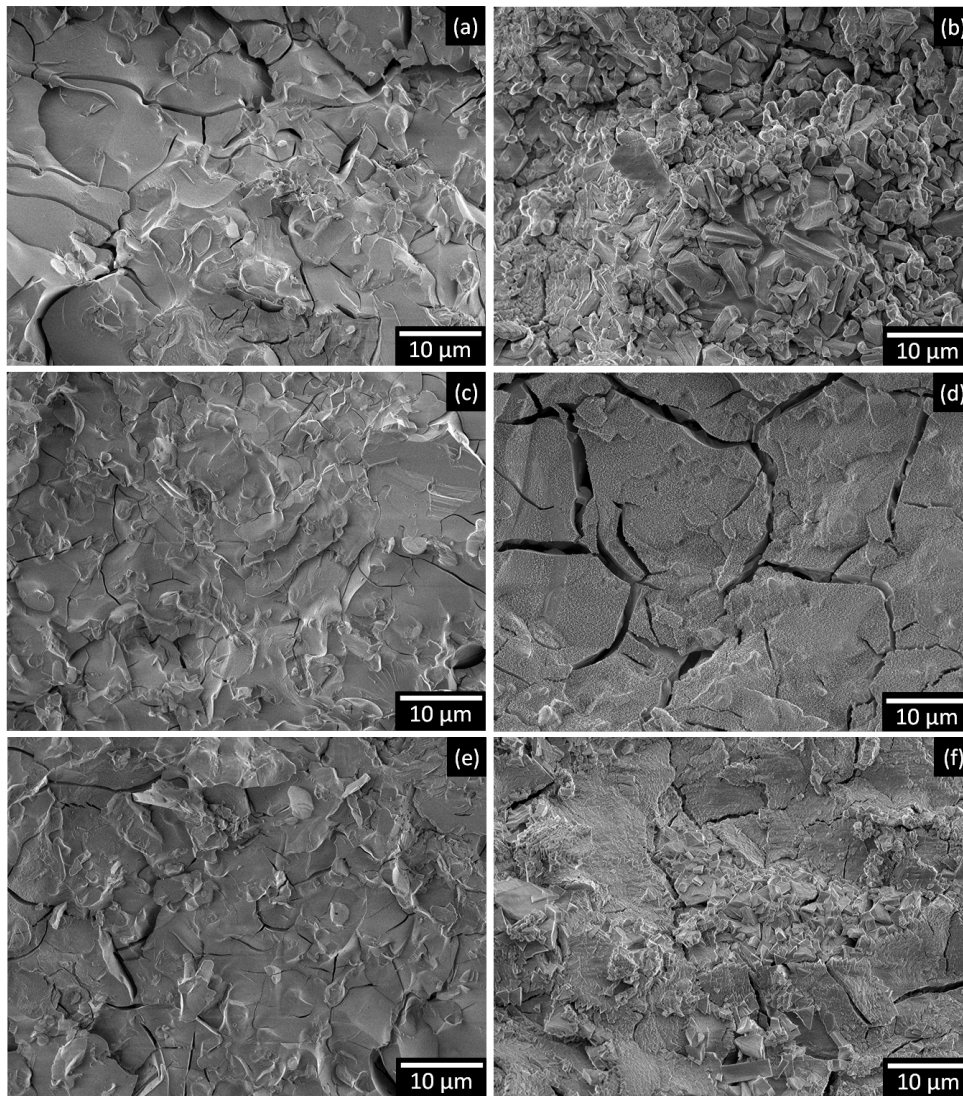
Figure 7.26. Microstructure at 2000x of fracture surfaces of the RAD-MPC formulations after immersion in Ringer's solution for 1 h at 37°C: a) NH$_4$-MPC, c) Na-MPC and e) NH$_4$+Na-MPC, and for 7 days: b) NH$_4$-MPC, d) Na-MPC and f) NH$_4$+Na-MPC.

Table 7.5 shows the chemical analysis of fracture surfaces of the RAD-MPC formulations after 1 h and 7 days. For Na-MPC (Figure 7.25 b), the chemical analysis was performed focusing separately on the particles (coded as P) and on the matrix (coded as M). Without taking into consideration the particles found in Na-MPC, it can be generalized that the matrix of three RAD-MPC formulations had 34–42 wt% Mg, 26–41 wt% P and 7–13 wt% Bi. NH$_4$-MPC and NH$_4$+Na-MPC had 8–18 wt% N, and Na-MPC and NH$_4$+Na-MPC had 4–15 wt% Na. In contrast, the particles embedded in Na-MPC contained a lower amount of Mg and Bi, and higher amount of P and Na than the matrix.

Table 7.5. Chemical analysis (EDS) of the fracture surfaces of the three RAD-MPC formulations after 1 h and 7 days in Ringer's solution. M stands for matrix and P for particle, which is indicated in Figure 7.25 b. The chemical composition of the initial powder of each formulation is included for comparison. The standard deviation associated to the technique is $\pm$ 2%.

Formulation	Time	Elements (wt%)				
		Mg	P	N	Na	Bi
NH$_4$-MPC	Powder	61.2	20.5	9.3	–	9.0
	1 h	38.5	36.0	15.6	–	9.9
	7 d	33.7	41.2	18.0	–	7.1
Na-MPC	Powder	57.7	19.3	–	14.4	8.6
	1 h (M)	42.2	25.6	–	18.8	13.4
	1 h (P)	13.6	45.2	–	33.0	8.2
	7 d (M)	37.9	31.0	–	23.1	8.0
	7 d (P)	28.9	40.8	–	29.1	1.2
NH$_4$+Na-MPC	Powder	59.4	19.9	4.6	7.2	8.8
	1 h	36.3	30.8	9.0	11.9	12.0
	7 d	39.1	36.6	7.6	8.3	8.3

7.4.3.5 Specific surface area, skeletal density and porosimetry

Table 7.6 shows the specific surface area (SSA) and the skeletal density of the three RAD-MPC formulations immersed in Ringer's solution for 7 days. The trend of the MPC formulations for SSA (NH$_4$-MPC > NH$_4$+Na-MPC > Na-MPC) was the opposite than for the skeletal density (Na-MPC > NH$_4$+Na-MPC > NH$_4$-MPC).

Table 7.6. Specific surface area (SSA, m^2/g) and skeletal density (g/cm^3) of the three formulations of MPC after 7 days of immersion in Ringer's solution. The average $\pm$ standard deviation is shown, n = 2.

	SSA (m^2/g)	Skeletal density (g/cm^3)
NH$_4$-MPC	30.37 $\pm$ 0.09	2.65 $\pm$ 0.07
Na-MPC	1.38 $\pm$ 0.01	2.77 $\pm$ 0.01
NH$_4$+Na-MPC	13.68 $\pm$ 0.04	2.71 $\pm$ 0.02

Figure 7.27 shows the distribution of the entrance pore size diameter for the three RAD-MPC formulations immersed in Ringer's solution for 7 days. NH$_4$-MPC had a bimodal distribution,

with a wide peak around 6.5 µm and a very sharp one centered at 32 µm. Both Na-MPC and NH$_4$+Na-MPC formulations had a unique peak around 7 µm. NH$_4$+Na-MPC showed another peak around 250 µm that was associated to the cracks appearing in the material during the drying process, as observed in Figure 7.26 f.
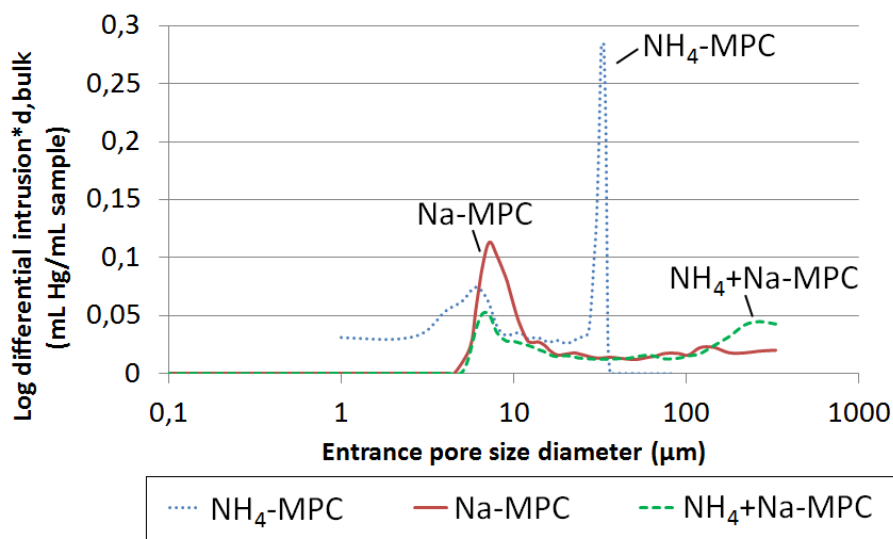
Figure 7.27. Distribution of the entrance pore size diameter of NH$_4$-MPC, Na-MPC and NH$_4$+Na-MPC after being immersed in Ringer's solution for 7 days at 37°C.

Table 7.7 shows the total open porosity of the three RAD-MPC formulations after 7 days of immersion in Ringer's solution. The total open porosity of the three formulations was lower than 11.0 %, following the trend NH$_4$-MPC > Na-MPC > NH$_4$+Na-MPC.

Table 7.7. Total open porosity of the three RAD-MPC formulations after 7 days of immersion in Ringer's solution.

NH$_4$-MPC	Na-MPC	NH$_4$+Na-MPC
11.0	5.0	4.2

7.4.4 Specific characterizations for endodontic cements

In the following section, the results of the characterizations performed to the RAD-MPC with the aim to determine if these cements could be applied in endodontic applications are

described. Specifically, the stability with time, the bonding strength to dentin and the sealing ability of the cements were evaluated.

7.4.4.1 Material stability

In the degradation study, the weight of each specimen was monitored every 3.5 days and the weight change was calculated (Figure 7.28). After 1 day, NH$_4$-MPC, Na-MPC and NH$_4$+Na-MPC increased their weight about 0.8, 1.8 and 3.3 wt%, respectively. However, after this time, the weight of NH$_4$-MPC and Na-MPC started decreasing continuously. The weight remained constant between 14 and 35 days for NH$_4$-MPC and between 14 and 42 days for Na-MPC. Afterwards, both formulations dropped their weight slightly and, finally, they remained again stable with time until the end of the study. NH$_4$+Na-MPC maintained the reached weight after 1 day stable for the initial 21 days and, afterwards, it decreased slightly with time. After 60 days, the weight loss was 4.3 $\pm$ 0.6, 5.2 $\pm$ 0.8 and 2.4 $\pm$ 1.6 wt% for NH$_4$-MPC, Na-MPC and NH$_4$+Na-MPC, respectively. Significant differences were only found between the Na-MPC and the NH$_4$+Na-MPC.

Figure 7.28. Weight change of the three MPC formulations immersed in PBS solution for 60 days at 37°C, the medium being refreshed every 3.5 days. Error bars indicate the standard deviation, n = 5.

The three MPC formulations released Mg ions continuously with time (Figure 7.29 a). For the initial 24 days, the trend of [Mg] was NH_4-MPC > NH_4+Na-MPC > Na-MPC, although the fast increasing release of Mg ions of NH_4+Na-MPC led to a similar [Mg] than that of NH_4-MPC after 24 days. After 28 days, the continuous release of Mg ions by both Na-MPC and NH_4+Na-MPC formulations produced a constant [Mg] with time and, in contrast, NH_4-MPC tended to decrease the [Mg] with time.

After 3.5 days, the three MPC formulations released phosphate ions, causing a [P] of 21.3 ± 2.1, 30.2 ± 2.7 and 14.7 ± 0.9 mM for NH_4-MPC, Na-MPC and NH_4+Na-MPC, respectively (Figure 7.29 b). However, after 7 days, whilst NH_4-MPC still released P ions causing a slightly higher [P] than that of PBS, Na-MPC and NH_4+Na-MPC did not significantly modify the [P] of PBS (Figure 7.29 b). At longer times, no significant release of P ions was detected.

For the initial 31 days, both Na-MPC and NH_4+Na-MPC released Na ions producing a [Na] slightly higher than that in PBS (Figure 7.29 c). Afterwards, the [Na] of media remained similar to that in PBS, showing that the cements did not release Na ions anymore.

Finally, during the whole period of study, the three MPC formulations increased the pH of PBS medium from 7.4 to around 8.5 (Figure 7.29 d). The general trend observed was that Na-MPC increased the pH slightly less than the other two formulations and, after 35 days, NH_4-MPC was the formulation that most increased the pH.
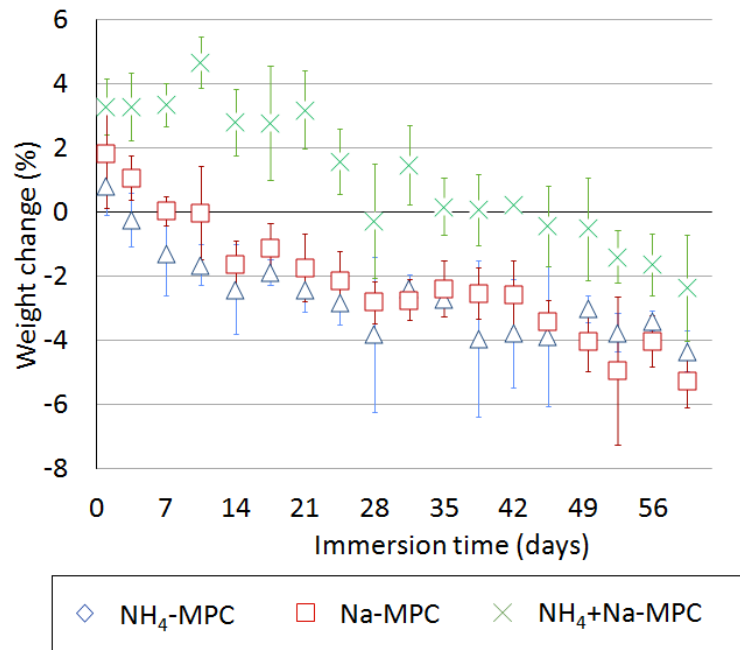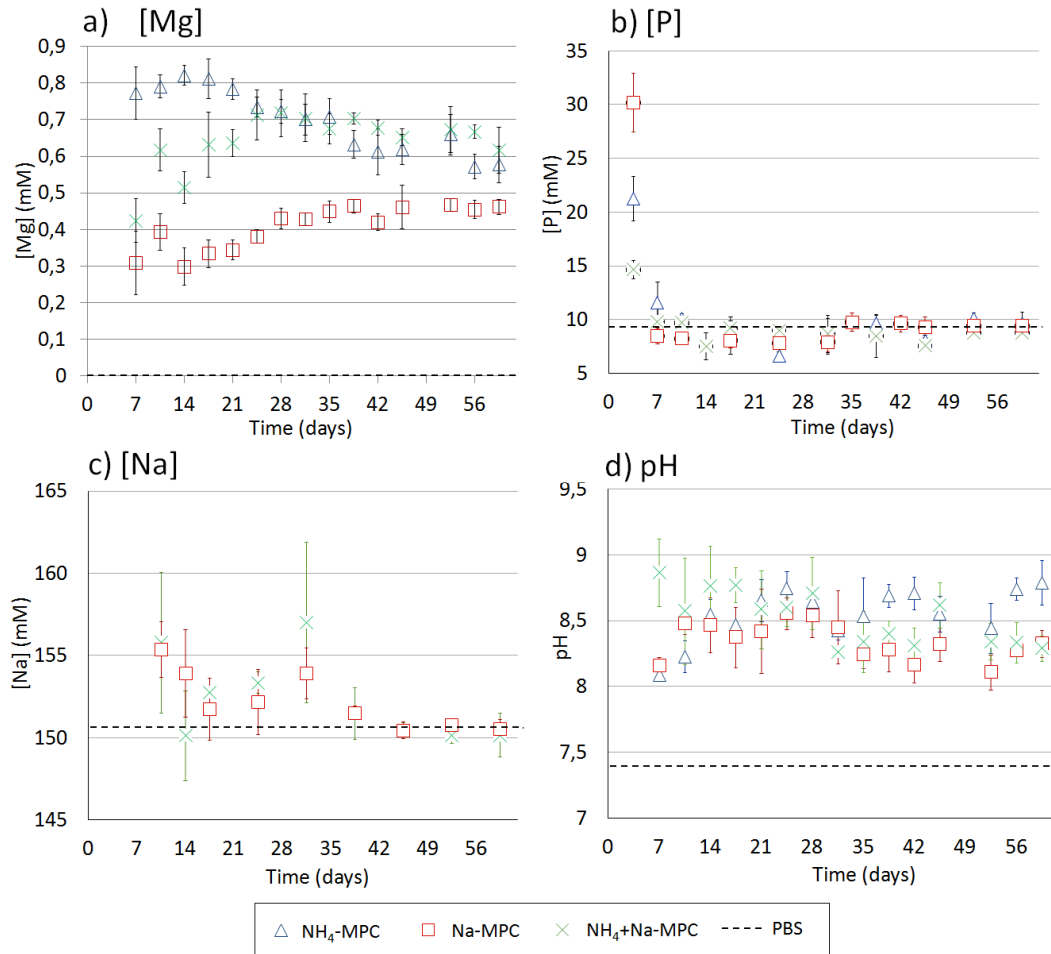
Figure 7.29. Degradation study in which the three RAD-MPC formulations were immersed in PBS solution for 60 days at 37°C, the medium being refreshed every 3.5 days: a) [Mg], b) [P], c) [Na] and d) pH. The dash lines indicate the concentrations or pH of pristine PBS. Error bars indicate the standard deviation, n = 5 for a, c and d, and n = 9 for b.

7.4.4.2 Dentin-cement bonding strength (push-out test)

First of all, it should be highlighted that this study has been included in this Chapter because the dentin-cement bonding strength is a characterization specific for materials aimed to be used for endodontic applications. Nevertheless, the family of MPCs optimized in Chapter 6 was used, which contained 6 wt% borax and 0 wt% Bi_2O_3.

Figure 7.30 shows the surface of tooth slices after the root canal was obturated with Na-MPC, observed with an optical microscope (Olympus MVX10) at different magnifications.
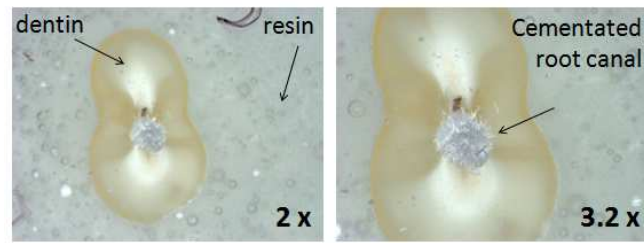
Figure 7.30. Images of root slices with the root canal cemented with Na-MPC, observed with an optical microscope (the magnifications applied are indicated in every picture).

Figure 7.31 shows the images of the three MPC formulations and the control (grey MTA) filling the root canal, viewed with the optical microscope.
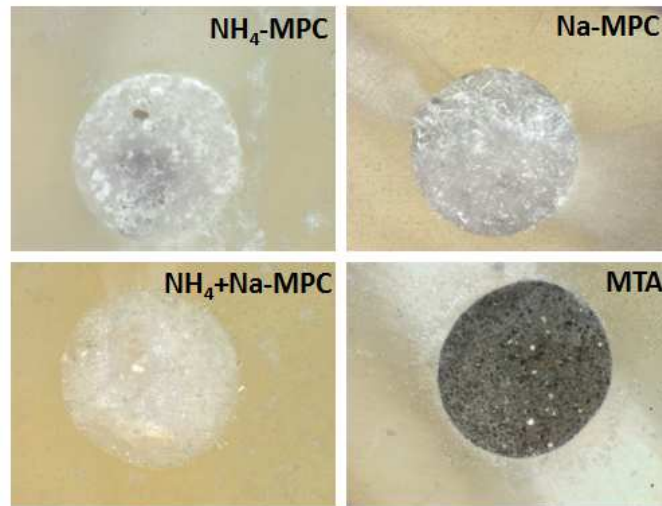
Figure 7.31. Images of root slices, the root canal cemented with NH_4-MPC, Na-MPC, NH_4+Na-MPC and MTA (control), observed with an optical microscope at a magnification of 10x.

The bonding strength between the cements under study (3 formulations of MPC and grey MTA as control) and the dentin of the root canal is shown in Figure 7.32. NH_4-MPC, Na-MPC and NH_4+Na-MPC had a bonding strength between 20.5 and 22.0 MPa, which was significantly higher ($p < 0.05$) than that of MTA (13.8 ± 5.3 MPa). Samples that fractured during the test (4.2 % of total) were not included in the analysis.
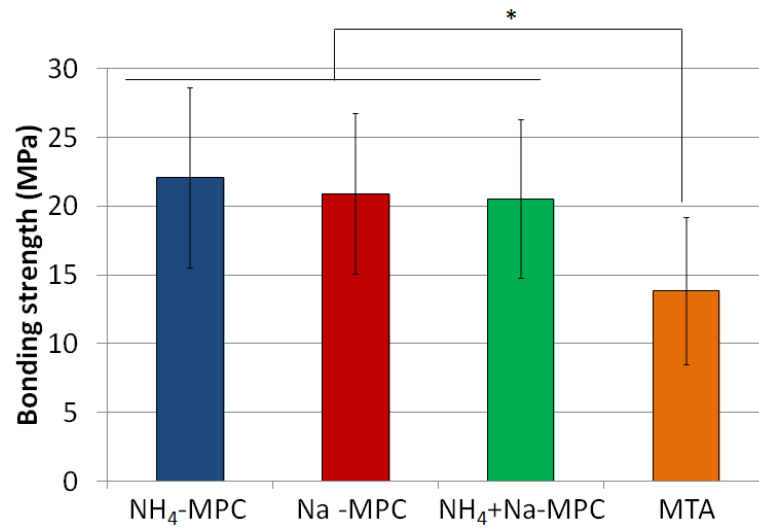
Figure 7.32. Dentin-cement bonding strength, evaluated with the push-out test, between the cement formulations (NH$_4$-MPC, Na-MPC, NH$_4$+Na-MPC and MTA) and the dentin. Error bars indicate standard deviation, n = 12. * indicates statistical significant differences between MTA and the other formulations ($p < 0.05$).

7.4.4.3 Sealing ability (microleakage test)

Figure 7.33 shows the X-ray images of the root canals obturated with the three formulations of RAD-MPC and with grey MTA (used as control). For each cement formulation and procedure of obturation (with or without gutta-percha) the cement was clearly distinguished from the anatomic structure of the root, which demonstrates that the amount of radiopacifying agent was adequate. However, the contrast of some of the X-ray images is low.

Figure 7.33. X-ray images of the root canal obturated with NH$_4$-MPC, Na-MPC, NH$_4$+Na-MPC and grey MTA, with gutta-percha (cement used as sealer) or without gutta-percha (cement used as filler). GP stands for gutta-percha.
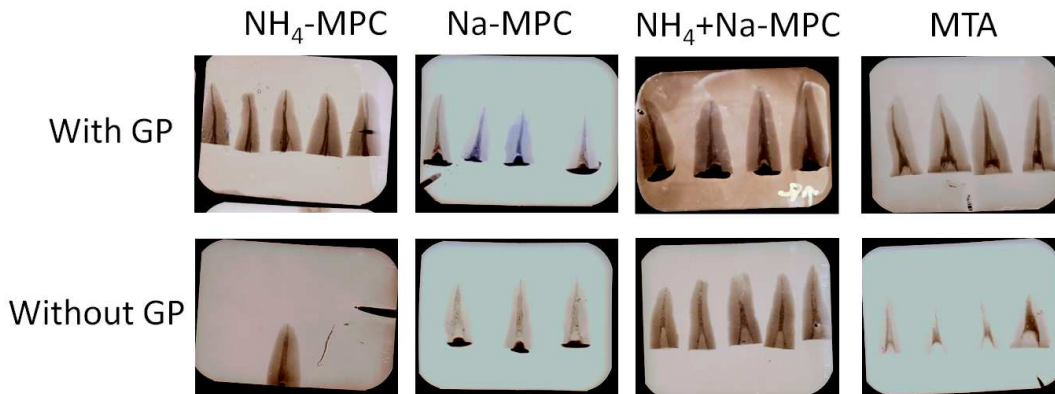
In this study, the microleakage of the root canal fillings was evaluated in function of several parameters:

a) Time: 24 h, 48 h, 72 h, 1 week, 2 weeks, 1 month, 3 months and 6 months;

b) Formulation of cements: three experimental ones within the family of RAD-MPC (NH_4-MPC, Na-MPC, NH_4+Na-MPC) and a control (grey MTA);

c) Procedure of obturation, using the cements as sealers (together with gutta-percha) or as fillers (without gutta-percha).

The results are summarized in Figure 7.34 and in Table 7.8, where the statistically significant differences are included.
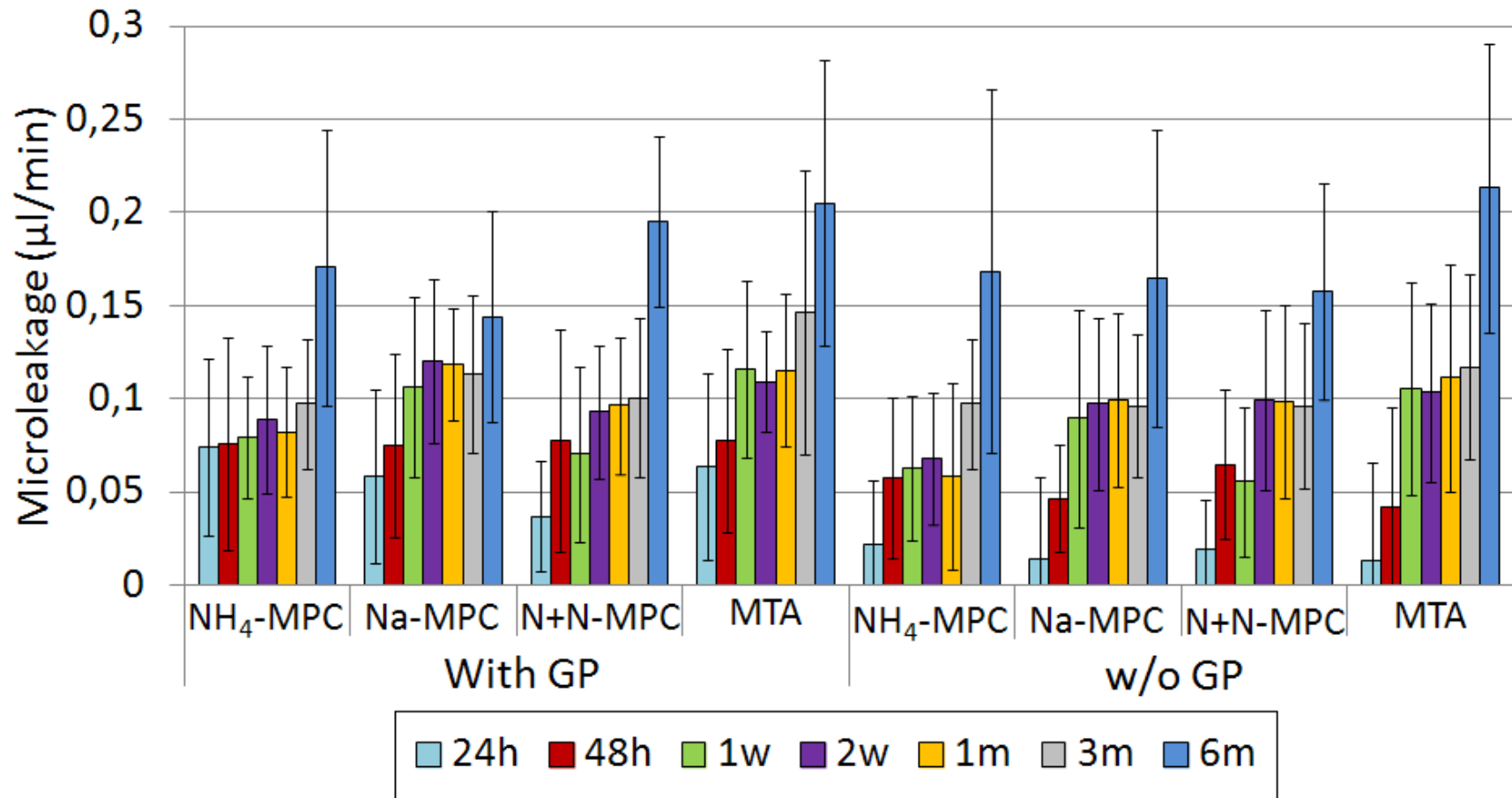
Figure 7.34. a) Microleakage of different cement formulations in function of three parameters: i) the time of immersion in PBS (24 h, 48 h, 1 week, 2 weeks, 1 month and 3 months and 6 months, h stands for hour, w stands for week and m stands for month), ii) the cement formulation (NH$_4$-MPC, Na-MPC, NH$_4$+Na-MPC and MTA; N+N-MPC stands for NH$_4$+Na-MPC) and iii) the obturation procedure of the root canal, which was either with cement and gutta-percha (with GP) or only with cement (w/o GP). Error bars indicate the standard deviation, n = 100.

Table 7.8. Microleakage of different cement formulations represented in Figure 7.34. Statistical analyses were carried out among each parameter, fixing the other conditions: i) the time of immersion in PBS (numbers 1-5), ii) the cement formulation (letters A-C) and iii) obturation of the root canal using either cement and gutta-percha (with GP) or only cement (w/o GP) (symbols ψ, *, $,and χ). For (i) and (ii), groups marked with the same letter or with the same number were not statistically different, for (iii) groups marked with the same number of symbols (one or two) were not statistically different.

		24 hours	48 hours	1 week	2 weeks	1 month	3 months	6 months
With GP	NH_4-MPC	0,074±0.047 1-A-ψ	0,076±0.057 1-A-ψ	0,080±0.033 1-A-ψ	0,089±0.039 1-A-ψ	0,082±0.035 1-B-ψ	0,097±0.035 2-A-ψ	0.195±0.046 3-B-ψ
	Na-MPC	0,059±0.046 1-B-*	0,075±0.049 2-A-*	0,106±0.048 3-B-*	0,120±0.044 3-B-*	0,119±0.030 3-A-*	0.113±0.042 3-A-*	0.144±0.056 4-C-*
	NH_4+Na-MPC	0,037±0.030 1-C-$	0,078±0.060 2-A-$	0,070±0.047 2-A-$	0,093±0.035 3-A-$	0,097±0.037 3-C-$	0,100±0.043 3-A-$	0.171±0.074 4-A-$
	MTA	0,063±0.050 1-A,B-χ	0,077±0.049± 2-A-χ	0.115±0.041 3-B-χ	0,114±0.028 3-C-χ	0,115±0.041 3-A-χ	0,147±0.076 4-B-χ	0.205±0.077 5-A-χ
w/o GP	NH_4-MPC	0,022±0,034 1-A-ψψ	0,058±0,043 2-A,B-ψψ	0.063±0.038 2-A-ψψ	0,068±0,035 2-B-ψψ	0,059±0,050 2-B-ψψ	0,097 ±0,035 3-A-ψ	0.168±0.097 4-A- ψ
	Na-MPC	0,014±0,043 1-A-**	0,046±0,029 2-B,C-**	0,089±0,058 3-B-*	0,097±0,046 3-A-**	0.100±0.047 3-A-**	0,096 ±0,038 3-A-**	0.165±0.079 4-A-*
	NH_4+Na-MPC	0,019±0,026 1-A-$$	0,065±0,040 2-A-$	0,055±0,040 2-A-$	0,099±0,049 3-A-$	0.099±0.052 3-A-$	0,096±0,044 3-A-$	0.157±0.058 4-A-$$
	MTA	0,013±0,052 1-A-χχ	0,042±0,054 2-C-χχ	0,105±0,057 3-B-χ	0.103±0.048 3-A-χ	0,111±0,061 3-A-χ	0,117 ±0,049 3-B-χχ	0.213±0.077 4-B-χ

In order to analyze more easily the effect of each parameter, the results are represented in three separate graphs, one for each variable to evaluate. Figures 7.35, 7.36 and 7.37 show the microleakage of the three RAD-MPC formulations and the MTA used to obturate the root canal of human teeth in function of the immersion time, the tested formulation and whether gutta-percha was used or not, respectively.

a) Microleakage *versus* time

Figure 7.35 shows the root canal microleakage in function of the immersion time. The general trend for both the roots obturated with cement and gutta-percha and those obturated only with cement shown a moderate increase of the microleakage with time, being more relevant between 24 h and 1 week and, afterwards, between 3 and 6 months. The microleakage monitored was between 0.05 to 0.2 µl/min for all formulations and times, either when gutta-percha was used or not for the root obturation.

Specifically for those roots obturated with cement and gutta-percha (Figure 7.35 a), NH_4-MPC was the formulation that maintained the initial value of microleakage constant for a longer period of time, from 24 h to 1 month. In contrast, the other three formulations had lower microleakage values than those of NH_4-MPC after 24 h, but their microleakage increased significantly ($p < 0.05$) after 48 h, reaching a similar microleakage than that of NH_4-MPC. The microleakage of Na-MPC and MTA significantly increased ($p < 0.05$) between 48 h and 1 week, whilst that of NH_4+Na-MPC suffered a similar increase between 1 and 2 weeks. The four formulations reached a stable value of microleakage ($p > 0.05$) for a period of time, NH_4-MPC between 24 h and 1 month, Na-MPC between 1 week and 3 months, NH_4+Na-MPC between 2 weeks and 3 months, and MTA between 1 week and 1 month. Finally, the four formulations viewed a significant increase ($p < 0.05$) between 3 and 6 months.

The microleakage of the teeth obturated without gutta-percha (Figure 7.35 b) significantly increased ($p < 0.05$) between 24 and 48 h for the four formulations. Afterwards, the four formulations maintained a constant value of microleakage ($p > 0.05$) for a period of time that was

between 48 h and 1 month for NH$_4$-MPC, between 1 week and 3 months for Na-MPC, between 2 weeks and 3 months for NH$_4$+Na-MPC, and between 1 week and 3 months for MTA. Finally, the microleakage significantly raised (p < 0.05) for all of them between 3 and 6 months.

Figure 7.35. a) Microleakage of root canals *versus* time: a) root canals obturated with cements and gutta-percha (with GP), b) root canals obturated only with cements (without GP). Error bars indicate the standard deviation, n = 100. The significant differences have been evaluated within consecutive times, groups identified by the same superscript letters are not significantly different (p > 0.05).

b) Microleakage *versus* formulation

Figure 7.36 shows the microleakage in function of the cement formulation at fixed immersion times. Regarding the teeth obturated with cement and gutta-percha (Figure 7.36 a), there were significant differences between formulations after 24 h, the NH$_4$+Na-MPC having a significantly lower microleakage than the other three formulations (p < 0.05). However, there were no significant differences between formulations (p > 0.05) after 48 h. Between 1 week and 1 month, in general, two differentiated groups appeared, Na-MPC and MTA had a significantly higher microleakage (p < 0.05) than NH$_4$-MPC and NH$_4$+Na-MPC. After 3 months, the microleakage of MTA was significantly higher (p < 0.05) than that of the other three formulations, whose microleakage values were not statistically different (p > 0.05) between them. Finally, the microleakage after 6 months was significantly higher (p < 0.05) for NH$_4$+Na-MPC and MTA than for NH$_4$-MPC, and Na-MPC had a significantly lower microleakage (p < 0.05) than the other three formulations.

The microleakage trends of the root canals filled only with cement (Figure 7.36 b) were different than those observed for roots obturated with gutta-percha and cement. Significant differences (p < 0.05) between formulations appeared after 48 h and at longer times. After 1 week, Na-MPC and MTA had a significantly higher microleakage (p < 0.05) than those of NH$_4$-MPC and

NH_4+Na-MPC. After 2 weeks and 1 month, NH_4-MPC had a significantly lower microleakage ($p < 0.05$) than the other three formulations. Finally, after 3 and 6 months, MTA had a significantly higher microleakage ($p < 0.05$) than the other three formulations.
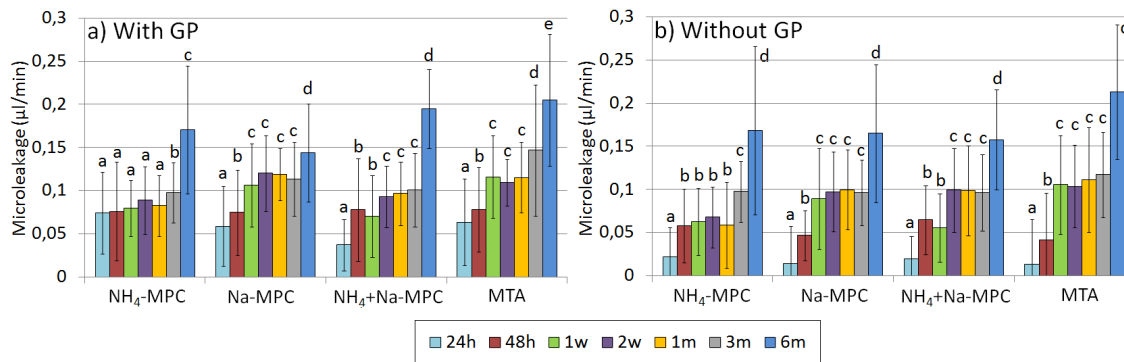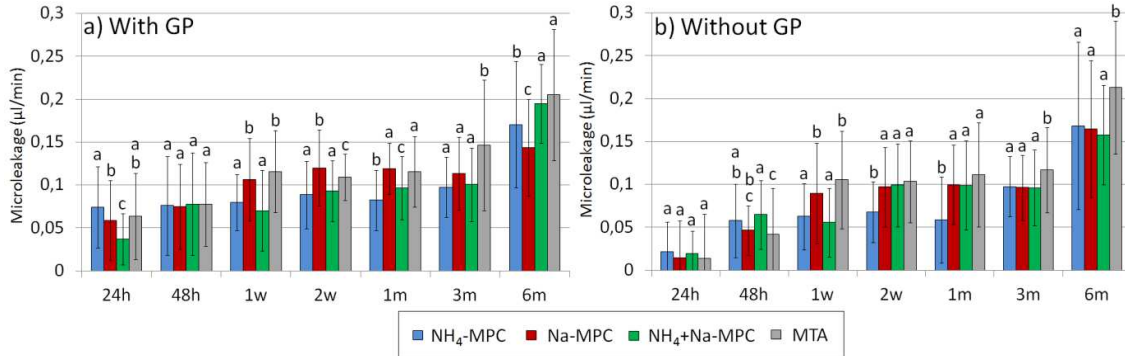

Figure 7.36. Microleakage *versus* cement formulation: a) root canals obturated with cements and gutta-percha (with GP), b) root canals obturated only with cements (without GP). Error bars indicate the standard deviation, n = 100. Groups identified by the same superscript letters are not significantly different ($p > 0.05$).

c) Microleakage *versus* use or not of gutta-percha

Figure 7.37 shows the microleakage of each formulation in function of whether or not gutta-percha was used to obturate the root canal, together with the cement. It is interesting to note that when differences appeared for different formulations and times, the roots sealed with cement and gutta-percha had a significantly higher ($p < 0.05$) microleakage than those obturated only with cement. The differences were more pronounced at short times, mainly at 24 h and 48 h, which were indistinctive of the formulation.
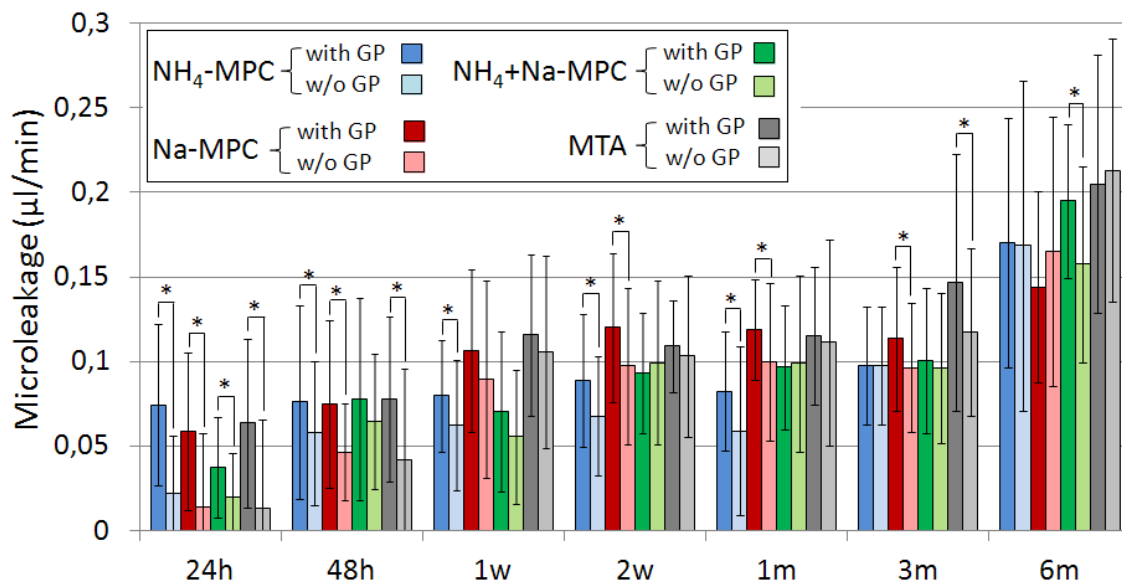
Figure 7.37. Microleakage *versus* use of gutta-percha: "with GP" stands for with gutta-percha; "w/o GP" stands for without gutta-percha, namely the root canals obturated only with cement. Error bars indicate the standard deviation, n = 100. The significant differences have been evaluated within samples of the same formulation that were immersed in PBS for the same time. * indicates statistically significant differences (p < 0.05).

7.5 Discussion

7.5.1 Radiographic assessment

Interestingly, the MPCs had certain radiopacity by themselves. Table 7.9 shows the elements making up the MPC powder, sorted in ascending atomic number. Regardless Bi (Z = 83), Mg and P (Z = 12 and 15, respectively) were the atoms present in the MPCs with a higher atomic number. The radiopacity of the MPC formulations showed the trend: Na-MPC > NH$_4$+Na-MPC > NH$_4$-MPC. The higher radiopacity of Na-MPC was due to the presence of Na ions (Z = 11), which have higher atomic number than N (Z = 7). The radiopacity of NH$_4$+Na-MPC, which was in between to that of the other two formulations, was in accordance with its formulation, containing an equimolar ratio of NH$_4$H$_2$PO$_4$ and NaH$_2$PO$_4$, used for the preparation of NH$_4$-MPC and Na-MPC, respectively.

Table 7.9. Atoms making up the RAD-MPC formulations sorted by ascending atomic number (Z).

Atom	B	N	O	Na	Mg	P	Bi
Atomic number (Z)	5	7	8	11	12	15	83

Bi_2O_3, which had a high absorption capacity, was added as a radiopacifying agent. The addition of Bi_2O_3 to the cement powder increased the radiopacity of the cements linearly in the range between 0 and 20 wt % (Figure 7.19). When 30 wt% Bi_2O_3 was added, the cement radiopacity reached the maximum level of grey (R = G = B = 255) that, with the used quantification method, was assimilated to the maximum optical density. Therefore, it could not be distinguished any increase on the radiopacity of the cement when adding more Bi_2O_3.

When 10 wt% Bi_2O_3 was added to the cement powder and 2 mm-thickness cement disks were prepared, the sodium-containing MPCs had a radiopacity higher than 6 equivalent millimeters of aluminum thickness. Since this radiopacity satisfied the UNE-EN ISO 6876 standard for dental root canal filling materials (1 mm-thickness disk should have a minimum radiopacity of 3 equivalent millimeters of aluminum thickness) [7], 10 wt% Bi_2O_3 was the selected amount. It should be mentioned that only NH_4-MPC did not strictly fulfill the ISO standard. Nevertheless, it was selected 10 wt% Bi_2O_3 because the two novel formulations developed in this Thesis, which were free of ammonium ions (Na-MPC) or contained a reduced amount (NH_4+Na-MPC), did meet the standard. Moreover, the selected amount of Bi_2O_3 was enough to easily distinguish the three MPC formulations from the surrounding anatomical structures, as observed by the X-ray images of the root canals obturated with RAD-MPCs (Figure 7.33).

The amount of raciopacifying agent added to the RAD-MPCs was lower than that in the commercial root canal sealer MTA, which contains 16 wt% Bi_2O_3 [8]. In this work, the addition of Bi_2O_3 was minimized on purpose because even though it has been proved that compound is not harmful to the human body, since it is insoluble in water, this compound could decrease the material biocompatibility if it is leached out when the cement is degraded [23].

7.5.2 Assessment of the exothermy and the setting times

The factors influencing the exothermy and the setting times of the three MPC formulations have been extensively discussed in Chapter 5 (Section 5.5.1 and 5.5.2, respectively). Therefore, these topics will only be briefly discussed in this section, and Chapter 5 should be addressed for further details.

When the MPCs were provided with 10 wt% Bi_2O_3 and 0 wt% borax was added, the maximum temperature reached by NH_4-MPC (62°C) was significantly higher than that of Na-MPC (46°C) (Figure 7.20). The higher exothermy of NH_4-MPC was associated to the higher acidity of $NH_4H_2PO_4$ in comparison to its analogous phosphate salt, NaH_2PO_4, used for the preparation of Na-MPC. However, Na-MPC reached the maximum temperature earlier (3 min) than NH_4-MPC (3.5 min), due to the higher solubility of NaH_2PO_4 (94.5 wt%) than that of $NH_4H_2PO_4$ (40.5wt%) [24]. Nevertheless, the difference was rather small, since $NH_4H_2PO_4$ had a smaller particle size distribution than NaH_2PO_4 (Figure 7.2), favoring the solubilization of the former salt.

Interestingly, the addition of 1 wt% borax reduced significantly the exothermy of NH_4-MPC and, in contrast, Na-MPC was almost not affected by the addition of the retardant (Figure 7.20). This was attributed to the better solubilization of borax, a sodium tetraborate decahydrate, into NH_4-MPC, since Na-MPC contains sodium ions that may hinder the process. In fact, this behavior was more accentuated when 3 wt% borax was added. Whereas the setting times of Na-MPC only increased slightly, NH_4-MPC triplicated its setting time (Figure 7.21).

When MPCs contained 10 wt% Bi_2O_3 and 1 wt% borax, the setting time of the cements followed the trend Na-MPC < NH_4-MPC < NH_4+Na-MPC (Figure 7.21). This correlated well with the evolution of temperature observed for the three formulations. As already stated, the faster setting of Na-MPC in comparison with that of NH_4-MPC could be related to two complementary factors: i) the higher solubility in water of NaH_2PO_4 (94.5 wt%) with respect to that of $NH_4H_2PO_4$ (40.5wt%) [25] [24] accelerated the reaction; and ii) the sodium ions present in Na-MPC hindered the dissolution of borax, the retardant was less effective and thus the cement set faster. Surprisingly, even though it would be expected that NH_4+Na-MPC would have setting times between the ones of the other two formulations, it showed the longest values.

The addition of 10 wt% Bi_2O_3 decreased the exothermy and increased the setting times of the MPCs. Thus, only 1 wt% borax was needed in order to have a cement with appropriate exothermy (thermal coefficient lower than 1, Table 7.3) and an adequate setting time (final setting times between 7.4 and 11.4 min, Figure 7.21), in comparison with the 6 wt% added to the MPCs optimized in Chapter 6.

7.5.3 Physico-chemical characterization of the RAD-MPC

The factors that determine the physico-chemical properties of the MPC formulations have been extensively explained in Chapters 5 and 6. Thus, this section is mainly focused on discussing the differences brought by the incorporation of the radiopacifying agent.

7.5.3.1 Injectability

The load/displacement curves (Figure 7.22) correlated well with the total amount of injected paste: the longer the displacement of the piston, the higher amount of paste injected (Table 7.4). The NH_4-MPC was hardly injectable, whereas Na-MPC and NH_4+Na-MPC showed a good injectability. These results matched with the better moldeability of both Na-MPC and NH_4+Na-MPC.

The addition of 10 wt% Bi_2O_3 slightly increased the injectability of Na-MPC and NH_4+Na-MPC in comparison with the MPCs optimized in Chapter 6 (comparison shown at Table 7.10). This was attributed to the unreactivity of the radiopacifying agent, which did not set with time. Another parameter that could have an effect on the different injectability between the MPCs and the RAD-MPCs is the fineness of the $NH_4H_2PO_4$, being finer in the RAD-MPC. The finer $NH_4H_2PO_4$ would have a higher specific surface area, thus increasing the viscosity of the cement.

Table 7.10. Injectability of the three formulations of RAD-MPC and MPC. The data indicate mean ± standard deviation, n = 3.

Family of MPC	NH$_4$-MPC	Na-MPC	NH$_4$+Na-MPC
MPCs (Chapter 6)	41.4 ± 14.0	74.4 ± 13.0	86.4 ± 3.4
RAD-MPCs (Chapter 7)	35.8 ± 1.0	88.9 ± 0.6	90.3 ± 0.2

7.5.3.2 Phase composition

In comparison with the MPCs optimized in Chapter 6, the addition of Bi$_2$O$_3$ only affected the phases composition by the presence of Bi$_2$O$_3$ as an extra crystalline phase. Briefly, NH$_4$-MPC and NH$_4$+Na-MPC formulations formed schertelite and struvite, which evolved with time (Figure 7.24), the amount of struvite (MgNH$_4$PO$_4$·6H$_2$O) increasing in detriment to schertelite (Mg(NH$_4$·HPO)$_2$·4H$_2$O). As explained in Section 5.5.3, the initial formation of schertelite was associated to a kinetic limitation, since struvite can only be formed when enough Mg atoms and molecules of water are available [26] [27]. Therefore, at longer times, the higher amount of MgO dissolved and the higher amount of molecules of water available, which permeated through the cement, favored the reorganization of the crystalline structure giving place to struvite, a phase thermodynamically more stable than schertelite [26] [27].

The end-product formed by Na-MPC was amorphous, and although the hump centered at $2\theta \sim 31°$ was consistent with the formation of an amorphous magnesium sodium phosphate phase, it was difficult to specify which one was it by means of XRD. The observation of an amorphous phase was not clear for the NH$_4$+Na-MPC because peaks of struvite masked the presence of the hump. However, since NH$_4$+Na-MPC had an equimolar content of NH$_4$H$_2$PO$_4$ and NaH$_2$PO$_4$, it was assumed that the amorphous phase coexisted with the crystalline one.

While the phosphate salts were dissolved quickly with time, the intensity of the XRD peaks of MgO decreased very slightly with time (Figure 7.24). This can be attributed to the low solubility of this compound in water [24] and to its addition in excess in order to have a core material that enhances the strength development [28] [26] [29]. The radiopacifying agent, Bi$_2$O$_3$, remained unaltered with time since it is insoluble in water [24].

7.5.3.3 Reaction kinetics: compressive strength and setting times

The hardening kinetics was NH_4-MPC > NH_4+Na-MPC > Na-MPC, although the three formulations reached their higher compressive strength after 1 day (Figure 7.23). The longer period of time required by Na-MPC to reach its maximum compressive strength was associated to the slow formation of end-products, which provided the strength to the material. In fact, the formation of an amorphous phase was almost negligible after 1 h by XRD and a hump around $2\theta \sim 31°$ did not clearly appear until 1 day (Figure 7.24), which indicated the slow reaction kinetics of Na-MPC. As previously explained, it could be hypothesized that the dissolution of the retardant, a sodium borate decahydrate, was hindered in the Na-MPC matrix due to the presence of sodium ions, being thus less effective at short times (fast setting times) (Figure 7.21) and delaying the reaction at longer times, as well as the attainment of compressive strength (Figure 7.23). In contrast, NH_4-MPC had longer setting times due both to the slower dissolution of $NH_4H_2PO_4$ in water and the higher efficiency of borax. Nevertheless, the faster formation of struvite and schertelite end-products (Figure 7.24), which enhanced the attainment of higher compressive strength after 1 and 2 h for NH_4-MPC (Figure 7.23). Surprisingly, NH_4+Na-MPC was the formulation with longer setting times. However, its speed to increase the compressive strength was in between to that of NH_4-MPC and Na-MPC, and the formation of struvite and schertelite after 1 h could be assimilated to that of NH_4-MPC.

Regarding the compressive strength, it is worth noting that the maximum values attained by the different MPC formulations were not significantly ($p > 0.05$) different after 1 day (Figure 7.23), regardless of the crystalline or amorphous nature of the end-product.

7.5.3.4 Morphology, chemical analysis, specific surface area, skeletal density and porosity

a) Morphology and porosity

The three RAD-MPC formulations showed a glassy-like morphology, probably due to the formation of a borate compound layer on the surface of the material (Figure 7.26), as explained in Chapter 5 (Section 5.5.6). The elongated particles observed after 7 days in Figure 7.26 b and f could

be associated with the formation of struvite and schertelite. It was difficult to discern between the MPC matrix and the added Bi_2O_3.

At a low magnification, it was observed that NH_4-MPC had pores around 50 µm distributed along the surface fracture, which were not observed on Na-MPC and were present in a much lower quantity on NH_4+Na-MPC (Figure 7.25). The pores observed on the NH_4-MPC surface were in accordance with the pore size distribution of this formulation (Figure 7.27), which showed a peak centered at 32 µm. The mentioned pores could correspond to the voids left after the dissolution of $NH_4H_2PO_4$, particles embedded in the matrix of the set cement. This hypothesis was also in agreement with the broad particle size distribution of $NH_4H_2PO_4$, between 1 and 300 µm, with the highest amount of particles with a size around 43 µm (Figure 7.2). In contrast, no pores were observed in the morphology of Na-MPC. The fact that only $NH_4H_2PO_4$ particles resulted in pores within a matrix was attributed to the lower solubility of this salt (40.5 wt%) than that of NaH_2PO_4 (94.5 wt%) [24]. The higher solubility of NaH_2PO_4 allowed the total dissolution of the salts prior to the cement setting, and thus the spaces left for the salt were filled by the cement paste. The morphology of NH_4+Na-MPC showed only the presence of few pores that could also be associated to the dissolution of $NH_4H_2PO_4$, whose amount was half than that of Na-MPC.

The low liquid to powder ratio needed to produce MPC with adequate viscosity (L/P = 0.13 ml/g) leaded to set cement with a low total open porosity, between 4 and 11 wt% (Table 7.7). This is a good property for cements aimed to be used for endodontic applications, where leakage through the material and its degradation has to be minimized. For comparison, the MTA cements used for endodontic applications have a porosity comprised between 30.2 and 38.4% for a liquid to powder ratio comprised between 0.26 and 0.33 ml/g, respectively [30]. The higher porosity of MTA could be mainly associated to the higher liquid to powder ratio needed to have workable cements.

It should be highlighted that the porosity was significantly lower for the RAD-MPC formulations than for the MPCs optimized in Chapter 6 (comparison shown at Table 7.11). This was associated to the addition of Bi_2O_3 that could fill voids between particles, allowing a better compaction of the end-products. Nevertheless, these results differed from the work of Lumley *et al.* [31] that showed that the incorporation of 20 wt% Bi_2O_3 increased the porosity of the material. However, the amount of Bi_2O_3 used in the current work was half of the one used by Lumley *et al.*

and, moreover, the porosity is known to be a parameter highly dependent on the particle size of the reactants and the liquid to powder ratio, among several other variables, being therefore not possible to directly compare the results of porosity with other works.

Table 7.11. Total open porosity (%) for the MPC formulations optimized in Chapter 6 and for the RAD-MPC formulations.

Family of MPC	NH_4-MPC	Na-MPC	NH_4+Na-MPC
MPC (Chapter 6)	30.8	28.8	35.1
RAD-MPC (Chapter 7)	11.0	5.0	4.2

b) Morphology and chemical analysis

The atomic ratio obtained from the punctual chemical analysis of NH_4-MPC after 7 days was $MgP_{0.96}N_{0.93}$ (excluding Bi), which indicated the presence of struvite ($MgNH_4PO_4 \cdot 6H_2O$). However, it should be stressed that NH_4-MPC is a multiphasic material, constituted by a mixture of struvite (end-product), MgO (reactant in excess) and Bi_2O_3 (insoluble radiopacifying agent).

The morphology of Na-MPC showed the presence of some particles (Figure 7.25 b). The fracture surfaces of the cements was analyzed by EDS, which allowed determining that the particles found in Na-MPC had a higher ratio of Na and P atoms, and a lower ratio of Mg and Bi atoms than the matrix (Table 7.5).

The chemical analysis showed a high dispersion in the amount of Bi_2O_3 for each sample, between 8.0 and 13.4 wt% after 1 h (Table 7.5), which indicated that this compound was not homogeneously distributed along the matrix. In fact, agglomerates of the radiopaque agent were also observed in the X-ray images of cement disks as white dots (Figure 7.18). The same problem was reported by Tadier *et al.* [9], which showed that similar agglomerates of their radiopaque agent ($SrCO_3$) appeared in a cement, and reported that this agent could be homogeneously distributed by milling together all the reactants composing the powder. This procedure could be also applied for the RAD-MPC powders, although some time should be invested to find a milling protocol that would not alter the physical properties of cements, and the borax amount should be readjusted to maintain the exothermy and setting times within adequate ranges.

c) Specific surface area, skeletal density and porosity

The specific surface area (SSA) followed the trend NH_4-MPC > NH_4+Na-MPC > Na-MPC (Table 7.6). The higher SSA of NH_4-MPC was associated to the elongated particles of struvite and schertelite, which also produced a higher porosity of the material (Table 7.7), in contrast with the flat surface and glassy-like morphology of Na-MPC, which produced very low SSA and porosity. The NH_4+Na-MPC, which had a morphology with characteristics of both NH_4-MPC and Na-MPC, had as well a value of SSA between the other two formulations. However, the NH_4+Na-MPC had a porosity slightly lower than Na-MPC. Surprisingly, the NH_4-MPC and NH_4+Na-MPC exhibited values of SSA significantly high, even though their porosity was low.

The trend of the skeletal density values were the opposite than those of the SSA: Na-MPC > NH_4+Na-MPC > NH_4-MPC (Table 7.6). The amorphous phase formed in Na-MPC resulted to be denser than struvite and schertelite phases formed in NH_4-MPC. Again, NH_4+Na-MPC had values of skeletal density between the other two formulations. The skeletal density for the of NH_4-MPC was higher than the expected value for struvite (skeletal density of 1.71 g/cm^3 [24]. This could be associated to the addition of 10 wt% Bi_2O_3 (skeletal density 8.9 g/cm^3 [24]) and to the potentially high amount of unreacted MgO (skeletal density of 3.6 g/cm^3 [24]), since 50.8 wt% MgO was added and only 25.9 wt% MgO should react (1 mol MgO should stoichiometrically react with 1 mol of $NH_4H_2PO_4$). Indeed, the skeletal values of the RAD-MPC formulations were higher than those of the MPCs optimized in Chapter 6 (Table 7.12) due to the presence of the radiopacifying agent.

Table 7.12. Skeletal density (g/cm^3) for the MPC formulations optimized in Chapter 6 and for the RAD-MPC formulations.

Family of MPC	NH_4-MPC	Na-MPC	NH_4+Na-MPC
MPC (Chapter 6)	2.43 ± 0.02	2.64 ± 0.02	2.59 ± 0.02
RAD-MPC (Chapter 7)	2.65 ± 0.07	2.77 ± 0.01	2.71 ± 0.02

7.5.4 Specific characterization for endodontic cements

The aim of a root filling material is to seal the access of microorganisms through the root canal, since otherwise a secondary infection could occur. In order to ensure this permanent

sealing, the material has to intrinsically be a good sealer and it must be stable with time. In other words, it must not dissolve or disintegrate as a result of the contact with physiological fluids. Moreover, the root canal filling material should adapt to the dentin's shape, thus reducing the risk of leakage. Furthermore, the root canal filling material should remain fixed in its original position, enduring to mechanical charges present during the normal activities of a patient [32].

The root canal filling material should also be biocompatible and produce minimal irritation to the apical tissues, and it cannot be toxic or carcinogenic. Moreover, a material with antimicrobial properties is desired, to kill any bacteria remaining in the root canal after the disinfection process done by mechanical and chemical procedures. Chapter 6 has dealt with the evaluation of some of these biological properties. Finally, for practical reasons, the material should be easy to manipulate and radiopaque to allow its control by means of X-rays [1–3,6].

In this section, the stability with time, the bonding strength to dentin and the sealing ability of the three MPC formulations are discussed.

7.5.4.1 Material stability

The degradation assay was performed in order to evaluate the stability of cements with time when immersed in an aqueous solution. It is important to note that the conditions of this assay were not the actual ones in the root canal, but more drastic due to the high volume of liquid used, which was periodically refreshed in order to accelerate the degradation pattern of the materials.

The total weight loss was 4.3 ± 0.6, 5.2 ± 0.8 and 2.4 ± 1.6 wt% for NH_4-MPC, Na-MPC and NH_4+Na-MPC, respectively (Figure 7.28). However, if the weight loss was calculated considering as initial weight the maximum value reached for each formulation (*i.e.* after 1 day), the total weight loss would be 5.1 ± 1.0, 7.1 ± 0.8 and 5.7 ± 0.4 wt% for NH_4-MPC, Na-MPC and NH_4+Na-MPC, respectively, although no significant differences were found between formulations ($p > 0.05$). The weight loss was associated with the solubilization of the cements in PBS. The solubilization of the set cements started from the surface and also from the micropores and canals containing trapped water, which diffused out when the medium was refreshed [30,33].

The key parameters involved in the solubility of a material are the temperature (in this case, 37°C), the pH (7.4 for pristine PBS) and the ionic concentration of the medium (pristine PBS contains [P] ~ 9 mM and [Na] ~ 151 mM). The small degradation of NH$_4$-MPC and NH$_4$+Na-MPC, which are mainly formed by struvite and MgO in excess, could be explained by the solubility of these two compounds at the exposed conditions. The solubility product (pK$_s$) of struvite is between 9.41 and 13.36 [34–41], and of magnesium hydroxide (the compound that forms MgO in water) is 11.25 [24]. The solubility of struvite can be considered to be very low [34] or relatively high [42], in function of the application given to this compound. However, both struvite and magnesium hydroxide are more soluble than α-TCP (pK$_s$ = 25.5) and much more soluble than calcium deficient hydroxyapatite (pK$_s$ = 85.1). The solubility of Na-MPC, which contained an amorphous magnesium sodium phosphate product and unreacted MgO, is unknown.

The weight changes observed for the three MPC formulations in the first day (Figure 7.28) were the balance of two processes occurring at the same time. On one hand, the formation of hydrated phases such as struvite, schertelite or a magnesium sodium phosphate phase increased the weight. On the other hand, the release of ions such as Mg, P and Na (Figure 7.29), counteracted this effect. In fact, the formulations that released a higher amount of P after 3.5 days, namely NH$_4$-MPC and Na-MPC, matched to be the ones that also gained a lower amount of weight in the same period of time. And vice versa for NH$_4$+Na-MPC. The high [P] produced at the very beginning could be partially due to the dissolution of the phosphate salts, which occurred in a few hours (Figure 7.24). The fast dissolution of the phosphate salts was in accordance with the high solubility of the phosphate salts in water, the NaH$_2$PO$_4$ (94.5 wt%) being more soluble than the NH$_4$H$_2$PO$_4$ (40.5 wt%) [24].

The continuous weight loss observed after 1 day for NH$_4$-MPC and Na-MPC, and after 21 days for NH$_4$+Na-MPC, was associated to the degradation of the end-products (*i.e.* schertelite, struvite or amorphous phase) or the remaining reactants (*i.e.* MgO). The dissolution of these compounds with time produced a [Mg] between 0.3 and 0.8 mM (Figure 7.29 a) and contributed to the decrease of weight. The ions released to the medium, for instance, the hydroxyl ions formed during the dissociation of MgO increased the pH of the medium to about 8.5 during the entire study (Figure 7.29 d). In general, NH$_4$-MPC was the formulation that released the highest amount

of Mg ions with time, consequently increasing more the pH of the medium, whilst Na-MPC released the lowest amount of Mg ions and also caused the minor increase of pH. The release of Na ions by Na-MPC and NH$_4$+Na-MPC, which occurred for a period of 31 days (Figure 7.29 c), also might decrease the samples weight. The period of time during which Na ions were released was not limited to the initial stages, associated to the dissolution of NaH$_2$PO$_4$. Therefore, the release of Na ions could be associated to the dissolution of the amorphous magnesium sodium phosphate phase. It is interesting to note that whilst the [Na] of the PBS medium was increased in about $1 - 5$ mM at each time point, the [Mg] was increased in only $0.3 - 0.8$ mM. Thus, the Na ions probably had a higher influence on the weight loss than the Mg ones, which was in accordance with the higher weight loss observed for Na-MPC, although it was the formulation that released a lower amount of Mg ions.

Similar degradation studies have been published for MTA. Vivan *et al.* [43] reported that disks of MTA (20 mm diameter and 1.5 mm height) immersed in 50 ml of distilled water for a time period of 7 days experienced a weight loss of 3.5 wt%. Another study that used the same experimental conditions determined that the degradation of the MTA after 7 days was between 1.8 and 2.8 wt% when a liquid to powder ratio between 0.26 and 0.33 ml/g was used, respectively [30]. For comparison, in the current work, the degradation observed after 7 days showed that NH$_4$-MPC decreased about 1.8 wt%, whereas NH$_4$+Na-MPC increased 3.3 wt% and Na-MPC remained with the same weight. However, it should be considered that the study carried out by Vivan *et al.* was conducted in distilled water, whereas our studies were performed in PBS. Other degradation studies, conducted for a longer period of time, reported that when disks of MTA were immersed in distilled water for 78 days the weight loss was 16 and 24 wt% for liquid to powder ratios between 0.28 and 0.33 ml/g, respectively [44].

The low solubility found for the MPCs is quite in contradiction with other works conducted with similar procedures, immersing ammonium-magnesium phosphate cements disks in SBF or in Tris/HCl (pH = 7.4) and showed a weight loss between 50 and 80 wt% after 90 days of immersion [45–49]. These differences could be ascribed mainly to the phase composition of the materials, the mentioned works using farrangstonite (Mg$_3$(PO$_4$)$_2$ and ammonium phosphate as reactants of the cement [47–49] or not using any retardant of the reaction [45–47].

7.5.4.2 Dentin-cement bonding strength (push-out test)

It should be highlighted that the bonding strength characterization was performed with the MPCs optimized in Chapter 6, which contained 6 wt% borax, instead of the 10 wt% Bi_2O_3 and 1 wt% borax present in RAD-MPC. However, since the amount of reactants aimed to the formation of the magnesium phosphate matrix was 94 wt% for MPCs and 89 wt% for the RAD-MPCs, it was expected that both families of cements would have very similar adhesive properties. Nevertheless, this assay should be validated with RAD-MPC in a future study.

The bonding strength between the three formulations of MPC and dentin was significantly higher than that of MTA and dentin (Figure 7.32). The bonding between the cements and the dentin was most probable mechanical, without the establishment of chemical bonds. Probably, the cement paste was introduced into microporosities of the dentin before setting, producing a strong mechanical anchorage [50].

Reyes-Carmona *et al.* performed a push-out test study with MTA [51] by introducing the cement into root canals of 1.3 mm of diameter. They evaluated the dentin-cement bonding strength after storing the obturated roots in different conditions: a) covering the cement with a wet cotton pellet for 72 h at 37°C or b) immersing the teeth in PBS for 2 months at 37°C. Reyes-Carmona *et al.* reported values of dentin-cement bonding strength of 4.67 ± 1.35 MPa after 72 h and of 7.14 ± 0.42 after 2 months. The differences between their results and the results reported in this Chapter for MTA (13.8 ± 5.3 MPa) could be mainly attributed to the different experimental conditions such as storage of the samples, diameter of the roots or speed rate during the test.

The adhesion between the material and the dentin is important in order to ensure the success of an endodontic treatment, since the anchorage allows the material to keep fixed to its original position even though the presence of dislocation forces, such as mechanical stress [4]. Furthermore, a high bonding strength to dentin also allows to expect a lower risk of interfacial bacterial leakage [6].

7.5.4.3 Sealing ability (microleakage test)

Although several methodologies have been described to evaluate the microleakage of materials, in this work, the liquid pressure method proposed by Derkson *et al.* for restorative

materials [52] was selected since it is a quantitative and non-destructive method. Moreover, this method has a higher reliability than others such as dye penetration, bacterial penetration or fluid transport [6].

The microleakage of the three formulations of RAD-MPC and MTA was evaluated by obturating the root canal of human teeth, using the cement either as root canal filler or as root canal sealer together with gutta-percha. The microleakage was monitored at different times for a period of 6 month, during which the teeth were soaked in a PBS solution. The study aimed at evaluating the microleakage of MPCs and the influence that the immersion time, the cement formulation and the use of gutta-percha had on the microleakage.

The microleakage was mainly influenced by the period of time that the teeth had been immersed in PBS (Figure 7.35). Although the microleakage of all formulations remained stable for a considerable period of time, afterwards, all of them suffered a significant increase ($p < 0.05$) between 3 and 6 months. The fact that the microleakage increased with time was associated with the degradation of the cement, which probably increased its total porosity making an easier path for water to go through it. For the teeth obturated with cement and gutta-percha, the degradation of the cement could make some voids between the gutta-perchas, also creating a kind of microcanals through which water could leak.

The four tested formulations had a value of microleakage of the same order (Figure 7.36). However, whilst NH_4-MPC was one of the MPC formulations that, in general, had a lower microleakage for a longer period of time, MTA could be pointed as the tested cement with the highest microleakage, especially at long times (3 and 6 months). This result would indicate that MTA had a higher degradation rate that the MPCs.

Finally, the effect that the use of gutta-percha had on the microleakage was assessed (Figure 7.37). At short times (24 h and 48 h) it was very clear that the use of gutta-percha had a negative influence on the teeth obturation, since the microleakage was significantly higher in those formulations sealed with gutta-percha and cement than in their counterparts sealed only with cement. This may indicate that the cement alone was more effectively compacted into the root canal than the combination of gutta-percha and cement. Nevertheless, this effect was reduced with the immersion time, the microleakage for those root canals obturated only with cement

increasing between 24 h and 48 h, probably due to the changes in microstructure of the transforming cement or its partial degradation, and after 6 months differences due to the gutta-percha were only observed for NH_4+Na-MPC. In contrast, whilst the root canals obturated with gutta-percha initially had a higher microleakage, the lower amount of present degradable material, in other words, the lower amount of cement added in the root canals maintained the initial microleakage stable for a longer period of with time.

After 6 months, the microleakage of the three formulations of RAD-MPC was significantly lower than that of MTA, applying the cements into the root canal with and without gutta-percha (except for NH_4+Na-MPC used with gutta-percha). Since MTA is a commercially used sealer for endodontic applications, the three RAD-MPC formulations could be considered as potentially good candidates as root canal filler or sealer.

The results reported in literature regarding microleakage of root canal filling materials depend greatly upon the method being used. Therefore, data should be regarded with caution. Nevertheless, the microleakage values obtained in the current work were in the order of other studies. For instance, Gandolfi *et al.* [53] found that when root canals were filled with warm vertical compaction of gutta-percha and sealer, which was either an experimental MTA (cement) or AH plus (resin), the microleakage was between 0.13 and 0.26 µl/min for a period of time between 24 h and 6 months, although the values did not follow any clear trend. Interestingly, Brackett *et al.* [54] found that the microleakage of root canals filled with GuttaFlow (powdered gutta-percha with nanosilver particles) increased with time (evaluated after 1, 6 and 12 weeks), as observed in the current study. In contrast, Gandolfi *et al.* [55] reported that when retrograde filling of the root-end canal was performed using white-MTA (ProRoot), the microleakage diminished with time for a period comprised between 4 h and 12 weeks, which was associated with the formation of hydroxyapatite that would obliterate voids, pores and capillary channels.

7.6 Conclusions

In this Chapter, the MPCs formulations optimized in Chapter 6 were modified with the aim to make them suitable for endodontic applications such as root canal filling (coded as RAD-MPC). Both physico-chemical characterizations and studies focused on evaluating the potential performance of the cement for endodontic applications have been carried out. The main conclusions extracted from this work are indicated below.

1. The addition of 10 wt% Bi_2O_3 to the MPC powder resulted in cements that fulfilled the radiopacity requirement established in UNE-EN ISO 6876 standard, the anatomic structure of the root being visible in X-ray images. The addition of 1 wt% borax allowed tailoring the exothermy of the reaction to physiological requirements.

2. The three RAD-MPC formulations had adequate setting times, and NH_4-MPC and NH_4+Na-MPC were almost completely injectable using a syringe of 2 mm-aperture and a maximum load of 100 N.

3. NH_4-MPC and NH_4+Na-MPC resulted into a mixture of struvite and schertelite compounds, whilst Na-MPC resulted in an amorphous magnesium sodium phosphate. MgO remained in excess and Bi_2O_3 was unaltered with time.

4. The three RAD-MPC formulations attained their maximum compressive strength after 1 day, regardless of the nature of the end-products. The compressive strength was reached significantly faster than in calcium phosphate cements.

5. The total porosity of the three RAD-MPC formulations was low, between 4 and 11 %.

6. Cements were quite stable with time in the experimental conditions used, which could be attributed to their composition, as well as to their low porosity.

7. The bonding strength between the cements and the dentin was significantly higher for the three MPCs than for MTA.

8. The microleakage of the three RAD-MPCs suffered a moderate increase with time when the root canal was obturated with or without gutta-percha. After 3 and 6 months, the microleakage was

significantly lower for the three RAD-MPC formulations than for MTA when the root canal was obturated with or without gutta-percha. The gutta-percha increased the microleakage of the root canal at short times, but the root canals obturated with gutta-percha suffered a lower increase in microleakage with time.

7.7 Acknowledgements

7.8 References

[1] Tronstad L. Clinical endodontics: a textbook. New York, USA: Thieme, 2003.

[2] Vasudev S, Goel B, Tyagi S. Root end filling materials: a review. Dental Traumatology 1996; 12: 161–178.

[3] Gartner A, Doran S. Advances in endodontic surgery. Dental Clinics of North America 1992; 36: 357–337.

[4] Saghiri MA, Shokouhinejad N, Lotfi M, Aminsobhani M. Push-out bond strength of mineral trioxide aggregate in the presence of alkaline pH. Journal of Endodontics 2010; 36: 1856–1859.

[5] van Noort R. Introduction to dental materials. London: Mosby, Elsevier, 2007.

[6] Bergenholtz G, Hørsted-Bindslev P, Reit C, editors. Textbook of endodontology. Chichester: Wiley-Blackwell, 2009.

[7] Norma Española UNE-EN ISO No.6876. Dental root canal sealing materials, 2003.

[8] Roberts HW, Toth JM, Berzins DW, Charlton DG, Mi M. Mineral trioxide aggregate material use in endodontic treatment: a review of the literature. Dental Materials 2007; 4: 149–164.

[9] Tadier S, Le Bolay N, Girod-Fullana S, Cazalbou S, Charvillat C, Labarrère M, Boitel D, Rey C, Combes C. Co-grinding significance for calcium carbonate-calcium phosphate mixed cement. Part II: effect on cement properties. Journal of Biomedical Materials Research B 2011; 99: 302–313.

[10] Carvalho-Junior JR, Correr-Sobrinho L, Correr AB, Sinhoreti MAC, Consani S, Sousa-Neto MD. Radiopacity of root filling materials using digital radiography. International Endodontic Journal 2007; 40: 514–520.

[11] Joint Committee for Powder Diffraction Studies (JCPDS). International Center for Diffraction Data and American Society for Testing Materials. Powder diffraction file (Inorganic and Organic). Swarthmore (USA) 1991.

[12] Lacy J. Semi-automatic determination of calcium and magnesium hardness in water. Talanta 1963; 10: 1031–1040.

[13] Chen PS, Toribara TY, Warner R. Microdetermination of phosphorus. Atomic Energy, 1956; 28: 1756–1758.

[14] O'Connell MS, Morgan, LA, Beeler, WJ, Baumgartner JC. A comparative study of smear layer removal using different salts of EDTA. Journal of Endodontics 2000; 26: 739–743.

[15] Vizgirda PJ, Liewehr FR, Patton, WR, Mcpherson, JC, Buxton TB. A comparison of laterally condensed gutta-percha, thermoplasticized gutta-percha and mineral trioxide aggregate as root canal filling materials. Journal of Endodontics 2004; 30: 103–106.

[16] Monticelli F, Osorio R, Toledano M, Ferrari M, Pashley DH, Tay FR. Sealing properties of one-step root-filling fibre post-obturators *vs.* two-step delayed fibre post-placement. Journal of Dentistry 2010; 38: 547–552.

[17] Yildirim T, Tas T. The evaluation of the influence of using MTA in teeth with post indication on the apical sealing ability. Oral Surgery Oral Medicine Oral Pathology 2009; 108: 471–474.

[18] Monticelli F, Sword J, Martin R, Schuster G, Weller R, Ferrari M, Pashley DH, Tay FR. Sealing properties of two contemporary single-cone obturation systems. International Endodontic Journal 2007; 40: 374–385.

[19] Santos J, Tja L, Ferraz C, Zaia A, Alves M, Goes MD, Carrilho M. Long-term sealing ability of resin-based root canal fillings. International Endodontic Journal 2010; 43: 455–460.

[20] Dunne NJ, Orr J. Thermal characteristics of curing acrylic bone cement. ITBM-RBM 2001; 22: 88–97.

[21] Khairoun I, Boltong M, Driessens FCM, Planell JA. Limited compliance of some apatitic calcium phosphate bone cements with clinical requirements. Journal of Materials Science: Materials in Medicine 1998; 9: 667–671.

[22] Ginebra MP, Fernández E, De Maeyer EA, Verbeeck RM, Boltong MG, Ginebra J, Driessens FCM, Planell JA. Setting reaction and hardening of an apatitic calcium phosphate cement. Journal of Dental Research 1997; 76: 905–12.

[23] Cutajar A, Mallia B, Abela S, Camilleri J. Replacement of radiopacifier in mineral trioxide aggregate: characterization and determination of physical properties. Dental Materials 2011; 27: 879–891.

[24] Lide D. CRC Handbook of Chemistry and Physics (internet version). Boca Raton: CRC, 2010.

[25] Wagh AS. Chemically bonded phosphate ceramics: 21st century materials with diverse applications. Hurst E, editor. Oxford: Elsevier, 2004.

[26] Sarkar AK. Phosphate Cement-Based Fast-Setting Binders. Ceramic Bulletin 1990; 69: 234–238.

[27] Sarkar AK. Hydration/dehydration characteristics of struvite and dittmarite pertaining to magnesium ammonium phosphate cement systems. Journal of Materials Science 1991; 26: 2514–2518.

[28] Abdelrazig B, Sharp J, Siddy P, El-Jazairi B. Chemical reactions in magnesia-phosphate cement. Proceedings of the British Ceramic Society 1984; 35: 141–154.

[29] Soudée E, Péra P. Mechanism of setting reaction in magnesia-phosphate cements. Cement and Concrete Research 2000; 30: 315–321.

[30] Fridland M, Rosado R. Mineral trioxide aggregate (MTA) solubility and porosity with different water-to-powder ratios. Journal of Endodontics 2003; 29: 814–817.

[31] Lumley P, Shelton RM, Hofmann M, Coomaraswamy K. Evaluation of different radiopacifiers for an MTA-like dental cement. Bioceramics 20 2008; 361-363: 885-888.

[32] Wu M, van der Sluis L, Ardila C, Wesselink P. Fluid movement along the coronal two-thirds of root filling placed by three different gutta-percha techniques. International Endodontic Journal 2003; 36: 533–540.

[33] Neville AM. Properties of concrete. London: Pitman Pub, 1975.

[34] Harrison ML, Johns MR, White ET, Mehta CM. Growth rate kinetics for struvite crystallization 1992; 1939: 3–8.

[35] Rahaman MS, Mavinic DS, Bhuiyan MIH, Koch FA. Exploring the determination of struvite solubility product from analytical results. Environmental Technology 2006; 27: 951–961.

[36] Bhuiyan MIH, Mavinic DS, Beckie R. A solubility and thermodynamic study of struvite. Environmental Technology 2007; 28: 1015–1026.

[37] Burns J, Finlayson B. Solubility product of magnesium ammonium phosphate hexahydrate at various temperatures. Journal of Urology 1982; 128: 426–428.

[38] Abbona F, Madsen H, Boistelle R. Crystallization of two magnesium phosphates, struvite and newberyite: effects of pH and concentration. Journal of Crystal Growth 1982; 57: 6–14.

[39] Wu Q, Bishop P. Enhancing struvite crystallization from anaerobic supernatant. Journal of Environmental Engineering and Science 2004; 3: 21–29.

[40] Snoeyink V, Jenkins D. Water chemisty. New York: John Wiley & Sons, 1980.

[41] Booram C, Smith R, Hazen T. Crystalline phosphate precipitation from anaerobic animal waste treatment lagoon liquors. Trans ASAE 1975; 18: 340–343.

[42] Moseke C, Saratsis V, Gbureck U. Injectability and mechanical properties of magnesium phosphate cements. Journal of Materials Science: Materials in Medicine 2011; 22: 2591–2598.

[43] Vivan RR, Zapata RO, Zeferino MA, Bramante CM, Bernardineli N, Garcia RB, Hungaro-Duarte MA, Tanomaru Filho M, Gomes de Moraes I. Evaluation of the physical and chemical properties of two commercial and three experimental root-end filling materials. Oral Surgery, Oral Medicine, Oral Pathology, Oral Radiology and Endodontics 2010; 110: 250–256.

[44] Fridland M, Rosado R. MTA solubility: a long term study. Journal of Endodontics 2005; 31: 376–379.

[45] Wu F, Su J, Wei J, Guo H, Liu C. Injectable bioactive calcium-magnesium phosphate cement for bone regeneration. Biomedical Materials 2008; 3: 1–7.

[46] Wu F, Wei J, Guo H, Chen F, Hong H, Liu C. Self-setting bioactive calcium-magnesium phosphate cement with high strength and degradability for bone regeneration. Acta Biomaterialia 2008; 4: 1873–1884.

[47] Wei J, Jia J, Wu F, Wei S, Zhou H, Zhang H, Shin JW, Liu C. Hierarchically microporous/macroporous scaffold of magnesium-calcium phosphate for bone tissue regeneration. Biomaterials 2010; 31: 1260–1269.

[48] Jia J, Zhou H, Wei J, Jiang X, Hua H, Chen F, Wei S, Shin J, Liu C. Development of magnesium calcium phosphate biocement for bone regeneration. Journal of the Royal Society, Interface 2010; 7: 1171–1180.

[49] Lu J, Wei J, Yan Y, Li H, Jia J, Wei S, Guo H, Xiao T, Liu C. Preparation and preliminary cytocompatibility of magnesium doped apatite cement with degradability for bone regeneration. Journal of Materials Science: Materials in Medicine 2011; 22: 607–615.

[50] Zou L, Liu J, Yin S, Li W, Xie J. *In vitro* evaluation of the sealing ability of MTA used for the repair of furcation perforations with and without the use of an internal matrix. Oral Surgery, Oral Medicine, Oral Pathology, Oral Radiology and Endodontics 2008; 105: 61–65.

[51] Reyes-Carmona JF, Felippe MS, Felippe WT. The biomineralization ability of mineral trioxide aggregate and Portland cement on dentin enhances the push-out strength. Journal of Endodontics 2010; 36: 286–291.

[52] Derkson GD, Pashley DH, Derkson ME. Microleakage measurement of selected restorative materials: a new *in vitro* method. The Journal of Prosthetic Dentistry 1986; 56: 435–440.

[53] Gandolfi MG, Prati C. MTA and F-doped MTA cements used as sealers with warm gutta-percha. Long-term study of sealing ability. International Endodontic Journal 2010; 43: 889–901.

[54] Brackett MG, Martin R, Sword J, Oxford C. Comparison of seal after obturation techniques using a polydimethylsiloxane-based root canal sealer. Techniques 2006; 32: 1188–1190.

[55] Gandolfi MG., Sauro S, Mannocci F. New tetrasilicate cements as retrograde filling material: an *in vitro* study on fluid penetration. Journal of Endodontics 2007; 33: 742–745.

Chapter 8.

General conclusions and future perspectives

I. General conclusions

This Thesis addresses the development of two novel families of inorganic cements for hard tissue regeneration or substitution: silicon-doped calcium phosphate cements and magnesium phosphate cements. Below are summarized the main findings for each of them.

➢ Regarding the **silicon-doped calcium phosphate cements:**

1. A new method to stabilize α-tricalcium phosphate with silicon was developed and optimized. The high temperature polymorph α-tricalcium phosphate was stabilized by the presence of silicon, which inhibited the reversion of the $\beta \rightarrow \alpha$ transformation. This was achieved by the addition of 2.54 wt% colloidal silicon oxide to a calcium deficient hydroxyapatite and subsequent sintering at 1250°C for 2 h, followed by slow cooling. In the Si-free sample α-tricalcium phosphate completely reverted to the β-polymorph. The addition of Si did not modify the $\beta \rightarrow \alpha$ transformation temperature, which took place between 1148 and 1150°C. Fourier Transform Infrared analysis suggested the formation of $Si_2O_7^{6-}$ groups within the α-TCP structure, following an oxygen-vacancy formation mechanism.

2. The Si-stabilized α-tricalcium phosphate was a suitable reactant for the preparation of silicon-containing calcium phosphate cements with adequate setting and cohesion times for clinical applications. Si-stabilized α-tricalcium phosphate was completely hydrolyzed to a calcium deficient hydroxyapatite, showing faster reaction kinetics than its Si-free counterpart, as proved by its shorter setting and cohesion times, as well as by its higher earlier compressive strength. Upon complete reaction, the crystalline phases, morphology and mechanical properties of both cements were similar.

3. The *in vitro* bioactivity of the calcium phosphate cements was enhanced by the addition of Si. The formation of an apatite layer when immersed in simulated body fluid was accelerated in the Si-containing calcium phosphate cements as compared to the Si-free calcium phosphate cements. This formed apatite layer had a higher Ca/P ratio and a higher Si content than the core material.

4. An *in vitro* cell culture study, in which osteoblastic-like cells were exposed to the medium modified by the Si-containing calcium phosphate cement and the undoped calcium phosphate cement, showed a delay in cell proliferation and stimulation of cell differentiation in both cases, the latter effect being more marked for the Si-containing cement. These results can be attributed to a strong modification of the ionic concentrations of the culture medium by both materials. Ca depletion from the medium was similarly observed for both cements, whereas continuous Si release was detected for the Si-containing cement.

➤ Regarding the **magnesium phosphate cements**:

1. A novel family of magnesium phosphate cements with different compositions was developed. The MPC reactants consisted of magnesium oxide and a phosphate salt, either $NH_4H_2PO_4$ or NaH_2PO_4 or a mixture of both.

2. The exothermy and setting times of the three magnesium phosphate cements were tailored for clinical applications by sintering the magnesium oxide, adjusting the particle size of the reactants and adding sodium tetraborate decahydrate (borax) as retardant. The cements exhibited very similar initial and by final setting times due to their fast setting. The sodium-containing formulations were injectable using a 2 mm-aperture syringe and a maximum load of 100 N.

3. The main product of the ammonium-containing cements was struvite ($MgNH_4PO_4 \cdot 6H_2O$), schertelite ($Mg(NH_4 \cdot HPO_4)_2 \cdot 4H_2O$) being an intermediate product of the reaction. An amorphous phase was formed in the magnesium phosphate cements prepared with NaH_2PO_4. Unreacted MgO was found in all formulations due to the addition of this reactant in excess.

4. The MPCs displayed high early compressive strength, reaching $30 - 50$ MPa after $1 - 2$ h, whereas conventional calcium phosphate cements only reached $1 - 5$ MPa at the same time. After 1 day, the magnesium phosphate cements reached their maximum compressive strength, which was close to 50 MPa.

5. The morphology of ammonium-containing cements showed elongated particles covered by a glassy layer, which was associated to the precipitation of a borate compound on the surface of magnesium oxide particles, thus retarding the reaction between the magnesium oxide and the

phosphate salts. The amorphous product of the magnesium phosphate cements prepared with NaH_2PO_4 resulted in a glassy-like microstructure.

6. In general, extracts of fresh magnesium phosphate cement prepared with NaH_2PO_4 had bactericidal properties against *Escherichia coli*, *Pseudomonas aeruginosa* (as free floating bacteria or as biofilm) and *Aggregatibacter actinomycetemcomitans*, whilst extracts of fresh magnesium phosphate cement prepared with $NH_4H_2PO_4$ or with an equimolar mixture of $NH_4H_2PO_4$ and NaH_2PO_4 had bacteriostatic properties against the same bacterial strains. The antimicrobial potency of these extracts was associated to the synergic effect of the high osmolarity and the pH modification.

7. Fresh magnesium phosphate cement extracts reduced osteoblastic-like cell viability. However, the cell viability increased by aging the cements, probably due to the lower osmolarity of these extracts.

8. The magnesium phosphate cement formulations were also optimized for endodontic applications. Radiopaque magnesium phosphate cements were developed, their physico-chemical properties not being substantially modified in comparison to magnesium phosphate cements. The cements showed to be quite stable with time, with a high cement-dentin bonding strength and a low microleakage up to 6 months, similar to that of commercial cements used for endodontic applications.

II. Future perspectives

This Thesis represents a step forward in the development of novel inorganic phosphate cements which have shown to present interesting outstanding properties for clinical applications. However, some of the studies should be continued by providing a more in depth characterization and other potential applications should be explored.

➢ Regarding **silicon-doped calcium phosphate cements**:

The physico-chemical modifications that silicon may induce upon incorporation into the α-tricalcium phosphate structure should be investigated through further characterization. Similar analysis should also be performed on the silicon-doped calcium deficient hydroxyapatite to prove introduction of Si into the structure.

Moreover, different strategies should be undertaken in order to be able to suggest possible mechanisms by which silicon increases the bioactivity of the doped-calcium phosphate cement and also stimulates the cell differentiation.

An additional study of potential interest would be to develop porous scaffolds of silicon-containing calcium deficient hydroxyapatite in order to improve cell colonization in bone regeneration applications. Cell seeding on these materials should be performed to evaluate cell colonization, proliferation and differentiation in these porous samples.

Finally, *in vivo* studies should be carried out to evaluate the real performance of these materials. In order to study the stimulation of new bone growth by the ceramic scaffolds, these scaffolds could be introduced in a previously drilled cavity in the femur of a small animal model like rabbit.

➢ Regarding **magnesium phosphate cements**:

Despite the great potential of the family of magnesium phosphate cements and its interesting properties, there are several aspects that should be addressed in view to their application in endodontic treatments. On the one hand, the paste should be optimized in order to guarantee its injectability by means of cannulae typically used in these applications. On the other hand, a more homogeneous radiopacity of the material should be achieved. From a more fundamental perspective, further studies should be performed to deeply understand the setting reaction mechanism of these cement formulations at short times. Further *in vitro* studies should be carried out to know in more detail the effect of cement aging on the cell response. Finally, *in vivo* studies should be performed using big animal models like dogs. In this study, root canals with vital pulp should be instrumented and obturated in a single session with the magnesium phosphate cements, which could be used as filler or as sealer materials.

The magnesium phosphate cements could also be considered for other clinical applications. On the one hand, the intrinsic high exothermy of the magnesium phosphate cements could be exploited in vertebroplasty, after removing a tumor confined in the vertebral column. Ideally, the cements would restore the mechanical properties of the injured site, at the same time that would destroy any remaining malign tissue. On the other hand, the magnesium phosphate cements as dense or porous structures could be used for bone regeneration applications after ensuring a good biocompatibility of the cements, which might restrict the use of only aged cements. It should be pointed out that these potential future applications are, by now, only ideas that require further studies at different levels to corroborate their feasibility.

Appendix.

Table of Contents

A1. Acronyms

α-TCP alpha-tricalcium phosphate

ALP alkaline phosphatase

β-TCP beta-tricalcium phosphate

BET Brunnauer – Emmet – Teller theory

CDHA calcium deficient hydroxyapatite

CPC calcium phosphate cement

DTA differential thermal analysis

FTIR fourier transform infrared spectra

FWHM full width at half maximum

HA hydroxyapatite

ICP-OES inductively coupled plasma-optical emission spectrometry

ICP-MS inductively coupled plasma-mass spectrometry

ICSD inorganic crystal structure database

JCPDS joint committee on powder diffraction standards

L/P liquid to powder ratio

LDH lactate dehydrogenase

MIP mercury intrusion porosimetry

MPC magnesium phosphate cement

MTA mineral trioxide aggregate

PBS phosphate buffers solution

SBF simulated body fluid

SEM scanning electron microscope

Si-α-TCP silicon-doped-alpha-tricalcium phosphate

SSA specific surface area

TEM transmission electron microscope

XRD X-ray diffraction

A.2. Data used to calculate the time-temperature damage threshold

Dunne *et al.* determined the maximum exothermy that the tissues surrounding a material can bear without suffering any harmful effect [1]. Figure A.1 was used to determine the maximum time that tissues could bear a determined temperature without suffering any irreversible damage.
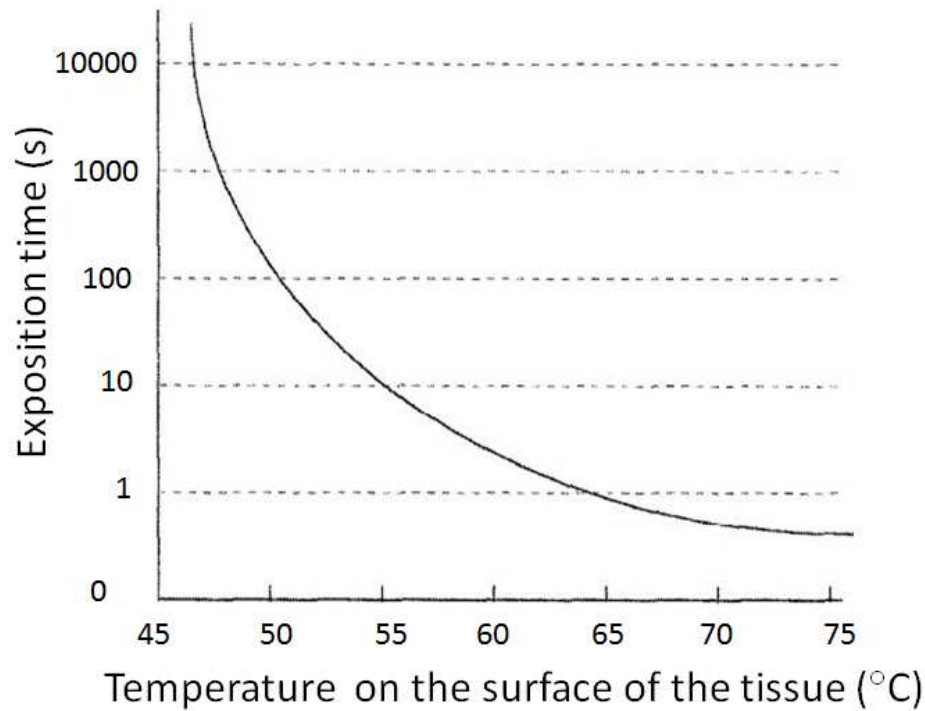
Figure A.1. Experimental curve that indicates the periods of time during which a determined temperature can be maintained causing just a mild damage to the surrounding tissue (left bottom) or an irreversible one (right top) (modified from [1], which extracted the data from [2]).

The data to calculate the time-temperature damage threshold was extracted from Figure A.1, and it is displayed in Table A.1. Thus, Table A.1 shows the exposition time that a tissue can bear a temperature without suffering irreversible damages.

---

[1] Dunne NJ, Orr J. Thermal characteristics of curing acrylic bone cement. ITBM-RBM 2001; 22: 88–97.
[2] Moritz AR, Henriques FC Jr. Studies of thermal injury, II: the relative importance of time and surface temperature in the causation of cutaneous burns. The American Journal of Pathology 1947; 23: 695–720.

Table A2.1. Exposition time that a tissue can bear a temperature without suffering irreversible damages (extracted from Figure A.1).

Exposition temperature (°C)	Exposition time (s)
46	10,000
48	1,000
50	100
55	10
60	2
65	0.8
70	0.6
75	0.5

Afterwards, a more extended Table (Table A.2) was done from the information extracted from Figure A.1. However, it has to be considered that the values of exposition times were approximated. Moreover, it was considered that temperature between 37 and 46°C would only cause irreversible damage if they were maintained for times longer than 10,000 s and that temperature between room temperature and 37°C would not cause any damage regardless the exposition time.

Table A2.2. Detailed values of the exposition time that a tissue can bear a temperature without suffering irreversible damages (approximated from Figure A.1).

Exposition temperature (°C)	Exposition time (s)	Exposition temperature (°C)	Exposition time (s)
45	1000	58.5	3
46	1000	59	2.3
47	1000	59.5	2.1
48	1000	60	2
48.5	500	60.5	1.8
49	210	61	1.5
49.5	120	61.5	1.2
50	100	62	1.1
50.5	70	62.5	1
51	52	63	1
51.5	40	63.5	1
52	32	64	1
52.5	28	64.5	1
53	20.5	65	1
53.5	18	65.5	1
54	12	66	1
54.5	10.8	66.5	1
55	10	67	1
55.5	8	67.5	1
56	7	68	1
56.5	6	68.5	1
57	5	69	1
57.5	4	69.5	1
58	3.2	70	1

A3. Growth curve values

A3.1. Fresh-cement extract

Table A3.3. Data of the growth curve of *E. coli* incubated in fresh-NH_4-MPC, Na-MPC and NH_4+Na-MPC broth-extract or in broth (control). The mean and standard deviation are indicated, n = 4.

Time (h)	NH_4-MPC-extract	Na-MPC-extract	NH_4+Na-MPC-extract	Broth (control)
0	$2.2 \cdot 10^5 \pm 2.6 \cdot 10^4$	$2.4 \cdot 10^5 \pm 2.5 \cdot 10^4$	$2.0 \cdot 10^5 \pm 2.3 \cdot 10^4$	$2.3 \cdot 10^5 \pm 2.5 \cdot 10^4$
1	$1.7 \cdot 10^5 \pm 5.7 \cdot 10^3$	$1.3 \cdot 10^5 \pm 1.1 \cdot 10^3$	$1.1 \cdot 10^5 \pm 1.2 \cdot 10^4$	$1.8 \cdot 10^5 \pm 2.5 \cdot 10^4$
2	$1.5 \cdot 10^5 \pm 2.9 \cdot 10^4$	$7.6 \cdot 10^4 \pm 9.9 \cdot 10^3$	$1.5 \cdot 10^5 \pm 1.4 \cdot 10^4$	$4.4 \cdot 10^5 \pm 7.7 \cdot 10^4$
4	$2.0 \cdot 10^5 \pm 4.8 \cdot 10^4$	$9.6 \cdot 10^4 \pm 1.7 \cdot 10^4$	$1.8 \cdot 10^5 \pm 1.6 \cdot 10^5$	$1.4 \cdot 10^6 \pm 5.9 \cdot 10^5$
8	$2.4 \cdot 10^5 \pm 1.9 \cdot 10^4$	$1.0 \cdot 10^4 \pm 9.9 \cdot 10^3$	$1.7 \cdot 10^5 \pm 1.8 \cdot 10^4$	$6.0 \cdot 10^7 \pm 6.4 \cdot 10^5$
24	$1.4 \cdot 10^5 \pm 4.2 \cdot 10^4$	0 ± 0	$2.4 \cdot 10^5 \pm 2.8 \cdot 10^3$	$1.0 \cdot 10^9 \pm 3.2 \cdot 10^8$

Table A3.4. Data of the growth curve of *P. aeruginosa* incubated in fresh-NH_4-MPC, Na-MPC and NH_4+Na-MPC broth-extract or in broth (control). The mean and standard deviation are indicated, n = 4.

Time (h)	NH_4-MPC-extract	Na-MPC-extract	NH_4+Na-MPC-extract	Broth (control)
0	$1.4 \cdot 10^5 \pm 5.3 \cdot 10^4$	$1.3 \cdot 10^5 \pm 5.3 \cdot 10^4$	$1.5 \cdot 10^5 \pm 5.3 \cdot 10^4$	$1.1 \cdot 10^5 \pm 5.3 \cdot 10^4$
1	$1.1 \cdot 10^5 \pm 5.1 \cdot 10^4$	$6.5 \cdot 10^3 \pm 7 \cdot 10^2$	$1.6 \cdot 10^5 \pm 1.5 \cdot 10^4$	$7.5 \cdot 10^4 \pm 3.4 \cdot 10^4$
2	$1.2 \cdot 10^5 \pm 4.1 \cdot 10^4$	$2.0 \cdot 10^3 \pm 1.4 \cdot 10^3$	$8.9 \cdot 10^4 \pm 4.9 \cdot 10^3$	$2.6 \cdot 10^5 \pm 8.5 \cdot 10^4$
4	$1.5 \cdot 10^5 \pm 4.9 \cdot 10^3$	0 ± 0	$9.1 \cdot 10^4 \pm 1.4 \cdot 10^3$	$1.3 \cdot 10^7 \pm 6.1 \cdot 10^6$
8	$1.2 \cdot 10^5 \pm 1.5 \cdot 10^4$	0 ± 0	$9.5 \cdot 10^4 \pm 3.2 \cdot 10^4$	$2.0 \cdot 10^8 \pm 3.7 \cdot 10^7$
24	$8.6 \cdot 10^4 \pm 6.4 \cdot 10^3$	0 ± 0	$6.9 \cdot 10^4 \pm 1.7 \cdot 10^4$	$2.2 \cdot 10^9 \pm 4.2 \cdot 10^8$

Table A3.5. Data of the growth curve of *A. actinomycetemcomitans* incubated in fresh-NH_4-MPC, Na-MPC and NH_4+Na-MPC broth-extract or in broth (control). The mean and standard deviation are indicated, n = 4.

Time (h)	NH_4-MPC-extract	Na-MPC-extract	NH_4+Na-MPC-extract	Broth (control)
0	$8.7 \cdot 10^5 \pm 1.4 \cdot 10^5$	$8.9 \cdot 10^5 \pm 1.2 \cdot 10^4$	$8.6 \cdot 10^5 \pm 1.8 \cdot 10^5$	$9.2 \cdot 10^5 \pm 2.0 \cdot 10^5$
2	$3.3 \cdot 10^4 \pm 3.5 \cdot 10^3$	0 ± 0	$1.5 \cdot 10^6 \pm 2.1 \cdot 10^3$	$1.4 \cdot 10^6 \pm 1.6 \cdot 10^5$
4	0 ± 0	0 ± 0	0 ± 0	$2.3 \cdot 10^6 \pm 3.7 \cdot 10^5$
8	0 ± 0	0 ± 0	0 ± 0	$7.2 \cdot 10^6 \pm 4.2 \cdot 10^6$
24	0 ± 0	0 ± 0	0 ± 0	$2.8 \cdot 10^8 \pm 5,6 \cdot 10^7$

A3.2 Aged-cement extract

Table A3.6. Data of the growth curve of *E. coli* incubated in aged-NH_4-MPC, Na-MPC and NH_4+Na-MPC broth-extract or in broth (control). The mean and standard deviation are indicated, n = 4.

Time (h)	NH_4-MPC-extract	Na-MPC-extract	NH_4+Na-MPC-extract	Broth (control)
0	$2.4 \cdot 10^5 \pm 4 \cdot 10^4$	$2.8 \cdot 10^5 \pm 6.0 \cdot 10^4$	$2.6 \cdot 10^5 \pm 5.0 \cdot 10^4$	$2.7 \cdot 10^5 \pm 2.8 \cdot 10^4$
1	$2.6 \cdot 10^5 \pm 3.6 \cdot 10^4$	$5.0 \cdot 10^2 \pm 7.1 \cdot 10^2$	$2.8 \cdot 10^5 \pm 1.5 \cdot 10^4$	$2.7 \cdot 10^5 \pm 4.2 \cdot 10^3$
2	$1.6 \cdot 10^5 \pm 2.1 \cdot 10^4$	0 ± 0	$3.0 \cdot 10^5 \pm 3.2 \cdot 10^4$	$3.9 \cdot 10^5 \pm 1.1 \cdot 10^4$
4	$2.5 \cdot 10^5 \pm 6.3 \cdot 10^4$	0 ± 0	$9.9 \cdot 10^5 \pm 8.4 \cdot 10^4$	$2.7 \cdot 10^6 \pm 1.8 \cdot 10^5$
8	$1.4 \cdot 10^6 \pm 5.2 \cdot 10^5$	0 ± 0	$2.8 \cdot 10^7 \pm 5.7 \cdot 10^5$	$5.1 \cdot 10^7 \pm 3.5 \cdot 10^6$
24	$1.4 \cdot 10^8 \pm 1.7 \cdot 10^7$	0 ± 0	$5.4 \cdot 10^8 \pm 8.5 \cdot 10^7$	$4.3 \cdot 10^8 \pm 5.7 \cdot 10^7$

Table A3.7. Data of the growth curve of *P. aeruginosa* incubated in aged-NH_4-MPC, Na-MPC and NH_4+Na-MPC broth-extract or in broth (control). The mean and standard deviation are indicated, n = 4.

Time (h)	NH_4-MPC-extract	Na-MPC-extract	NH_4+Na-MPC-extract	Broth (control)
0	$7.9 \cdot 10^4 \pm 3.0 \cdot 10^4$	$7.7 \cdot 10^4 \pm 4.0 \cdot 10^4$	$7.6 \cdot 10^4 \pm 4.0 \cdot 10^4$	$7.3 \cdot 10^4 \pm 3.0 \cdot 10^4$
1	$7.9 \cdot 10^4 \pm 9.9 \cdot 10^3$	$1.9 \cdot 10^4 \pm 2.8 \cdot 10^3$	$9.3 \cdot 10^4 \pm 2.9 \cdot 10^4$	$2.1 \cdot 10^5 \pm 1.3 \cdot 10^5$
2	$9.3 \cdot 10^4 \pm 3.5 \cdot 10^3$	$4.0 \cdot 10^3 \pm 1.4 \cdot 10^3$	$2.7 \cdot 10^5 \pm 2.1 \cdot 10^5$	$1.8 \cdot 10^5 \pm 2.0 \cdot 10^4$
4	$3.3 \cdot 10^5 \pm 1.8 \cdot 10^5$	0 ± 0	$9.9 \cdot 10^5 \pm 2.0 \cdot 10^4$	$1.5 \cdot 10^6 \pm 8.8 \cdot 10^5$
8	$1.0 \cdot 10^6 \pm 1.2 \cdot 10^5$	0 ± 0	$3.6 \cdot 10^7 \pm 4.5 \cdot 10^6$	$6.1 \cdot 10^7 \pm 3.8 \cdot 10^6$
24	$3.0 \cdot 10^8 \pm 1.2 \cdot 10^7$	0 ± 0	$1.5 \cdot 10^9 \pm 1.7 \cdot 10^8$	$2.5 \cdot 10^9 \pm 4.2 \cdot 10^8$

Table A3.8. Data of the growth curve of *A. actinomycetemcomitans* incubated in aged-NH_4-MPC, Na-MPC and NH_4+Na-MPC broth-extract or in broth (control). The mean and standard deviation are indicated, n = 4.

Time (h)	NH_4-MPC-extract	Na-MPC-extract	NH_4+Na-MPC-extract	Broth (control)
0	$1.3 \cdot 10^6 \pm 5.4 \cdot 10^5$	$1.5 \cdot 10^6 \pm 7.7 \cdot 10^4$	$1.4 \cdot 10^6 \pm 6.2 \cdot 10^5$	$1.3 \cdot 10^6 \pm 4.5 \cdot 10^5$
2	$4.5 \cdot 10^5 \pm 8.6 \cdot 10^4$	0 ± 0	$5.7 \cdot 10^5 \pm 6.0 \cdot 10^4$	$1.3 \cdot 10^6 \pm 6.4 \cdot 10^4$
4	$3.5 \cdot 10^4 \pm 1.7 \cdot 10^4$	0 ± 0	$1.4 \cdot 10^5 \pm 7 \cdot 10^3$	$2.2 \cdot 10^6 \pm 8.8 \cdot 10^4$
8	0 ± 0	0 ± 0	0 ± 0	$1.1 \cdot 10^7 \pm 8,8 \cdot 10^6$
24	0 ± 0	0 ± 0	0 ± 0	$2.0 \cdot 10^8 \pm 2.8 \cdot 10^7$

A4. Publications

The publications are shown in inverse chronological order

1. Mestres G, Ginebra MP. Desarrollo de cementos de fosfato de magnesio con alta resistencia mecánica y propiedades antimicrobianas. Congreso Nacional de Materiales.

2. Mestres G, Le-Van C, Ginebra MP. Preparation of Si-α-TCP by wet milling and its corresponding silicon doped calcium phosphate cements. Acta Biomaterialia 8 (2012) 1169-1179.

3. Mestres G, Ginebra MP. Novel magnesium phosphate cements with high early strength and antibacterial properties. Acta Biomaterialia 7 (2011) 1853–1861.

4. Ginebra MP, Espanol M, Montufar EB, Perez RA, Mestres G. New processing approaches in calcium phosphate cements and their applications in regenerative medicine. Acta Biomaterialia 6 (2010) 2863–2873.

5. Mestres G, Castano O, Navarro M, Almirall A, Ginebra MP, Planell JA. Micro and nanostructure evolution study of novel injectable calcium phosphate cements prepared by ceramic and sol-gel processes. Tissue Engineering (2007) 13 (7):1726-1726 274.

A5. Participation in congresses

The conference communications are shown in inverse chronological order. The presenting author is underlined.

1. <u>Mestres G</u>, Manzanares N, Ginebra MP. Radiopaque Magnesium Phosphate Cements. GRIBOI Congress (Society for Injectable Osteoarticular Biomaterials). Uppsala (Sweden), 2012. Oral presentation

2. <u>Mestres G</u>, Ginebra MP. Desarrollo de cementos de fosfato de magnesio con alta resistencia mecánica y propiedades antimicrobianas. XII Congreso Nacional de Materiales. Alicante (Spain), 2012. Oral presentation.

3. <u>Kent N</u>, Karpukhina N, Hill R, Ginebra MP, Mestres G. ^{31}P MAS NMR characterization of the cement setting reaction in magnesium phosphate cements. Bioengineering 11 (Queen Mary University of London). London (United Kingdom), 2011. Oral presentation.

4. <u>Mestres G</u>, Abdolhosseini M, Pastorino D, Bowles W, Huang SH, Aparicio C, Ginebra MP. Antimicrobial sodium magnesium phosphate cement: resorbability, bonding strength and sealability study. 24th European Conference on Biomaterials (ESB 2011). Dublin (Ireland), 2011. Oral presentation.

5. Mestres G, Abdolhosseinic M, Ginebra MP, <u>Gorr SU</u>. Antimicrobial properties of novel magnesium phosphate cements for endodontic treatment. International Association for Dental Research & American Association for Dental Research (89th General Session, IADR 2011). San Diego (California, US), 2011. Poster.

6. Mestres G, <u>Ginebra MP</u>. Magnesium phosphate cements for bone regeneration. 23rd European Conference on Biomaterials (ESB 2010). Tampere (Finland), 2010. Oral presentation.

7. <u>Mestres G,</u> Ginebra MP. Novel magnesium phosphate cements for endodontic treatment. International Association for Dental Research & American Association for Dental Research (88th General Session, IADR 2010). Barcelona (Spain), 2010. Poster

8. <u>Mestres G,</u> Le Van C, Ginebra MP. Silicon doped calcium phosphate cement: physical chemical properties and *in vitro* cell response. GRIBOI Congress 2010 (Society for Injectable Osteoarticular Biomaterials). Turin (Italy), 2010. Oral presentation.

9. <u>Ginebra MP</u>, Espanol M, Montufar EB, Perez RA, Mestres G. New processing approaches in calcium phosphate cements and their applications in regenerative medicine. V Congreso Internacional de Biomateriales BIOMAT 2010. La Habana (Cuba), 2010. Oral presentation.

10. <u>Mestres G,</u> Le Van C, Ginebra MP. New calcium phosphate cement doped with silicon for bone regeneration. 5th EEIGM/AMASE International Conference on Advanced Materials Research. Nancy (France), 2009. Poster.

11. <u>Mestres G,</u> Le Van C, Ginebra MP. New method to prepare silicon stabilized α-tricalcium phosphate. European Society of Biomaterials 2009 (ESB 2009). Lausanne (Switzerland), 2009. Oral presentation.

12. <u>Mestres G</u>, Castaño O, Navarro M, Almirall A, Sanzana ES, Ginebra MP, Planell JA A novel hybrid calcium phosphate/autocross linked polysaccharide injectable cement. 8th World Biomaterials Congress (WBC 2008). Amsterdam (The Netherlands), 2008. Poster.

13. Mestres G, <u>Castaño O</u>, Navarro M, Almirall A, Sanzana ES, Ginebra MP, Planell JA. Injectable calcium phosphate cements prepared by liquid-phase synthesis. Journées Sol-Gel du CEA. Tours (France), 2008. Oral presentation.

14. Mestres G, Rajzer I, <u>Castaño O</u>, Navarro M, Almirall A , Sanzana ES, Ginebra MP, Planell JA. Novel modified in-vivo casting for a Na-K doped calcium phosphate cement. 3rd World Congress Regenerative Medicine (WCRM). Leipzig (Germany), 2007. Oral presentation.

15. Mestres G, <u>Castaño O</u>, Navarro M, Almirall A, Sanzana ES, Ginebra MP, Planell JA. Micro and nanostructure evolution study of novel injectable calcium phosphate cements prepared by ceramic and sol-gel processes. Termis-EU meeting. London (United Kingdom), 2007. Oral presentation.

A6. Patents

1. Inventors   Ginebra MP, Mestres G

   Title   *"Cementos de fosfato de magnesio y sodio con propiedades antimicrobianas para aplicaciones óseas y dentales"* (Magnesium sodium phosphate cements with antimicrobial properties for osseous and dental applications)

   Application number   P201000359

   Application date   March 17th 2010

   Country of priority   Spain

2. Inventors   Ginebra MP, Mestres G

   Title   *"Método de obtención de fosfato tricálcio α estabilizado con elementos alfágenos y fosfato tricálcio α estabilizado obtenido"* (Method to obtain α tricalcium phosphate stabilized with alphagen elements and α tricalcium phosphate obtained)

   Application number   0300E-8796

   Application date   February 2nd 2009

   Country of priority   Spain